

Synthesis of Telechelic Polymers as
Functional Building Blocks in Material
Science and Biomedical Applications
Based on Thermoresponsive
Poly(2-Oxazoline)s and *N*-Substituted
Poly(Acrylamide)s

DISSERTATION

zur Erlangung des Grades eines Doktors
der Naturwissenschaften

vorgelegt von

M.Sc. Niklas Jung

eingereicht bei der Naturwissenschaftlich-Technischen Fakultät
der Universität Siegen
Siegen 2021

Die vorliegende Arbeit wurde in der Zeit von Oktober 2016 bis Juli 2021 in der Arbeitsgruppe der Makromolekularen Chemie an der Universität Siegen angefertigt.

Dekan:	Prof. Dr. Holger Schönherr
1. Gutachter:	Prof. Dr. Ulrich Jonas
2. Gutachter:	Prof. Dr. Holger Schönherr
Übrige Mitglieder der Prüfungskommission:	Prof. Dr. Heiko Ihmels Dr. Tony Le Gall
Tag der mündlichen Prüfung:	21.Dezember 2021

Content

1	Summary	1
	Zusammenfassung.....	4
2	Structures and Abbreviations	7
3	Aim and Outline of the Thesis	23
4	Introduction	27
4.1	Thermoresponsive Polymers.....	27
4.2	Cationic Ring Opening Polymerization (CROP) of 2-Oxazolines	30
4.3	Reversible Addition-Fragmentation Chain Transfer Polymerization (RAFT Polymerization).....	35
5	Results and Discussion	39
5.1	Synthesis and Post-functionalization Strategies of Poly(2-alkyl-2-oxazoline)s.....	39
5.1.1	Synthesis of Hemi-Telechelic Poly(2-oxazoline)s.....	40
5.1.2	Synthesis of Hetero-Telechelic Poly(2-oxazoline)s.....	59
5.1.3	Thiol-Substituted Poly(2-oxazoline)s with Photolabile Protecting Groups-Tandem Network Formation by Light	79
5.2	Synthesis and (Post-)Functionalization Strategies of <i>N</i> -Substituted Poly(acrylamide)s	112
5.2.1	Synthesis of Hemi-Telechelic Poly(NiPAm) Derivatives.....	112
5.2.2	Pendant Group Modification of Poly(<i>N</i> -hydroxyalkyl acrylamide)s.....	126
5.3	Synthesis of thermoresponsive Polymer-DNA Conjugates as Building Blocks for Smart Materials	141
5.4	Hetero-Telechelic Poly(2-oxazoline)s as Linkers for Biosensing Assays.....	155
5.5	Amino-Functionalized Poly(acrylamide)s as Alternative Safe Non-viral DNA Carriers for Transfection Applications: An <i>In Vitro</i> Study	169
6	Experimental Section	185
6.1	Equipment and Methods	185
6.2	Chemicals.....	186
6.3	Synthesis of Initiators and Oxazolines for CROP.....	188
6.3.1	Functionalized Tosylates as Initiators for CROP.....	188
6.3.2	2-Alky-2-Oxazolines	194
6.4	Synthesis of Acrylamide Monomers and RAFT-Agents	195

6.4.1	RAFT Agent and their Modifications	195
6.4.2	Synthesis of Amino-Functionalized Acrylamides.....	200
6.5	Experimental Procedures for Synthesis of Poly(2-Oxazoline)s.....	207
6.6	Post-functionalization Reactions of Poly(2-Oxazoline)s.....	222
6.7	General Procedures for RAFT-Polymerizations	234
6.8	Post-functionalization Reactions of Poly(acrylamide)s.....	239
6.9	Procedures for UV/Vis and Irradiation Experiments.....	247
6.10	Experimental Details of Surface Plasmon-Enhanced Fluorescence Spectroscopy (SPFS).....	249
6.11	Experimental Details of the Cell and Transfection Experiments.....	253
7	Appendix.....	255
7.1	Spectra of Non-Polymeric Compounds	255
7.1.1	Additional Spectra of Synthesized Tosylate Initiators.....	255
7.1.2	NMR-Spectra of Oxazoline Monomers	264
7.1.3	RAFT-Agents and their Modifications	266
7.1.4	Spectra of Amino-Functionalized Acrylamides and their Precursors.....	270
7.1.5	Additional Experimental Details for the Preparation of Multi-functional Hydrogels.....	284
7.2	Polymer Spectra	288
7.2.1	Spectra of Postfunctionalized Poly(2-Oxazoline)s	292
7.3	Poly(Acrylamide) Spectra.....	296
7.3.1	Spectra of Post functionalized Poly(Acrylamide)s	298
7.4	Additional UV/Vis Spectra	301
7.5	Additional Data Gel Electrophoresis Experiments	305
7.6	Additional Data of the SPFS Measurements.....	305
7.7	Additional Data of Transfection Experiments	306
8	References.....	311
	Acknowledgements.....	331

1 Summary

Thermoresponsive and biocompatible polymers attend nowadays great attention in research areas like DNA nanotechnology, continuous monitoring of analytes in biosensing assays and gene therapy as non-viral vectors. Therefore, it is crucial to design and adjust the molecular architecture of such polymers to the corresponding requirements of the targeted application, e.g., by the specific structure of the monomers, by the choice of comonomer composition, and by the introduction of functional groups within the backbone or at the chain ends. The main focus of this thesis was directed towards the synthetic development of thermoresponsive polymer systems and study of their applicability as polymer-DNA-conjugates, as biosensor matrix, and as non-viral transfection vectors.

The design of *polymer-DNA conjugates* to achieve complex structure formation by hierarchical self-assembly with respect to responsive and reconfigurable matter combines the self-assembly pathways of block copolymers and DNA. Such conjugates allow the design of scaffolds with arbitrary and programmable shape, which can be applied e.g., as templates for the fabrication of nanoobjects with specific geometries. Thus, thermoresponsive polymer-DNA conjugates and their resulting superstructures are intensely studied in various research disciplines to understand their self-assembly mechanism. In the context of the collaboration with Dr. Emmanuel Stiakakis at the Forschungszentrum Jülich, synthetic routes based on cationic ring-opening polymerization (CROP) of 2-alkyl-2-oxazolines were developed in this thesis to obtain well-defined and thermoresponsive poly(2-oxazoline)s as co- and terpolymers carrying azide end groups. These functional end groups were introduced via 3-azidopropyl tosylate as initiator and sodium azide as termination agent. Furthermore, thermoresponsive NiPAm-based polymers were synthesized by reversible addition-fragmentation chain transfer (RAFT) polymerization, in which an azide-functionalized chain transfer agent was employed. A two-step post-functionalization strategy was developed, which includes the transformation of the respective azide group into an amino group by a Staudinger reduction and subsequent coupling of dibenzylcyclooctyne (DBCO)-groups via the *N*-hydroxysuccinimide (NHS) active ester. It was found that this efficient two-step post-functionalization strategy could be exploited for both, the poly(2-oxazoline) and the poly(NIPAm) derivatives carrying azide moieties. Efficient coupling of the azide- and DBCO-functionalized polymers with the respective azide-modified DNA derivative was demonstrated by gel electrophoresis experiments by the Stiakakis group in

Jülich. These experiments showed also that the poly(2-oxazoline)s react more efficiently with the DNA than the poly(NIPAm) derivatives.

The application of *hetero-telechelic poly(2-oxazoline)s as flexible linkers* in surface plasmon resonance (SPR) spectroscopy-based sensors are considered for the design of different biosensing assay architectures that allow continuous monitoring of small analytes. This research topic was investigated in collaboration with Dr. Jakub Dostalek at AIT in Vienna. For this purpose, well-defined, thermoresponsive and hetero-telechelic poly(2-oxazoline) copolymers were prepared by CROP, which carried an azide end group on one side for coupling to a fluorescent dye. The other chain end was modified with either an amine- or a (protected) thiol-end group for coupling to the sensor surface. Successful coupling of the thermoresponsive copolymers to the sensor surface could be demonstrated after deshielding the amine- or thiol-end groups, followed by conjugation of the fluorescent dye Alexa Fluor 647 to the azide groups. In order to mimic affinity interactions, temperature-modulated surface plasmon-enhanced fluorescence spectroscopy (SPFS) experiments were conducted with these polymer layers in the labs of the Dostalek group. A promising sensor design was identified, in which the fluorescence intensity could be reversibly switched upon modulation of the temperature. However, in all performed SPFS measurements photobleaching was observed as undesired side effect.

In another research focus, a novel polymer architecture based on *poly(2-oxazoline)s bearing protected thiol functionalities* was investigated, which can be selectively liberated by irradiation with UV light. Whereas free thiol groups often suffer from oxidation or other spontaneous reactions that degrade polymer performance, this strategy with masked thiol groups offers the possibility of photodeprotection on demand with spatio-temporal control while maintaining the polymer integrity. In order to gain access to thiol-containing poly(2-oxazoline)s as gel precursors, a novel oxazoline monomer 2-{2-[(2-nitrobenzyl)thio]ethyl}-4,5-dihydrooxazole (NbMEtOxa) carrying a 2-nitrobenzyl-shielded thiol group was synthesized and copolymerized with 2-ethyl-2-oxazoline (EtOxa) in varying ratios. Moreover, the concept of tandem network formation was exemplarily demonstrated by using the photoinitiator 2-hydroxy-2-methylpropiophenone (HMPP) and pentaerythritol tetraacrylate (PETA), a commercially available, tetrafunctional vinyl crosslinker. The crosslinking experiments indicate that a minimal ratio of ~10% NbMEtOxa repeat units in the polymer backbone is necessary for network formation and in-situ gelation in *N,N*-dimethylformamide.

Novel non-viral polymer-based vectors in gene therapy require several attributes like biocompatibility, the ability for strong DNA complexation, and an appropriate molar mass range. Further, the balance between hydrophobic moieties and charge influences their performance. The ability for complexation and the hydrophobicity of such carriers can be adjusted e.g., by varying the spacer lengths of the side chains carrying a positive charge or the number of amino groups at the side chain ends. The size of such a carrier molecule can be tailored with controlled polymerization techniques. Therefore, a series of copolymers composed of the biocompatible (2-hydroxyethyl) acrylamide (HEAm) and one of four different masked amino-functionalized acrylamides with different side chain lengths were prepared by RAFT polymerization with a targeted ratio of 30% side chains containing amino group. After removal of the amino protecting groups, the copolymers were scrutinized in *in vitro* experiments with different cell lines and compared to polyethyleneimine (PEI) as commonly adopted reference. The cell experiments were performed in collaboration with Dr. Tony Le Gall in the laboratories at the Université de Bretagne Occidentale in Brest. These studies demonstrated that the specifically synthesized polymers were tolerated by all tested cell types even at high polymer/DNA mass ratios. DNA complexation assays corroborated the ability to bind DNA for all tested polymers, in which the polymers carrying amino groups that are connected through a C12-spacer to the polymer backbone showed the best results. Further, in cell transfection experiments, the copolymers with the amino groups bound to the backbone by a C6-spacer yielded the best gene transfection efficiency. These results suggested that complexation of DNA outside of the cells and its release once inside target cells was best achieved with the latter compound under the experimental conditions explored. However, the transfection efficiency was lower compared to the gold standard polyethyleneimine (PEI).

Zusammenfassung

Thermoresponsive und biokompatible Polymere erhalten heutzutage große Aufmerksamkeit in Forschungsgebieten wie DNA-Nanotechnologie, kontinuierliche Detektion von Analyten in Biosensoren und in Gentherapie als nicht-viraler Vektor. Daher ist es von entscheidender Bedeutung, die molekulare Architektur solcher Polymere auf die entsprechenden Anforderungen der Zielanwendung abzustimmen, z. B. durch die spezifische Struktur der Monomere, durch die Wahl der Comonomerzusammensetzung und durch die Einführung von funktionellen Gruppen innerhalb der Kette oder an den Kettenenden. Der Schwerpunkt dieser Arbeit lag dabei auf der synthetischen Entwicklung thermoresponsiver Polymersysteme und der Untersuchung ihrer Anwendbarkeit als Polymer-DNA-Konjugate, als Biosensor-Matrix und als nicht-virale Transfektionsvektoren.

Das Design von *Polymer-DNA-Konjugaten* zur Erzielung komplexer Strukturbildung durch hierarchische Selbstorganisation in Bezug auf reaktionsfähige und rekonfigurierbare Materie kombiniert die Selbstorganisationswege von Blockcopolymeren und DNA. Solche Konjugate ermöglichen den Entwurf von Gerüsten mit beliebiger und programmierbarer Form, die z. B. als Vorlagen für die Herstellung von Nanoobjekten mit bestimmten Geometrien verwendet werden können. Dafür werden thermoresponsive Polymer-DNA-Konjugate und die daraus resultierenden Überstrukturen intensiv in verschiedenen Forschungsdisziplinen untersucht, um ihren Selbstorganisationsmechanismus zu verstehen. Im Rahmen der Zusammenarbeit mit Dr. Emmanuel Stiakakis vom Forschungszentrum Jülich wurden Synthesestrategien entwickelt, die auf der kationischen ringöffnenden Polymerisation (CROP) von 2-Alkyl-2-oxazolinen basieren, um definierte und thermoresponsive Poly(2-Oxazolin)e als Co- und Terpolymere mit Azid-Endgruppen zu erhalten. Die funktionellen Endgruppen wurden mittels 3-Azidopropyltosylat als Initiator und Natriumazid als Abbruchsreagenz eingeführt. Weiterhin wurden thermoresponsive NiPAm-basierte Polymere durch „Reversible Additions-Fragmentierungs Kettenübertragungs-Polymerisation“ (RAFT-Polymerisation) synthetisiert, bei der ein azidfunktionalisierter Kettenüberträger verwendet wurde. Es wurde eine zweistufige Postfunktionalisierungsstrategie entwickelt, die die Umwandlung der jeweiligen Azidgruppe in eine Aminogruppe durch eine Staudinger-Reduktion und die anschließende Kopplung von Dibenzylcyclooctin (DBCO)-Gruppen mittels *N*-Hydroxysuccinimid (NHS) Aktiv-Ester beinhaltet. Es wurde festgestellt, dass diese effiziente zweistufige Postfunktionalisierungs-

strategie sowohl für die Poly(2-Oxazolin)e als auch für die Poly(NIPAm) Derivate, die Azid-Gruppen enthalten, genutzt werden kann. Die effiziente Kopplung der Azid- und DBCO-funktionalisierten Polymere mit dem jeweiligen Azid- oder DBCO-modifizierten DNA-Derivat wurde in Gelelektrophorese-Experimenten von der Stiakakis-Gruppe in Jülich nachgewiesen. Diese Experimente zeigten auch, dass die Poly(2-Oxazolin)e effizienter mit der DNA reagieren als die vergleichbaren Poly(NIPAm) Derivate.

Der Einsatz von *heterotelechelischen Poly(2-Oxazolin)en als flexible Linker* in Oberflächen-Plasmonresonanz- (SPR) -Spektroskopie-basierten Sensoren wird für den Aufbau unterschiedlicher Sensor-Architekturen in Betracht gezogen, die eine kontinuierliche Detektion kleiner Moleküle ermöglichen. Dieses Forschungsthema wurde zusammen mit Dr. Jakub Dostálek am AIT in Wien untersucht. Zu diesem Zweck wurden durch CROP thermoresponsive und heterotelechelische Poly(2-Oxazolin) Copolymere mit definierten Molmassen hergestellt, die an einem Ende der Polymerkette eine Azidgruppe trugen, um sie an einen Fluoreszenzfarbstoff zu binden. Das andere Kettenende wurde entweder mit einer Amin- oder einer (geschützten) Thiol-Endgruppe zur Bindung an die Sensoroberfläche modifiziert. Die erfolgreiche Kupplung der thermoresponsiven Copolymere an die Sensoroberfläche konnte nach dem Entschützen der Amin- oder Thiol-Endgruppen und nach der Konjugation des Fluoreszenzfarbstoffs Alexa Fluor 647 an die Azid-Gruppen nachgewiesen werden. Um Affinitäts-Wechselwirkungen imitieren zu können, wurden mit diesen Polymerschichten Versuche zur temperaturmodulierten Oberflächenplasmon-verstärkten Fluoreszenzspektroskopie (SPFS) in Laboren der Dostálek-Gruppe durchgeführt. Dabei wurde ein vielversprechender Sensoraufbau identifiziert, bei dem die Fluoreszenzintensität bei Modulation der Temperatur reversibel geschaltet werden konnte. Jedoch wurde in allen durchgeführten SPFS-Messungen lichtinduziertes Ausbleichen des Farbstoffes als unerwünschte Nebenwirkung beobachtet.

In einem anderen Forschungsprojekt wurde eine neuartige Polymerarchitektur basierend auf *Poly(2-Oxazolin)en, die Thiol-Funktionalitäten tragen*, untersucht, welche durch Bestrahlung mit UV-Licht selektiv freigesetzt werden können. Während freie Thiol-Gruppen oft anfällig für Oxidation oder andere spontane Reaktionen sind, welche die Polymerleistung beeinträchtigen, bietet diese Strategie mit maskierten Thiol-Gruppen die Möglichkeit der gezielten Photoentschützung mit räumlicher und zeitlicher Kontrolle bei gleichzeitiger Aufrechterhaltung der Polymerintegrität. Um Zugang zu thiolhaltigen Poly(2-oxazolin)en als Gel-Vorstufen zu erhalten, wurde das neuartige Oxazolinmonomer 2-{2-[(2-nitrobenzyl)

thio]ethyl}-4,5-dihydrooxazol (NbMEtOxa) mit einer durch 2-Nitrobenzyl-geschützten Thiol-Gruppe synthetisiert und in unterschiedlichen Comonomerverhältnissen mit 2-Ethyl-2-oxazolin (EtOxa) copolymerisiert. Darüber hinaus wurde das Konzept einer Tandem-Netzwerkbildung exemplarisch mit dem Photoinitiator 2-Hydroxy-2-methylpropiophenon (HMPP) und Pentaerythritoltetraacrylat (PETA), einem gebräuchlichen, tetrafunktionellen Vinylvernetzer, demonstriert. Die Vernetzungsexperimente zeigen, dass ein Mindestverhältnis von ~10% NbMEtOxa-Wiederholungseinheiten im Polymer-Rückgrat für die Netzwerkbildung und die *In-situ*-Gelierung in *N,N*-Dimethylformamid erforderlich ist.

Neuartige, nicht-virale Polymer-basierte Vektoren in der Gentherapie erfordern mehrere Eigenschaften wie Biokompatibilität, die Fähigkeit zur starken DNA-Komplexierung und eine definierte Molmasse. Darüber hinaus beeinflusst das Gleichgewicht zwischen hydrophoben Anteilen und Ladung ihre Leistung. Die Komplexierungsfähigkeit und der hydrophobe Charakter solcher Träger können z. B. durch Variation der Spacer-Länge der positiv geladenen Seitenketten oder der Anzahl der Aminogruppen an den Seitenkettenenden eingestellt werden. Die Größe eines solchen Trägermoleküls kann mit kontrollierte Polymerisationstechniken angepasst werden. Daher wurde eine Reihe von Copolymeren bestehend aus dem biokompatiblen (2-Hydroxyethyl) Acrylamid (HEAm) und einem von vier verschiedenen maskierten aminfunktionalisierten Acrylamiden mit unterschiedlichen Seitenkettenlängen durch RAFT-Polymerisation mit einer angestrebten Menge von 30% Aminogruppen mit Seitenketten synthetisiert. Nach Entschützung der Aminogruppen wurden die Copolymeren in *in vitro* Experimenten hinsichtlich Zelltoxizität, DNA-Komplexierung und Transfektionseffizienz mit verschiedenen Zelllinien untersucht und Polyethylenimin (PEI) als Standard verglichen. Diese Zellexperimente wurden in Zusammenarbeit mit Dr. Tony Le Gall in den Laboren der Université de Bretagne Occidentale in Brest durchgeführt. Diese Studien zeigten, dass die speziell hergestellten Polymere von allen getesteten Zelltypen selbst bei hohen Polymer/DNA Massenverhältnissen toleriert wurden. DNA-Komplexierungstests zeigten eine gute Bindungsfähigkeit für alle getesteten Polymere. Insbesondere die Polymere mit Aminogruppen, die über einen C12-Spacer verbunden waren, zeigten die höchste DNA-Beladung. In Zelltransfektionsexperimenten wurden unter den gegebenen experimentellen Bedingungen die beste Gentransfektionseffizienz für die Copolymeren mit C6-Spacern zwischen den Aminogruppen und dem Polymer-Rückgrat gefunden. Allerdings war die Transfektionseffizienz im Vergleich zum Goldstandard Polyethylenimin (PEI) geringer.

2 Structures and Abbreviations

In the following chapter, the structure of all initiators (Table 2.2), monomers (Table 2.3 and Table 2.5), RAFT agents (Table 2.4) as well as basic polymeric structures (Table 2.6 and Table 2.7) are listed. For compounds, which were synthesized according to a procedure reported in literature the corresponding reference is stated. The abbreviation given for the corresponding structure will be used in the following chapters.

For each synthesized polymer, a unique label will be used, as explained below in Figure 2.1.

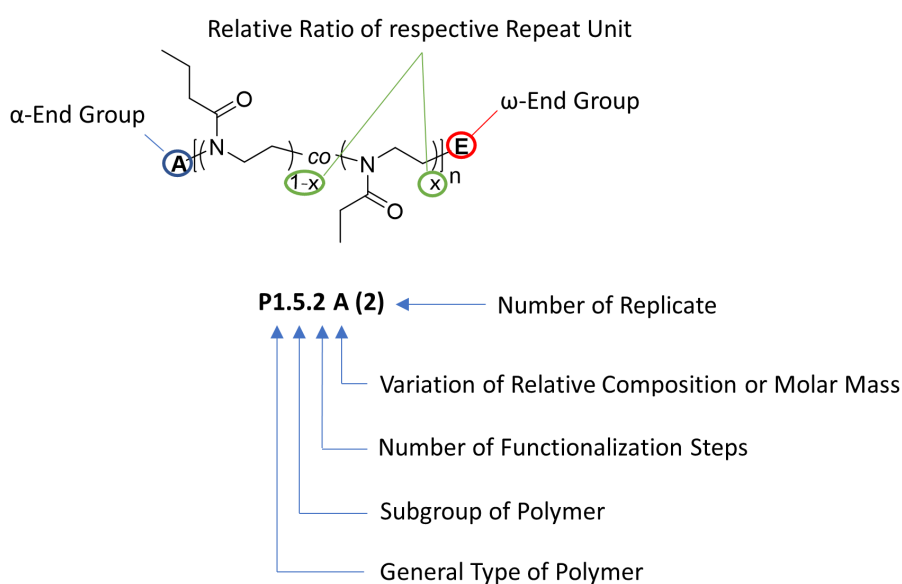


Figure 2.1: Illustration of the labeling code for the synthesized polymers which is used throughout the thesis.

This label includes information about the general type of the polymers as well as the subgroup, number of functionalization steps, and number of replicate. An example is explained in the following Table 2.1.

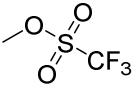
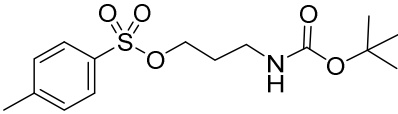
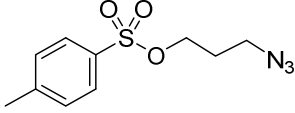
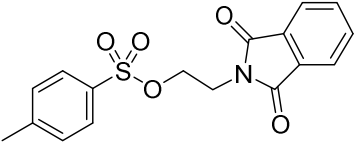
2 Structures and Abbreviations

Table 2.1: Explanation of example shown in Figure 2.1.

	Example	Explanation
General Type of Polymer	P1	Poly(2-oxazoline) [P2: Poly(acrylamide)]
Subgroup of Polymer	5	Copolymer composed of ethyl-2-oxazoline and <i>n</i> -propyl-2-oxazoline
Number of Functionalization Steps	2	2: DBCO-functionalization of amine end group (1: Staudinger reaction of N ₃ - end group)
Variation Relative Composition or Molar Mass	A	Molar mass: 30 kDa
Number of Replicate	(2)	The copolymer was synthesized in a second approach which was performed under the same conditions as the first synthesis

Further, the placeholder for the end groups A (α -end group) and E (ω -end group) as well as the structural format used for illustrating co- and terpolymers throughout the thesis are explained.

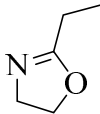
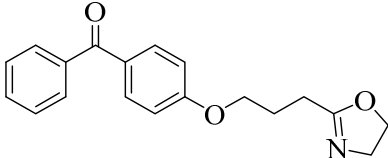
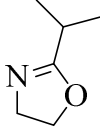
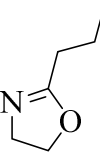
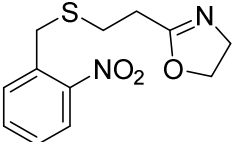
Table 2.2: Summary of initiators for cationic ring-opening polymerization (CROP).

Structure	Name	Abbreviation	Reference
	Methyl trifluoro-methanesulfonate	MeOTf	--- ^a
	3-[(<i>tert.</i> -Butoxycarbonyl)amino]propyl 4-methyl-benzenesulfonate	<i>N</i> -Boc-Prop-Tos	1
	3-Azidopropyl 4-methyl-benzenesulfonate	N ₃ -Prop-Tos	2
	2-(1,3-dioxo- <i>iso</i> indolin-2-yl)ethyl 4-methyl-benzenesulfonate	Pht-Et-Tos	3 ^b

^a commercially available ; ^b modified procedure

2 Structures and Abbreviations

Table 2.3: List of 2-oxazoline monomers used for different projects of the thesis.

Structure	Name	Abbreviation	Reference
	2-Ethyl-4,5-dihydrooxazole	EtOxa	--- ^a
	{4-[3-(4,5-Dihydro-oxazol-2-yl)propoxy]phenyl} (phenyl)methanone	BP-Oxa	4
	2-Isopropyl-4,5-dihydrooxazole	iPrOxa	5 ^b
	2-Propyl-4,5-dihydrooxazole	nPrOxa	5 ^b
	2-{2-[(2-Nitrobenzyl)thio]ethyl}-4,5-dihydrooxazole	NbMEtOxa	--- ^c

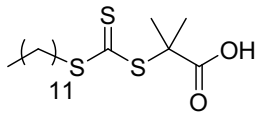
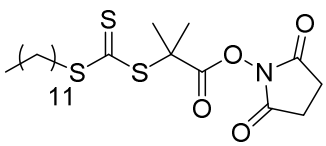
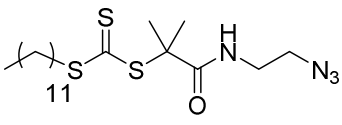
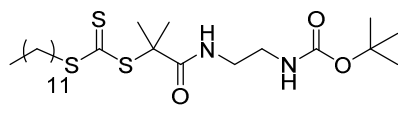
^a commercially available

^b modified procedure

^c new compound synthesized in this thesis

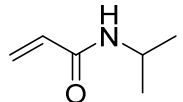
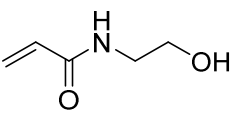
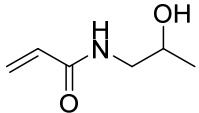
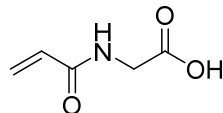
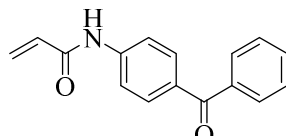
2 Structures and Abbreviations

Table 2.4: Register of RAFT-Agents used in this thesis.

Structure	Name	Abbreviation	Reference
	2-[[[(Dodecylthio)-carbonothioyl]thio]-2-methylpropanoic acid	DMP	6
	2,5-Dioxopyrrolidin-1-yl 2-[[[(ethylthio)carbonothioyl]thio]-2-methylpropanoate	DMP-NHS	7
	1-((2-Azidoethyl)amino)-2-methyl-1-oxopropan-2-yl ethyl carbonotrithioate	DMP-N ₃	--- ^a
	<i>tert.</i> -Butyl (2-(2-[[[(ethylthio)carbonothioyl]thio]-2-methylpropanamido)ethyl] carbamate	DMP-NH-Boc	8

^a new compound synthesized in this thesis

Table 2.5: Overview of acrylamide monomers used for synthesizing various polymers of the thesis.

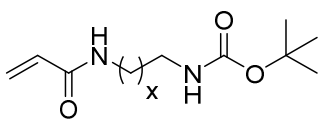
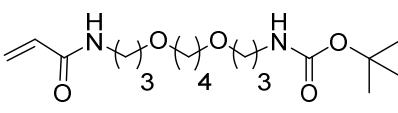
Structure	Name	Abbreviation	Reference
	<i>N</i> -(Isopropyl) acrylamide	NiPAm	--- ^a
	<i>N</i> -(2-Hydroxyethyl) acrylamide	HEAm	--- ^a
	<i>N</i> -(2-Hydroxypropyl) acrylamide	HPAm	9
	<i>N</i> -(2-Acetic acid) acrylamide	AaAm	10,11
	<i>N</i> -(4-Benzoylphenyl) acrylamide	BPAm	12b

^a commercially available

^b modified procedure

2 Structures and Abbreviations

Table 2.5 continued

Structure	Name	Abbreviation	Reference
			
x = 1	<i>N</i> -(2-Aminoethyl) acrylamide (Boc-protected)	AEAm (-Boc)	13,14
x = 2	<i>N</i> -(3-Aminopropyl) acrylamide (Boc-protected)	APAm (-Boc)	13,15
x = 5	<i>N</i> -(6-Aminohexyl) acrylamide (Boc-protected)	AHexAm (-Boc)	13,16
x = 11	<i>N</i> -(12-Aminododecyl) acrylamide (Boc-protected)	ADodAm (-Boc)	13,16
	<i>N</i> -{3-[(3-Aminopropoxy) butoxy]propyl} acrylamide	APOAm (-Boc)	13,17

2 Structures and Abbreviations

Table 2.6: Overview of all 2-oxazoline based polymers and their molar mass as well as their corresponding location in the thesis. The indices correspond to the relative composition of the co- or terpolymer (1-x, x) and the total number of repeat units (n). The abbreviation for each polymer stated in the table will be used throughout the thesis.

Structure	Name	Chapter	Abbreviation (Molar Mass / g·mol ⁻¹)
$R^1 =$ $R^2 =$	CH ₃ - Poly(nPrOxa) _n - NH ₂	5.1.1	P1.1
$R^1 =$ $R^2 =$	CH ₃ - Poly(iPrOxa) _n - NH ₂	5.1.1	P1.2
$R^1 =$ $R^2 =$	CH ₃ - Poly[(nPrOxa) _{1-x} - co-(iPrOxa) _x] _n - NH ₂	5.1.1	P1.3 A (3.2 k) B (5.0 k) C (6.8 k) D (10.5 k) E (15.2 k) F (18.1 k) G (10.2 k) H (18.9 k) I (22.6 k)
$A =$ $E =$	Pht-Et- Poly[(nPrOxa) _{1-x} - co-(iPrOxa) _x] _n -N ₃	5.1.2	P1.4 (9.9 k)
$A =$ $E =$	Pht-Et- Poly[(nPrOxa) _{1-x} - co-(iPrOxa) _x] _n -NH ₂	5.1.2	P1.4.1 (10.8 k)
$A =$ $E =$	H ₂ N-Et- Poly[(nPrOxa) _{1-x} - co-(iPrOxa) _x] _n -N ₃	5.1.2	P1.4.2 (14.9 k)
$A =$ $E =$	H ₂ N-Et- Poly[(nPrOxa) _{1-x} - co-(iPrOxa) _x] _n -NH ₂	5.1.2	P1.4.3 (16.3 k)

2 Structures and Abbreviations

Table 2.6 continued

Structure	Name	Chapter	Abbreviation (Molar Mass / g·mol ⁻¹)
A = E =	CH ₃ -Poly[(nPrOxa) _{1-x-} co-(EtOxa) _x] _n -N ₃	5.1.1	P1.5 A (---) ^a B (5.4 k) C (1) (9.0 k) C (2) (9.7 k) C (3) (10.1 k) C (4) (18.2 k) D (9.4 k) E (20.0 k) F (21.5 k)
A = E =	CH ₃ -Poly[(nPrOxa) _{1-x-} co-(EtOxa) _x] _n -NH ₂	5.1.1	P1.5.1 C (2) (9.5 k) C (3) (9.9 k) C (4) (17.9 k)
A = E =	CH ₃ -Poly[(nPrOxa) _{1-x-} co-(EtOxa) _x] _n -NH-C ₄ - DBCO	5.1.1 / 5.3	P1.5.2 C (3) (11.3 k) C (4) (17.9 k)
A = E =	CH ₃ -Poly[(nPrOxa) _{1-x-} co-(EtOxa) _x] _n -NH-C ₂ - DBCO	5.1.1 / 5.3	P1.7 (11.1 k)
A = E =	CH ₃ -Poly[(nPrOxa) _{1-x-} co-(EtOxa) _x] _n -OOC- C ₄ -DBCO	5.1.1 / 5.3	P1.8 (11.3 k)

^a no molar mass was determined

2 Structures and Abbreviations

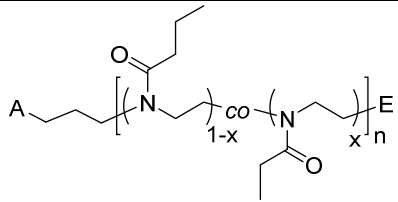
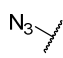
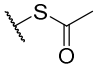
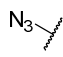
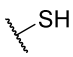
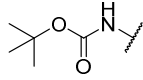
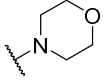
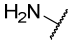
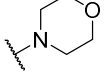
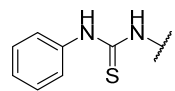
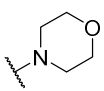
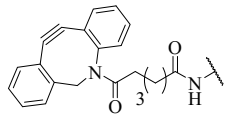
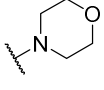
Table 2.6 continued

Structure	Name	Chapter	Abbreviation (Molar Mass / g·mol ⁻¹)
A = E =	CH ₃ -Poly[(nPrOxa) _{1-x-y} -co-(EtOxa) _x -co-(BP-Oxa) _y] _n -N ₃	5.1.1	P1.6 (8.2 k)
A = E =	CH ₃ -Poly[(nPrOxa) _{1-x-y} -co-(EtOxa) _x -co-(BP-Oxa) _y] _n -NH ₂	5.1.1	P1.6.1 (8.5 k)
A = E =	CH ₃ -Poly[(nPrOxa) _{1-x-y} -co-(EtOxa) _x -co-(BP-Oxa) _y] _n -NH-C ₄ -DBCO	5.1.1 / 5.3	P1.6.2 (9.4 k)
	N ₃ -Prop-Poly[(nPrOxa) _{1-x} -co-(EtOxa) _x] _n -N ₃	5.1.2 / 5.3	P1.9 (9.4 k)
	N ₃ -Prop-Poly[(nPrOxa) _{1-x-y} -co-(EtOxa) _x -co-(BP-Oxa) _y] _n -N ₃	5.1.2	P1.10 (---) ^b

^b polymer could not be isolated due to undesired side reactions

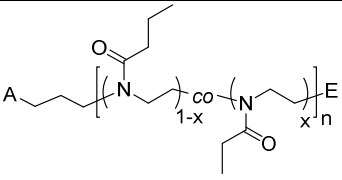
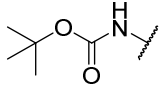
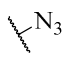
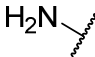
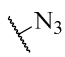
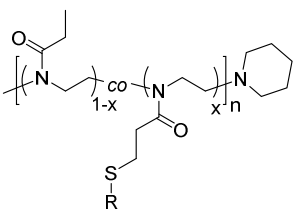
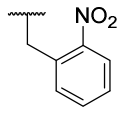
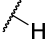
2 Structures and Abbreviations

Table 2.6 continued

Structure	Name	Chapter	Abbreviation (Molar Mass / g·mol ⁻¹)
			
A = 	E = 	N ₃ -Prop- Poly[(EtOxa) _{1-x} - co-(nPrOxa) _x] _n - S-Ac	5.1.2 / 5.3 P1.11 (8.0 k)
A = 	E = 	N ₃ -Prop- Poly[(EtOxa) _{1-x} - co-(nPrOxa) _x] _n -SH	5.1.2 / 5.3 P1.11.1 (9.3 k)
A = 	E = 	<i>N</i> -Boc-Prop- Poly[(EtOxa) _{1-x} - co-(nPrOxa) _x] _n -N ₃	5.1.2 P1.12 (1) (4.6 k) (2) (6.7 k)
A = 	E = 	<i>N</i> -Boc-Prop- Poly[(EtOxa) _{1-x} - co-(nPrOxa) _x] _n -N ₃	5.1.2 P1.12.1 (1) (4.4 k) (2) (6.5 k)
A = 	E = 	<i>N</i> -Boc-Prop- Poly[(EtOxa) _{1-x} - co-(nPrOxa) _x] _n -N ₃	5.1.2 P1.12.2 (1) (5.5 k) (2) (7.0 k)
A = 	E = 	DBCO-C ₄ -NH- Prop- Poly[(EtOxa) _{1-x} - co-(nPrOxa) _x] _n -N ₃	5.1.2 P1.12.3 (7.4 k)

2 Structures and Abbreviations

Table 2.6 continued

Structure	Name	Chapter	Abbreviation (Molar Mass / g·mol ⁻¹)
			
A = 	E = 	<i>N</i> -Boc-Prop- Poly[(EtOxa) _{1-x} - <i>co</i> -(<i>n</i> PrOxa) _x] _n -N ₃	5.1.2
			P1.13 A (1) (7.3 k) A (2) (7.1 k) B (9.5 k) C (10.9 k) D (12.4 k) E (14.7 k) F (16.1 k) G (16.0k) H (19.7 k) I (24.7 k)
A = 	E = 	H ₂ N-Prop- Poly[(EtOxa) _{1-x} - <i>co</i> -(<i>n</i> PrOxa) _x] _n -N ₃	5.1.2 / 5.3
			P1.13.1 A (1) (6.3 k) B (10.0 k) E (15.3 k) G (16.9 k) H (19.6 k) I (24.3 k)
			
R = 		Poly[(EtOxa) _{1-x} - <i>co</i> -(NbMEtOxa) _x] _n	5.1.3
			P1% (16.1 k) ^c P2.5% (13.7 k) P5% (8.0 k) P10% (5.6 k)
R = 		Poly[(EtOxa) _{1-x} - <i>co</i> -(MEtOxa) _x] _n	5.1.3
			P1% ^d P2.5% ^d P5% ^d P10% ^d

^c Abbreviation refer to the label used in the paper reproduced in chapter 5.1.3

^d no molar mass was determined after deprotection

2 Structures and Abbreviations

Table 2.7: Overview of all acrylamide-based polymers synthesized and their corresponding molar mass as well as the location within the thesis. The indices correspond to the relative composition of the co- or terpolymer (1-x, x or 1-x-y, x, y) and the total number of repeat units (n). The abbreviation for each polymer stated in the table will be used throughout the thesis.

Structure	Name	Chapter	Abbreviation (Molar Mass / g·mol ⁻¹)
E =	Poly(NiPAm) _n -N ₃	5.2.1	P2.1 A (4.7 k) B (1) (26.3 k) B (2) (23.4 k) B (3) (24.1 k) C (32.4 k) D (38.9 k)
E =	Poly(NiPAm) _n -NH ₂	5.2.1	P2.1.1 A (6.2 k) B (1) (23.9 k) B (2) (23.3 k) B (3) (26.0 k) C (32.5 k) D (21.7 k)
E =	Poly(NiPAm) _n -NH-C ₄ - DBCO	5.2.1 / 5.3	P2.1.2 A (6.0 k) B (1) (27.7 k) B (2) (20.9 k) B (3) (25.8 k) C (32.4 k) D (21.5 k)

Table 2.7 continued

Structure	Name	Chapter	Abbreviation (Molar Mass / g·mol ⁻¹)
E =	Poly[(NiPAm) _{1-x} -co-(BPAm) _x] _n -N ₃	5.2.1	P2.2 A (10.0 k) B (1) (16.9 k) B (2) (16.0 k) C (12.1 k) D (12.7 k) E (12.9 k)
E =	Poly[(NiPAm) _{1-x} -co-(BPAm) _x] _n -NH ₂	5.2.1	P2.2.1 A (22.0 k) B (1) (21.1 k) B (2) (22.2 k) C (20.8 k) D (22.6 k) E (16.9 k)
E =	Poly[(NiPAm) _{1-x} -co-(BPAm) _x] _n -NH-C ₄ -DBCO	5.2.1 / 5.3	P2.2.2 A (19.8 k) B (1) (25.5 k) B (2) (22.1 k) C (22.2 k) D (23.0 k) E (18.9 k)

Table 2.7 continued

Structure	Name	Chapter	Abbreviation (Molar Mass / g·mol ⁻¹)
R =	Poly[(HPAm) _{1-x} -co-(APAm{-Boc}) _x] _n	5.2.2	P2.3 (33.2 k)
R =	Poly[(HPAm) _{1-x} -co-(AHexAm{-Boc}) _x] _n	5.2.2	P2.4 (34.2 k)
R =	Poly[(HPAm) _{1-x} -co-(ADodAm{-Boc}) _x] _n	5.2.2	P2.5 (27.0 k)
R =	Poly[(HPAm) _{1-x} -co-(APOAm{-Boc}) _x] _n	5.2.2	P2.6 (21.7 k)
R =	Poly[(HPAm) _{1-x} -co-(APAm) _x] _n	5.2.2 / 5.5	P2.3.1 (15.2 k)
R =	Poly[(HPAm) _{1-x} -co-(AHexAm) _x] _n	5.2.2 / 5.5	P2.4.1 (21.0 k)
R =	Poly[(HPAm) _{1-x} -co-(ADodAm) _x] _n	5.2.2 / 5.5	P2.5.1 (18.8 k)
R =	Poly[(HPAm) _{1-x} -co-(APOAm) _x] _n	5.2.2 / 5.5	P2.6.1 (14.8 k)

Table 2.7 continued

Structure	Name	Chapter	Abbreviation (Molar Mass / g·mol ⁻¹)
$R^1 = $ $R^2 = $	Poly[(HEAm) _{1-x-y} - co-(HPAm) _x -co- (BPAm) _y] _n	5.2.2	P2.7 A (36.1 k) B (39.4 k) C (34.9 k)
$R^1 = $ $R^2 = $	Poly[(HEAm) _{1-x-y} - co-(AaAm) _x -co- (BPAm) _y] _n	5.2.2	P2.8 (31.9 k)
$R^1 = $ $R^2 = $	Poly[(HEAm) _{1-x-y} - co-(PrAm) _x -co- (BPAm) _y] _n	5.2.2	P2.9 (---) ^a
$R^1 = $ $R^2 = $	Poly[(HEAm) _{1-x-y} - co-(AEAm{-Boc}) _x - co-(BPAm) _y] _n	5.2.2	P2.10 (38.0 k)
$R^1 = $ $R^2 = $	Poly[(HEAm) _{1-x-y} - co-(APAm{-Boc}) _x - co-(BPAm) _y] _n	5.2.2	P2.11 (34.7 k)
$R^1 = $ $R^2 = $	Poly[(HPAm) _{1-x-y} - co-(AaAm) _x -co- (BPAm) _y] _n	5.2.2	P2.12 (34.0 k)
$R^1 = $ $R^2 = $	Poly[(HPAm) _{1-x-y} - co-(PrAm) _x -co- (BPAm) _y] _n	5.2.2	P2.13 (---) ^a
$R^1 = $ $R^2 = $	Poly[(HPAm) _{1-x-y} - co-(AEAm{-Boc}) _x - co-(BPAm) _y] _n	5.2.2	P2.14 (32.0 k)
$R^1 = $ $R^2 = $	Poly[(HPAm) _{1-x-y} - co-(APAm{-Boc}) _x - co-(BPAm) _y] _n	5.2.2	P2.15 (39.3 k)

^a no polymer could be isolated^b After deprotection the corresponding polymers are named **P2.10.1**, **P2.11.1**, **P2.14.1** and **P2.15.1**, respectively.

2 Structures and Abbreviations

Table 2.7 continued

Structure	Name	Chapter	Abbreviation (Molar Mass / g·mol ⁻¹)
$R^1 = $ $R^2 = $	Poly[(HEAm) _{1-x-} _{y-co-(AEAm)_{x-}} _{co-(BPAm)_y]} _n	5.2.2	P2.10.1 (33.3 k)
$R^1 = $ $R^2 = $	Poly[(HEAm) _{1-x-} _{y-co-(APAm)_{x-}} _{co-(BPAm)_y]} _n	5.2.2	P2.11.1 (34.6 k)
$R^1 = $ $R^2 = $	Poly[(HPAm) _{1-x-} _{y-co-(AEAm)_{x-}} _{co-(BPAm)_y]} _n	5.2.2	P2.14.1 (11.0 k)
$R^1 = $ $R^2 = $	Poly[(HPAm) _{1-x-} _{y-co-(APAm)_{x-}} _{co-(BPAm)_y]} _n	5.2.2	P2.15.1 (14.5 k)

In the following, abbreviations that are used in this thesis are listed:

AIBN	Azobisisobutyronitrile	M_p	Peak maximum of molar mass distribution
ATP	Adenosine triphosphate		
BP	Benzophenone	MWCO	Molecular weight cut-off
Boc	Tertiary butyloxycarbonyl	NHS	<i>N</i> -Hydroxysuccinimide
CROP	Cationic ring-opening polymerization	NMR	Nuclear magnetic resonance spectroscopy
CRC	Coil-Rod-Coil conjugate	OEI	Oligo(ethyleneimine)
<i>D</i>	Dispersity	OEG	Oligo(ethylene glycol)
DBCO	Dibenzylcyclooctyne	PEI	Poly(ethyleneimine)
DCM	Dichloromethane	PEG	Poly(ethylene glycol)
DMAc	<i>N,N</i> -Dimethylacetamide	PETA	Pentaerythritol tetraacrylate
4-DMAP	<i>N,N</i> -Dimethyl-4-aminopyridine	PMMA	Polymethylmethacrylate
DNA	Deoxyribonucleic acid	POxa	Poly(2-oxazoline)
DTPA-NHS	Bis(2,5-dioxopyrrolidin-1-yl) 3,3'-disulfanedioldipropanoate	RCR	Rod-Coil-Rod conjugate
EDC-HCl	1-Ethyl-3-(3-dimethylamino propyl)carbodiimide hydrochloride	RNA	Ribonucleic acid
EtOH	Ethanol	SAM	Self-assembled monolayer
EtOAc	Ethyl acetate	SP(R)	Surface plasmon (resonance)
equiv.	Equivalent	SPFS	Surface plasmon-enhanced fluorescence spectroscopy
FRET	Förster resonance energy transfer	r.t.	Room temperature
GP	General procedure	r.u.	Repeat units
h	Hour	SEC/GPC	Gel permeation chromatography
MeCN	Acetonitrile	TFA	Trifluoroacetic acid
MeOH	Methanol	THF	Tetrahydrofuran
MeOTf	Methyl trifluoromethanesulfonate	TLC	Thin layer chromatography
min	Minute	TMS	Tetramethylsilane
\bar{M}_n	Number-average molar mass	TosCl	4-Methylbenzene-1-sulfonyl chloride
\bar{M}_w	Weight-average molar mass	TPP	Triphenylphosphine
		TPPO	Triphenylphosphine oxide
		\bar{X}_n	Number-average degree of polymerization

3 Aim and Outline of the Thesis

In this thesis, the synthesis of different copolymers based on 2-oxazolines and acrylamides as well as their characterization and post-functionalization is presented. These functionalized copolymers were used in different projects. The structure of the thesis is shown below in Figure 3.1. In the chapters 5.1 and 5.2, results of the synthesis and the respective type of modification of either poly(2-oxazoline)s or poly(acrylamide)s will be presented and discussed. Then, the application of these functionalized polymers in the corresponding project (chapter 5.3-5.5) will be described.

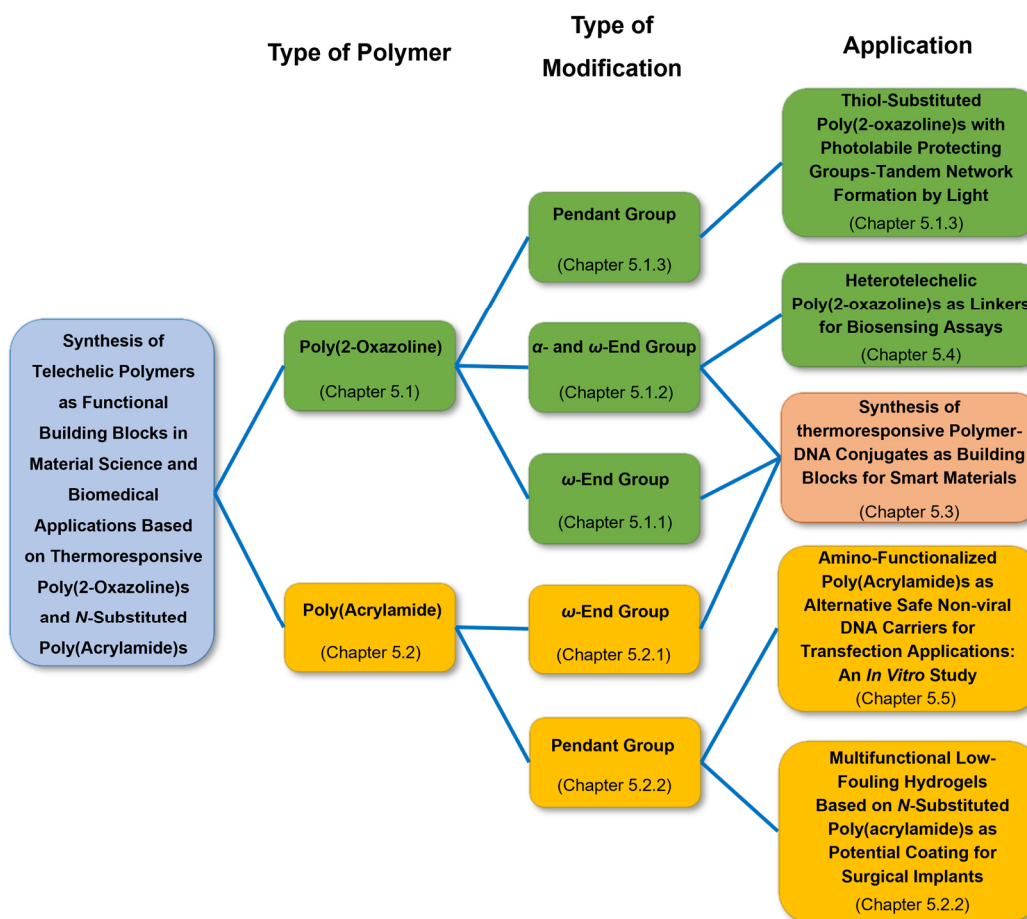


Figure 3.1: Schematic outline of the different polymers, types of modification and their relation to the respective application discussed in this thesis. References to the respective chapters are provided in brackets.

In the first project, end group-functionalized poly(NiPAm)s and poly(2-oxazoline)s were chosen as building blocks for the preparation of thermoresponsive polymer-DNA conjugates, which should be investigated by our collaboration partner Dr. Emmanuel Stiakakis at the

Forschungszentrum Jülich with respect to their temperature dependent self-assembly behavior (chapter 5.3) based on a recently published paper.^{18,19} Therefore, different approaches for both types of polymers (chapter 5.1.1 and chapter 5.2.1) should be tested in order to find an efficient synthesis and functionalization strategy that allows the preparation of hemi-telechelic copolymers with dibenzylcyclooctyne (DBCO) units as functional end groups. DBCO is known as highly reactive group, that couples efficiently and fast with azide-containing molecules. Thus, this so-called strain-promoted azide-alkyne click (SPAAC) chemistry might be suitable for the coupling of azide-functionalized DNA with DBCO-functionalized polymers to yield the desired polymer-DNA conjugates. Additionally, photocrosslinkable derivatives of the above-mentioned DBCO-functionalized polymers should be prepared to facilitate the investigation of the polymer-DNA architectures by immobilizing the shape via formation of crosslinks. These systems may find also application as templates for organizing gold nanoparticles into a diamond lattice to fabricate photonic crystals.^{20,21} Further, in this project a novel homo-telechelic poly(2-oxazoline) should be prepared that permits the coupling of two Y-shaped DNA strands, which can be used as core for the synthesis of a DNA dendrimers. These charged structures hold great promise in targeted self-assembly of soft matter, which can be very interesting in material sciences.²²

As a second objective, poly(2-oxazoline)s should be investigated with respect to their usability as flexible, thermoresponsive linkers in different SPR (surface plasmon resonance)-based biosensor architectures. The idea is to use these structures as smart molecular connector between the sensor surface and a specific ligand molecule that is responsible for capturing the analyte of interest (chapter 5.3). Therefore, different hetero-telechelic copolymers should be prepared (chapter 5.1.2), which carry at one distal end a reactive group for specific coupling of the targeting ligand. The other end group should be able to bind either to the sensor surface itself or should couple efficiently to an existing self-assembled monolayer e.g. by active ester chemistry. The reactive end groups will be introduced into the polymer chain by an appropriate functionalized initiator and a suitable termination agent. Initially, for demonstrating the working principle, the targeting ligand is to be replaced by a fluorescent dye in the anticipated sensor devices. Temperature modulation experiments should lead to a change in intensity of the fluorescence signal in response to the thermally dependent coiling behavior of the poly(2-oxazoline). From these experiments, the averaged distance of the fluorophore from the metal surface, and thus the coil dimensions of the polymer chain, can be estimated as reported by Sergelen and coworkers.²³

In a further synthetic challenge, an alternative approach to the strategy of Cesana and coworkers for the introduction of thiol units as pendant groups in poly(2-oxazoline)s should be developed since these are not tolerated during cationic ring-opening polymerization (CROP) (chapter 5.1.3). These authors masked the thiol functions with a 4-methoxybenzyl substituent during the polymerization step. However, the deprotection required harsh conditions.²⁴ In an alternative approach, the thiol groups should be masked with a photolabile protecting group, which can be cleaved by UV light under mild reaction conditions. Moreover, the idea is to combine the UV light induced thiol deprotection and subsequent network formation by photocrosslinking via thiol-ene coupling.²⁵

With respect to functional biocompatible macromolecules, different poly(acrylamide) copolymers containing various pendant functional groups should be synthesized and characterized (chapter 5.2.2) for the preparation of multifunctional and photocrosslinkable systems. Therefore, different acrylamides, which contain amino-, hydroxy- or carboxylic acid groups, should be prepared and characterized. Subsequently, these monomers should be used in combination with a photocrosslinkable monomer as toolbox for the synthesis of a library of co- and terpolymers. The systems containing photocrosslinkable groups should be tested as potential non-cell toxic and adhesive coating for surgical implants. Moving a step beyond, biocompatible copolymers composed of amino- and hydroxy group-containing acrylamides should be tested as potential non-viral vectors in gene delivery (chapter 5.5), since these copolymers possess a certain structural similarity to poly(amido amines) (PAA), a well-known class of gene delivery vectors.^{26,27}

4 Introduction

In the following sections the utilized polymerization techniques as well as the class of thermoresponsive polymers will be briefly described. The more specific topics like click chemistry and DNA-nanotechnology (chapter 5.3), surface plasmon-enhanced fluorescence spectroscopy (chapter 5.4) and transfection (chapter 5.5) will be introduced in the respective chapter.

4.1 Thermoresponsive Polymers

Synthetic, stimuli responsive polymers are nowadays of particular interest for biomedical applications. Many different external stimuli as e.g. light, temperature, pH or magnetic fields have been considered in the context of novel smart materials.²⁸ Especially, thermoresponsive polymers hold great promise for potential therapeutics^{29–31} or for tissue engineering.^{32,33} Their ability to respond to local increased body temperature, which is e.g. caused by inflammation, can be used for releasing appropriate drugs (targeted drug release).

Such polymers can be divided into two different classes, depending on their phase separation behavior from (here specifically aqueous) solution upon lowering or rising the temperature (Figure 4.1). Polymers, which exhibit a lower critical solution temperature (LCST), are soluble in aqueous media at low temperatures, because the solvent-polymer interactions caused by hydrogen bonding prevail the less pronounced inter- and intramolecular hydrogen bonding. With increasing temperature, the solvent-polymer interactions become less favored, and are superposed by the inter- and intramolecular forces leading to a change in solubility.^{34,35} This so-called LCST behavior is an entropically driven effect releasing the water molecules from the polymer chains, which in turn precipitate upon heating (hydrophobic effect).^{35,36} The opposite phenomenon, in which a polymer abruptly dissolves with increasing temperature, is called upper critical solution temperature (UCST) behavior and represents an enthalpically driven effect.³⁰ Reviews about UCST polymers have been published by different research groups.^{37–39}

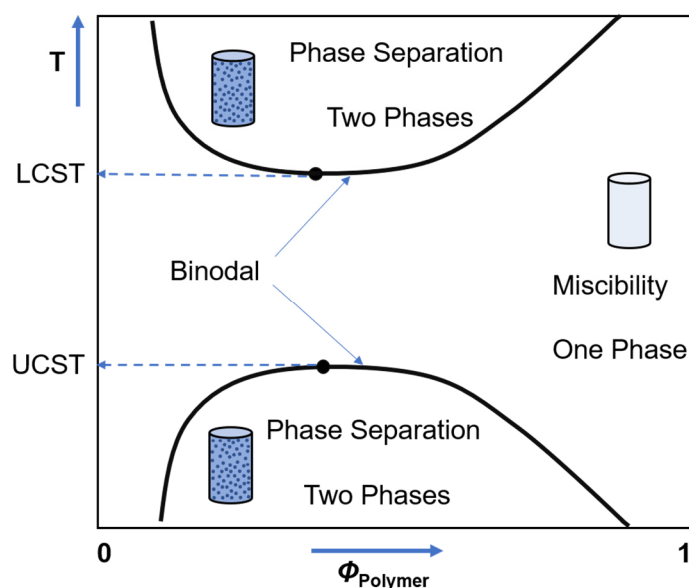


Figure 4.1: Simplified phase diagram with temperature T versus polymer volume fraction of a polymer-solvent mixture ϕ_{Polymer} , which either exhibit a LCST and/or a UCST behavior.

Further, the phase transition temperature depends strongly on the volume fraction of the polymer as shown in (Figure 4.1) as well as on the presence of cosolvents or, more important, dissolved salts. The type and concentration of those additives influence the strength of the solvent-polymer hydrogen bonding.⁴⁰ The LCST, as well as the UCST, are defined as minimum or maximum of the binodal curve in the respective phase diagrams.⁴¹

An interesting class of thermoresponsive polymers are poly(2-oxazoline)s (POxa), which is described in chapter 4.2. A selection of other polymers exhibiting a LCST behavior are shown in Figure 4.2. and described shortly below.

Poly(*N*-isopropylacrylamide) (PNiPAm) is the earliest reported⁴² and probably most investigated thermoresponsive polymer.²⁸ It possesses a phase transition temperature at around 30-34 °C, which is near body temperature and thus gaining a lot of interest for applications in targeted drug delivery systems.^{34,43} However, PNiPAm owns some disadvantages such as a phase transition hysteresis as well as a limited biocompatibility.^{28,44,45}

In contrast, poly(ethylene oxide) (PEO) and poly(propylene oxide) (PPO) as well as their copolymers are known to be highly biocompatible.^{46,47} Their phase transition temperature or cloud point temperature (T_c) can be varied from 20-85 °C depending on the molar ratio of ethylene oxide and propylene oxide in the copolymer. Further, these copolymers are commercially available.⁴⁸

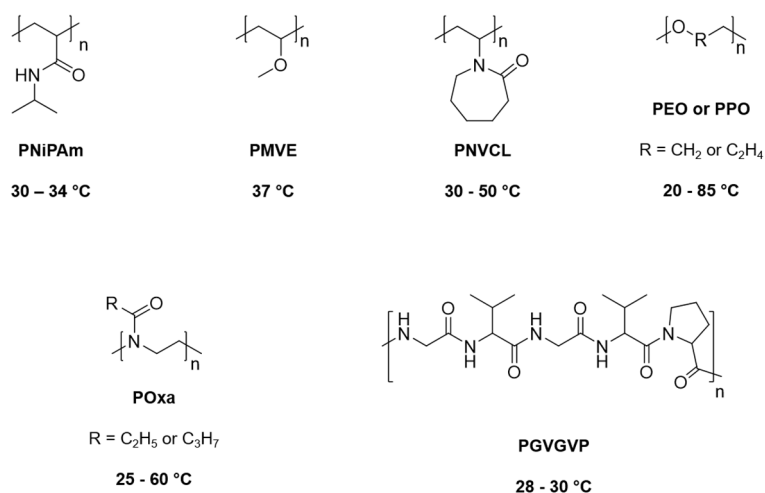


Figure 4.2: Selection of commonly used LCST polymers and their abbreviations. The corresponding temperature range given indicate the reported phase transition temperature.

Poly(methyl vinyl ether) (PMVE) possesses a transition temperature at 37 °C,²⁹ which is exactly human body temperature and thus very attractive for biomedicine. Another interesting polymer is poly(*N*-vinylcaprolactam) (PNVCL), which exhibits a cloud point around 32 °C⁴⁹ similar to PNiPAm. This non-ionic, water soluble polymer possess high biocompatibility, which renders the corresponding gels especially attractive for biomedical applications.⁵⁰

Elastin-like polymers are poly(pentapeptide)s composed of glycine (G), valine (V) and proline (P) (PGVGVP), where one of the valine units can be replaced by any natural amino acid except proline.^{35,51} Interestingly, these polymers are not described as classical LCST polymers in the literature, but as polymers with an inverse solubility temperature. This means that a different mechanism is responsible for the reversible phase transition upon temperature modulation compared to the classical mechanism described for PNiPAm.³⁵ A main difference to the classical LCST polymers is the fact that elastin-like polymers are weakly charged.³⁵

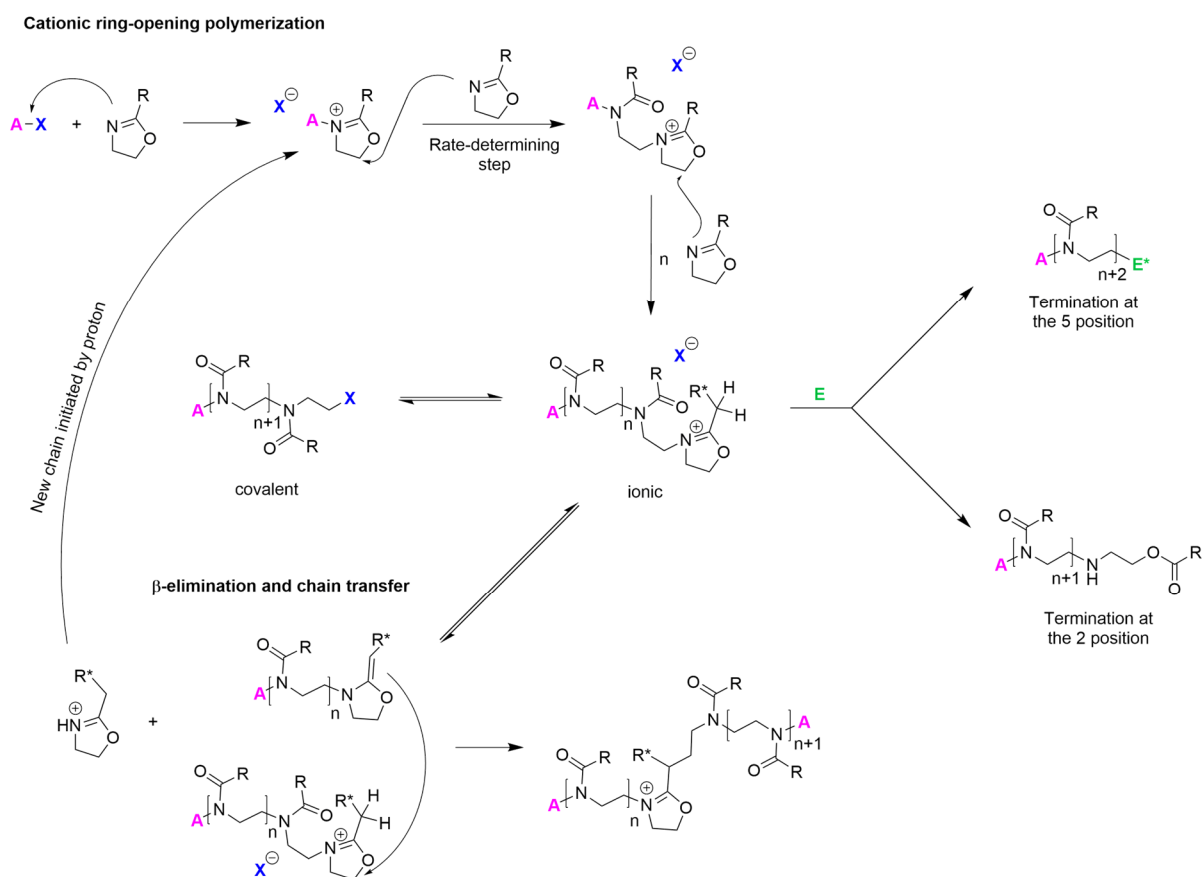
However, it could be shown that the phase separation process is much faster than the dissolution, which is similar to the hysteresis obtained e.g. for PNiPAm.³⁵ Below the phase transition temperature, water molecules are ordered in neighborhood to the polymer. By increasing the temperature of the solution, the structured water molecules become disordered due to weakening of attractive forces and thus resulting in a transition of the polymer into a bulky phase similar to the known mechanism for LCST-polymers.^{29,52} Above the transition temperature, however, the poly(pentapeptide)s form a secondary supramolecular structure (β -spiral), which favors hydrophobic interactions. This leads to the formation of nano- and microaggregates, and eventually to separation from solution.^{52,53}

4.2 Cationic Ring Opening Polymerization (CROP) of 2-Oxazolines

Cationic ring-opening polymerization (CROP) is beside anionic polymerization one of the controlled or ionic polymerization techniques, which allows the synthesis of well-defined polymers, and is the technique of choice for the polymerization of 2-oxazolines. First successful polymerizations of 2-oxazolines were reported in the 1970's by different groups.⁵⁴⁻⁵⁷ Nowadays a broad variety of 2-oxazoline derivatives is available. The most common substitution and functionalization of the 2-oxazolines is done in the 2-position. Substitution at the 4- and 5-position is also possible, but it will lead to the generation of a chiral center, which in case of polymerization, sterically hinders the chain propagation. Therefore, the propagation rate drops dramatically and thus, these oxazoline isomers are less used as monomers in research.⁵⁸⁻⁶²

CROP can be assigned to the chain-growth polymerization mechanism, which is subdivided into the initiation, propagation, and termination step. Driving force of the CROP of 2-oxazolines is the isomerization of the cyclic imino ether into a thermodynamically more favored tertiary amide.⁶³

Similar to the anionic living polymerization, the employed components like initiators, monomers and solvents have to be absolutely pure to avoid undesired reactions like termination, especially caused by traces of water, which leads to broadening of the molar mass distributions. The mechanism of CROP of 2-oxazolines is depicted in Scheme 4.1 on the next page. In the initiation step, the 2-oxazoline reacts by an exothermic nucleophilic attack with the electrophilic initiator forming a 2-oxazolinium cation. In dependence of the type of initiator, monomer and solvent, the counterion has an influence on the equilibrium between the cyclic cationic 2-oxazoline species and the covalent species.⁶⁴ Lewis acids, alkylating agents, iodine and even oxazolinium salts can initiate the CROP of 2-oxazolines.^{63,65-67} The most popular initiators are based on tosylates or triflates. Further, these initiators can be modified to allow the introduction of certain functionalities, like e.g. (protected) amino-,⁶⁸⁻⁷⁰ azide-^{71,72} or vinylic-^{73,74} groups at the α -chain end of the polymer (A). Additionally, different architectures of polymers could be obtained by using multifunctional initiators, which define the later shape.⁶³



Scheme 4.1: Simplified CROP mechanism of 2-oxazolines. “A” indicates the initiation species, “X” the corresponding counter ion and “E” represents the termination agent. (Adapted from literature with modifications.⁶³)

The propagation step is described as a two-step mechanism: A monomer molecule is added to the 2-oxazolinium species, which was formed in the initiation process. This addition step is very slow and is therefore the rate-determining step. Again an equilibrium between cationic- and covalent species is present, which depends on the type of counter ion, monomer and solvent.⁶³ After this addition, the propagation rate drastically increases, because of an intramolecular dipole-ion polarization effect that stabilizes the transition state and shifts the equilibrium towards the cationic species, which is more reactive than the covalent species.^{75,76} The addition rate of 2-oxazoline units depends on the nucleophilic character of the imine group and the partial positive charge at the 5-position of the propagating species.⁶³ Both effects are opposing to each other. An electron-donating substituent in the side chain of such a 2-oxazoline leads to an increased nucleophilicity of the imine group and thus the monomer is more reactive, while the partial cationic charge in the 5-position of the propagating chain damps the reactivity. Contrary trends are observed if an electron-withdrawing group is attached as a side group of

the 2-oxazoline.⁶³ Additionally, the steric demand of the monomer unit has to be considered when estimating the propagation rate. Further, many nucleophiles like e.g. primary and secondary amines, carboxylic acids and thiols are not tolerated by CROP, since they terminate the polymerization.⁷⁷ Nevertheless, in literature many of these functional groups, attached at the 2-position of a 2-oxazoline monomer, are reported, which were previously masked with suitable protecting groups.^{24,25,78–80}

The termination reaction of CROP can occur in either the kinetically controlled 2-position or the thermodynamically favored 5-position of the oxazolinium species, depending on the termination agent. In literature this behavior is discussed on the basis of the hard and soft acid and bases theory.⁶³ The authors argue that in contrast to the harder termination agents like amines, carboxylates or thiolates, the relative softer quenchers (like water and ammonia) tend to terminate at the 2-position,⁶³ leading to a secondary amine and an ester-containing group.^{81,82} The harder termination agents attack at the 5-position of the oxazolinium ring, resulting in the corresponding end capping functionality.⁸¹ The rate of termination depends, similar to the other reaction steps, on the equilibrium between covalent species and the more reactive cationic species. Further, the termination allows the introduction of a large variety of functional groups, even those that are not suitable during the polymerization process. This option offers the possibility to obtain various telechelic polymers.^{63,83} It should be denoted that side reactions decrease the number of active cationic chains and thus have a significant influence on the degree of functionalization at the ω -chain end (E), while each polymer chain can be functionalized at the α -chain end (A) by using a functionalized initiator.⁶³

As mentioned in the beginning, under ideal reaction conditions no side reactions should occur during the CROP of 2-oxazolines. However, chain transfer reactions are not avoidable even under laboratory conditions and thus present to a small extent. This leads to a loss of active chain ends and, hence, a broadening of the molar mass distribution. Litt and coworkers found that the main side reaction arises from a β -elimination, which is formally an imine-enamine rearrangement, leading to a proton-initiated oxazolinium cation, which can initiate a new polymer chain, and a polymer chain that loses its active center.^{84,85} This latter species may act as nucleophile, which can react with another active chain (chain coupling) to form a branching point.⁸⁴ Further, it was found that the chain transfer rate is much slower than the propagation rate and the chain coupling becomes more important at high conversions of monomer (> 75%).^{63,84} Also, an increased acidity of the α -protons in the 2-oxazoline derivative leads to

a more likely chain transfer⁸⁶ as well as elevated temperatures.⁸⁷ Opposite to this, an increasing steric hindrance of the α -position and lower reaction temperatures decreases the rate of chain transfer.^{84,87-89} However, a low reaction temperature leads to extended reaction times, because the propagation rate significantly drops.⁶³

Important is also the chain transfer activity of the utilized solvent. For example, acetonitrile, the mostly used solvent for CROP, exhibits a moderate chain transfer rate in which the nitrile group acts as the chain transfer active group.^{63,90} It has to be mentioned that for most of the solvent chain transfer reactions the exact mechanisms are still unknown.⁶³

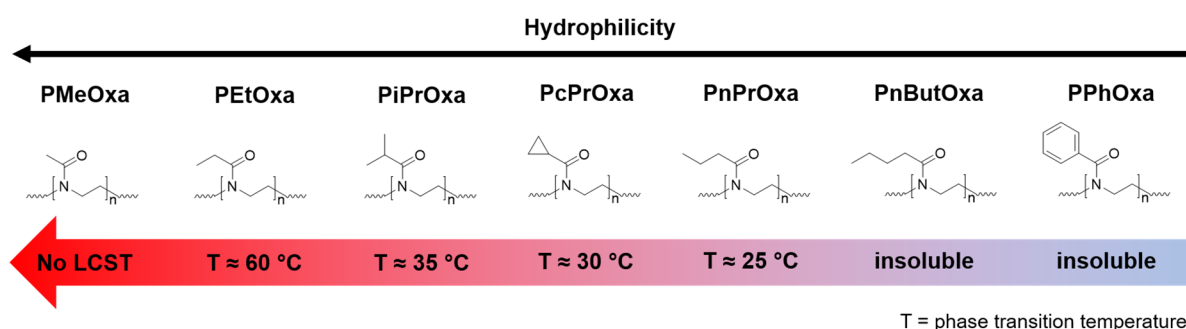


Figure 4.3: Schematic representation of the lower critical solution behavior of different poly(2-oxazoline)s.^{91,92} It should be denoted that most of the reported phase transition temperatures are not the absolute LCST values.

Various potential applications have been suggested by researchers investigating poly(2-oxazoline)s. However, due to the restrictive reaction conditions the synthesis of these polymers cannot be scaled up easily from laboratory to industrial quantities, which hamper the industrial implementation of this interesting class of polymers.⁶³

The thermoresponsive behavior of poly(2-oxazoline)s with short alkyl side chains in aqueous solutions (see above in chapter 4.1) is one of the most remarkable properties beside their biocompatibility.⁹²⁻⁹⁶ The combination of both properties renders them as very interesting polymers for biomedical applications. In Figure 4.3, representative examples of poly(2-oxazoline)s are illustrated. Poly(2-ethyl-2-oxazoline) (PEtOxa) and poly(2-propyl-2-oxazoline)s P(PrOxa) as well as their copolymers exhibit a lower critical solution temperature (LCST), whereas poly(2-methyl-2-oxazoline) (PMeOxa) is fully soluble in water between the freezing and the boiling point. In general, the solubility depends on the length of the alkyl side chain decreasing with increasing number of carbon atoms. For example, neither poly(2-n-butyl-2-oxazoline) (PnButOxa) nor the aromatic derivatives like poly(2-phenyl-2-oxazoline) (PPhOxa) are soluble in water under ambient pressure at any temperature. PEtOxa possesses a

LCST around 60 °C,⁹⁷ when the degree of polymerization is larger than 100.⁹⁸ The three poly(2-propyl-2-oxazoline) derivatives possess LCSTs in the range of room and human body temperature between 25 °C and 35 °C.⁹⁷

Poly(2-isopropyl-2-oxazoline) (PiPrOxa) shows the highest LCST and poly(2-*n*-propyl-2-oxazoline) (PnPrOxa) the lowest of these well-investigated polymers.^{91–93} In contrast, the third derivative poly(2-cyclopropyl-2-oxazoline) (PcPrOxa), which possesses a LCST around 30 °C, is less thoroughly examined, but it is anticipated as potential material in biomedicine.⁹⁹ Each of the presented 2-alkyl-2-oxazolines can be copolymerized with the others, which leads to a shift in the phase transition temperature in dependence of the composition. Hence, a tool box is available that allows the preparation of copolymers with the targeted thermoresponsive behavior or structure.^{62,88,97,100–105} Further, the LCST depends on the hydrophobicity of the end groups, chain length and salts present in the aqueous medium similar as for other thermoresponsive polymers.^{106–108}

Beside the thermoresponsivity and the good biocompatibility, poly(2-oxazoline)s offer other beneficial properties like high thermal stability⁶³ and low surface energy,¹⁰⁹ which make them interesting e.g. for building blocks in antifouling,⁴⁶ or therapeutic^{110,111} applications or as antimicrobial surface coatings.¹¹²

4.3 Reversible Addition-Fragmentation Chain Transfer Polymerization (RAFT Polymerization)

Another polymerization technique used in this thesis is the reversible addition-fragmentation chain transfer polymerization (RAFT-polymerization), which is beside atom transfer radical polymerization (ATRP) and nitroxide-mediated radical polymerization (NMP), one of the most used reversible-deactivation radical polymerization (RDRP) techniques to achieve well-defined polymers with narrow molar mass distributions.^{113–118} RAFT polymerization is probably the most versatile process due to its tolerance towards a wide variety of different reaction conditions and monomer functionalities compared to e.g. ATRP and NMP.¹¹⁹ Furthermore, the RAFT process can be performed in existing free radical polymerization set-ups, which is another benefit with respect to “green” chemistry.^{120,121}

Among these advantages, the chain transfer agent (CTA) is an indispensable molecule in this technique since it is responsible for controlling the radical polymerization in the RAFT process. Further, the CTA offers the possibility to introduce various functional motifs as end groups at the polymer chains.^{6,122–127} Additionally, these end groups can be subsequently converted into other functional groups,^{128–130} which are suitable for the synthesis of e.g. polymer-protein/peptide-^{131–133} or polymer-drug conjugates^{134–136} as therapeutics. Furthermore, a CTA allows the sequential introduction of different monomers yielding multi block copolymers.^{114,137–139}

In Scheme 4.2, the general structure of such a CTA featuring a thiocarbonyl group is shown **(1)**. The Z-group effects the stability of the intermediate radicals **(2)** and **(4)**, which influences the rate of adding the propagating radicals as well as the rate of fragmentation of the intermediates. In general, electron-withdrawing groups (EWG) at the Z-group lead to higher transfer coefficients, but also to more side reactions like aminolysis or hydrolysis at these groups.^{114,140}

The R-group must provide a good homolytic leaving group, which is also able to reinitiate the polymerization efficiently, otherwise retardation results as consequence. Researchers found that the transfer rate increases from primary to secondary to tertiary alkyl groups.¹⁴¹ Introduction of substituents with the capability to delocalize the radical center leads to the same effect.¹⁴² However, it is not sufficient that the leaving group is a monomeric analogue to the propagating chain, because the unit next to the radical unit possesses a large effect on the radical, especially

for tertiary R-groups. EWGs attached to the R-group lead on one hand to a decrease of chain additions at the thiocarbonyl fragment and on the other hand to an increasing rate of fragmentation of the radical intermediates (2) and (4).

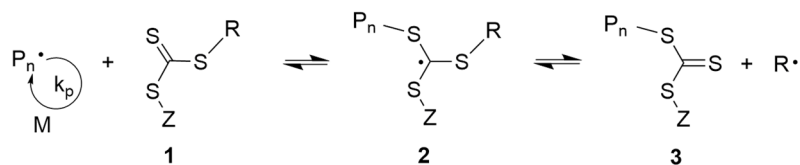
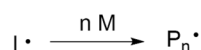
The most reactive CTAs are dithioesters and trithiocarbonates, wherein a sulfur or carbon atom is attached to the thiocarbonyl group. In contrast, RAFT agents carrying free electron pairs on nitrogen- or oxygen atoms, neighbored to the thiocarbonyl group, are less prone to radical addition reactions.¹⁴² This is a consequence of the conjugation of the free electron pair and the C=S double bond, which reduces the double-bond character and at the same time increase the stability of the RAFT agent against the addition of the reactive polymer chain.^{113,118,143,144}

For selecting an appropriate CTA, monomers can be subdivided into two groups. The group of “more activated monomers” (MAMs) contains monomers, in which the double bond is adjacent to an electron-withdrawing group like an aromatic system, a carbonyl or a nitrile group. Polymerizations of MAMs are best controlled by RAFT agents, which possess primary or secondary R-groups. In most cases the tertiary alkyl R-group is inefficient to reinitiate the polymerization.¹⁴⁵ In contrast, the class of “less activated monomers” (LAM) includes monomers, wherein the double bond is adjacent to a saturated carbon, an oxygen or a nitrogen that carry free electron pairs.¹⁴² Consequently, LAM monomers must be polymerized by using a less active CTA to achieve well-defined polymers.^{142,146}

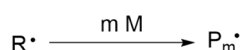
Since the versatility of classical CTAs is limited, Moad and coworkers designed RAFT agents, which are switchable to overcome this problem. Therefore, they designed dithiocarbamates, which preferentially polymerize LAM monomers with good control, but in the presence of a strong protic or Lewis acid the RAFT agent switches into a species, which preferentially polymerizes MAM monomers. Moreover, they could demonstrate that with such CTAs the preparation of block-copolymers composed of monomers possessing different reactivities is possible.^{141,146–148}

The simplified RAFT process is illustrated in Scheme 4.2. In most cases azo-initiators are used, but also peroxides are appropriate to initiate the polymerization. In the case of peroxides, irradiation with UV light leads to the generation of radicals, whereas azo-initiators are mostly activated by thermolysis.¹⁴⁹ The generated radical I \cdot , reacts with the monomer M. The formed polymeric radical P $_n\cdot$ reacts with the C=S double-bond of the CTA, resulting in a deactivation of the active propagating chain, and the RAFT species is in a so-called dormant state (2 and 4).

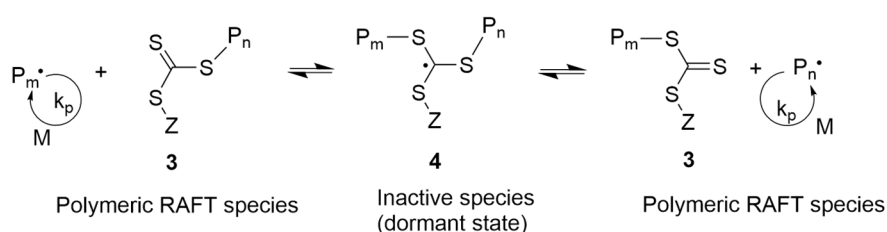
Initiation, propagation and chain transfer to RAFT agent



Reinitiation



Chain transfer to polymeric RAFT species and propagation



Termination



Scheme 4.2: Simplified mechanism of RAFT-Polymerization; M represents the monomer and R· represents the initial radical species, $P_n\cdot$ and $P_m\cdot$ indicate different polymer chains. (Adapted and modified from literature.^{150,151})

Subsequently, the CTA cleaves off the radical $R\cdot$, which can be the R-group of the CTA or the R-group with attached polymeric chain (more likely with progressing reaction time) that is able to reinitiate the polymerization and forms another polymeric species $P_m\cdot$.¹⁴⁹ In general, the polymerization rate rises with increasing concentration of the monomer.¹⁵² The combination of $P_n\cdot$ and $P_m\cdot$ leads to a dead polymer. This termination reaction is widely suppressed in an ideal RAFT process throughout the polymerization. But only in the early stage of a RAFT polymerization, where only low molecular-weight polymers are formed, this reaction is completely suppressed.¹⁵¹

Investigations of the RAFT process showed, that the molar ratio between the CTA and the initiator has to be as large as possible to achieve narrowest molar mass distributions.¹⁵³ By adjusting the molar ratio between monomer and CTA, it is possible to synthesize well-defined molar masses. The number average molar mass ($\bar{M}_{n,theo}$) can be calculated according to the formula shown on the next page

$$\bar{M}_{n,theo} = conversion \times M_{Monomer} \times \frac{[Monomer]_0}{[CTA]_0} + M_{CTA} \quad (1)$$

in which $M_{Monomer}$ and M_{CTA} are the molar masses of the monomer and the CTA, respectively. $[Monomer]_0$ and $[CTA]_0$ are the concentrations of the monomer and the chain-transfer agent at the start of the polymerization. The conversion is usually determined from a recorded 1H NMR spectrum by integrating a signal that corresponds to distinct protons in the polymer chain and a signal, which corresponds to protons within the monomer.

Although the general mechanism of RAFT-polymerization is well accepted, there are remaining discussions about the detailed kinetics of the different equilibria and the influence of side reactions on the efficiency of this technique.^{142,154} Recent investigations focus on e.g. the purpose of light as trigger for the RAFT polymerization processes,^{121,155} RAFT-mediated polymerization-induced self-assembly (PISA)¹¹⁹ or the application of RAFT polymerization in surfactant-free emulsion polymerization.¹⁵⁶

5 Results and Discussion

In the following subsections, first various polymerization strategies and the different types of modification methods of poly(2-oxazoline)s (chapter 5.1.1-5.1.3) and *N*-substituted poly(acrylamide)s (chapter 5.2.1 and 5.2.2) that were performed during the thesis, will be presented and discussed. Afterwards, results of different projects (5.3-5.5), in which these functionalized (co-)polymers were tested, will be debated. Initial results of the smaller projects (chapter 5.1.3 and 5.2.2) were discussed at the end of the respective chapter about the synthesis of the copolymers.

5.1 Synthesis and Post-functionalization Strategies of Poly(2-alkyl-2-oxazoline)s

In the following chapters, first the synthesis as well as the (post)functionalization of hemitelechelic, thermoresponsive poly(2-oxazoline) derivatives (see chapter 5.1.1) is discussed. In general, the thermoresponsiveness can be tuned by varying the monomer composition of different 2-alkyl-2-oxazolines. The functional end group of these polymers can be used for preparing thermoresponsive polymer-DNA conjugates (see chapter 5.3). The thermoresponsiveness will lead to a reversible structural change of such conjugates and thus also an alterable change in the phase behavior. In chapter 5.1.2, the synthesis and modification of hetero-telechelic polymers with different end groups like (protected) amino-, azide and (protected) thiols will be debated. These polymers were tested as thermoresponsive linkers that connected the sensor surface and a fluorescent dye (see chapter 5.4). The thermoresponsiveness of these polymers allow a modulation of the emitted fluorescence by changing the distance between the sensor surface and the dye molecule. In the last subchapter, the synthesis of a novel oxazoline monomer carrying 2-nitrobenzyl-shielded thiol groups will be presented as an alternative approach for the introduction of (masked) thiol moieties into poly(2-oxazoline)s. Also, the tandem network formation upon irradiation with UV light by thiol deprotection and concurrent crosslinking via thiol-ene coupling of the synthesized masked thiol-containing poly(2-oxazoline)s will be discussed (see chapter 5.1.3).

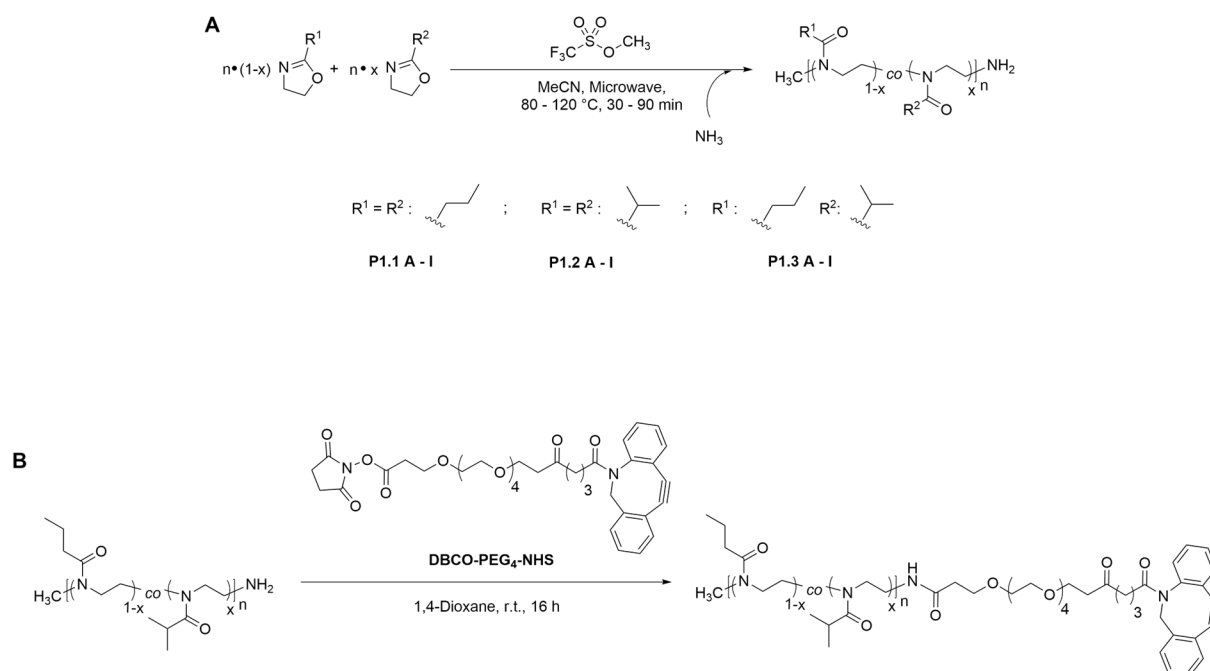
5.1.1 Synthesis of Hemi-Telechelic Poly(2-oxazoline)s

In this chapter, the synthesis of different end group-functionalized poly(2-oxazoline)s (POxa) are described and discussed. The copolymers composed of 2-ethyl-2-oxazoline (EtOxa) or *iso*-2-propyl-2-oxazoline (iPrOxa) and 2-*n*-propyl-2-oxazoline (nPrOxa) were synthesized as thermoresponsive building blocks for polymer-DNA systems, which are discussed in chapter 5.3. These three 2-oxazolines were chosen, since their combinations shows a LCST behavior depending of the molar ratio of incorporated comonomers into the polymer chain.^{88,97} As additional monomer {4-[3-(4,5-dihydrooxazol-2-yl)propoxy]phenyl} (phenyl)methanone (BP-Oxa) was used, which was previously synthesized within the group.⁴ The incorporation of such a monomer, which carries the photoactive benzophenone group, allows the crosslinking of polymer chains by irradiation with light.⁴ Further, the CROP of 2-oxazolines allow the introduction of various functional end groups beside highly defined molar masses and narrow molar mass distributions.⁹³

In a previous work, the influence of high reaction temperatures ($T = 120\text{ }^{\circ}\text{C} - 140\text{ }^{\circ}\text{C}$), induced by microwave irradiation, onto the molar mass and their distributions as well as the number of accessible end groups of different homopolymers composed of EtOxa, iPrOxa and nPrOxa was investigated. Key findings of this studies were the increased occurrence of side reactions during polymerization with increasing temperature as well as the influence of the chemical structure of the corresponding 2-oxazoline derivative.⁴ Further, it was found that a reaction temperature of $T = 120\text{ }^{\circ}\text{C}$ and a reaction time of $t = 90\text{ min}$ showed best results for the 2-alkyl-2-oxazoline homopolymers. The copolymerization of nPrOxa and iPrOxa possess the advantage that the LCST can be tuned from $T = 24 - 38\text{ }^{\circ}\text{C}$ depending on the molar ratio of these 2-oxazolines.⁹⁷

Optimization of reaction conditions for poly[(nPrOxa)-co-(iPrOxa)]-NH₂:

In literature, these copolymers were prepared by conventional heating and not by microwave irradiation. In order to refine reaction conditions for the copolymerization of iPrOxa and nPrOxa a series of corresponding homo- and copolymers with different reaction times ($t = 30\text{-}90\text{ min}$) and temperatures ($T = 80\text{ }^{\circ}\text{C} - 120\text{ }^{\circ}\text{C}$) were prepared. The reaction scheme is shown below in Scheme 5.1 A.



Scheme 5.1: Schematic overview of the cationic ring-opening homopolymerization of nPrOxa (**P1.1 A-I**) and iPrOxa (**P1.2 A-I**) and the copolymerization of iPrOxa and nPrOxa (**P1.3 A-I**) at various reaction conditions. The reaction was quenched by using gaseous ammonia (A). **P1.3 I** was further functionalized with DBCO-PEG₄-NHS as depicted in (B).

The polymerization was initiated by using commonly used methyl trifluoromethanesulfonate (MeOTf) and quenched by purging with gaseous ammonia to introduce an amino group at the end of the polymer backbone (**P1.3 A-I**). The termination procedure is described in literature.¹⁵⁷ As targeted molar mass $17.0 \text{ kg}\cdot\text{mol}^{-1}$ was chosen, which was adjusted by a monomer-to-initiator ratio of 150 to 1. The relative comonomer ratio of iPrOxa and nPrOxa was adjusted to 50:50 to yield thermoresponsive polymers that possess a cloud point temperature T_c around 32°C , which is comparable to the phase transition temperature of poly(NiPAm).^{43,158} Experimental details are provided in the experimental section (page 207). The yielded polymers were investigated by proton NMR spectroscopy. The molar mass at peak maximum (M_p) was determined by GPC and used as a reference for evaluation of the respective polymerization since this parameter is independent of the shape of the molar mass distribution peak and the integration thresholds that are used for the calculation of \bar{M}_n and \bar{D} . In **Fehler! Verweisquelle konnte nicht gefunden werden.**, the measured molar mass parameters and the calculated built-in of iPrOxa as well as the corresponding yields are listed. As expected, the yield of the polymerizations increased with reaction time and reaction temperature. Obviously, high temperatures ($T \geq 100^\circ\text{C}$) are necessary, to yield polymers with reliable M_p , because at $T = 80$

°C only short polymers with low masses ($M_p = 2.6\text{-}4.8 \text{ kg}\cdot\text{mol}^{-1}$) are obtained, which indicate an incomplete conversion of the comonomers and thus led to low yields. Further, the series showed that with increasing reaction time at constant temperature the yield as well as the M_p and their molar mass distribution (\mathcal{D}) increased.

Table 5.1: Overview of the different reaction conditions of the poly(nPrOxa-co-iPrOxa)s (P1.3 A-I) and the corresponding yields as well as the built-in of iPrOxa, determined by ^1H NMR spectroscopy. The M_p and \mathcal{D} were measured by GPC.

Polymer	T_{Reaction} / °C	t_{Reaction} / min	Built-In of iPrOxa (NMR) / %	M_p (GPC ^a , RI) / $\text{kg}\cdot\text{mol}^{-1}$	\mathcal{D}	Yield / mg (%)
P1.3 A		30	34	3.2	1.18	72 (18)
P1.3 B	80	60	34	5.0	1.19	96 (23)
P1.3 C		90	39	6.8	1.22	164 (40)
P1.3 D		30	40	10.5	1.30	163 (40)
P1.3 E	100	60	41	15.2	1.43	193 (47)
P1.3 F		90	44	18.1	1.47	276 (67)
P1.3 G		30	46	10.2	1.27	313 (76)
P1.3 H	120	60	46	18.9	1.49	323 (79)
P1.3 I		90	47	22.6	1.48	358 (87)

^a eluent : DMAc containing LiBr ($\beta = 1 \text{ g}\cdot\text{l}^{-1}$); PMMA standards were used for calibration

The increase in yield and M_p can be explained by increased consumption of monomer units, whereas the increase of the \mathcal{D} indicate the occurrence of intrinsic side reactions, which become more pronounced with increasing reaction time. The built-in of iPrOxa was determined by ^1H NMR spectroscopy. Therefore, the integral of the signal corresponding to the protons of the methyl groups of iPrOxa ($\delta = 1.09 \text{ ppm}$) and the integral of the signal assigned to the methyl group of nPrOxa ($\delta = 0.93 \text{ ppm}$) were compared (see Figure S58). In Figure 5.1, calculated built-in ratios of iPrOxa for **P1.3 A-I** and the corresponding M_p for different reaction times are plotted against the reaction temperature. The plot of the built-in ratios at different reaction times indicates that long reaction times of $t = 90 \text{ min}$ and high temperatures of $T = 120 \text{ °C}$ are needed to obtain the desired comonomer ratio in which equal numbers of iPrOxa and nPrOxa units are incorporated into the same polymer chain. Further, the increasing content of iPrOxa in the

polymer chains with increasing reaction time and reaction temperature indicated different copolymerization parameters of iPrOxa and nPrOxa.

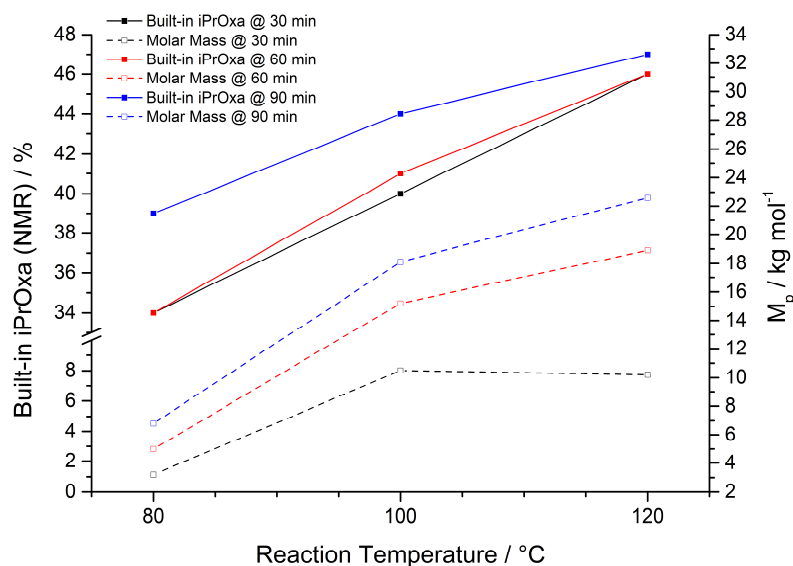
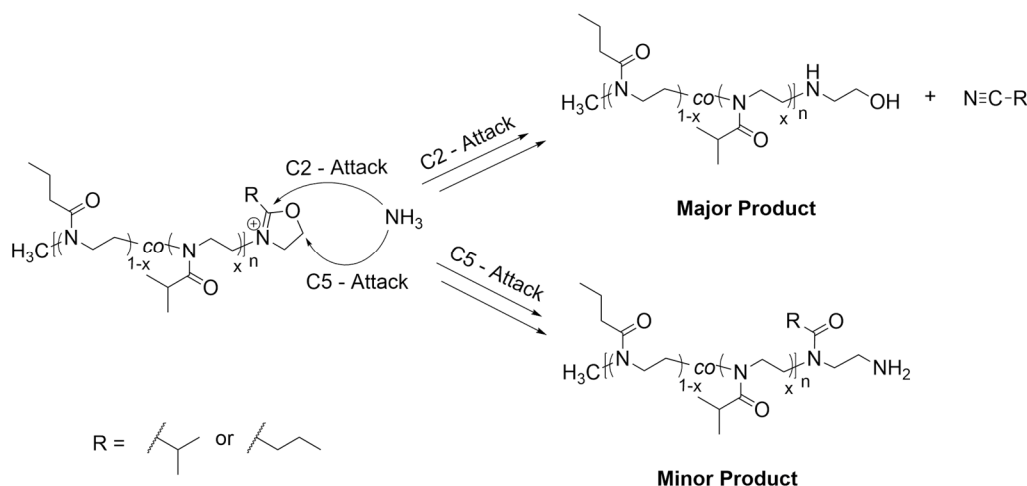


Figure 5.1: Illustration of the dependency of the built-in of iPrOxa and M_p on the reaction temperature as well as the reaction time (indicated by the different colors). The solid lines represent the built-in of iPrOxa into the polymer and the corresponding dashed line the measured M_p .

The lower reactivity of iPrOxa compared to nPrOxa can be explained with the inductive effect of the isopropyl group, which is able to stabilize the cationic charge in the oxazolinium ring at the propagating chain.¹⁵⁹ This leads to polymer chains in which preferentially nPrOxa units and less iPrOxa units were incorporated. With progressed reaction time most of the nPrOxa units are built-in and thus the consumption of iPrOxa become more likely, leading to a gradient-like structure with the overall comonomer ratio adjusted at reaction start. The above described results are in accordance to observations discussed in literature.⁹⁷ The depiction of the measured M_p values for the different reaction times indicate that high reaction temperatures of $T = 120$ °C and long reaction times of $t = 60-90$ min are needed for this copolymer system to obtain molar masses that were close to the targeted molar mass of $17.0 \text{ kg}\cdot\text{mol}^{-1}$. In contrast, the broad D values at elevated reaction times and temperatures indicated intrinsic side reactions. Nevertheless, **P1.3 I** was used for further functionalization with NHS-PEG₄-dibenzylazacyclooctyne (NHS-PEG₄-DBCO) for the formation of Polymer-DNA conjugates. The reaction is depicted in Scheme 5.1 B. However, the obtained DBCO-functionalized copolymer showed poor coupling efficiency to DNA (chapter 5.3, Figure 5.21). A possible

explanation can be the loss of reactive end groups of the propagating chains by side reactions like chain transfer and chain coupling reactions,^{84,160} which is indicated by the unusual broad D of 1.48.

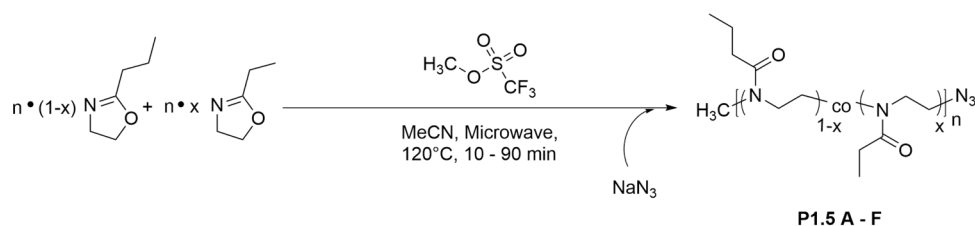


Scheme 5.2: Simplified reaction pathway of the possible termination reaction, proposed in literature,⁸² which occurs by quenching the polymerization with ammonia.

Another explanation for the insufficient number of amino groups could be the termination with ammonia, which led to an unwanted side reaction. Kosakowska and coworkers investigated termination reactions of propagating poly(EtOxa) chains by using mass spectrometry.⁸² Nuyken and coworkers proposed that small termination agents like water, hydroxides or ammonia are able to overcome the sterical hindrance around the C2 position of the oxazolinium ring and can attack there instead of the C5 carbon which is the more favored reaction site for bulky termination agents.⁸¹ As consequence of the preferred C2 attack of ammonia, a hydroxyl end group will be formed as major product instead of the desired amino group, which is supported by the mass spectrometry measurements performed by Kosakowska and coworkers.⁸² The proposed reaction pathway for the C2 attack and the expected C5 attack are depicted in Scheme 5.2. The resulting hydroxyl group is rather insensitive to active ester chemistry, which was used for coupling the DBCO moieties to the polymer, resulting in a reduced degree of functionality and would explain the resulting poor DNA coupling efficiency (see chapter 5.3).

Therefore, instead of ammonia for the following reactions sodium azide was used as termination agent to introduce the amino group masked as azide at the distal end of the polymer backbone.¹⁶¹ Additionally, in order to suppress possible intrinsic side reactions, iPrOxa was replaced by EtOxa, which possess similar polymerization parameters as nPrOxa.⁹⁷ Advantages

of the EtOxa/nPrOxa copolymer system could be decreased reaction times compared to the iPrOxa/nPrOxa copolymer system, that should result in narrower \mathcal{D} values.



Scheme 5.3: Copolymerization of nPrOxa and EtOxa in MeCN at different reaction times using microwave irradiation.

Optimization of reaction conditions for poly[(nPrOxa)-co-(EtOxa)]-N₃:

The reaction time was varied from $t = 10$ min to $t = 90$ min, whereas the reaction temperature was kept constant at $T = 120$ °C following the results obtained for the series of **P1.3**. As targeted molar mass $9.8 \text{ kg}\cdot\text{mol}^{-1}$ was chosen, which was adjusted by a monomer-to-initiator ratio of 90 to 1 (see General Procedure 5 on page 212). The relative comonomer ratio of nPrOxa and EtOxa was adjusted to 70:30 in order to obtain thermoresponsive copolymers possessing a T_c around $T = 32$ °C. The obtained copolymers were characterized by ^1H NMR spectroscopy and GPC. In the following Table 5.2 the calculated built-in of EtOxa as well as molar mass parameters and the corresponding yield are listed.

Table 5.2: Summarizing of the different reaction times of the azide-terminated poly(nPrOxa-co-EtOxa)s (**P1.5 A-F**) and the corresponding yields as well as the built-in of EtOxa, determined by ^1H NMR spectroscopy. The molar mass M_p was calculated by both ^1H NMR spectroscopy and GPC. The dispersities \mathcal{D} were also obtained by GPC. The reaction temperature was kept constant at $T = 120$ °C.

Polymer	t_{Reaction} / min	M_p	\mathcal{D}	Yield / mg (%)
		(GPC ^a , RI) / $\text{kg}\cdot\text{mol}^{-1}$		
P1.5 A	10	--- ^b	--- ^b	30 (5)
P1.5 B	15	5.4	1.09	82 (13)
P1.5 C	22.5	9.0	1.11	351 (56)
P1.5 D	45	9.4	1.12	478 (77)
P1.5 E	60	20.0	1.20	474 (76)
P1.5 F	90	21.5	1.17	474 (76)

^a eluent : DMAc containing LiBr ($\beta = 1 \text{ g}\cdot\text{l}^{-1}$); PMMA standards were used for calibration

^b no GPC measurement was performed

From the recorded proton NMR spectra, the built-in of EtOxa along the polymer chains dispersity (\mathcal{D}) was determined by comparing the integral of the signal that corresponds to the methyl group of EtOxa ($\delta = 1.10$ ppm) and the integral of the signal, which could be assigned to the methyl group of nPrOxa ($\delta = 0.93$ ppm). The calculated content of EtOxa units in the polymers was close to the targeted 30% at reaction start and independent of the reaction time, which is in accordance to the literature.⁹⁷ As expected, the obtained yields increased with increasing reaction time until $t = 45$ min. The \mathcal{D} values obtained for each polymer revealed a good control of the copolymerizations with minor side reactions. Again, M_p was determined since this parameter is independent of the shape of the molar mass peak and the integration thresholds in the GPC traces. The comparison of the M_p values indicate that a reaction time of $t = 22.5$ min (**P1.5 C**) seemed to be sufficient, since an increase to $t = 45$ min lead to no significant increase in the obtained M_p as illustrated below (Figure 5.2).

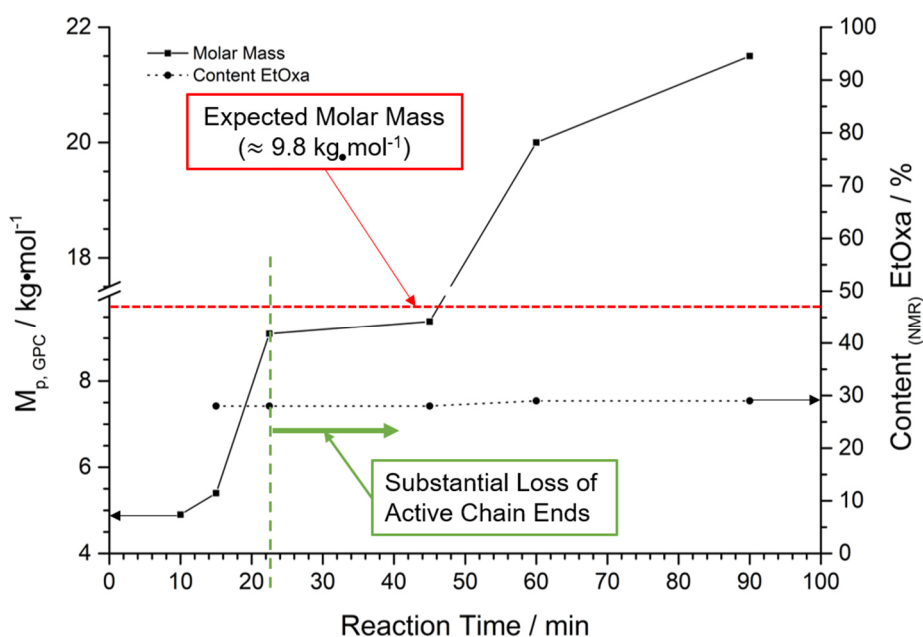


Figure 5.2: $M_{p, GPC}$ (solid black line) and content of EtOxa (dashed black line) versus the reaction time diagram. The dashed colored lines indicate significant points for the molar mass curve. The black arrow indicates the corresponding y-axis.

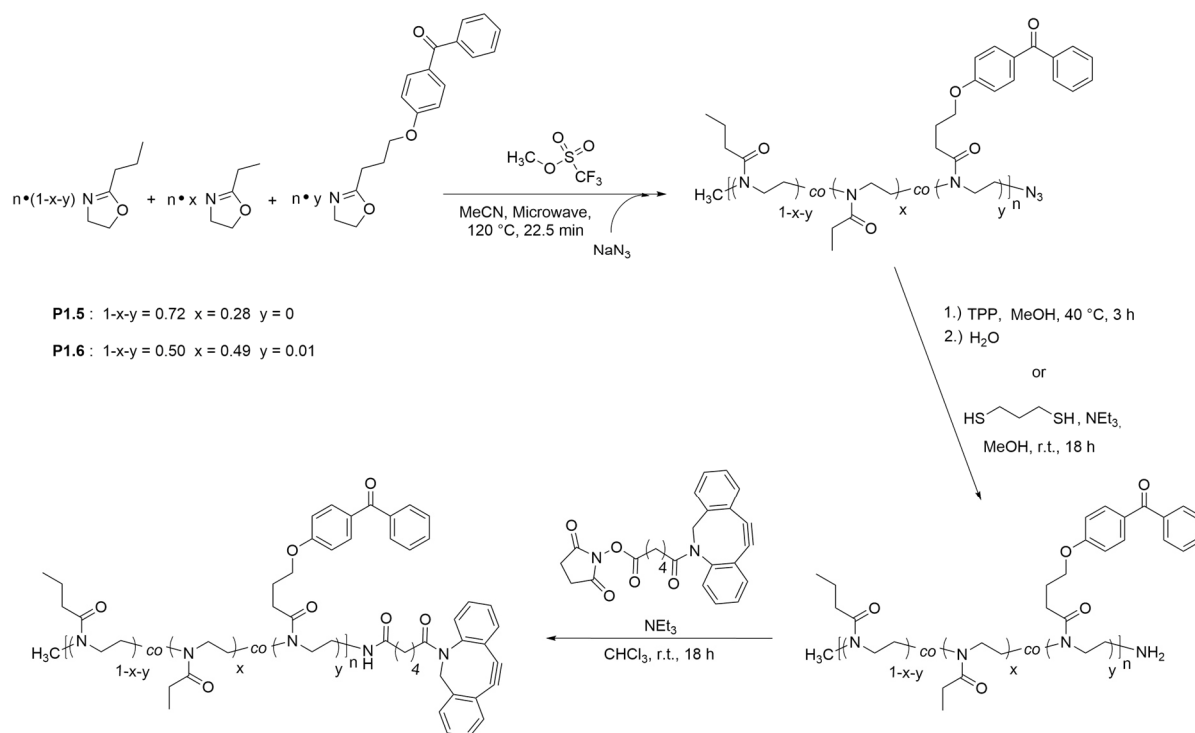
Interestingly, for the longest reaction times of $t = 60$ min and $t = 90$ min the obtained M_p values were more than doubled (20.0 and 21.5 $\text{kg}\cdot\text{mol}^{-1}$, respectively) compared to the targeted mass, whereas the \mathcal{D} values only slightly increased implying that the copolymerizations were well controlled. Probably, the remaining monomer, present at shorter reaction times, act as solvent for the reactive chain ends. After full consumption of the monomer, the chain ends can interact

with each other, which may lead to termination reactions like chain coupling.¹⁶² This chain coupling also result in a loss of reactive chain ends in accordance with the previous described copolymer **P1.3 A-I**.

Moreover, extended reaction times favor the occurrence of side reactions, which lead to a loss of active centers and in consequence the loss of end groups, since the plateau ($t = 22.5-45$ min) in the graph indicates no significant propagation of the polymer chains. Therefore, in following copolymerizations of EtOxa and nPrOxa the reaction time was kept constant at $t = 22.5$ min in order to exploit a reasonable yield and at the same time to obtain a maximum of possible azide end groups (General Procedure 6 on page 214), for further functionalization as depicted in Scheme 5.4.

In addition, a terpolymer composed of EtOxa, nPrOxa and BP-Oxa was synthesized (**P1.6**) following the same protocol as developed for **P1.5 C**. The incorporation of BP-Oxa allows the intermolecular crosslinking of the polymer chains by irradiation with UV-light after coupling of the polymer to DNA. This irreversible crosslinking allows the isolation and investigation of the formed superstructures (depending on the environmental temperature) of the polymer-DNA systems (see chapter 5.3).

The content of BP-Oxa was adjusted to 1%, which was suggested to be sufficient for crosslinking polymer chains, but low enough to not influence the overall polarity (and transition temperature) of the polymer too much. In order to obtain a similar LCST of around $T = 32^{\circ}\text{C}$ as for **P1.5 C**, the content of EtOxa in **P1.6** was increased from 30% to 49%.



Scheme 5.4: Schematic overview of the cationic ring-opening copolymerization of EtOxa and nPrOxa (**P1.5**) and the terpolymerization of EtOxa, nPrOxa and BP-Oxa (**P1.6**). Further, the corresponding functionalization steps to obtain the DBCO-functionalized derivatives (**P1.5.2** and **P1.6.2**) are illustrated.

In Table 5.3, the molar mass values and yields as well as the content of EtOxa and BP-Oxa are listed. Based on the recorded ^1H NMR spectra of **P1.5 C (2)-(4)** and **P1.6** (Figure 5.3 top), the \bar{X}_n was determined by comparing the integrals of the signal of the distal methyl group ($\delta = 3.02$ ppm) and the integral of the signal which corresponds to the polymer backbone ($\delta = 3.44$ ppm). The \bar{M}_n was then calculated by multiplying the average molar mass of a repeat unit with \bar{X}_n . The calculated \bar{M}_n of $15.1 \text{ kg}\cdot\text{mol}^{-1}$ - $16.4 \text{ kg}\cdot\text{mol}^{-1}$ for **P1.5 C** are in good agreement to the targeted molar masses of $16.4 \text{ kg}\cdot\text{mol}^{-1}$. Similar, \bar{M}_n calculated for **P1.6** ($16.4 \text{ kg}\cdot\text{mol}^{-1}$) matched well to the targeted molar mass of $16.3 \text{ kg}\cdot\text{mol}^{-1}$. The contents of EtOxa and BP-Oxa in the synthesized co- and terpolymers were in accordance with the adjusted co- and termonomer ratios at reaction start (**P1.5 C**: 30% EtOxa; **P1.6**: 49% EtOxa, 1% BP-Oxa). Similar to the results observed for the reaction optimization of **P1.5 C**, the obtained D of 1.07-1.10 for the corresponding co- or terpolymer were in the typical range ($D \leq 1.20$) as reported for poly(2-alkyl-2-oxazoline)s prepared by microwave synthesis,^{160,163,164} suggesting a well-controlled polymerization process with minor side reactions.

Table 5.3: Listing of the measured molar masses \bar{M}_n and dispersities \mathcal{D} of the azide-functionalized poly(nPrOxa-co-EtOxa)s (**P1.5 C**) and poly(nPrOxa-co-EtOxa-co-BPOxa) (**P1.6.2**) as well as the calculated built-in of BP-Oxa, determined by ^1H NMR. Further, the corresponding yield of the polymerization is given. The mass values were measured using GPC and were calculated by from the ^1H NMR spectroscopic data. The relative yield (%) was calculated by comparison the initial mass of monomer and the obtained mass of polymer.

Polymer	Built-in EtOxa (NMR) /%	Built-in BP-Oxa (NMR) /%	\bar{M}_n (NMR) / $\text{kg}\cdot\text{mol}^{-1}$	\bar{X}_n (NMR)	\bar{M}_n (GPC ^a) / $\text{kg}\cdot\text{mol}^{-1}$	\mathcal{D}	Yield / g (%)
P1.5 C (2)	28	---	15.9	145	9.7	1.10	0.26 (43)
P1.5 C (3)	28	---	15.1	138	10.1	1.10	0.55 (45)
P1.5 C (4)	28	---	16.4	150	18.2	1.07	4.02 (66)
P1.6	49	0.7	16.4	151	8.2	1.33	0.28 (48)

^a eluent : DMAc containing LiBr ($\beta = 1 \text{ g}\cdot\text{l}^{-1}$); PMMA standards were used for calibration

The broadening of the molar mass distribution ($\mathcal{D} = 1.33$) of **P1.6** can be assigned to possible aggregation reactions of the benzophenone moieties. Interestingly, the determined \bar{M}_n of 18.2 $\text{kg}\cdot\text{mol}^{-1}$ for **P1.5 C (4)** was close to the expected molar mass (16.4 $\text{kg}\cdot\text{mol}^{-1}$), whereas the \bar{M}_n values for the other copolymers, measured under same conditions, were significant lower. Probably, the temperature control by the microwave is not as accurate for using small reaction vials as for reactions performed on larger scale, leading to lower reaction temperatures that also decreases the rate of chain propagation. The discrepancy can probably be explained by the higher susceptibility of the small-scale attempts **P1.5 C (2)** and **P1.5 C (3)** for termination reactions caused by humidity diffusing into the reaction vial, than the large-scale attempt **P1.5 C (4)**. The successful termination of the chain ends by azide groups was determined by appearance of the azide stretching vibration ($\bar{\nu} = 2100 \text{ cm}^{-1}$) in the recorded IR spectra (Figure 5.3 below)

5 Results and Discussion

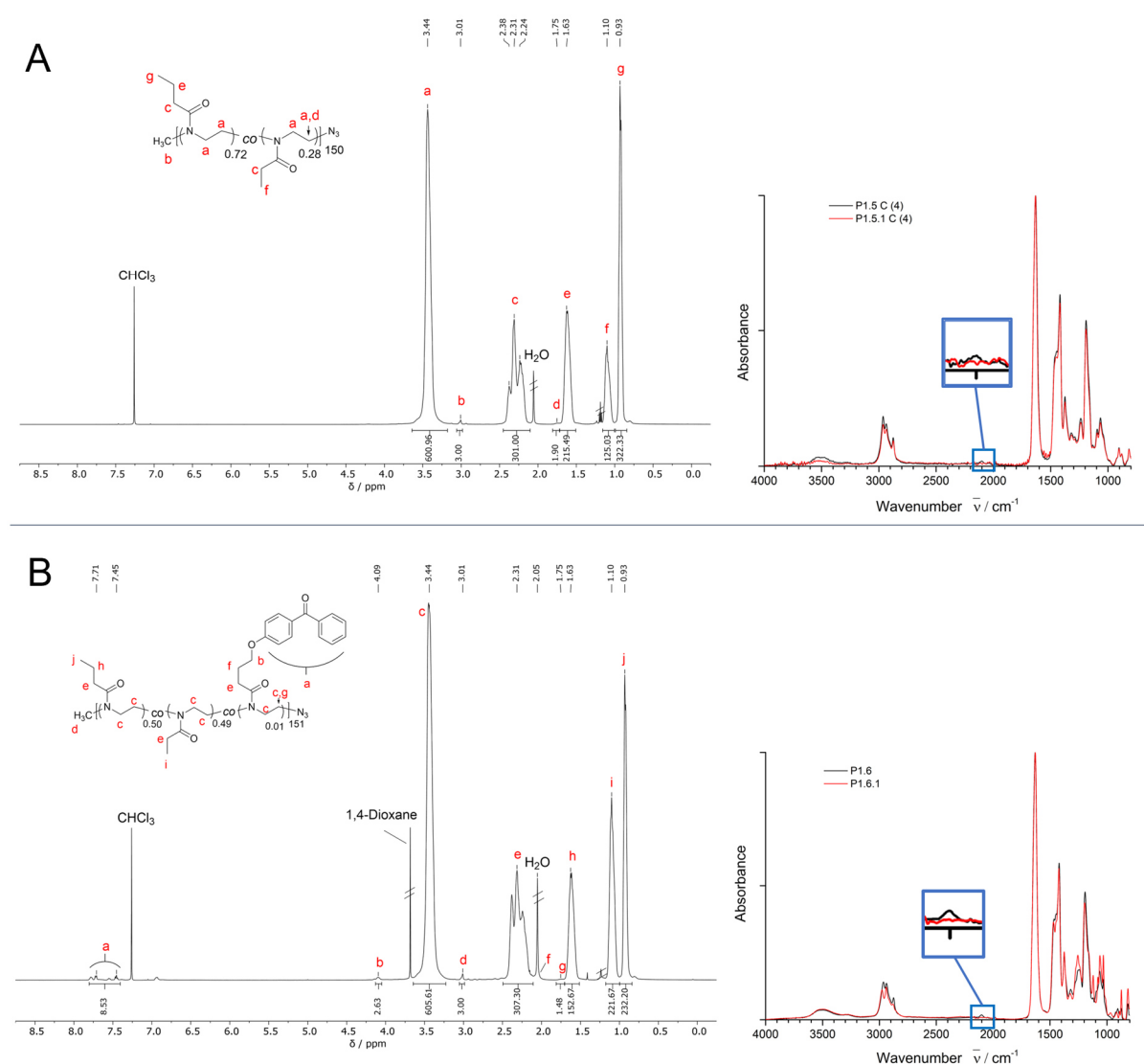


Figure 5.3: Representative depiction of the recorded ^1H NMR spectra (400 MHz) of **P1.5 C (4)** (A, top) and **P1.6 C** (B, below) as well as the corresponding normalized IR spectra (right), recorded before (black line) and after Staudinger reaction (red line). The regions where the azide stretching vibration typically appears is enlarged to illustrate the disappearance after successful reduction of the azide.

The quantification of the azide content from the recorded IR spectra was not possible, because of the small intensity of the azide vibrational band and the overlapping of absorption bands in the region $\bar{\nu} = 1700\text{-}1000\text{ cm}^{-1}$.

Reduction of the azide group to an amino group:

The azide end groups of **P1.5 C (2)-(4)** were reduced by a Staudinger reaction (General Procedure 10 on page 222) using triphenylphosphine (TPP) and the success of this reaction was proven by IR spectroscopy. The superimposition of the normalized IR spectrum

of **P1.5 C (4)** (Figure 5.3, left: black line) and **P1.5.1 C (4)** (Figure 5.3, left: red line) showed a vanishing of the absorption band of the azide stretching vibration at $\bar{\nu} = 2100 \text{ cm}^{-1}$, indicating a successful reduction.

Table 5.4: Tabulation of the measured molar masses \bar{M}_n and dispersities \mathcal{D} of the amine-functionalized poly(nPrOxa-co-EtOxa)s (**P1.5 C**) and poly(nPrOxa-co-EtOxa-co-BPOxa) (**P1.6.1**). Further, the corresponding yield of the azide-reduction reaction is given. The mass values were measured using GPC. The relative yield (%) was calculated by comparing the initial mass of azide-terminated polymer used as educt and the obtained mass of the amino-functionalized polymer after reduction.

Polymer	\bar{M}_n (GPC ^a) / $\text{kg}\cdot\text{mol}^{-1}$	\mathcal{D}	Yield / g (%)
P1.5.1 C (2)	9.5	1.11	0.09 (86)
P1.5.1 C (3)	9.9	1.11	0.25 (93)
P1.5.1 C (4)	17.9	1.08	2.88 (84)
P1.6.1^b	8.5	1.29	250 (99)

^a eluent : DMAc containing LiBr ($\beta = 1 \text{ g}\cdot\text{l}^{-1}$); PMMA standards were used for calibration

^b reduced by using 1,3-propanedithiol

For all attempts of **P1.5.1 C** good yields were obtained between 84% and 93%. Recorded proton NMR spectra showed traces of remaining TPP or the formed byproduct triphenylphosphine oxide (TPPO), which in general are difficult to remove. As expected, the measured \bar{M}_n and \mathcal{D} of **P1.5.1 C** (Table 5.4) were similar to the results obtained for the corresponding precursor polymer **P1.5. C** (Table 5.3) since the theoretical loss of $26 \text{ g}\cdot\text{mol}^{-1}$ by conversion of the azide to an amino group is below the detection limit of the used GPC.

For the reduction of the azide moieties in **P1.6** an alternative route was tested, in which 1,3-propanedithiol was used instead of TPP (see Experimental Part on page 226).¹⁶⁵ The usage of this dithiol avoids the difficult removal of the TPP and TPPO, which should simplify the purification. The successful reduction was demonstrated by the recorded and superimposed IR spectra of **P1.6** and **P1.6.1**, which showed a vanishing of the azide vibration (Figure 5.3B, bottom). In addition, the amino-functionalized polymer was obtained in an almost quantitative yield (99%). As expected, the recorded molar mass values of **P1.6.1** were similar to the values obtained for **P1.6**.

DBCO-functionalization of the amino group:

In the next step, DBCO moieties were coupled to the distal amino group of the polymer backbone by using active ester chemistry (General Procedure 12 on page 227), which enables the coupling of azide-containing building blocks without using an additional catalyst like Cu^+ ions (see chapter 5.3). Good yields of 73-92% were obtained for the DBCO-functionalized polymers. The recorded ^1H NMR spectra of **P1.5.2 C** and **P1.6.2** (Figure 5.4) indicated a successful coupling of the DBCO moieties to the corresponding polymers by appearing of additional proton signals in the aromatic region ($\delta = 7.80\text{-}7.20$ ppm).

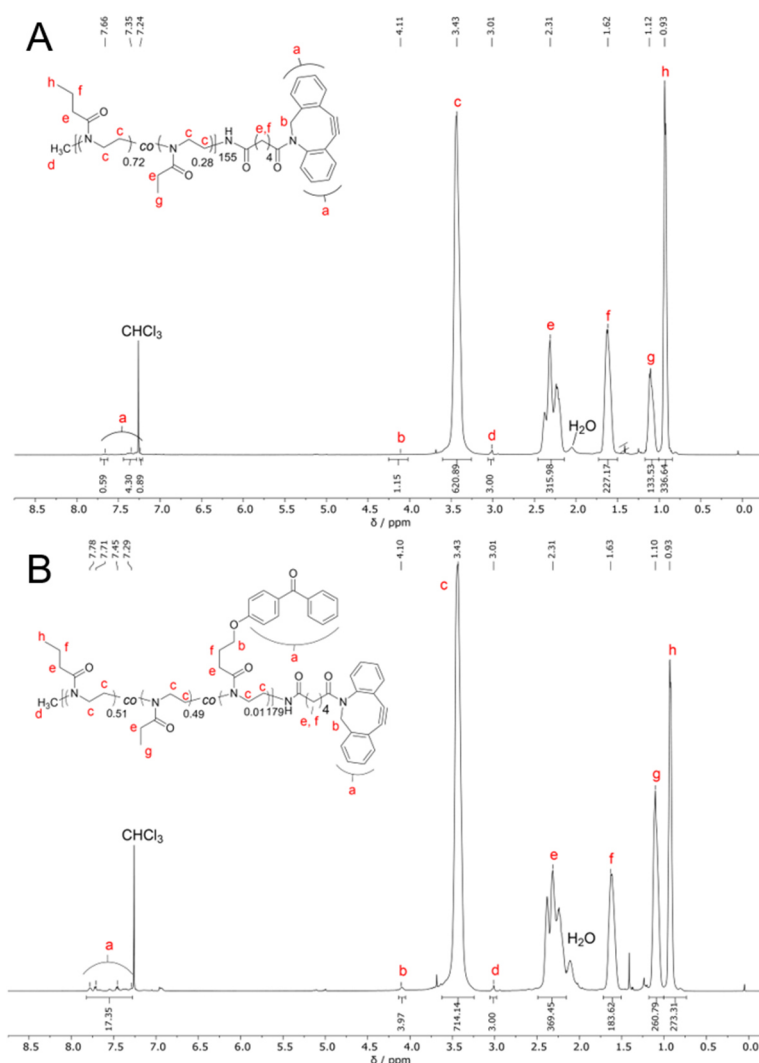


Figure 5.4: ^1H NMR spectra (400 MHz) of **P1.5.2 C** (4) (A) and **P1.6.2** (B).

The degree of functionalization of **P1.5.2 C** was determined by comparison the integrals of the aromatic proton signals that could be assigned to DBCO and the integral of the signal, which belongs to the protons of the methyl end group at the polymer backbone. For both **P1.5.2 C**

polymers high degrees of functionalization were calculated (83% and 96%) that indicate an effective modification procedure. The determination of the degree of functionalization of **P1.6.2** was difficult, because the protons of the benzophenone moiety and the DBCO moiety overlapped in the aromatic region of the ^1H NMR spectrum (Figure 5.4 B). Assuming a BP-Oxa content of 0.7%, which was determined previously for **P1.6**, yields a degree of functionality of 89% for **P1.6.2**, which is similar to the values obtained for the **P1.5.2 C** polymers as listed in Table 5.5.

The \bar{M}_n values of $17.1 \text{ kg}\cdot\text{mol}^{-1}$ and $17.2 \text{ kg}\cdot\text{mol}^{-1}$ for **P1.5.2 C (3)-(4)** and $22.0 \text{ kg}\cdot\text{mol}^{-1}$ for **P1.6.2**, calculated from the corresponding ^1H -NMR spectra, were close to the calculated molar masses with the DBCO fragment of $16.8 \text{ kg}\cdot\text{mol}^{-1}$ and $16.7 \text{ kg}\cdot\text{mol}^{-1}$, respectively. The increased \bar{M}_n of **P1.6.2** may be explained by integration errors, because of overlapping signals of the methyl end group and the polyethyleneimine backbone.

Table 5.5: Listing of the measured molar masses \bar{M}_n and dispersities D of the DBCO-functionalized poly(nPrOxa-co-EtOxa)s (**P1.5 C**) and poly(nPrOxa-co-EtOxa-co-BPOxa) (**P1.6.2**) as well as the degree of functionalization with DBCO, determined by ^1H NMR. Further, the corresponding yield of the reaction is given. The mass parameters were measured using GPC and calculated by ^1H NMR spectroscopy. The relative yield (%) was calculated by comparison the initial mass of polymer which was used as educt and the obtained mass of polymer after DBCO-functionalization.

Polymer	Degree of	\bar{M}_n (NMR) / $\text{kg}\cdot\text{mol}^{-1}$	\bar{M}_n (GPC ^a) / $\text{kg}\cdot\text{mol}^{-1}$	D	Yield / g (%)
	Functionalization DBCO /%				
P1.5.2 C (3)	83	17.1	11.3	1.14	0.18 (73)
P1.5.2 C (4)	96	17.2	17.9	1.08	2.79 (92)
P1.6.2	89	22.0	9.4	1.38	0.18 (83)

^a eluent : DMAc containing LiBr ($\beta = 1 \text{ g}\cdot\text{l}^{-1}$); PMMA standards were used for calibration

In addition, the \bar{M}_n and D values for **P1.5.2 C** and **P1.6.2** were determined by GPC. As expected, the measured molar masses of the DBCO-functionalized polymers did not differ from the molar mass obtained for the polymer precursors. Again, the \bar{M}_n obtained in GPC for the small-scale attempts **P1.5.2 C (3)** and **P1.6.2** were significantly lower than the expected molar mass and the \bar{M}_n calculated by ^1H NMR spectroscopy, which was already obtained and

explained for the precursor polymers, whereas the obtained molar masses for **P1.5.2 C (4)** are close to the calculated theoretical molar mass. The comparison of the dispersities of the DBCO-functionalized polymers with the molar mass distributions observed for the precursor polymers showed a broadening as illustrated in Figure 5.5.

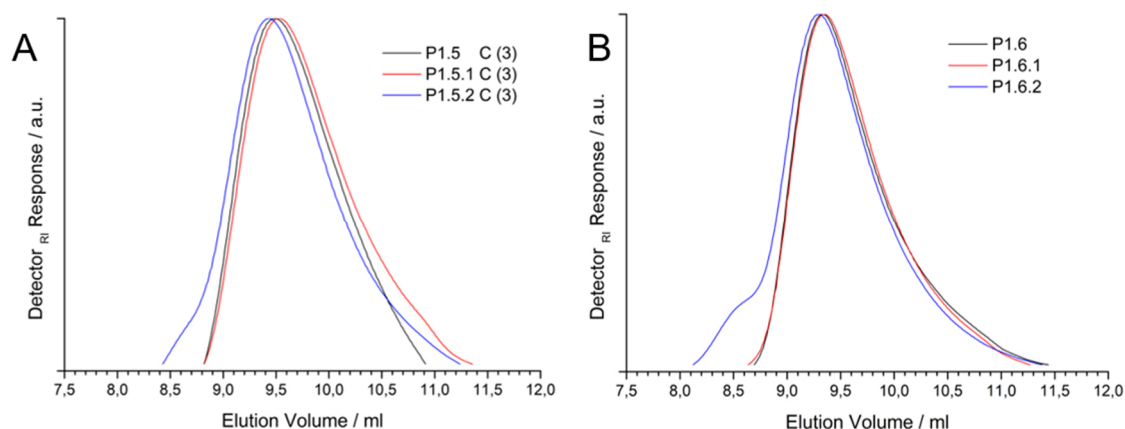
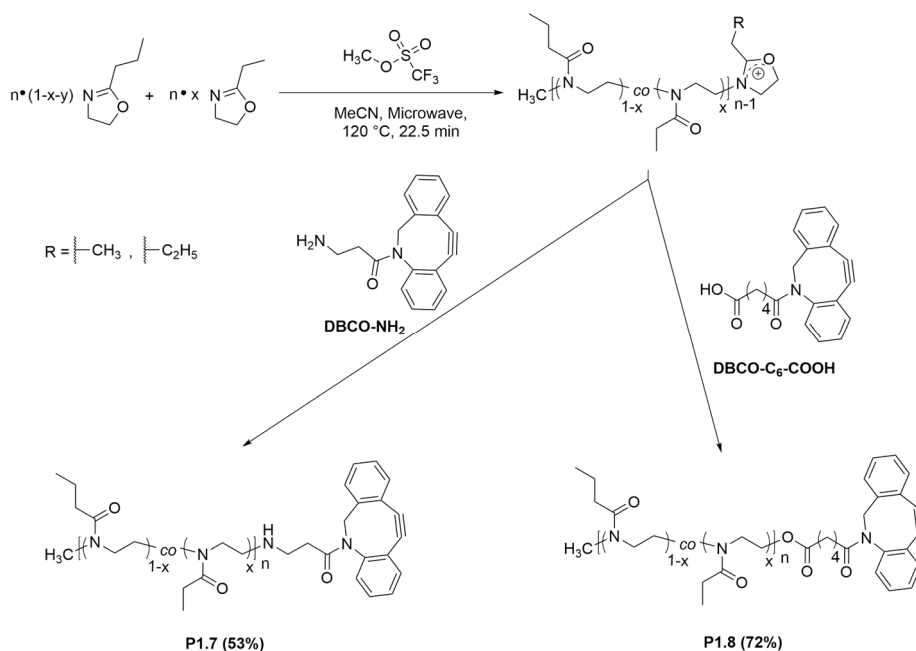


Figure 5.5: Superimposed elugrams of the three GPC (eluent: DMAc containing LiBr, $\beta = 1 \text{ g}\cdot\text{l}^{-1}$) traces of **P1.5 C(3)**, **P1.5.1 C(3)** and **P1.5.2 C(3)** (Elugram A) and **P1.6**, **P1.6.1** and **P1.6.2** (Elugram B).

The small shoulders of the molar mass peaks at an elution volume of $V = 8.5 \text{ ml}$ for both type of polymers may arise from aggregation of at least two polymer chains with the respective DBCO end group or a possible complexation of Li^+ ions, present in the eluent used for GPC. Interestingly, this shoulder is more pronounced for **P1.6.2**, which may suggest the participation of the benzophenone groups in the aggregation of the polymer species.

Direct termination of the CROP using DBCO derivatives:

As alternative approach to the above-described procedure for **P1.5.2 C** and **P1.6.2** two different DBCO derivatives as termination reagents were tested. Advantages of this proposed procedure would be the direct DBCO-functionalization without intermediate modification reactions, which may lead to improved yields and decreased reaction time. As first DBCO termination agent DBCO- NH_2 was chosen, because it is known that amine-based termination reagents react fast with the active center of the POxa chains.⁸¹ As second termination agent DBCO- $\text{C}_6\text{-COOH}$ was tested, which possess a carboxylic acid group that deprotonates in the presence of a base generating a carboxylate-anion, which then can react efficiently with the cationic charge of the propagating POxa species.



Scheme 5.5: Reaction scheme of the copolymerization of EtOxa and nPrOxa which were terminated using DBCO-NH₂ (**P1.7**) and DBCO-C₆-COOH (**P1.8**). In brackets the corresponding yield of the polymerization is given.

The copolymers were prepared using the same protocol and ratios as described for **P1.5 C** and **P1.6** (General Procedure 6 on page 214). Polymerization chains were quenched after a reaction time of $t = 22.5$ min by either using DBCO-NH₂ to yield **P1.7** or using DBCO-C₆-COOH to yield **P1.8** (Scheme 5.5). Both copolymers were received in reasonable yields of 53% (**P1.7**) and 72% (**P1.8**). The lower yield obtained for **P1.7** can be attributed to losses during purification of the polymer. A successful termination of the polymer chains with the different DBCO derivatives was confirmed by ¹H NMR spectroscopy. The corresponding spectra are illustrated below (Figure 5.6). Both spectra showed a successful coupling of the DBCO moieties to the polymer backbone by appearance of proton signals in the aromatic region ($\delta = 7.20$ - 7.80 ppm). The degrees of functionalization were determined by NMR signal integration as described for **P1.5.2 C**. For **P1.7** and **P1.8** significant lower degrees of DBCO-functionalization of 65% and 43%, compared to **P1.5.2 C**, were observed. This may arise from a decreased coupling efficiency caused by undesired side reactions and lower reaction efficiencies of the DBCO-amine and DBCO-COOH derivative with the reactive chain end, compared with the DBCO active ester coupling of the amino-functionalized polymer chain. Additionally, the DBCO-COOH derivative is rather unstable resulting in even lower coupling efficiencies explaining the lower degree of functionalization of **P1.8**.

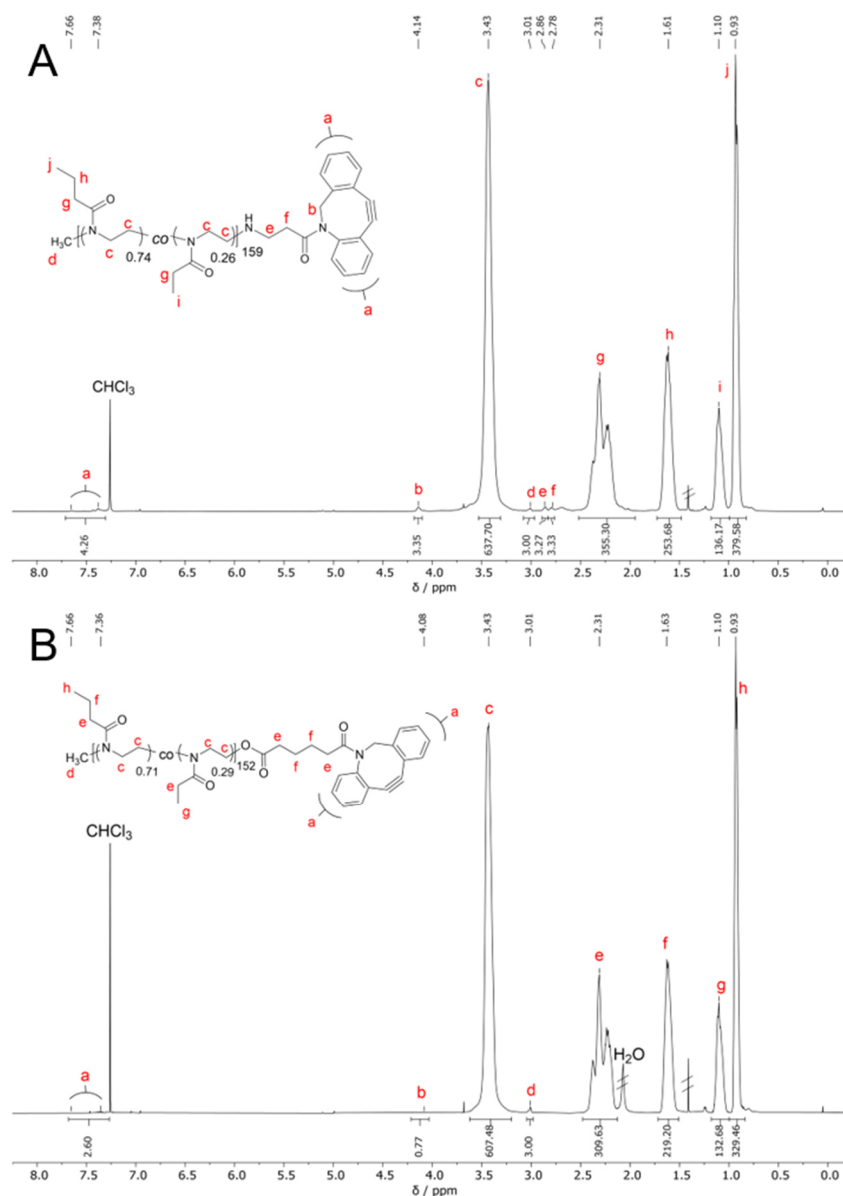


Figure 5.6: ¹H NMR spectra (400 MHz) of **P1.7**(A) and **P1.8** (B).

In addition, the built-in as well as the \bar{M}_n could be calculated from the corresponding proton NMR spectra. The built-in of EtOxa of 26% (**P1.7**) and 29% (**P1.8**) along the polymer chain was in both cases close to the targeted built-in of 25% (**P1.7**) and 30% (**P1.8**), respectively. The \bar{M}_n of **P1.7** (17.7 kg·mol⁻¹) and **P1.8** (16.9 kg·mol⁻¹), which were calculated from the corresponding ¹H NMR spectrum, were close to the targeted molar mass of 16.7 kg·mol⁻¹. In contrast the corresponding \bar{M}_n for **P1.7** (11.1 kg·mol⁻¹) and **P1.8** (11.3 kg·mol⁻¹) that was determined by GPC deviate from the targeted and calculated molar mass, which may be addressed to a change in the polymer conformation and interactions of the DBCO end group with the eluent. The observed \bar{D} values of 1.10 (**P1.7**) and 1.20 (**P1.8**) indicate slightly

broadened molar mass distributions, which may arise from the formation of aggregates by interactions of the aromatic groups of the terminal DBCO moieties, as discussed for **P1.5.2 C** and **P1.6**, or other side reactions.

Summary:

In this chapter, copolymerization procedures of nPrOxa and iPrOxa or EtOxa using microwave heating were discussed. First different copolymers composed of nPrOxa and iPrOxa were prepared under different reaction times and temperatures to find the optimal reaction conditions. The polymers were quenched with ammonia introducing an amino functionality at the terminal end of the polymer backbone. This series revealed that high temperatures ($T = 120\text{ }^{\circ}\text{C}$) and long reaction times ($t = 90\text{ min}$) are necessary to obtain copolymers with targeted comonomer ratios, which is in accordance to observations made within the work group.⁴ However, high reaction temperatures and long reaction times increase the probability of intrinsic side reactions, which lead to a loss of accessible end groups.⁴ Moreover, investigations of the termination using ammonia by Kosakowska and coworkers suggested that unexpectedly instead of an amino group at the distal end of the polymer backbone, a hydroxyl group will be formed.⁸² This together with the increased probability of side reactions led to the replacement of iPrOxa by EtOxa. Again, the optimal reaction time was found by synthesizing a series of copolymers composed of EtOxa and nPrOxa using different reaction times. It was found that EtOxa could be copolymerized with nPrOxa in much shorter reaction times (22.5 min) to yield the desired polymer composition and targeted molar mass. Instead of ammonia, sodium azide was used as termination agent to introduce an azide-functionality. The azide group was subsequently reduced to an amino group by a Staudinger reaction and the reduction was confirmed by IR spectroscopy. DBCO moieties were introduced by NHS active ester chemistry with a high degree of functionality (83% and 96%), determined by ¹H NMR spectroscopy. Following the above-mentioned synthesis protocol, EtOxa and nPrOxa were terpolymerized with BP-Oxa, which was used as photocrosslinkable group. Again, the termination was accomplished by using sodium azide, but the reduction of the azide moiety was performed by using 1,3-propanedithiol instead of using TPP to improve the purity amino-functionalized terpolymer. The DBCO-functionalization was performed again according to the procedure for the above-mentioned copolymers and yielded a high degree of functionality (89%).

In alternative approaches, the usage of DBCO-NH₂ and DBCO-C₆-COOH as termination agents were investigated. ¹H NMR spectra recorded for both products revealed a significant lower degree of functionalization (65% and 43%) compared to the DBCO-functionalized co- and terpolymer prepared from the corresponding azide-functionalized derivative. The application of the above-mentioned co- and terpolymers will be discussed in chapter 5.3.

5.1.2 Synthesis of Hetero-Telechelic Poly(2-oxazoline)s

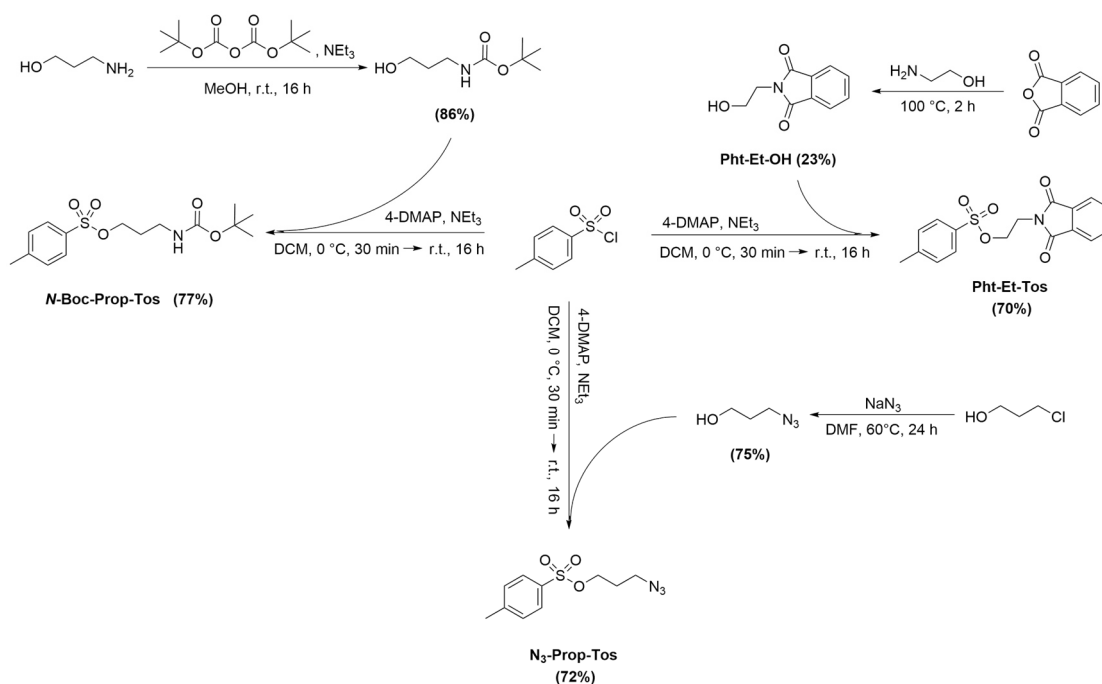
Polymers containing functional groups as chain ends are interesting as potential junctions in biosensor devices. Such linkers should be able to connect e.g., a surface and a specific molecule or functional group for example in a sensor device (see chapter 5.3) or they should act as a conjugation between DNA molecules, which can form different arrangements depending on the environmental temperature (see chapter 5.3). Therefore, properties like a certain chain flexibility or pH-responsiveness as well as thermoresponsiveness are required. CROP features the possibility to introduce such functional groups in α - and ω -end group by using modified initiators or termination agents. Since some functional groups like amino groups are not tolerated during the polymerization, the introduction of protecting groups in the initiators as well as the termination agents is necessary. Poly(2-oxazoline)s are well-known thermoresponsive polymers whose LCST can be varied using different comonomers and compositions.

Synthesis of functional initiators for CROP:

A series of initiators based on 4-methylbenzene-1-sulfonyl chloride (TosCl) were prepared (Scheme 5.6). The desired functional group was introduced in the initiator using ω -end-functionalized alcohols. As mentioned above, the introduction of amino groups is only possible if they are masked before polymerization either by forming a carbamate or as phthalimide derivative, since the free amino groups would react with the positive charge of the terminal oxazolinium ring of the propagating chain leading to termination of the polymerization.

For the first amine-containing tosylates 2-(2-hydroxyethyl)isoindoline-1,3-dione (Pht-Et-OH) was synthesized by reacting ethanolamine and phthalic anhydride at elevated temperatures ($T = 100\text{ }^{\circ}\text{C}$).¹⁶⁶ However, the yield of 23% was poor which might be assigned to the short reaction time ($t = 2\text{ h}$). It is expected that extended reaction times will improve the yield of the product, but no attempts with increased reaction times were performed, because sufficient mass for the tosylate reaction of Pht-Et-OH was obtained in the initial attempt.

5 Results and Discussion



Scheme 5.6: Outline of the synthesis of different ω -functionalized initiators for CROP of 2-oxazolines. All initiators were prepared by using previously synthesized ω -end functionalized alcohols and TosCl. The number in brackets indicate the obtained yields.

In a second step, the Pht-Et-OH was reacted with TosCl according to a procedure described in literature (see General Procedure 1 on page 191) to produce Pht-Et-Tos.^{2,3} The structure of the pure compound was confirmed by IR and NMR spectroscopy (Figure S14-20). The obtained yield of 70% is slightly lower than reported for other tosylation reactions,^{1,2} but the yielded mass was sufficient to initiate several polymerizations. The conversion of the phthalimide group into an amino group requires harsh conditions (hydrazinolysis under acidic conditions), which is discussed below.

Therefore, another approach for preparing poly(2-oxazoline)s with amino end groups was explored, which includes shielding of the amino groups by forming the *tert*-butyl carbamate (Boc) derivative. The reaction of 3-aminopropanol with di-*tert*-butyldicarbonate was performed using modified procedures described in literature (General Procedure 2 on page 200).¹ For the protected amino group derivative a good yield (86%) was obtained in accordance with the yields reported in the literature.^{1,167} The tosylation reaction was again performed using the protocol described on page 191. The obtained yield of 77% was slightly lower than reported for other tosylation reactions,^{1,2} but were sufficient to perform various polymerization reactions. The recorded NMR spectra of *N*-Boc-Prop-Tos (Figure S9 and Figure S10) showed small impurities, which may have been introduced during purification by using column

chromatography. Probably, this compound slightly decomposes in the presence of the weakly acidic silica gel that can be avoided by using other purification methods like recrystallization. Additional to the above described functionalized tosylates another initiator was prepared that is able to introduce an azide group at the distal end from the termination group of the polymer backbone.

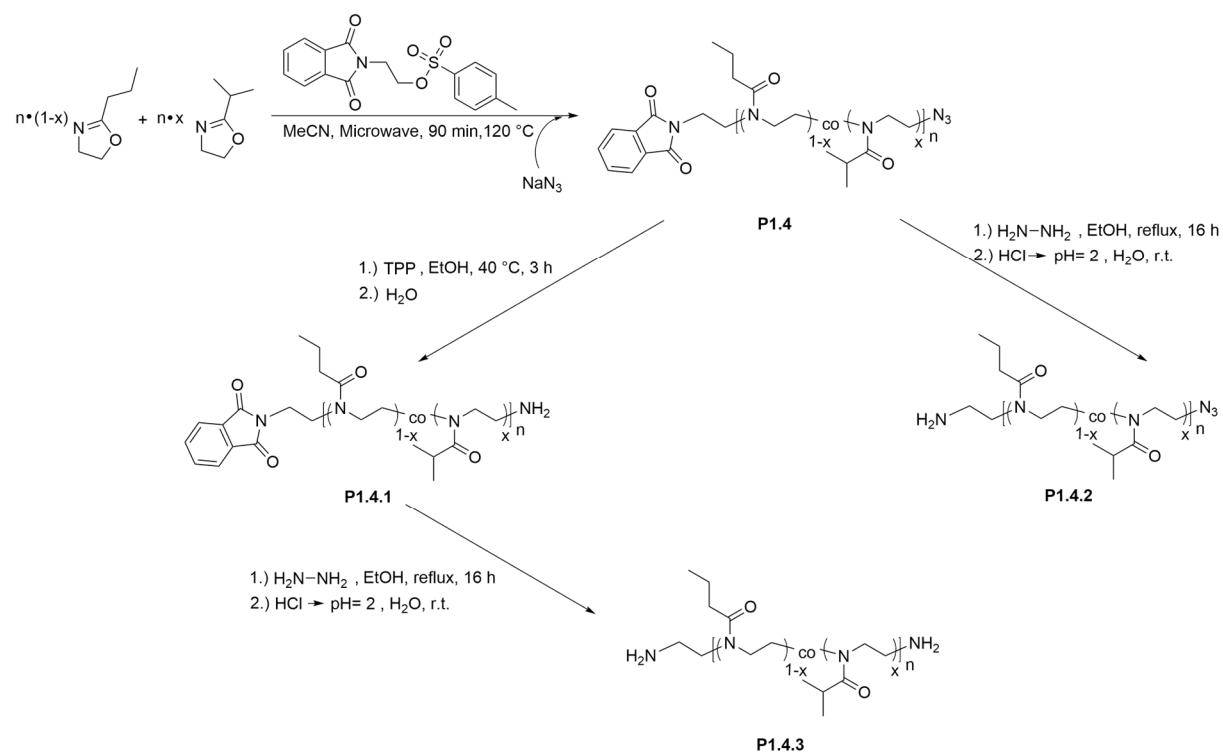
Azide moieties along the polymer chain are very helpful for postmodification reactions, because azide moieties can be used e.g. in azide-alkyne click reactions^{168,169} or can be reduced to amino groups e.g. in a Staudinger reduction with phosphines¹⁷⁰⁻¹⁷² or by using dithiols.^{165,173} Therefore, 3-chloropropanol was converted into 3-azidopropanol using NaN_3 in DMF at elevated temperature as described in the literature.² The product was obtained in a larger amount than the theoretical quantitative yield, which was due to traces of DMF found in ^1H NMR and ^{13}C NMR spectra. No further purification was performed, since no interference in the tosylation reaction, caused by the DMF, was expected.

N_3 -Prop-Tos was prepared using the same protocol as described above. Also, the obtained yield (72%) was in the same range as observed for the other tosylate derivatives (70%-80%). An absorption band at $\bar{\nu} = 2107 \text{ cm}^{-1}$ in the IR spectrum showed the presence of the azide group in N_3 -Prop-Tos (Figure S11). Small impurities arising from 3-azidopropanol, which probably result from decomposition of N_3 -Prop-Tos during the purification procedure, were observed in the recorded ^1H and ^{13}C NMR spectra (Figure S12 and Figure S13). However, further purification using recrystallization showed no significant improvement of the purity. It was expected that the small impurities may have a small influence on the molar mass and the dispersity of polymers initiated by N_3 -Prop-Tos, because of possible termination reactions caused by 3-azidopropanol.

Synthesis of hetero-telechelic poly(2-alkyl-2-oxazoline)s their postfunctionalization:

First copolymerizations of iPrOxa and nPrOxa using Pht-Et-Tos as initiator were performed according to a procedure developed within the group.⁴ The copolymers made of the two 2-propyl-2-oxazoline derivatives are known to be thermoresponsive, possessing a LCST of 24 °C-38 °C in dependence of their compositions.⁹⁷ As termination agent NaN_3 ¹⁶¹ was chosen to obtain **P1.4** as hetero-telechelic copolymer. **P1.4** served as a basis for preparing different derivatives (**P1.4.1-P1.4.3**) by postmodification reactions (Scheme 5.7) like hydrazinolysis or Staudinger reduction. The composition of the obtained copolymer was determined by

integration of the proton signals in the ^1H NMR spectra at $\delta = 1.09$ ppm, which correspond to the methyl groups of the *iso*-propyl sidechain and the signal at $\delta = 0.91$ ppm that arise from the terminal methyl group of the *n*-propyl side chain (Figure 5.7).



Scheme 5.7: Schematic overview of the cationic ring-opening copolymerization of *i*PrOxa and *n*PrOxa (**P1.4**) using Pht-Et-Tos as functionalized initiator. The different functionalization strategies to obtain various α - and ω -end group-functionalized copolymers (**P1.4.1**, **P1.4.2** and **P1.4.3**) are illustrated.

The integration derived compositions of *n*PrOxa to *i*PrOxa along the polymer of 51 : 49 (refer to Table 5.6) were in good agreement to the initial adjusted ratio of 50 : 50. The calculation of the \bar{M}_n by ^1H NMR was only possible for **P1.4** and **P1.4.1**. The calculated \bar{M}_n of $7.2 \text{ kg}\cdot\text{mol}^{-1}$ (**P1.4**) and $8.4 \text{ kg}\cdot\text{mol}^{-1}$ (**P1.4.1**) were higher than the expected molar masses of $4.2 \text{ kg}\cdot\text{mol}^{-1}$, which may arise from heterogeneities of the reaction mixture before polymerization because Pht-Et-Tos was not fully soluble at reaction start in MeCN. This may result in a decreased concentration of initiator molecules that could initiate the chain propagation, and consequently lead to an increased initiator-to-monomer ratio. Notably, the calculated \bar{M}_n for **P1.4** and **P1.4.1** by NMR spectroscopy and the values obtained by GPC (eluent: DMAc + LiBr [$1 \text{ g}\cdot\text{l}^{-1}$], PMMA standards as reference) were similar, supporting the above-mentioned hypothesis. **P1.4.1** was synthesized by Staudinger reduction using a published procedure.¹⁶¹

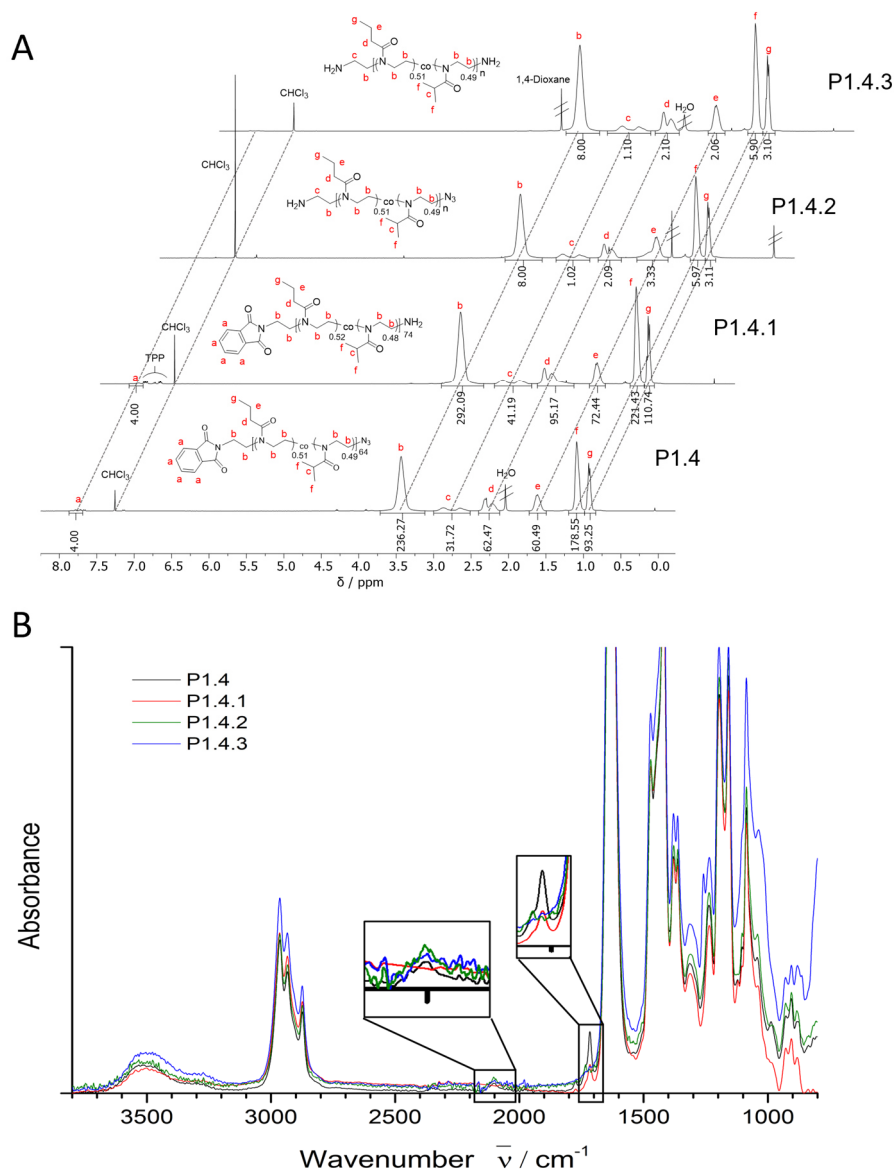


Figure 5.7: (A) Overview of the recorded ^1H NMR (400 MHz) spectra of **P1.4-P1.4.3** and the corresponding assignment of the signals to the structure. The dashed lines are drawn for better visualization. (B) Comparison of recorded IR spectra of the polymers **P1.4-P1.4.3**. The enlargements of the azide stretching vibration band ($\bar{\nu} \approx 2100 \text{ cm}^{-1}$) and the carbonyl stretching vibration band ($\bar{\nu} \approx 1700 \text{ cm}^{-1}$) are shown in the inserts.

The recorded ^1H NMR spectra indicated an insufficient removal of excess of TPP and formed TPPO, because of the presence of aromatic signals at $\delta = 7.30\text{-}7.70$ ppm (Figure 5.7). Repetition of the purification procedure led to a decrease of signal intensity, but TPP and TPPO could not be removed quantitatively. Integration errors due to partially overlapping signals of the aromatic phthalimide and protons of remaining TPP after Staudinger reduction could be an additional explanation for the observed higher molecular masses of **P1.4.1**. Comparison of the IR spectra of **P1.4** (black line, Figure 5.7 B) with **P1.4.1** (red line, Figure 5.7 B) indicate reduction of the azide group to amino groups by vanishing of the absorption band at

$\bar{\nu} = 2100 \text{ cm}^{-1}$. However, the quantification of the azide content in the polymer was not possible, because of the low intensity of the band for the azide stretching vibration due to the high molecular mass of the polymers ($\bar{M}_n \approx 8.0 \text{ kg}\cdot\text{mol}^{-1}$, refer to Table 5.6) and the corresponding low abundance of azide groups in the measured sample. The deshielding of the phthalimide-capped amino groups by hydrazinolysis (see General Procedure 11 on page 224) to yield **P1.4.2**, was successful as indicated by the recorded ^1H NMR spectra (Figure 5.7; P1.4 and P1.4.2) in which the signals of the aromatic protons ($\delta = 7.20\text{-}7.80 \text{ ppm}$) disappeared after hydrazinolysis. This evidence was clearly supported by comparison of the IR spectrum traces of **P1.4** (black line, Figure 5.7 B) with **P1.4.2** (green line, Figure 5.7 B). After the Staudinger reaction, the carbonyl stretching vibration band at $\bar{\nu} = 1720 \text{ cm}^{-1}$ could be observed, which can be assigned to the carbonyl groups of the phthalimide moiety. This demonstrates that it is possible to reduce the azide- independent of the phthalimide group, which enables a new synthetic pathway that may be helpful for different applications where either the amine- or the azide group are not tolerated. Further, no distinct vibration band from the poly(2oxazoline) backbone could be observed due to the overlapping of the absorption bands that is typical for polymers. Similar problems occurred for the quantification of the phthalimide end groups by using the carbonyl stretching vibration ($\bar{\nu} \approx 1720 \text{ cm}^{-1}$) as indicator for those groups. Therefore, only qualitative statements regarding the success of the corresponding postmodification reactions could be done.

P1.4.3 was prepared by hydrazinolysis of **P1.4.1**. The success of this reaction was confirmed by disappearance of the phthalic protons at $\delta = 7.20\text{-}7.80 \text{ ppm}$ (Figure 5.7 A) as well as the vanishing of the carbonyl stretching vibration band $\bar{\nu} \approx 1720 \text{ cm}^{-1}$ (carbonyl stretching vibration of phthalimide) in the IR spectrum (Figure 5.7 B). Further, this reaction demonstrated the orthogonal reactivity of both end groups again. The calculation of \bar{M}_n by ^1H NMR was not possible for **P1.4.2** and **P1.4.3** since no distinct signal for a respective end group was obtained. The \bar{M}_n obtained by GPC (Table 5.6) for the polymers differ from the targeted molar mass of $4.2 \text{ kg}\cdot\text{mol}^{-1}$. These deviations can be partially ascribed to the eluent and standards used in the GPC, which may be not ideal, especially the usage of PMMA standards can cause a significant difference. Compared to the calculated \bar{M}_n obtained by ^1H NMR spectroscopy, the differences are much smaller, supporting the evidence that, probably the initiator efficiency was hampered as described above.

Table 5.6: Tabulation of the measured molar masses and dispersities of the hetero-telechelic poly(nPrOxa-co-iPrOxa)s (**P1.4-P1.4.3**) as well as the corresponding yield of the reaction. The mass parameters were measured using GPC and calculated by ¹H NMR spectroscopy. The relative yield (%) was calculated by comparing the initial mass of polymer which was used as educt and the obtained mass of polymer after postmodification reaction.

Polymer	Built-In ratio		\bar{M}_n	\bar{M}_n	\bar{D}	Yield / mg (%)
	nPrOxa :	iPrOxa ^a	(NMR) / kg·mol ⁻¹	(GPC ^b) / kg·mol ⁻¹		
P1.4 (1)	51 : 49		7.2	9.9	1.27	860 (67)
P1.4.1	52 : 48		8.4	10.8	1.39	82 (82)
P1.4.2	51 : 49		--- ^c	14.9	1.21	50 (50)
P1.4.3	51 : 49		--- ^c	16.3	1.26	25 (50)

^a determined by ¹H NMR spectroscopy

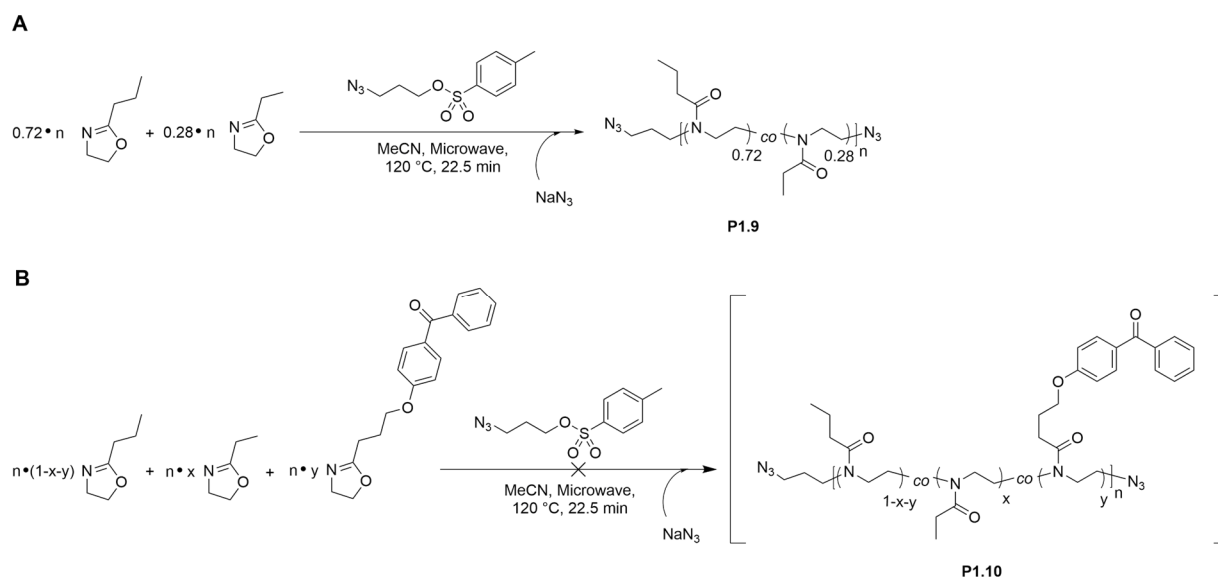
^b eluent : DMAc containing LiBr ($\beta = 1 \text{ g}\cdot\text{l}^{-1}$); PMMA standards were used for calibration

^c could not be determined by ¹H NMR spectroscopy

The drastic increase of the apparent molar masses for **P1.4.2** and **P1.4.3** obtained by GPC, compared to the molar mass of the precursor **P1.4**, can be attributed to the conversion of the phthalimide to an amino group. This could increase the overall polarity of the polymer and thus lead to expanded coiling behavior in DMAc. However, since only a single end group should not cause such a strong change in coiling behavior, the potential occurrence of side reactions may be indicated. Such a possible side reaction could be the partial hydrolysis of the polymer by hydrazine, forming ethyleneimine repeat units and hydrazides as side products. Further, the presence of the amino group as end group can cause aggregations of at least two polymer chains leading to the larger measured molar mass.

Preparation of homo-telechelic copolymers using N₃-Prop-Tos:

The copolymer system was changed from a copolymer composed of 2-propyl-2-oxazoline derivatives to a system based on EtOxa and nPrOxa as discussed previously (see chapter 5.1.1). Besides, the copolymers (**P1.5 C**), which contain an azide group as ω -end group, another copolymer was prepared that carries azide groups at both polymer backbone ends (**P1.9**). The reaction is illustrated in the scheme below (Scheme 5.8 A).



Scheme 5.8: (A) Illustration of polymerization of α - and ω -azide-functionalized Poly(EtOxa-co-nPrOxa) (**P1.9**) and (B) the corresponding terpolymer using BP-Oxa as additional photocrosslinkable comonomer (**P1.10**). Latter reaction failed as indicated by the brackets.

P1.9 was prepared using the synthesized N_3 -Prop-Tos as initiator and NaN_3 as termination agent. The polymerization was performed according to the polymerization procedure described previously in chapter 5.1.1 (experimental details can be found in General Procedure 7 on page 217). The obtained yields in both attempts of 48% and 54% were in accordance to yields obtained for polymers prepared by using the same polymerization protocol. From the recorded 1H NMR (Figure 5.8 A) the \bar{M}_n could be calculated comparing the integral of the signal, that represents the protons in the backbone ($\delta = 3.44$ ppm) and the signal, which corresponds to the methylene group of the 3-azidopropyl group next to the first nitrogen of the backbone ($\delta = 2.68$ ppm). Both the \bar{M}_n of $17.3 \text{ kg}\cdot\text{mol}^{-1}$, calculated from the 1H NMR spectrum, as well as the \bar{M}_n of $13.7 \text{ kg}\cdot\text{mol}^{-1}$, obtained by GPC, are close to the theoretical \bar{M}_n of $16.4 \text{ kg}\cdot\text{mol}^{-1}$. The narrow molar mass distribution ($D = 1.16$) indicates a good control over the polymerization reaction with only few side- or termination reactions. Further, the content of EtOxa in **P1.9** was determined by integration of the proton signals at $\delta = 1.11$ ppm, which correspond to the methyl group of EtOxa and the signal at $\delta = 0.93$ ppm that arise from the terminal methyl group of the *n*-propyl side chain.

The comparison showed an EtOxa content of 27% which is close to the targeted 30% at reaction start.

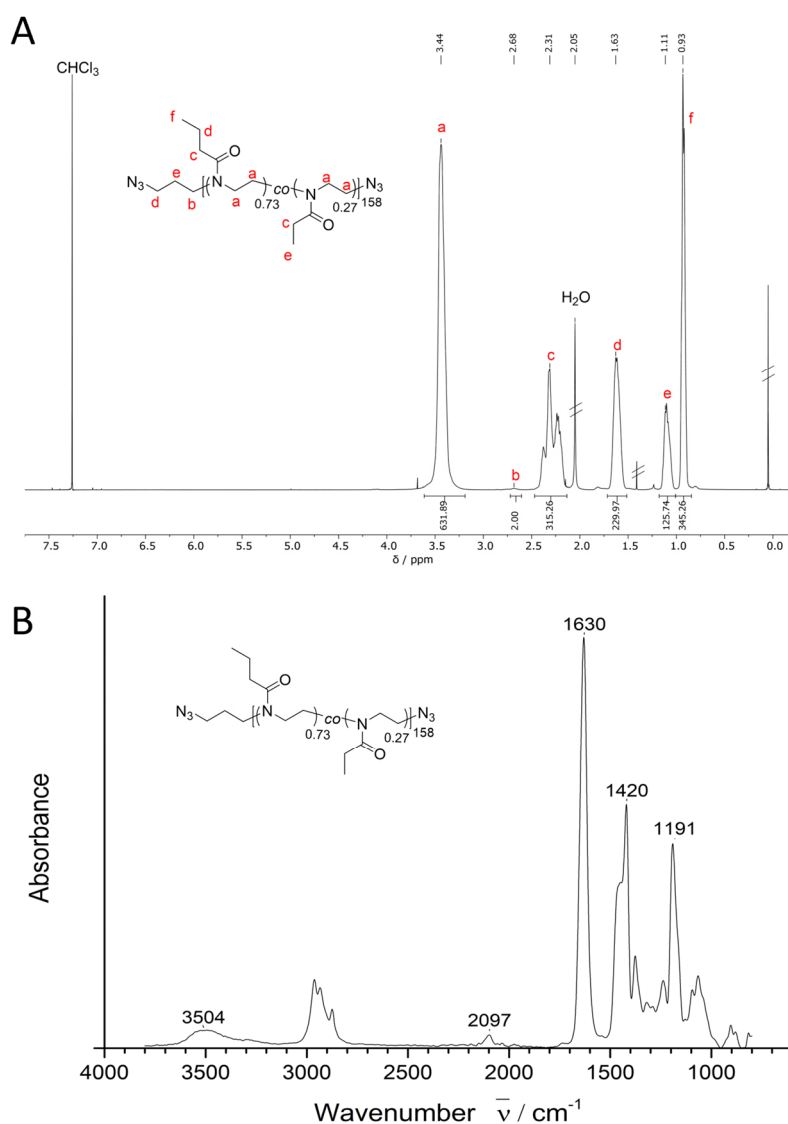
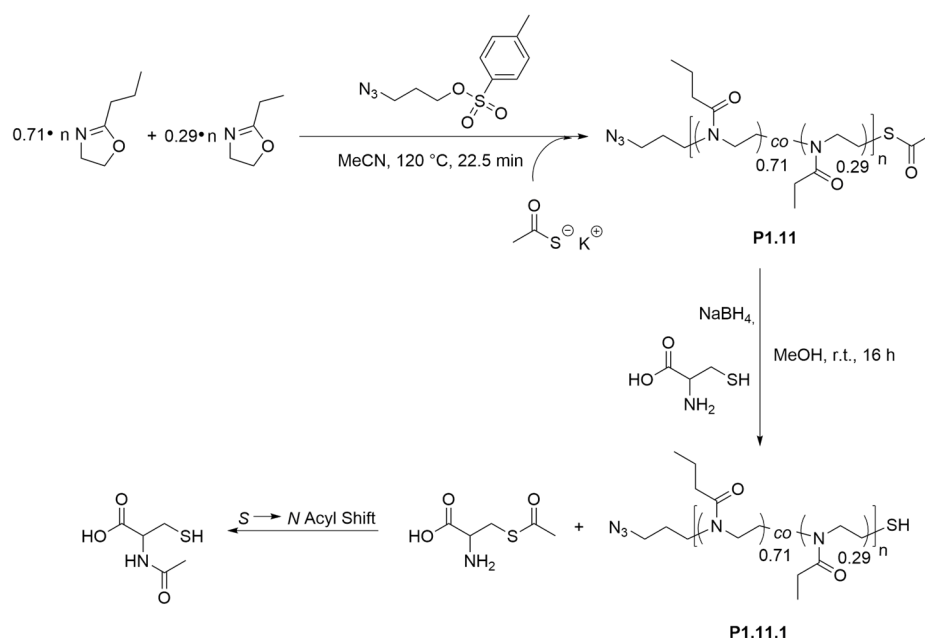


Figure 5.8: (A) Depiction of the recorded ¹H NMR (500 MHz) spectrum of **P1.9** and the corresponding assignment of the signals to the structure. (B) Illustration of the recorded IR spectrum.

The recorded IR spectrum showed the successful azide-functionalization of **P1.9** by the appearance of the azide stretching vibration at $\bar{\nu} \approx 2097 \text{ cm}^{-1}$. However, quantification by IR was not possible, due to the low signal intensity of the azide vibration. Additionally, a derivative of **P1.9** should be synthesized that carries BP-Oxa units for photo crosslinking (**P1.10**) (Scheme 5.8 B). The preparation of the photocrosslinkable **P1.10** failed, which was indicated by forming of a precipitate during the polymerization reaction. After, isolation of the product the polymer was insoluble in all typical solvents for poly(2-oxazoline)s, implying a crosslinking reaction during the polymerization. Obviously, the incorporation of BP-Oxa units caused this undesired side reaction since the polymerization without BP-Oxa worked well as described above.

Synthesis of hetero-telechelic copolymers using N₃-Prop-Tos:

For the potential application of poly(2-oxazoline)s as linker in SPR based biosensing devices, it is favorable to prepare polymers containing two distinct end groups. This structure should avoid undesired coupling reactions e.g. of the targeted analyte or the sensing molecule, which should be attached to only one of the polymeric linker. In first experiments to explore the suitability of such polymers as junctions between the metal surface and the sensing molecule or ligand, different copolymers were used that possess asymmetric end groups (see chapter 5.3), with one being a thiol anchor group for gold surfaces.



Scheme 5.9: Outline of the copolymerization of nPrOxa and EtOxa using N₃-Prop-Tos as initiator and potassium thioacetate as termination agent to yield **P1.11**. The conversion of the thioacetate end group to a thiol group (**P1.11.1**) was performed by a native chemical ligation (NCL) reaction.

Again, as comonomers EtOxa and nPrOxa were chosen to yield thermoresponsive copolymers. The copolymerization can be good controlled, meaning that side reactions can be widely suppressed by using short polymerization times. N₃-Prop-Tos was used as initiator to introduce the azide group at one end of the chain and potassium thioacetate was chosen to terminate the chain propagation as reported in the literature.¹⁷⁴ This termination agent allows the introduction of a thioacetate group at the distal end of the polymer, which acts as protecting group for the thiol group.

The synthetic pathway to obtain **P1.11** and **P1.11.1** is shown in Scheme 5.9. The copolymerization was performed according to previous synthesized polymers (see above) and the procedure as well as the experimental details for the native chemical ligation (NCL) -reaction are described in General Procedure 7 on page 217. The liberation of the thiol groups, in a NCL-reaction, which is well-known in synthesis of proteins^{175,176} as well as technique to form hydrogels,^{177,178} can be accomplished by using cysteine and sodium borohydride as reagents. First, the deprotonated thiol group of the cysteine reacts with the carbonyl of the thioacetate group coupled to the polymer chain (transthioesterification). After cleavage of the carbon-sulfur bond, the polymer chain bearing the thiol group at the end will be released and the resulting thioester of the cysteine undergoes a rapid intramolecular rearrangement reaction in which an acyl shift from the sulfur to the nitrogen occurs that leads to *N*-acetylcysteine amide as byproduct.^{175,178} **P1.11** could be obtained in a reasonable yield of 54%, which is in accordance to the obtained yields for other copolymers prepared by the same polymerization procedure. The presence of the azide groups at the α -chain end could be confirmed by the presence of the absorption band at $\bar{\nu} \approx 2100 \text{ cm}^{-1}$ in the IR spectrum (Figure 5.9 A). The content of azide groups could not be quantified from the IR spectrum as already discussed previously in this chapter.

The recorded ^1H NMR spectrum indicate small impurities that may arise from remaining potassium thioacetate. The content of EtOxa present in the polymer chains, determined as described previously, was found to be 30%, which is equal to the monomer ratio at reaction start. The $\bar{X}_{n,NMR}$ and the corresponding $\bar{M}_{n,NMR}$ could be determined by comparing the integrals of the signals that represent the protons in the backbone ($\delta = 3.44 \text{ ppm}$) and the signal, which correspond to the methylene group of the 3-azidopropyl group next to the first nitrogen of the backbone and the methylene group next to the thioacetate group ($\delta = 2.95 \text{ ppm}$). The calculated values of $\bar{X}_n = 83$ and $\bar{M}_n = 9.0 \text{ kg}\cdot\text{mol}^{-1}$ were close to the theoretical values adjusted at polymerization start ($\bar{X}_n = 74$ and $\bar{M}_n = 8.0 \text{ kg}\cdot\text{mol}^{-1}$). The deviation may occur from integration inaccuracies of the signal at $\delta = 2.95 \text{ ppm}$, because of overlapping signals, which arise from impurities. In GPC experiments (eluent: DMAc + LiBr [$1 \text{ g}\cdot\text{l}^{-1}$], PMMA standards as reference), a $\bar{M}_n = 9.3 \text{ kg}\cdot\text{mol}^{-1}$ was found. The low D of 1.20, obtained in GPC, indicate a good control of the molar masses in this polymerization. The thiol-terminated **P1.11.1**, prepared by NCL reaction, was obtained in a yield of 69% which is reasonable.

5 Results and Discussion

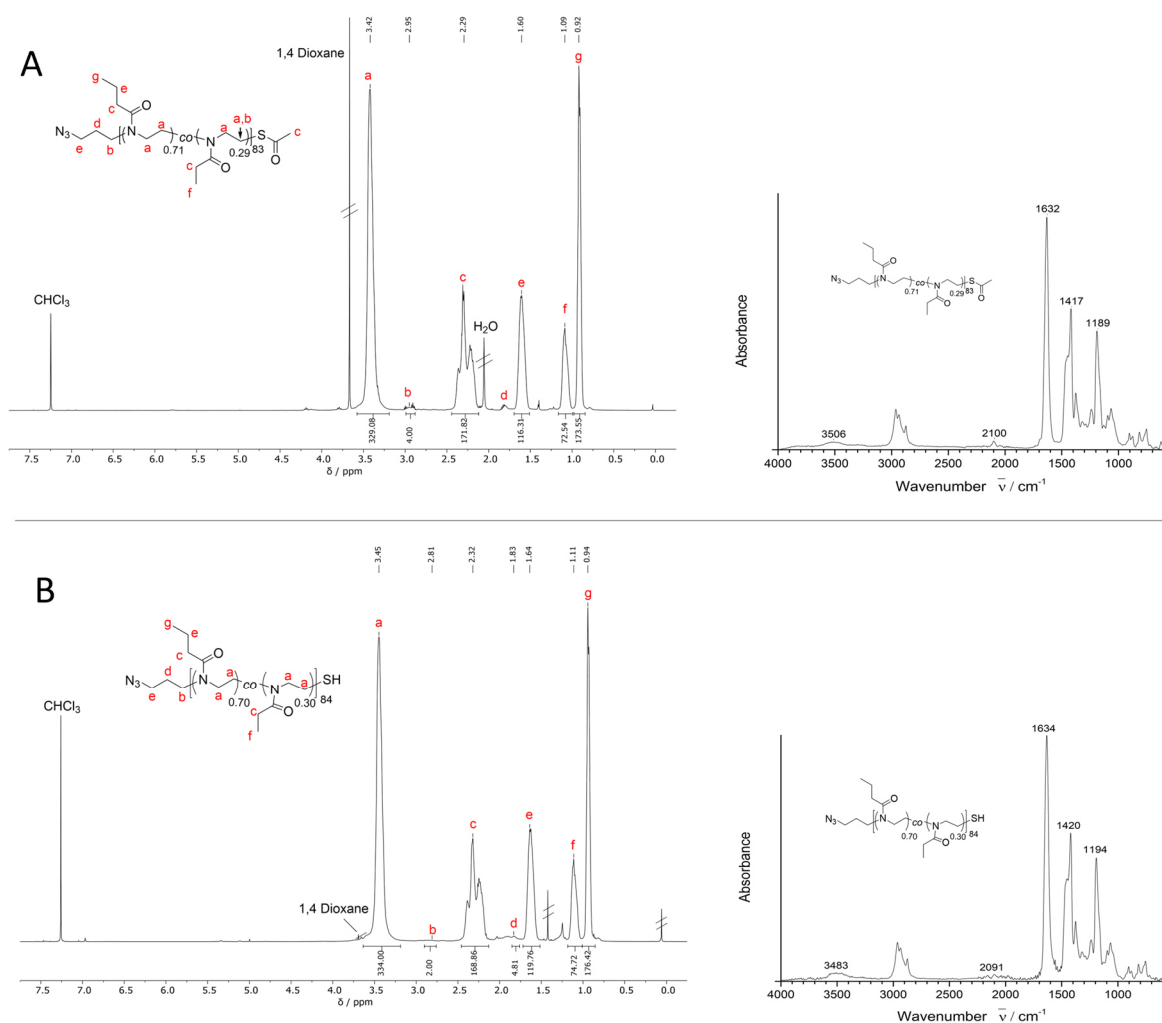


Figure 5.9: (A) Illustration of the recorded $^1\text{H NMR}$ (500 MHz) spectrum of **P1.11** and the corresponding IR spectrum. (B) Depiction of the recorded $^1\text{H NMR}$ (500 MHz) and IR spectrum after deprotection (**P1.11.1**).

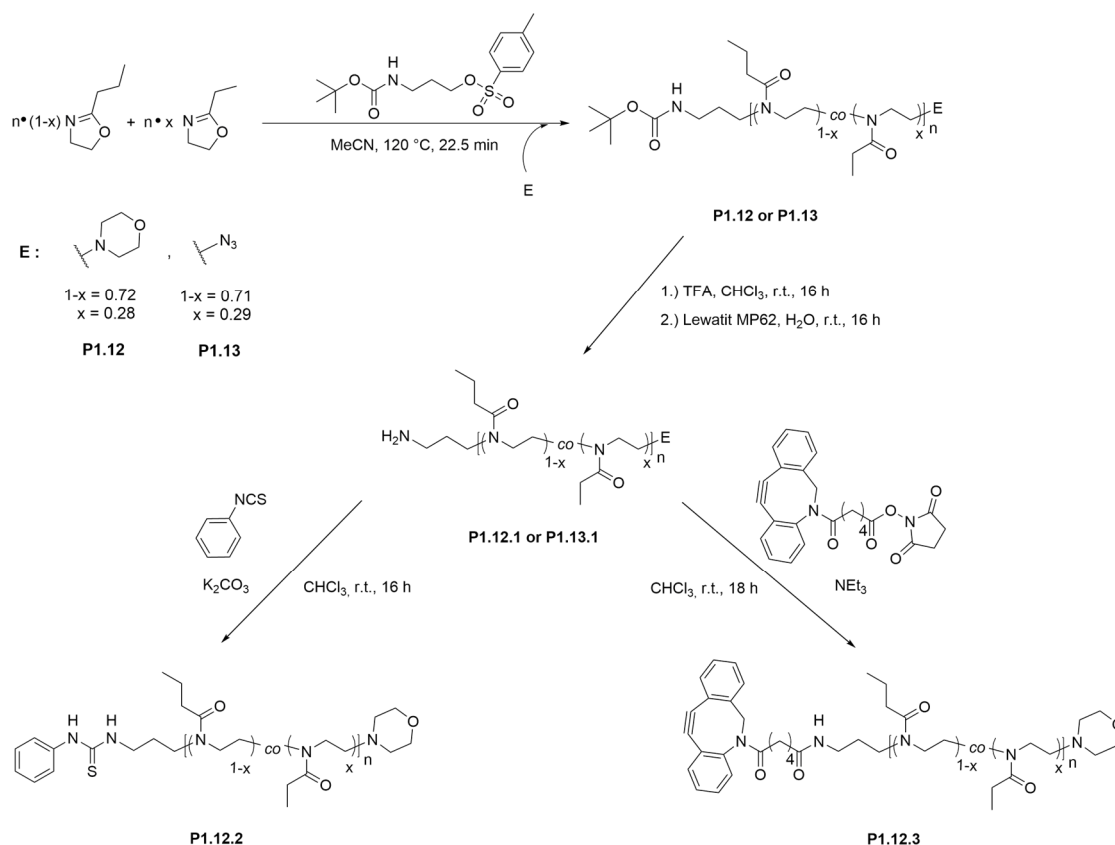
Clear evidence for a successful liberation of the thiol groups at the ω -chain end by $^1\text{H NMR}$ or IR spectroscopy was not possible since the methyl group of the thioacetate overlapped with the methylene groups next to the carbonyl groups of the amide side chains in NMR and the carbonyl stretching vibration of the thioacetate possess the same absorption wavenumber as the other carbonyls present in the polymer chain. However, in $^1\text{H NMR}$ a shift of the signal assigned to methylene group adjacent to the ω -end group was observed, indicated by the decrease of the integral at $\delta = 2.95$ ppm, which could be a hint for the liberation of the thiol group (Figure 5.9 B). It is suspected that the signal assigned to the methylene group next to the thiol group leads, due to a downfield shift after deshielding of the thiol, to an overlap with the broadened signal of the methylene groups of the polymer backbone ($\delta = 3.44$ ppm). Further, the recorded GPC data showed a shift towards higher molecular masses ($\bar{M}_n = 13.1 \text{ kg}\cdot\text{mol}^{-1}$), whereas the molar mass distribution remained almost constant ($D = 1.22$) compared to the mass parameters

before deprotection ($\bar{M}_n = 9.3 \text{ kg}\cdot\text{mol}^{-1}$ and $\bar{D} = 1.20$) indicating increased hydrodynamic radii of the polymer chains. The recorded IR spectrum (Figure 5.9 B) also implied a side reaction since the absorption band of the azide stretching vibration at $\bar{\nu} \approx 2100 \text{ cm}^{-1}$ almost vanished. Sodium borohydride acts as strong reducing agent and thus the azide could be converted to an amino group, which amplifies the polarity of the polymer chains resulting in larger hydrodynamic radii as observed by GPC after deprotection. The obvious loss of azide groups led to an alternative approach to prepare suitable linker for biosensing devices. This synthetic route is related to the strategy discussed at the beginning of the chapter (**P1.4**) in which an azide group as well as an amino group were introduced at the distal ends of the polymer backbone. Instead of PhT-Et-Tos now *N*-Boc-Prop-Tos is used as initiator, which enables a mild and more selective deprotection method by using TFA compared to the hydrazinolysis of the phthalimide-capped amino groups (see above). Again, EtOxa and nPrOxa were used as comonomers. The linkage to the metal surface should be accomplished by either using carboxylate-terminated alkanethiols or by using bis(2,5-dioxopyrrolidin-1-yl) 3,3'-disulfanedioldipropanoate (DTPA-NHS) as gold anchor, which was prepared and investigated within the work group previously.⁴ The polymer will be bound to the NHS activated carboxyl sites of the alkanethiol or DTPA-NHS, which is able to chemisorb onto gold. Further details will be discussed in chapter 5.3.

Preparation of copolymers using N-Boc-Prop-Tos:

Waschinski and coworkers as well as Qiu and coworkers demonstrated the suitability of a Boc-protected amino-functionalized tosylate for initiating the CROP of EtOxa.^{179,69} Initially, copolymers were prepared using *N*-Boc-Prop-Tos as initiator and morpholine as termination agent (**P1.12**). Later, in a series of poly[(EtOxa)-*co*-(nPrOxa)] with different masses, morpholine was replaced by sodium azide to obtain hetero-telechelic copolymers (**P1.13**). Both reaction pathways and their post-functionalization reactions are depicted in Scheme 5.10

5 Results and Discussion



Scheme 5.10: Schematic overview of the synthesis of distinct α -amino-functionalized poly[(EtOxa)-*co*-(nPrOxa)] copolymers bearing different ω -end groups (**P1.12**: -morpholine, **P1.13**: $-N_3$). After deprotection of the amino group, different coupling reactions were accomplished.

The yields for **P1.12** and **P1.13 A** (75%-85%) were higher than the yields obtained for the other prepared copolymers **P1.13 B-P1.13 I** (Table 5.7). Obviously, the preparation in larger scales led to a lower relative loss of polymer mass during the purification procedure. **P1.13 B-P1.13 I** (26%-63%) were obtained in yields that were also obtained for other polymer systems prepared by the same polymerization protocol. Interestingly, the yields for **P1.13 F** (26%) and **P1.13 G** (29%) were lower than acquired for the other polymers. Additionally, the obtained \bar{M}_n of $16 \text{ kg}\cdot\text{mol}^{-1}$ were similar for both copolymers and significantly lower than expected. The monomer to initiator ratio was adjusted to yield a theoretical \bar{M}_n of $29.8 \text{ kg}\cdot\text{mol}^{-1}$ for **P1.13 F** and for **P1.13 G** a theoretical \bar{M}_n of $41.0 \text{ kg}\cdot\text{mol}^{-1}$. However, the low \bar{D} of 1.11 and 1.14, respectively indicated a well-controlled copolymerization, but the monomer conversion was too low. Thus, the polymerization time of $t = 22.5 \text{ min}$ was obviously too short.

Therefore, **P1.13 H** and **P1.13 I** were synthesized using the same monomer-to-initiator ratio of 375 : 1 (same as for **P1.13 G**), but with different reaction times ($t = 37.5 \text{ min}$ and $t = 45 \text{ min}$).

Table 5.7: Listing of the built-in of nPrOxa and EtOxa, the expected and measured molar masses as well as the corresponding dispersity of Boc protected amine-functionalized poly(nPrOxa-co-EtOxa) (**P1.12**) and poly(nPrOxa-co-EtOxa) (**P1.13**) and the yield of the polymerization. The mass parameters were measured using GPC and the built-in was calculated by ¹H NMR spectroscopy. The relative yield (%) was calculated by comparison of the initial mass of monomer and the obtained mass of polymer.

Polymer	Built-In ratio ^a nPrOxa : EtOxa / %	Theoretical \bar{M}_n / kg·mol ⁻¹	\bar{M}_n (GPC ^b) / kg·mol ⁻¹	\bar{D}	Yield / mg (%)
P1.12 (1)	72 : 28	4.8	4.6	1.22	532 (82)
P1.12 (2)	72 : 28	4.3	6.7	1.12	984 (75)
P1.13 A	71 : 29	5.5	7.3	1.09	475 (75)
P1.13 A (2)	“ ^c	4.4	7.1	1.09	1040 (82)
P1.13 B	“	8.4	9.5	1.09	400 (63)
P1.13 C	“	11.0	10.9	1.10	341 (54)
P1.13 D	“	16.4	12.4	1.07	261 (41)
P1.13 E	“	19.9	14.7	1.11	263 (42)
P1.13 F	“	29.8	16.1	1.11	164 (26)
P1.13 G	“	41.0	16.0	1.14	185 (29)
P1.13 H^d	“	41.6	19.7	1.20	266 (41)
P1.13 I^e	“	41.6	24.7	1.13	338 (52)

^a determined by ¹H NMR spectroscopy

^b eluent : DMAc containing LiBr ($\beta = 1 \text{ g}\cdot\text{l}^{-1}$); PMMA standards were used for calibration

^c same built-in ratio as described for P1.13 A

^d reaction time 37.5 min at 120 °C

^e reaction time 45 min at 120 °C

The measured \bar{M}_n of 19.7 kg·mol⁻¹ (**P1.13 H**) and 24.7 kg·mol⁻¹ (**P1.13 I**) implied a higher conversion of the monomers, but still the theoretical \bar{M}_n was not reached. For **P1.12** and **P1.13 A-P1.13 D**, the measured \bar{M}_n were in good agreement to the corresponding theoretical molar mass. The overall low \bar{D} of 1.07-1.22 indicates a good control polymerization. The \bar{M}_n of **P1.13 E** (14.7 kg·mol⁻¹) already showed a significant deviation from the theoretical value (20.0 kg·mol⁻¹) supporting the evidence that with decreasing initiator concentration longer reaction times are necessary to reach full conversion of the monomers. Additionally, side reactions like chain coupling reactions become more apparent, which lead to a small broadening

of the molar mass distribution.¹⁸⁰ The built-in ratios of EtOxa and nPrOxa were determined by ¹H NMR spectroscopy as described above. For all copolymers, the calculated built-in ratio was in good agreement to the initial monomer ratio at reaction start.

Removal of the Boc-protecting group at the amino groups was accomplished by using TFA followed by an anion exchange reaction to obtain primary amino-moieties as α -end groups.

The procedure is described in General Procedure 13 on page 230. Success of the deprotection reaction was confirmed by comparison the recorded ¹H NMR spectra before and after deprotection. Below, a representative comparison of **P1.13 A** and **P1.13.1 A** is shown (Figure 5.10). The corresponding ¹H NMR of **P1.12** and **P1.12.1** are depicted in Figure S61 and Figure S67.

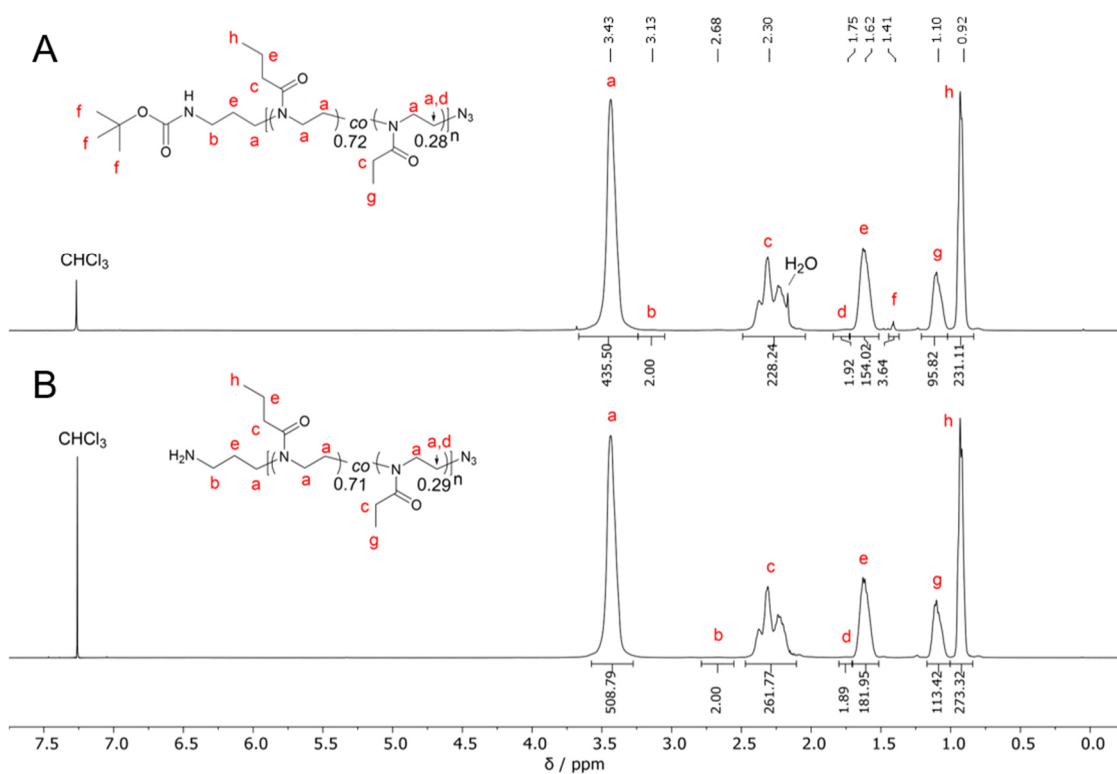


Figure 5.10: Comparison of recorded ¹H NMR spectra (500 MHz) of **P1.13** before (A) and after deprotection (B)

The successful removal of the Boc-protecting group could be identified by disappearance of the signal at $\delta = 1.41$ ppm, which correspond to their methyl groups. Further, a high field shift of the signal b, which is assigned to the methylene group next to the protect amino moiety, from $\delta = 3.13$ ppm to $\delta = 2.68$ ppm can be observed giving evidence for the success of above-mentioned reaction. Determination of the \bar{X}_n and the \bar{M}_n by ¹H NMR was not possible, because of overlapping signals. Interestingly, the integral of signal assigned to the methyl groups of the

tert.-butyl-moiety ($\delta = 1.41$ ppm) indicate that the protecting group was partially removed during polymerization (Integral value 3.6 instead of 9) that is potentially caused by the cationic chain ends. The liberated amino groups can in turn act as termination agents for the cationic chain ends, leading to a broadening of the molar mass distribution and lower molar masses than expected. The ability of small oligomers to react with the secondary amino group may decrease during the polymerization time due to the increasing spatial demand of the growing polymer chains, which may explain the quite narrow molar mass distributions ($\mathcal{D} = 1.07$ -1.22) and reliable molar masses observed by GPC. Similar results were also obtained for **P1.12** and **P1.12.1** indicating an intrinsic side reaction. Cesana and coworkers observed a similar side reaction of Boc-protected amino groups at the side chains of poly(2-oxazoline)s initiated by using a classical initiator for CROP like MeOTf.⁷⁹ The presence of the azide group at the ω -chain end was confirmed by IR spectroscopy.

Table 5.8: Summarization of the obtained molar masses and dispersities of the amine-functionalized poly(nPrOxa-co-EtOxa) (**P1.12.1**) and poly(nPrOxa-co-EtOxa) (**P1.13.1**) after removal of the Boc-protecting group as well as the corresponding yield of the reaction. The mass parameters were measured using GPC. The relative yield (%) was calculated by comparison the initial used mass of polymer which was used as educt and the obtained mass of polymer after postmodification reaction.

Polymer	Polymer / mg (μmol)	\bar{M}_n (GPC ^a) / kg·mol ⁻¹	\mathcal{D}	Yield / mg (%)
P1.12.1 (1)	125 (4.0)	4.4	1.26	106 (86) ^b
P1.12.1 (2)	500 (66.7)	6.5	1.14	235 (47)
P1.13.1 A	250 (31.5)	6.3	1.12	174 (69)
P1.13.1 B	200 (19.0)	10.0	1.06	45 (23)
P1.13.1 E	250 (14.9)	15.3	1.07	128 (51)
P1.13.1 G	200 (10.4)	16.9	1.09	95 (48)
P1.13.1 H	250 (9.8)	19.6	1.19	122 (49)
P1.13.1 I	250 (8.6)	24.3	1.13	196 (78)

^a eluent : DMAc containing LiBr ($\beta = 1 \text{ g}\cdot\text{l}^{-1}$); PMMA standards were used for calibration

^b no anion exchange reaction was performed

In both, the recorded spectrum of **P1.13 A** before deprotection and the spectrum of **P1.13.1 A** after deprotection the azide stretching vibration band at $\bar{\nu} \approx 2100 \text{ cm}^{-1}$ was observed (compare Figure S62 and Figure S68). In Table 5.8, the corresponding mass parameters as well as the yield of each post-functionalization reaction are listed. The yields of the deprotection reactions were around 50% for **P1.12.1 (2)** and **P1.13.1 A-I**. The loss of polymer mass may be explained by partial adsorption of polymer at the used an anion exchanger (Lewatit MP62). This also explains the higher yield (86%) of **P1.12.1 (1)**, which was determined before the use of the anion exchanger. As expected, the \bar{M}_n and \mathcal{D} , obtained after deprotection reaction, showed no significant deviation compared to the mass parameters before deprotection. The liberated amino groups at the α -chain end of **P1.12.1** were exemplarily converted to a thiourea derivative using phenyl isothiocyanate (**P1.12.2 (1)**). The idea was a feasible quantification of the primary amino groups by $^1\text{H NMR}$, which additionally allows the determination of the corresponding \bar{X}_n and the \bar{M}_n values of the corresponding polymer. The recorded $^1\text{H NMR}$ spectrum of **P1.12.2 (1)** indicate a successful linkage of the isothiocyanate to the copolymer and thus also confirming the presence of a primary amino group at the distal end of the backbone. Comparison of the integral of the aromatic proton signals at $\delta = 7.80\text{-}7.40 \text{ ppm}$ with the integral of the signal assigned to the polymer backbone ($\delta = 3.44 \text{ ppm}$) a \bar{X}_n of 58 and a \bar{M}_n of $6.3 \text{ kg}\cdot\text{mol}^{-1}$, which is close to the \bar{M}_n of $5.5 \text{ kg}\cdot\text{mol}^{-1}$ measured by GPC (see Table 5.9).

Table 5.9: Tabularization of the measured molar masses and dispersities of the functionalized poly(nPrOxa-co-EtOxa) **P1.12.2** and **P1.12.3** as well as the corresponding yield of the coupling reaction with phenyl isothiocyanate (**P1.12.2**) and with DBCO-C6-NHS (**P1.12.3**). The mass parameters were measured using GPC. The relative yield (%) was calculated by comparison the initial used mass of polymer which was used as educt and the obtained mass of polymer after postmodification reaction.

Polymer	Educt Polymer	Polymer / mg (μmol)	\bar{M}_n (GPC ^a) / $\text{kg}\cdot\text{mol}^{-1}$	\mathcal{D}	Yield / mg (%)
P1.12.2 (1)	P1.12.1 (1)	103 (17.1)	5.5	1.15	54 (52)
P1.12.2 (2)	P1.12.1 (2)	100 (16.6)	7.0	1.11	54 (52)
P1.12.3 (2)	P1.12.1 (2)	100 (16.6)	7.4	1.12	80 (80)

^a eluent : DMAc containing LiBr ($\beta = 1 \text{ g}\cdot\text{l}^{-1}$); PMMA standards were used for calibration

Together with the good control of the polymerization, indicated by the low molar mass distributions, the above discussed synthesis route defines an efficient strategy towards hetero-telechelic copolymers. This approach could be used as alternative route to the proposed postfunctionalization strategy discussed in chapter 5.1.1 that was used for preparing polymer-DNA conjugates (chapter 5.3). The reaction pathway is shown above (Scheme 5.10) in which the primary amino moiety of the copolymer **P1.12.2** react with the NHS activated carbonyl group of the DBCO derivative.

A possible advantage of the proposed pathway could be the fact, that each polymer chain carries an amino group incorporated by the initiator, which might improve the coupling efficiency of the functionalized DNA. Co- and terpolymers that were terminated by azide (**P1.5** and **P1.6**) and then further functionalized (refer to chapter 5.1.1), may suffer from intrinsic side reactions during polymerization, which lead to a loss of active centers (termination reactions) and thus to a lower coupling efficiency. The recorded ^1H NMR spectrum of **P1.12.3 (2)** (Figure S70) indicate a successful coupling of the DBCO functionality to the copolymer by appearing of the signals assigned to the DBCO functionality at $\delta = 7.50\text{-}7.00$ ppm and $\delta = 4.29$ ppm. However, the integrals of these signals demonstrated, that only low degree of functionalization of around 17%, calculated by comparison the integrals of the aromatic protons of the DBCO moiety and the methylene group adjacent to the first repeat unit ($\delta = 3.13$ ppm), was obtained. The sterical demand of the DBCO derivative may lead to decreased coupling efficiency.

Another explanation could be the orientation of the polymer coils in chloroform, which may surround the polar amino groups by the more hydrophobic chain segments, so that the bulky DBCO moieties can hardly reach these amino groups. Improved coupling efficiencies of DBCO to **P1.12.1** may can be observed by extending the reaction time as well as a change to a more polar solvent.

Summary:

Different tosylate-based initiators with either protected amino functionalities or an azide group were prepared for the synthesis of telechelic POxas according to procedures described in literature.¹⁻³ First, novel hetero-telechelic copolymers composed of nPrOxa and iPrOxa were prepared with Pht-Et-Tos as initiator and sodium azide as termination agent (**P1.4**). The reduction of the azide group by Staudinger reaction yielded the desired amino-functionalized copolymer carrying an azide group at the other distal end (**P1.4.1**). The orthogonality of both

used masked amino groups was demonstrated by hydrazinolysis of the phthalimide-capped amino group of **P1.4** whereas the azide end group remained unaffected (**P1.4.2**).

Further, a novel copolymer composed of EtOxa and nPrOxa carrying at both distal ends an azide group (**P1.9**) was synthesized by using N₃-Prop-Tos and sodium azide as termination agent. This homo-telechelic copolymer features the possibility to couple to equivalent building blocks, which is interesting for the preparation of polymer-DNA conjugates (chapter 5.3).

For the potential use as flexible linker in biosensing assays (see chapter 5.4), a series of novel hetero-telechelic copolymers composed of nPrOxa and EtOxa were prepared, which carry a (protected) thiol- and an azide end group, as well as copolymers that bear amino- and azide end groups. Therefore, sodium azide was replaced by potassium thioacetate as termination agent and N₃-Prop-Tos was used as initiator to obtain **P1.11**. The presence of the azide group after copolymerization was successfully confirmed by IR spectroscopy. The acetate group was removed by a NCL reaction yielding the free thiol end group (**P1.11.1**). However, the comparison of the IR spectra before and after NCL reaction indicates that a partially reduction of the azide moieties as side reaction occurred, which will lead to a reduced coupling efficiency in azide-alkyne based click reactions.

In an alternative approach, first a model copolymer was prepared using *N*-Boc-Prop-Tos as initiator and morpholine as termination agent (**P1.12**). The ¹H NMR spectrum of **P1.12** revealed a possible side reaction of the cationic oligomers, present at short reaction times, which may lead to a partial deprotection of the masked amino end group. The liberated amino groups could cause combination reactions with propagating chains, which would explain the observed increased molar masses and the broadening of the molar mass distributions. In a model reaction, a DBCO-NHS ester was chosen for further functionalization of the polymers that carry an amino groups at one of the distal end (**P1.12.2**). However, a poor degree of functionalization was obtained by ¹H NMR spectroscopy for **P1.12.3**, which could be explained by the sterical demand of the bulky DBCO group and the shielding of the polar amino groups by the more hydrophobic polymer backbone in chloroform.

Based on the results obtained for **P1.12** and **P1.12.1**, a series of copolymers with different molar masses were prepared in which the termination agent morpholine was replaced by sodium azide (**P1.13 A-I**). The amino groups of six copolymers (**P1.13 A**, **P1.13 B** and **P1.13 G-P1.13 I**) were deprotected using the previously mentioned protocol and the resulting copolymers were tested as potential linkers in biosensors (chapter 5.4).

5.1.3 Thiol-Substituted Poly(2-oxazoline)s with Photolabile Protecting Groups-Tandem Network Formation by Light

The following manuscript was submitted to *Polymers* an online journal of MDPI and was accepted for publication on 4th of August 2020. Below the accepted manuscript is presented and the online version can be found at <https://doi.org/10.3390/polym12081767>.

Thiol-Substituted Poly(2-oxazoline)s with Photolabile Protecting Groups—Tandem Network Formation by Light

Niklas Jung, Fiona Diehl and Ulrich Jonas *

Macromolecular Chemistry, Department Chemistry-Biology, University of Siegen, Adolf-Reichwein-Strasse 2, 57076 Siegen, Germany; Niklas.Jung@uni-siegen.de (N.J.); Fiona.Diehl@uni-siegen.de (F.D.)

* Correspondence: jonas@chemie.uni-siegen.de

Received: 21 July 2020; Accepted: 4 August 2020; Published: 7 August 2020

Abstract: Herein, we present a novel polymer architecture based on poly(2-oxazoline)s bearing protected thiol functionalities, which can be selectively liberated by irradiation with UV light. Whereas free thiol groups can suffer from oxidation or other spontaneous reactions that degrade polymer performance, this strategy with masked thiol groups offers the possibility of photodeprotection on demand with spatio-temporal control while maintaining polymer integrity. Here, we exploit this potential for a tandem network formation upon irradiation with UV light by thiol deprotection and concurrent crosslinking via thiol-ene coupling. The synthesis of the novel oxazoline monomer 2-{2-[(2-nitrobenzyl)thio]ethyl}-4,5-dihydrooxazole (NbMEtOxa) carrying 2-nitrobenzyl-shielded thiol groups and its cationic ring-opening copolymerization at varying ratios with 2-ethyl-2-oxazoline (EtOxa) are described. The tandem network formation was exemplarily demonstrated with the photoinitiator 2-hydroxy-2-methylpropiophenone (HMPP) and pentaerythritol tetraacrylate (PETA), a commercially available, tetrafunctional vinyl crosslinker. The key findings of the conducted experiments indicate that a ratio of ~10% NbMEtOxa repeat units in the polymer backbone is sufficient for network formation and in-situ gelation in *N,N*-dimethylformamide.

Keywords: in situ-forming gels; polymer network; chemical bonding; thiol-ene click; poly(2-oxazoline)s; photoremoveable protecting group (PPG)

Introduction

Poly(2-oxazoline)s are a class of pseudo-polyamides with a polyethyleneimine backbone and pendant amide substituents [1]. Interesting features of this polymer class encompass antifouling [2], biocompatibility [3–5] or therapeutic [1,6] properties. Consequently, in recent years, a large body of research was addressed to this domain [7–9]. For many applications of these poly(2-oxazoline)s, e.g. antifouling surface coatings, crosslinked networks are required [10]. In the literature, various

crosslinking mechanisms are described to yield such network architectures, specifically as water-swollen hydrogels. Pioneering work was reported by Seagusa and coworkers at the end of the last century [11–14]. Several years later, different research groups regained interest in poly(2-oxazoline)s as potential precursor for hydrogels [15,16]. A particular elegant strategy to crosslink poly(2-oxazoline)s harnesses the power of the thiol-ene click reaction, as demonstrated by many groups [10,17–24]. There, vinyl-functionalized poly(2-oxazoline)s as network backbone and multi-functional thiol derivatives as small crosslinker units were utilized [22].

To our knowledge, so far no gel is reported, which is formed from a thiol-functionalized poly(2-oxazoline) and a crosslinker with unsaturated carbon bonds. One advantage of this novel concept concerns the increased stability (e.g. against oxidation) and accessibility of numerous vinyl- or alkyne-functionalized crosslinker derivatives opposed to their corresponding thiol analogues. Furthermore, the complementary thiol-substituted poly(2-oxazoline)s represent by themselves an interesting class of functional polymers:

- a. Targeted functionalization of poly(2-oxazoline)s may be conveniently performed utilizing thiol groups.
- b. The biological activity of free thiol groups (e.g. after conversion to asymmetric disulfides) as biologically cleavable linker which has been proposed in advanced transfection methodologies [25].
- c. The thiol group can serve as anchor group for immobilization of poly(2-oxazoline)s on metal surfaces like Au and Ag [26,27].
- d. In self-healing materials, the thiol moieties can undergo so-called thiol-disulfide exchange reactions, which is an interesting motive for repair processes [28,29].

Despite these advantages of free thiol groups, such SH-modified poly(2-oxazoline) derivatives may be affected by the following complications:

- a. 2-Oxazoline monomers bearing free thiol groups are not applicable in cationic ring opening polymerization (CROP), since the thiol is a nucleophile which acts as termination agent for the cationic active centers [30].
- b. Further, unprotected thiol groups are susceptible to oxidation to disulfides (e.g. with oxygen from air), which renders them inactive in thiol-ene click reactions and consequently may lead in poly(2-oxazoline)s to uncontrolled crosslinking, making storage and handling under ambient conditions difficult.
- c. Free thiol-groups in poly(2-oxazoline)s could also interfere in biological applications with sulfur-containing biomolecules (in particular in living organisms) by nucleophilic or disulfide exchange reactions [10].

Furthermore, thiol moieties may adversely transform other reactive groups within the same polymer backbone, e.g. reduction of azide moieties [31]. Consequently, protection of these free thiol moieties along the polymer backbone is necessary. For many side chain functionalities in poly(2-oxazoline)s, e.g. aldehyde [32], amino [33], and carboxylic acid groups [34], a large number of protecting groups is reported in the literature. But so far, for mercapto-modified poly(2-oxazoline)s, only the 4-methoxybenzyl substituent is discussed as protecting group [35]. Its cleavage requires quite harsh conditions with trifluoroacetic acid and anisole under elevated temperatures over extended periods of time [35], which may cause damage to sensitive moieties in the polymer.

An alternative approach employs photoremovable protecting groups (PPGs), which have been reported for various functionalities [36–44]. One of the early PPGs, which found broad application, is based on the 2-nitrobenzyl motif and till the 1980s about six main classes of different PPG classes were described [41]. Until 2013, the spectrum of PPG systems was significantly enhanced as elaborated by the exhaustive review of Klán et al. [36]. Maybe some current research directions worthwhile to point out are as follows: Concurrent implementation of complementary PPGs at solid interfaces, which allow selective deprotection in a lithographic manner [42]; long-wavelength-sensitive PPGs for biological and biomedical *in vivo* applications [43]; two-photon-sensitive PPGs, which combine the advantages of

longer wavelengths for deprotection with high spatial resolution [44]. Generally, PPGs provide the advantage of using light as sole means for cleavage under mild conditions, allowing good spatio-temporal control and obviating the need for chemical reagents in the deprotection reaction [36,40].

In the present publication, we focus on the well-known photolabile 2-nitrobenzyl unit as PPG for novel thiol-modified poly(2-oxazoline)s. The efficient synthesis of an oxazoline monomer carrying a 2-nitrobenzyl-shielded thiol group and its copolymerization with 2-ethyl-2-oxazoline (EtOxa) is reported. As a proof of principle, the tandem reaction cascade depicted in Figure 1 was investigated with the synthesized polymer system by preliminary gelation experiments. This cascade comprises photodeprotection and simultaneous thiol-ene click coupling to result in network formation.

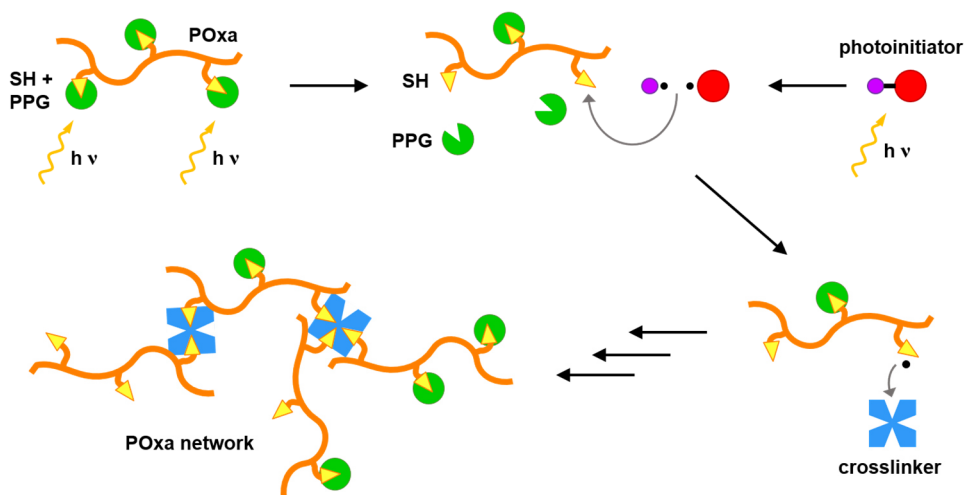


Figure 1. Schematic strategy of the tandem network formation by concurrent photodeprotection and thiol-ene click crosslinking ('POxa': poly(2-oxazoline), 'PPG': photoremovable protecting group, 'SH': thiol group).

Materials and Methods

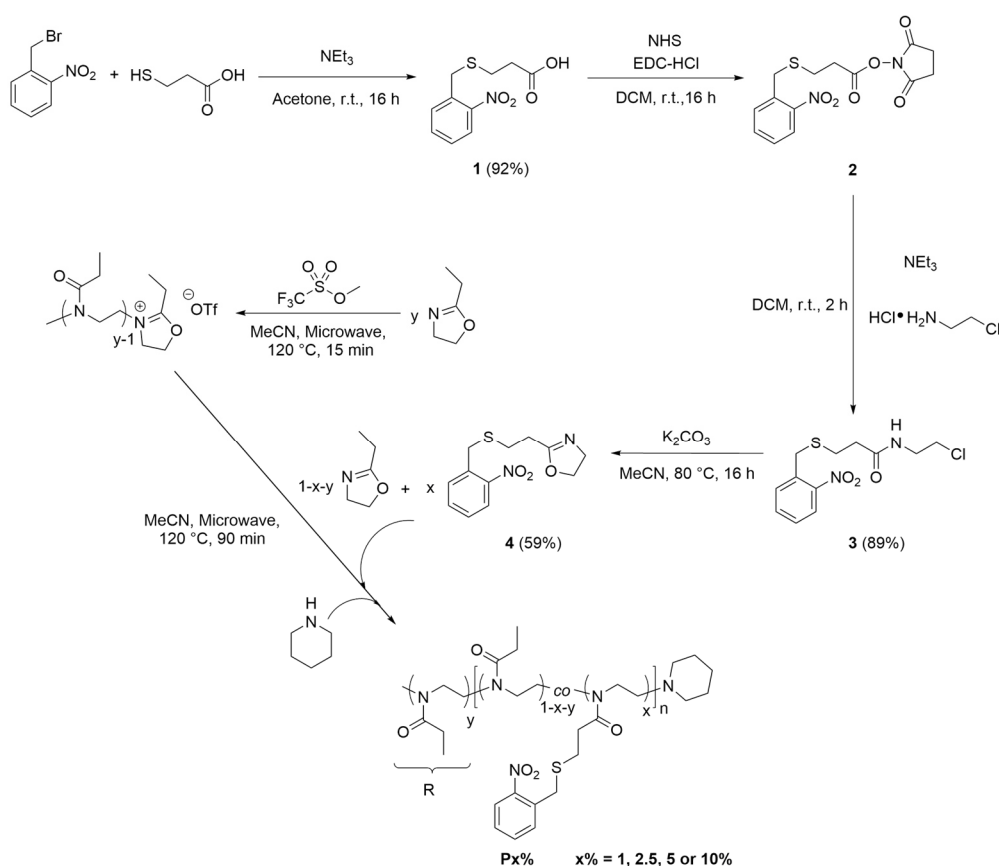
Experimental details about the synthetic procedures and characterization methods are provided in the Supporting Information.

Results and Discussion

Monomer synthesis:

The novel monomer 2-[2-[(2-nitrobenzyl) thio]ethyl]-4,5-dihydrooxazole (**4**), abbreviated NbMEtOxa, was prepared in four steps partially based on concepts from the literature (see Scheme 1) [45]. For the synthesis of 3-[(2-nitrobenzyl)thio] propanoic acid (**1**), the thiol group of mercaptopropionic acid was protected with *o*-nitrobenzyl bromide, according to reaction procedures published by Hensarling et al. and Pauloehrl et al. [46,47]. In the subsequent step, the carboxyl group was converted to the *N*-hydroxysuccinimide ester **2** and directly coupled with 2-chloroethylamine to yield amide **3**. Ring closure to the 2-oxazoline **4** was accomplished with potassium carbonate at elevated temperatures in acetonitrile. The overall yield of the 4-step synthesis route amounted to 47% and corresponding ¹H and ¹³C NMR spectra (see ESI, Figures S1 to S6) confirmed the presence of the title compound **4**.

5 Results and Discussion



Scheme 1. Synthesis route for 2-{2-[(2-nitrobenzyl)thio]ethyl}-4,5-dihydrooxazole (NbMEtOxa) and the corresponding copolymerization using 2-ethyl-2-oxazoline (EtOxa) as comonomer. The label R in the polymer structure denotes the EtOxa-homoblock of the initiator species with degree of polymerization y .

Polymer synthesis:

Copolymerization of NbMEtOxa with other 2-oxazolines allows to incorporate properties of the respective comonomers into a single polymer architecture. The copolymer composition can be conveniently controlled by this approach via the comonomer mixing ratio in the reaction feed. In particular, for copolymers based on 2-alkyl-2-oxazolines, the thermoresponsiveness in aqueous solution can be controlled by the types of alkyl groups and their combinations [8]. In our study, we employed commercially available EtOxa as a comonomer, which has been extensively used by many groups. After deprotection of the NbMEtOxa repeat unit, the free thiol groups were exploited for crosslinking of the copolymer, with the crosslinking density being tailored by the comonomer ratio of NbMEtOxa and EtOxa. Several polymerization attempts of the novel NbMEtOxa indicated problems with the common initiator methyl trifluoromethanesulfonate (MeOTf), as no reasonable amounts of polymer could be obtained. A potential impediment may be S-methylation by MeOTf, analogous to issues reported by Cesana and coworkers for the copolymerization of amino-functionalized oxazolines [33]. Various literature reports suggest a strategy with a preinitiator species for functionalized 2-oxazolines to circumvent such side reactions. There, a preceding reaction of an appropriate 2-alkyl-2-oxazoline and methylation agent (e.g. MeOTf or methyl tosylate) generates an initiator species for the subsequent polymerization of the problematic oxazoline monomers [32,33,35,48]. Based on these reports, we found that oligo(2-ethyl-2-oxazoline)-2-ethyl-2-oxazolinium trifluoromethanesulfonate (EtOxaOTf, formed from EtOxa and MeOTf) allowed successful copolymerization of EtOxa and NbMEtOxa. The copolymers with different NbMEtOxa content (**P1%**, **P2.5%**, **P5%**, **P10%**) were characterized by ^1H NMR

spectroscopy, gel permeation chromatography (GPC), and UV/Vis spectroscopy. Integration of both types of monomers into the same polymer backbone is corroborated by their respective proton signals in the ^1H NMR spectrum, as exemplarily shown for **P10%** in Figure 2A. The relative ratio of 8.5 mol% for the NbMEtOxa repeat units in the polymer could be determined by comparing the integral of signal **a** ($\delta = 3.02$ ppm) with that of signals **f** ($\delta = 7.41\text{--}7.93$ ppm), which is in good agreement with the monomer feed of 10 mol%. The molar mass at peak maximum (M_p) of the copolymers, as determined by GPC (see ESI, Figure S14), matches for the low NbMEtOxa content with the target molar mass of 15 kg mol^{-1} , but decreases with higher comonomer content (M_p for **P1%**: 16.1 kg mol^{-1} ; **P2.5%**: 13.7 kg mol^{-1} ; **P5%**: 8.0 kg mol^{-1} ; **P10%**: 5.6 kg mol^{-1}). For an ideal Gaussian curve, \bar{M}_n corresponds to M_p , but due to the broader molar mass distributions and the presence of several polymer species \bar{M}_n is not well defined and thus we provide M_p for the maximum of the GPC trace. Molar mass distributions ($\mathcal{D} = 1.3\text{--}3.2$) were broader than expected for CROP of 2-oxazolines (\mathcal{D} typically around 1.2). These GPC traces show several local maxima that indicate the presence of multiple species. In addition, the UV detector signal deviates significantly from the RI detector signal. The aromatic protecting group of NbMEtOxa is the only functionality that can contribute to a UV absorption at the specific detector wavelength ($\lambda = 280$ nm for DMAc), while the EtOxa repeat unit possesses no such UV absorption. A deviation between the shapes of the UV and RI detector signal traces reflects a compositional drift for different molar masses. In order to quantify the absolute number of incorporated comonomer units, the corresponding response factors of each repeat unit type and both detectors must be known [49]. The response factor is defined by the specific detector sensitivity for a given type of repeat unit. For the copolymers discussed in this paper, no response factors can be determined, neither for the EtOxa repeat unit, as it does not show any UV absorption, nor for the NbMEtOxa repeat unit, as it does not form defined homopolymers. Nevertheless, a qualitative analysis of the compositional drift is possible by the following procedure to generate a UV-RI difference plot: (a) first the UV and RI traces are normalized by dividing all signal intensity values with the one at the respective trace maxima and (b) then the normalized RI trace is subtracted from the normalized UV trace. Even though this normalization procedure does remove information on the absolute number of repeat units in the polymer backbone and thus prevents quantitative analysis, this internal calibration yet allows qualitative comparison of the compositional drift between different samples.

5 Results and Discussion

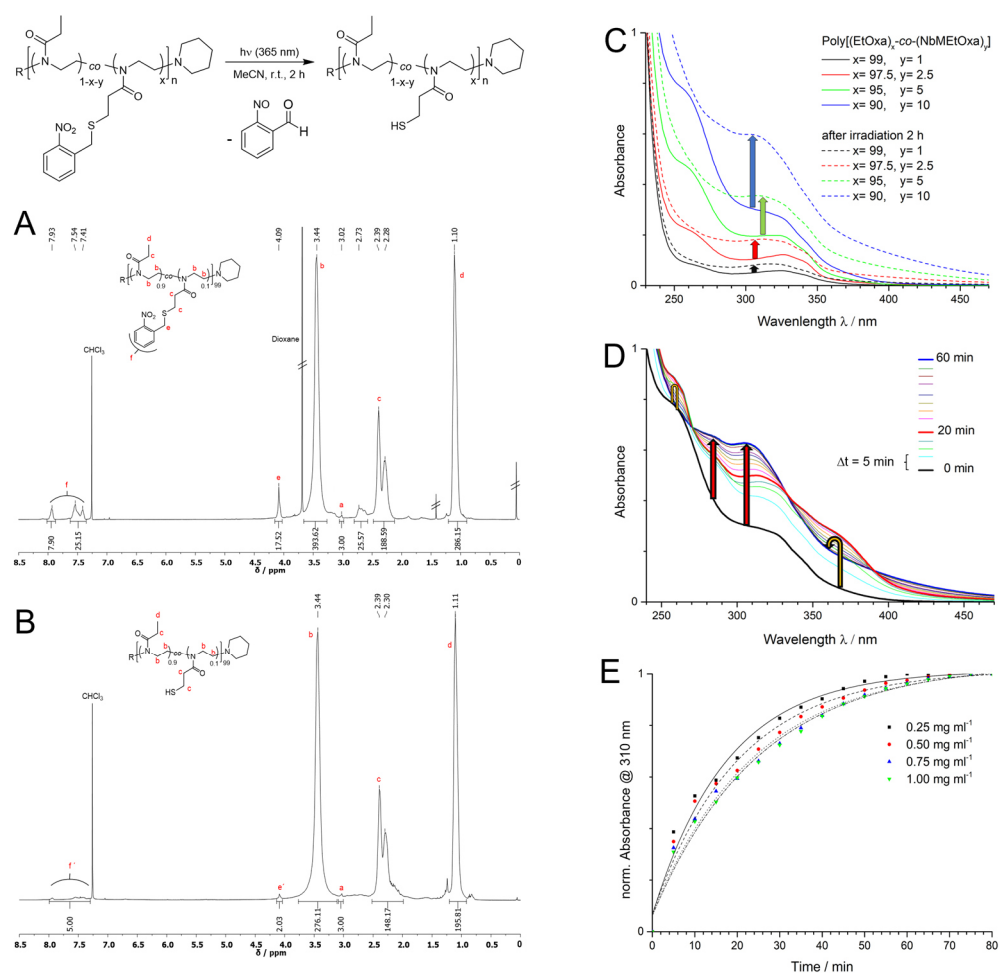


Figure 2. Deprotection reaction scheme for copolymer **P10%** and the corresponding ¹H NMR spectra recorded before (A) and after irradiation with UV light ($\lambda = 365$ nm) (B). R = EtOxa-homoblock of initiator species, signals **a** and **a'** correspond to the terminal methyl group of the initiator block R (the corresponding integrals are normalized to three protons), signals **e'** and **f'** in (B) indicate residual PPGs after the deprotection step. These signals were used to calculate the degree of polymerization. In graph (C), UV/Vis spectra of polymers containing different amounts of protected thiol moieties in acetonitrile solution ($c = 0.25$ mg ml⁻¹) are depicted. Spectrum (D) shows the time-dependent absorbance change during deprotection of **P10%**. Deprotection kinetics (E) are shown for different polymer concentrations. The absorbance was measured at its maximum for *o*-nitrosobenzaldehyde at $\lambda_{\max} = 310$ nm. The dashed lines are drawn to guide the eye. The arrows indicate the change in absorbance with increasing time.

For the example of a perfectly random copolymer with fixed comonomer ratio, the proportionality between the UV and RI detector traces is independent of the degree of polymerization, as the overall composition is identical for every chain length. As consequence, the UV-RI difference plot would result in a straight line at zero value. In the case of a polymer composed of non-UV-active monomers, this procedure would yield the inverse of the normalized RI trace with -1 at minimum. In contrast, if the copolymer composition of UV-absorbing and non-UV-active comonomers varies for different chain lengths, non-zero values are expected in such a UV-RI difference plot. Positive values in the UV-RI difference plot indicate polymer chains containing higher amounts of UV-absorbing units, while negative values represent such with higher content of non-UV-active comonomer in reference to the chain composition at the elution volume, where the normalized intensity of the UV trace equals that of the RI trace (intersection of both curves).

In our polymers, the significant deviations from the zero-line (abscissa) imply that the ratio between the UV-absorbing NbMEtOxa-related repeat units and the non-UV-active EtOxa repeat units is not uniform for all polymer chain lengths (see ESI, Figure S15). In essence, the UV-RI difference plots for all polymer samples (**P1%**, **P2.5%**, **P5%**, **P10%**) show a positive peak at low molar masses (short chain lengths at high elution volumes) and a negative deflection in the intermediate region, while at high molar masses (long chains at low elution volumes) the amount of UV-absorber seems to increase again. The data suggest the coexistence of three different polymer architectures:

- Low molar mass polymers (fraction 1) with high NbMEtOxa content that can be removed by deprotection (see discussion on photodeprotection further below),
- polymer chains (fraction 2) consisting of high EtOxa and low NbMEtOxa content,
- and high molar mass species (fraction 3) with UV-active groups.

The low molar mass polymers (fraction 1) with high content of UV-active species may be explained by a tendency for early chain termination of NbMEtOxa. This assumption is supported by the fact that the homopolymerization of NbMEtOxa solely led to oligomers even by employing the above presented two-step initiation strategy (see ESI, Table S1). In contrast, the EtOxa monomer supports extended chain growth leading to longer polymer chains with lower NbMEtOxa content (fraction 2). Furthermore, the *o*-nitrosobenzaldehyde PPGs from the NbMEtOxa repeat units in the polymer backbone may undergo side-reactions that lead to branched polymer species with high molar masses (fraction 3) and a high content of UV-active groups.

Photodeprotection:

Deprotection of the copolymers was performed in acetonitrile solution ($c = 0.25 \text{ mg ml}^{-1}$) by irradiation with UV light at a wavelength of $\lambda = 365 \text{ nm}$ and radiant exposure of up to $H_e = 24 \text{ J cm}^{-2}$ (exposure time up to 2 h). Under these conditions, photoinduced cleavage of the *o*-nitrobenzyl PPG follows the mechanism of a Norrish type II reaction, forming 2-nitrosobenzaldehyde as side product (chemical reaction depicted in Figure 2) [36,39,40]. Successful fragmentation is clearly indicated by the decrease of the *o*-nitrobenzylic ^1H NMR signal intensities at $\delta = 4.09 \text{ ppm}$ (signal **e**) and $\delta = 7.41\text{--}7.93 \text{ ppm}$ (signal **f**) in Figure 2A and B. The deprotection efficiency was determined by comparison of the signal integrals at $\delta = 4.09 \text{ ppm}$ (signals **e** and **e'**) before and after irradiation, amounting to 90% after 2 h irradiation. Similar values are reported in the literature for carboxylates, which were protected with the same PPG [40]. Delaittre and coworkers reported quantitative deprotection of *o*-nitrobenzyl-masked thiol groups in polyacrylamide RAFT copolymers after 2 h irradiation time and workup [50]. In our case, extended irradiation times beyond 2 h showed no further increase in deprotection yield, potentially due to side reactions during CROP of the incorporated NbMEtOxa units, as discussed above for the high molar mass species (fraction 3). After deprotection, the UV-RI difference curves show a substantial loss of UV-active components for the low molar mass region (see ESI, Figure S15). The GPC traces indicate a high molar mass fraction with residual UV absorbance that result from persistent UV-active moieties that cannot be removed by light (see ESI, Figure S14). These moieties may be a consequence from NbMEtOxa side-reactions that yield branched polymers, which become insensitive to UV deprotection. Furthermore, additional high molar mass species are observed in the GPC traces of the deprotected samples, which may result from oxidative coupling of the liberated thiol groups.

Comparison of the UV/Vis spectra (Figure 2C), recorded before (solid lines) and after 2 h irradiation (dashed lines), showed an absorbance increase in the range of $\lambda = 300\text{--}350 \text{ nm}$, proportional to the concentration of the liberated *o*-nitrosobenzaldehyde with two local absorption maxima at 285 nm and 310 nm [50,51]. In Figure 2D, the time-dependent change of absorbance during deprotection is exemplarily shown for **P10%** at a concentration of $c = 0.25 \text{ mg ml}^{-1}$. With progressing time, the *o*-nitrosobenzaldehyde absorbance in the range of $\lambda = 270\text{--}350 \text{ nm}$ steadily increases, as indicated by the red arrows. Interestingly, two additional temporary absorbance maxima around $\lambda = 265$ and 350 nm appear during the first 20 minutes of irradiation and decrease again (indicated by the bent yellow arrows), which may be attributed to reactive intermediates [40,51–53]. The kinetic measurements in

Figure 2E were performed using four different concentrations of **P10%**, as indicated in the figure legend, by following the absorbance of the *o*-nitrosobenzaldehyde maximum at $\lambda = 310$ nm. Independent of the polymer concentration, the UV/Vis measurements show no further change in absorbance beyond 80 minutes of irradiation, indicating maximal deprotection of the thiol moieties. The small variations (flattening) in the kinetic curves for the different polymer concentrations can be attributed to an internal filter effect caused by the released *o*-nitrosobenzaldehyde that absorbs the incident light [36,40] and therefore decreases the amount of photons triggering the photoelimination.

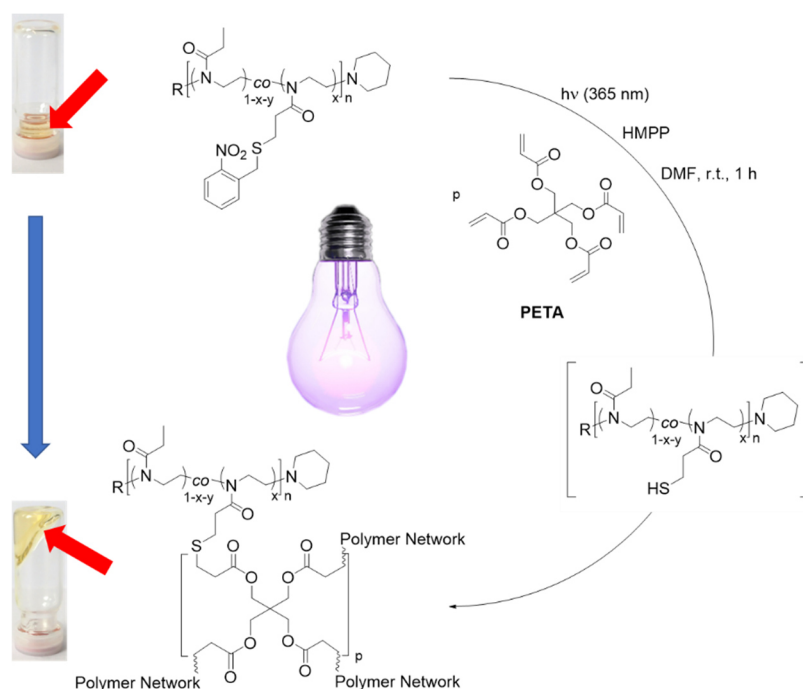


Figure 3. Tandem network formation by in situ photodeprotection and concurrent crosslinking of **P10%** with pentaerythritol tetraacrylate (PETA). The label R in the polymer structure denotes the initiator EtOxa-homoblock with degree of polymerization y . The photos (left) show the liquid-to-gel transition induced by UV irradiation of the tilted vial resulting in a rigid gel. Red arrows indicate liquid and gel, respectively.

Tandem network formation:

The free thiol groups along the polymer backbone provided by photodeprotection are a prerequisite for network formation by reaction with a separate crosslinker unit. Our proposed tandem reaction cascade employs photoactivated thiol-ene click coupling between such liberated thiol groups and vinyl moieties in the crosslinker. Specifically, pentaerythritol tetraacrylate (PETA) was used as tetrafunctional crosslinker and 2-hydroxy-2-methylpropiophenone (HMPP) as photoinitiator for radical activation. The reaction conditions reported by Ooi and coworkers were adapted to the increased molar ratio of thiol groups along the polymer backbone [54]. Crosslinking tests (Figure 3) were performed with 15 wt% polymer solutions of **P1%**, **P2.5%**, **P5%**, and **P10%** in DMF using UV light at a wavelength of $\lambda = 365$ nm and radiant exposure of up to $H_e = 24$ J cm⁻² (exposure time up to 2 h, each experiment with five replicates). Successful network formation is demonstrated in Figure 3 with a firm gel that retains its oblique shape when inverting the vial containing the mixture that was irradiated in a tilted position. Even though the initial photoexcited state during deprotection of the *o*-nitrobenzyl PPG may involve radical species [39], it was found that addition of the photoinitiator HMPP was crucial for gel formation via the thiol-ene click process. As no gel formation was observed in the absence of the photoinitiator, spontaneous thiol-Michael addition is excluded under these conditions. Neither did

irradiation of a DMF solution of photoinitiator HMPP and the tetrafunctional acrylate crosslinker PETA (ESI, Figure S22, vial 2) nor irradiation of a mixture of HMPP and P10% (ESI, Figure S22, vial 1) alone lead to gel formation. In the presence of photoinitiator and crosslinker, successful network formation was achieved for P10% with a higher NbMEtOxa content after an irradiation time of 1 h by the formation of a non-flowing gel. In contrast, for copolymers containing lower amounts of NbMEtOxa (P1%, P2.5%, P5%) no gel formation was observed, even after doubling either the irradiation time, or the photoinitiator concentration, or the polymer mass concentration. In order to preserve the positive intrinsic properties of poly(EtOxa), the NbMEtOxa content was limited to 10%, as this amount was already sufficient for crosslinking.

Conclusions

In summary, we could demonstrate a novel tandem process for the photoinduced formation of a poly(oxazoline) network involving concurrent photodeprotection of polymer-associated thiol units and their thiol-ene click coupling to a vinyl crosslinker agent. For this purpose, a synthesis route for the novel monomer NbMEtOxa with overall yield of 47% was developed. Copolymerization with EtOxa led to polymers with masked thiol functions, for which nearly quantitative photodeprotection could be achieved within 2 h at $\lambda = 365$ nm ($H_e = 24$ J cm⁻²). Successful network formation via the tandem deprotection-crosslinking route requires a minimum ratio of NbMEtOxa repeat units (in the investigated system around 10%) in the macromolecular structure.

The unique feature of this strategy lies in the concurrent activation of functional groups and induction of a crosslinking reaction both triggered by light with high spatio-temporal control. This approach circumvents potential side reactions of free thiol groups that affect polymer stability and allows storage and convenient handling of a thiol-containing polymer.

Further studies will be directed to the improvement of the gelation efficiency at lower thiol group content (other types of crosslinkers, initiators, and solvents), extension of the tandem network formation concept to responsive polymer systems, and the exploration of potential applications in materials, biomedical, and surface sciences.

Supplementary Materials: The following are available online at <http://www.mdpi.com/2073-4360/12/8/1767/s1>.

Author Contributions: Conceptualization, N.J.; Investigation, N.J. and F.D.; Project administration and funding acquisition, U.J.; Writing—original draft, N.J., F.D. and U.J.; Writing—review & editing, N.J., F.D. and U.J. All authors have read and agreed to the published version of the manuscript.

Funding: Financial support from Deutsche Forschungsgesellschaft (DFG) Application D-A-CH Lead Agency Program “Self-Assembly of DNA Dendrimers in the Bulk and at Interfaces” (JO 370/5-1) is gratefully acknowledged.

Acknowledgments: N.J. thanks the Deutsche Forschungsgesellschaft (DFG) for funding (JO 370/5-1). Max Meier, Petra Frank, and Thorben Jaik are acknowledged for helpful discussions. We thank Thomas Paululat for help with the NMR measurements.

Conflicts of Interest: The authors declare no conflict of interest.

References

1. R. Luxenhofer, Y. Han, A. Schulz, J. Tong, Z. He, A. V. Kabanov, R. Jordan Poly(2-oxazoline)s as Polymer Therapeutics. *Macromol. Rapid Commun.* **2012**, *33*, 1613–1631.
2. K. Knop, R. Hoogenboom, D. Fischer, U. S. Schubert Poly(ethylene glycol) in Drug Delivery: Pros and Cons as Well as Potential Alternatives. *Angewandte Chemie International Edition* **2010**, *49*, 6288–6308.
3. N. Adams, U. S. Schubert Poly(2-oxazolines) in biological and biomedical application contexts. *Advanced Drug Delivery Reviews* **2007**, *59*, 1504–1520.
4. T. X. Viegas, M. D. Bentley, J. M. Harris, Z. Fang, K. Yoon, B. Dizman, R. Weimer, A. Mero, G. Pasut, F. M. Veronese Polyoxazoline: Chemistry, Properties, and Applications in Drug Delivery. *Bioconjugate Chemistry* **2011**, *22*, 976–986.

5. L. Tauhardt, K. Kempe, M. Gottschaldt, U. S. Schubert Poly(2-oxazoline) functionalized surfaces: From modification to application. *Chem. Soc. Rev.* **2013**, *42*, 7998.
6. T. Lorson, M. M. Lübtow, E. Wegener, M. S. Haider, S. Borova, D. Nahm, R. Jordan, M. Sokolski-Papkov, A. V. Kabanov, R. Luxenhofer Poly(2-oxazoline)s based biomaterials: A comprehensive and critical update. *Biomaterials* **2018**, *178*, 204–280.
7. R. Hoogenboom Poly(2-oxazoline)s: Alive and Kicking. *Macromolecular Chemistry and Physics* **2007**, *208*, 18–25.
8. R. Hoogenboom Poly(2-oxazoline)s: A Polymer Class with Numerous Potential Applications. *Angewandte Chemie International Edition* **2009**, *48*, 7978–7994.
9. D. Pizzi, J. Humphries, J. P. Morrow, N. L. Fletcher, C. A. Bell, K. J. Thurecht, K. Kempe Poly(2-oxazoline) macromonomers as building blocks for functional and biocompatible polymer architectures. *European Polymer Journal* **2019**, *121*, 109258.
10. N. Ahmad, B. Colak, M. J. Gibbs, D.-W. Zhang, J. E. Gautrot, M. Watkinson, C. R. Becer, S. Krause Peptide Cross-Linked Poly(2-oxazoline) as a Sensor Material for the Detection of Proteases with a Quartz Crystal Microbalance. *Biomacromolecules* **2019**, *20*, 2506–2514.
11. Y. Chujo, Y. Yoshifuji, K. Sada, T. Saegusa A Novel Nonionic Hydrogel from 2-Methyl-2-oxazoline. *Macromolecules* **1989**, *22*, 1074–1077.
12. Y. Chujo, K. Sada, T. Saegusa Polyoxazoline Having a Coumarin Moiety as a Pendant Group. *Macromolecules* **1990**, *23*, 2693–2697.
13. Y. Chujo, K. Sada, T. Saegusa Reversible Gelation of Polyoxazoline by Means of Diels-Alder Reaction. *Macromolecules* **1990**, *23*, 2636–2641.
14. Y. Chujo, K. Sada, A. Naka, R. Nomura, T. Saegusa Synthesis and Redox Gelation of Disulfide-Modified Polyoxazoline. *Macromolecules* **1993**, *26*, 883–887.
15. A. M. Kelly, A. Hecke, B. Wirnsberger, F. Wiesbrock Synthesis of Poly(2-oxazoline)-Based Hydrogels with Tailor-Made Swelling Degrees Capable of Stimuli-Triggered Compound Release. *Macromol. Rapid Commun.* **2011**, *32*, 1815–1819.
16. M. Hartlieb, D. Pretzel, K. Kempe, C. Fritzsche, R. M. Paulus, M. Gottschaldt, U. S. Schubert Cationic poly(2-oxazoline) hydrogels for reversible DNA binding. *Soft Matter* **2013**, *9*, 4693–4704.
17. A. Gress, A. Völkel, H. Schlaad, Thio-Click Modification of Poly[2-(3-butenyl)-2-oxazoline]. *Macromolecules* **2007**, *40*, 7928–7933.
18. K. Kempe, M. Lobert, R. Hoogenboom, U. S. Schubert Synthesis and characterization of a series of diverse poly(2-oxazoline)s. *J. Polym. Sci. A Polym. Chem.* **2009**, *47*, 3829–3838.
19. K. Kempe, A. Vollrath, H. W. Schaefer, T. G. Poehlmann, C. Biskup, R. Hoogenboom, S. Hornig, U. S. Schubert Multifunctional Poly(2-oxazoline) Nanoparticles for Biological Applications. *Macromolecular Rapid Communications* **2010**, *31*, 1869–1873.
20. K. Kempe, R. Hoogenboom, M. Jaeger, U. S. Schubert Three-Fold Metal-Free Efficient (“Click”) Reactions onto a Multifunctional Poly(2-oxazoline) Designer Scaffold. *Macromolecules* **2011**, *44*, 6424–6432.
21. K. Kempe, C. Weber, K. Babiuch, M. Gottschaldt, R. Hoogenboom, U. S. Schubert Responsive Glycopoly(2-oxazoline)s: Synthesis, Cloud Point Tuning, and Lectin Binding. *Biomacromolecules* **2011**, *12*, 2591–2600.
22. T. R. Dargaville, R. Forster, B. L. Farrugia, K. Kempe, L. Voorhaar, U. S. Schubert, R. Hoogenboom Poly(2-oxazoline) Hydrogel Monoliths via Thiol-ene Coupling. *Macromolecular Rapid Communications* **2012**, *33*, 1695–1700.
23. J. Blöbbaum, I. Paulus, A.-C. Pöppler, J. Tessmar, J. Groll Influence of charged groups on the cross-linking efficiency and release of guest molecules from thiol-ene cross-linked poly(2-oxazoline) hydrogels. *Journal of Materials Chemistry B* **2019**, *7*, 1782–1794.
24. J. Liebscher, J. Teßmar, J. Groll In Situ Polymer Analogue Generation of Azlactone Functions at Poly(oxazoline)s for Peptide Conjugation. *Macromol. Chem. Phys.* **2019**, 1900500.
25. Y. Wang, M. Zheng, F. Meng, J. Zhang, R. Peng, Z. Zhong Branched Polyethylenimine Derivatives with Reductively Cleavable Periphery for Safe and Efficient In Vitro Gene Transfer. *Biomacromolecules* **2011**, *12*, 1032–1040.

26. J. C. Love, L. A. Estroff, J. K. Kriebel, R. G. Nuzzo, G. M. Whitesides Self-Assembled Monolayers of Thiolates on Metals as a Form of Nanotechnology. *Chemical Reviews* **2005**, *105*, 1103–1170.
27. P. J. Roth, C. Boyer, A. B. Lowe, T. P. Davis RAFT Polymerization and Thiol Chemistry: A Complementary Pairing for Implementing Modern Macromolecular Design. *Macromolecular Rapid Communications* **2011**, *32*, 1123–1143.
28. J. A. Yoon, J. Kamada, K. Koynov, J. Mohin, R. Nicolaÿ, Y. Zhang, A. C. Balazs, T. Kowalewski, K. Matyjaszewski Self-Healing Polymer Films Based on Thiol–Disulfide Exchange Reactions and Self-Healing Kinetics Measured Using Atomic Force Microscopy. *Macromolecules* **2012**, *45*, 142–149.
29. M. Pepels, I. Filot, B. Klumperman, H. Goossens Self-healing systems based on disulfide–thiol exchange reactions. *Polym. Chem.* **2013**, *4*, 4955.
30. M. Glassner, M. Vergaelen, R. Hoogenboom Poly(2-oxazoline)s: A comprehensive overview of polymer structures and their physical properties. *Polymer International* **2017**, DOI 10.1002/pi.5457.
31. I. L. Cartwright, D. W. Hutchinson, V. W. Armstrong The reaction between thiols and 8-azidoadenosine derivatives. *Nucleic Acids Research* **1976**, *3*, 2331–2340.
32. C. Taubmann, R. Luxenhofer, S. Cesana, R. Jordan First Aldehyde-Functionalized Poly(2-oxazoline)s for Chemoselective Ligation. *Macromol. Biosci.* **2005**, *5*, 603–612.
33. S. Cesana, J. Auernheimer, R. Jordan, H. Kessler, O. Nuyken First Poly(2-oxazoline)s with Pendant Amino Groups. *Macromol. Chem. Phys.* **2006**, *207*, 183–192.
34. M. T. Zarka, O. Nuyken, R. Weberskirch Amphiphilic Polymer Supports for the Asymmetric Hydrogenation of Amino Acid Precursors in Water. *Chemistry - A European Journal* **2003**, *9*, 3228–3234.
35. S. Cesana, A. Kurek, M. A. Baur, J. Auernheimer, O. Nuyken Polymer-Bound Thiol Groups on Poly(2-oxazoline)s. *Macromolecular Rapid Communications* **2007**, *28*, 608–615.
36. P. Klán, T. Šolomek, C. G. Bochet, A. Blanc, R. Givens, M. Rubina, V. Popik, A. Kostikov, J. Wirz, Photoremovable Protecting Groups in Chemistry and Biology: Reaction Mechanisms and Efficacy. *Chemical Reviews* **2013**, *113*, 119–191.
37. C. G. Bochet Wavelength-selective cleavage of photolabile protecting groups. *Tetrahedron Letters* **2000**, *41*, 6341–6346.
38. C. G. Bochet Orthogonal Photolysis of Protecting Groups. *Angewandte Chemie International Edition* **2001**, *40*, 2071–2073.
39. C. G. Bochet Photolabile protecting groups and linkers. *J. Chem. Soc., Perkin Trans. 1* **2002**, 125–142.
40. P. Wang Photolabile Protecting Groups: Structure and Reactivity. *Asian Journal of Organic Chemistry* **2013**, *2*, 452–464.
41. V. N. Rajasekharan Pillai Photoremoveable Protecting Groups in Organic Synthesis. *Synthesis* **1980**, *1980*, 1–26.
42. A. del Campo, D. Boos, H. W. Spiess, U. Jonas Surface Modification with Orthogonal Photosensitive Silanes for Sequential Chemical Lithography and Site-Selective Particle Deposition. *Angew. Chem. Int. Ed.* **2005**, *44*, 4707–4712.
43. A. Y. Vorobev, A. E. Moskalensky Long-wavelength photoremovable protecting groups: On the way to in vivo application. *Computational and Structural Biotechnology Journal* **2020**, *18*, 27–34.
44. A.-L. K. Hennig, D. Deodato, N. Asad, C. Herbivo, T. M. Dore Two-Photon Excitable Photoremovable Protecting Groups Based on the Quinoline Scaffold for Use in Biology. *J. Org. Chem.* **2020**, *85*, 726–744.
45. A. Levy, M. Litt Polymerization of cyclic iminoethers. V. 1,3-oxazolines with hydroxy-, acetoxy-, and carboxymethyl-alkyl groups in the 2 position and their polymers. *J. Polym. Sci. A-1 Polym. Chem.* **1968**, *6*, 1883–1894.
46. R. M. Hensarling, E. A. Hoff, A. P. LeBlanc, W. Guo, S. B. Rahane, D. L. Patton Photocaged pendent thiol polymer brush surfaces for postpolymerization modifications via thiol-click chemistry. *Journal of Polymer Science Part A: Polymer Chemistry* **2013**, *51*, 1079–1090.
47. T. Pauloehrl, G. Delaittre, M. Bastmeyer, C. Barner-Kowollik Ambient temperature polymer modification by in situ phototriggered deprotection and thiol–ene chemistry. *Polym. Chem.* **2012**, *3*, 1740–1749.
48. S. Kobayashi, S. Iijima, T. Igarashi, T. Saegusa Synthesis of a Nonionic Polymer Surfactant from Cyclic Imino Ethers by the Initiator Method. *Macromolecules* **1987**, *20*, 1729–1734.

49. Kilz, P. Copolymer Analysis by LC Methods, including 2D Chromatography. In *Encyclopedia of Chromatography*; Cazes, J., Ed.; Marcel Dekker: New York, NY, USA, 2001; pp. 195–200.
50. G. Delaittre, T. Pauloehrl, M. Bastmeyer, C. Barner-Kowollik Acrylamide-Based Copolymers Bearing Photoreleasable Thiols for Subsequent Thiol–Ene Functionalization. *Macromolecules* **2012**, *45*, 1792–1802.
51. Y. V. Il'ichev, M. A. Schwörer, J. Wirz Photochemical Reaction Mechanisms of 2-Nitrobenzyl Compounds: Methyl Ethers and Caged ATP. *Journal of the American Chemical Society* **2004**, *126*, 4581–4595.
52. Abraham. Patchornik, B. Amit, R. B. Woodward Photosensitive Protecting Groups. *Journal of the American Chemical Society* **1970**, *92*, 6333–6335.
53. J. A. Barltrop, P. J. Plant, P. Schofield Photosensitive protective groups. *Chemical Communications (London)* **1966**, 822–823.
54. H. W. Ooi, K. S. Jack, A. K. Whittaker, H. Peng Photo-initiated Thiol–Ene “Click” Hydrogels from RAFT-Synthesized Poly(N-isopropylacrylamide). *Journal of Polymer Science Part A: Polymer Chemistry* **2013**, 4626–4636.



© 2020 by the authors. Licensee MDPI, Basel, Switzerland. This article is an open access article distributed under the terms and conditions of the Creative Commons Attribution (CC BY) license (<http://creativecommons.org/licenses/by/4.0/>).

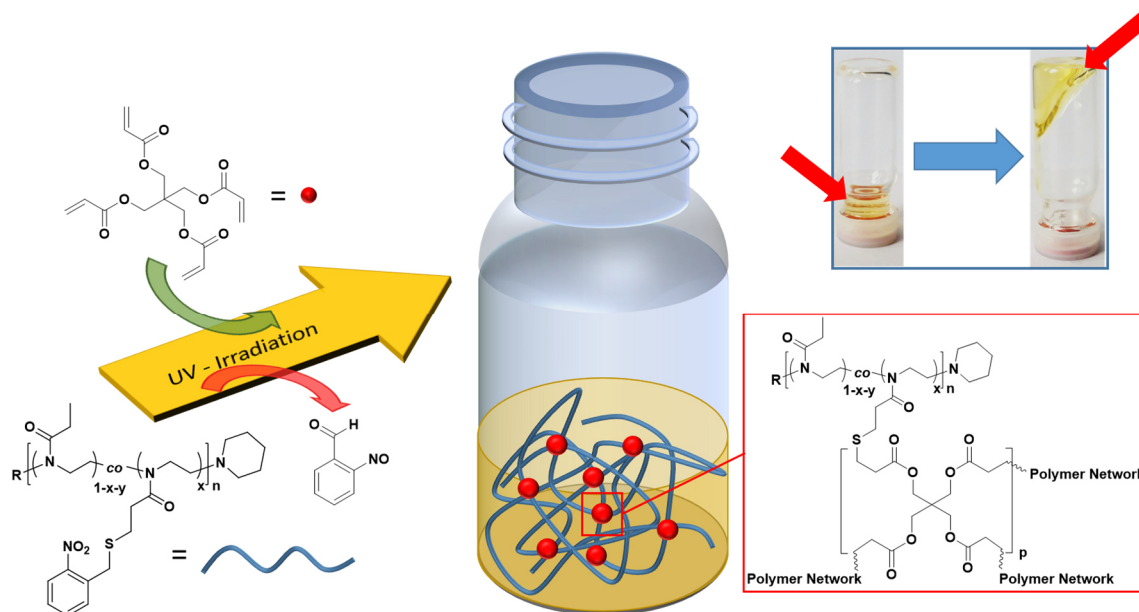
Supporting Information

Thiol-Substituted Poly(2-Oxazoline)s with Photolabile Protecting Groups - Tandem Network Formation by Light

*Niklas Jung, Fiona Diehl, Ulrich Jonas**

Macromolecular Chemistry, University of Siegen, Adolf-Reichwein Strasse 2, 57076 Siegen, Germany

*corresponding author Email address: jonas@chemie.uni-siegen.de



Schematic representation of tandem network formation by concurrent photodeprotection and thiol-ene click coupling (red arrows indicate liquid and gel, respectively).

Experimental Part

Materials

Acetone (VWR Chemicals, 99.8%) was distilled before use. Further, 2-ethyl-2-oxazoline (EtOxa, Alfa Aesar 99%), methyl trifluoromethanesulfonate (MeOTf, Alfa Aesar, 97%), triethylamine (NEt₃, ChemSolute, 99%), and 2-methyl-2-oxazoline (MeOxa, Sigma Aldrich, 98%) were dried over CaH₂ and distilled under inert gas or vacuum prior to use. For polymerizations anhydrous acetonitrile (MeCN, VWR, max. 0.001% H₂O) and for further experiments acetonitrile (MeCN, VWR Chemicals, 99+%) was used. Deuterated solvents were purchased from Deutero GmbH. 2-Chloroethylamine hydrochloride (Alfa Aesar, 98+%), dichloromethane (DCM, Fisher Scientific, 99.8%), diethyl ether (Acros Organics, 99.5%), *N,N*-dimethylformamide (DMF, Carl Roth, 99.8%), 1,4-dioxane (Carl Roth, 99.5%), ethyl acetate (EtOAc, VWR Chemicals, 99.8%), 1-ethyl-3-(3-dimethylaminopropyl)carbodiimide hydrochloride (EDC-HCl, Carl Roth, 99+%), hexanes (Fisher Scientific), hydrochloric acid (VWR Chemicals, 37%), 2-hydroxy-2-methylpropiophenone (HMPP, CIBA, 97%), *N*-hydroxysuccinimide (NHS, Alfa Aesar, 98+%), 3-mercaptopropionic acid (Alfa Aesar, 99%), magnesium sulfate hexahydrate (Carl Roth, 99+%), methanol (MeOH, Fisher Scientific, 99.8%), 2-nitrobenzyl bromide (Alfa Aesar, 98+%), pentaerythritol tetraacrylate (PETA, Sigma Aldrich), piperidine (Alfa Aesar, 99%), potassium carbonate (Bernd Kraft) and sodium hydrogencarbonate (J.T. Baker) were used as received.

Methods

The molar masses and the molar mass distribution (\bar{M}) of the synthesized poly(2-oxazoline)s were measured using a PSS system (Agilent 1260) equipped with an autosampler, RI detector and an UV-detector type Agilent VWD Series 1260. The absorption was measured at $\lambda = 280$ nm. A so-called Gram Linear M column, equipped with a 10 μm particle size precolumn was utilized at $T \approx 60$ °C. As eluent dimethylacetamide (DMAc) mixed with 1 g l⁻¹ LiBr was used and 20 μl of the polymer-samples were injected. The flow rate of the system was 1 ml min⁻¹. The calibration curve was measured using PMMA standards (PSS, Mainz). Other gel permeation chromatography (SEC) experiments were carried out on an Agilent 1200-System consisting of a degasser, an isocratic pump, an autosampler, a RI-detector, a UV-detector (Lambda 1010, Bischoff), and a SDV Linear M column. THF was used as eluent with a flow rate of 1 ml min⁻¹. Calibration was performed with polystyrene standards (PSS, Mainz). The UV/Vis measurements were performed using an Evolution 220 UV-Visible spectrophotometer and a PCCU 1 Peltier control and cooling unit from Thermo Scientific. NMR

spectroscopy was performed using a Bruker AV 400 spectrometer or a Joel ECZ 500 spectrometer. All measurements were performed at room temperature. The ^1H NMR spectra were recorded at 400 or 500 MHz and ^{13}C NMR spectra at 101 or 126 MHz. Chemical shifts (δ) are given in ppm and are referenced to the undeuterated signal of the used solvent. Polymerizations were performed using a Discover SP Microwave System equipped with an Explorer 12 Hybrid Autosampler from CEM. Crosslinking and photodeprotection experiments were carried out in a UV-crosslinker UVP-CL1000, operating at $\lambda = 365$ nm ($H_e = 12.0$ J cm $^{-2}$ per 1 h).

Synthesis of 2-{2-[(2-Nitrobenzyl)thio]ethyl}-4,5-dihydrooxazole (NbMEtOx)

A: Synthesis of 3-[(2-Nitrobenzyl)thio]propanoic acid (1)

3-Mercaptopropionic acid (1.98 g, 18.7 mmol, 1.62 ml) and anhydrous NEt_3 (1.44 g, 14.2 mmol, 1.98 ml) were stirred in anhydrous acetone (60 ml) for 30 min at 0 °C. Then 2-nitrobenzyl bromide (2.02 g, 9.4 mmol) was added in portions under nitrogen. The reaction was stirred overnight at room temperature. The formed triethylamine hydrobromide was filtered-off and the crude product was isolated via rotary evaporation. The crude product was redissolved in dichloromethane (60 ml), washed with 0.5 M HCl (4 x 20 ml) and brine (20 ml). The organic phase was dried over MgSO_4 , filtrated and the product was concentrated via rotary evaporation. The obtained yellowish, highly viscous residue was stirred with hexanes (60 ml) for 30 min to obtain a yellowish-white powder as product. The title compound was filtered-off, washed with small portions of cold hexanes and dried in vacuo. TLC: R $_f$: 0–0.32 (EtOAc : hexanes 2:1) - Yield: 2.08 g (8.62 mmol, 92%) - ^1H NMR (400 MHz, CDCl_3) δ 10.90 (s, 1H), 7.98 (dd, 1H, $J = 8.1, 1.3$ Hz), 7.57 (td, 1H, $J = 7.5, 1.3$ Hz), 7.51–7.39 (m, 2H), 4.10 (s, 2H), 2.75–2.69 (m, 2H), 2.65–2.59 (m, 2H) ppm; ^{13}C NMR (101 MHz, CDCl_3) δ 177.7, 148.9, 134.0, 133.3, 132.0, 128.5, 125.6, 34.4, 33.8, 26.7 ppm.

B: Synthesis of 2,5-Dioxopyrrolidin-1-yl 3-[(2-nitrobenzyl)thio]propanoate (2)

3-((2-Nitrobenzyl)thio)propanoic acid (2.08 g, 8.62 mmol), NEt₃ (1.43 g, 14.1 mmol, 2.0 ml) and NHS (1.62 g, 14.1 mmol) were dissolved in DCM (60 ml). To the yellowish mixture, EDC-HCl (2.70 g, 14.1 mmol) was added and the mixture was stirred at room temperature overnight. The mixture was washed with 1 M HCl (3 x 40 ml), water (3 x 40 ml) and brine (2 x 40 ml). The aqueous phases were combined and extracted with DCM (30 ml). The solvent was evaporated, and the crude product was directly used for preparation of compound **3**.

C: Synthesis of N-(2-chloroethyl)-3-[(2-nitrobenzyl)thio]propenamide (3)

Compound **2** (2.98 g, 8.8 mmol) was dissolved in DCM (30 ml) and cooled to 0 °C. To this solution 2-chloroethylamine hydrochloride (2.05 g, 17.6 mmol) and NEt₃ (1.78 g, 17.6 mmol, 2.5 ml) were added and the mixture was stirred for 45 min at 0 °C. Afterwards, the cooling bath was removed and the solution was stirred until TLC (EtOAc : hexanes 4:1, R_f: 0.65 [product **3**]) showed complete conversion (around 2 h). The mixture was diluted with DCM (30 ml) and 1 M HCl (20 ml) was added. The organic phase was further washed with 1 M HCl (2 x 20 ml), brine (20 ml) and saturated aq. NaHCO₃ (3 x 20ml) The organic phase was dried with MgSO₄, filtrated and the solvent was evaporated under reduced pressure. The product was isolated as yellow-white solid. Yield: 2.34 g (7.7 mmol, 89%) - ¹H NMR (400 MHz, CDCl₃) δ 7.96 (dd, 1H, *J* = 8.1, 1.3 Hz), 7.56 (td, 1H, *J* = 7.5, 1.3 Hz), 7.49 (dd, 1H, *J* = 7.7, 1.4 Hz), 7.45–7.39 (m, 1H), 6.09 (br.s, 1H), 4.09 (s, 2H), 3.64–3.56 (m, 4H), 2.76 (t, 2H, *J* = 7.1 Hz), 2.44 (t, 2H, *J* = 7.1 Hz) ppm. ¹³C NMR (101 MHz, CDCl₃) δ 171.3, 148.8, 134.0, 133.3, 132.2, 128.5, 125.5, 44.0, 41.4, 36.5, 33.8, 27.8 ppm.

D: Ring formation to 2-[2-[(2-Nitrobenzyl)thio]ethyl]-4,5-dihydrooxazole (NbMEtOxa) (4)

Amide **3** (2.31 g, 7.7 mmol) was dissolved in MeCN (50 ml). Anhydrous K₂CO₃ (2.74 g, 19.9

mmol) was added to the solution and stirred at 80 °C until TLC (EtOAc, R_f: 0.20 [product 4]) showed full conversion (around 16 h). After cooling the reaction suspension, the solids were decanted and then passed through a syringe filter (PTFE, 0.45 μm). Then, the solvent was evaporated, and the product was dried in vacuum overnight. The obtained yellow oil was dissolved in DCM, passed through a syringe filter (PTFE, 0.45 μm), and the solvent was removed in vacuo. Afterwards the crude product was passed through a short silica column (eluent: EtOAc) and then the solvent was evaporated. The product appeared as light brownish solid after drying in vacuum overnight. Yield: 1.22 g (4.57 mmol, 59%) - ¹H NMR (400 MHz, CDCl₃) δ 7.96 (dd, 1H, *J* = 8.1, 1.3 Hz), 7.55 (td, 1H, *J* = 7.5, 1.3 Hz), 7.48 (dd, 1H, *J* = 7.7, 1.5 Hz), 7.44–7.37 (m, 1H), 4.21 (t, 2H, *J* = 9.5 Hz), 4.09 (s, 2H), 3.81 (t, 2H, *J* = 9.5 Hz), 2.76–2.70 (m, 2H), 2.55–2.48 (m, 2H) ppm. ¹³C NMR (101 MHz, CDCl₃) δ 166.6, 148.8, 134.1, 133.2, 132.0, 128.3, 125.5, 67.5, 54.5, 33.7, 28.5, 28.2 ppm.

Synthesis of CH₃-Poly[(2-ethyl-2-Oxazoline)_{1-x}-co-(NbMEtOx)_x]-piperidine (Px%)

All polymerizations were performed according to the following procedure. As example, the polymerization using 10 mol% NbMEtOxa is described.

Briefly, MeOTf (5.61 mg, 34 μmol) and EtOxa (10.17 mg, 100 μmol) were dissolved in anhydrous MeCN (1091 mg) in a glovebox. Then the mixture was stirred under microwave irradiation for 15 min at 120 °C. Afterwards, the solution was transferred into a glovebox, in which EtOxa (384 mg, 3.88 mmol) and NbMEtOxa (103.3 mg, 0.38 mmol) were added to the vial. The final concentration was adjusted to *c* = 2 mol l⁻¹ by adding anhydrous MeCN. Then, the mixture was stirred under microwave irradiation for 90 min at 120 °C. The polymerization was stopped by adding 1 M methanolic piperidine solution (0.2 ml) and the resulting mixture was stirred at room temperature overnight. The polymer was precipitated in ice-cold diethyl ether, redissolved in 1,4-dioxane, filtrated and freeze dried. Yield: 370 mg (74%) - ¹H NMR

(500 MHz, CDCl_3) δ 8.02–7.87 (8H), 7.62–7.35 (25H), 4.15–4.03 (17H), 3.66–3.27 (401H), 3.06–2.98 (3H), 2.80–2.58 (26H), 2.48–2.12 (192H), 1.21–0.89 (292H) ppm.

Deprotection Procedure

The corresponding copolymer (100 mg, 6.7 μmol) was filled into a microwave vial and dissolved in MeCN (30 ml). The vial was sealed with a silicone cap and the mixture was purged with Ar for 15 min. Afterwards, the vial was placed in a UV crosslinking chamber with a wavelength of $\lambda = 365$ nm for 2 h ($H_e = 24$ J cm^{-2}). Then the polymer was recovered by precipitation into ice-cold diethyl ether. The precipitate was collected and thoroughly washed with diethyl ether. Finally, the product was dried in vacuum overnight.

Kinetics of Photodeprotection

Solutions of different polymer concentrations were prepared in MeCN. Each solution was added to a 1 cm square quartz cell. The cells were irradiated at $\lambda = 365$ nm in a UV crosslinking chamber ($H_e = 12$ J cm^{-2} per 1 h). After 5 min, the irradiation was stopped and the cells immediately transferred to a UV spectrometer, where the absorbance was recorded at $\lambda = 310$ nm.

Gelformation using Pentaerythritol tetraacrylate (PETA)

The polymer **P10%** containing protected thiol groups (50 mg, 3.3 μmol , 36.3 μmol thiol groups) and PETA (0.7 equiv. with respect to thiol groups) were dissolved in degassed DMF to obtain a concentration of 15 wt%. Then HMPP (2.7×10^{-3} mg, 1.64×10^{-2} μmol , 2.5 μl) was added. The vial was sealed, and remaining oxygen was removed by a freeze-pump-thaw cycle. Afterwards, the vial was placed in a UV crosslinker ($\lambda = 365$ nm, $H_e = 12$ J cm^{-2}) for 1 h.

Attempts to synthesize a NbMEtOxa Homopolymer

MeOTf and MeOxa were dissolved in anhydrous MeCN and stirred for 15 minutes in the microwave oven at 120 °C with an initial power of 140 W. Then, NbMEtOxa was added in a glovebox to the reaction mixture. The reaction vial was transferred back to the microwave oven and further stirred for 90 min (120 °C, initial power 140 W). Subsequently, the polymerization was quenched by adding water (0.2 ml) and stirred for 4 hours at room temperature. The polymer was precipitated into ice-cold diethyl ether, dissolved in 1,4-dioxane and dried via lyophilization. The individual reaction parameters are listed in the following table.

Table S1: Tabular representation of the initial weights of MeOTf, MeCN, MeOxa, NbMEtOxa, yields, and GPC analysis data for NbMEtOxa homopolymers.

No.	MeOTf /mg (μmol)	MeCN /g	MeOxa /mg (μmol)	NbMEtOxa /g (mmol)	Yield /mg (%)	\bar{M}_n /kDa	\bar{D}
1	3.1 (19)	1.2	3.8 (45)	0.20 (0.77)	- ^a	- ^a	- ^a
2	4.4 (27)	1.8	5.1 (60)	0.27 (1.0)	- ^a	- ^a	- ^a
3	2.9 (17)	2.3	6.2 (73)	0.19 (0.72)	20 (10)	1.3	2.9

^a Homopolymer could not be isolated.

NMR Spectra of NbMEtOxa and Precursors

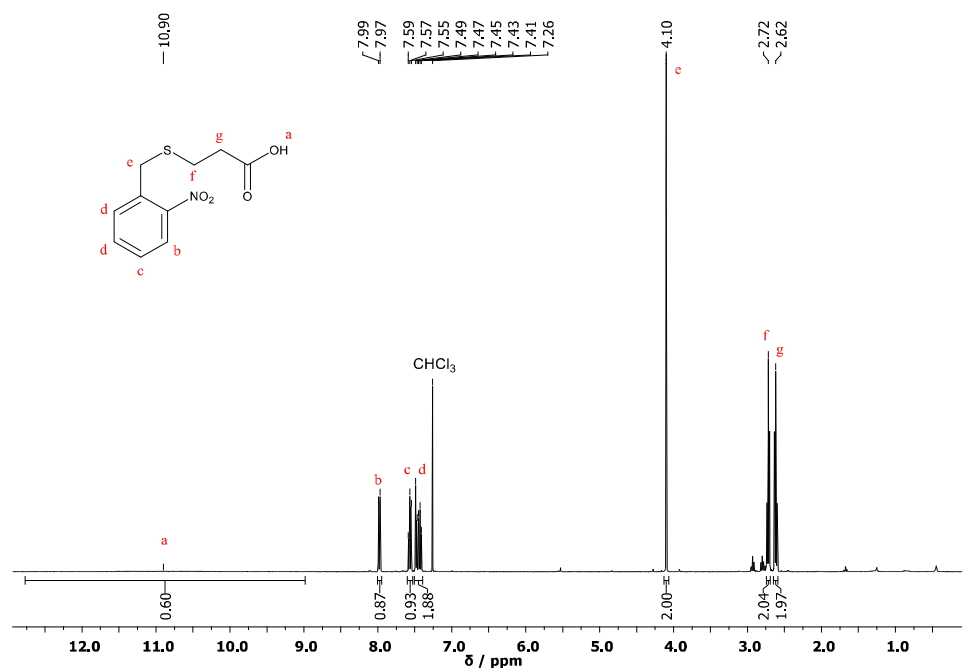


Figure S1: ¹H NMR (400 MHz) spectrum of 3-[(2-nitrobenzyl)thio]propanoic acid (1) recorded in CDCl₃.

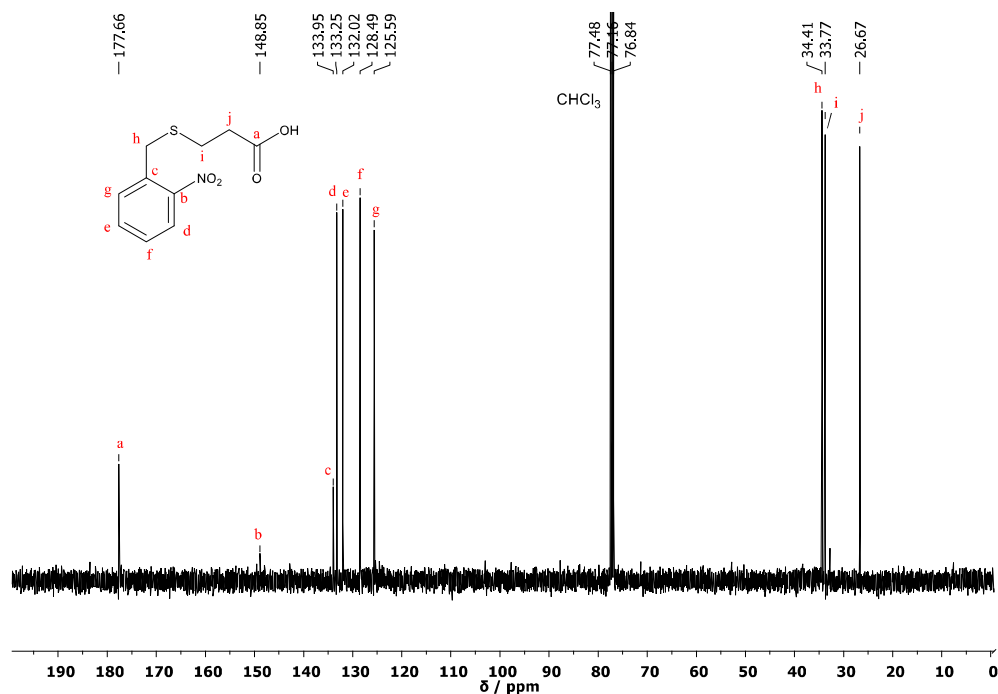


Figure S2: ¹³C NMR (101 MHz) spectrum of 3-[(2-nitrobenzyl)thio]propanoic acid (1) recorded in CDCl₃.

5 Results and Discussion

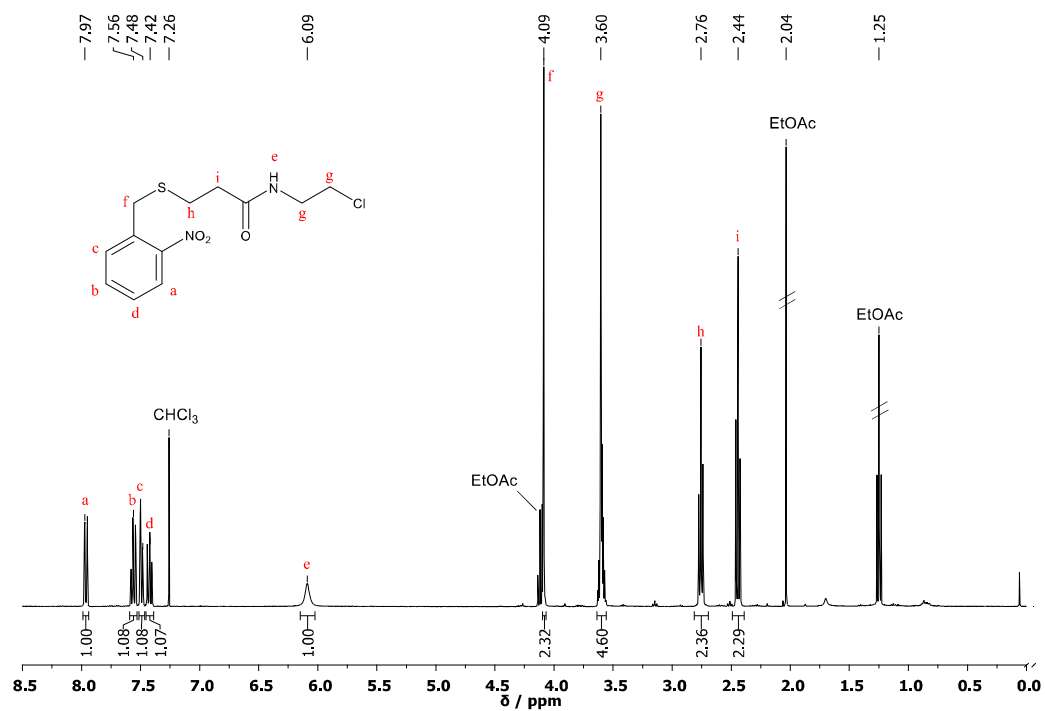


Figure S3: ^1H NMR (400 MHz) spectrum of *N*-(2-chloroethyl)-3-[(2-nitrobenzyl)thio]propanamide (**3**) recorded in CDCl_3 .

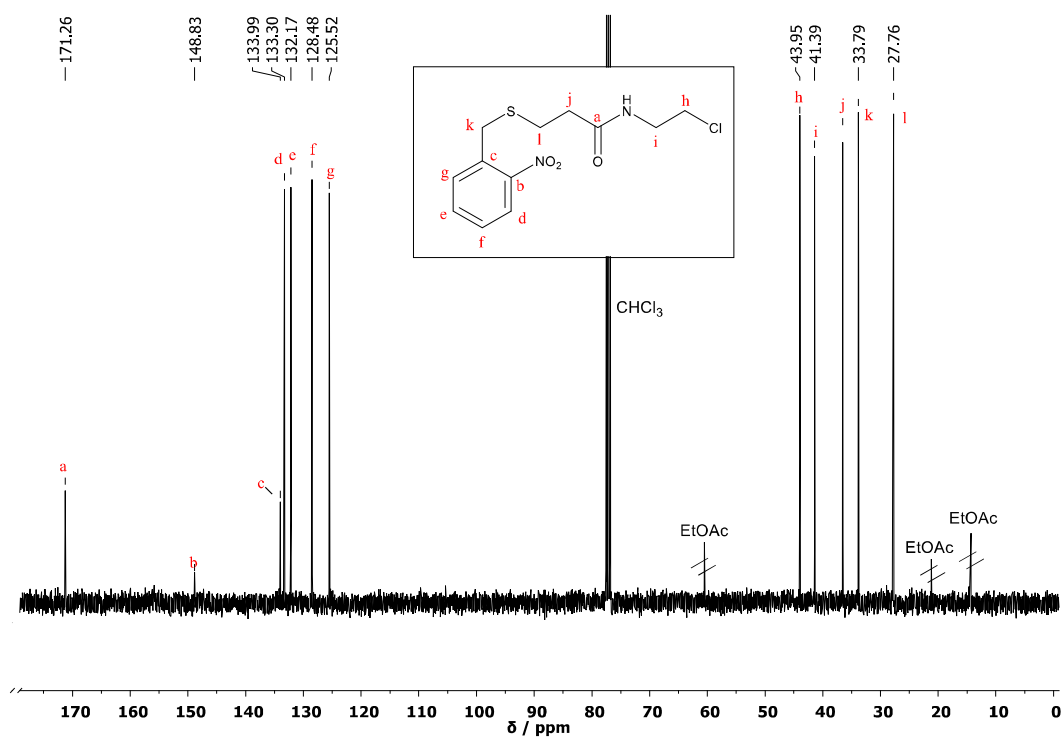


Figure S4: ^{13}C NMR (101 MHz) spectrum of *N*-(2-chloroethyl)-3-[(2-nitrobenzyl)thio]propanamide (**3**) recorded in CDCl_3 .

5 Results and Discussion

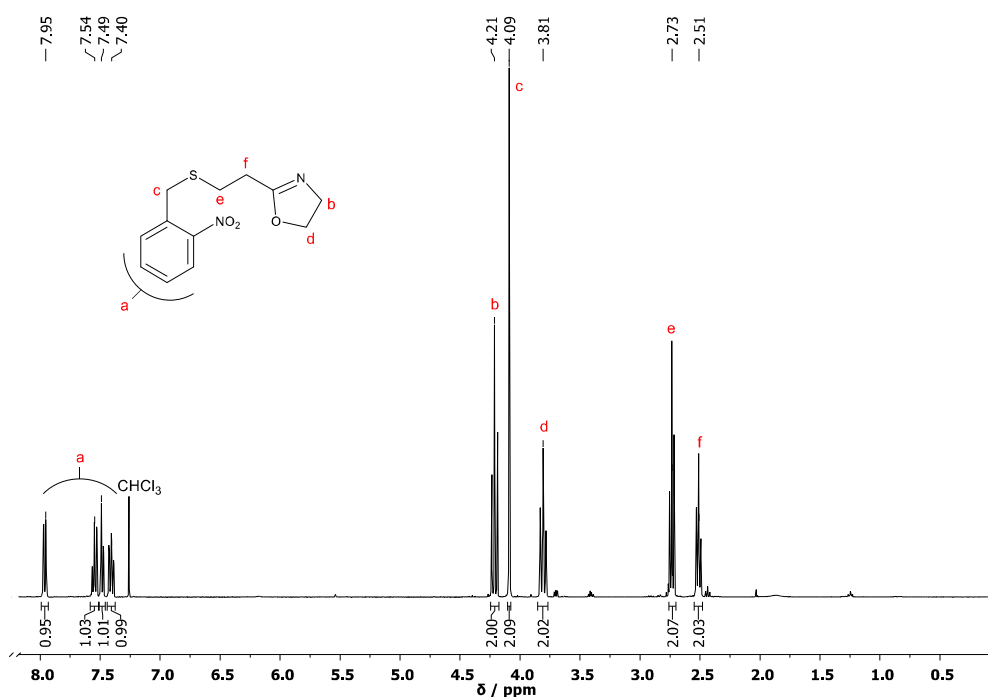


Figure S5: ¹H NMR (400 MHz) spectrum of 2-{2-[(2-nitrobenzyl)thio]ethyl}-4,5-dihydrooxazole (NbMEtOx) (**4**) recorded in CDCl₃.

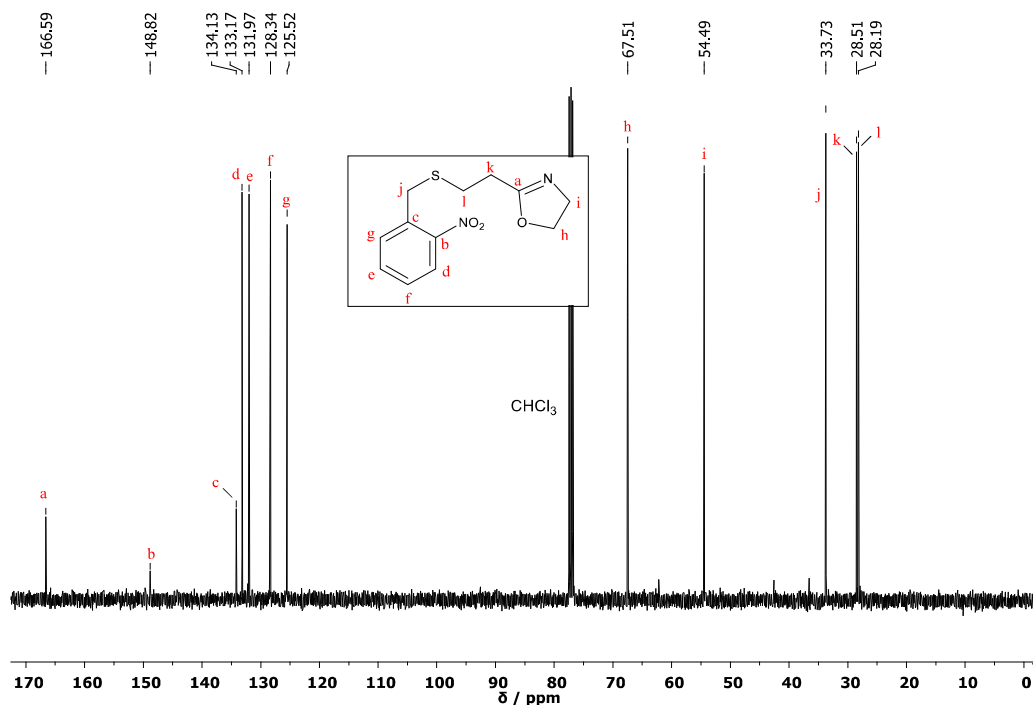
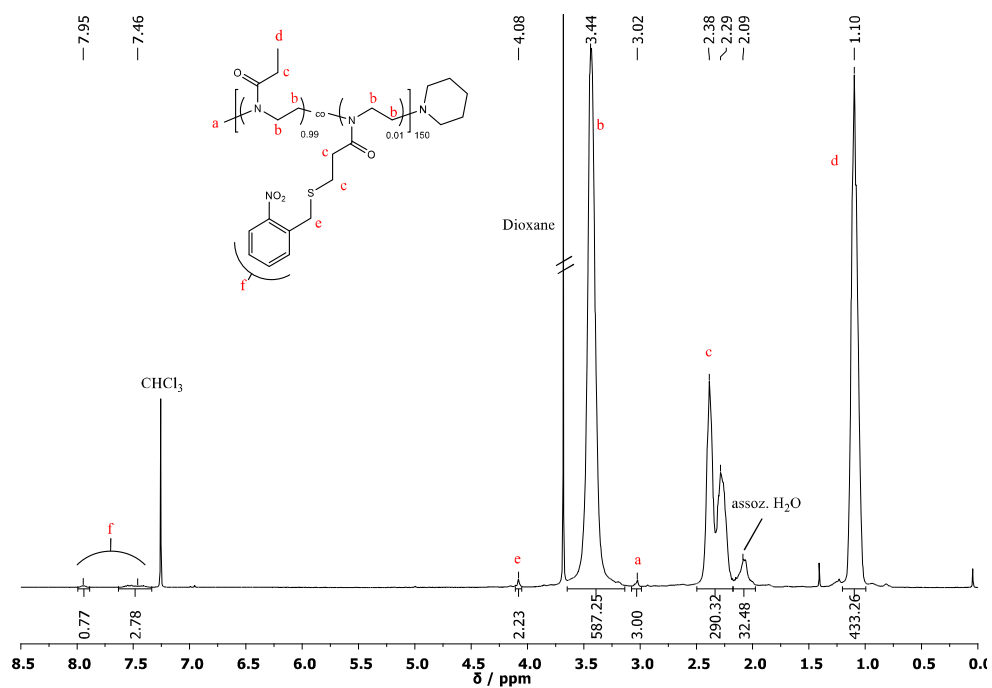
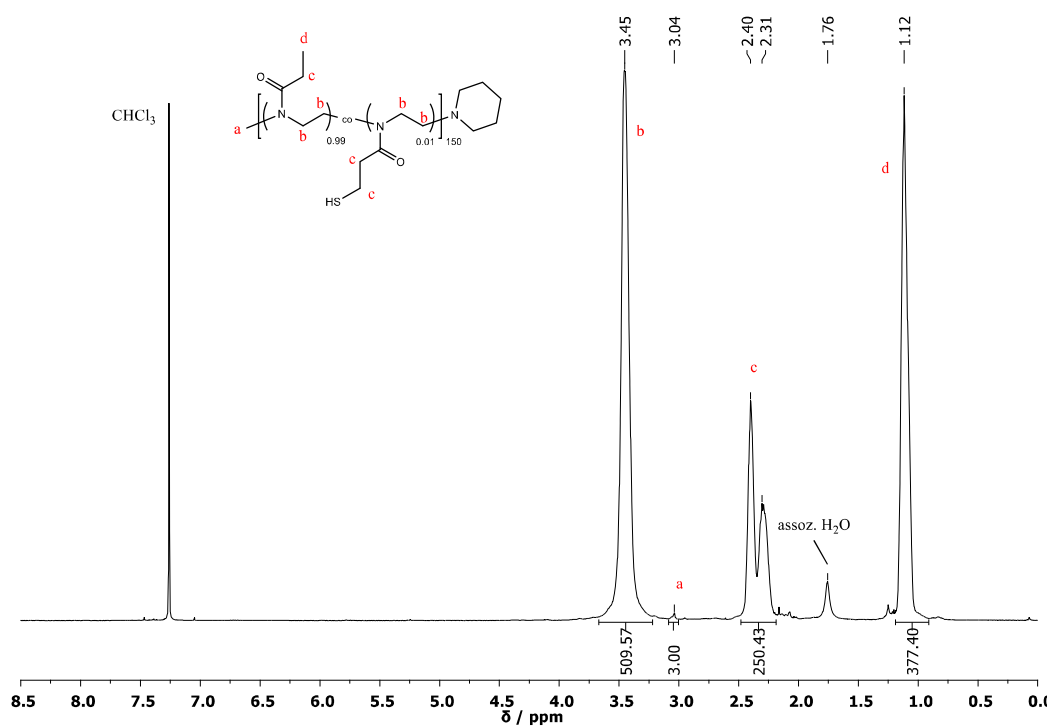


Figure S6: ¹³C NMR (101 MHz) spectrum of 2-{2-[(2-nitrobenzyl)thio]ethyl}-4,5-dihydrooxazole (NbMEtOx) (**4**) recorded in CDCl₃.

NMR Spectra of Polymers before and after Deprotection

Figure S7: ¹H NMR (500 MHz) spectrum of P1% recorded in CDCl₃.Figure S8: ¹H NMR (500 MHz) spectrum of P1% after deprotection recorded in CDCl₃.

5 Results and Discussion

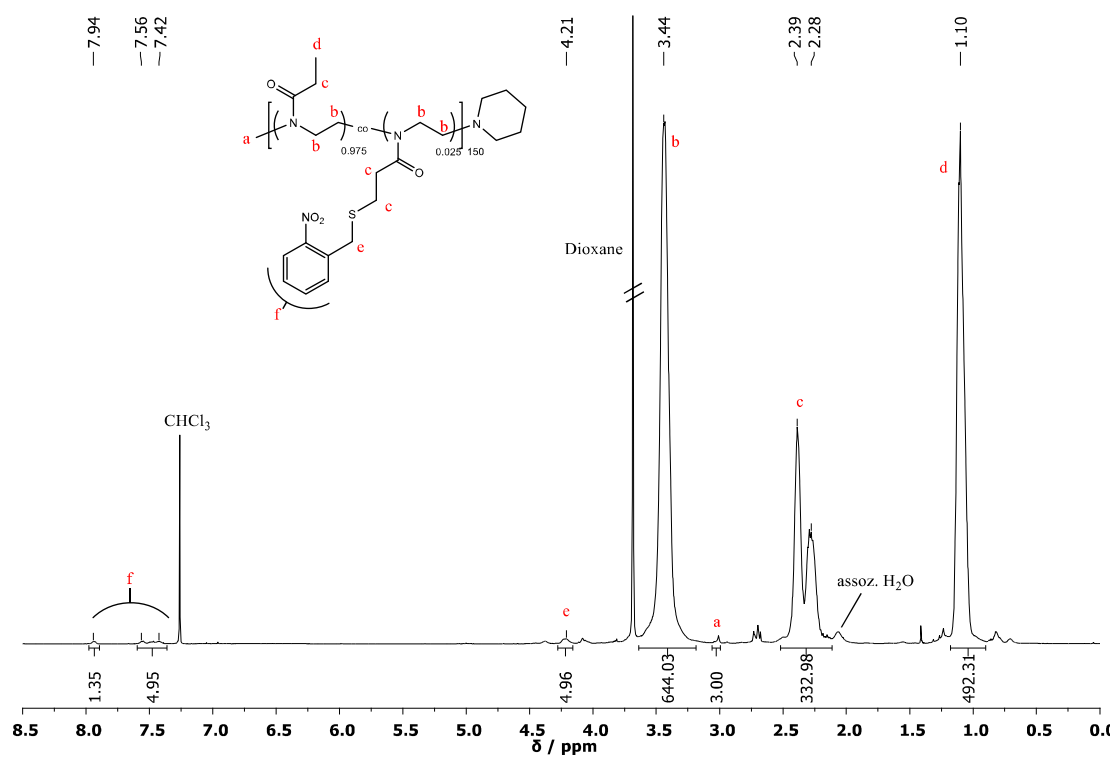


Figure S9: ^1H NMR (500 MHz) spectrum of **P2.5%** recorded in CDCl_3 .

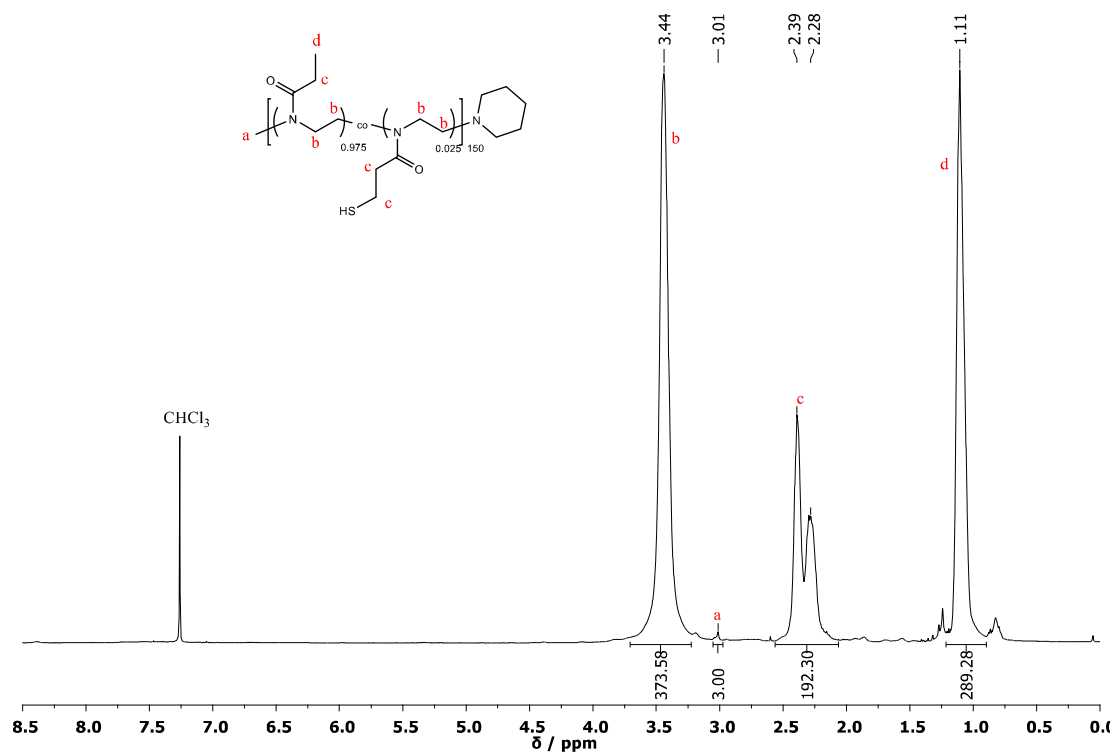


Figure S10: ^1H NMR (500 MHz) spectrum of **P2.5%** after deprotection, recorded in CDCl_3 .

5 Results and Discussion

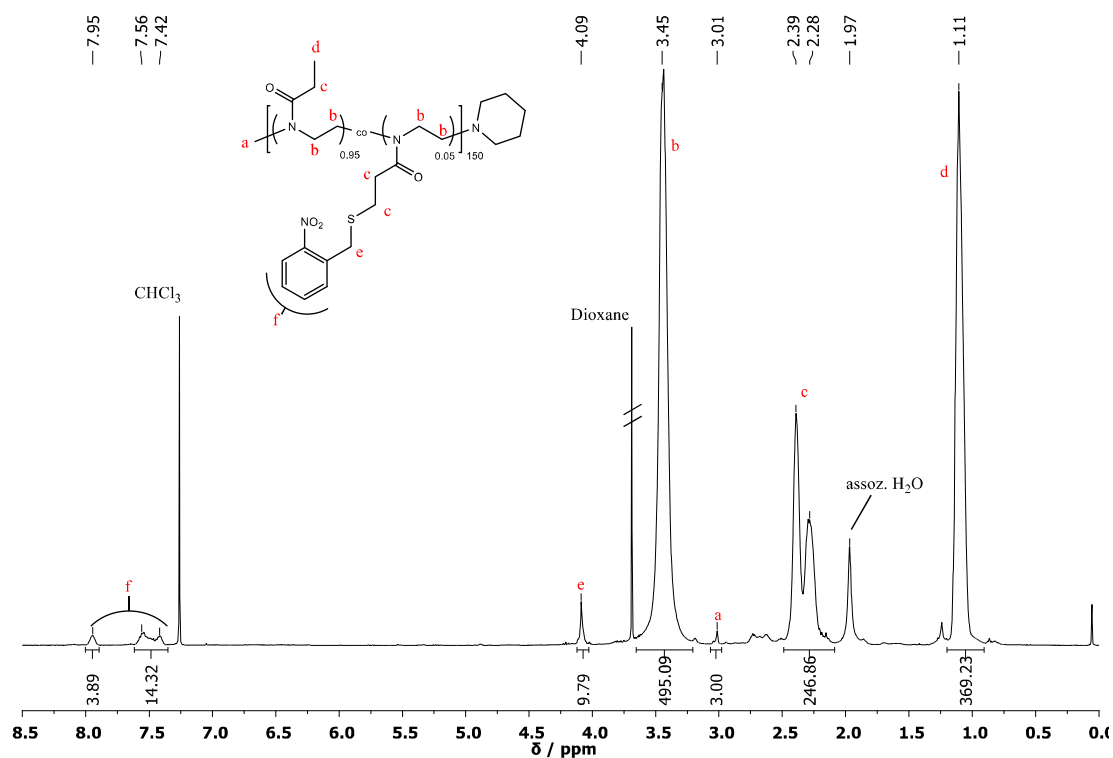


Figure S11: ^1H NMR (500 MHz) spectrum of **P5%** recorded in CDCl_3 .

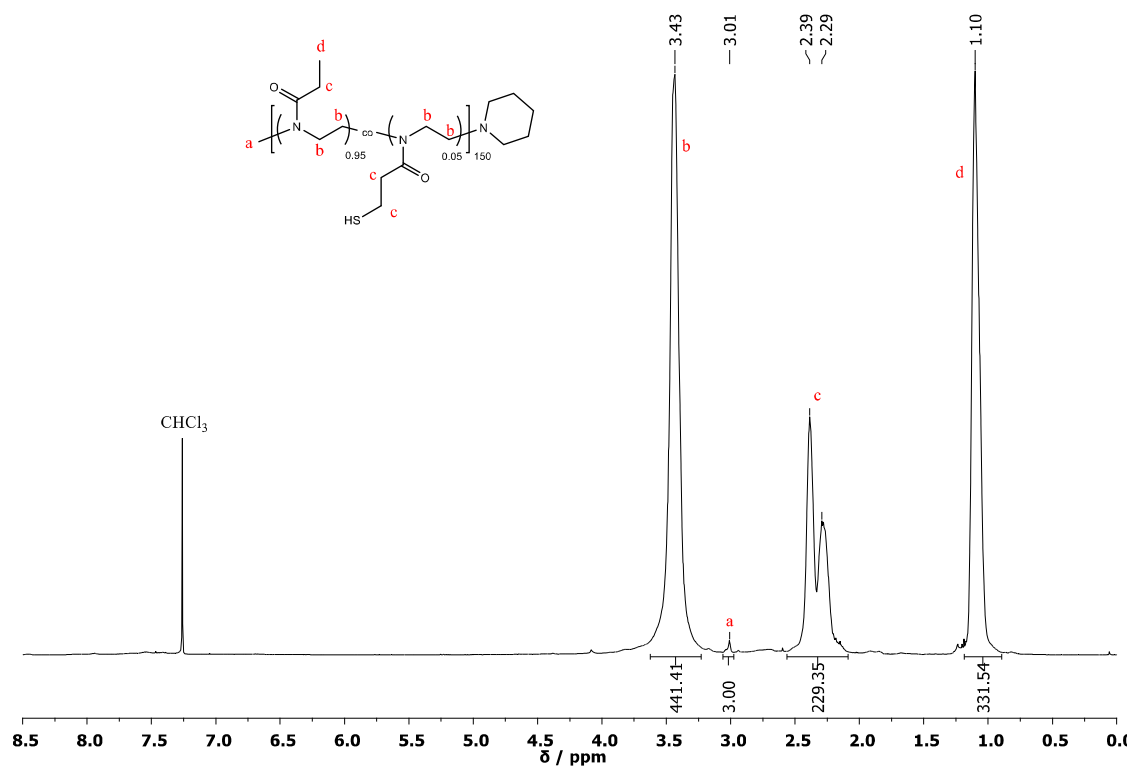


Figure S12: ^1H NMR (500 MHz) spectrum of **P5%** after deprotection, recorded in CDCl_3 .

5 Results and Discussion

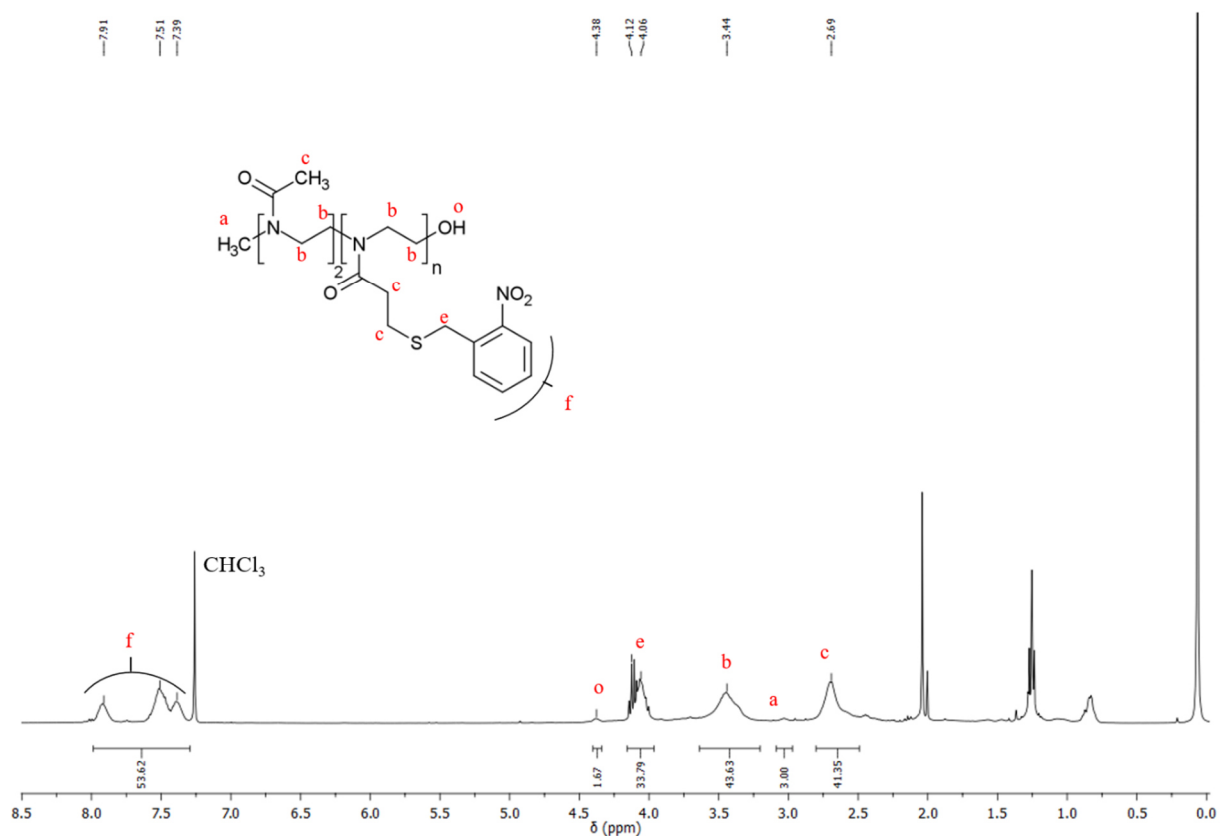


Figure S13: ¹H NMR (400 MHz) spectrum of the NbMEOxa homopolymer, recorded in CDCl₃.

GPC Data of Polymers

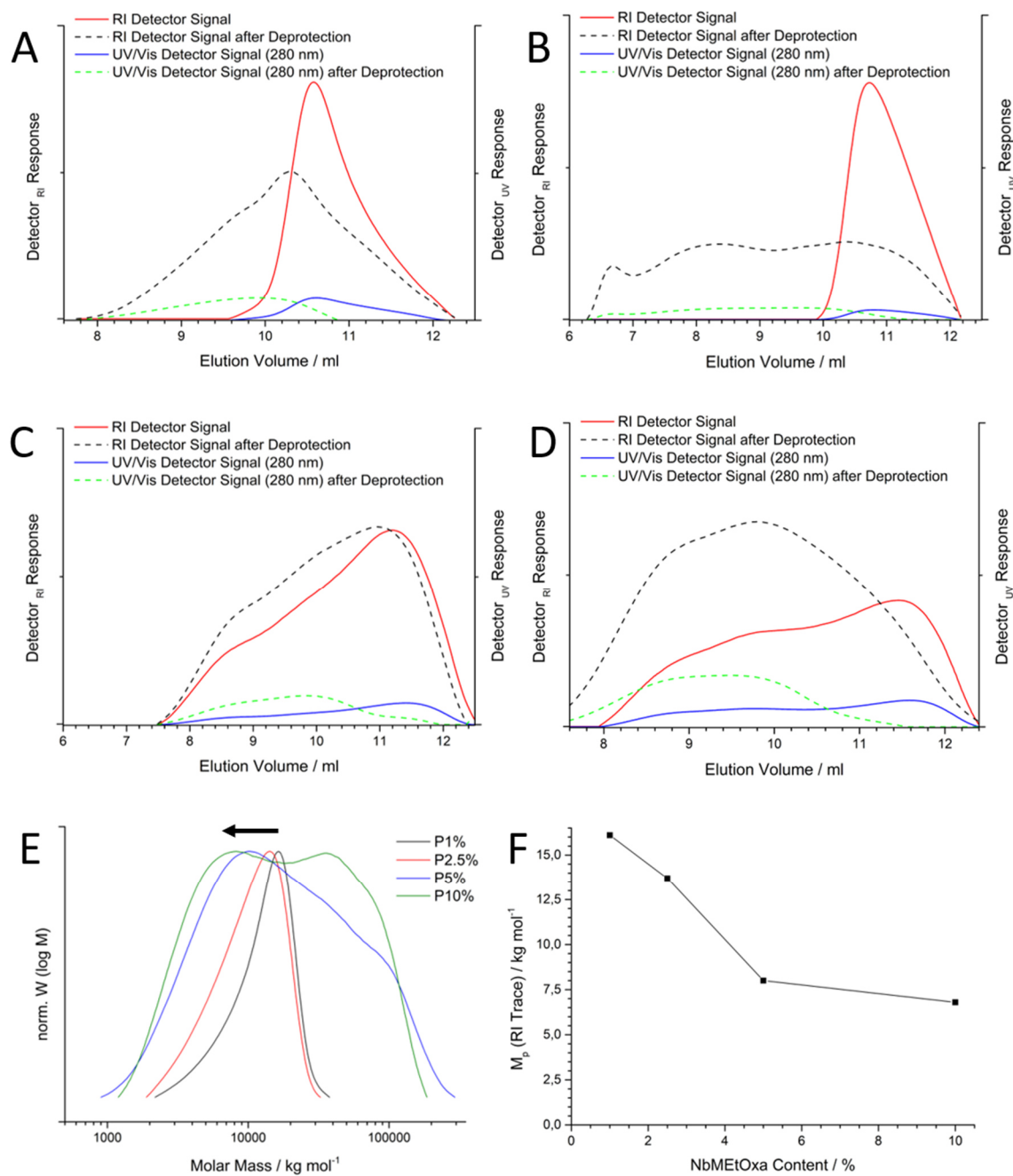


Figure S14: GPC elugrams of the different copolymers containing NbMEtOxa. The content of NbMEtOxa increased in the order from **P1%** (A), **P2.5%** (B), **P5%** (C) to **P10%** (D). DMAc containing LiBr (1 g l⁻¹) was used as eluent for each measurement. In graph (E), the RI GPC traces for all copolymers (**P1%**, **P2.5%**, **P5%**, **P10%**) are plotted to illustrate the change in molar mass at peak maximum (M_p), as indicated in panel (F).

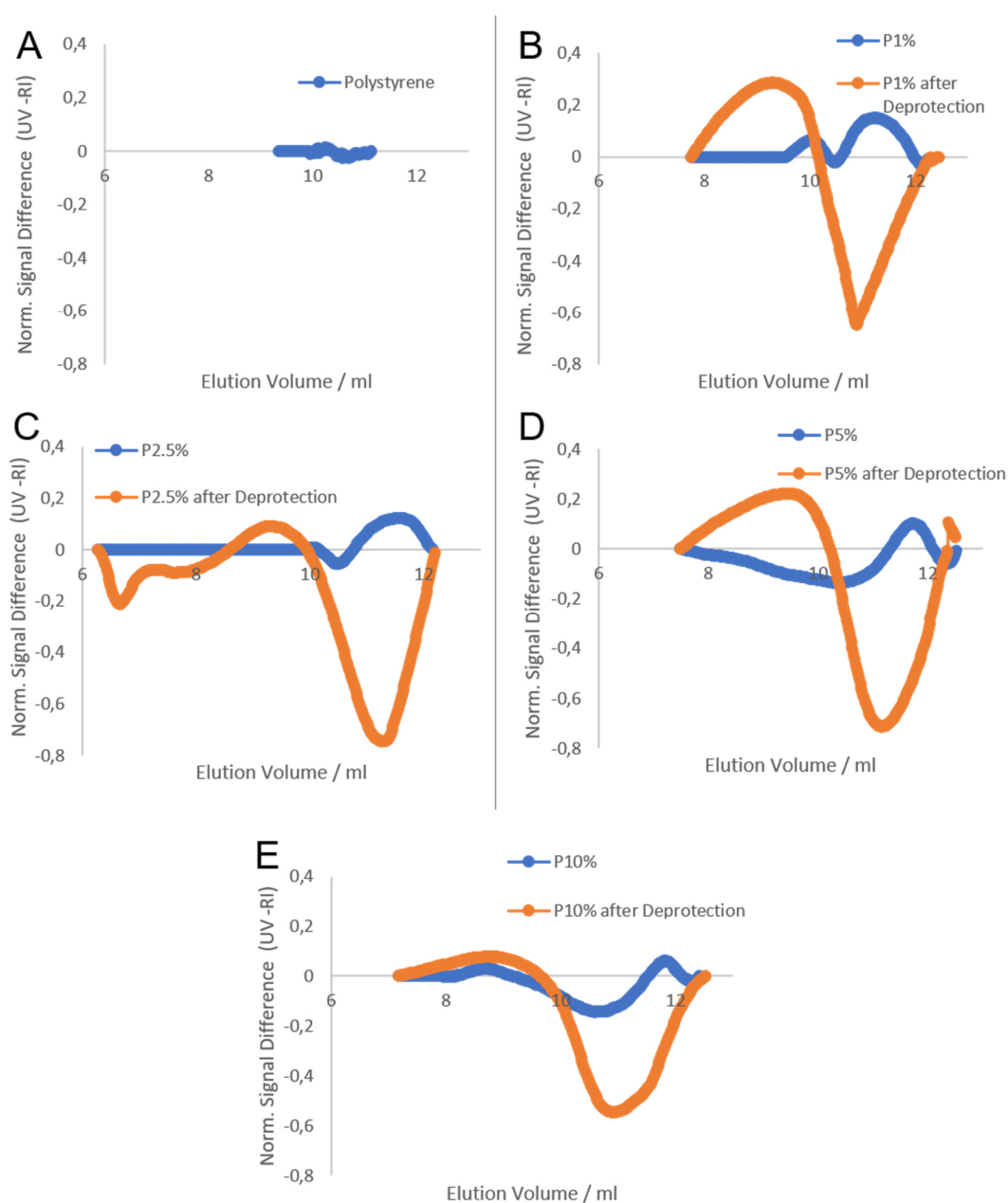


Figure S15: Qualitative analysis of the compositional drift by UV-RI difference plots for a polystyrene (PS) standard 5630 g mol^{-1} (A), **P1%** (B), **P2.5%** (C), **P5%** (D) to **P10%** (E) based on the following procedure: (1) first the UV and RI traces were normalized by dividing all signal intensity values with the one at the respective trace maxima and (2) then the normalized RI trace was subtracted from the normalized UV trace. The reference trace (A) shows a close to zero-value line as expected for the PS homopolymer. The blue lines show the copolymer systems before and the orange lines after irradiation with UV light ($\lambda = 365 \text{ nm}$, $H_e = 12 \text{ J cm}^{-2}$, 1 h).

UV/Vis Spectra of Polymers

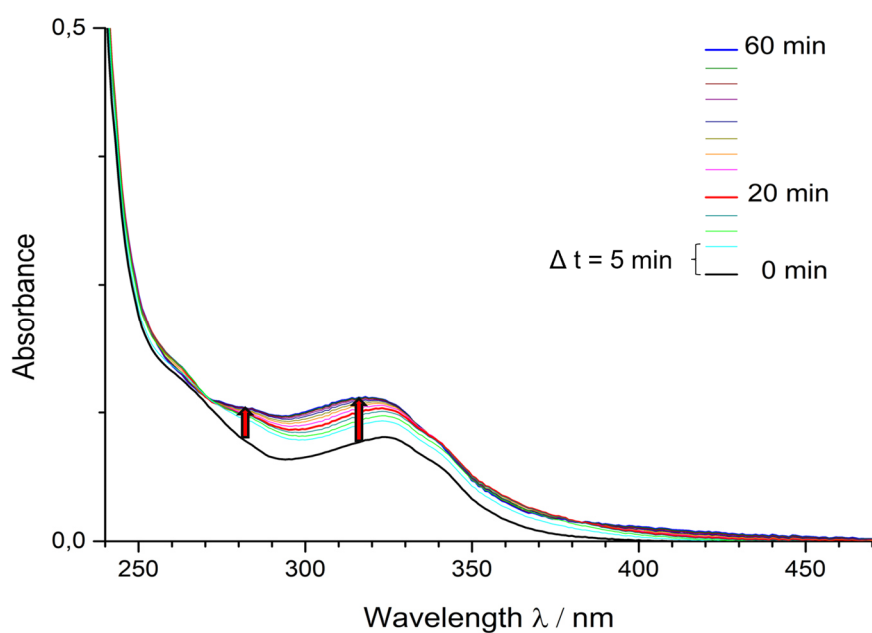


Figure S16: Time-dependent UV/Vis absorbance vs. wavelength scans of **P1%**. Red arrows indicate the change in absorbance with increasing time.

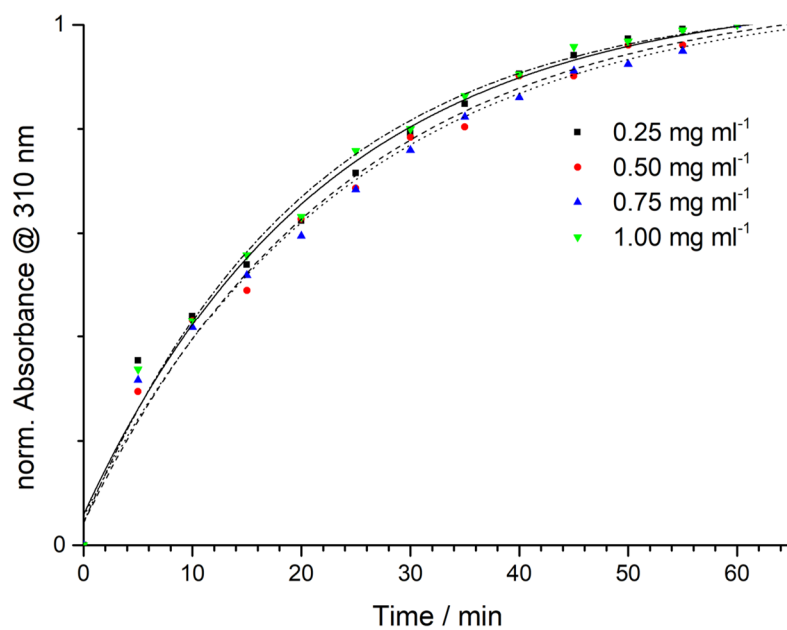


Figure S17: Deprotection kinetics of **P1%** at different concentrations. The absorbance was measured at $\lambda = 310$ nm.

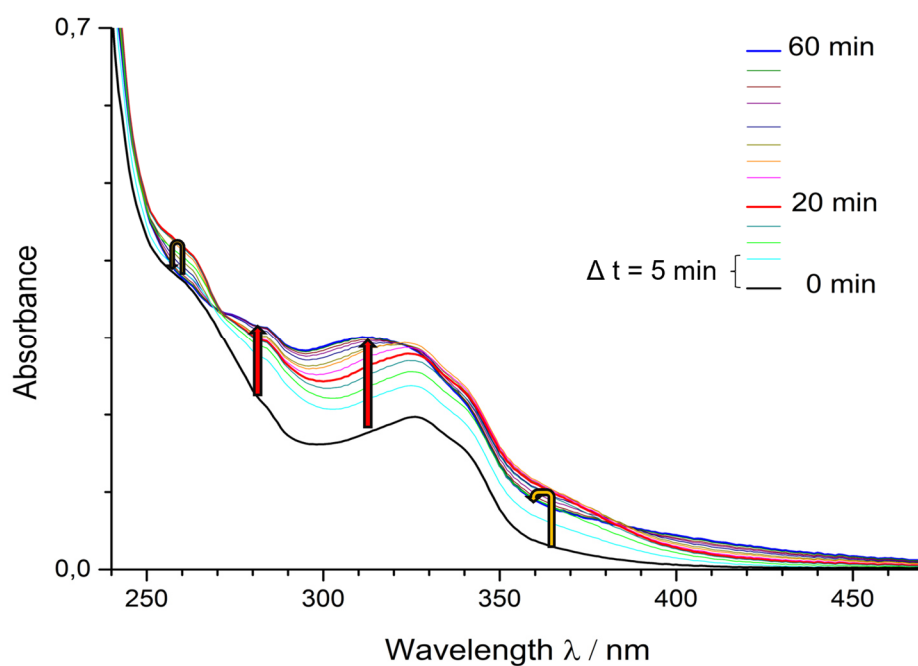


Figure S18: Time-dependent UV/Vis absorbance vs. wavelength scans of **P2.5%**. Red and yellow arrows indicate the change in absorption with increasing time.

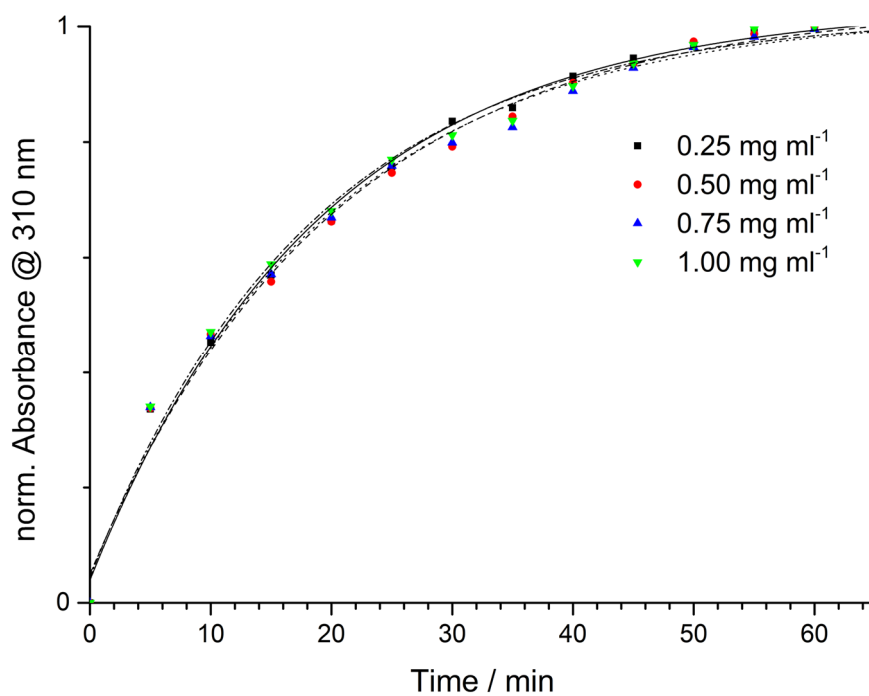


Figure S19: Deprotection kinetics of **P2.5%** at different concentrations. The absorbance was measured at $\lambda = 310$ nm.

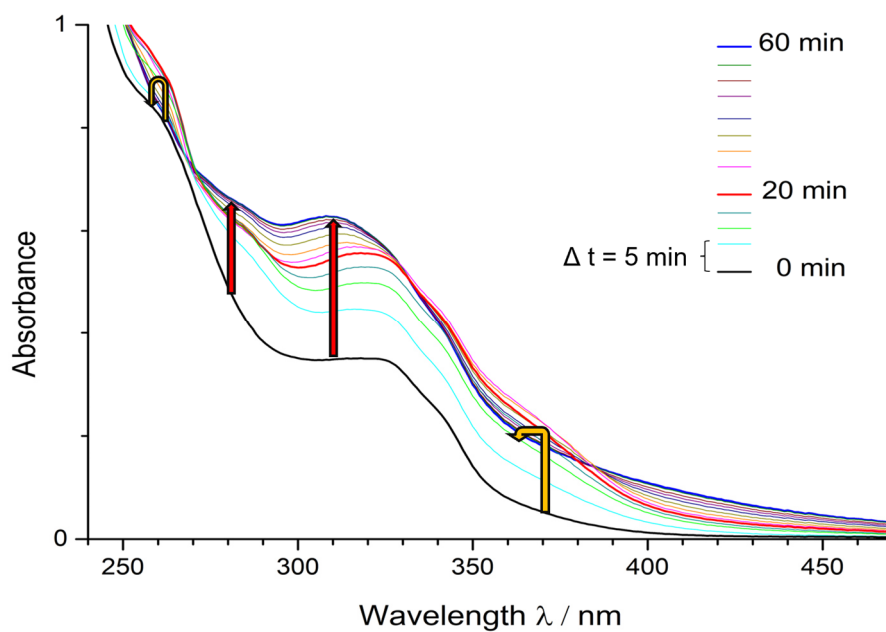


Figure S20: Time-dependent UV/Vis absorbance vs. wavelength scans of **P5%**. Red and yellow arrows indicate the change in absorption with increasing time.

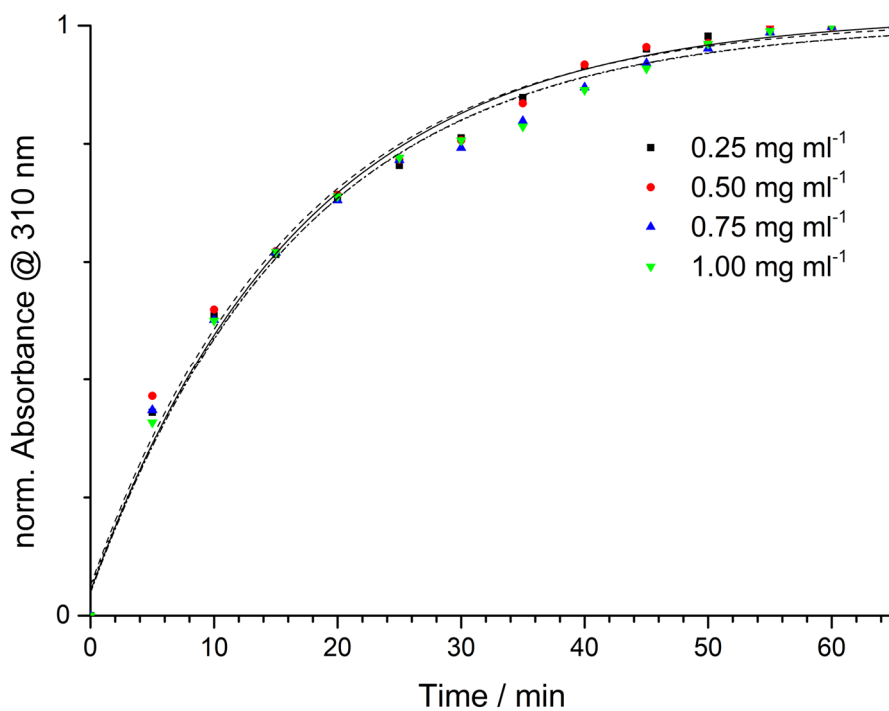


Figure S21: Deprotection kinetics of **P5%** at different concentrations. The absorbance was measured at $\lambda = 310$ nm.

Gel Formation

Table S2: Quantities of polymer, crosslinker PETA and DMF used for crosslinking tests.

Vial	Polymer	Mass Polymer / mg (content of Thiols / μmol)	Mass PETA ^a / mg (μmol , μl)	Total Volume DMF / μl
1	P10%	50 (36.3)	-	331
2 ^b	-	-	2.3 (25.4, 21.5)	350
3 ^b	P1%	50 (3.4)	0.21 (2.4, 2.0)	348
4 ^b	P2.5%	50 (10.4)	0.65 (7.3, 6.1)	344
5 ^b	P5%	50 (18.1)	1.15 (12.7, 10.7)	340
6 ^b	P10%	50 (36.3)	2.3 (25.4, 21.5)	331

^a Mass of PETA was taken from a freshly prepared stock solution in DMF ($\beta = 107 \text{ mg ml}^{-1}$).

^b HMPP was used as photoinitiator (2.7 μg , $1.64 \times 10^{-2} \mu\text{mol}$, 2.5 μl)

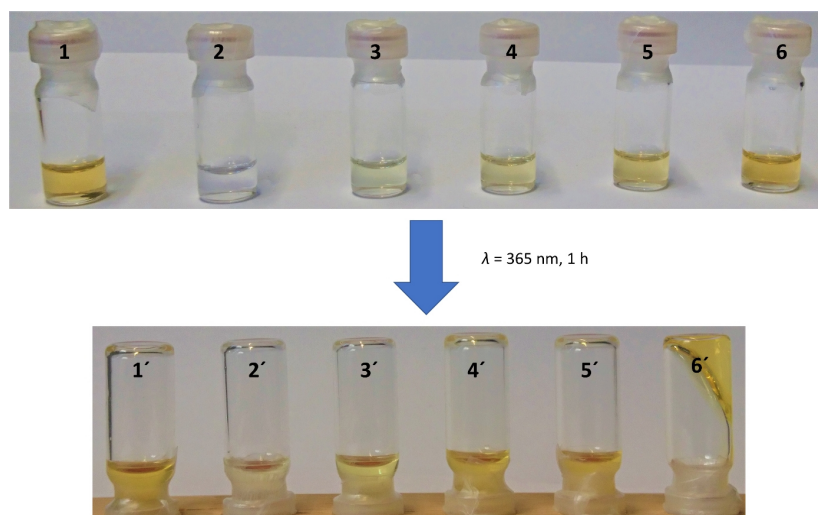


Figure S22: Images of reaction vials before (upper picture) and after irradiation (lower picture, vial numbers are marked with a prime). The vial numbers correspond to numbering in Table S2. The concentration of polymer was 15 wt% in DMF. Vials **1** and **2** were used as control. Successful network formation in vial **6'** is corroborated by the triangular shape of the rigid gel after irradiation of the tilted vial.

5.2 Synthesis and (Post-)Functionalization Strategies of *N*-Substituted Poly(acrylamide)s

In the following chapters, first the synthesis as well as the (post)functionalization of hemitelechelic, thermoresponsive PNiPAm derivatives (chapter 5.2.1) will be discussed. These polymers were investigated as building blocks for thermoresponsive polymer-DNA conjugates (discussed in chapter 5.3) as alternative to the hemitelechelic poly(2-oxazoline)s. In chapter 5.2.2, the synthesis of biocompatible *N*-substituted poly(acrylamide)s will be presented and discussed. The different functional groups like amino-, carboxylic acid- or hydroxy groups can be introduced into such polymers by preparing the corresponding *N*-substituted acrylamides as monomer. The combination of hydroxy-functionalized acrylamides, a photocrosslinkable acrylamide derivative and either amino- or carboxylic acid-functionalized acrylamides as additional binding sites e.g., for coupling of drugs, allow the design of precursors for low-fouling hydrogels. Similar, copolymers composed of hydroxy-functionalized- and amino-functionalized acrylamides were synthesized, in which the pendant amino groups can condense DNA by electrostatic interactions. These polymers were examined as vectors in gene delivery (discussed in chapter 5.5).

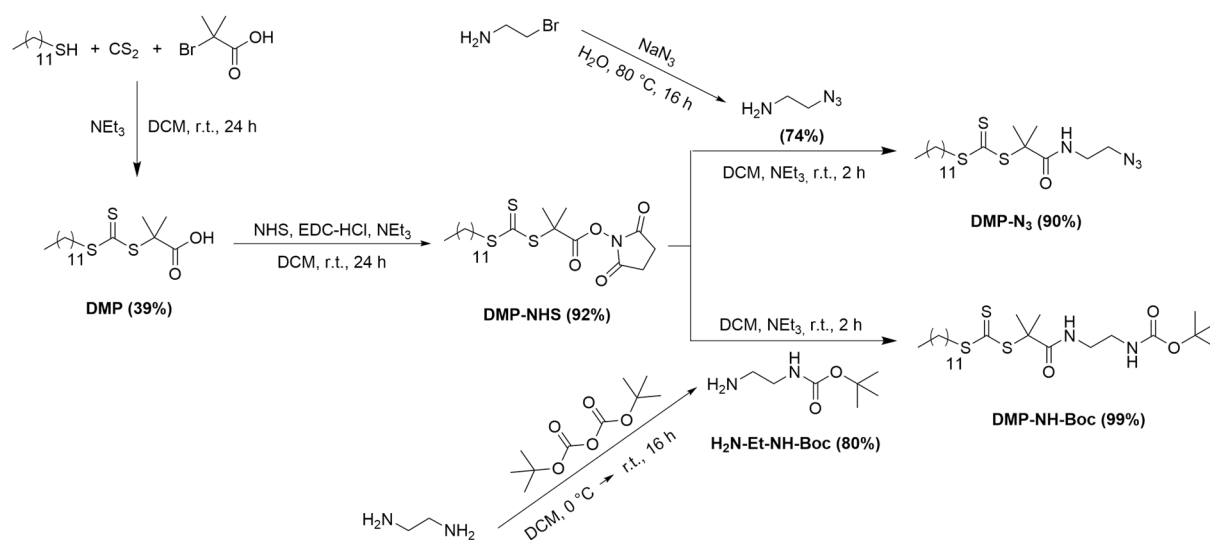
5.2.1 Synthesis of Hemi-Telechelic Poly(NiPAm) Derivatives

In this chapter, the synthesis of different end group-functionalized NiPAm homo- and copolymers are described and discussed. This monomer and the corresponding polymers were chosen as alternative system to the previous described poly(2-oxazoline) copolymers (chapter 5.1.1), which were synthesized as building blocks for polymer-DNA conjugates (discussed in chapter 5.3), because PNiPAm is similar to the previously described POxas also biocompatible and water-soluble below its LCST. The phase transition temperature of poly(NiPAm) is at $T = 32\text{ }^{\circ}\text{C}^{43,158}$ (depending on the environment like pH- or salt effects^{181,182} and molar mass³⁴), which is close to the targeted LCST ($T \approx 30\text{ }^{\circ}\text{C}$) of the prepared poly(EtOxa-co-nPrOxa)-derivatives (**P1.5** and **P1.6**). RAFT polymerization was chosen as reversible-deactivation radical polymerization (RDRP) to ensure low molar mass distributions of the prepared homo- and copolymers. The introduction of functional groups at the end of the polymer backbone can be achieved by functionalization of the respective CTA. Therefore, 2-[[[(dodecylthio)carbono

thiyl]thio}-2-methylpropanoic acid (DMP) was chosen as CTA, because of the ease of synthesis (depicted in Scheme 5.11) as well as the versatility of trithiocarbonates to control radical polymerization for a broad range of vinylic monomers.¹⁸³ Further, the carboxylic acid group of DMP can be easily modified, e.g. by active ester chemistry, enabling the introduction of various functional groups and linkers.

Functionalization of DMP:

First, DMP was prepared by a modified procedure of Postma and coworkers⁶ using *n*-dodecanethiol, carbon disulfide and α -bromoisobutyric acid as reagents. A poor yield of 39% was obtained, which can be explained by losses of product during the purification process (see Experimental Part on page 195). The success of the reaction was confirmed by NMR spectroscopy (see Figure S21 and Figure S22). Further functionalization reactions of DMP are illustrated in Scheme 5.11. First, DMP was transformed into the more reactive NHS derivative DMP-NHS by reaction of the carboxylic group with *N*-hydroxysuccinimide (NHS) in the presence of 1-ethyl-3-(3-dimethylaminopropyl)carbodiimide hydrochloride that is known in protein chemistry as efficient coupling agent.¹⁸⁴



Scheme 5.11: Synthesis route for the preparation of end-functionalized RAFT-agents by activation of the carboxylic group of DMP by NHS-ester chemistry followed by coupling with previously functionalized primary amine derivatives.

DMP-NHS can react under mild conditions preferentially with primary or secondary amino-groups. Thus, two different amino ethyl derivatives as coupling agents were prepared. First,

2-bromoethylamine hydrobromide was modified in a nucleophilic substitution reaction using sodium azide to obtain 2-azidoethylamine (see Experimental Part on page 195) in a good yield of 74%. The success of the reaction was confirmed using IR spectroscopy by appearing of the azide stretching vibration at $\bar{\nu} \approx 2090 \text{ cm}^{-1}$ and NMR spectroscopy.

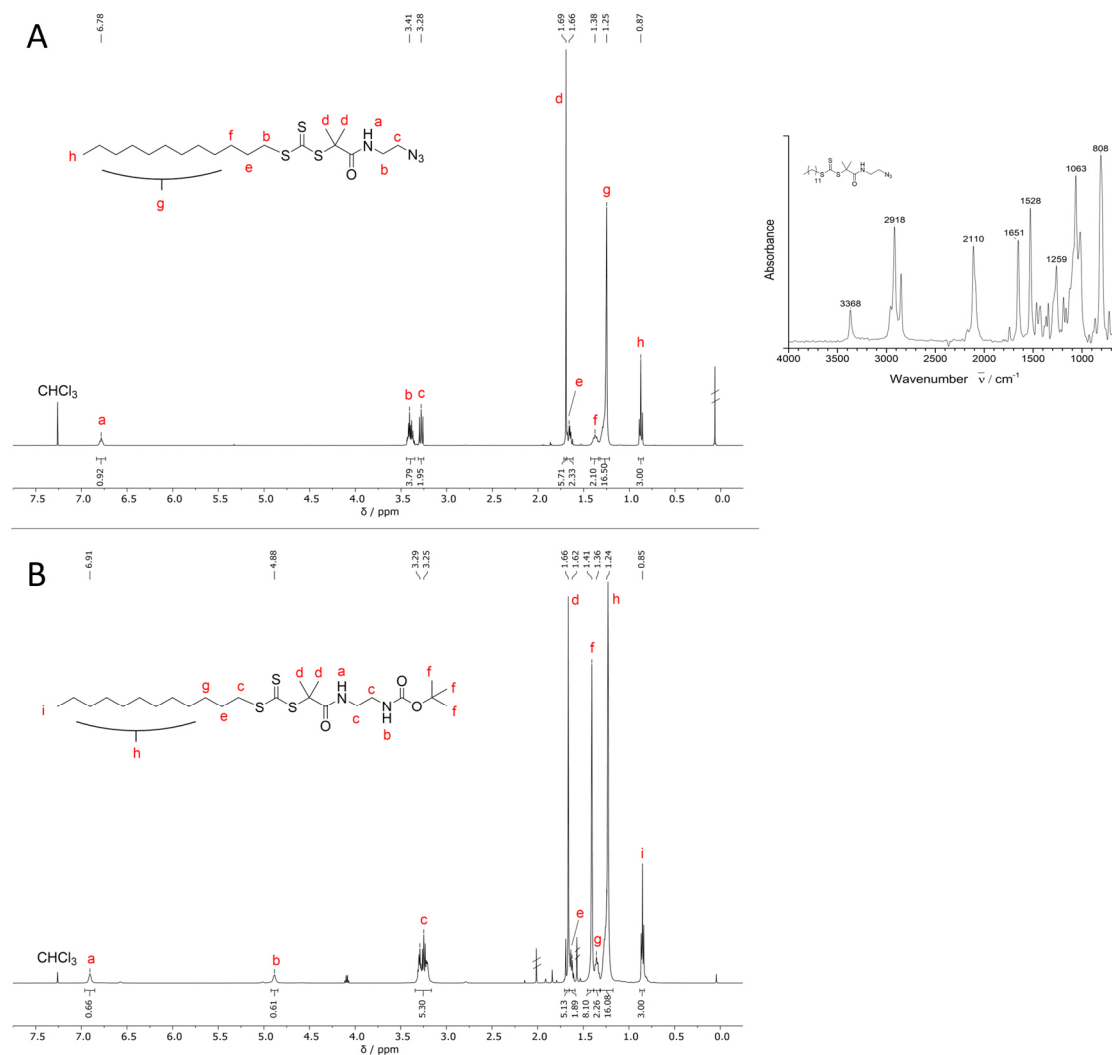
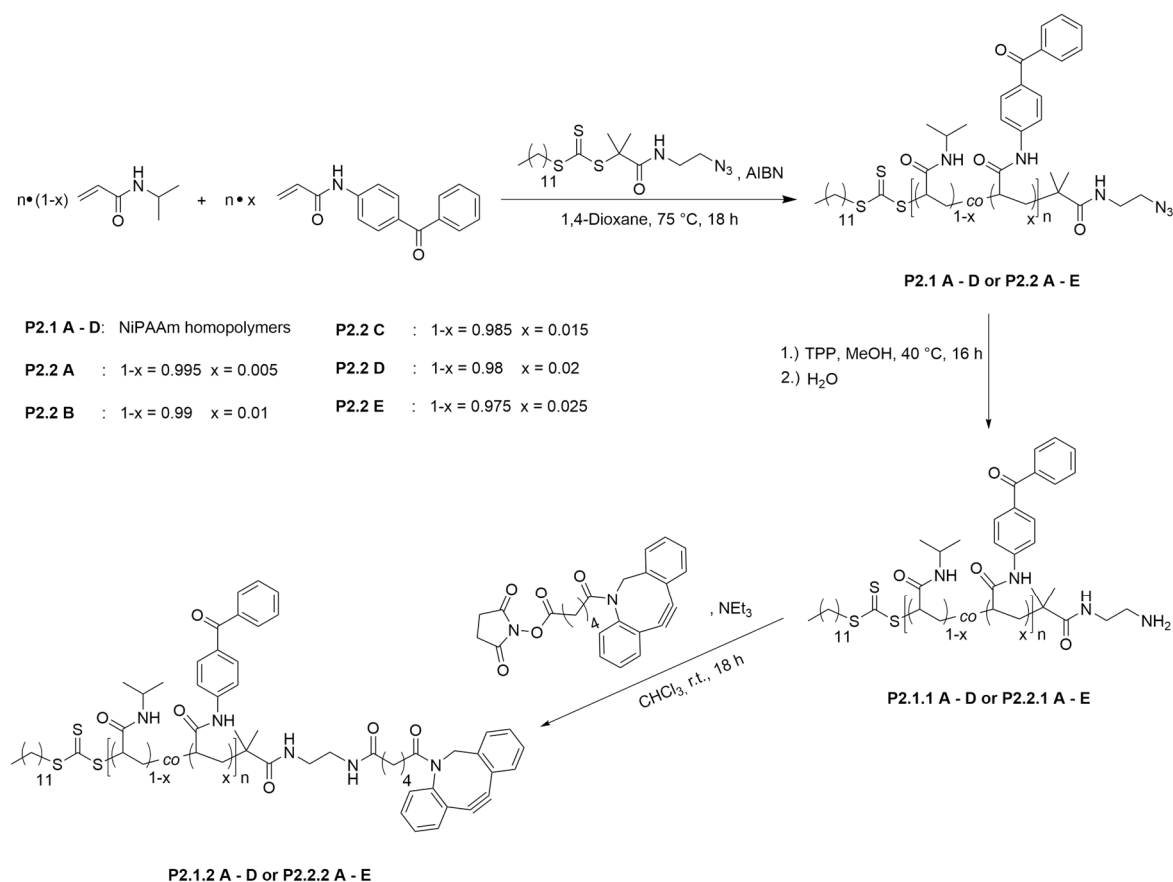


Figure 5.11: Illustration of the recorded ¹H-NMR (400 MHz) and IR spectra of DMP-N₃ (A). Below, the ¹H-NMR (500 MHz) spectrum of DMP-NH-Boc is shown (B). Both NMR spectra were recorded in CDCl₃.

The corresponding spectra are shown in Figure S25-Figure S27. In a subsequent reaction, DMP-NHS and 2-azidoethylamine were coupled using NEt₃ as additional base. The product DMP-N₃ was obtained in particularly good yield of 90% and the recorded NMR spectra as well as the recorded IR spectrum confirmed the success of the reaction (Figure 5.11 A and Figure S28). As second derivative, one amino group of ethylenediamine was protected using di-*tert*.butyl dicarbonate to yield *tert*.-butyl (2-aminoethyl)carbamate (H₂N-Et-NH-Boc). The

reaction is described in the General Procedure 2 on page 200 and discussed in chapter 5.2.2 together with other *mono*-Boc-protected diaminoalkanes. The corresponding NMR spectra, which confirmed the presence of the title compound, are depicted in Figure 5.11 and Figure S29. DMP-NH-Boc was prepared using the same procedure as for the coupling of DMP-NHS and 2-azidoethyl amine. An excellent yield of 99% was obtained and the success of the reaction was confirmed by NMR spectroscopy (Figure 5.11 B and Figure S29), which showed only small impurities present in the proton NMR spectrum. DMP-NH-Boc was prepared as alternative to DMP-N₃ for the synthesis of poly(NiPAm) homo- and copolymers. However, no polymers were prepared by using this DMP derivative for the coupling of polymers and DNA, since the postmodification route using the azide containing CTA derivative DMP-N₃ was successful (chapter 5.3) and was comparable to the postmodification route of the azide terminated poly(2-oxazoline)s (chapter 5.1.1).

Synthesis of azide end-functionalized poly(NiPAm) derivatives:



Scheme 5.12: Schematic overview of the RAFT-polymerization of NiPAm (**P2.1 A-D**) and the RAFT-copolymerization of NiPAm and BPAm (**P2.2 A-E**) using DMP-N₃ as CTA and the corresponding further functionalization steps to obtain the DBCO-functionalized derivatives (**P2.1.2 A-D** and **P2.2.2 A-E**).

DMP-N₃ was used as functional CTA to introduce an azide group at the distal end of the polymer backbone. Then, analogue to the functionalization pathway of the poly(2-oxazoline)s (see chapter 5.1.1), the azide moiety was reduced by a Staudinger reduction and the yielded amino group was subsequently modified with DBCO-C₆-NHS in order to introduce an highly reactive alkyne-group that can be utilized in SPAAC reactions to couple azide-functionalized molecules (Scheme 5.12). A series of azide-functionalized poly(NiPAm)s with different molar masses were prepared (**P2.1A-D**) using DMP-N₃ as CTA and azobisisobutyronitrile (AIBN) as common thermal initiator. The polymerization was performed in 1,4-dioxane at $T = 75\text{ }^{\circ}\text{C}$ for $t = 18\text{ h}$ with a monomer concentration of $\beta = 130\text{ mg}\cdot\text{ml}^{-1}$ (General Procedure 16 on page 234). Different molar masses between $3.2\text{ kg}\cdot\text{mol}^{-1}$ and $50\text{ kg}\cdot\text{mol}^{-1}$ were achieved by varying the monomer-to-CTA ratios from 25 : 1 to 400 : 1. Furthermore, five copolymers of NiPAm with different contents of *N*-(4-benzoylphenone) acrylamide (BPAm), varying from 0.5 mol% to 2.5 mol%, were prepared (**P2.2 A-E**) using the same polymerization protocol as for **P2.1A-D**. The monomer-to-CTA ratio was kept constant at 150 : 1 to obtain molar masses of $17.4\text{ kg}\cdot\text{mol}^{-1}$. The yields observed for all homo- and copolymers (79%-93%) were in good agreement to yields that were observed for similar polymers prepared within the work group. For **P2.1 B (3)** a yield larger than the theoretical value was obtained, which was caused by the presence of 1,4-dioxane in the polymer sample that was observed in the recorded ¹H NMR spectrum. The presence of the azide group ($\bar{\nu} \approx 2090\text{ cm}^{-1}$) at the chain end of the homo- and copolymers were confirmed by IR spectroscopy. The built-in of BPAm in **P2.2 A-E** as well as the molar masses were calculated by ¹H NMR spectroscopy. Exemplarily, the recorded ¹H NMR and IR spectra of **P2.1 A** and **P2.2 C** are depicted in Figure 5.12. The broadening of the signals in the NMR spectra and the presence of the azide stretching vibration in the IR spectra confirmed the successful polymerization of both the homo- (**P2.1**) and the copolymers (**P2.2**). The calculation of the \bar{X}_n was possible by NMR spectra by comparison the integral of the signal, which corresponds to the terminal methyl group of the CTA ($\delta = 0.86\text{ ppm}$) and the integral of the signal that belongs to the proton of the methine group in the isopropyl side chain ($\delta \approx 3.94\text{ ppm}$) and additionally, the integral of the aromatic protons of BPAm ($\delta \approx 7.80\text{-}7.40\text{ ppm}$) for the copolymers **P2.2 A-E**. The \bar{X}_n was used to calculate the \bar{M}_n values and the built-in of BPAm, which are listed in Table 5.10. Both, the \bar{M}_n calculated by ¹H NMR spectroscopy or measured by GPC differ strongly from the theoretical value particularly for the high monomer-to-CTA ratio polymers **P2.1 C** and **P2.1 D**. The large discrepancy between the

5 Results and Discussion

theoretical and calculated \overline{M}_n by ^1H NMR may be explained by the low intensity of the signal assigned to the methyl group of the CTA, which additionally overlaps with the broad signal of the methyl protons of the isopropyl group.

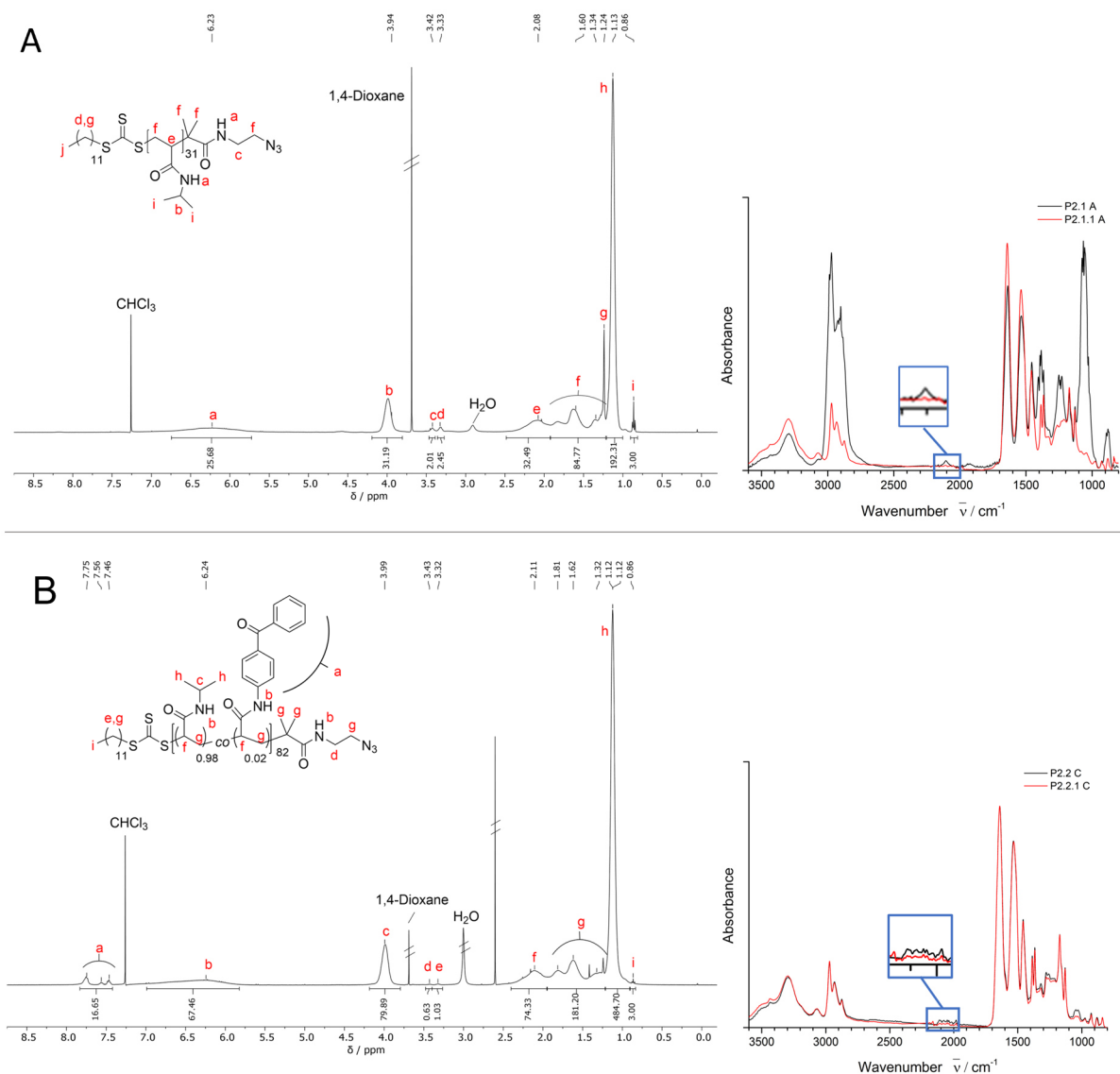


Figure 5.12: Depiction of the recorded ^1H NMR spectra (400 MHz) of **P2.1 A** (A, left) and **P2.2 C** (B, left) and the corresponding IR spectra (right), recorded before (black line) and after Staudinger reduction (red line). The regions where the azide stretching vibration typically appears is enlarged to illustrate the disappearance after successful reduction of the azide.

Further, the GPC data compared with the theoretical values implied that the solvent system and PMMA as standard are not ideal for determining molar mass of NiPAM based homo- and copolymers, since strong deviations were observed. In literature, Mark-Houwink parameters are reported for GPC measurements of poly(NiPAM) in THF, which would allow a more

precisely determination of the molar masses. However, the authors claimed that the purification of the poly(NiPAm)s has a strong influence on the deviation between measured molar mass and the theoretical molar mass.¹⁸⁵

Table 5.10: Tabulation of the theoretical and obtained molar masses and dispersities of the PNiPams **P2.1 A-D** and **P2.2 A-E** measured by GPC and calculated by ¹H NMR spectroscopy. The theoretical as well as the calculated content of BPAm, determined by ¹H NMR, are listed. The relative yield (%) was calculated by comparing the initial monomer feed with the obtained mass of polymer after polymerization.

Polymer	BPAm	Theor. \bar{M}_n	\bar{M}_n	\bar{M}_n	\mathcal{D}	Yield
	Content / % (theor.% ^a)	/ kg·mol ⁻¹ ([M] ₀ : [CTA])	(NMR) / kg·mol ⁻¹	(GPC ^b) / kg·mol ⁻¹		
P2.1 A	---	3.2 (25 : 1)	3.9	4.7	1.19	0.80 (80)
P2.1 B (1)	---	17.4 (150 : 1)	14.0	26.3	1.18	0.79 (79)
P2.1 B (2)	---	17.4 (150 : 1)	11.4	23.4	1.17	9.32 (93)
P2.1 B (3)	---	17.4 (150 : 1)	15.1	24.1	1.15	22.0 (110) ^c
P2.1 C	---	28.4 (247 : 1)	19.1	32.4	1.27	0.84 (84)
P2.1 D	---	45.7 (400 : 1)	17.9	38.9	1.37	0.88 (88)
P2.2 A	0.7 (0.5)	17.5 (150 : 1)	10.0	22.1	1.24	0.83 (83)
P2.2 B (1)	1.3 (1.0)	17.6 (150 : 1)	16.9	22.9	1.30	0.79 (79)
P2.2 B (2)	1.3 (1.0)	17.6 (150 : 1)	16.0	21.9	1.25	8.75 (88)
P2.2 C	1.7 (1.5)	17.7 (150 : 1)	12.1	21.2	1.29	0.86 (86)
P2.2 D	1.9 (2.0)	17.8 (150 : 1)	12.7	22.7	1.24	0.81 (81)
P2.2 E	1.9 (2.5)	17.9 (150 : 1)	12.9	21.8	1.27	0.86 (86)

^a theoretical content in percent of BPAm adjusted by monomer feed-in

^b eluent: DMAc containing LiBr, $\beta = 1 \text{ g} \cdot \text{l}^{-1}$; PMMA standards were used for calibration

^c 1,4-dioxane present in the polymer

The feed of BPAm compared to calculated contents from ^1H NMR indicates a nearly uniform polymerization of both acrylamide derivatives. The obtained values slightly differ from the theoretically possible contents, which could be addressed to integration errors due to the overlapping of the signals (especially the signal of the terminal methyl-group of the CTA) used for calculation. This could be the reason for the significant deviation of 0.6% in the built-in ratios of **P2.2 E**. Additionally, the molar mass distributions became broader ($\mathcal{D} = 1.15\text{-}1.37$) for **P2.1 A-D** with increasing monomer-to-initiator ratio and for the copolymers **P2.2 A-E** dispersities around 1.28 were obtained. The broader molar mass distributions of **P2.1 C** and **P2.1 D** suggested a less controlled RAFT polymerization, which is caused by insufficient CTA concentration present in the polymerization mixture. The broadening of the molar mass distributions **P2.1 A-D** and **P2.2 A-E** can be assigned to an aggregation of at least two polymer chains, which lead to a second species at double of molar mass of the M_p that is more predominant for **P2.2 A-E** (see Figure 5.13, black lines).

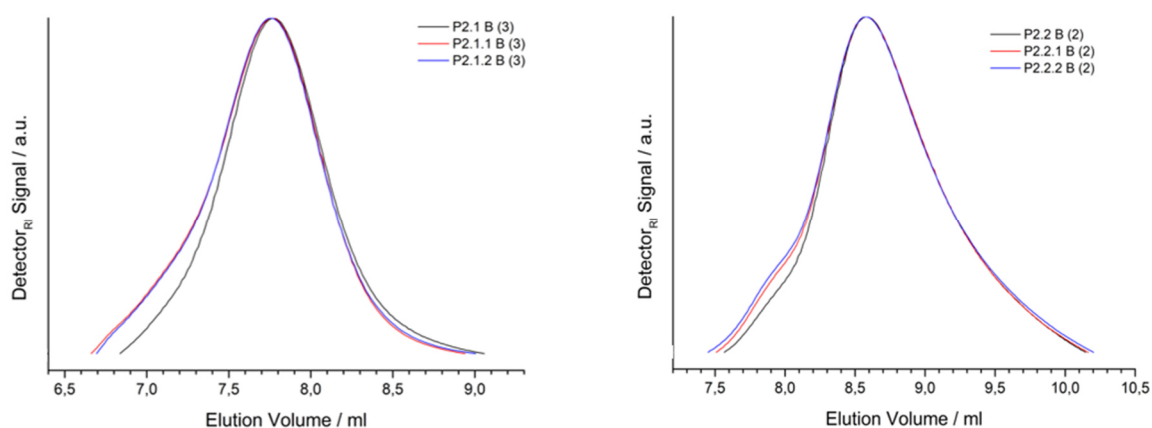


Figure 5.13: Superimposed GPC elugrams of **P2.1 B (3)** and their further functionalization (left) and the corresponding elugrams of **P2.2 B (2)** (right). The measurements were performed in DMAc containing LiBr ($\beta = 1 \text{ g}\cdot\text{l}^{-1}$) as eluent.

Responsible for the aggregation may be intermolecular interactions of CTA groups present in the polymer chains of the prepared homo- and copolymers. In case of copolymers **P2.2 A-E**, the aggregation behavior seemed to be supplemented by the presence of benzophenone groups, leading to an increased broadening of the molar mass distribution.

Staudinger reduction of the azide group:

The azide-end group was reduced by Staudinger reaction using TPP, according to the poly(2-oxazoline) analogues (see General Procedure 18 on page 239). The removal of the

formed TPPO and remaining TPP by repeated precipitation in water led to poor yields (13%-56%), especially for the small-scale attempts caused by losses of polymer, which may be encapsulated by the precipitate. However, for the large-scale attempts **P2.1.1 B (3)** and **P2.2.1 B (2)** good yields of 75% and 87% were obtained. Extensive washing of the precipitate did not lead to a significant increase of polymer yield. Moreover, the proposed purification procedure showed no quantitative removal of the byproducts. In particular, for the low molar mass **P2.1.1 A**, aromatic protons could be detected in ^1H NMR. In Table 5.11, the yields of the polymers and the corresponding measured molar mass parameters are listed.

Table 5.11: Listing of the measured molar masses and dispersities of the amino-functionalized PNIPAMs **P2.1.1 A-D** and **P2.2.1 A-E** as well as the corresponding yield of the Staudinger reaction.

Polymer	\overline{M}_n (GPC ^a) / kg·mol ⁻¹	\overline{D}	Yield / g (%)
P2.1.1 A	6.2	1.34	0.24 (49)
P2.1.1 B (1)	23.9	1.29	0.28 (56)
P2.1.1 B (2)	23.3	1.29	3.62 (44)
P2.1.1 B (3)	26.0	1.18	12.50 (75)
P2.1.1 C	32.5	1.29	0.13 (26)
P2.1.1 D	21.7	1.43	0.10 (20)
P2.2.1 A	22.0	1.28	0.12 (24)
P2.2.1 B (1)	21.1	1.40	0.38 (76)
P2.2.1 B (2)	22.2	1.27	6.58 (87)
P2.2.1 C	20.8	1.33	0.18 (35)
P2.2.1 D	22.6	1.26	0.20 (38)
P2.2.1 E	16.9	1.37	0.06 (13)

^a eluent: DMAc containing LiBr, $\beta = 1 \text{ g}\cdot\text{l}^{-1}$; PMMA standards were used for calibration

A small broadening of the molar mass distribution for the homopolymers **P2.1.1 A-D** compared to those after polymerization (Table 5.10) were observed, which may be assigned to present amino groups that is probably able to form aggregates mediated by Li^+ present in the eluent system, which was used for GPC measurements as suggested by the GPC elugrams (Figure

5.13 left). Interestingly, this a significant broadening of the molar mass distribution was not observed for the corresponding copolymers **P2.2.1 A-E**, which may indicate that the possible aggregation primarily is caused by benzophenone groups present along the polymer chains for **P2.2.1 A-E**. For all prepared homo- and copolymers slightly higher molar mass distributions after reduction of the distal azide end groups were observed that may arise due to an aggregation behavior of polymer chains with their amino groups. In contrast, the occurrence of possible side reactions, like aggregation, is not clearly supported by the comparison of the \bar{M}_n , before and after reduction, which shows that in almost all cases the \bar{M}_n were similar or only slightly increased after reduction of the azide group (e.g. **P2.1.1 A**). Therefore, the proposed aggregation obviously plays a minor role. However, for **P2.1.1 D** a drastic decrease in \bar{M}_n (21.7 kg·mol⁻¹) compared to the polymer precursor ($\bar{M}_n = 38.9$ kg·mol⁻¹) was observed, which cannot be explain yet. Both, the precursor **P2.1 D** and amino-functionalized homopolymer **P2.1.1 D** were measured under same conditions in the GPC. Obviously, an unexpected side reaction led to degradation of the polymer. In an alternative approach, the azide reduction was tested using propane-1,3-dithiol, according to the poly(2-oxazoline)s (chapter 5.1.1), in order to avoid TPP and TPPO traces in the amino-functionalized polymer. However, a partially crosslinked polymer was obtained, which might be result from a reduction of the trithiocarbonate by the dithiol and subsequent intermolecular disulfide formation or other side reactions. The recorded GPC elugram from the soluble part of this mixture showed a distribution of polymer over the whole separation range of the used column (GRAM 100A, 1.0 kg·mol⁻¹-100 kg·mol⁻¹), which implies that this is no practical alternative. Therefore, traces of TPP and TPPO were tolerated, since the subsequent DBCO-functionalization should not be affected and the traces could be removed during the purification of the DBCO-functionalized polymers.

DBCO-functionalization:

DBCO-C₆-NHS was coupled to the amino-functionalized homo- and copolymers in CHCl₃ (details provided in General Procedure 19 on page 242). The yields of around 80% that were obtained for most of the described polymers, were in good agreement to yields, which are reported for the same type of coupling reaction. The majority of loss of polymer probably occurred during purification by dialysis. The significant lower yields of **P2.1.2 B** and **P2.2.2 B (2)** of 54% and 63% can be explained by additional removal of the remaining TPP and TPPO by dialysis that was present in the polymer samples after the Staudinger reduction.

The signals of the aromatic protons of the DBCO at $\delta = 7.70\text{--}7.20$ ppm in the recorded ^1H NMR spectrum confirmed the successful coupling reaction. In Figure 5.14 representative spectra of **P2.1.2 A** and **P2.2.2 B (2)** are depicted.

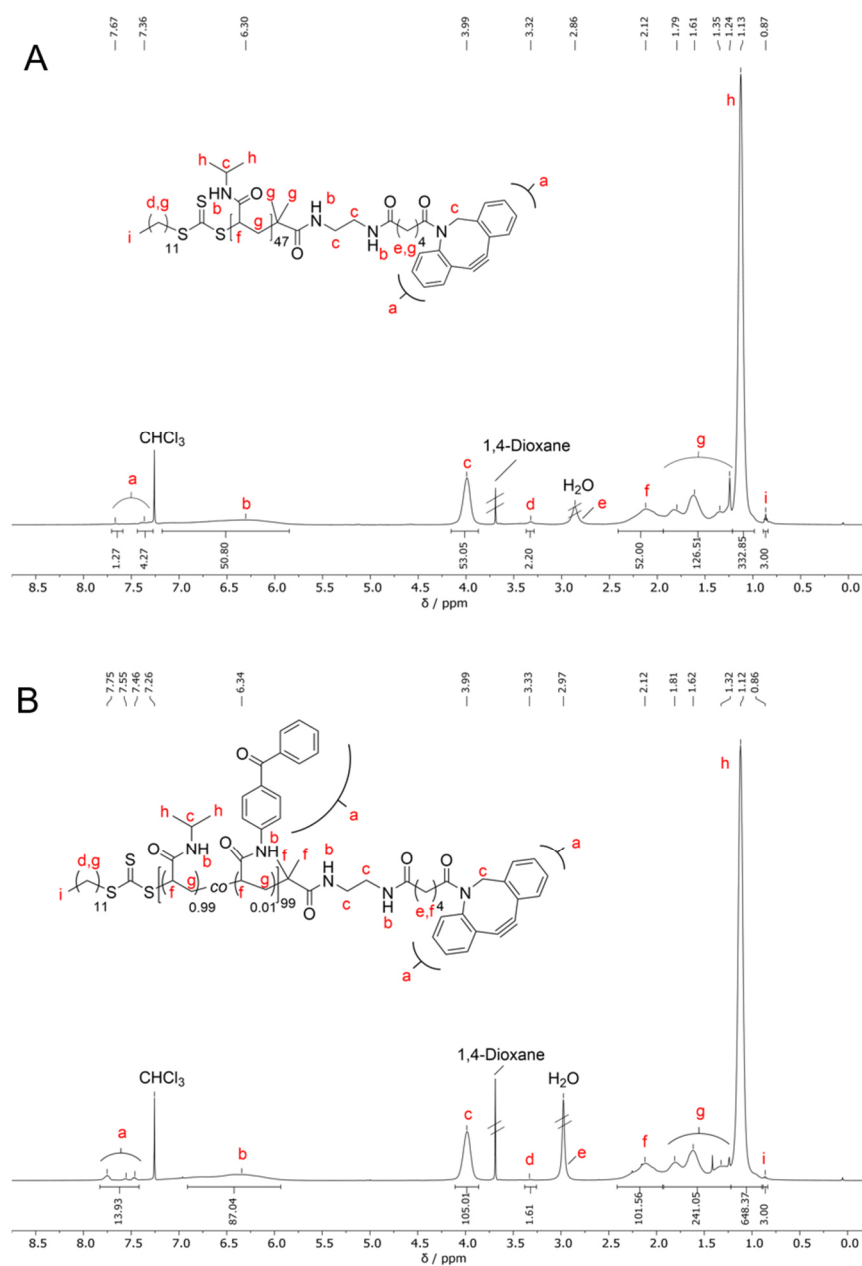


Figure 5.14: Depiction of the recorded ^1H NMR spectra (500 MHz, CDCl_3) of **P2.1.2 A** (A) and **P2.2.2 B (2)** (B).

The signals of protons assigned to the benzophenone group and to the DBCO moiety overlapped for the copolymers **P2.2.2 A-E**, which restricted the calculation of the degree of DBCO functionalization. For **P2.1.2 A**, a degree of functionalization of 92% (refer to Table 5.12) was calculated by adding the values of the integrals of $\delta = 7.70\text{--}7.20$ ppm and dividing the sum by

the theoretical number of aromatic protons present for a quantitative DBCO functionalization (six protons).

The degrees of functionalization for the other DBCO-functionalized homopolymers **P2.1.2 B** and **P2.1.2 C** were in the range of 75% and 90%, whereas for **P2.1.2 D** no degree could be determined accurately since the signal intensities of both polymer backbone end groups were too low.

Table 5.12: Tabulation of the measured molar masses and dispersities of the DBCO-functionalized PNIPAMs **P2.1.2 A-D** and **P2.2.2 A-E** obtained by GPC and by ¹H NMR spectroscopy as well as the yields of the coupling reactions and the corresponding degree of DBCO-functionalization.

Polymer	Degree of DBCO-functionalization (NMR) / %	\bar{M}_n (NMR) / kg·mol ⁻¹	\bar{M}_n (GPC ^a) / kg·mol ⁻¹	<i>D</i>	Yield / g (%)
P2.1.2 A	92	6.0	6.0	1.31	0.22 (88)
P2.1.2 B (1)	90	14.4	27.7	1.21	0.15 (54)
P2.1.2 B (2)	75	14.2	20.9	1.32	3.07 (85)
P2.1.2 B (3)	79	16.0	25.8	1.18	7.25 (92)
P2.1.2 C	90	16.7	32.4	1.27	0.09 (70)
P2.1.2 D	--- ^b	17.5	21.5	1.43	0.09 (85)
P2.2.2 A	--- ^c	11.3	19.8	1.35	0.08 (65)
P2.2.2 B (1)	--- ^c	14.8	25.5	1.28	0.30 (74)
P2.2.2 B (2)	--- ^c	13.2	22.1	1.29	3.71 (63)
P2.2.2 C	--- ^c	11.3	22.2	1.30	0.14 (80)
P2.2.2 D	--- ^c	11.8	23.0	1.29	0.17 (89)
P2.2.2 E	--- ^c	10.8	18.9	1.28	0.04 (67)

^a eluent: DMAc containing LiBr, $\beta = 1 \text{ g}\cdot\text{l}^{-1}$; PMMA standards were used for calibration

^b due to low signal intensities, no degree of functionalization could be calculated

^c could not be determined because of overlapping signals of the aromatic protons of benzophenone and DBCO

Again, the calculation of the \bar{M}_n by NMR for the polymers **P2.1.2 A-D** and **P2.2.2 A-E** led to large differences between the theoretical molar masses and the calculated values. Also, the

comparison of the measured molar mass parameters with the calculated molar mass from the NMR spectra showed large deviations caused by the above discussed issues. Thus, the calculation of the \bar{M}_n by NMR is not suitable for the here described homo- and copolymer systems.

As expected, the obtained \bar{M}_n of **P2.1.2 A-D** and **P2.2.2 A-E**, measured by GPC (Table 5.12) show no significant deviations from the mass parameters of the amino-functionalized precursors **P2.1.1 A-D** and **P2.2.1 A-E**, and thus indicating no undesired side reaction. As expected, the obtained D values are similar to those values of the corresponding precursors.

Summary:

In this chapter, the three-step synthesis of novel DBCO-end group functionalized homopolymers of NiPAm (**P2.1.2 A-D**) with different molar masses as well as photocrosslinkable copolymers, using BPAm (**P2.2.2 A-E**), were described for the preparation of thermoresponsive polymer-DNA conjugates (chapter 5.3).

Therefore, a novel azide-functionalized trithiocarbonate as CTA (DMP-N₃) was synthesized for the RAFT (co-)polymerization. As alternative, DMP-NH-Boc was synthesized according to the procedure used for the synthesis of DMP-N₃. DMP-NH-Boc was not used as CTA, since the polymers prepared with DMP-N₃ allow the application of the previously developed DBCO-functionalization protocol for the poly(2-oxazoline) derivatives (Chapter 5.1.1).

Azide-end group functionalized homopolymers of NiPAm (**P2.1 A-D**) with different molar masses as well as five photocrosslinkable copolymers, using BPAm (**P2.2 A-E**) in different ratios, were synthesized by RAFT polymerization using DMP-N₃ as CTA.

For the copolymers **P2.2 A-E**, a broader molar mass distribution than for **P2.1 A-D** were obtained, which might arise from possible aggregation of two or more polymer chains by their benzophenone moieties. The successful reduction of the azide moieties by Staudinger reaction was confirmed by the disappearance of the azide stretching vibration in the corresponding IR spectrum. Similar to the poly(2-oxazoline) analogues, also for **P2.1.1 A-D** and **P2.2.1 A-E** low yields (around 40%) were obtained caused by substantial losses during purification. Traces of TPP and TPPO remained after purification, but repetition of the purification did not lead to a significant improvement of the purity. DBCO was coupled to the amino group containing (co-)polymers by NHS active ester chemistry (**P2.1.2 A-D** and **P2.2.2 A-E**) in high yields. Further, high degrees of DBCO-functionalization (75-97%) were obtained for **P2.1.2 A-D**. However, for the copolymers carrying photocrosslinkable groups a calculation of the degree of

functionalization was not possible, because the signals of the DBCO and the benzophenone protons overlapped in the recorded ^1H NMR spectra.

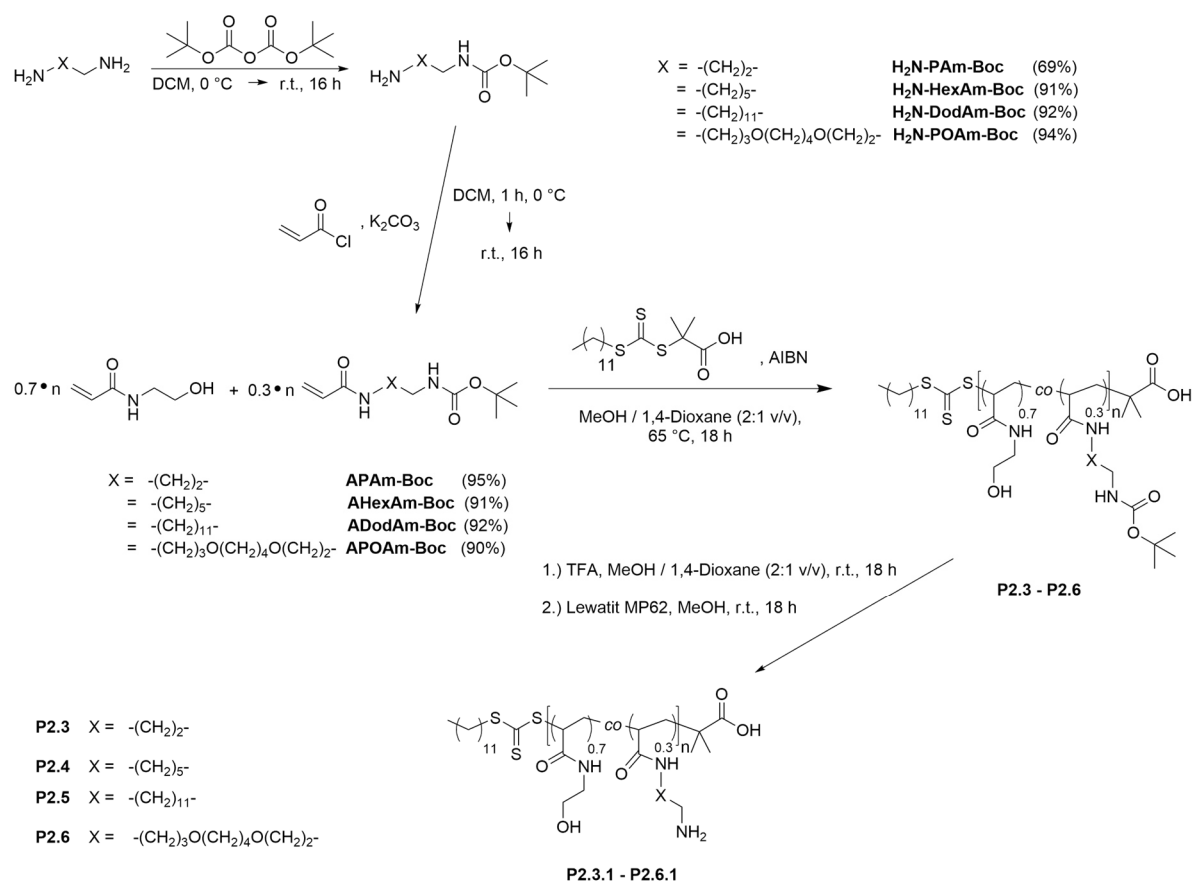
5.2.2 Pendant Group Modification of Poly(*N*-hydroxyalkyl acrylamide)s

The introduction of different side groups like amino- or carboxylic acid groups in polymers allows preparation of multifunctional macromolecular architectures by specific coupling reactions to these side groups with effective conjugation reactions, which can be orthogonally modified if more than one distinguished functional group will be needed. Further, this pendant group modification e.g. amino groups into the side chain of polymers, may be very interesting for different applications, like in biomedicine as antimicrobial agent^{186–188} or as non-viral vector in gene delivery.^{189–191} Amino groups possess interesting features like the ease of further functionalization by many different reaction mechanisms or pH responsiveness, which means that depending on the pH value of the environment the amino groups are either charged by proton abstraction or uncharged that lead to a change in their hydrophilicity.¹⁹² Further, preferentially secondary and tertiary amino groups containing polymers are often used as chelating agent for the complexation of metal ions.^{193,194} However, these groups are in radical polymerization techniques problematic since they can act as retarder.¹⁹⁵ Further, the acrylamide monomers, which contain free amino groups, could not be isolated because these monomers immediately polymerized. Additionally, the handling and storage of free amines can be problematic in terms of their stability since they tend to oxidize with oxygen from air over time. Therefore, shielding of the amino groups is needed, which can be achieved by the introduction of a protecting group. The common strategy for shielding amines is the protection as *tert.*-butylcarbamate (Boc) derivative,^{196–198} because this provides several practical advantages. First, the removing of the protection groups can be simply achieved by using an acidic environment yielding exclusively gaseous byproducts like isobutylene and CO₂.¹⁹⁹ Second, the introduction can be accomplished under mild conditions and thus allowing the protection of a large variety of (unstable) molecules containing amino groups. It should be noted that Boc-derivatives are only stable in weakly basic and neutral environment and therefore acidic environments should be avoided.¹⁹⁹

Synthesis of copolymers for application as non-viral gene vector:

Below the synthetic overview of copolymerization of **P2.3-P2.6** (Scheme 5.13) is illustrated. For the mono protection of the diaminoalkanes a general procedure was developed, which was suitable for all used educts (General Procedure 2 on page 200). H₂N-Dod-NH-Boc and H₂N-PO-NH-Boc (precursor of ADodAm-Boc and APOAm-Boc) were purified by column

chromatography because the purification protocols for the other mono-*N*-Boc protected diaminoalkanes using extraction did not lead to a satisfying purification.



Scheme 5.13: Exemplification of the synthesis of *N*-Boc aminoalkyl acrylamides and their RAFT-copolymerization using HEAm as comonomer and DMP as CTA (**P2.3-P2.6**). Values in brackets shown the yield of the corresponding acrylation reaction. The final polymers were obtained after removing of the Boc-group to yield amino-functionalized copolymers (**P2.3.1-P2.6.1**).

H₂N-PAm-Boc seemed to be slightly water soluble, which obviously led to losses during purification because the obtained yield (69%) is lower than the yields obtained for the other mono-*N*-Boc protected diaminoalkanes (>90%). The recorded ¹H NMR and ¹³C NMR (exemplarily shown in Figure S32 to Figure S43) showed that during the reaction also the di-*N,N'*-Boc diaminoalkanes were formed as byproducts. In these derivatives, the reactive amino groups are blocked and were not accessible for further reactions like the acrylation with acryloyl chloride or in radical polymerization. These byproducts (disubstituted diamines) could be removed in the purification after the acrylation reaction. The experimental details of the acrylation are described in General Procedure 3 on page 203. All mono-Boc protected acrylamides (AXAm-Boc) could be obtained in high yields (>90%) and the presence of the

target molecules was confirmed by NMR spectroscopy. Corresponding ^1H and ^{13}C NMR spectra are shown in Figure S44 to Figure S55. The obtained mono-Boc protected acrylamides were used as comonomers in RAFT polymerizations using *N*-hydroxyethyl acrylamide (HEAm) as second monomer. These monomers were selected to fulfill specific requirements as potential non-viral vector in gene delivery (chapter 5.5). The content of amino-functionalized monomer in the polymer was adjusted to 30% at the beginning of the polymerization. Details of cell experiments with these polymers will be discussed in chapter 5.5. The polymerization was started using azobisisobutyronitrile (AIBN) as common thermal initiator and DMP was used as chain-transfer agent (CTA) in a MeOH / 1,4-dioxane (2:1 v/v) mixture at $T = 65\text{ }^\circ\text{C}$.

Table 5.13: List of the total monomer to CTA ratio $[\text{M}_0] : [\text{CTA}]$ as well as the yields of the synthesized *N*-substituted poly(acrylamide)s and their corresponding molar mass parameters. The targeted molar mass was adjusted to $25.0\text{ kg}\cdot\text{mol}^{-1}$. The ratio of the comonomers HEAm and the corresponding amino-functionalized acrylamide $[\text{HEAm}] : [\text{AXAm-Boc}]$ was adjusted to 70 : 30 at start of the polymerization. The relative yields (%) are calculated according to the corresponding mass of the monomers.

Polymer	Comonomer AXAm-Boc	$[\text{M}_0] : [\text{CTA}]$	Built-in of AXAm-Boc (NMR) / %	Yield / mg (%)
P2.3	APAm-Boc	170 : 1	26	359 (70)
P2.4	AHexAm-Boc	156 : 1	25	343 (69)
P2.5	ADodAm-Boc	133 : 1	26	148 (28)
P2.6	APOAm-Boc	134 : 1	19	205 (40)

The reaction parameters were adapted from previous synthesis of poly(HEAm) homo- and copolymers (Master's Thesis "*Synthesis of Multifunctional Hydrogel Coatings Using RAFT Polymerization for Potentially Improved Cell-Material Interactions*" Niklas Jung, Universität Siegen, 2016). Experimental details are given in General Procedure 17 on page 237. In Table 5.13, the corresponding reaction parameters as well as the obtained yields of the polymers and the build-in of the corresponding AXAm-Boc, determined by ^1H NMR spectroscopy, are listed. The yields of the shorter side chain containing polymers **P2.3** and **P2.4** of $\approx 70\%$ are in a typical range for yields of RAFT polymerizations. Interestingly, the yields of the polymers **P2.5** and **P2.6** (28% and 40% respectively) were lower compared to the other reported yields, which could be explained by the overall polarity of the copolymers. It seemed, that these longer side

chain copolymers were more hydrophobic than the other two copolymers, which cause a better solubility in the precipitation agent EtOAc, than the polymers with shorter side chains. The build-in of the corresponding AXAm-Boc was determined from recorded ^1H NMR spectra.

In Figure 5.15, exemplarily the spectrum of **P2.3** before (A) and after deprotection (B) is shown. The corresponding ^1H NMR of the other copolymers are shown in Figure S72 to Figure S74 and Figure S78 to Figure S80, respectively. The corresponding content of AXAm-Boc along the copolymer was determined by comparison of the integral of signal b ($\delta \approx 3.65$ ppm), which correspond to the protons of the methylene group next to the carbamate group, and signal d ($\delta \approx 1.90$ - 2.37ppm), that correspond to the hydrogen of the methine group in the polymer backbone. The calculated amounts of the corresponding AXAm-Boc incorporated into the polymers **P2.3-P2.5** (25-26%) were in good agreement to the initial monomer ratio of [HEAm] : [AXAm-Boc] of 70 : 30. The small deviations between monomer feed-in and calculated ratio could be assigned to integration errors of the corresponding signals because of signal overlapping due to the typical broadening of polymeric signals. However, the calculated content of APOAm-Boc in copolymer **P2.6** (19%) is much lower than expected. Probably, HEAm and APOAm-Boc possess different reaction parameters, which result in a preferred incorporation of HEAm molecules into the copolymer. Owing to the flexibility of the ether moieties in APOAm-Boc the vinyl group could be sterically hindered that hampers the accessibility of the double bond.

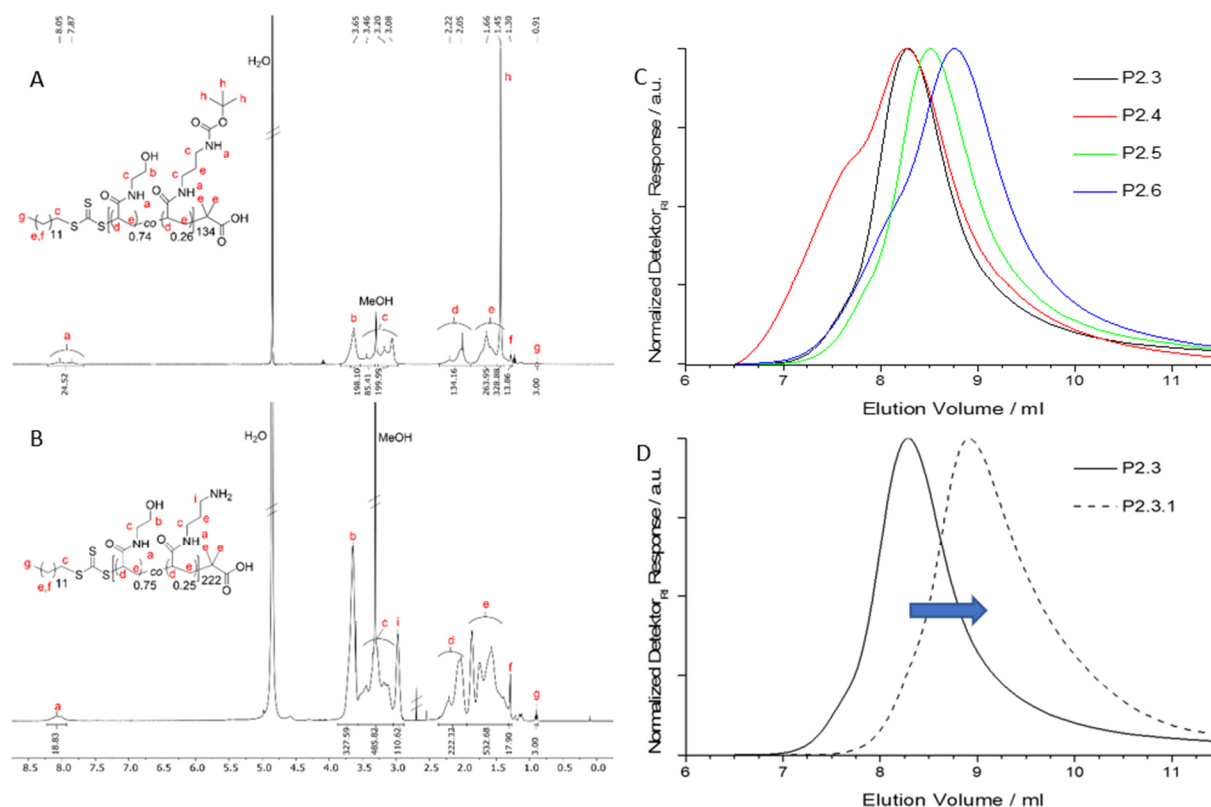


Figure 5.15: On the left side, $^1\text{H-NMR}$ (500 MHz) spectra of poly[(HEAm) $_{0.7}$ -co-(APAm-Boc) $_{0.3}$] $_{134}$ (**P2.3**) before (A) and after deprotection using TFA (B) are illustrated. Both spectra were recorded in CD_3OD . On the right side, GPC traces of the different copolymers **P2.3-P2.6** (C) and the change of the elution volume of **P2.3** before and after deprotection are depicted (D). For the GPC measurements DMAc containing LiBr ($\beta = 1 \text{ g}\cdot\text{l}^{-1}$) were used as eluent. (The NMR spectra and GPC traces were kindly provided by Fiona Diehl.)

If the masked amino groups containing monomer act as retarder, the reduced copolymerization rate of HEAm and APOAm-Boc would not lead to full conversion of the monomers during the giving reaction time. Contrary, the obtained molar mass of **P2.6** indicate a quite high conversion of the monomers (Table 5.14). According to the build-in of the corresponding AXAm-Boc, the \bar{X}_n and \bar{M}_n could be also determined by $^1\text{H NMR}$ spectroscopy. Therefore, the signal g ($\delta \approx 0.91 \text{ ppm}$), which correspond to the protons of the methyl end group of the CTA and signal d ($\delta \approx 2.05 \text{ ppm}$), corresponding to the methine group of the polymer backbone, were compared. The calculated number of repeat units, which is the same as \bar{X}_n , deviate strongly from the monomer to CTA ratio at reaction start. A possible error in calculation could be caused by integration of overlapping signals due to the typical signal broadening of polymeric signals or the low intensity of the peak assigned to the end group of the polymer chain. Furthermore, the comparison of the recorded $^1\text{H NMR}$ spectra (exemplarily shown in Figure 5.15) revealed that the number of repeat units increases after deprotection, which is contrary to the observations

made by GPC (compare Table 5.14). These false number of repeat units after deprotection, calculated from the ^1H NMR spectra, indicated side reaction like a partial aminolysis of the trithiocarbonate groups of the CTA induced by the liberated amino groups, which led to a loss of the dodecyl end group.

Therefore, the determination of the molar mass by ^1H NMR is not suitable. The obtained GPC data of the copolymers **P2.3-P2.6** as well as the change in the elution volume of **P2.3** after deprotection of the masked amino groups and anion exchange reaction (**P2.3.1**) is shown above in Figure 5.15. The elugrams of the copolymers **P2.4** and **P2.6** show that a second peak is overlapping with the main peak and its maximum is located at the double of the molar mass of the main peak revealing an aggregation of at least two polymer chains. This second peak is more distinct for **P2.4** than for **P2.6**, which may be explained by increased intermolecular hydrophobic interactions of the hexamethylene spacer compared to propylene oxide-containing spacer (Figure 5.15 C, red and blue line). Interestingly, the copolymers with smallest and largest hydrophobic linkers in the side group **P2.3** and **P2.5** showed no increased quantity of possible aggregated polymer chains. Moreover, almost no second species is observable in the elugrams for these polymers (Figure 5.15 C, black and green line).

In case of **P2.3**, the propylene spacer may be too short to undertake intermolecular hydrophobic interactions with other polymer chains. The increased flexibility of the Boc-protected amino groups-functionalized sidechains in **P2.6**, caused by the ether moieties, may hinder the formation of aggregates. The obtained molar mass parameters of the copolymer before and after deprotection are listed in Table 5.14. The measured \bar{M}_n of the copolymers before deprotection were higher for **P2.3-P2.5** ($\bar{M}_n = 27.0\text{-}34.2 \text{ kg}\cdot\text{mol}^{-1}$) than the desired molar mass ($\bar{M}_n = 25 \text{ kg}\cdot\text{mol}^{-1}$), which could be arise by more likely solvent-polymer interaction, resulting in expanded polymer coils.

For **P2.6**, a lower molar mass than expect was obtained ($\bar{M}_n = 21.7 \text{ kg}\cdot\text{mol}^{-1}$), which may be addressed to the different side chain of APOAm-Boc, which contains additional ether groups beside the aliphatic segments. The flexible side chain could lead to different coiling behavior and thus leading to a more compact polymer coil. The dispersities of **P2.3** and **P2.5** ($\mathcal{D} = 1.22$) were typically for RAFT polymerizations, but the dispersities for **P2.4** and **P2.6** ($\mathcal{D} = 1.55$ and 1.38 , respectively) were broader than expected. The broadening of these molar mass distributions arised from the appearance of a second peak in the elugram. After deprotection

and removing of the TFA-anion by anion exchanger, significant lower \bar{M}_n were obtained for all copolymers.

Table 5.14: Listing of the molar masses and the dispersities of the different poly(*N*-hydroxyalkyl acrylamide) derivatives before (P2.3-6) and after deprotection (P2.3.1-P2.6.1), which were obtained by GPC. The obtained values were calculated from the signal of the respective refractive index detector (RI-detector).

Polymer	Before Deprotection		After Deprotection		Relative Loss of Molar Mass /%
	\bar{M}_n^a / kg·mol ⁻¹	\mathcal{D}	\bar{M}_n^a / kg·mol ⁻¹	\mathcal{D}	
P2.3	33.2	1.22	15.2	1.31	-54
P2.4	34.2	1.55	21.0	1.40	-38
P2.5	27.0	1.22	18.8	1.42	-30
P2.6	21.7	1.38	14.8	1.46	-32

^a eluent: DMAc containing LiBr, $\beta = 1 \text{ g}\cdot\text{l}^{-1}$; PMMA standards were used for calibration

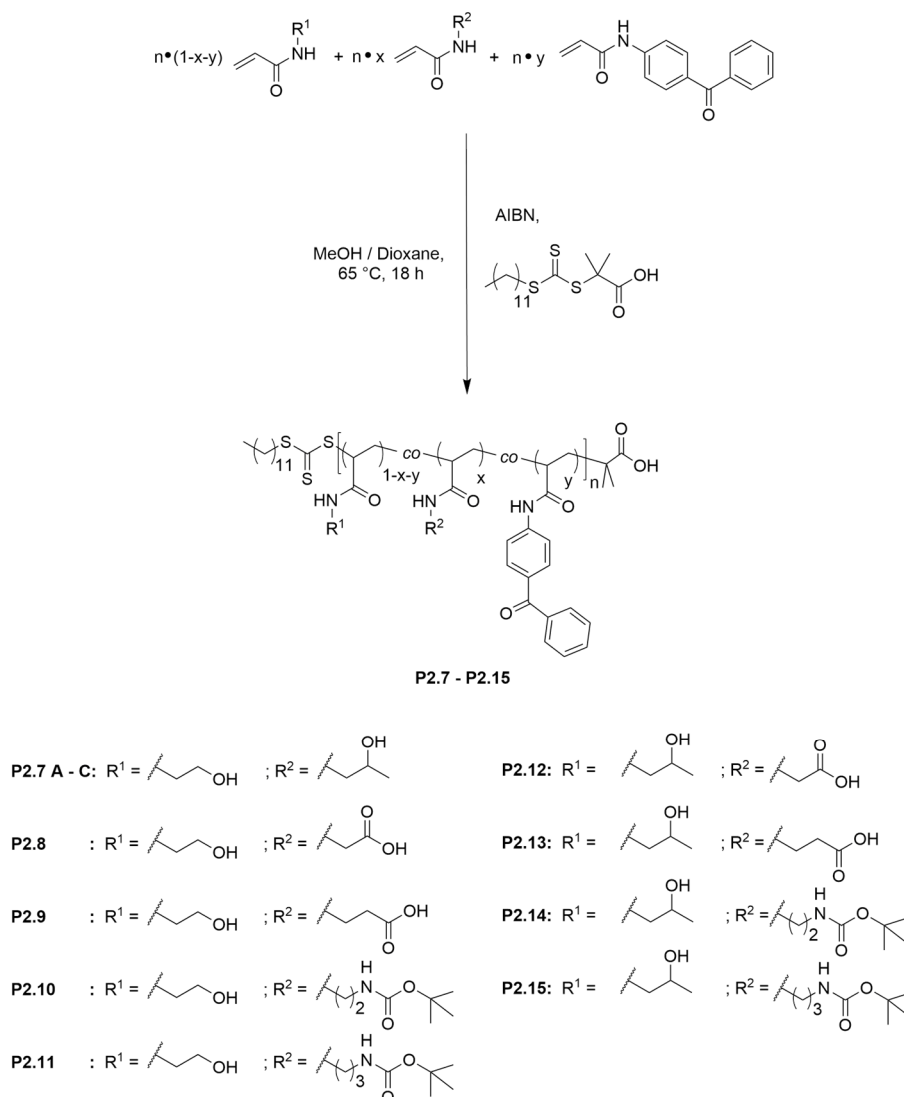
The calculated relative loss of molar mass was between 30-54%. Partially, this could be addressed to liberation of CO₂ and isobutylene, which led to a loss of molar mass. At full conversion of all monomers the relative loss of molar mass after deprotection of the amino groups and successful removal of salt moieties by anion exchange should be around 15-20% compared to the molar mass obtained before deprotection. The significant higher loss of molar mass indicates a change in the coiling behavior of the polymer chains due to an increase in polarity caused by the deshielding of the amino groups. Thus, polymer segment-polymer segment interactions become more likely than polymer segment-solvent interactions, which cause a shrinkage of the polymer coils.

Synthesis of N-substituted acrylamide terpolymers as hydrogel precursors:

For another project different acrylamide terpolymers containing two distinct functional groups in the side chain as well as a photocrosslinkable unit for gel formation were synthesized by RAFT polymerization. The synthesis protocols for *N*-(2-hydroxypropyl) acrylamide (HPAm) and *N*-(2-acetic acid) acrylamide (AaAm) were adapted from literature.^{9,11} *N*-(4-Benzoylphenyl) acrylamide was prepared according to a modified procedure, which is described in chapter 7.1.5 on page 284. The polymerization protocol was developed previously

during another thesis (*Synthesis of Multifunctional Hydrogel Coatings Using RAFT Polymerization for Potentially Improved Cell-Material Interactions*”, Master’s Thesis, Niklas Jung, 2016) and is similar to the above-mentioned polymerization route (Scheme 5.14).

Fairbanks and coworkers reported the synthesis of the novel HPAm and the polymerizability. Further, they could show that polymers containing HPAm possess low-fouling properties.⁹ The structural similarity of (2-hydroxyethyl) acrylamide (HEAm) compared to HPAm, which is commercially available, suggested the assumption that HEAm containing polymers could show a similar behavior in biological environment. Indeed, Zhao and coworkers could show that the cell cytotoxicity and protein absorption is low for copolymers of HEAm and acrylic acid.²⁰⁰ Therefore, the two monomers HEAm and HPAm were chosen to be the main components in the terpolymers. A second distinct functional group was introduced to use the resulting multifunctional polymers for further modification reactions, e.g. attachment of drugs. The second side chain functionality should be incorporated in low amounts (around 5%) to ensure the biocompatibility of the terpolymers. As photocrosslinkable monomer BPAm was used to prepare gels, which is extensively studied within the work group. From different synthesized copolymers containing BPAm, prepared in the work group, it was found that 2 mol% incorporated into co- and terpolymers is sufficient to form stable hydrogels. The used BPAm was prepared from 4-amino benzophenone and acryloyl chloride as described previously.¹² Since all monomers are acrylamides, it is expected that there is no crucial difference in their polymerization behavior. Hence, the initial weight ratios should be close to the build-in ratios along the polymer chain. The synthesis of the monomers HPAm and BPAm is discussed in the above-mentioned Master’s Thesis in detail.



Scheme 5.14: Schematic overview of the RAFT polymerization to obtain photocrosslinkable hydrophilic terpolymers which possess different functional groups for further reactions (**P2.7-P2.15**). **P2.7 A-C** are terpolymers possessing different ratios of HPAm to HEAm. The synthetic route was adapted from a previous thesis (*“Synthesis of Multifunctional Hydrogel Coatings Using RAFT Polymerization for Potentially Improved Cell-Material Interactions”*, Master’s Thesis, Niklas Jung, 2016).

The terpolymers were synthesized in MeOH/1,4-dioxane (2:1 v/v) as solvent mixture at $T = 65\text{ °C}$ for 18 h using AIBN as initiator. DMP was used as CTA and the ratio of all monomers to CTA again was set to 200:1 to obtain molar masses of $27.5\text{ kg}\cdot\text{mol}^{-1}$, theoretically. It was found, that for terpolymerization of the amino acid derivatives a more polar solvent is necessary, because during polymerization using the standard solvent mixture a precipitation of oligomers occurred. Therefore, the content of MeOH was increased, yielding a ratio of MeOH / 1,4-dioxane of 2.4 : 1 (v/v). The corresponding yields of **P2.7-15** and the

corresponding mass parameters of the obtained terpolymers, measured by GPC, are depicted in Table 5.15.

Table 5.15: Overview of the recorded molar masses and their distribution of the different *N*-substituted poly(acrylamide) terpolymers (**P2.7-15**) measured by GPC. The obtained values were calculated from the signal of the respective refractive index detector (RI-detector) using PMMA standards. The additional values in brackets (columns Monomer A and Monomer B) for the entries **P2.7 A-C** describe the relative monomer ratio of [HEAm] : [HPAm] at reaction start. The relative yields (%) are calculated according to the corresponding masses of the monomers.

Polymer ^a	Monomer A	Monomer B	\bar{M}_n^b / kg·mol ⁻¹	\mathcal{D}	Yield / mg (%)
P2.7 A	HEAm (0.25)	HPAm (0.75)	36.3	1.36	327 (78)
P2.7 B	HEAm (0.50)	HPAm (0.50)	39.4	1.19	308 (73)
P2.7 C	HEAm (0.75)	HPAm (0.25)	34.9	1.23	283 (66)
P2.8^c	HEAm	AaAm	31.9	1.25	286 (67)
P2.9^c	HEAm	PrAm	---	---	---
P2.10^c	HEAm	AEAm-Boc	38.0	1.18	302 (71)
P2.11^c	HEAm	APAm-Boc	34.7	1.31	332 (79)
P2.12^c	HPAm	AaAm	34.0	1.38	280 (66)
P2.13^c	HPAm	PrAm	---	---	---
P2.14^c	HPAm	AEAm-Boc	32.0	1.30	150 (36)
P2.15^c	HPAm	APAm-Boc	39.3	1.17	147 (35)

^a the monomer to CTA ratio [M₀] : [CTA] was adjusted to 200 : 1, yielding polymers of $\bar{M}_n \approx 27.5$ kg·mol⁻¹.

^b eluent: DMAc containing LiBr, $\beta = 1$ g·l⁻¹; PMMA standards were used for calibration

^c the relative ratio of the monomers [Monomer A] : [Monomer B] : [BPAm] was adjusted to 93 : 5 : 2 at reaction start

Terpolymers containing *N*-(3-propionic acid) acrylamide (PrAm) could not be successfully isolated (**P2.9** and **P2.13**). Probably, an undesired side reaction, like self-polymerization, occurred upon storage of PrAm, because the monomer did not dissolve completely in the solvent mixture used as medium for the copolymerization. The other terpolymers could be

isolated in typical yields for polymers (66%-79%), except terpolymers **P2.14** and **P2.15**, which contained the *N*-Boc-(2-aminoethyl) acrylamide (AEAm-Boc) and APAm-Boc. For these two terpolymers yields of 36% and 35% were obtained, respectively. The obtained \bar{M}_n and D , measured by GPC measurements, indicated successful polymerization in both cases, that led to the suggestion, that the loss of polymer mass caused by an insufficient workup.

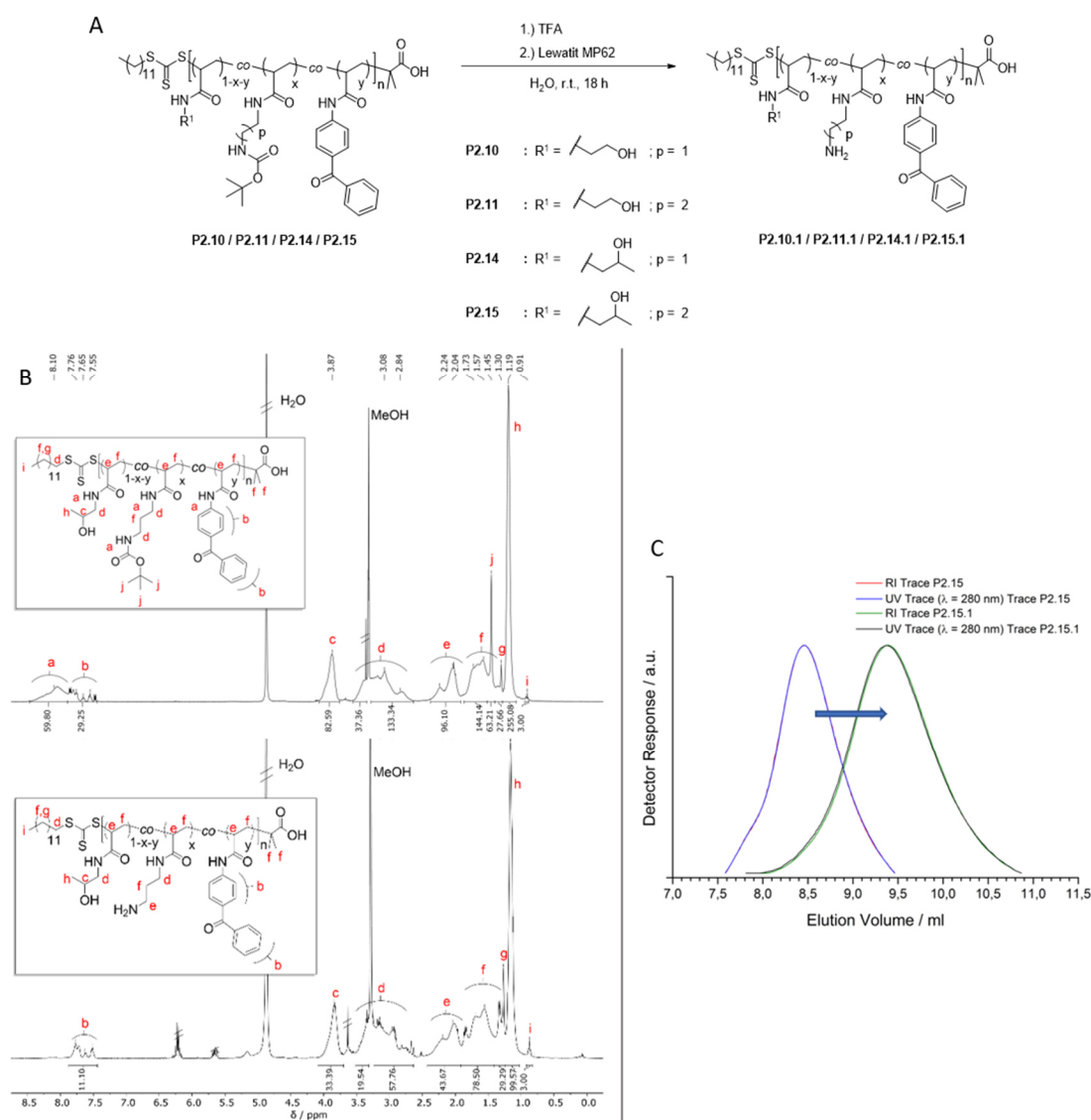


Figure 5.16: General outline of deprotection of the amino-functionalized photocrosslinkable RAFT terpolymers (A). On the left side, ¹H-NMR (400 MHz) spectra of **P2.15** before (above) and after deprotection using TFA (below) are illustrated (B). Both spectra were recorded in CD₃OD. On the right side, GPC traces of **P2.15** (red and blue line) and **P2.15.1** (green and black line) and the change of the elution volume are depicted (indicated by the blue arrow) (C). For the GPC measurements DMAc containing LiBr ($\beta = 1$ g·l⁻¹) was used as eluent.

The measured \bar{M}_n of all terpolymers **P2.7-P2.15** (31.9-40.0 kg·mol⁻¹) were larger than the calculated theoretical molar mass of 27.5 kg·mol⁻¹. The same trend was observed by the previous discussed copolymers **P2.3-P2.6**. Again, the solvent-polymer interaction became more likely, resulting in expanded polymer coils, which led to shorter elution times and higher molar masses. The dispersities varied from 1.17 (**P2.15**) to 1.36 (**P2.7 A**) and were in good agreement to dispersities observed for other polymers prepared by RAFT polymerization. The broadening of the molar mass distributions could be explained by the appearance of a second peak in the elugrams, similar to results obtained at the beginning of the chapter. Probably, an aggregation of polymer chain occurred that was induced by the hydrophobic dodecyl group of DMP or the hydrophobic benzophenone moieties. Compared to the relative peak heights in the elugrams described in Figure 5.15, the peak heights of the second mass peaks in the corresponding elugrams of **P2.15** and **P2.15.1** (depicted in Figure 5.16) are significant lower, which may led to the conclusion, that the number of potentially aggregated polymer chains increased with increasing content of amino-functionalities as pendant group implying a participation of those functionalities in the aggregation reaction. In general, the calculation of the built-in of the respective monomers was not possible, because overlapping of the signals in ¹H NMR spectroscopy. But as mentioned before, the high molar masses indicate a high conversion of the monomers. Together with the assumption of nearly equal reactivity of the acrylamide monomers it can be concluded that the built-in ratio is in the same range as the adjusted monomer ratio at reaction start.

Further, the content of photocrosslinkable groups in the polymers could not be well estimated since the overlapping of the signals b assigned to the aromatic systems ($\delta = 7.40-7.80$ ppm) and the signals a related to the protons of the amide groups ($\delta = 7.80-8.30$ ppm) as exemplarily shown in Figure 5.16. Deprotection of the Boc-protected amino groups along the polymer chains of **P2.10**, **P2.11**, **P2.14** and **P2.15** could be established by using TFA as shown in Figure 5.16. The experimental details are illustrated in General Procedure 20 on page 245. For this deprotection reaction MeOH was replaced by H₂O. The vanishing of signal j ($\delta = 1.45$ ppm), which correspond to methyl groups of *tert.*-butyloxycarbonyl group, indicate a successful deshielding of the amino groups. (Figure 5.16, right side). Interestingly, also the proton signals of the amide groups at signal a ($\delta = 7.80-8.30$ ppm) are not observable after deprotection, which could be attributed to a shift or the broadening due to the change of the local environment by the presence of free amino groups or the change of relative water content. Based on the

comparison of signal i ($\delta = 0.91$ ppm, CH₃- group of DMP) and signal b ($\delta = 7.40$ - 7.80 ppm, aromatic protons of benzophenone) as well as signal c ($\delta = 3.87$ ppm, CH₃- group of HPAm), the number of repeat units could be calculated. The calculation indicated a number around 35 repeat units, which is far too low compared to the desired 200 repeat units. Therefore, the calculation of the molar mass by using ¹H NMR spectroscopy is not suitable for this polymer system.

A better method for estimating the molar mass of **P2.10**, **P2.11**, **P2.14** and **P2.15** before and after deprotection (**P2.10.1**, **P2.11.1**, **P2.14.1** and **P2.15.1**) is the use of GPC. The obtained \bar{M}_n and \bar{D} values as well as the yield of the deprotection reactions for the terpolymers are listed in Table 5.16. The yields of the HEAm containing terpolymers **P2.10.1** and **P2.11.1** were higher (92% and 98%) than for the HPAm based terpolymers **P2.14.1** and **P2.15.1** (78% and 76%). The difference could be attributed to losses of polymer mass during the workup.

Table 5.16: Comparison of the molar masses and their distributions of the different amino group containing *N*-substituted poly(acrylamide) terpolymers before (**P2.10**, **P2.11**, **P2.14** and **P2.15**) and after deprotection (**P2.10.1**, **P2.11.1**, **P2.14.1** and **P2.15.1**) obtained by GPC. The obtained values were calculated from the signal of the respective refractive index detector. The relative yields (%) are calculated according to the corresponding masses of the monomers.

Polymer	Before Deprotection		After Deprotection		Yield / mg (%)
	\bar{M}_n^a / kg·mol ⁻¹	\bar{D}	\bar{M}_n^a / kg·mol ⁻¹	\bar{D}	
P2.10	38.0	1.18	33.3	1.18	98 (98)
P2.11	34.7	1.31	34.6	1.33	92 (92)
P2.14	32.0	1.30	11.0	1.18	39 (78)
P2.15	39.3	1.17	14.5	1.24	38 (76)

^a eluent: DMAc containing LiBr, $\beta = 1$ g·l⁻¹; PMMA standards were used for calibration

The dispersities are in a typical range for RAFT polymers. The change in the molar mass distribution is negligible and can be assigned to integration errors for **P2.10** and **P2.11**. More interesting is the comparison of the molar masses before and after deprotection of the masked amino groups (**P2.14** and **P2.15**). Whereas the measured molar mass of **P2.10** and **P2.11** stayed almost constant between 33.3 and 38.0 kg·mol⁻¹, a significant loss of molar mass is observed for the HPAm containing terpolymers **P2.14.1** and **P2.15.1**. The \bar{M}_n of both polymers dropped

from $32.0 \text{ kg}\cdot\text{mol}^{-1}$ (**P2.14**) and $39.3 \text{ kg}\cdot\text{mol}^{-1}$ (**P2.15**) to $11.0 \text{ kg}\cdot\text{mol}^{-1}$ (**P2.14.1**) and $14.5 \text{ kg}\cdot\text{mol}^{-1}$ (**P2.15.1**), which is in both cases a relative loss of 66% and 63%, respectively. This significant loss of molar mass give evidence for a degradation of the polymer chains during the deprotection. This is supported by the obtained lower yields and the comparison of the NMR spectra before and after deprotection, which demonstrate that the integrals of the backbone significantly decrease. Probably, an intramolecular chain transfer reaction from the active center of the propagating backbone to the isopropyl moiety of HPAm led to the formation of amide units within the polymer backbone that might be cleaved under the acidic conditions used for the deprotection of the amino functionalities.

Cell Studies:

The motivation for the above-described synthesis of the terpolymers is the potential application of such coatings for surgical implants. Therefore, these coatings have to fulfill different requirements like e.g., biocompatibility and adhesion of the coatings at the implant itself.

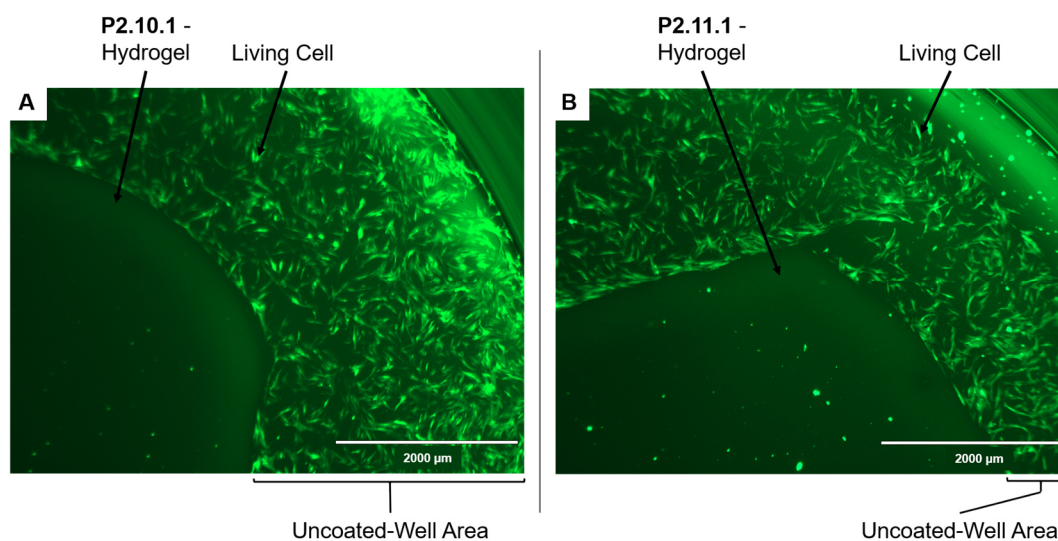


Figure 5.17: Fluorescence microscopy images of NHDF cells cultured on TCPS in the presence of a hydrogel made of **P2.10.1** (A) and a hydrogel made of **P2.11.1** (B). The living cells were stained green. (Kindly provided by Kira Vogel and PD Dr. Ulrike Ritz, University of Mainz)

First, tissue culture grade polystyrene (TCPS) well-plates were coated with the prepared terpolymers and irradiated at $\lambda = 365 \text{ nm}$ for 60 min according to the procedure described in chapter 7.1.5 on page 287. Initial cell viability experiments of all synthesized and photo-crosslinked copolymers **P2.7-P2.15.1** were performed by Kira Vogel under supervision of PD Dr. Ulrike Ritz at the university of Mainz.

Exemplarily, fluorescence microscope images of cell viability tests of wells, which were

partially coated with **P2.10.1** and **P2.11.1** hydrogels, are depicted in Figure 5.17. Both pictures demonstrate that normal human dermal fibroblasts (NHDF) cells do not accumulate on both hydrogels. Further, no dead cells are present in the medium, implying that the cells are not affected by the presence of the hydrogel. Similar results were obtained with the other tested hydrogels composed of **P2.14.1** and **P2.15.1**, respectively. In following experiments, these hydrogels will be tested as coatings for titanium, which is used as material for surgical implants.

Summary:

In this chapter, the synthesis of *N*-substituted polyacrylamides carrying different functionalities like amino-, hydroxy- and carboxylate units as pendant groups by RAFT polymerization is discussed. Therefore, a set of protected amino group containing monomers (AXAm-Boc) with different spacer lengths were successfully prepared in a two-step synthesis involving first the mono-Boc protection of one amino group and subsequent functionalization by an acrylation of the respective unprotected amino group. The yielded protected amino-functionalized monomers were copolymerized with HEAm in a RAFT polymerization (**P2.3-P2.6**). The deshielding of the amino groups after successful polymerization was accomplished by using TFA. The resulting novel copolymers with hydroxy- and amino groups were tested as candidates in gene delivery (chapter 5.5).

Further, unique photocrosslinkable terpolymers carrying hydroxy groups and carboxylic acid or amino groups were prepared as precursor of hydrogels, which may find application as biocompatible coating for implants (described above). Therefore, the above-described library of *N*-substituted acrylamides was extended by the synthesis of the hydroxy group carrying HPAm and the carboxylic acid containing AaAm. The novel co- and terpolymers **P2.7-P2.15** could be synthesized with the same reaction conditions as developed for **P2.3-P2.6**. Again, the deshielding of the amino groups in the respective terpolymer was done by using TFA (**P2.10.1**, **P2.11.1**, **P2.14.1** and **P2.15.1**). Initial cell viability experiments of these terpolymers demonstrated that NHDF cells did not accumulate on the resulting hydrogels, which implied a good tolerance of this cell type. Further experiments will be direct towards testing these hydrogels as potential coatings on surgical implants.

5.3 Synthesis of thermoresponsive Polymer-DNA Conjugates as Building Blocks for Smart Materials

Deoxyribonucleic acid (DNA) is nowadays a powerful building block in terms of nanotechnology,^{201–203} which was first suggested by Seeman in the 1980s.²⁰⁴ Features like the high selective (self-) assembly, the spontaneous arrangement of compounds into ordered structures, and the well-defined, rigid structure allows the design of objects in nanoscale precision.^{201–203} Further, the sequence of the base pairs can be controlled during synthesis, which directly influences the assembly behavior.^{202,203}

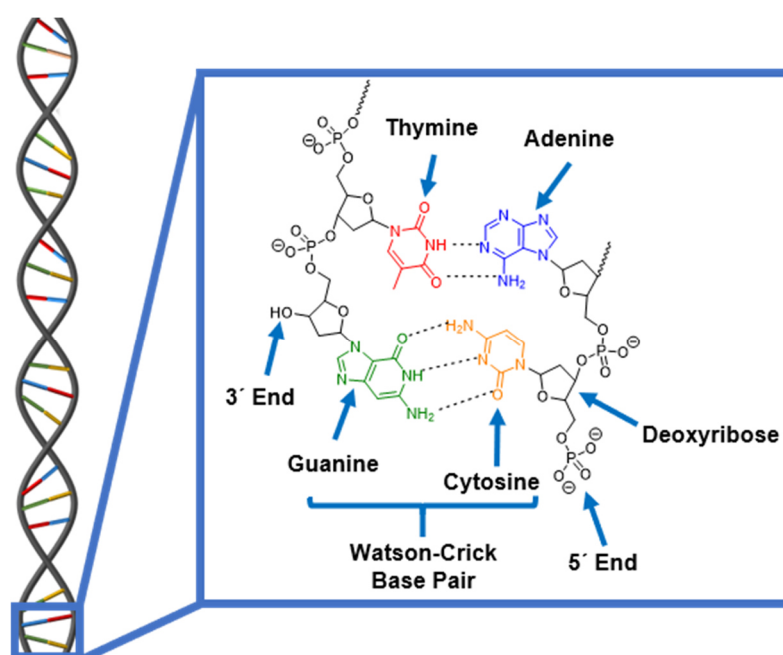


Figure 5.18: Simplified structure of a double-stranded DNA molecule (left) with an enlargement to visualize the chemical structure (right).

In general, DNA consists of four different nucleobases, which are attached to five-membered deoxyribose units that are again interconnected by phosphate groups. The nucleobases adenine and guanine belong to the class of purines and can form specifically hydrogen bonds to the pyrimidine derivatives thymine and cytosine, respectively. These specific hydrogen-bond motifs are called Watson-Crick base pairs (Figure 5.18).²⁰⁵ Together with the π - π stacking of the nucleobases, which is more important for the stability of the double-stranded DNA than the base pairing itself,²⁰⁶ two DNA strands can arrange into a double helix, which is called DNA hybridization. Further, the two associated strands are antiparallel, which means that the 3'-deoxyribose end is aligned with the 5'-sugar-end of the other strand (Figure 5.18).

Typically, the so-called double-stranded or duplex DNA (dsDNA) is a highly charged molecule that possess a geometrical diameter of 2 nm and helical pitch length of 3.4 nm. Each helical turn consist in average of 10.5 base pairs.²⁰³ It could be demonstrated that this type of DNA behaves like a rigid rod, because the contour length is smaller than its persistence length (50 nm), which is an indicator for the stiffness of a macromolecule.²⁰³

DNA as motif in nanoscience:

DNA is nowadays used as a nanoscale programable motif in the area of nanotechnology based on bottom-up self-assembly. Two different approaches are used that are inspired from molecular biology to generate structures with DNA strands.²⁰³ The first concept is called DNA crossover junction and is based on a strand that starts in one DNA helix and switch over to a second helix yielding branched DNA molecules that can assemble in two- or three dimensional constructions.²⁰⁴ The second approach is known as sticky-end cohesion. Requirement for this very specific and programmable interaction, is the presence of a short single-stranded end (sticky-end) at one end of the duplex DNA, which can interact with e.g. a duplex DNA containing a complementary single-stranded end.^{203,204} Over the years, several research groups extended the above described concepts towards more complicated shapes by increasing e.g. the number of crossover points^{207,208} or the development of other complex motifs^{209–212} and crossover techniques.²¹³

In 2006, Rothmund reported a technique that can significantly increase the complexity and extend the range of DNA nanostructures.²⁰³ Single-stranded DNA (ssDNA) is folded by the presence of hundreds of other ssDNA strands, which act as staples that direct and connect the scaffold leading to a variety of two-dimensional patterns with arbitrary complexity.²¹⁴ Over the years, this approach was extended by different groups to obtain three-dimensional structures.^{215–217} Contrary, Yin and coworkers developed a concept, which creates also complex objects, but without using a scaffold.²¹⁸ They used ssDNA containing four different sections that are able to build DNA lattices, which are formed of neighbored strands by specific interactions of the different sections of the DNA. Consequently, these pattern can be used as template that can be modified for different arbitrary shapes by variation of the sequences of the used ssDNA strands.^{203,218}

Nevertheless, the high selectivity of the nucleobases can also cause several issues like the limited scalability of the designed DNA strands or errors in the self-assembly, which may lead

to short-ranged ordered systems.¹⁸ Further, a large number of unique sequences is needed to achieve the desired self-assembly behavior.

A completely different approach in soft matter science is based on microphase separation of copolymers composed of blocks that are chemically different.^{219,220} A recently published paper suggests that this approach can be a parallel mode of self-assembly in DNA nanotechnology.¹⁸ The combination of these dissimilar blocks within one macromolecule enables interesting assembly phenomena in nanoscale range, which also affect the macroscale behavior of such systems.^{220,221} Furthermore, many physical properties of such systems cannot be obtained by simple blending of the non-linked blocks. Most block copolymer systems in solution are composed of a more hydrophilic and a more hydrophobic block.^{222,223} The self-assembly of such amphiphilic molecules in one-, two- and three-dimensional systems is mostly driven by the tendency of hydrophobic moieties to aggregate in aqueous environment.^{224,225} Depending on different parameters, like volume fraction of the hydrophilic and hydrophobic blocks, the steric repulsion of the hydrophilic chains as well as the interfacial energy between the hydrophobic moieties and the aqueous environment various geometries like vesicles, spheres or cylinder can be obtained.^{224,226} This results in nanostructures like micelles and liposomes,²²⁷ which can be used in applications like biocatalysis,²²⁸ nanomedicine²²⁹ as well as drug delivery^{230,231} or microencapsulation.²³²

The combination of the DNA-based self-assembly mechanism and the self-assembly mechanism of block copolymers held promise to circumvent the above-mentioned problems in the self-assembly of DNA while retaining e.g. information encoded in the DNA sequence.¹⁸ To date this approach is limited to the construction of programmable micelles, vesicles and nanotubes or nanofibers.^{233–237}

Click chemistry:

A well-established coupling technique for combining two different blocks^{169,220} is the so-called “Click” chemistry, which was described by Sharpless and coworkers in 2001.²³⁸ The features of this class of reactions are the high yields, easy purification of the products, regio- and stereoselectivity, insensitivity to oxygen and water, orthogonality to other organic reactions and versatility of compounds that can be used as starting materials.²³⁹ One of the most applied reaction is the copper-catalyzed azide-alkyne cycloaddition reaction (CuAAC),²⁴⁰ because of the very efficient reaction of a terminal alkyne group connected to one building block and an

azide group containing block, which form a stable 1,2,3-triazole. The reaction itself was described in the 1960s by Huisgen,²⁴¹ but the usage of catalysts like copper, reported independently by Sharpless and coworkers²³⁸ and Meldal and coworkers,²⁴² gained attention to this reactions, since mild conditions could be used in presence of the catalysts instead of the harsher requirements typically necessary for these 1,3-dipolar cycloadditions without such a stimulant. However, the usage of Cu-based catalysts can cause problems, especially if reactions are performed in biological environment, since copper is cell-toxic.²⁴⁰ Additionally, Cu^+ , which is the catalytic active species, is rather unstable and will be oxidized to Cu^{2+} in solution.^{238,240} Thus, the active species Cu^+ is typically formed *in situ* by using a reducing agent like sodium ascorbate.²⁴³ Unlikely, it could be shown that the combination of Cu^+ and sodium ascorbate support the oxidation of biomolecules like histidine and arginine.²⁴⁴ In 2004, Bertozzi and coworkers reported a different approach, called strain-promoted azide-alkyne cycloaddition, which make the use of catalysts expendable (Figure 5.19).²⁴⁵

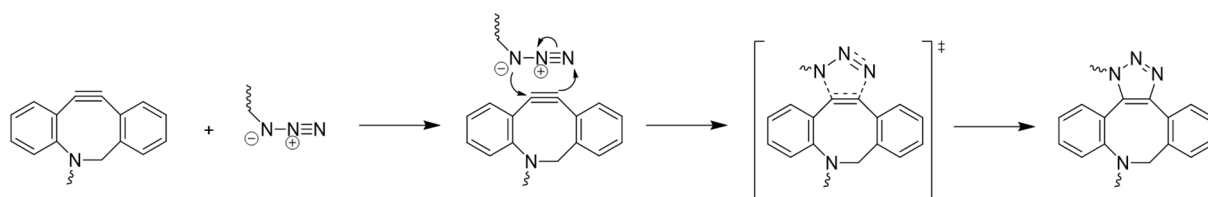


Figure 5.19: Simplified mechanism of the SPAAC reaction

Key feature of this reaction pathway is the replacement of the terminal aliphatic alkyne group by a strained cyclooctyne moiety. Driving force of the fast reaction of the cyclooctyne and the azide is the high degree of ring strain ($75.3 \text{ kJ}\cdot\text{mol}^{-1}$), which allows mild reaction conditions.^{240,246} It has to be mentioned, that contrary to the CuAAC pathway, the SPAAC pathway do not provide regioselectivity, resulting in a mixture of 1,4-substituted products.²⁴⁰ Further, the low solubility of the cyclooctyne moieties in aqueous mediums is a disadvantage, but the solubility could be improved e.g. by introduction of PEG moieties²⁴⁰ or the coupling to other hydrophilic polymers like poly(2-oxazoline)s or poly(NiPAm) as described in chapter 5.1.1 and 5.2.1.

Background for the recent investigation:

In a recent publication, both above described self-assembly mechanisms, borrowed from block copolymers and DNA, were combined and used for designing different architectures consist of DNA and poly(NiPAm), which was prepared by free radical polymerization.¹⁸

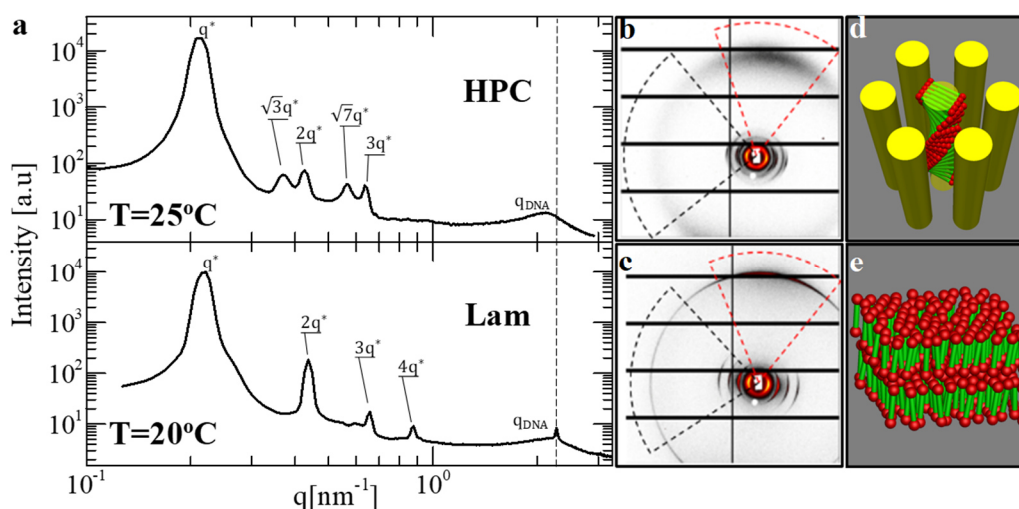


Figure 5.20: (a) 1D small-angle X-ray scattering (SAXS) measurements of the poly(NiPAm)-DNA-poly(NiPAm) (linear coil-rod-coil) conjugates at $T = 20^\circ\text{C}$ (bottom) and $T = 25^\circ\text{C}$ (top) and the corresponding 2D-SAXS patterns (b and c). Schemes of the packing arrangement of the coil-rod-coil (L-CRC) molecules inside the lamellar (e, Lam) and hexagonally packed cylinders (d, HPC) structures. The DNA and polymer segments are illustrated as green cylinder and red ball, respectively. Reprinted with permission from Reference 18. Copyright © 2020 American Chemical Society.

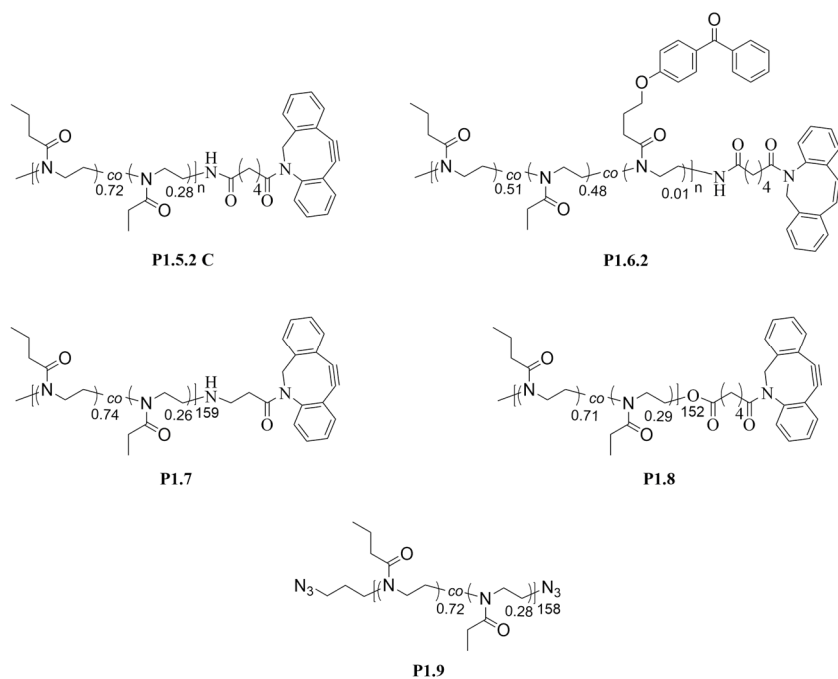
It was found by small-angle X-ray scattering (SAXS) experiments that these systems formed several different phases ranging from a lamellar to ordered bicontinuous double diamond phase depending on the concentration and the temperature.¹⁸ In Figure 5.20 a, selected 1D-SAXS patterns at concentrations above the liquid crystal ordering of DNA are shown, which demonstrate the change in the self-assembly behavior of the investigated L-CRC system upon temperature modulation. The corresponding 2D-SAXS profiles (Figure 5.20 b and c) revealed that this system arrange in lamellar packed cylinders (Figure 5.20 e) at $T = 20^\circ\text{C}$. Interestingly, a chiral hexagonally packed cylinder phase (Figure 5.20 d) was detected at $T = 25^\circ\text{C}$, which is typically found in liquid crystals and cannot be stabilized for bare DNA rod-like motifs.¹⁸

In order to extend this approach and to understand the self-assembly behavior of such polymer-DNA conjugates in more detail, different linear systems composed of rigid DNA molecules and flexible, thermoresponsive (co-)polymers should be prepared by combining the toolkit from synthetic polymer chemistry and DNA nanotechnology, which will be demonstrated by integrating the block copolymer approach to DNA nanotechnology.

Therefore, two different sets of DBCO-functionalized thermoresponsive polymers were synthesized, which both exhibit a T_c in the range of 30°C . NiPAm-based (co-)polymers were prepared by RAFT polymerization and oxazoline-based co- and terpolymers were prepared by

CROP, in order to obtain polymers with defined molar masses and narrow molar mass distributions (chapter 5.1.1 and 5.2.1). In addition, crosslinkable derivatives were prepared by incorporation of benzophenone units into the polymers. These derivatives allow a better investigation of the corresponding self-assembly behavior of the polymer-DNA system since the shape can be locked by irreversible crosslinking. Moreover, these systems may find application as templates for organizing gold nanoparticles into a diamond lattice to fabricate photonic crystals.^{20,21}

A relative cheap, fast and powerful way to test the coupling reactions is based on the migration of the Polymer-DNA complexes in a gel matrix. These gel electrophoresis experiments were performed by Dr. Emmanuel Stiakakis and Sanja Novak at the Research Centre Jülich and were kindly provided for discussing the efficiency of the coupling reactions. Experimental details for the coupling reactions and the gel electrophoresis experiments are specified in literature.¹⁸



Determination of the phase transition temperatures of the copolymers:

Prior the coupling of the polymers to DNA, cloud point temperatures (T_c) were determined by UV-Vis spectroscopy (see chapter 6.9), which could be a first indication for possible phase

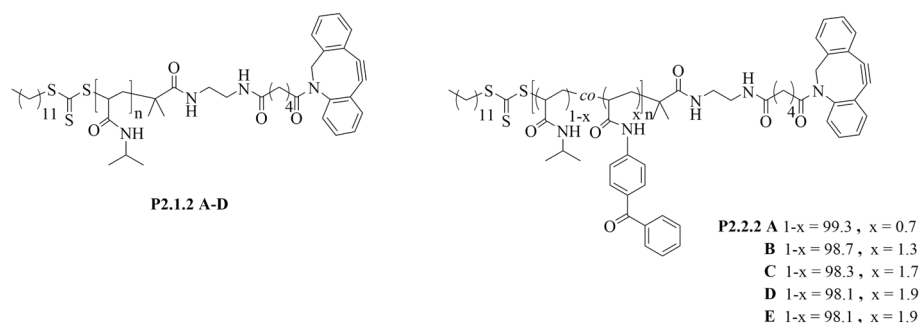
transition temperatures of the polymer-DNA systems. In the following Table 5.17, the measured T_c for each poly[(EtOxa)-co-(nPrOxa)], used for preparing these conjugates, is listed.

Table 5.17: Listing of the obtained molar masses and dispersities of poly(2-oxazoline) derivatives, discussed in this chapter, as well as the corresponding cloud point temperature (T_c) determined by UV/Vis spectroscopy. The mass parameters were measured using GPC. Structures are depicted above.

Polymer P1.	\bar{M}_n^a (RI Signal) / kg·mol ⁻¹	\bar{D}	T_c (UV-Vis) / °C
5.2 C (3)	11.3	1.14	28.8
5.2 C (4)	17.9	1.08	28.4
6.2	9.4	1.38	34.1
7	11.1	1.10	30.9
8	11.3	1.20	32.8
9	13.7	1.16	35.1

^a eluent: DMAc containing LiBr, $\beta = 1 \text{ g}\cdot\text{l}^{-1}$; PMMA standards were used for calibration

For the copolymers **P1.5.2 C**, **P1.7** and **P1.8** cloud points were obtained that are close to the targeted temperature of 30 °C, respectively. The higher T_c obtained for **P1.6.2** ($T_c = 34.1 \text{ °C}$) may arise from the increased EtOxa content (49% instead of 30% for **P1.5.2 C**, **P1.7** and **P1.8**) incorporated into the polymer, which was used to compensate the influence of the hydrophobic benzophenone moieties that would lead to a decreased T_c . **P1.9** carries instead of a bulky, hydrophobic DBCO moiety two azide groups at its distal ends, which may explain the higher T_c of 35.1 °C compared to those copolymers with same EtOxa-to-nPrOxa ratio (**P1.5.2 C**, **P1.7** and **P1.8**). The same measurements were done for the NiPAm based homo- and copolymers and the results are listed in Table 5.18. The trend for the DBCO-functionalized homopolymers indicates that the end group has a negligible influence on the T_c in polymers with molar masses larger than 25.8 kg·mol⁻¹, which is in agreement with observations reported by other groups.^{45,247–249}



For **P2.1.2 A** a lower T_c was observed, since the hydrophobic DBCO group attached to the short polymer chain decreases the overall hydrophilicity of the chains. Further, Table 5.18 shows that with increasing content of benzophenone moieties in the polymer chains the observed T_c decreased, which can be assigned to the hydrophobic character of these moieties.

Table 5.18: Overview of the obtained molar masses and dispersities of poly(NiPAm) derivatives, discussed in this chapter, as well as the corresponding cloud point temperature (T_c) determined by UV/Vis spectroscopy. The mass parameters were measured using GPC. Structures are depicted above.

Polymer P2.	\overline{M}_n^a (RI Signal) / $\text{kg}\cdot\text{mol}^{-1}$	\overline{D}	T_c (UV-Vis) / $^\circ\text{C}$
1.2 A	6.6	1.31	27.6
1.2 B	25.8	1.18	32.7
1.2 C	32.4	1.27	32.8
1.2 D	21.5	1.43	32.8
2.2 A	19.8	1.35	31.6
2.2 B	22.1	1.29	29.1
2.2 C	22.2	1.30	27.7
2.2 D	23.0	1.29	26.9
2.2 E	18.9	1.28	24.7

^a eluent: DMAc containing LiBr, $\beta = 1 \text{ g}\cdot\text{l}^{-1}$; PMMA standards were used for calibration

Polymer-DNA coupling experiments:

Initially, **P1.13 I** was functionalized with a PEG-derivative of DBCO as shown in Figure 5.21. This copolymer was tried to couple to a dsDNA, which is composed of 48 base pairs and carries at both 5' ends an azide group [N3-dsDNA-N3 (ds48b0T)]. Below, the gel electrophoresis pattern, containing 5% polyacrylamide (PAGE, 5%), of the coupling experiments with varying polymer to DNA ratios is illustrated (Figure 5.21). The migration of the stained dsDNA indicated in both tested coupling ratios an unsuccessful coupling of the DBCO-functionalized

polymer to the azide-functionalized dsDNA. As discussed in chapter 5.1.1, the poor coupling arises from an insufficient degree of DBCO functionalization of the copolymer caused by an unexpected termination reaction using ammonia and a loss of reactive end groups during polymerization.

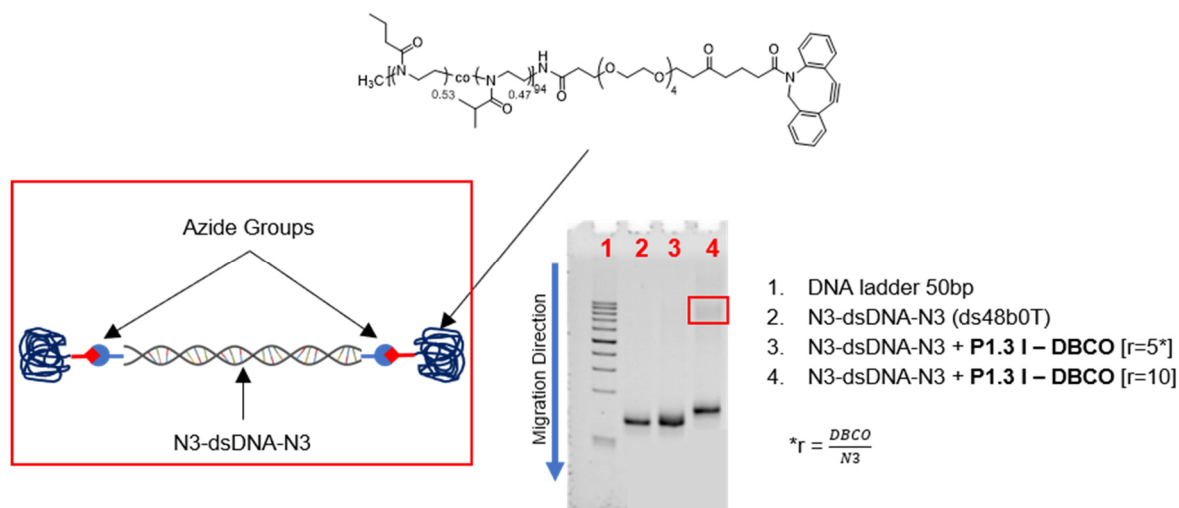


Figure 5.21: Poly(acrylamide) (PAGE) electrophoresis pattern of **P1.13 I-DBCO** after coupling of N3-dsDNA-N3 in different ratios. The red frame indicates the location of the L-CRC conjugate in the gel. The gel electrophoresis patterns were kindly provided by Emmanuel Stiakakis.

Therefore, the copolymer system (replacement of iPrOxa by EtOxa) as well as the functionalization strategy was changed, which is described previously. The electrophoresis pattern of **P1.5.2 C (3)** and its photocrosslinkable derivative **P1.6.2** showed that the dsDNA could be quantitatively functionalized with both poly(2-oxazoline) derivatives (Figure 5.22) since a broad band was observed in both patterns, which did not migrate as fast as bare dsDNA (compare line 2) due to the larger size of the polymer-DNA complexes. Further, no band arising from migration of bare DNA in the lines 3-5 were observed.

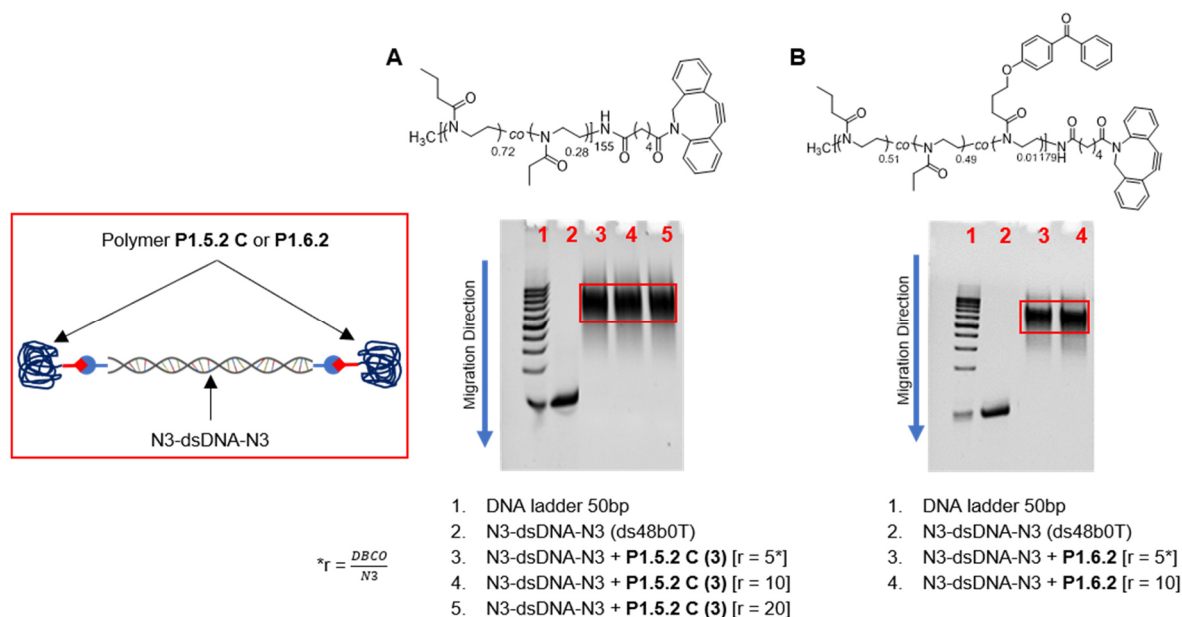


Figure 5.22: PAGE (5%) electrophoresis pattern of **P1.5.2 C (3)** (A) and **P1.6.2** (B) after coupling of N3-dsDNA-N3 in different ratios. The red frame indicates the location of the L-CRC conjugate in the gel. The gel electrophoresis patterns were kindly provided by Emmanuel Stiakakis.

P1.6.2 possess the advantage that the polymer chains can be crosslinked by irradiation of UV light due to the incorporated benzophenone groups. Therefore, the corresponding structure of the polymer-DNA-polymer conjugates, in the following denoted as linear coil-rod-coil (L-CRC) conjugates, formed by changes of the temperature or concentration can be immobilized, which facilitate its investigation. It was found that even small ratios $r = \frac{DBCO}{N3}$ of 5 were sufficient to obtain L-CRC conjugates. The broadening of the stained polymer-DNA systems may arise from overloading of the wells or the dispersity of the polymers.

Basically, the copolymers **P1.7** and **P1.8**, which were directly terminated with DBCO-amine and DBCO-COOH, showed a significant decreased ability to form L-CRC architectures. A lower coupling efficiency of **P1.7** was expected, since the obtained degree of DBCO-functionalization (65%) was significantly lower compared to the degrees calculated for **P1.5.2 C** and **P1.6.2** (83-96%), as described in chapter 5.1.1. Surprisingly, the gel electrophoresis pattern of **P1.7** demonstrated that almost no polymer-DNA conjugate was formed (Figure 5.23 A) in all tested polymer-to-DNA ratios.

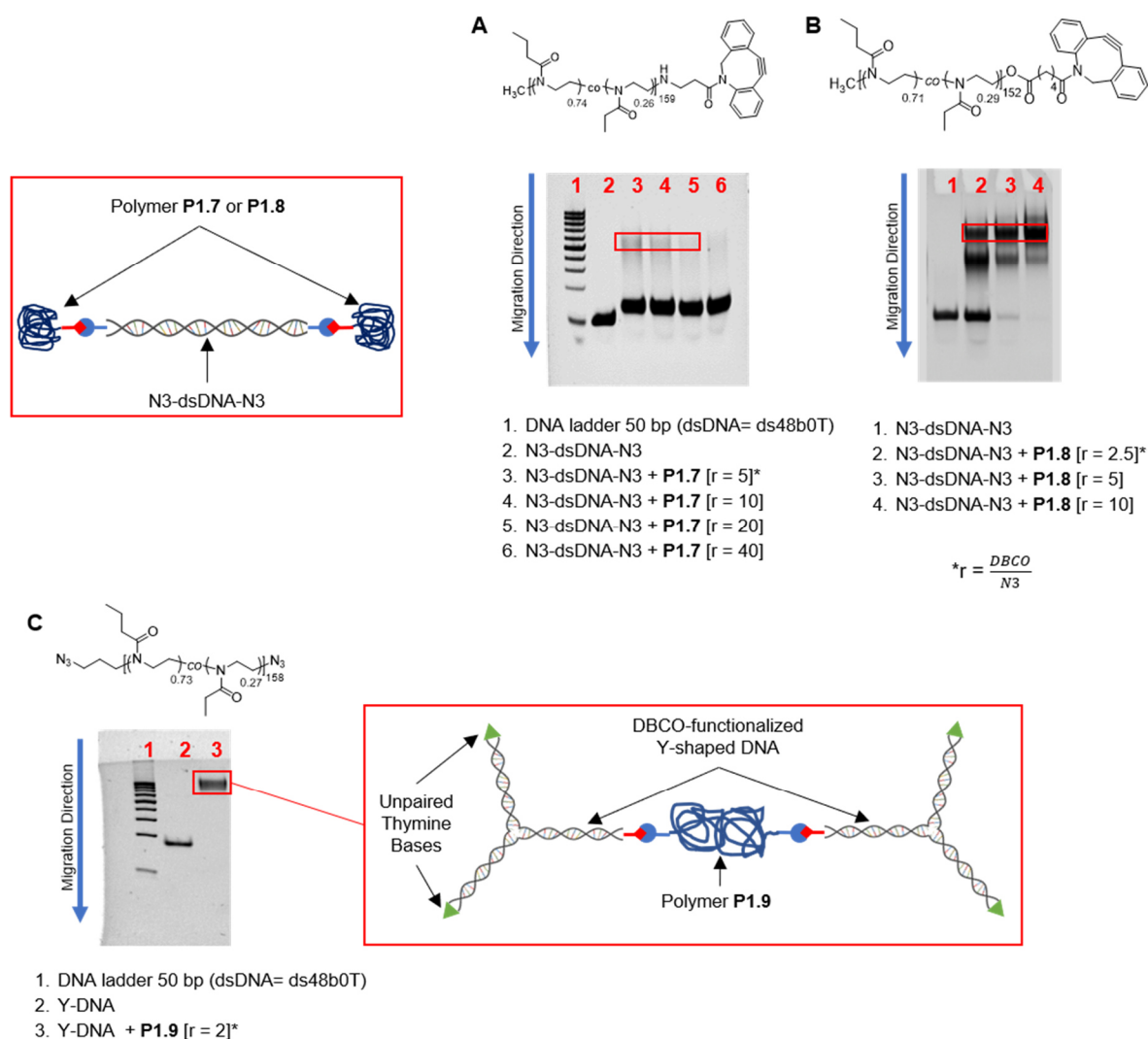


Figure 5.23: PAGE (5%) electrophoresis pattern of **P1.7** (A) and **P1.8** (B) after coupling of N3-dsDNA-N3 in different ratios. **P1.9** was coupled in different ratios to Y-shaped DNA, which was functionalized with DBCO groups (C). The red frame indicates the location of the L-CRC- or RCR-conjugate in the gel. The gel electrophoresis patterns were kindly provided by Emmanuel Stiakakis.

Further, the slightly slower migrating bands (line 3-6) indicate that the dsDNA had reacted with a small molecule like free DBCO-amine. This might be arising from an insufficient DBCO-functionalization of the polymer chains, which probably led to the formation of an ionic structure with DBCO moieties as counter ion. For the coupling reaction of **P1.8** with dsDNA, the gel electrophoresis pattern (Figure 5.23 B) implies that no quantitative reaction of the azide groups of the dsDNA with the DBCO-functionalized polymer occurred. However, the coupling efficiency increased with increasing r , but even at the highest tested ratio of $r = 10$ a mixture of unreacted and partial modified DNA beside the targeted polymer-DNA-polymer conjugate was observed. Interestingly, the degree of DBCO functionalization (43%) was lower than for **P1.5.2**

(83-96%) and **P1.7** (65%), but it showed a much better coupling ability than **P1.7**, supporting the hypothesis that the termination reaction with DBCO-amine in case of **P1.7** did not lead to a formation of the desired DBCO end group.

Polymer **P1.9**, which carries two azide groups at both distal chain ends, was prepared to fabricate DNA-based dendritic-linear-dendritic copolymers. The copolymer was coupled to 5' DBCO-functionalized all-DNA dendrons of the first generation (Y-DNA)²⁵⁰ in which the other 5' ends were terminated with unpaired thymine bases. The gel electrophoresis pattern (Figure 5.23 C) illustrates, that these rod-coil-rod (RCR) conjugates could be efficiently prepared even in small DNA-to-polymer ratios ($r = 2$), indicating a high degree of azide groups at the chain ends of **P1.9**. The obtained conjugates were the subject of SAXS experiments. These measurements demonstrated that such polymer-DNA conjugates can assemble in a unique type of phase, which is called cluster crystals.¹⁹ This phase behavior was predicted by theory but has not been experimentally realized so far.^{251–253}

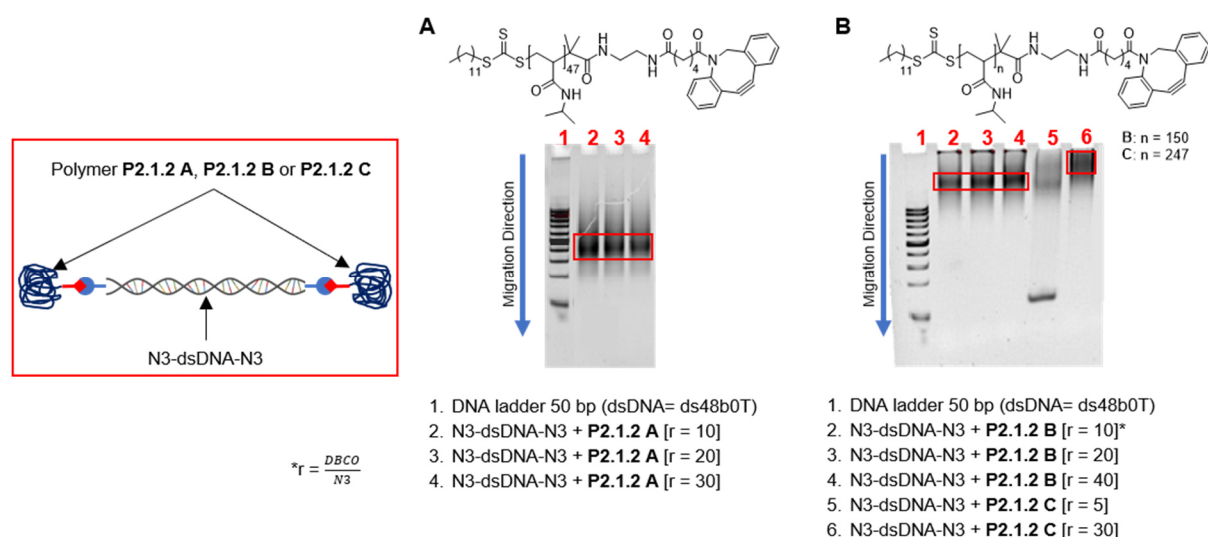


Figure 5.24: PAGE (5%) electrophoresis pattern of **P2.1.2 A** (A) and **P2.1.2 B** and **C** (B) after coupling of N3-dsDNA-N3 in different ratios. The red frame indicates the location of the L-CRC conjugate in the gel. The gel electrophoresis patterns were kindly provided by Emmanuel Stiakakis.

Poly(NiPAm) derivatives, prepared by RAFT polymerization, were used for preparing polymer-DNA-systems in order to extend the investigations and results, which were recently published.¹⁸ Similar to the polyoxazoline derivatives **P1.5** and **P1.6**, DBCO-functionalized homopolymers of NiPAm (**P2.1.2**) were prepared with molar masses ranging from $\bar{M}_n = 4.7$ to $32.4 \text{ kg}\cdot\text{mol}^{-1}$. The gel electrophoresis patterns for DBCO to azide ratios are illustrated above (Figure 5.24). Both patterns indicate, that independent of the molar mass a ten-fold excess of

DBCO-functionalized polymer in relation to one azide group of the DNA must be used to obtain L-CRC conjugates, which is twice as for **P1.5.2** and **P1.6.2**. Obviously, the coupling efficiency of PNiPAm is decreased compared to the poly(2-oxazoline) derivatives. This is contradictory, since the molar masses and their distributions indicated a controlled polymerization process and thus the RAFT agent, which carries the reactive end group, has to be incorporated into the poly(NiPAm) chains. Probably, unexpected side reactions led to a loss or degradation of DBCO end groups. Noticeable is that for **P2.1.2 C** an even higher excess of $r = 30$ was necessary to obtain polymer-DNA-polymer systems, which might be explained by the loss of reactive end groups during polymerization, as described in chapter 5.2.1.

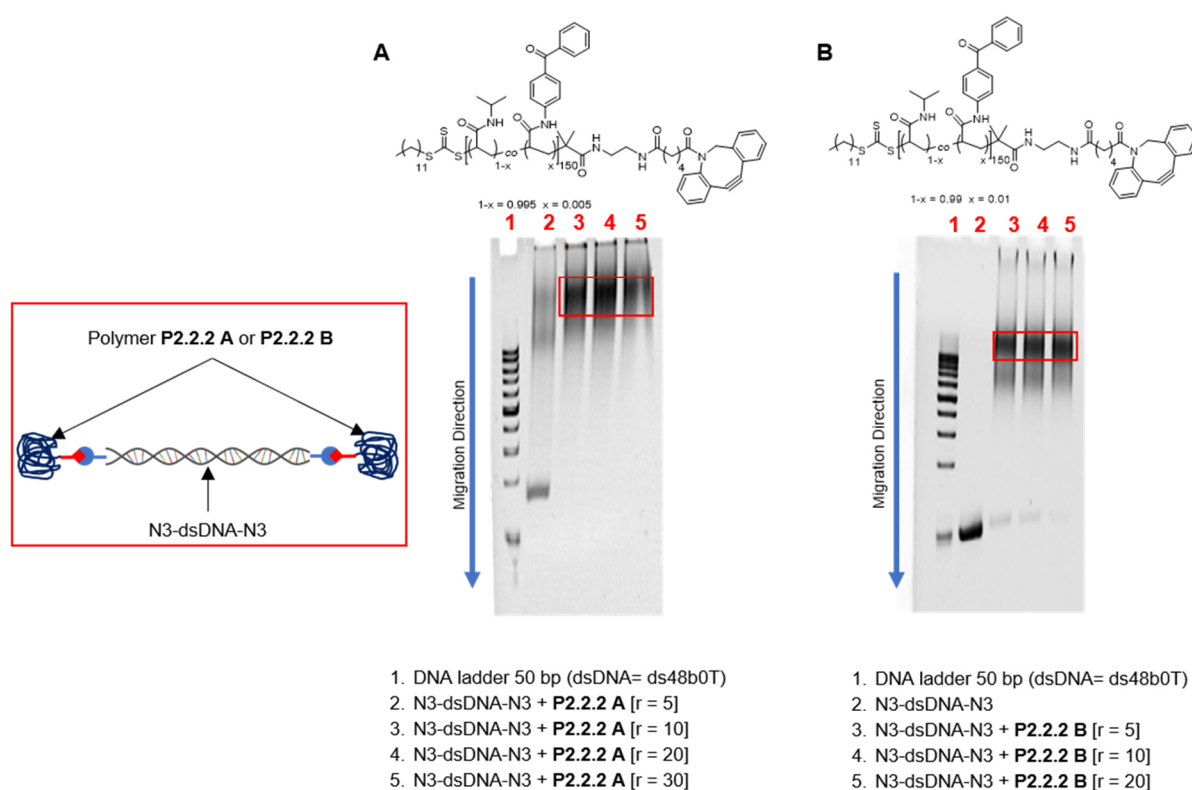


Figure 5.25: PAGE (5%) electrophoresis pattern of **P2.2.2 A** (A) and **P2.2.2 B** (B) after coupling of N3-dsDNA-N3 in different ratios. The red frame indicates the location of the L-CRC conjugate in the gel. The gel electrophoresis patterns were kindly provided by Emmanuel Stiakakis.

According to the photocrosslinkable poly(2-oxazoline) **P1.6.2**, also photocrosslinkable poly(NiPAm) copolymers with varying content of benzophenone moieties (0.5%-2.5%) were synthesized. The crosslinking of the prepared polymer-DNA systems at a certain temperature facilitates the investigation of the aggregation behavior since the formed superstructure is irreversible locked. Exemplarily, the prepared gel electrophoresis patterns for the two

copolymers containing the lowest amounts of the photo-crosslinker **P2.2.2 A** (0.5%) and **P2.2.2 B** (1.0%) are depicted in Figure 5.25. For both copolymers it was found, in accordance with **P2.1.2 A-C**, that a minimum ratio of DBCO to azide of 10 is needed to obtain an almost quantitative SPAAC reaction at both azide ends of the DNA. The gel electrophoresis pattern, which demonstrate the coupling efficiency of the copolymer with higher content of benzophenone (**P2.2.2 C** and **P2.2.2 D**) showing the same trends as observed for the above-described copolymers (Figure S88).

Summary:

In summary, it could be demonstrated that integration of synthetic polymer chemistry into the field of DNA nanotechnology is possible by combining the concepts of block-copolymers and DNA technology. The coupling reaction of DBCO-functionalized poly(2-oxazoline)s with dsDNA was successful even at comparable low DBCO-to-azide ratios ($r = 5$) indicating an efficient DBCO-post-functionalization strategy of the hemi-telechelic POxas. However, the copolymers **P1.7** and **P1.8**, prepared by quenching the CROP with DBCO-amine and DBCO-COOH respectively, showed significant lower (**P1.8**) or even no coupling to DNA (**P1.7**), which may arise from undesired side reactions of the labile DBCO moieties. Additionally, a homo-telechelic POxa copolymer (**P1.9**) that carries azide groups at both backbone ends, was very efficiently in even low polymer-to-DNA ratios coupled to y-shaped DNA, which carries a DBCO-group at one 5'-end. The obtained conjugates showed in SAXS experiments a unique self-assembly into a so-called cluster crystal phase, which has not been experimentally realized so far.¹⁹

Based on recently published results,¹⁸ DBCO-functionalized poly(NiPAM)s were prepared by RAFT polymerization with varying molar masses (**P2.1.2 A-C**) and different content of photocrosslinkable groups (**P2.2.2 A-E**). The coupling experiments with azide-functionalized DNA indicated that large DBCO to azide ratios of 10 were necessary for almost quantitative conjugation of the DNA. Further, these reactions implied that with increasing molar mass of the DBCO-functionalized (co-)polymers a larger DBCO to azide ratio is necessary to obtain fully functionalized DNA rods.

Overall, the coupling efficiency of the NiPAM based copolymers was significantly lower than for the poly(2-oxazoline) derivatives, which could arise from unexpected side reactions of the DBCO moieties and should be further investigated.

5.4 Hetero-Telechelic Poly(2-oxazoline)s as Linkers for Biosensing Assays

Optical Sensors based on surface plasmon resonance (SPR) spectroscopy are well-known and are commonly used as analytical tool for label-free and real-time probing of targeted analytes that interact with binding partners, which are immobilized at the surface.^{254–257}

The most common SPR configuration was developed by Kretschmann²⁵⁸ in which a thin metal layer (typically around 50 nm of gold) is placed at the interface of two dielectric media with distinct refractive indices (Figure 5.26 A).

The underlying principle is the interaction of incident light with a metal leading to occurrence of an oscillating surface charge density, which propagates parallel to the interface of a metal surface (e.g. gold) and a dielectric medium (e.g. H₂O).^{254,257} Incident light is typically refracted at the interface of two transparent media with two different refractive indices n_1 and n_2 according to Snell's law. When the impinging light first passes through the optically denser medium, the angle of refraction is larger than the angle of incidence and vice versa. Further, if the angle of incident light approaches the so-called critical angle θ_c , the light will propagate along the interface of both transparent mediums.^{255,259,260} The θ_c can be derived from Snell's law

$$\frac{\sin\theta_1}{\sin\theta_2} = \frac{n_2}{n_1} \rightarrow \sin\theta_c = \frac{n_2}{n_1} \quad (2)$$

in which n_1 is the refractive index of the optically denser medium (here: a glass prism) and n_2 the refractive index of the optically less dense medium e.g., an analyte solution or air. Angles of incident light larger than θ_c lead to total internal reflection, which cause the formation of an evanescent field that penetrates into the less dense medium.^{259,261} An exponential decay for this field with a distance to the interface is observed.^{259,261} The evanescent field can only excite surface plasmons (SP), when parallel- (p-) polarized light is used and the wave vector of the evanescent field and the wave vector of the surface plasmon match.^{256,261} The angle at which resonant coupling of the evanescent field with the collective oscillation of electrons takes place is called the resonance angle θ_{SPR} . The resulting decreased intensity of the reflected light beam lead to a minimum of the recorded reflectivity or reflectance (R) curve.^{259,261}

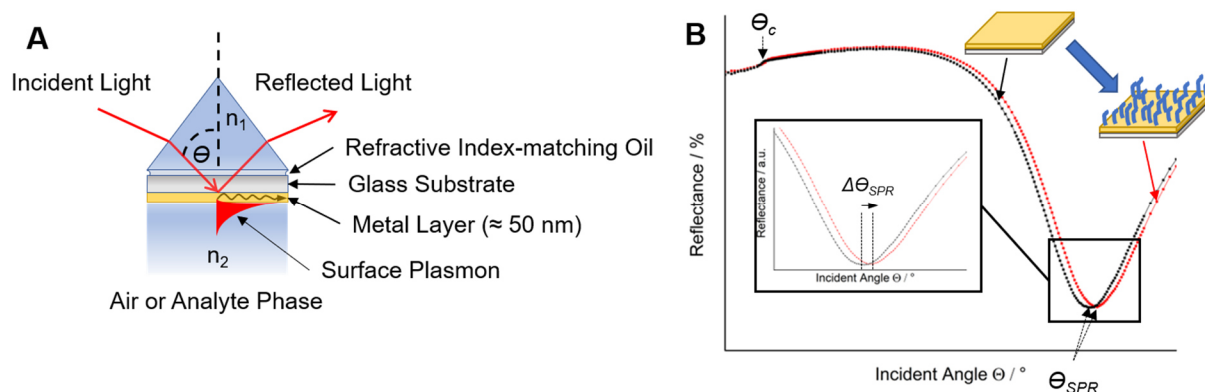


Figure 5.26: Depiction of the setup of the commonly used Kretschmann configuration (A) and a reflectance vs. incident angle diagram, which indicates an angular shift ($\Delta\theta_{SPR}$) caused by the absorption of molecules onto a metal surface.

The damping of the excited SPs is caused by an energy conversion of the SPs to photons and phonons.²⁵⁹ The θ_{SPR} can be determined by the comparison of the wavevector of the evanescent field and the wavevector of the surface plasmon and rearranging the equation to θ_{SPR}

$$\theta_{SPR} = \sin^{-1} \left(\frac{1}{n_1} \sqrt{\frac{n_2^2 n_{Gold}^2}{n_2^2 + n_{Gold}^2}} \right) \quad (3)$$

in which n_1 is the refractive index of the glass prism and n_{Gold} the refractive index of the gold surface. If n_1 and n_{Gold} are fixed parameters, the θ_{SPR} is only influenced by local changes of n_2 , which can be caused by e.g. absorption or desorption of analytes on the surface that lead to a shift of θ_{SPR} (Figure 5.26 B).^{254,259} Thus, the observation of angular shifts in SPR spectroscopy can be used for analyzing interactions of (bio)molecules and the gold sensor surface. However, if only low concentrations of analyte can be absorbed onto the surface, very small angular shifts will be observed, which might be too small for detection.²⁶² Therefore, labeling techniques were combined with SPR spectroscopy in order to improve the sensitivity for low analyte concentrations of such sensors. In the so-called surface plasmon-enhanced fluorescence spectroscopy (SPFS), fluorescence spectroscopy is combined with SPR spectroscopy, which drastically increase the sensitivity of such biosensor devices.^{254,255} Fluorescent molecules can absorb photons upon irradiation with a specific wavelength and emit photons with a longer wavelength. The absorption of photons of a specific wavelengths lead an excitation from the ground state of the fluorophore (S_0) to an excited singlet state (S_1 or S_2). If the molecule is excited to S_2 the energy level will be lowered to S_1 by an internal conversion or

vibrational relaxation.²⁶³ Typically, the relaxation of the excited fluorophore (S_1) to S_0 lead to the emission of photons with longer wavelength (fluorescence) or non-radiative relaxation processes (Figure 5.27 A).²⁶³ The fluorescence emission rate (P_{em}) is proportional to the excitation rate (P_{ex}), when it is far from saturation, as can be derived from equation

$$P_{em} \propto P_{ex} \frac{P_r}{P_r + P_{nr}} \quad (4)$$

in which P_r is the radiative decay rate and P_{nr} the nonradiative decay rate. Consequently, P_{em} can be increased by placing fluorescent molecules in the evanescent field of the surface plasmons.²⁵⁴ If the fluorescent-molecule is in the vicinity of a metallic surface, an additional excitation pathway arise from the coupling of the SP modes with the fluorophore.^{254,255} However, the maximum fluorescence appears at slightly smaller angles than the minimum of reflectance, which is addressed to the coherent superposition of a partial wave, which is reflected from the metal-prism interface, and a re-radiated surface mode.²⁵⁵ As consequence, the minimum of the observed total reflection is the destructive interference of the two partial waves.²⁵⁵ Beside the two relaxation channels that are existing for fluorophores in free space, two additional decay channels can be observed, if the orbitals of such a molecule are able to interact with the extended electronic band structure of a metal.²⁵⁵

This interaction lead also to strong modifications of radiative lifetimes and obtained fluorescent intensities.²⁵⁵ In the first SPR induced relaxation channel, a strong coupling of the emitted fluorescence light to the SP occurred (up to several hundreds of nanometers).²⁶⁴ The second new occurring relaxation pathway is nonradiative due to the Förster resonance energy transfer (FRET) between the excited fluorophore and the electrons of the metal surface. This phenomenon predominantly occurs at low separation distances below 10-15 nm.²⁵⁴ At larger distances between metal surface and fluorophore the FRET pathway as well as other interference effects are negligible. When the fluorescent molecule is excited by the evanescent field of the SP no fluorescence can be observed, if the separation distance is larger than the decay length of the SP (typically around 200 nm).

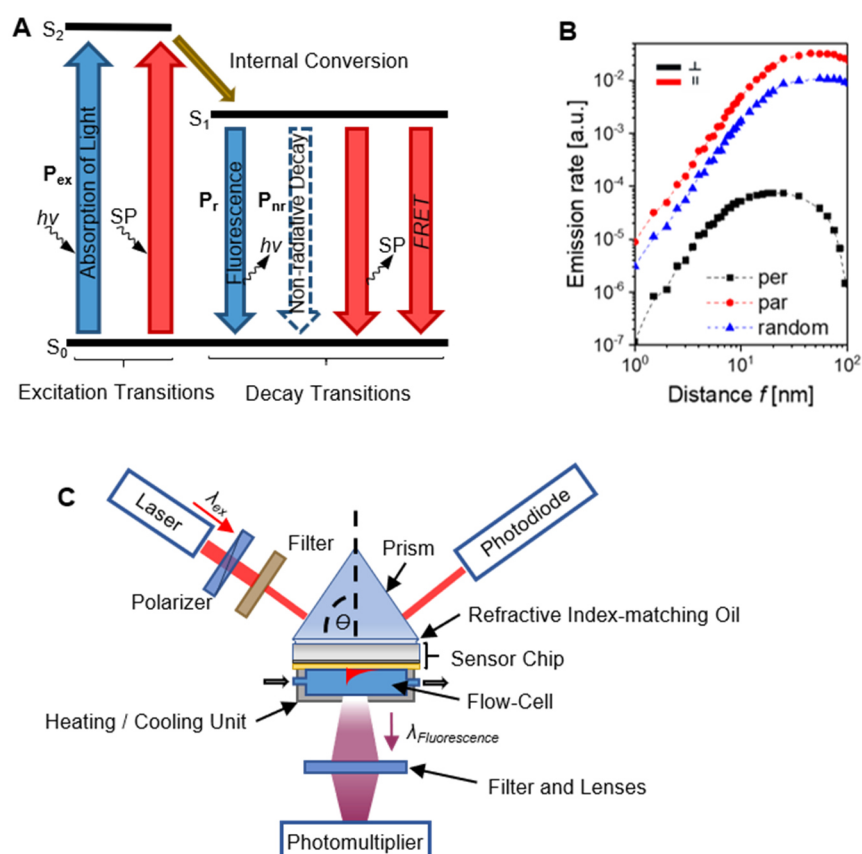


Figure 5.27: (A) Simplified Jablonski diagram indicating transitions of the fluorescent molecule in free space (blue) and additional excitation and decay channels of a fluorophore close to a metal surface (red). (B) Emission rate versus distance (f) diagram of a fluorophore that is perpendicular (per), parallel (par) or randomly oriented to the direction of the exciting propagating surface plasmons (SPs) at $\lambda_{ex} = 633$ nm. (C) Simplified setup for SPFS measurements. Figure A was adapted from Ref. 254 with permission. Copyright © 2008 American Vacuum Society. Figure B and C were reprinted with modifications from Ref. 23 with permission. Copyright © 2017 American Chemical Society

Overall, the fluorescence intensities observed by using SPs compared to intensities obtained in conventional fluorescence spectroscopy can be enhanced by a factor of 50 (Ag used as metal) or 16 (Au).²⁵⁵ In recent years, several approaches for further enhancement were reported in literature using nanostructured metal layers.^{257,265}

Further, simulations predicted that the fluorescence emission rate strongly increases with increasing distance between the surface and the fluorescent molecule and reaches a plateau at $f \approx 15$ nm (Figure 5.27 B). The diagram also demonstrates that the orientation of the fluorescent dye influences the rate of emission. A parallel or randomly oriented emitter lead to higher fluorescence intensity than a fluorescent dye that is perpendicular oriented to the propagating SPs.²³

A common setup for SPFS measurements is shown in Figure 5.27 C. Beside the classical SPR setup using Kretschmann configuration, an additional transparent flow-cell is employed. For temperature-dependent measurements this flow-cell can be cooled or heated. The fluorescence light, which is emitted perpendicular to the metal surface will be collected by a lens, will be passed through filters in order to decrease the background signal that occurs from the scattering of the excitation light beam. Finally, the emitted light will be collected by a photomultiplier.^{23,254}

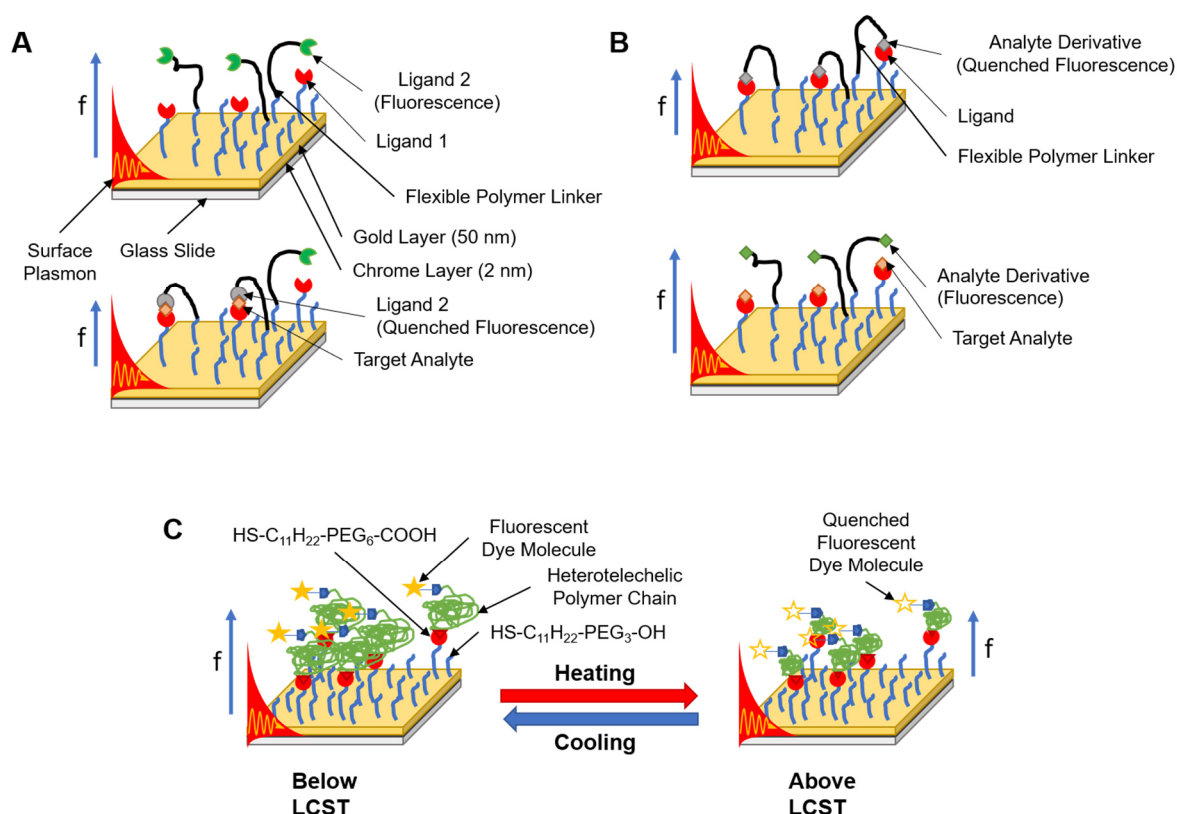
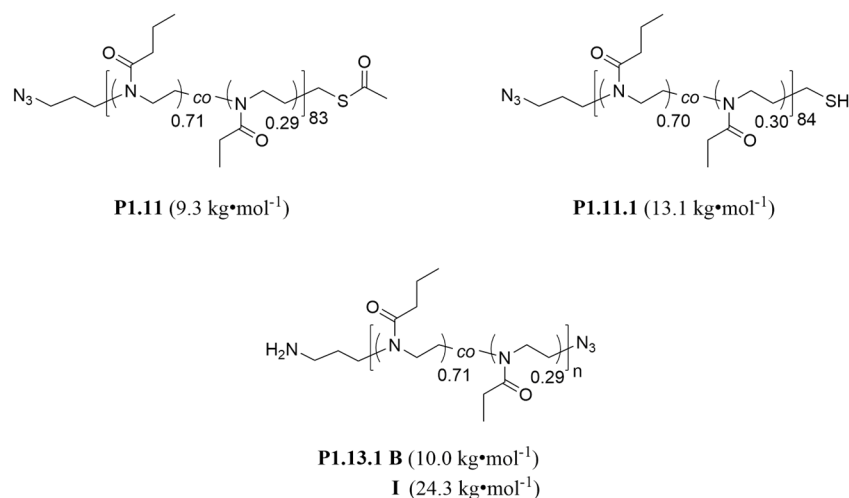


Figure 5.28: Schematic representation of the sandwich assay (A) and competitive assay (B) configuration. In (C), a scheme of the temperature-modulated SPFS measurement is illustrated.

Basically, two different biosensor setups for continuous monitoring are conceivable, in which flexible linkers can be suitable. In so-called sandwich assays (Figure 5.28 A), the analyte molecule of interest will be bound to the surface by a specific ligand and subsequent a second fluorescent ligand, which is connected with the surface by a flexible (polymeric) linker, binds additionally to the analyte. This later binding leads to a decrease of the fluorescent ligand-surface distance and thus a quenching of fluorescence, which is proportional to the number of analytes.²⁶⁶ However, this approach lacks in sensing small analytes.²⁶⁶ In order to overcome this disadvantage, researchers developed so-called competitive assays (Figure 5.28 B).²⁶⁶ In this

devices, an analyte derivative is labeled with a fluorescent tag, and coupled to the surface by a flexible linker. At the surface, a specific ligand is attached, which catch the analyte derivative and cause a quenching of the fluorescence. If the assay is incubated with a medium containing the analyte of interest, the fluorescent analyte derivative will be displaced by the analyte of interest and the flexible linker cause an increase in the fluorescent analyte-surface distance, which lead to emission of fluorescence.²⁶⁶ The reversibility of these binding events in both mentioned sensor architectures with flexible linkers allow the continuous monitoring of analytes of interest, which distinguishes them from other regular assays.



Aim of the experiments is to test the synthesized hetero-telechelic, thermoresponsive copolymers (**P1.11** and **P1.11.1**, **P1.13.1 B** and **P1.13.1 I**) as potential flexible linkers between the gold surface and specific targeting ligand (see chapter 5.1.2) for preparing such as above-mentioned sensor devices. In this early experiments, a DBCO-functionalized fluorescent dye (Alexa Fluor 647) was used instead of a DNA-based ligand. The coupling of the poly(2-oxazoline) derivatives to the gold surface should be achieved by reaction of the sulfur containing end groups of **P1.11** (thioacetate) or **P1.11.1** (thiol), which was already demonstrated for shorter aliphatic thiol or thioacetate compounds.^{267–269} The amino-functionalized derivatives **P1.13.1 B** and **P1.13.1 I** should be linked to previously prepared self-assembled monolayers (SAM). These layers contain carboxylic acid groups that can be used for coupling amino-functionalized polymers by applying NHS active-ester chemistry. Alexa Fluor 647 should be connected to the distal azide groups of the respective copolymer by SPAAC chemistry. The fluorescent tag in combination with the tested thermoresponsive copolymers can be used in temperature-modulated SPFS measurements in order to mimic

affinity interactions of a regular biosensor. Therefore, the prepared sensors will be heated above the corresponding critical temperature (T_c) of the used copolymer, which should lead to a collapsing of the polymer coil and thus result in a quenching of the fluorescence signal. Cooling the sensor below the T_c should lead to an increase of the fluorescence signal (Figure 5.28 C).

The following discussed SPR spectroscopy measurements were performed under supervision of PhD Jakub Dostálek in the laboratories at the Austrian Institute of Technology (AIT) in Tulln.

Determination of T_c :

Table 5.19: Listing of the obtained molar masses and dispersities of the polymers **P1.11**, **P1.11.1**, **P1.13.1 B** and **P1.13.1 I** as well as the corresponding cloud point temperature (T_c) determined by UV/Vis spectroscopy. The mass parameters were measured using GPC.

Polymer	\bar{M}_n (RI Signal) ^a / kg·mol ⁻¹	\bar{D}	T_c (UV-Vis) / °C
P1.11	9.3	1.20	36.4
P1.11.1	13.1	1.22	30.6
P1.13.1 B	10.0	1.06	36.8
P1.13.1 I	24.3	1.13	36.8

^a eluent: DMAc containing LiBr, $\beta = 1 \text{ g}\cdot\text{l}^{-1}$; PMMA standards were used for calibration

First, the phase transition temperatures were determined by UV-Vis spectroscopy (see chapter 6.9) in order to find suitable temperatures (below and above the corresponding T_c) for the temperature-modulation measurements. In Table 5.19, the used copolymers for SPR measurements together with the corresponding molar masses and T_c are listed. The turbidity measurements are shown in Figure S89. Except the T_c of **P1.11.1** ($T = 30.6 \text{ °C}$), all other measured phase transition temperatures were around $T = 36 \text{ °C}$. The comparison of the T_c of **P1.11** and **P1.11.1** revealed a difference of 5.8 °C . This difference may arise from similar effects as discussed for the deprotection of the thioacetate group with respect to the large discrepancy in the obtained molar masses (see chapter 5.1.2). Based on the measured T_c for the copolymers $T = 25 \text{ °C}$ and $T = 45 \text{ °C}$ were chosen as suitable temperatures for the SPFS experiments.

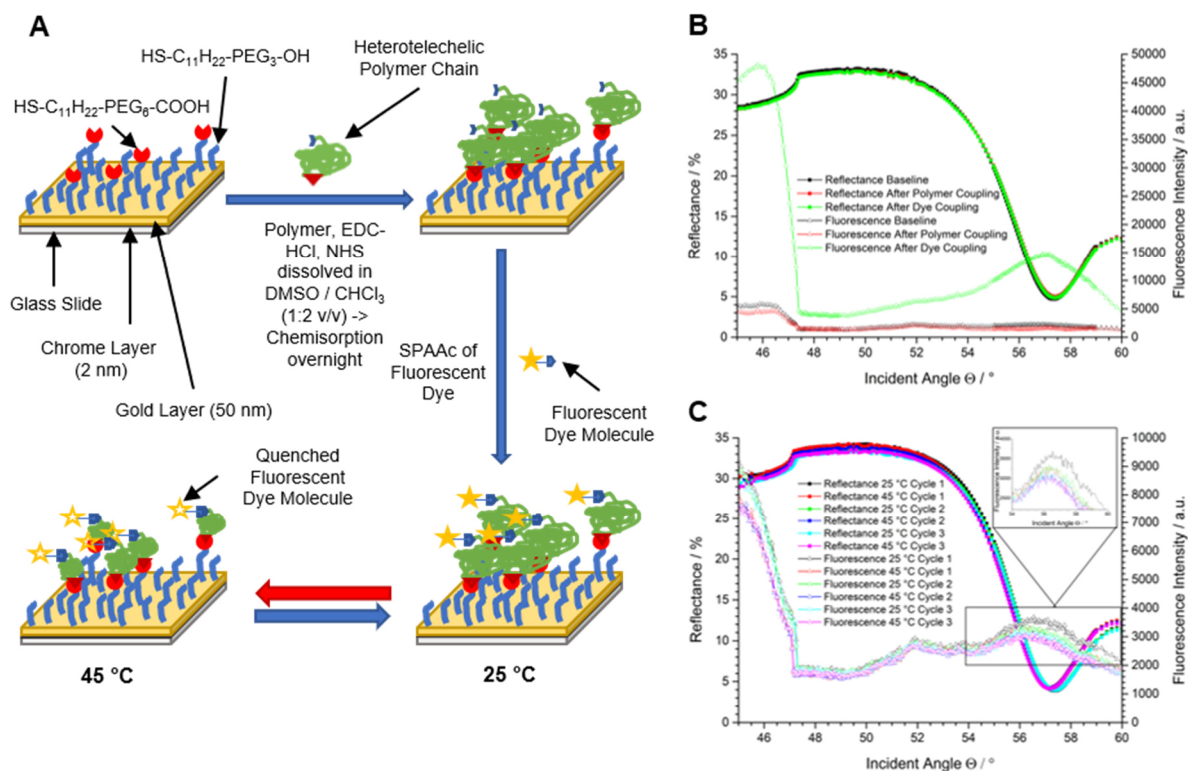
In-situ coupling of hetero-telechelic poly(2-oxazoline) linkers to a SAM:

Figure 5.29: Depiction of the coupling of the hetero-telechelic copolymer **P1.13.1 I** to the mixed thiol SAM followed by attachment of the fluorescent dye and subsequent temperature modulation experiments (A). The corresponding angular scans after the coupling reactions (B) and during the temperature modulation experiments are shown (C).

In a first approach, **P1.13.1 I** was dissolved together with the EDC-HCl and the NHS in a mixture of DMSO and chloroform that was rinsed over the surface of the mixed thiol-SAM (Figure 5.29 A). Subsequently, the fluorescent dye was coupled by SPAAC reaction to the azide end groups of the polymer chains. Comparison of the angular scans (Figure 5.29 B) before coupling of the polymer and afterwards revealed an angular shift of 0.05° that may indicate successful coupling of the polymer chains to the mixed thiol-SAM. After coupling of the fluorescent dye and rinsing with PBS solution no further change in the θ_{SPR} was observed. However, a distinct fluorescence signal close to the θ_{SPR} could be observed, which indicates the successful coupling of the fluorescent dye to the polymeric linkers. The temperature modulation from $T = 25^\circ\text{C}$ to $T = 45^\circ\text{C}$ and *vice versa* (Figure 5.29 C) caused no distinguishable change in the fluorescence intensity, which is contrary to expected decrease of fluorescence intensity for a decrease in the dye-surface distance caused by the collapsing of

polymer chains. It seemed that photobleaching of the dye occurred, which is probably responsible for the low fluorescence intensity.

Coupling of the copolymers to a disulfide linker and subsequent SPR experiments:

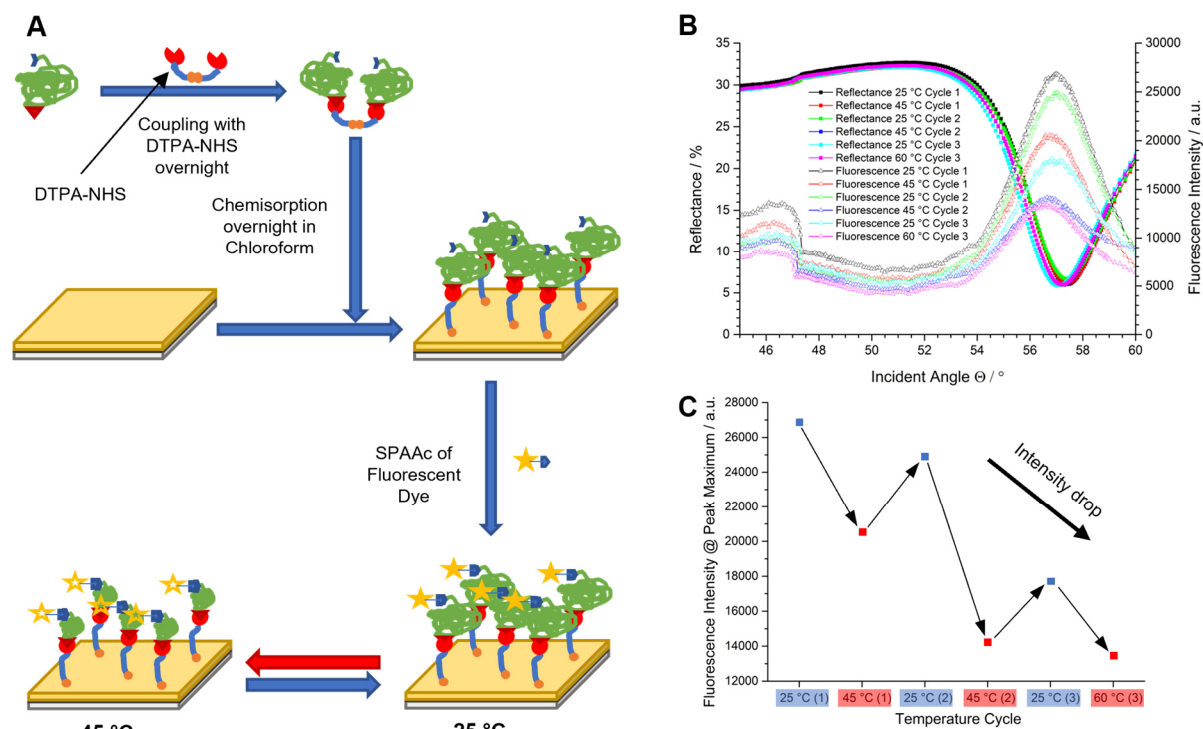


Figure 5.30: Scheme of the reaction pathway in which the hetero-telechelic copolymer **P1.13.1 I** were first coupled to the linker DTPA-NHS and subsequent these structures were attached to the gold surface of the sensor device by chemisorption. The fluorescent dye was coupled during the SPR measurement (A). On the right side, the corresponding angular scans during the temperature modulation experiments (B) as well as a graph (C) visualizing the change in fluorescence intensity at peak maximum are shown. The number in brackets indicates the number of the temperature cycle.

Based on this results, the grafting density was increased in the next experiment by replacing the mixed thiol-SAM by bis(2,5-dioxopyrrolidin-1-yl) 3,3'-disulfanediyldipropionate (DTPA-NHS) as gold anchor, which was previously synthesized within the work group.⁴ First, **P1.13.1 I** was coupled to DTPA-NHS in chloroform and a freshly prepared gold substrate was immersed into the resulting mixture overnight.

Afterwards the SPAAC reaction of Alexa Fluor 647-DBCO with the azide groups of the polymeric linkers was monitored by SPR (Figure 5.30 A). After rinsing the coated surface of the chip with the fluorescent dye solution a strong fluorescence signal close to the θ_{SPR} could be found, whereas no significant change in the θ_{SPR} after coupling of the dye could be observed.

After rinsing the surface of the chip with water, three temperature modulation cycles were performed (Figure 5.30 B). In the last cycle, the temperature was increased to $T = 60\text{ }^{\circ}\text{C}$ instead of $T = 45\text{ }^{\circ}\text{C}$ to test if the fluorescence intensity decreased further. As expected, the recorded profiles showed a decrease of fluorescence intensity when the flow-cell was heated above the T_c of **P1.13.1 I** and increases when the flow cell was cooled down. Further, the comparison of the cycles demonstrated that this modulation was reversible as expected for the temperature-dependent phase transition of the copolymer.

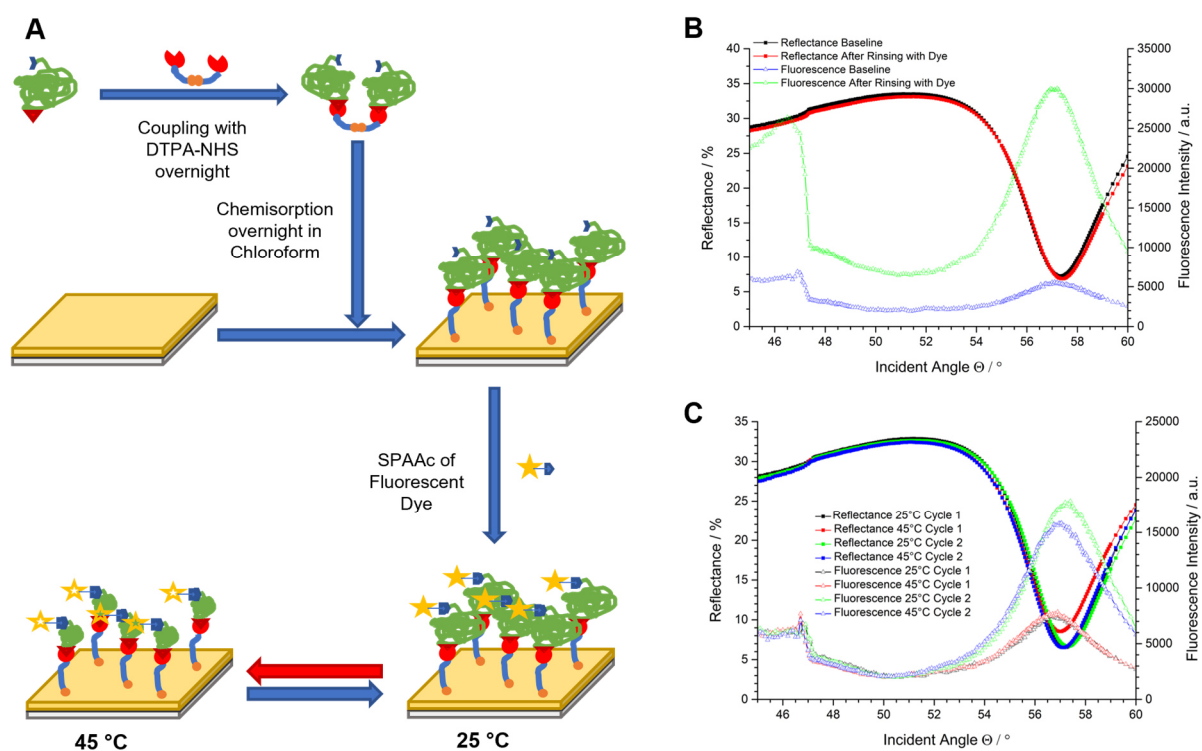


Figure 5.31: Schematic representation of the coupling of the hetero-telechelic copolymers **P1.13.1 B** to DTPA-NHS and subsequent coupling to the gold surface. Afterwards the fluorescent dye was coupled, and the prepared chip was used for temperature modulation experiments (A). On the right side, the corresponding angular scans after the coupling reaction (B) is shown. Additionally, angular scans recorded during the temperature modulation experiments are depicted (C).

The plot, which correlates the fluorescence intensity and the number of cycles at $T = 25\text{ }^{\circ}\text{C}$, demonstrates that the fluorescence intensity decreases with increasing number of cycles (see Figure 5.30 C). A similar decrease of the intensity was also observed for fluorescence intensities above the T_c of the copolymer. Both comparisons imply that photobleaching occurred during the measurement.

The experiment was repeated with **P1.13.1 B** under same conditions in order to investigate the influence of the polymer chain length onto the fluorescence intensity changes upon temperature modulation (Figure 5.31 A). The SPR profiles (Figure 5.31 B) after coupling of the fluorescent dye showed similar results as described for **P1.13.1 I**.

Interestingly, the fluorescence signal increased during the measurement of the second cycle, which is contrary to the expected behavior and also contrary to the results obtained for **P1.13.1 I** (Figure 5.31 C). It seemed that after chemisorption on the surface, the end groups of copolymer chains are closer to each other than expected, which result in a decreased dye-surface distance. After cooling from $T = 45\text{ }^{\circ}\text{C}$ to $T = 25\text{ }^{\circ}\text{C}$ in the first cycle, the polymer chains could probably re-assemble in a more expanded coil conformation than in the first cycle, which leads to an increase in the dye-surface distance and thus a larger fluorescence intensity. It would be also possible that a re-orientation of the dye molecule led to this behavior.

Direct chemisorption of the sulfur containing copolymers and subsequent SPFS measurements:

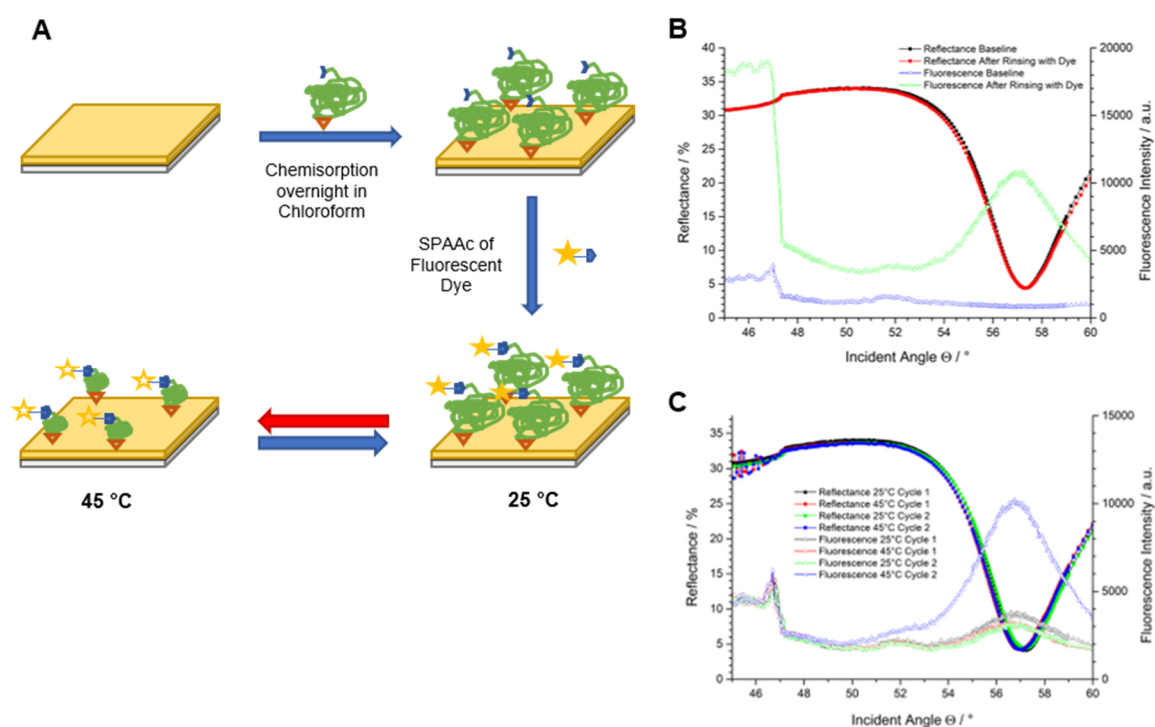


Figure 5.32: Sketch of the chemisorption of **P1.11** onto the gold surface of the sensor device followed by coupling of the fluorescent dye during the SPR measurement and subsequent modulation of the temperature (A). On the right side, the corresponding angular scan after coupling of the fluorescent dye (B) and during the temperature modulation experiments are shown (C).

As expected, the difference in fluorescence intensity below ($T = 25\text{ }^{\circ}\text{C}$) and above ($T = 45\text{ }^{\circ}\text{C}$) the T_c is less distinct as observed for the device with **P1.13.1 I** as linker, because of the lower molar mass and thus the smaller relative shrinkage of the polymer coil during phase transition. Also, the sulfur containing copolymers **P1.11** and **P1.11.1** were tested as possible linkers between the sensor surface and the fluorescent dye. At first **P1.11**, which carries a thioacetate as end group, was tested. The copolymer was directly grafted onto the gold surface of the sensor chip by chemisorption and subsequently the dye was coupled by SPAAC chemistry (Figure 5.32 A). The recorded SPR profiles demonstrated similar trends as observed for the copolymer **P1.13.1 B**.

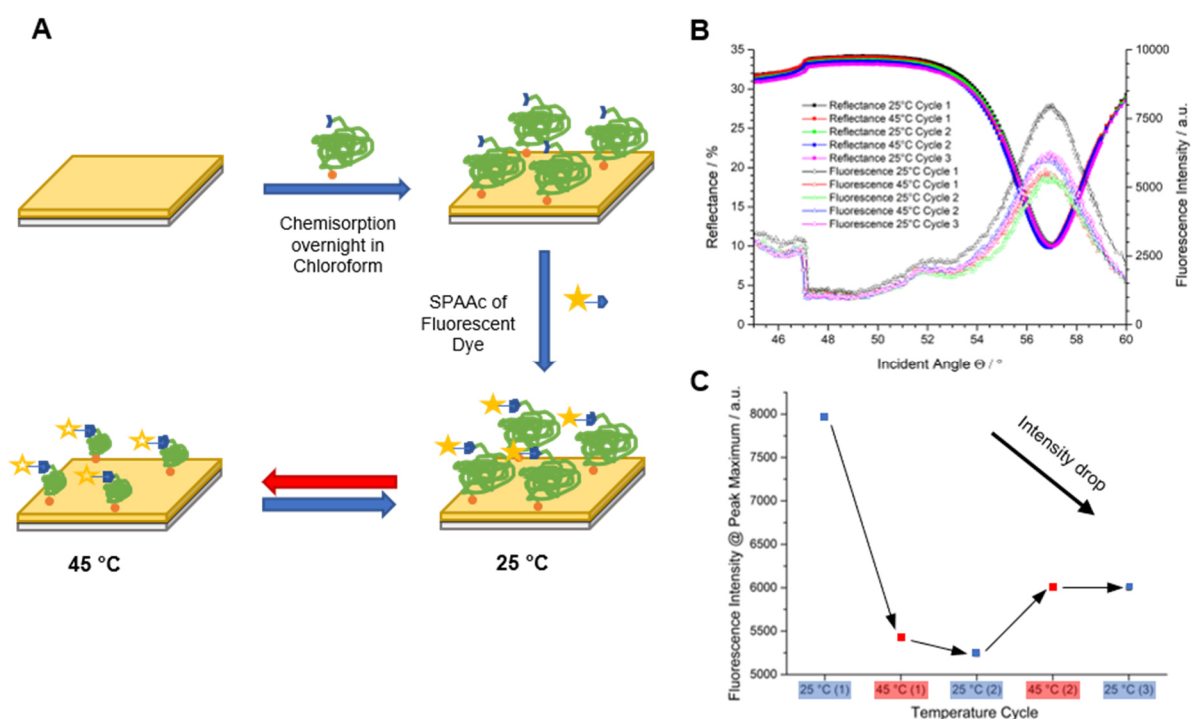


Figure 5.33: Schematic representation of the chemisorption of **P1.11.1** onto the gold surface of the sensor device followed by coupling of the fluorescent dye during the SPR measurement and subsequent modulation of the temperature (A). On the right side, the corresponding angular scans during the temperature modulation experiments (B) as well as a graph (C) visualizing the change in fluorescence intensity at peak maximum (indicated by the black arrow) are shown. The number in brackets indicate the number of the temperature cycle.

A fluorescent signal was obtained after rinsing the flow-cell with the dye-solution indicating the successful coupling of the dye to the linker (Figure 5.32 B). Similar to the previous described experiment, the fluorescence intensity below ($T = 25\text{ }^{\circ}\text{C}$) and above the T_c ($T = 45\text{ }^{\circ}\text{C}$) showed a small distinct deviation in the first cycle, which may arise from the collapsing polymer coils and thus the partially quenching of the fluorescence by FRET (Figure 5.32 C).

Interestingly, the highest fluorescence intensity in this experiment was observed in the second cycle at $T = 45\text{ }^{\circ}\text{C}$ at which the copolymer is in a collapsed state. Again, a re-orientation of the fluorescent dye or a change in the chain conformation of the linker could be responsible for this observations. In the last experiment, **P1.11** was replaced by **P1.11.1**, which carries a thiol group instead of the thioacetate group (Figure 5.33 A). Similar to the previous described experiments, a significant fluorescence intensity signal close to θ_{SPR} was obtained, indicating the successful coupling of the fluorescent dye to the polymeric linker. The first cycle of the temperature modulation experiments showed the expected behavior, in which the increase of temperature led to a decrease of fluorescence intensity. In the second cycle, the fluorescence intensity at $T = 25\text{ }^{\circ}\text{C}$ was similar to the fluorescence intensity at $T = 45\text{ }^{\circ}\text{C}$ of the previous cycle indicating no increase in the dye-surface distance. However, the increase in temperature to $T = 45\text{ }^{\circ}\text{C}$ in the second cycle led to an increase of the fluorescence intensity compared to the intensity obtained at $T = 25\text{ }^{\circ}\text{C}$ of the same cycle. Interestingly, the fluorescence remained constant after cooling down to $T = 25\text{ }^{\circ}\text{C}$. Probably, the modulation of the temperature led to a re-orientation of the dye molecules, and thus resulting in an increased dye-surface distance. Further, the trend also gives evidence for a possible photobleaching of the dye during the SPFS measurements.

Summary:

In this chapter, novel hetero-telechelic and thermoresponsive POxas carrying an azide group and a (protected) thiol group at the distal ends (**P1.11** and **P1.11.1**) as well as a unique lower molar mass and a higher molar mass copolymer with an azide- and an amino end groups (**P1.13.1 B** and **P1.13.1 I**) were tested as potential linkers for biosensing applications. Therefore, these hetero-telechelic copolymers were coupled to a DBCO-functionalized fluorescent dye (Alexa Fluor 647) by SPAAc and to the surface of a sensor chip by the respective amino- or (protected) thiol end group.

First coupling experiments with the copolymers carrying an amino end group (**P1.13.1 B** and **P1.13.1 I**), which should be coupled to a SAM containing carboxylic acid groups by NHS active ester chemistry, failed. Therefore, in the following experiments these copolymers were pre-reacted with a disulfide linker molecule (DTPA-NHS) and subsequent coupled onto the gold surface of a sensor chip. After successful coupling of the fluorescent dye, temperature-modulation experiments with three cycles between 25 and 45 $^{\circ}\text{C}$ demonstrated for **P1.13.1 I** the expected reversible change in fluorescence intensity depending on the coiling behavior of

the polymer chains. However, a steady decrease in the fluorescence signal within these cycles was observed, which gave evidence for photobleaching of the dye.

Contradictory results were obtained for low molar mass **P1.13.1 B**, which was coupled to the fluorescent dye and the gold surface similar to **P1.13.1 I**, because a higher fluorescence intensity was observed in the second temperature modulation cycle than in the first cycle. This may indicate that the orientation of the dye molecule at the surface is locked, and modulation of the temperature probably led to a re-orientation of the dye.

Similar results were obtained for the copolymers carrying a (protected) thiol end group (**P1.11** and **P1.11.1**), which allowed the direct coupling to the gold surface of the sensor chip. However, the temperature modulation experiments showed only in the first cycle the expected modulation of the fluorescence intensity depending on the phase behavior of the polymers, indicating occurrence of undesired side effects. Overall, the experiments demonstrated that the preparation of biosensing setups with hetero-telechelic copolymers is possible. Further, the temperature modulation experiments showed an increase or decrease of the fluorescence intensity due to the decreased or increased dye-surface distance, caused by the thermoresponsive behavior of the copolymers. However, further investigations must be performed to understand the experimental deviations from the expected behavior.

5.5 Amino-Functionalized Poly(acrylamide)s as Alternative Safe Non-viral DNA Carriers for Transfection Applications: An *In Vitro* Study

Gene therapy continues gaining more interests in the biomedical field since it holds great promise for treating genetic disorders²⁷⁰ like severe combined immunodeficiency^{271,272} or cystic fibrosis,^{273,274} Parkinson's disease^{275,276} as well as cancers.^{277–279} The underlying DNA or gene delivery mechanism was recently adapted by different companies to develop novel types of highly effective vaccines to treat the currently ongoing COVID-19 pandemic.^{280,281} Therefore, so-called therapeutic genes have to be introduced into target cells to stop disease progression and/or cure or alleviate the causative genetic defect.²⁸² The introduction of free DNA into cells is usually hindered by the size, hydrophilicity, and polyanionic character of the DNA backbone. Therefore, several physical methods to transfer naked DNA into target cells to be treated have been developed like electroporation^{283,284} or direct injection.^{285,286} However, their applications can be limited by the presence of DNA nucleases in biological fluids.²⁷⁰

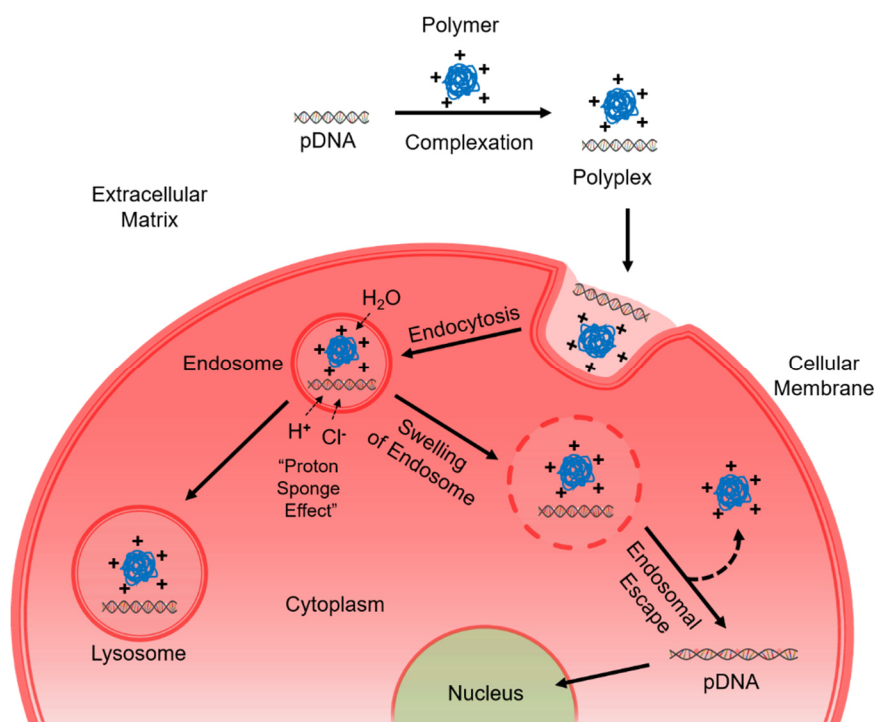


Figure 5.34: Simplified schematic representation of the DNA delivery process into a eukaryotic cell using a polymer as non-viral vector. Adapted from Ref. 287 with permission. Copyright © 2013 The Royal Society of Chemistry

In Figure 5.34, the simplified pathway is shown, in which DNA will be introduced into a eukaryotic cell by using a non-viral carrier, here a polymer. First, the negatively charged

plasmid-DNA (pDNA) interacts with cationic moieties of the polymer to form a so-called polyplex. Also, the negative charges of the DNA backbone are screened/neutralized, which facilitates the penetration of target cell membrane. Before penetration of the cell membrane, the cationic moieties of the carrier interact with the negatively charged proteoglycans present on the surface of the cell membrane.²⁸⁸ However, it has been demonstrated that the cellular uptake is strongly influenced by the nature of the cationic carrier, cell type as well as the number of glycosaminoglycans on the membrane surface.²⁸⁹ Further, it is proposed that the cellular uptake can occur via different endocytic routes depending on the gene carrier used.^{270,290} After penetration of the cell membrane, the DNA-carrier system will be encapsulated into an endosome (endocytosis). The polyplex must then cross the endosomal membrane (endosomal escape) before fusion with lysosomes, to reach the cytoplasm and traffic towards the nucleus.²⁹¹ Additionally, cationic carriers made of secondary or tertiary amines can be protonated due to the acidic environment of the endosome. This will lead to an osmotic diffusion of water from the cytoplasm into the vesicles, which cause a swelling of the endosome. If the inner pressure of the endosome is too high, the vesicles will burst and liberate the DNA-carrier system into the cytoplasm. This effect, called proton-sponge effect,²⁹² is believed to be responsible for the high transfection efficiency of PEI.²⁹³

If the DNA/carrier system is not able to penetrate through the endosomal membrane before reaching lysosomes, the polyplex will be degraded.²⁹¹ After release of the DNA-carrier system, the plasmid DNA (pDNA) must cross the membrane of the nucleus, which can happen through nuclear pore complexes²⁷⁰ or during mitosis (when the nuclear membrane transiently disappear). pDNA, which is complexed by a cationic carrier, showed superior gene expression efficiency compared to free pDNA, indicating a so called nuclear-localizing effect.²⁹⁴ For the above described pathway, carrier molecules, also called vectors, are needed that can transport molecules like deoxyribonucleic acid (DNA) or ribonucleic acid (RNA) through the cell membrane into the targeted cell.²⁷⁰

Viral and non-viral vectors in gene delivery:

First, research was focused on so-called viral carriers like retroviruses and adenoviruses.²⁷⁰ The use of retroviruses as viral vector is suitable, if permanent modification of the diseased cell genome is required,²⁹⁵ because this class of virus is able to transcribe their own RNA into DNA, using a reverse transcriptase, which then will be firmly integrated into the genome of the host

cell.²⁹⁶ Adenoviruses are nonenveloped linear double stranded DNA viruses that are used as carriers in gene therapy since two decades, because of their high *in vivo* delivering efficiencies of genes into most of the human cells.^{297,298} Drawbacks of using viral vectors are toxicity, immunogenicity and their preparation in large scales.²⁷⁰ Alternatively, non-viral vectors like cationic lipids, nanoparticles, polycations or peptides were explored to overcome this disadvantages. Advantages of this class is the ability to produce such systems in large scale as well as their improved biocompatibility and safety compared to viral vectors.^{270,282} Positively charged carriers are promising candidates for gene therapy because of their good water solubility and ability to pack the DNA by electrostatic interactions.²⁸² Well examined representatives of linear polymeric vectors are poly(amido-amine)s (PAA), polymethacrylates or poly(ethylene imine) (PEI).²⁷⁰ Especially, the last mentioned PEI gained a lot of interest in research since the first reported transfection by Boussif and coworkers.²⁹⁹ Over the years PEI was modified to improve the biocompatibility and physicochemical properties of the formed DNA-PEI systems.^{300,301} Commercially available are various PEI based transfection agents,²⁷⁰ which are often used as benchmark compounds for studies of new carrier molecules with respect to transfection efficiency. Poly[(2-dimethylamino)ethyl] methacrylate was also considered as potential gene carrier because of its inherent cationic charges.^{302,303} Over the years, several improvements regarding the transfection efficiency in combination with no or low cytotoxicity of these systems were tried by incorporation of different comonomers. However, in most cases, the transfection efficiency dropped with improved biocompatibility.^{304–306}

Another interesting class of potential non-viral vectors are PAAs, which are synthesized by hydro-transfer polyaddition of primary amines or bis(secondary amines) and bisacrylamides forming polymeric structures with amide and tertiary amino functionalities.²⁶ Different transfection studies based on the PAAs and modified PAAs containing disulfide linker showed good efficiencies and low cytotoxicity.^{27,307,308} PAAs are commonly used as building blocks for dendrimers in gene therapy applications.^{270,309,310} Besides, a lot of research was performed in designing polypeptides³¹¹ as well as nanoparticles³¹² as efficient gene carrier molecules. However, the gene delivery efficiency of non-viral vectors is reduced significantly because of various extra- and intracellular problems.²⁸² For example, the presence of an excess of cationic charges at the DNA-carrier systems can lead to formation of aggregates with charged serum proteins resulting in a decreased transfection efficiency by stimulating immune responses.³¹³ A decrease of the unwanted side reactions was achieved by introduction of polyethylene glycol

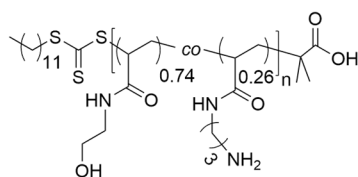
moieties^{314,315} or shielding of the positive charges by using polyanions.³¹⁶ The resulting extend in blood circulation time leads to an enhanced permeation and retention (EPR) effect, which increases the delivery efficiency of the DNA-carrier system.²⁸² Another issue that must be considered is the particle size of such DNA-carrier systems, because the spatial demand influence the encapsulation efficiency, stability, endocytosis and endosomal escape behavior.^{270,282} Generally, small polyplexes showed poor gene delivery efficiency whereas it has been shown that large polyplexes can be rapidly cleared from blood circulation indicating an ideal size of about 90 nm for the polyplexes.³¹⁷⁻³¹⁹

Cytotoxicity is also an important parameter that influences the performance of synthetic molecules as carriers. The interaction of cationic components with proteins or the proteoglycans attached to the cell wall of eukaryotic cells can cause destabilization of the cytoplasmic membrane and lead to necrosis of the cells.³²⁰ The cytotoxicity increases usually with increasing charge density along the carrier molecule. Unfortunately, also the delivery efficiency decreases in most cases. PEI with molar masses of 5 to 25 kg·mol⁻¹ show good complexation and gene transfection abilities, whereas a significant cytotoxicity is observed. In contrast the oligo(ethyleneimine) (OEI) showed lower cytotoxicity, but also lower transfection efficiencies.^{300,321,322} Attempts to improve the gene delivery performance and biocompatibility of such carrier systems utilize e.g. the grafting of small OEI units to an hydrophilic polymer backbone³²³ or the introduction of disulfide moieties along the polymer backbone, which leads to a reductive cleavage of the disulfide bonds in the intracellular environment resulting in a decreased charge density.^{324,301,325} Another interesting approach is the introduction of hydrophobic segments into the polycations which might have several advantages³²⁶ like the ability to promote the charge inversion of the DNA-carrier polyplexes, which eases the attachment to the negatively charged cell membrane^{327,328} or the improved complex formation by cooperative binding of the genes.³²⁹ Also, the incorporation of bioligands that can interact with receptors of the cell can positively influence the performance of non-viral cationic vectors.^{270,316,330} Gene carriers must be additionally able to pack the DNA into stable polyplexes to prevent degradation in the specific microenvironment of the cell.³³¹ Again, the introduction of thiols by incorporation of cysteine building blocks improved the stability of DNA-carrier systems. After binding of the DNA, the thiol groups were oxidized by low molar mass peptides, which led to formation of intermolecular disulfide bridges resulting in more stable polyplexes.³³² However, DNA/carrier assemblies have to reach a compromise between stability

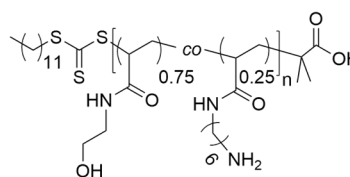
needed outside the cells (to efficiently compact and protect DNA) and instability once inside the cell (for a productive release of DNA).³³³

Poly(N-alkyl acrylamide)s as potential non-viral vector:

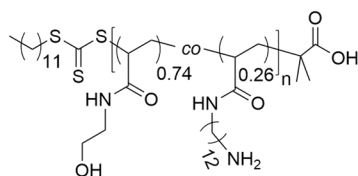
Poly(*N*-alkyl acrylamide) possess a structural similarity to poly(amido amines). Therefore, these polymers were synthesized with amino moieties in the sidechain for investigation as potential gene delivery vectors. Interestingly, no published reports on the transfection efficiency of polyacrylamides could be found in literature.



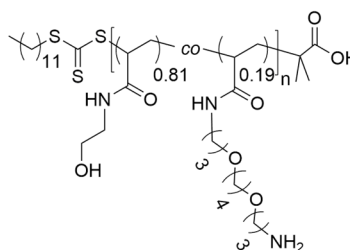
P2.3.1 ($15.2 \text{ kg}\cdot\text{mol}^{-1}$)



P2.4.1 ($21.0 \text{ kg}\cdot\text{mol}^{-1}$)



P2.5.1 ($18.8 \text{ kg}\cdot\text{mol}^{-1}$)



P2.6.1 ($14.8 \text{ kg}\cdot\text{mol}^{-1}$)

For the synthesis of the copolymers (**P2.3.1** to **P2.6.1** and **P2.3.1*** to **P2.6.1***), different amine-containing monomers were prepared and chosen as comonomers in order to investigate the transfection efficiency and biocompatibility according to the side chain length. Additionally, APOAm was prepared that carried a propylene oxide derivative as spacer between the amide- and amino group as it was demonstrated that introduction of PEG moieties can help to improve the performance of non-viral cationic gene vectors (see above). The content of this amine-containing monomer along the polymer chain was adjusted to 30%. To ensure an uniform distribution of the amino groups along the polymer, another acrylamide derivative, named *N*-(2-hydroxyethyl) acrylamide (HEAm), was used since it is known to possess good biocompatibility as polymer.³³⁴

RAFT polymerization was chosen to adjust the molar mass and to obtain narrow molar mass distribution of the polymers. The molar mass was adjusted to $25 \text{ kg}\cdot\text{mol}^{-1}$, which allows direct

comparison to branched PEI (bPEI, $M = 25 \text{ kg}\cdot\text{mol}^{-1}$) that is used as standard for evaluating the transfection efficiencies of the prepared polymers. Eight polymers were tested, namely **P2.3.1** to **P2.6.1** and **P2.3.1*** to **P2.6.1***, the latter polymers specified with an asterisk being those isolated before the ion exchange reaction (meaning that the ammonium moieties possess a triflate as counter anion). The synthesis of the polymers is discussed in chapter 5.2.2. All polymers were tested first according to their capacity to condense a reporter pDNA. Further studies were conducted with respect to their *in vitro* transfection ability in different cell lines [human epithelial lung carcinoma cells (A549), human epithelial ovarian carcinoma cells (HeLa) and murine myoblast cells (C2C12)] as well as their potential cytotoxicity for those cell lines. The DNA used in these experiments was a 3.7 kb luciferase-encoding pDNA.³³⁵

All above-mentioned biological experiments were performed in the context of a research program exchange (PHC PROCOPE 2017, Project no. 37733UM, Dr. Tony Le Gall and Prof. Dr. Holger Schönherr), with Dr. Tony Le Gall and Dr. Yann Le Guen in the laboratory headed by Prof. Tristan Montier at the Université de Bretagne Occidentale in Brest.

DNA-complexation assays:

The initial complexation ability of the polymers was tested using a fluorometric DNA-complexation assay. The procedure is described in chapter 6.10. Briefly, ethidium bromide (EtBr), which should not to be confused with ethyl bromide, is a well-known intercalator for DNA and a fluorescent tag, that can bind between base pairs of the double stranded helix of DNA resulting in a significant increase in fluorescence intensity.³³⁶ The intense fluorescence after binding to DNA may arise from a change in the equilibrium conformation of the intercalator or the change from a hydrophilic to a hydrophobic environment that is present between the base pairs. During the intercalation process into the DNA, the EtBr cation is forced to cast associated water molecules, which led to an increase in fluorescence intensity, because H₂O is known to be an efficient fluorescent quencher.³³⁷ Irradiation with light at $\lambda_{ex} = 530 \text{ nm}$ leads to a fluorescence emission at $\lambda_{em} = 590 \text{ nm}$ caused by the formed DNA-EtBr complexes. The DNA bound to EtBr was mixed with a given polymer (either **P2.3.1-P2.6.1**, **P2.3.1*-P2.6.1***, or bPEI) in 4-(2-hydroxyethyl)-1-piperazineethanesulfonic acid (HEPES) buffer (20 mM), respectively. If these polymers can more efficiently bind to the DNA than EtBr, this is expelled from DNA, which results in a drop of the measured fluorescence. It is

assumed that with increasing binding affinity of a given polymer to the DNA the fluorescence intensity decreases. For the complexation as well as for the other tests, different polymer-to-DNA mass ratios (MR) were tested. In the following Figure 5.35, heatmaps of the complexation assay performed at different temperatures ($T = 4\text{ }^{\circ}\text{C}$, $25\text{ }^{\circ}\text{C}$ and $45\text{ }^{\circ}\text{C}$) are shown. The obtained fluorescent values of each well were compared with the averaged fluorescence intensities of EtBr and DNA-EtBr, respectively. The relative fluorescence was calculated as follows:

$$Fluo (\% \text{ of max}) = \frac{(f_{\text{polymer-DNA}} - \bar{f}_{\text{EtBr}}) \times 100\%}{(\bar{f}_{\text{DNA-EtBr}} - \bar{f}_{\text{EtBr}})} \quad (5)$$

in which f is the intensity of fluorescence measured for the polymer-DNA polyplex and \bar{f} the average of all measured fluorescent intensities of DNA-EtBr complexes (in absence of polymer) or EtBr, respectively. The interaction between all tested polymers and pDNA increased with increasing mass ratio (Figure 5.35). The graph in Figure 5.35 (left) illustrates a strong decrease fluorescence intensity between $\text{MR} = 1$ and $\text{MR} = 10$ indicating that at least a $\text{MR} = 1$ is necessary to obtain good complexation of DNA by the tested polymers.

P2.3.1 as well as **P2.5.1** showed a stronger decrease in fluorescence at $\text{MR} > 1$ than **P2.4.1**, which is a hint for good complexation of the DNA by **P2.3.1** as well as **P2.5.1**. In contrast, for **P2.6.1** higher fluorescence intensities were measured indicating a decreased ability to form polyplexes with DNA. The further increase to $\text{MR} = 100$ led only to a small decrease in the fluorescence intensities. The graph indicated that polyplexes formed with **P2.5.1** emit the lowest fluorescence intensities of all tested polymers. Overall, these polymers were compared to the well-examined branched polyethyleneimine (bPEI), which demonstrate good transfection efficiency and is often used as reference for evaluating the efficiency of non-viral vectors.³³⁸ The graph also implied that the DNA complexation ability of bPEI is much higher than for the measured polymers **P2.3.1-P2.6.1** and **P2.3.1*-P2.6.1*** since a $\text{MR} = 1$ was sufficient to condense effectively DNA. Comparison of the fluorescence intensities (Figure 5.35 right side) measured for **P2.3.1-P2.6.1** and the fluorescence intensities of the corresponding **P2.3.1*-P2.6.1*** yield almost linear curves with coefficients of determination $R^2 = 0.92-0.99$ indicating almost similar fluorescence intensity values. Further, this graph demonstrated that the counterion has no effect on the complexation ability of the respective copolymers.

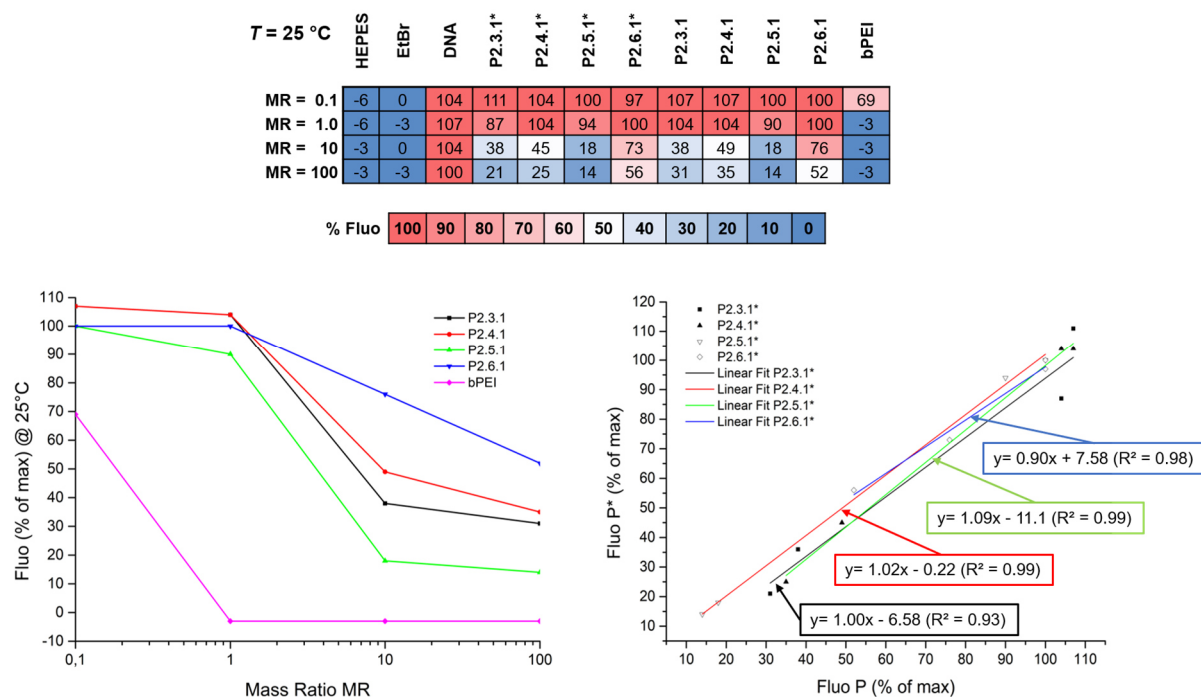


Figure 5.35: Depiction of the relative fluorescence intensity measured at $T = 25\text{ }^{\circ}\text{C}$: The normalized values of the fluorescence compared to the fluorescence of DNA-EtBr complexes were calculated according to equation (5) on page 175. The fluorescence is colored according to the scale bar to guide the eye. Below, the graphical evaluation for **P2.3.1-P2.6.1** compared to bPEI is shown (left). On the right side a diagram is depicted in which the fluorescence values of **P2.3.1-P2.6.1** were correlated to values observed for the corresponding **P2.3.1*-P2.6.1***.

Additional complexation experiments were performed in which the temperature was changed to $T = 4\text{ }^{\circ}\text{C}$ and $T = 45\text{ }^{\circ}\text{C}$ to see effects in the DNA complexation caused by temperature changes. The corresponding heatmaps indicate that the ability of complexation of **P2.3.1-P2.6.1** and **P2.3.1*-P2.6.1*** was not influenced by temperature (see Figure S90). The small deviations in the fluorescence intensities in both measurements ($T = 4\text{ }^{\circ}\text{C}$ and $T = 45\text{ }^{\circ}\text{C}$) compared to the measurement performed at $T = 25\text{ }^{\circ}\text{C}$ could be assigned to changes in the complexation kinetics caused by the lower or higher temperature. Successful complexation of DNA by the different measured polymer **P2.3.1-P2.6.1** and **P2.3.1*-P2.6.1*** was additionally confirmed by gel retardation experiments. The procedure is described in chapter 6.10. Pictures of the different gel retardation experiments were compiled and illustrated in Figure 5.36. The migration pattern of all polymers showed, that polyplexes were successfully formed, because the free DNA migrated (Figure 5.36, first column) faster than the formed polyplexes. Typically, two well-distinguished bands of pDNA could be observed with different migration velocities arising from different conformations of the DNA. The structure that moves faster can be assigned to supercoiled DNA because of a smaller spatial demanding of this structure compared to the

nicked/relaxed DNA, which needs more volume in space and migrates therefore slower.

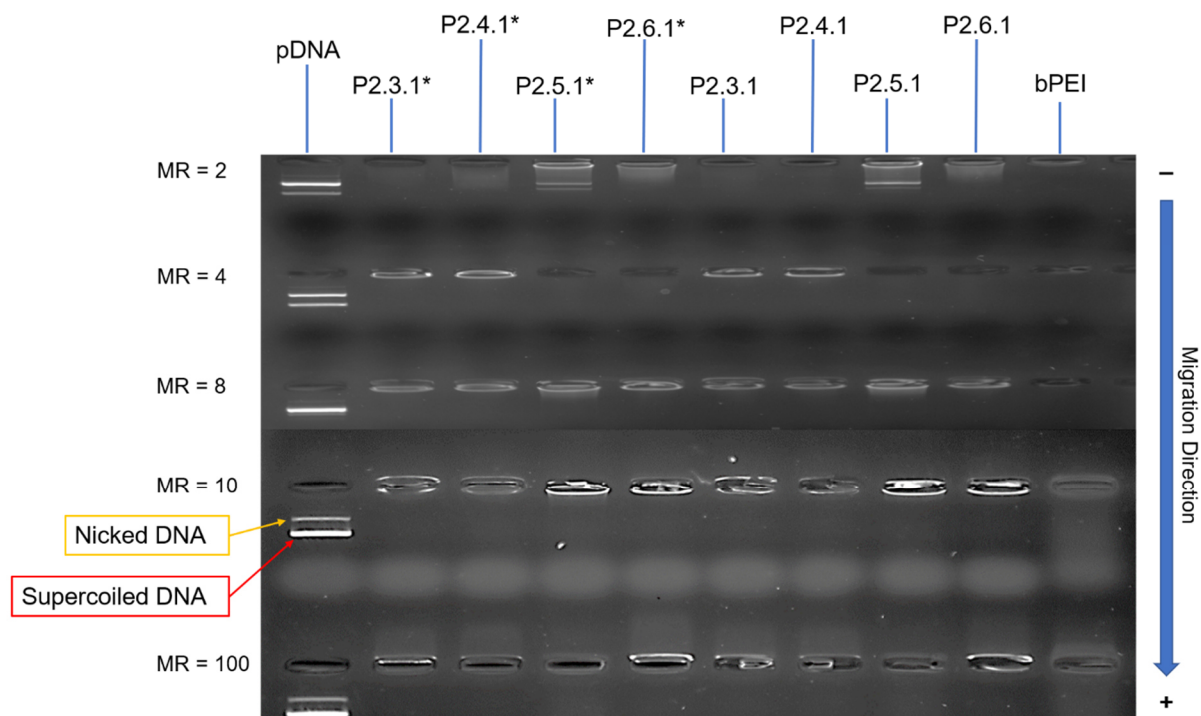


Figure 5.36: Compilation of pictures taken from different agarose (0.8%) gel retardation experiments. The experiments were performed at $U = 100$ mV for 20 min. Every column represents the migration of a corresponding polymer-DNA complex, and each line represents a different MR. The blue arrow indicates the migration direction (direction of the current).

Further, the gel retardation experiment showed, that the pDNA is obviously neutralized by the corresponding polymer, since no migration of the polyplexes is observed, but the remaining fluorescence indicate that the pDNA is not fully condensed, because it can still interact with EtBr. Overall, the results of these experiments confirmed the observations made for the DNA complexation assay shown above in Figure 5.35. The gel retardation pattern showed for low mass ratio (MR = 2) of **P2.5.1*** and **P2.5.1** an insufficient complexation of DNA indicated by the appearance of a second band which could be assigned to free DNA. Interestingly, at MR = 2 the polymer-DNA complexes of **P2.3.1*** and **P2.4.1*** as well **P2.3.1** and **P2.4.1** showed no fluorescence, indicating no contribution of EtBr within the complexes. Contrary, at higher mass ratios (MR = 4 and 8) the fluorescence unexpectedly appeared. The same phenomenon was observed for **P2.5.1*** and **P2.6.1*** as well **P2.5.1** and **P2.6.1** at MR = 4. This fact could not be clarified yet. However, the agarose (0.8%) gel retardation experiments confirmed the results obtained in the initial DNA-complexation assays.

Cell viability and transfection studies:

In the next experiments, the transfection efficiency as well as the cell viability were tested. For these experiments different cell lines namely A549 (human epithelial lung carcinoma cells), C2C12 (murine myoblast cells) and HeLa cells (human epithelial ovarian carcinoma cells), were used. $MR = 1.27$ instead of $MR = 1$ was chosen to minimize the error caused by dilution during preparation of the corresponding polymer-DNA mixtures. A critical parameter in terms of transfection efficiency is the ratio between amino groups in the polymer, which is related to the number of positive charges of the polymer, and the phosphate groups along the DNA backbone, which represent the number of negative charges. The so-called N/P ratio was calculated for all measured MR of each synthesized polymer-DNA- and bPEI-DNA conjugate (Table S7.2). For each tested MR, the calculated N/P ratio of bPEI, and thus the number of charges present in bPEI, is much higher compared to the N/P ratio of the synthesized polymers as indicated in Figure S91. The N/P ratio at $MR = 1.27$ is below one for **P2.3.1-P2.6.1**, which means that not all charges of the DNA were screened. In contrast, the N/P of bPEI at this MR is already about ten, which could explain the better DNA complexation ability of PEI compared to the other tested polymers. In the following, the results found for the A549 cell line are presented and discussed.

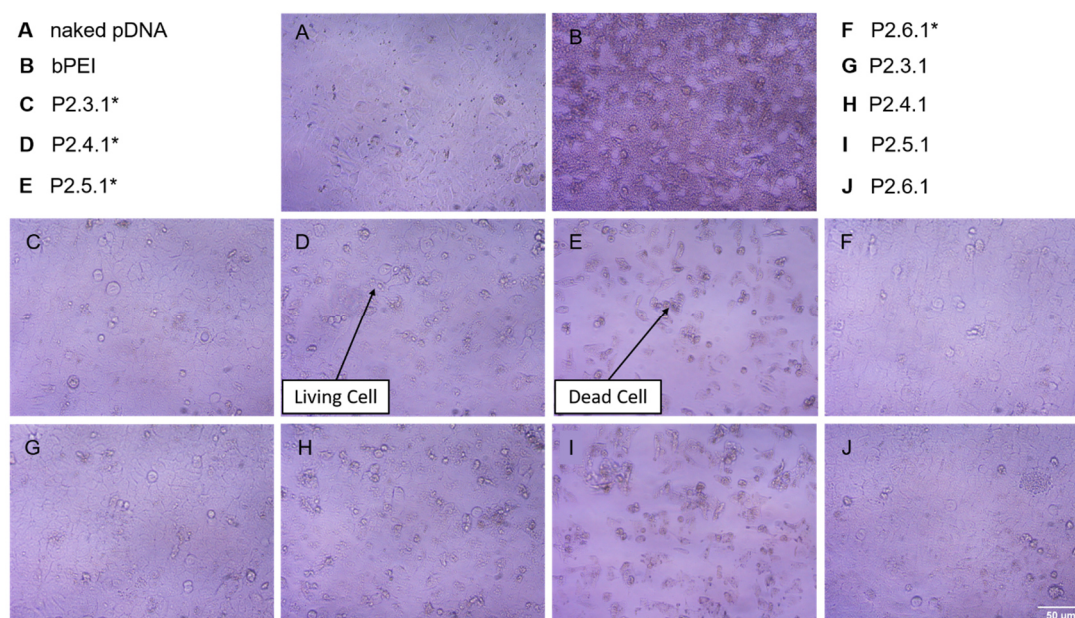
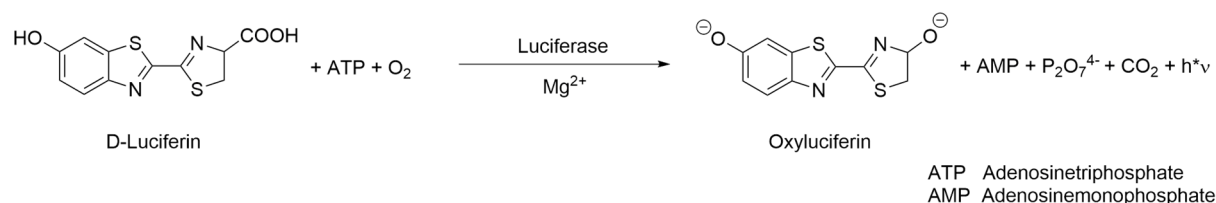


Figure 5.37: Microscope images of A549 cells treated with polyplexes of the tested polymers ($MR = 64$). In the top row cells are depicted which are employed with pDNA (A) and bPEI-DNA complexes (B). The middle row illustrates the viability of the cells treated with **P2.3.1*-P2.6.1*** polyplexes (C-F) and the bottom row represent the behavior of the cells treated with **P2.3.1-P2.6.1** polyplexes (G-J).

The corresponding results obtained for the other two cell lines are depicted in Figure S92 and Figure S93. Each cell line was cultured and incubated with the Polymer-DNA polyplexes for 36 h at $T = 37\text{ }^{\circ}\text{C}$. The biocompatibility was qualitatively evaluated by microscope images (Figure 5.37). The pictures were taken before lysis of the A549 cells after 36 h of incubation and as references naked pDNA (Figure 5.37A) and bPEI/pDNA (Figure 5.37B) were used. The corresponding polymers are shown in the rows below (Figure 5.37C-F). After 36 h incubation ($37\text{ }^{\circ}\text{C}$, $5\% \text{ CO}_2$) of the polyplexes with the A549 cells, the images showed that compared to bPEI almost no apparent cell injury of the cells occurred. Only for the polymers **P2.5.1*** and **P2.5.1** (Figure 5.37E and I) small necrosis could be observed. Probably, the increased hydrophobicity or the increased sterically demand of this polymer could lead to the cell death. In contrast, the polyplexes formed by DNA and **P2.6.1*** or **P2.6.1** were apparently well tolerated by the cells and showed no cell death. Due to the increased flexibility of such chains, the sterically demand could be decreased, compared to the dodecyl sidechain, which may lead to better tolerance by the cells. Comparison of the images showed that all measured polymers showed less cytotoxicity compared to bPEI. Contrary to the tested polymers at $\text{MR} = 64$, bPEI is highly cytotoxic at this MR, which is confirmed by the image that shows a cell death in large areas (Figure 5.37B).

Afterwards, the cells were disrupted by adding passive lysis buffer (PLB) (details provided in chapter 6.11). For the measurements of the transfection efficiency, the cell viability as well as the determination of the protein load, the same cell lysate was used. The transfection ability of the used polymers **P2.3.1-P2.6.1** and **P2.3.1*-P2.6.1*** were tested by using the so-called luciferase assay.



Scheme 5.15: Bioluminescence reaction of D-luciferin and luciferase in the presence of oxygen and adenosine triphosphate (ATP). The conversion to oxyluciferin and adenosine monophosphate (AMP) lead amongst other side products to emission of light at $\lambda = 540\text{ nm}$. The scheme was adapted from literature with modifications.³³⁹

The successful transfection of the luciferase-encoding pDNA into the cells leads to the production of the enzyme luciferase. The reaction of luciferin and luciferase in the presence of oxygen lead to oxyluciferin and other side products as well as to a bioluminescence that can be

detected at $\lambda = 540 \text{ nm}$.³⁴⁰ The intensity of this emission is proportional to the number of produced D-luciferin and therefore can be used to quantify the transfection efficiency of the respective polymer, which mediate the DNA delivery into the target cells (Scheme 5.15). The procedure of these experiments is described in chapter 6.11. From the obtained luminescence intensities of each well, the total number of relative light units (RLU) could be calculated using following equation

$$Total\ RLU = (I_{Well} - \bar{I}_{DNA}) \times \left(\frac{V_{Well}}{V_{Probe}}\right) \quad (6)$$

in which I_{Well} is the measured intensity of luminescence of the well, \bar{I}_{DNA} the average of luminescence intensities of the negative control (DNA on cells), V_{Well} total volume of the analytes inside the well and V_{Probe} the volume of cell lysis used for the measurement. Beside the transfection assay, the bicinchoninic acid (BCA) assay was performed to determine the total amount of protein in each cell lysate. The procedure is described in section 6.10. The reaction of bicinchoninic acid and copper leads to a color change of the sample solution from green to purple with increasing protein concentration. The assay is based on two reactions. In the first reaction, Cu^{2+} will be reduced to Cu^+ by the peptide bonds in the proteins (Biuret reaction). Consequently, the amount of reduced Cu^+ is proportional to the number of proteins present in the lysis of the cells. In the second reaction, two molecules of bicinchoninic acid form a purple-colored complex with Cu^+ as central atom.³⁴¹ This complex can be quantified by measuring the absorption at $\lambda = 560 \text{ nm}$. The total amount of proteins is related to the number of cells in each well. The transfection efficiency of a vector (given in $RLU \cdot mg^{-1}$) can be quantified by comparison the corresponding RLU of each well to the number of cells present in the respective well as follows

$$RLU \cdot mg^{-1} = \frac{Total\ RLU}{m_{Proteins}} \quad (7)$$

The results are given below in Figure 5.38 A. The comparison of the determined transfection efficiency (Figure 5.38 A) of all tested polymers indicated that **P2.4.1*** and **P2.4.1** possessed the best transfection abilities of the tested polymers, which is contrary to assumption stated after evaluation of the DNA-complexation assays and the gel retardation experiments in which **P2.3.1*** and **P2.3.1** as well as **P2.5.1*** and **P2.5.1** showed the best complexation behavior. Probably, the binding of the DNA to these polymers is too strong so that a release is hampered.

A	HEPES (20mM)	DNA	P2.3.1*	P2.4.1*	P2.5.1*	P2.6.1*	P2.3.1	P2.4.1	P2.5.1	P2.6.1	bPEI	HEPES (20mM)
	MR = 1.27	1.E+3	5.E+2	9.E+2	8.E+1	1.E+3	7.E+1	1.E+4	2.E+3	1.E+3	2.E+3	2.E+7
MR = 2	1.E+2	1.E+3	1.E+4	2.E+5	9.E+1	1.E+3	2.E+3	1.E+3	8.E+2	1.E+3	4.E+6	4.E+2
MR = 4	6.E+2	6.E+2	2.E+4	2.E+5	2.E+3	1.E+3	6.E+3	1.E+3	9.E+1	1.E+4	5.E+6	8.E+1
MR = 8	1.E+2	1.E+3	6.E+3	6.E+3	1.E+5	8.E+3	4.E+4	3.E+4	2.E+5	3.E+3	4.E+6	1.E+3
MR = 16	1.E+3	1.E+3	7.E+3	1.E+6	6.E+5	1.E+3	2.E+4	3.E+3	6.E+5	3.E+3	2.E+8	2.E+4
MR = 32	1.E+3	1.E+3	4.E+4	2.E+6	2.E+5	2.E+3	4.E+5	5.E+6	4.E+5	9.E+3	6.E+6	5.E+3
MR = 64	1.E+3	1.E+3	7.E+5	2.E+7	3.E+2	9.E+1	2.E+5	1.E+7	7.E+3	9.E+1	4.E+2	9.E+2
MR = 128	1.E+3	2.E+3	7.E+3	3.E+6	1.E+2	2.E+5	2.E+5	9.E+6	2.E+3	7.E+5	6.E+2	8.E+2

Values given in RLU / mg

B	HEPES (20mM)	DNA	P2.3.1*	P2.4.1*	P2.5.1*	P2.6.1*	P2.3.1	P2.4.1	P2.5.1	P2.6.1	bPEI	HEPES (20mM)
	MR = 1.27	97	103	115	106	105	118	120	112	116	121	109
MR = 2	74	95	108	96	103	111	111	110	111	117	104	120
MR = 4	88	98	104	93	111	114	107	106	115	118	103	119
MR = 8	84	101	108	95	112	111	107	105	116	116	93	114
MR = 16	77	96	103	86	87	108	108	104	91	112	24	112
MR = 32	93	104	105	91	34	107	110	100	37	112	1	117
MR = 64	100	105	100	78	0	101	106	84	0	107	0	112
MR = 128	86	98	84	46	0	106	91	48	0	105	0	115

Values given in %

Figure 5.38: Overview of the measured transfection efficiency (A) and the corresponding cell viability of A549 cells (B) after 36 h incubation with the polyplexes and lysis of the cells. In panel A, a different scale and color-code are used for denoting the luciferase activity measured with P and P* on one hand and bPEI on the other hand. Tests were performed in duplicates (n=2).

All other tested polymers showed only minor transfection abilities. The best transfection efficiencies of **P2.4.1*** and **P2.4.1** were obtained at MR = 64. Compared to the reference bPEI, the transfection efficiency is one order of magnitude lower. Further, the highest transfection ability of bPEI can be observed at MR = 16, which is a quarter of the needed MR of **P2.4.1*** and **P2.4.1**. The N/P ratio of bPEI at MR = 16 is around 123 revealing a large excess of positive charges, which can condense the DNA efficiently. In contrast, this N/P ratio were not reached for **P2.3.1-P2.6.1** and **P2.3.1*-P2.6.1*** even at the highest measured MR of 128 (N/P ratios between 43 and 75). Similar results were obtained for the other two cell lines C2C12 and HeLa (see Figure S94 and Figure S95). Beside the DNA-complexation and transfection efficiency, the biocompatibility of the polymers and their polyplexes with DNA was tested. The procedure of the cell viability assay is described in chapter 6.10. Adenosine triphosphate (ATP), which is crucial for living cells, are liberated after lysis, and can be used for measuring the cell viability. The ATP content reflects the number of living cells (transfected or not) in the culture, as a result of both cell proliferation and cell mortality (either normal or experimentally-induced) that

occurred during the transfection experiment. ATP reacts in the presence of Mg^{2+} ions, O_2 and luciferase with luciferin and forms oxyluciferin, adenosine-5'-monophosphate, CO_2 , and pyrophosphate as products.³³⁹ Thereby, light at $\lambda = 560$ nm will be emitted, which can be detected. The measured light intensity is proportional to the ATP content at low concentrations and therefore directly correlated to the number of living cells in the experiment.³⁴² The resulting luminescence intensities were compared to the negative control (cells mixed with naked pDNA) to obtain the relative cell viability by the following equation

$$rel. cell viability = \frac{I_{Well}}{\bar{I}_{DNA}} \times 100\% \quad (8)$$

I_{Well} is the measured fluorescence intensity of the content in the well and \bar{I}_{DNA} is the calculated averaged fluorescence of the wells, which were used as negative control. The obtained cell viabilities for all tested polymers at different MR are illustrated in Figure 5.38B. The polyplexes formed by the tested polymers **P2.3.1**, **P2.4.1** and **P2.6.1** were tolerated even at high MR < 64, which indicated a good biocompatibility as suggested by illustrated microscope images (Figure 5.37). Further, the tests showed that with increasing side chain length the cytotoxicity increased, which could be explained by the increasing sterical demanding with increasing chain length. Compared to bPEI, the biocompatibility of all tested polymers is better at MR > 8. It appears that the “utility window” (MR for which transfection is efficient while cell viability remains good) was larger for all tested polymers except **P2.6.1*** and **P2.6.1**, compared with bPEI as illustrated below (Figure 5.39).

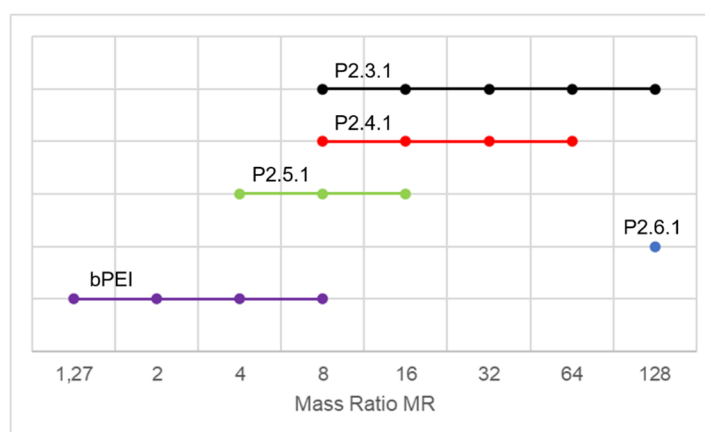


Figure 5.39: Illustration of the MR of **P2.3.1-P2.6.1** and **bPEI** that allow to obtain a transfection efficiency larger than $1.0 \cdot 10^4$ RLU·mg⁻¹ while a relative cell viability larger than 80% was measured.

This “utility window” was defined as MR at which a reliable transfection efficiency ($>1.0 \cdot 10^4$ RLU·mg⁻¹) as well as good biocompatibility (rel. cell viability above 80%) was obtained for the

measured polymer-DNA polyplexes. The cell viability of the tested C2C12 and HeLa cells (data presented in Figure S94 and Figure S95) indicated that even in the control deviations within the wells occurred. Probably, there is a problem with healthiness of the cells, which means that the cell viability data and the transfection efficiencies were also to be considered with caution.

Summary:

Overall, the cell experiments demonstrated that all novel *N*-substituted poly(acrylamide)s were able to condense pDNA and also *N*-substituted poly(acrylamide)s with C6 spacer between the amino groups and the polymer backbone were able to transport the pDNA into A549 cells.

The complexation assay indicated that high mass ratios ($MR \geq 10$) of **P2.3.1-P2.6.1** and **P2.3.1*-P2.6.1*** were needed to obtain similar complexation results as observed for bPEI (positive control). The polymers **P2.5.1** and **P2.5.1*** containing dodecyl side chains showed the most efficient complexation ability, whereas the polymers **P2.6.1** and **P2.6.1*** showed the worst complexation affinity. The measurements at three different temperatures ($T = 4\text{ }^{\circ}\text{C}$, $25\text{ }^{\circ}\text{C}$ and $45\text{ }^{\circ}\text{C}$) showed no significant improvement of the complexation ability of the polymers. Results of the gel retardation experiments were in accordance with the results obtained by the EtBr fluorescence exclusion assay. Further, these experiments showed that the pDNA is obviously neutralized by the corresponding polymer, since no migration of the polyplexes is observed, but the remaining fluorescence indicates that the pDNA is not fully condensed and it can still interact with EtBr.

The cell viability tests showed that all tested polymers were tolerated by the A549 cells even at high mass ratios ($MR < 64$). The best transfection efficiency could be observed for **P2.4.1** and **P2.4.1***, which possess a hexyl linker between the amino group and the polymer backbone. However, the observed transfection efficiency was one order of magnitude lower than for the reference bPEI. The comparison of the polymers that were stirred with an anionic exchanger (**P2.3.1-P2.6.1**) and those without an anion exchange reaction (**P2.3.1*-P2.6.1***) showed no significant difference indicating that the counterion has no effect on the performance of the polymers. The other tested cell lines C2C12 and HeLa showed strong deviations in both the transfection assays as well as the corresponding cell viability assays that might be explained by illness of the cells.

6 Experimental Section

6.1 Equipment and Methods

The molar masses and the molar mass distribution (\mathcal{D}) of the synthesized poly(2-oxazoline)s and poly(acrylamides) were measured using a PSS system (Agilent 1260) equipped with autosampler, RI detector and UV-Detector Type Agilent VWD Series 1260 were used. The absorption was measured at $\lambda = 280$ nm. A so-called Gram Linear M column or Gram 100 Å, equipped with a 10 μm particle size precolumn was utilized at $T \approx 60$ °C. As eluent dimethylacetamide (DMAc) mixed with $\beta = 1$ g·l⁻¹ LiBr was used. 20 μl of the polymer-samples were injected. The flow rate of the system was 1 ml·min⁻¹. The calibration curve was measured using PMMA standards (PSS, Mainz). Other gel permeation chromatography (SEC) experiments of poly(2-oxazoline)s were carried out on an Agilent 1200-System consisting of degasser, isocratic pump, autosampler, RI-detector, UV-detector (Lambda 1010, Bischoff, $\lambda = 254$ nm), and a SDV Linear M column. THF was used as eluent with a flow rate of 1 ml·min⁻¹. Calibration was performed with polystyrene standards (PSS, Mainz). The UV/Vis measurements were performed using an Evolution 220 UV-Visible spectrophotometer and a PCCU 1 Peltier control and cooling unit from Thermo Scientific. NMR spectroscopy was performed using a Bruker AV 400 spectrometer or a Joel ECZ 500 spectrometer. All measurements were performed at room temperature. The ¹H NMR spectra were recorded at 400 or 500 MHz and ¹³C NMR spectra at 101 or 126 MHz, respectively. Chemical shifts (δ) are given in ppm and are referenced to the non-deuterated signal of the used solvent. Polymerizations were performed using a Discover SP Microwave System equipped with an Explorer 12 Hybrid Autosampler from CEM. Details to the temperature program are provided in the corresponding experimental procedure. Crosslinking and photodeprotection experiments were carried out in a UV-crosslinker UVP-CL1000, operating at $\lambda = 365$ nm ($H_e = 12.0$ J cm⁻² per 1 h). IR spectra were recorded on a Bruker Tensor 28 equipped with ATR unit. Reaction mixtures for cationic ring-opening polymerization were prepared in a glovebox (MBraun LABstar) under N₂-atmosphere. If reactions were not performed in microwave, magnetic stirrers were used, and the reaction flasks were equipped with a stirring bar. The corresponding reaction temperatures were measured inside the oil bath.

6.2 Chemicals

Acetone for reactions (VWR Chemicals, 99.8%) was distilled before use. Further, 2-ethyl-2-oxazoline (Alfa Aesar 99%), methyl trifluoromethanesulfonate (Alfa Aesar, 97%), triethylamine (ChemSolute, 99%) were dried over CaH₂ and distilled under inert gas or vacuum prior to use. *N*-(2-Hydroxyethyl) acrylamide (HEAm, Sigma Aldrich, 97%) was passed through an aluminum oxide column prior to use. Water was demineralized by a MilliQ filtration unit ($\sigma = 18.2 \text{ M}\Omega\cdot\text{cm}$). Azobisisobutyronitrile (AIBN, Fluka, 99%) was recrystallized twice from methanol before usage. Dimethylsulfoxide (DMSO, 99.9, Fisher Scientific) was dried over molecular sieves 4 Å and ethylenediamine (J.T. Baker 99.9%) was dried over molecular sieves 5 Å prior usage. 4-Toluenesulfanyl chloride (Acros Organics, 98%) was purified according to a procedure described in literature prior usage.³⁴³ 4-*N,N*-Dimethylaminopyridine (4-DMAP, Alfa Aesar, 99%) was recrystallized from toluene. For cationic polymerizations anhydrous acetonitrile (VWR, max. 0.001% H₂O) and for other experiments acetonitrile (VWR Chemicals, 99+%) was used. Deuterated solvents were purchased from Deutero GmbH. DBCO derivatives were purchased from Lumiprobe GmbH.

Acryloyl chloride (Alfa Aesar, 96%), β -alanine (Alfa Aesar, 98%), Alexa Flour© 647-DBCO (Jena Bioscience), 1-amino-2-propanol (Fluka, 98%), 4-aminobenzophenone (Alfa Aesar, 98%), gaseous ammonia (Messer, 5.0), ammonium chloride (J.T. Baker, 99%), ammonia solution (Carl Roth, 25% w/w), 3-amino-1-propanol (Alfa Aesar, 99%), α -bromobutyric acid (Alfa Aesar, 98%), 2-bromoethylamine hydrobromide (Alfa Aesar, 98+%), *n*-butyronitrile (Alfa Aesar, 99%), *iso*-butyronitrile (Alfa Aesar, 99%), carbon disulfide (Acros Organics, 99.9%), 2-chloroethylamine hydrochloride (Alfa Aesar, 98+%), chloroform (VWR Chemicals, 99%), 3-chloro-1-propanol (Alfa Aesar, 98%), citric acid (Alfa Aesar, 99+%), *l*-cysteine (Alfa Aesar, 98%), 1,10-diaminododecane (J&K, 97%), 1,12-diaminododecane (Alfa Aesar, 98+%), 1,6-diaminohexane (Alfa Aesar, 98+%), 1,8-diaminooctane (Alfa Aesar 98%), 1,3-diaminopropane (Merck, 99%), di-*tert*.-butyl dicarbonate (Boc₂O, Alfa Aesar, 97+%), dichloromethane (DCM, Fisher Scientific, 99.8%), diethyl ether (Acros Organics, 99.5%), *N,N*-dimethylacetamide (DMAc, VWR Chemicals, 99.5%), *N,N*-dimethylformamide (DMF, Carl Roth, 99.8%), 1,4-dioxane (Carl Roth, 99.5%), 4,9-dioxadodecane-1,12-diamine (Merck, 99+%), *n*-dodecanethiol (Sigma Aldrich, 98%), dithiopropionic acid (Sigma Aldrich, 99%), ethanol (EtOH, VWR Chemicals, 99+%), ethyl acetate (EtOAc, VWR Chemicals, 99.8%), ethyl 4-bromobutyrate (Alfa Aesar, 98%), 1-ethyl-3-(3-dimethylaminopropyl)carbodiimide

hydrochloride (EDC-HCl, Carl Roth, 99+%), glycine (Sigma Aldrich, 99%), hexanes (Fisher Scientific), hydrochloric acid (VWR Chemicals, 37%), 2-hydroxy-2-methylpropiophenone (HMPP, CIBA, 97%), hydrazine monohydrate (Sigma Aldrich, 98%), *N*-hydroxysuccinimide (NHS, Alfa Aesar, 98+%), lithium bromide (Alfa Aesar, 98%), 3-mercaptopropionic acid (Alfa Aesar, 99%), (Mercaptoundecyl) triethylene glycol (SPT-0011, SensoPath Technologies) and (Mercaptoundecyl) pentaethylene glycol-2-ethoxyacetic acid (SPT-0012A, SensoPath Technologies), magnesium sulfate hexahydrate (Carl Roth, 99+%), methanol (MeOH, Fisher Scientific, 99.8%), 2-nitrobenzyl bromide (Alfa Aesar, 98+%), pentaerythritol tetraacrylate (PETA, Sigma Aldrich), phenyl isothiocyanate (Phenyl-NCS, Carl Roth, >99%), piperidine (Alfa Aesar, 99%), potassium carbonate (Bernd Kraft), potassium hydroxide (Carl Roth), potassium phthalimide (Alfa Aesar, 98+%), potassium thioacetate (Alfa Aesar, 98%), 1,3-propanedithiol (PDT, Alfa Aesar, 97%), sodium azide (Alfa Aesar, 99%), sodium hydrogencarbonate (J.T. Baker), sodium sulfate (Merck, 99+%), tetrahydrofuran (Fisher Scientific, 99%), trifluoroacetic acid (TFA, Roth, 99+%) and triphenylphosphine (TPP, Merck) were used as received. All other chemicals were purchased in highest quality available and were used as received.

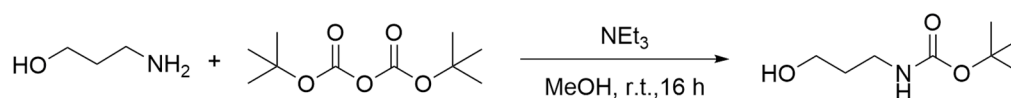
6.3 Synthesis of Initiators and Oxazolines for CROP

6.3.1 Functionalized Tosylates as Initiators for CROP

Synthesis of ω -functionalized Alcohols

Tert.-Butyl (3-hydroxypropyl)carbamate (N-Boc-Prop-OH)

The reaction was performed according to literature.¹



3-Aminopropanol (1.32 g, 17.54 mmol, 1.3 ml) was dissolved in methanol (20 ml) and successively di-tert-butyl dicarbonate (4.22 g, 19.30 mmol, 4.0 ml) was added. To the mixture triethylamine (3.55 g, 35.1 mmol, 4.9 ml) was added and the resulting mixture stirred overnight at room temperature. After removal of the solvent under reduced pressure, the product was redissolved in DCM (20 ml). The organic layer was washed with 10% citric acid (2 x 20 ml). The aqueous layers were extracted with DCM (3 x 20 ml). The combined organic layers were dried over sodium sulfate. Removal of the solvent under vacuum gave the title compound as colorless viscous oil. Yield: 2.63 g (15.0 mmol, 86%)

Spectral data:

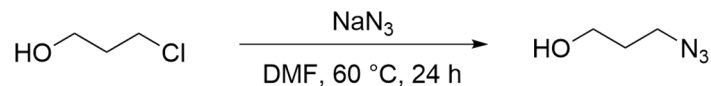
¹H NMR (500 MHz, CDCl₃): δ 4.85 (bs, 1H), 3.64 (t, J = 5.1 Hz, 2H), 3.26 (dd, J = 12.2, 6.2 Hz, 2H), 3.11 (bs, 1H), 1.65 (p, J = 5.9 Hz, 2H), 1.43 (s, 9H) ppm.

¹³C NMR (126 MHz, CDCl₃): δ 157.3, 79.7, 59.3, 37.0, 33.0, 28.5 ppm.

The NMR spectra are shown in Figure S1 and Figure S2.

3-Azidopropanol

The reaction was performed according to literature.²



3-Chloropropanol (5.65 g, 59.8 mmol, 5.0 ml) was dissolved in anhydrous DMF (40 ml). To this solution sodium azide (11.66 g, 0.18 mol) was added and the suspension stirred for 24 h at $T = 60\text{ }^\circ\text{C}$. Then the suspension was diluted four times with water and the title compound was extracted with diethyl ether (3 x 40 ml). The organic layer was dried over Na_2SO_4 , and the solvent removed in vacuo. The product was dried in vacuo overnight. Yield: 5.53 g* (44.9 mmol, 75 % of 3-azidopropanol).

*The recorded NMR spectra showed impurities caused by remaining DMF.

Spectral data:

^1H NMR (400 MHz, CDCl_3): δ 3.77–3.68 (m, 2H), 3.43 (t, $J = 6.7$ Hz, 2H), 2.16–2.06 (m, 1H), 1.87–1.75 (m, 2H) ppm.

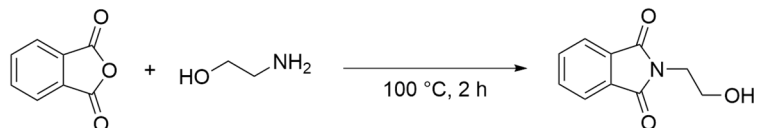
^{13}C NMR (101 MHz, CDCl_3): δ 59.9, 48.6, 36.6, 31.6 ppm.

IR (ATR): $\bar{\nu} = 3365, 2091, 1662, 1388, 1256, 1053\text{ cm}^{-1}$

The IR, NMR spectra are shown in Figure S3, Figure S4 and Figure S5, respectively.

2-(2-Hydroxyethyl)isoindoline-1,3-dione (Pht-Et-OH)

The reaction was performed according to literature.¹⁶⁶



Phthalic anhydride (5.94 g, 33.8 mmol) and ethanolamine (2.45 g, 40.0 mmol, 2.50 ml) were added to a flask equipped with magnetic stirrer and reflux condenser. The suspension was heated up to 100 °C and hold at this temperature for 2 h. Afterwards, the reaction cooled down to room temperature and was quenched by adding 1M HCl (25 ml). The formed white precipitate was filtered and recrystallized using ethanol. Afterwards, the product appeared as colorless crystals. Yield: 1.46 g (23%)

Spectral data:

¹H NMR (400 MHz, DMSO-d₆): δ 7.89–7.80 (m, 4H), 4.85 (t, *J* = 6.0 Hz, 1H), 3.68–3.60 (m, 2H), 3.62–3.53 (m, 2H) ppm.

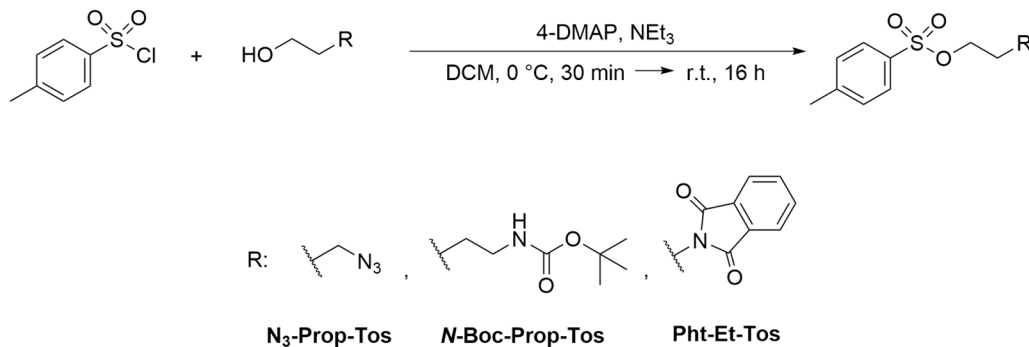
¹³C NMR (101 MHz, DMSO-d₆): δ 168.0, 134.3, 131.8, 122.9, 58.0, 40.4 ppm.

IR (ATR): $\bar{\nu}$ = 3498, 1691, 1392, 1055 cm⁻¹

The IR and NMR spectra are shown in Figure S6, Figure S7 and Figure S8, respectively.

General Procedure 1: Tosylation of ω -functionalized Alcohols

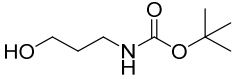
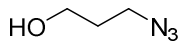
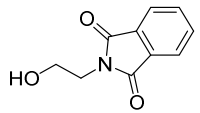
The tosylation of the different ω -functionalized alcohols was done according to literature.^{1,2}



The corresponding ω -functionalized alcohol (1 equiv.) was dissolved in DCM (15 ml). Then triethylamine (2 equiv.) and 4-DMAP (0.25 equiv.) were added and the mixture was cooled down to 0 °C. Afterwards a mixture of *p*-toluenesulfonyl chloride (1.4 equiv.), dissolved in DCM (10ml), was added dropwise to the solution. The mixture was stirred for further 30 min at 0 °C and then warmed to room temperature. Then, the mixture was diluted with DCM (25 ml) and washed with saturated NaHCO₃ solution (3 x 25 ml), 3M aqueous HCl (3 x 25 ml) and 10% brine (2 x 25 ml). The organic phase was dried with Na₂SO₄ and the solvent was removed in vacuo. Finally, the product was purified by column chromatography (for conditions see next page).

Pht-Et-Tos was purified by recrystallization from EtOAc / Hexane 2:1 (v/v). The weight-ins are listed in the following Table 6.1.

Table 6.1: Weight-ins of triethylamine, 4-DMAP, tosyl chloride and the corresponding ω -functionalized alcohol are listed. The concentration of the alcohol was adjusted to $\beta = 20 \text{ g l}^{-1}$. The yield of each reaction is given in the right column.

Product	Alcohol / g (mmol)	NEt ₃ / ml (g, mmol)	4-DMAP / mg (mmol)	Tosyl chloride / g (mmol)	Yield / g (mmol, %)
N-Boc-Prop-Tos	 0.52 (3.0)	0.8 (0.60, 6.0)	36 (0.3)	0.60 (3.1)	0.75 (2.3, 77)
N₃-Prop-Tos	 1.01 (7.8)	2.0 (1.46, 14.4)	242 (2.0)	2.08 (10.9)	1.43 (5.6, 72)
Pht-Et-Tos^b	 1.46 (7.6)	2.1 (1.55, 15.3)	--- ^a	2.02 (10.6)	1.84 (5.3, 70)

^a no 4-DMAP was used

^b purified by recrystallization from EtOAc / Hexane (2:1 v/v)

Spectral data:

N-Boc-Prop-Tos (NMR spectra are shown in Figure S9 and Figure S10.)

TLC / column chromatography: silica; eluent: hexanes / ethyl acetate 2 : 1 (v/v), $R_f = 0.72$

¹H NMR (500 MHz, CDCl₃): δ 7.77–7.74 (m, 2H), 7.34–7.30 (m, 2H), 4.69 (bs, 1H), 4.05 (t, $J = 6.1 \text{ Hz}$, 2H), 3.12 (t, $J = 6.4 \text{ Hz}$, 2H), 2.41 (s, 3H), 1.81 (p, $J = 6.3 \text{ Hz}$, 2H), 1.38 (s, 9H) ppm.

¹³C NMR (126 MHz, CDCl₃): δ 156.0, 145.0, 132.9, 130.0, 127.9, 79.4, 68.1, 36.9, 29.3, 28.4, 21.7 ppm.

N₃-Prop-Tos (IR and NMR spectra are shown in Figure S11, Figure S12 and Figure S13, respectively.)

TLC / column chromatography: silica; eluent: hexanes / ethyl acetate 3 : 1 (v/v), R_f: 0.64

¹H NMR (400 MHz, CDCl₃): δ 7.80–7.76 (m, 2H), 7.37–7.33 (m, 2H), 4.09 (t, *J* = 6.0 Hz, 2H), 3.36 (t, *J* = 6.5 Hz, 2H), 2.44 (s, 3H), 1.87 (p, *J* = 6.3 Hz, 2H) ppm.

¹³C NMR (101 MHz, CDCl₃): δ 145.1, 132.8, 130.0, 128.0, 67.1, 66.9, 47.3, 40.4, 31.8, 28.5, 21.7 ppm.

IR (ATR): $\bar{\nu}$ = 2096, 1356, 1172, 1096, 941 cm⁻¹

Pht-Et-Tos (The IR and NMR spectra are shown in Figure S14, Figure S15 and Figure S16, respectively.)

TLC / column chromatography: silica; eluent: hexanes / ethyl acetate 1 : 1, R_f: 0.54

¹H NMR (400 MHz, CD₃CN): δ 7.84–7.67 (m, 4H), 7.61–7.52 (m, 2H), 7.12–7.06 (m, 2H), 4.29 (s, 2H), 2.21 (s, 3H) ppm.

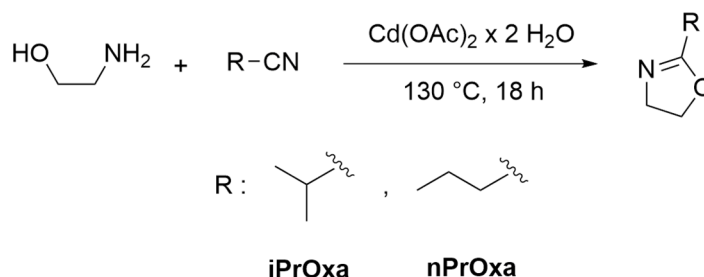
¹³C NMR (101 MHz, CD₃CN): δ 168.6, 146.3, 135.3, 133.3, 132.8, 130.9, 128.4, 124.0, 68.5, 37.6, 21.6 ppm.

IR (ATR): $\bar{\nu}$ = 1771, 1708, 1391, 1352, 1176 cm⁻¹

6.3.2 2-Alky-2-Oxazolines

Synthesis of Propyl-2-Oxazoline Derivatives

The reactions were performed according to a modified procedure described in literature.⁵



To a suspension of the respective butyronitrile (38.50 g, 0.556 mol, 48.6 ml), cadmium acetate dihydrat (7.32 g, 13.7 mmol) was added. Then, the reaction mixture was heated to 130 °C and ethanolamine (35.60 g, 0.582 mol, 36 ml) was added dropwise over a period of 1 h. The solution was stirred at this temperature overnight. After 18 h, the refluxing had stopped, and the product was isolated by fractional distillation in vacuo. Finally, the title compound was stirred with CaH₂ overnight followed by fractional distillation.

Analytical Data:

nPrOxa (NMR spectra are shown in Figure S17 and Figure S18.)

Yield: 38.4 g (0.34 mol, 61%)

Boiling point: $T = 68^\circ\text{C}$ at $p = 50$ hPa

¹H NMR (500 MHz, CDCl₃): δ 4.18 (t, $J = 9.5$ Hz, 2H), 3.79 (tt, $J = 9.3, 1.3$ Hz, 2H), 2.22 (tt, $J = 7.9, 1.4$ Hz, 2H), 1.67–1.58 (m, 2H), 0.94 (t, $J = 7.4$ Hz, 3H) ppm.

¹³C NMR (126 MHz, CDCl₃): δ 168.5, 67.2, 54.5, 30.0, 19.5, 13.8 ppm.

iPrOxa (NMR spectra are shown in Figure S19 and Figure S20.)

Yield: 32.2 g (0.29 mol, 51%)

Boiling point: $T = 63^\circ\text{C}$ at $p = 64$ hPa

¹H NMR (500 MHz, CDCl₃): δ 4.20 (t, $J = 9.4$ Hz, 2H), 3.79 (td, $J = 9.5, 1.2$ Hz, 2H), 2.55 (dtt, $J = 13.9, 7.0, 1.1$ Hz, 1H), 1.18 (d, $J = 6.9$ Hz, 6H) ppm.

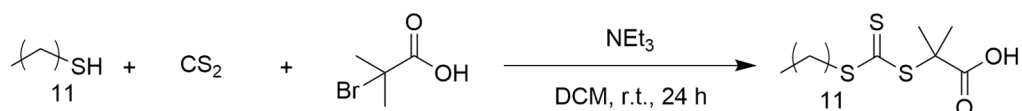
¹³C NMR (126 MHz, CDCl₃): δ 172.8, 67.4, 54.4, 28.2, 19.8 ppm.

6.4 Synthesis of Acrylamide Monomers and RAFT-Agents

6.4.1 RAFT Agent and their Modifications

Synthesis of RAFT-Agent 2-[[Dodecylthio]carbonothioyl]thio}-2-methylpropanoic acid (DMP)

DMP was synthesized according to a procedure reported in literature.⁶



n-Dodecanethiol (3.80 g, 18.8 mmol, 4.5 ml) and triethylamine (2.85 g, 28.2 mmol, 3.9 ml) were dissolved in DCM (50 ml) and stirred at room temperature under argon. After 20 min carbon disulfide (2.86 g, 37.6 mmol, 2.3 ml) was dropped into the solution and the reaction was carried out for further 3 h. Finally, α-bromoisobutyric acid (3.15 g, 18.8 mmol) was added and the mixture was stirred overnight. During the reaction, a white solid precipitated, which was removed by filtration. The clear yellowish solution was washed with 1M HCl solution (2 x 40 ml) and water (2 x 40 ml). The combined aqueous phase was extracted with DCM (40 ml). The organic phases were combined, dried over MgSO₄ and then the solvent was evaporated. The crude yellowish solid was recrystallized from hexane, to obtain DMP as pale-yellow crystals. Yield: 2.68 g (7.35 mmol, 39%)

Spectral data:

¹H NMR (500 MHz, CDCl₃): δ 3.28 (t, *J* = 7.4 Hz, 2H), 1.72 (s, 6H), 1.67 (dt, *J* = 15.0, 7.4 Hz, 2H), 1.41–1.34 (m, 2H), 1.34–1.21 (m, 16H), 0.88 (t, *J* = 7.0 Hz, 3H) ppm.

¹³C NMR (126 MHz, CDCl₃): δ 220.94, 178.93, 55.71, 37.22, 32.06, 29.78, 29.77, 29.71, 29.60, 29.49, 29.26, 29.12, 27.96, 25.36, 22.84, 14.26. ppm.

The NMR spectra are shown in Figure S21 and Figure S22.

Synthesis of RAFT-Agent DMP-Active ester (DMP-NHS)

DMP-NHS was synthesized according to a procedure reported in literature.⁷



DMP (500 mg, 1.4 mmol) and triethylamine (180 mg, 1.8 mmol, 247 μ l) were dissolved in DCM (30 ml) and stirred at room temperature under argon. Then EDC-HCl (341 mg, 1.4 mmol) and *N*-hydroxysuccinimide (241 mg, 1.8 mmol) was added and stirred overnight. The solvent was evaporated, and the product purified by a short silica column (eluent: hexanes : EtOAc 2 : 3 (v/v), R_f : 0.87). The solvents were evaporated, and the crude product further dried in vacuo overnight to obtain DMP-NHS as pale-yellow crystals. The product was directly used for the next step. Yield: 582 mg (1.3 mmol, 92%)

Spectral data:

¹H NMR (400 MHz, CDCl₃): δ 3.30 (t, J = 7.4 Hz, 2H), 2.90–2.72 (m, 4H), 1.91–1.82 (m, 6H), 1.68 (dt, J = 15.0, 7.3 Hz, 2H), 1.44–1.33 (m, 2H), 1.34–1.19 (m, 16H), 0.87 (t, J = 6.9 Hz, 3H) ppm.

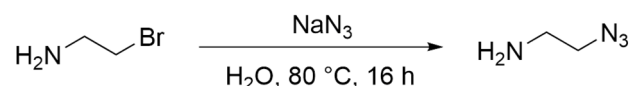
¹³C NMR (101 MHz, CDCl₃): δ 218.9, 169.2, 168.8, 54.4, 37.4, 32.0, 29.8, 29.8, 29.7, 29.6, 29.5, 29.2, 29.1, 27.9, 25.7, 22.8, 14.3 ppm.

The NMR spectra are shown in Figure S23 and Figure S24.

Synthesis of RAFT-Agent DMP-N₃

Synthesis of 2-Azidoethylamine

The reaction was performed according to a procedure reported in literature.³⁴⁴



2-Bromoethylamine hydrobromide (10.04 g, 48 mmol) was dissolved in water (50 ml). To this solution sodium azide (9.56 g, 147 mmol) was added and the suspension stirred for 16 h at 80 °C. Then the mixture was concentrated (~ 10 ml) and cooled in an ice bath. Afterwards, diethyl ether (100 ml) and subsequently solid KOH (8 g) were added, keeping the temperature below 10 °C. After phase separation, the aqueous phase was washed twice with diethyl ether (each 50 ml). The combined organic phases were dried over anhydrous K₂CO₃ and the solvent was evaporated. Finally, the title compound was purified by bulb-to-bulb distillation (T_{Boiling} : 63-65 °C at $p = 67$ hPa) on freshly grounded KOH (1 g). Yield: 3.05 g (35.4 mmol, 74%)

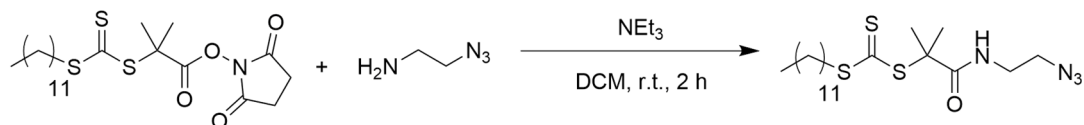
Spectral data:

¹H NMR (400 MHz, CDCl₃): δ 3.32 (t, $J = 5.8$ Hz, 2H), 2.87–2.81 (m, 2H), 1.17 (s, 2H) ppm.

¹³C NMR (101 MHz, CDCl₃): δ 54.7, 41.5 ppm.

IR (ATR): $\bar{\nu} = 3369, 2092, 1596, 1447, 1289, 838$ cm⁻¹

The IR and NMR spectra are shown in Figure S25, Figure S26 and Figure S27, respectively.

Synthesis of DMP-N₃

DMP-NHS (1.20 g, 2.6 mmol) and triethylamine (281 mg, 2.8 mmol, 385 μ l) were dissolved in DCM (30 ml) and stirred at room temperature under argon. Then 2-azidoethylamine (239 mg, 2.8 mmol, 239 μ l), was added and stirred until TLC (silica; eluent: hexanes : EtOAc 2 : 3 (v/v), R_f : 0.87) showed complete conversion (around 2 h). The reaction mixture was washed with 1M-HCl solution (3 x 30 ml) and brine (30 ml). The organic phase was dried over anhydrous Na_2SO_4 . Afterwards the solvent was evaporated in vacuo and the remaining yellow viscous liquid further dried in vacuo overnight. The product became a yellow solid during storage in a freezer. Yield: 908 mg (2.3 mmol, 90%)

Spectral data:

^1H NMR (400 MHz, CDCl_3): δ 6.78 (t, J = 5.3 Hz, 1H), 3.44–3.35 (m, 4H), 3.28 (t, J = 7.5 Hz, 2H), 1.69 (s, 6H), 1.68–1.62 (m, 2H), 1.42–1.33 (m, 2H), 1.32–1.22 (m, 16H), 0.87 (t, J = 6.9 Hz, 3H) ppm.

^{13}C NMR (101 MHz, CDCl_3): δ 220.31, 173.02, 57.11, 50.88, 39.74, 37.29, 32.04, 29.75, 29.68, 29.56, 29.47, 29.22, 29.09, 27.84, 25.88, 22.82, 14.26 ppm.

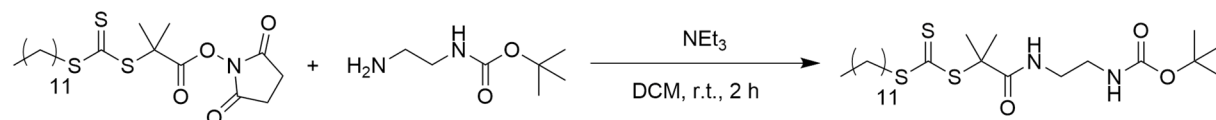
IR (ATR): $\bar{\nu}$ = 3368, 2918, 2110, 1723, 1651, 1528, 1259, 1063, 808 cm^{-1}

The IR and NMR spectra are shown in Figure 5.11 and Figure S28, respectively.

Synthesis of RAFT-Agent DMP-NH-Boc

DMP-NH-Boc was synthesized according to a procedure reported in literature.⁸

The synthesis of *tert.*-butyl (2-aminoethyl)carbamate is described in the chapter 6.4.2



DMP-NHS (619 mg, 1.3 mmol) and triethylamine (142 mg, 1.4 mmol, 194 μ l) were dissolved in DCM (30 ml) and stirred at room temperature under argon. Then *N*-Boc-ethylamine (216 mg, 1.4 mmol), was added and stirred until TLC (silica; eluent: hexanes : EtOAc 2 : 3 (v/v), R_f: 0.60) showed complete conversion (around 3.5 h). The solvent was evaporated, and the product purified by a short column chromatography. Afterwards the solvent was evaporated in vacuo and the remaining yellow viscous liquid further dried in vacuo overnight. The product became a yellow solid during storage in a freezer. Yield: 638 mg (1.3 mmol, 99%)

Spectral data:

¹H NMR (500 MHz, CDCl₃): δ 6.91 (s, 1H), 4.88 (s, 1H), 3.33–3.18 (m, 4H), 1.66 (s, 6H), 1.66–1.60 (m, 2H), 1.41 (s, 9H), 1.39–1.32 (m, 2H), 1.31–1.18 (m, 16H), 0.85 (t, J = 7.0 Hz, 3H) ppm.

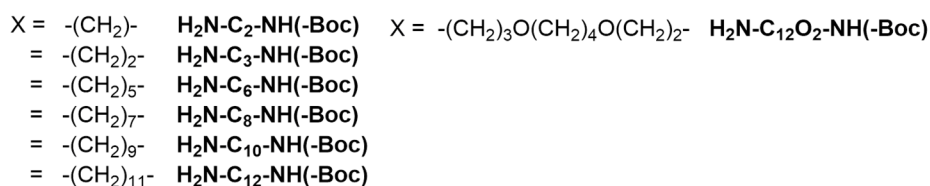
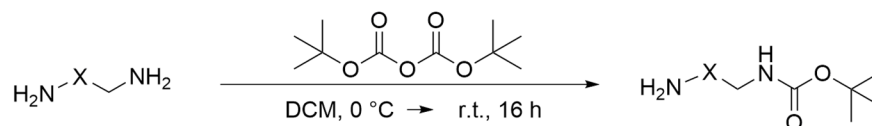
¹³C NMR (126 MHz, CDCl₃): δ 220.9, 173.1, 156.6, 79.5, 60.5, 57.1, 56.4, 41.1, 40.1, 37.2, 32.0, 29.7, 29.6, 29.5, 29.4, 29.2, 29.0, 28.5, 27.8, 25.9, 25.2, 24.0, 22.8, 14.2 ppm.

The NMR spectra are shown in Figure 5.11 and Figure S29.

6.4.2 Synthesis of Amino-Functionalized Acrylamides

General Procedure 2: Mono-Boc Protection of Diaminoalkanes

The *N*-Boc diamines were synthesized according to procedures reported in literature.^{14–17}



The corresponding diamine (2-10 equiv.) was dissolved in DCM ($\beta = 30 \text{ mg}\cdot\text{ml}^{-1}$) and cooled to 0 °C. Then a mixture of di-*tert*-butyl dicarbonate (1 equiv.) dissolved in DCM ($\beta = 90 \text{ mg}\cdot\text{ml}^{-1}$) was added dropwise. Afterwards, the reaction mixture was stirred for 16 hours at room temperature. Subsequently, the solvent was evaporated, and the residue dissolved in ethyl acetate (50 ml). The organic phase was washed with brine (3 x 30 ml), dried over anhydrous MgSO₄ and the solvent was removed under reduced pressure to yield the title compound. The weight-ins are listed in the following Table 6.2.

Table 6.2: Weight-ins of Boc₂O and the corresponding diamine are listed. The yield of each reaction is given in the right column.

Product	Diaminoalkane / g (mmol, ml)	Boc₂O / ml (mmol, g)	Yield / g (mmol, %)
H₂N-Et-NH-Boc	5.59 (93.0, 6.2)	2.0 (9.3, 2.03)	1.19 (7.4, 80)
H₂N-Prop-NH-Boc^a	2.02 (27.3, 2.3)	2.0 (9.3, 2.03)	1.05 (6.0, 69)
H₂N-Hex-NH-Boc	5.02 (43.2)	2.0 (9.3, 2.03)	1.72 (8.0, 91)
H₂N-Oct-NH-Boc	1.88 (13.1)	1.3 (5.8, 1.26)	1.27 (5.2, 90)
H₂N-Dec-NH-Boc	1.74 (10.0)	1.0 (4.7, 1.02)	0.99 (3.7, 81)
H₂N-Dod-NH-Boc^b	2.41 (12.1)	1.0 (4.7, 1.02)	1.21 (4.0, 92)
H₂N-PO-NH-Boc^b	4.82 (23.6, 5.0)	2.0 (9.3, 2.03)	2.49 (8.2, 94)

^a After DCM evaporation the crude product was redissolved in DCM and extracted with brine

^b Additional purification by column chromatography (silica; eluent: DCM : EtOH : TEA = 8 : 4 : 1)

Spectral data:

H₂N-Et-NH-Boc (Spectra are shown in Figure S30 and Figure S31.)

¹H NMR (500 MHz, CDCl₃): δ 4.92 (bs, 1H), 3.15 (dd, *J* = 11.3, 5.6 Hz, 2H), 2.77 (t, *J* = 5.9 Hz, 2H), 1.43 (s, 9H), 1.15 (s, 2H) ppm.

¹³C NMR (126 MHz, CDCl₃): δ 156.3, 79.3, 43.6, 42.0, 28.5 ppm.

H₂N-Prop-NH-Boc (Spectra are shown in Figure S32 and Figure S33.)

¹H NMR (500 MHz, CDCl₃): δ 4.94 (bs, 1H), 3.19 (dd, *J* = 12.1, 6.0 Hz, 2H), 2.74 (t, *J* = 6.6 Hz, 2H), 1.58 (p, *J* = 6.6 Hz, 2H), 1.41 (s, 9H), 0.87 (s, 2H) ppm.

¹³C NMR (126 MHz, CDCl₃): δ 156.3, 79.1, 39.8, 38.6, 33.6, 28.5 ppm.

H₂N-Hex-NH-Boc (Spectra are shown in Figure S34 and Figure S35.)

¹H NMR (500 MHz, CDCl₃): δ 4.55 (s, 1H), 3.09 (dd, *J* = 6.2 Hz, 6.2 Hz, 2H), 2.66 (t, *J* = 6.9 Hz, 2H), 1.51–1.36 (m, 13H), 1.35–1.25 (m, 4H), 1.17 (s, 2H) ppm.

¹³C NMR (126 MHz, CDCl₃): δ 156.1, 79.1, 42.3, 40.6, 33.9, 30.2, 28.5, 26.8, 26.7, 26.5 ppm.

H₂N-Oct-NH-Boc (Spectra are shown in Figure S36 and Figure S37.)

¹H NMR (500 MHz, CDCl₃): δ 4.54 (bs, 1H), 3.12–3.02 (m, 2H), 2.68–2.63 (m, 2H), 1.49–1.36 (m, 13H), 1.33–1.24 (m, 8 H), 1.07 (bs, 2H) ppm.

¹³C NMR (126 MHz, CDCl₃): δ 156.1, 79.1, 42.4, 40.7, 34.0, 30.2, 29.6, 29.5, 29.4, 28.6, 27.0, 26.9 ppm.

H₂N-Dec-NH-Boc (Spectra are shown in Figure S38 and Figure S39.)

¹H NMR (500 MHz, CDCl₃): δ 4.53 (bs, 1H), 3.08 (dd, *J* = 12.5, 6.1 Hz, 2H), 2.66 (t, *J* = 7.0 Hz, 2H), 1.48–1.37 (m, 13H), 1.26 (s, 12H), 1.17 (bs, 2H) ppm.

¹³C NMR (126 MHz, CDCl₃): δ 156.1, 79.1, 42.4, 40.7, 34.0, 30.2, 29.7, 29.6, 29.6, 29.4, 28.6, 27.0 ppm.

H₂N-Dod-NH-Boc (Spectra are shown in Figure S40 and Figure S41.)

TLC: silica; eluent: DCM : EtOH : NEt₃ = 8 : 4 : 1 (v/v/v); R_f: 0.55

¹H NMR (500 MHz, CD₃OD): δ 3.01 (t, *J* = 7.1 Hz, 2H), 2.65 (t, *J* = 7.2 Hz, 2H), 1.52–1.40 (m, 13H), 1.38–1.25 (m, 16H) ppm.

¹³C NMR (126 MHz, CD₃OD): δ 158.6, 79.7, 42.4, 41.4, 33.2, 31.0, 30.7, 30.6, 30.4, 28.8, 28.0, 27.9 ppm.

H₂N-PO-NH-Boc (Spectra are shown in Figure S42 and Figure S43.)

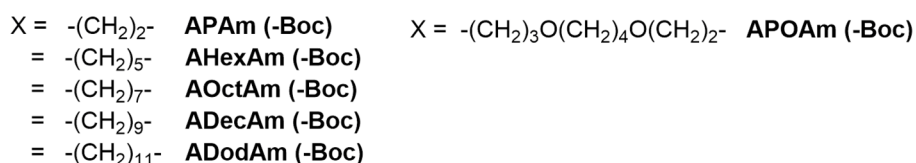
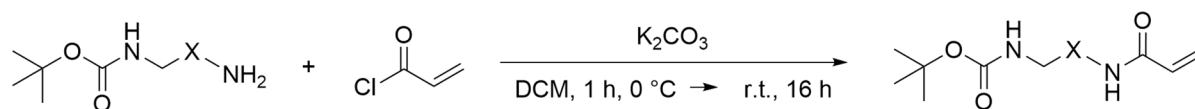
TLC: silica; eluent: DCM : EtOH : NEt₃ = 8 : 4 : 1 (v/v/v); R_f: 0.65

¹H NMR (500 MHz, CD₃OD): δ 3.53–3.42 (m, 8H), 3.12 (t, *J* = 6.9 Hz, 2H), 2.77 (t, *J* = 6.9 Hz, 2H), 1.78–1.68 (m, 4H), 1.65–1.60 (m, 4H), 1.43 (s, 9H) ppm.

¹³C NMR (126 MHz, CD₃OD): δ 158.5, 79.8, 71.8, 71.8, 69.9, 69.5, 40.0, 38.9, 32.9, 31.0, 28.8, 27.5 ppm.

General Procedure 3: Acrylation of *N*-Boc-Diaminoalkanes

The acrylation of the *N*-Boc-Diaminoalkanes, described in the previous section, was performed according to a procedure described in literature.¹³



The corresponding *tert.*-butyl-*N*-(aminoalkyl)carbamate (1 equiv.) was dissolved in DCM ($\beta = 30 \text{ mg}\cdot\text{ml}^{-1}$) and the solution was cooled down to 0 °C. Anhydrous potassium carbonate (1.2 equiv.) was added and the solution was stirred for 1 h. Acryloyl chloride (1.2 equiv.), dissolved in DCM ($\beta = 65 \text{ mg}\cdot\text{ml}^{-1}$), was added drop wise at 0 °C under vigorous stirring. The reaction was further continued for 16 h at room temperature. The reaction mixture was diluted with DCM (10 ml) and the solid materials were filtered-off. The organic layer was extracted with saturated sodium bicarbonate ($2 \times 25 \text{ ml}$) and saturated brine solution ($2 \times 25 \text{ ml}$). Anhydrous sodium sulfate was added to dry the organic layer, and the solvent was removed rotary evaporation. Finally, the product was dried in vacuum overnight.

Weight-in of the educts and the corresponding yields of the products are reported in the following Table 6.3.

Table 6.3: Weight-ins of acryloyl chloride, potassium carbonate and the corresponding mono-Boc protected diamine are listed. The yield of each reaction is given in the right column.

Product	mono-Boc protected diamine / g (mmol)	Acryloyl chloride / ml (mmol, g)	Potassium carbonate / g (mmol)	Yield / g (mmol, %)
APAm-Boc	H₂N-Prop-NH-Boc 1.05 (6.0)	0.58 (7.2, 0.65)	0.99 (7.2)	1.30 (5.7, 95)
AHexAm-Boc	H₂N-Hex-NH-Boc 1.72 (8.0)	0.77 (9.5, 0.86)	1.32 (9.5)	1.95 (7.2, 91)
AOctAm-Boc	H₂N-Oct-NH-Boc 1.25 (5.1)	0.50 (6.1, 0.56)	0.85 (6.1)	1.46 (4.9, 96)
ADecAm-Boc	H₂N-Dec-NH-Boc 1.00 (3.7)	0.36 (4.5, 0.40)	0.62 (4.5)	1.05 (3.2, 88)
ADodAm-Boc	H₂N-Dod-NH-Boc 0.83 (2.7)	0.27 (3.3, 0.30)	0.46 (3.3)	0.90 (2.54, 92)
APOAm-Boc	H₂N-PO-NH-Boc 1.00 (3.3)	0.32 (3.9, 0.36)	0.56 (4.0)	1.06 (3.0, 90)

Spectral data:

APAm-Boc (Spectra are shown in Figure S44 and Figure S45.)

¹H NMR (500 MHz, CDCl₃): δ 6.61 (bs, 1H), 6.25 (dd, *J* = 17.0, 1.5 Hz, 1H), 6.12 (dd, *J* = 17.0, 10.2 Hz, 1H), 5.61 (dd, *J* = 10.2, 1.6 Hz, 1H), 5.00 (bs, 1H), 3.36 (dd, *J* = 12.5, 6.3 Hz, 2H), 3.20–3.11 (m, 2H), 1.67–1.59 (m, 2H), 1.42 (s, 9H) ppm.

¹³C NMR (126 MHz, CDCl₃): δ 166.0, 156.9, 131.2, 126.1, 79.5, 37.1, 35.9, 30.2, 28.5 ppm.

AHexAm-Boc (Spectra are shown in Figure S46 and Figure S47.)

^1H NMR (500 MHz, CDCl_3): δ 6.26 (dd, $J = 17.0, 1.6$ Hz, 1H), 6.11 (dd, $J = 17.0, 10.3$ Hz, 1H), 5.99 (bs, 1H), 5.60 (dd, $J = 10.2, 1.6$ Hz, 1H), 4.58 (bs, 1H), 3.31 (dd, $J = 13.0, 7.0$ Hz, 2H), 3.13–3.04 (m, 2H), 1.49–1.38 (m, 13H), 1.38–1.26 (m, 4H) ppm.

^{13}C NMR (126 MHz, CDCl_3): δ 165.7, 156.3, 131.2, 126.2, 79.2, 40.2, 39.3, 30.1, 29.5, 28.6, 26.2, 26.1 ppm.

AOctAm-Boc (Spectra are shown in Figure S48 and Figure S49.)

^1H NMR (500 MHz, CDCl_3): δ 6.26 (dd, $J = 17.0, 1.5$ Hz, 1H), 6.09 (dd, $J = 17.0, 10.3$ Hz, 1H), 5.77 (bs, 1H), 5.61 (dd, $J = 10.3, 1.5$ Hz, 1H), 4.53 (bs, 1H), 3.33–3.28 (m, 2H), 3.12–3.02 (m, 2H), 1.56–1.48 (m, 2H), 1.48–1.37 (m, 11H), 1.34–1.23 (m, 8H) ppm.

^{13}C NMR (126 MHz, CDCl_3): δ 165.7, 156.2, 131.2, 126.2, 79.1, 40.7, 39.7, 30.1, 29.6, 29.2, 29.2, 28.6, 26.9, 26.8 ppm.

ADecAm-Boc (Spectra are shown in Figure S50 and Figure S51.)

^1H NMR (500 MHz, CDCl_3): δ 6.26 (dd, $J = 17.0, 1.5$ Hz, 1H), 6.08 (dd, $J = 17.0, 10.3$ Hz, 1H), 5.67 (bs, 1H), 5.61 (dd, $J = 10.3, 1.5$ Hz, 1H), 4.52 (bs, 1H), 3.34–3.29 (m, 2H), 3.09 (dd, $J = 12.8, 6.4$ Hz, 2H), 1.55–1.49 (m, 2H), 1.48–1.37 (m, 11H), 1.37–1.21 (m, 10H) ppm.

^{13}C NMR (126 MHz, CDCl_3): δ 165.6, 156.1, 131.2, 126.2, 79.1, 40.8, 39.7, 30.2, 29.7, 29.5, 29.3, 28.6, 27.0, 26.9 ppm.

ADodAm-Boc (Spectra are shown in Figure S52 and Figure S53.)

^1H NMR (500 MHz, CDCl_3): δ 6.25 (dd, $J = 17.0, 1.5$ Hz, 1H), 6.08 (dd, $J = 17.0, 10.3$ Hz, 1H), 5.75 (bs, 1H), 5.60 (dd, $J = 10.3, 1.4$ Hz, 1H), 4.53 (bs, 1H), 3.36–3.26 (m, 2H), 3.13–3.03 (m, 2H), 1.58–1.46 (m, 2H), 1.49–1.38 (m, 11H), 1.34–1.19 (m, 16H) ppm.

^{13}C NMR (126 MHz, CDCl_3): δ 165.6, 156.1, 131.2, 126.2, 79.1, 40.8, 39.8, 30.2, 29.7, 29.6, 29.4, 28.6, 27.0, 26.9 ppm.

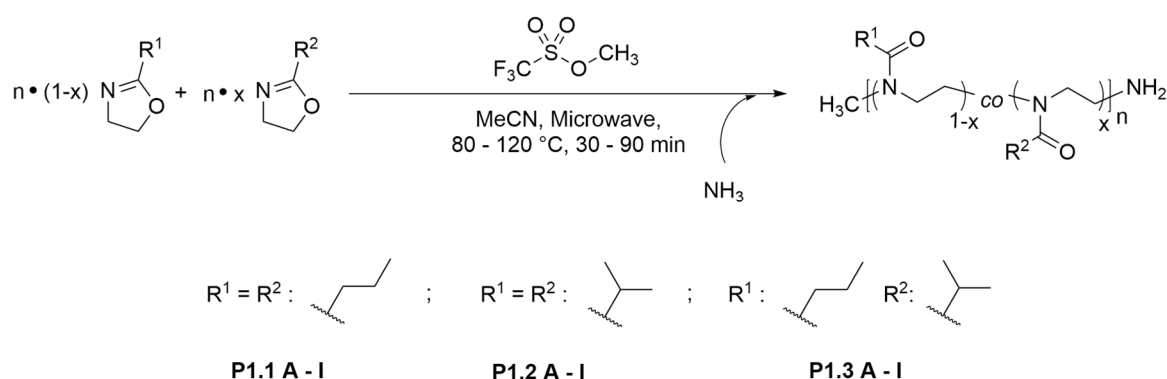
APOAm-Boc (Spectra are shown in Figure S54 and Figure S55.)

^1H NMR (500 MHz, CDCl_3): δ 6.55 (bs, 1H), 6.18 (dd, $J = 17.0, 1.7$ Hz, 1H), 6.05 (dd, $J = 17.0, 10.3$ Hz, 1H), 5.54 (dd, $J = 10.3, 1.7$ Hz, 1H), 4.96 (bs, 1H), 3.47 (t, $J = 5.8$ Hz, 2H), 3.42 (t, $J = 6.0$ Hz, 2H), 3.40–3.34 (m, 4H), 3.21–3.08 (m, 2H), 1.81–1.70 (m, 2H), 1.69 (p, $J = 6.3$ Hz, 2H), 1.64–1.51 (m, 4H), 1.37 (s, 9H) ppm.

^{13}C NMR (126 MHz, CDCl_3): δ 165.6, 156.1, 131.3, 125.7, 78.9, 70.8, 70.7, 69.8, 69.2, 38.8, 38.3, 38.1, 29.8, 29.0, 28.5, 26.5, 26.5 ppm.

6.5 Experimental Procedures for Synthesis of Poly(2-Oxazoline)s

General Procedure 4: Optimization of Reaction Conditions of Poly(2-Propyl-2-Oxazoline) Homo-and Copolymers



For the corresponding homopolymers either nPrOxa (401 mg, 3.5 mmol, **P1.1 A-I**) either iPrOxa (404 mg, 3.6 mmol, **P1.2 A-I**) were added from stock solutions, prepared in MeCN, into a glass vial in a glovebox. For the copolymer, mixtures of nPrOxa (209 mg, 1.8 mmol) and iPrOxa (201 mg, 1.8 mmol) (**P1.3 A-I**) were prepared under same conditions. Then MeOTf (7.72 mg, 0.05 mmol), dissolved in anhydrous MeCN, was added to the solution. The concentration of monomers was adjusted to $\beta = 200 \text{ mg}\cdot\text{ml}^{-1}$ ($V_{\text{MeCN}} = 2.0 \text{ ml}$). The polymerization was carried out in a microwave ($T_{\text{Reaction}} = 80 \text{ } ^\circ\text{C}$, $100 \text{ } ^\circ\text{C}$ or $120 \text{ } ^\circ\text{C}$) for different reaction times ($t_{\text{Reaction}} = 30 \text{ min}$, 60 min or 90 min). Afterwards the polymerization was quenched by purging the reaction mixture with gaseous NH_3 (1 h). The reaction mixture was stirred overnight at room temperature and concentrated by bubbling with N_2 , if necessary. The polymer solution was then dropwise added into ice-cold diethyl ether and the (co-)polymers appeared as white, sticky solid. The crude polymer was dissolved in 1,4-dioxane (20 ml) and lyophilized.

The detailed reaction parameter are provided in Table 6.4 (**P1.1 A-I**), Table 6.5 (**P1.2 A-I**) and Table 6.6 (**P1.3 A-I**).

6 Experimental Section

Table 6.4: Reaction conditions for the polymerization of different Poly(nPrOxa)-NH₂. The amounts of nPrOxa, and MeOTf were added each from a stock solution made in MeCN. The relative yields (%) are calculated according to the corresponding weight-in of monomer.

Polymer	T_{Reaction} / °C	t_{Reaction} / min	Yield / mg (%)
P1.1 A		30	22 (5)
P1.1 B	80	60	141 (35)
P1.1 C		90	298 (75)
P1.1 D		30	222 (56)
P1.1 E	100	60	239 (60)
P1.1 F		90	305 (76)
P1.1 G		30	127 (32)
P1.1 H	120	60	239 (60)
P1.1 I		90	314 (79)

Table 6.5: Reaction conditions for the polymerization of different Poly(iPrOxa)-NH₂. The amounts of iPrOxa and MeOTf were added each from a stock solution made in MeCN. The relative yields (%) are calculated according to the corresponding weight-in of monomer.

Polymer	T_{Reaction} / °C	t_{Reaction} / min	Yield / mg (%)
P1.2 A		30	43 (10)
P1.2 B	80	60	68 (17)
P1.2 C		90	66 (16)
P1.2 D		30	66 (16)
P1.2 E	100	60	168 (42)
P1.2 F		90	204 (50)
P1.2 G		30	117 (29)
P1.2 H	120	60	228 (57)
P1.2 I		90	286 (70)

Table 6.6: Reaction conditions for the polymerization of different Poly[(nPrOxa)-co-(iPrOxa)]-NH₂. The amounts of nPrOxa, iPrOxa and MeOTf were added each from a stock solution. The ratio [nPrOxa] : [iPrOxa] in the stock solution was adjusted to 51 : 49. The relative yields (%) are calculated according to the corresponding weight-in of monomer.

Polymer	T_{Reaction} / °C	t_{Reaction} / min	Yield / mg (%)
P1.3 A		30	72 (18)
P1.3 B	80	60	96 (23)
P1.3 C		90	164 (40)
P1.3 D		30	163 (40)
P1.3 E	100	60	193 (47)
P1.3 F		90	276 (67)
P1.3 G		30	313 (76)
P1.3 H	120	60	323 (79)
P1.3 I		90	358 (87)

Spectral data

Polymer P1.1 (Exemplarily shown in Figure S56)

¹H NMR (400 MHz, CDCl₃) δ 3.57–3.28 (1018H), 3.03–2.99 (3H), 2.39–2.14 (529H), 1.73–1.50 (529H), 0.98–0.84 (786H) ppm.

Polymer P1.2 (Exemplarily shown in Figure S57)

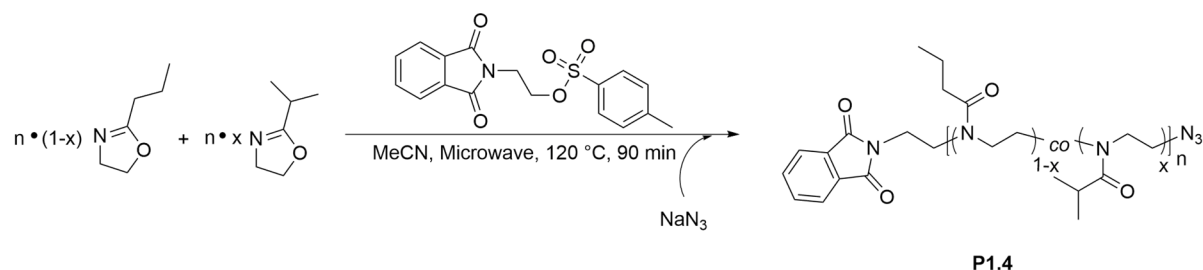
¹H NMR (400 MHz, CDCl₃) δ 3.62–3.24 (725H), 3.10–3.04 (3H), 2.99–2.48 (190H), 1.19–1.00 (1101H) ppm.

Polymer P1.3 (Exemplarily shown in Figure S58)

¹H NMR (400 MHz, CDCl₃) δ 3.59–3.27 (1084H), 3.13–3.09 (3H), 2.38–2.12 (303H), 1.16–0.99 (804H), 0.99–0.85 (442H) ppm.

Synthesis of Pht-Et-Poly[(nPrOxa)-*co*-(iPrOxa)]-N₃

The termination reaction was done according to a procedure described in literature.¹⁶¹



nPrOxa and iPrOxa were filled into a glass vial in a glovebox. Then a solution of Pht-Et-Tos, dissolved in anhydrous MeCN (3 ml), was added. The polymerization was carried out in a microwave at $T = 120\text{ }^{\circ}\text{C}$ for 90 min. Afterwards sodium azide was added under argon atmosphere. And the polymer solution was stirred 2 h at $70\text{ }^{\circ}\text{C}$. Afterwards, the mixture was cooled down to room temperature and the excess of sodium azide was filtered-off. Then acetonitrile was removed under reduced pressure and the remaining residue was redissolved in chloroform (20 ml). The organic phase was washed with saturated NaHCO_3 -solution (20 ml) and saturated brine (2 x 20 ml). The combined aqueous layers were extracted with chloroform (20 ml). Then both combined organic phases were combined, dried over anhydrous Na_2SO_4 and filtered. Then the polymer was concentrated ($\sim 5\text{ ml}$) and precipitated into ice-cold diethyl ether. Finally, the sticky polymer was dried in vacuo at $40\text{ }^{\circ}\text{C}$ for 1 h and then at room temperature overnight. The detailed weigh-ins are reported in the following Table 6.7.

Table 6.7: Weight-ins of nPrOxa, iPrOxa, Ph-Et-Tos and sodium azide and the corresponding yield of the reaction. For each reaction MeCN (3 ml) was used. The number in brackets indicates the number of e replicate. The relative yields (%) are calculated according to the corresponding weight-in of monomer.

Polymer	nPrOxa / mg (mmol)	iPrOxa / mg (mmol)	Ph-Et-Tos / mg (mmol)	MeCN / ml	NaN₃ / mg (mmol)	Yield / mg (%)
P1.4 (1)	596 (5.27)	608 (5.37)	103 (0.35)	3	229 (3.50)	860 (76)
P1.4 (2)	603 (5.32)	611 (5.40)	206 (0.60)	3	238 (3.66)	842 (64)
P1.4 (3)	631 (5.58)	623 (5.51)	108 (0.31)	3	228 (3.51)	857 (68)

Spectral data

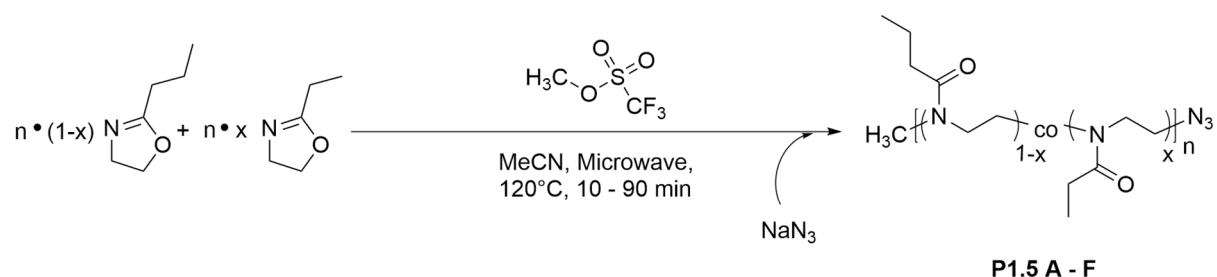
¹H NMR (400 MHz, CDCl₃) δ 7.87–7.69 (4H), 3.87–3.12 (244H), 3.00–2.51 (32H), 2.40–2.12 (62H), 1.72–1.49 (60H), 1.20–0.98 (179H), 0.98–0.83 (93H) ppm.

IR (ATR): $\bar{\nu}$ = 3510, 2107, 1714, 1628, 1419, 1198, 1087 cm⁻¹

The NMR and IR spectrum are shown in Figure 5.7.

General Procedure 5: Optimization of Reaction Conditions for Poly(*n*PrOxa-*co*-EtOxa) Copolymers

The termination reaction was done according to a procedure described in literature.¹⁶¹



*n*PrOxa (447 mg, 3.95 mmol) and EtOxa (147 mg, 1.48 mmol) were taken from a stock solution and filled into a glass vial in a glovebox. Methyl triflate (5.74 mg, 35 μmol), dissolved in anhydrous acetonitrile (1571 mg), was added and heated in a microwave at 120 $^\circ\text{C}$ for different reaction times ($t_{\text{Reaction}} = 10\text{-}90$ min) Afterwards the mixture was cooled to room temperature and sodium azide (60 mg, 0.92 mmol) was added under argon atmosphere. The polymer solution was stirred 2 h at 70 $^\circ\text{C}$. Afterwards, the mixture was cooled down to room temperature and the polymer precipitated into ice-cold diethyl ether. Then the polymer was redissolved in chloroform and washed with water (2 x 30 ml). The organic phase was concentrated and precipitated into ice-cold diethyl ether. The polymer was redissolved in 1,4-dioxane and freeze dried. The reaction times and corresponding yields are reported in the following Table 6.8.

Table 6.8: Reaction conditions for the polymerization of different Poly[(nPrOxa-co(EtOxa)]-N₃. The amounts of nPrOxa, EtOxa and MeOTf were added each from a stock solution made in MeCN. The relative yields (%) are calculated according to the corresponding weight-in of monomer.

Polymer	t_{Reaction} / min	Yield / mg (%)
P1.5 A	10	30 (5)
P1.5 B	15	82 (13)
P1.5 C	22.5	351 (56)
P1.5 D	45	478 (77)
P1.5 E	60	474 (76)
P1.5 F	90	474 (76)

Spectral data

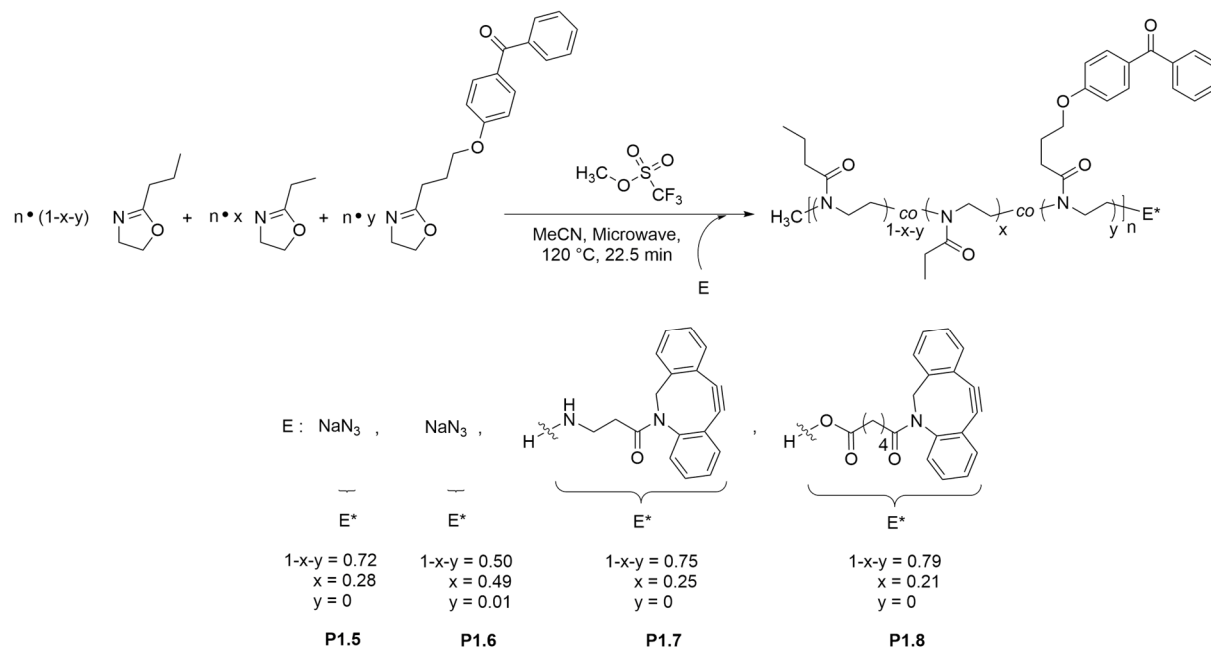
Polymer P1.5 D

¹H NMR (400 MHz, CDCl₃) δ 3.65–3.17 (581H), 3.12–2.98 (3H), 2.49–2.15 (287H), 1.72–1.48 (212H), 1.19–0.99 (122H), 0.99–0.83 (320H) ppm.

IR (ATR): $\bar{\nu}$ = 3498, 2100, 1629, 1418, 1191 cm⁻¹

The NMR and IR spectrum are shown in Figure S59 and Figure S60.

General Procedure 6: Polymerization of Poly(nPrOxa-co-EtOxa) Copolymers using Different Termination Agents



nPrOxa, EtOxa and BPOxa were filled into a glass vial. To this solution methyl triflate, dissolved in anhydrous acetonitrile, was added. The concentration of monomer to concentration of initiator was adjusted to $[M] : [I] = 150 : 1$. The overall monomer concentration was adjusted to $300 \text{ mg}\cdot\text{ml}^{-1}$. The polymerization was carried out in a microwave $T = 120 \text{ }^\circ\text{C}$ for 22.5 min. Afterwards the mixture was cooled to room temperature and the termination agent was added in excess with respect to the number of initiator molecules under argon atmosphere and stirred overnight. Afterwards, the polymer precipitated into ice-cold diethyl ether. Then, the polymer was redissolved in chloroform and filtrated through a syringe filter (PTFE, $0.2 \text{ }\mu\text{m}$). The solution was concentrated and precipitated into ice-cold diethyl ether. The polymer was finally redissolved in 1,4-dioxane and freeze dried.

The detailed weigh-ins and the yields are reported in the following Table 6.9.

Table 6.9: Weight-ins of nPrOxa, EtOxa, BP-Oxa, MeOTf, the termination agent and the corresponding yield of the reaction. The number in brackets indicates the number of replicate. The relative yields (%) are calculated according to the corresponding weight-in of monomer.

Polymer	nPrOxa / mg (mmol)	EtOxa / mg (mmol)	BP-Oxa / mg (mmol)	MeOTf / mg (μ mol)	MeCN / mg (ml)	Termination Agent E / mg (mmol)	Yield / mg (%)
P1.5 C (2)	447 (3.95)	147 (1.48)	---	5.7 (35.0)	1571 (2.0)	60 (0.92)	262 (43)
P1.5 C (3)	901 (7.96)	307 (3.10)	---	11.6 (70.9)	3089 (3.9)	120 (1.84)	548 (45)
P1.5 C (4)	4509 (39.85)	1538 (15.51)	---	58.4 (360)	15380 (19.7)	604 (9.29)	4020 (66)
P1.6	310 (2.74)	268 (2.71)	17 (0.06)	6.1 (37.1)	1588 (2.0)	26.2 (0.40)	280 (48)
P1.7	447 (3.95)	147 (1.48)	---	5.7 (35.0)	1574 (2.0)	19.3 (0.07)	323 (53)
P1.8	448 (3.95)	160 (1.61)	---	7.4 (45.1)	1575 (2.0)	18.0 ^a (54)	438 (72)

^a NEt₃ (7.3 mg, 72 μ mol, 10 μ l) was added additionally

Spectral data

Polymer P1.5 C (The NMR and IR spectrum are shown in Figure 5.3.)

¹H NMR (500 MHz, CDCl₃) δ 3.64–3.18 (601H), 3.06–2.98 (3H), 2.45–2.10 (301H), 1.81–1.72 (2H), 1.72–1.51 (215H), 1.16–1.00 (125H), 0.99–0.84 (322H).

IR (ATR): $\bar{\nu}$ = 3495, 2096, 1633, 1418, 1194 cm⁻¹ ppm.

Polymer P1.6 (The NMR and IR spectrum are shown in Figure 5.3.)

¹H NMR (500 MHz, CDCl₃) δ 7.80–7.41 (9H), 4.13–4.05 (2H), 3.65–3.23 (606H), 3.05–2.99 (3H), 2.49–2.11 (307H), 2.05 (2H), 1.81–1.70 (2H), 1.70–1.51 (153H), 1.18–1.00 (222H), 1.00–0.84 (232H) ppm.

IR (ATR): $\bar{\nu}$ = 3503, 2102, 1632, 1419, 1191 cm⁻¹

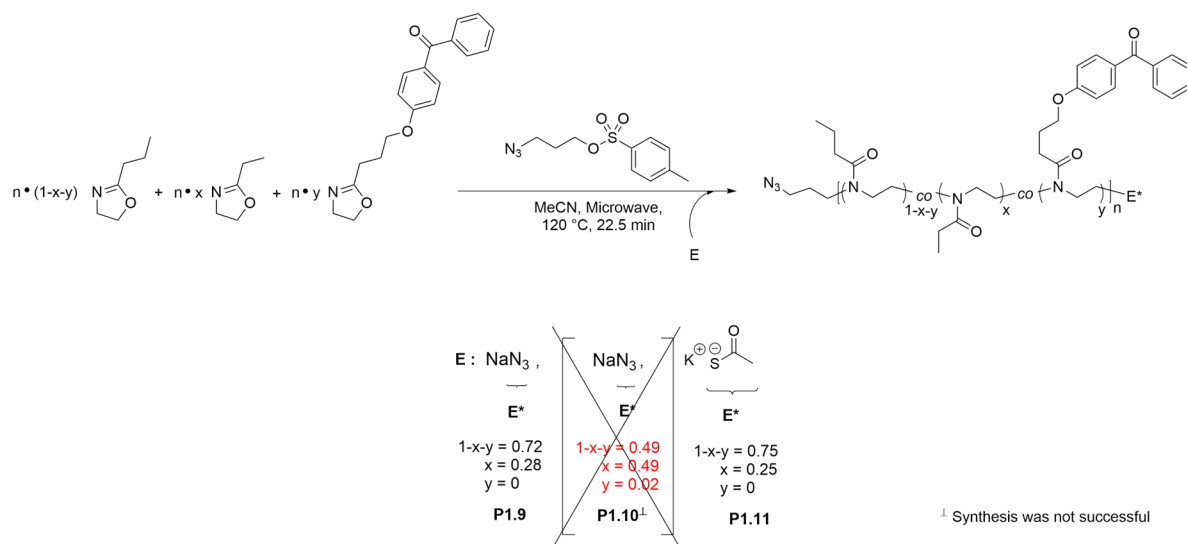
Polymer P1.7 (The NMR is shown in Figure 5.6.)

^1H NMR (400 MHz, CDCl_3) δ 7.70–7.60 (1H), 7.47–7.31 (4H), 4.18–4.10 (2H), 3.53–3.31 (644H), 3.05–2.99 (3H), 2.89–2.83 (m, 2H), 2.83–2.76 (m, 2H), 2.52–1.95 (359H), 1.73–1.48 (256H), 1.18–0.99 (137H), 0.99–0.82 (383H) ppm.

Polymer P1.8 (The NMR is shown in Figure 5.6.)

^1H NMR (500 MHz, CDCl_3) δ 7.68–7.27 (3H), 4.22–4.04 (1H), 3.62–3.20 (607H), 3.05–2.98 (3H), 2.48–2.13 (310H), 1.72–1.51 (219H), 1.18–1.00 (133H), 1.00–0.84 (329H) ppm.

General Procedure 7: Synthesis of N₃-Prop-Poly[(nPrOxa)-co-(EtOxa)] with different ω-End Groups



nPrOxa and EtOxa were filled into a glass vial. To this solution N₃-Prop-Tos, dissolved in anhydrous acetonitrile, was added in a glovebox. The concentration of monomer was adjusted to 265 mg·ml⁻¹. The polymerization was carried out in a microwave at 120 °C for 22.5 min. Afterwards the mixture was cooled to room temperature and quenched by adding the termination agent under argon atmosphere. The mixture was stirred overnight at room temperature. The solvent was evaporated, and the polymer redissolved in chloroform (20 ml). The organic phase was washed with saturated aqueous NaHCO₃-solution (2 x 20 ml). Afterwards, the solution was concentrated and precipitated into ice-cold diethyl ether. The polymer was finally redissolved in 1,4-dioxane and freeze dried. The detailed weigh-ins and the corresponding yields are reported in the following Table 6.10.

Table 6.10: Weight-ins of nPrOxa, EtOxa, N₃-Prop-Tos, the termination agent and the corresponding yield of the reaction. The number in brackets indicated the number of experiment. The relative yields (%) are calculated according to the corresponding weight-in of monomer.

Polymer	nPrOxa / mg (mmol)	EtOxa / mg (mmol)	N ₃ -Prop- Tos / mg (μ mol)	MeCN / mg (ml)	Termination Agent / mg (mmol)	Yield / mg (%)
P1.9 (1)	577 (5.12)	184 (1.86)	13.4 (52.4)	2240 (2.9)	34 (0.52)	370 (48)
P1.9 (2)	2320 (20.5)	745 (7.5)	54.1 (212.0)	8980 (11.5)	147 (2.26)	1700 (54)
P1.10^a	349 (3.08)	306 (3.08)	15.0 (58.8)	2016 (2.6)	35 (0.54)	--- ^b
P1.11	932 (8.23)	346 (3.49)	40.7 (159.4)	3150 (4.0)	78.4 (0.69)	696 (54)

^a additional BP-Oxa (31.0 mg, 0.1 mmol) was added

^b no polymer was obtained

Spectral data

Polymer P1.9 (The NMR and IR spectrum are shown in Figure 5.8.)

¹H NMR (500 MHz, CDCl₃) δ 3.65–3.22 (632H), 2.75–2.56 (2H), 2.47–2.13 (315H), 1.71–1.51 (230H), 1.18–1.01 (126H), 1.01–0.84 (345H) ppm.

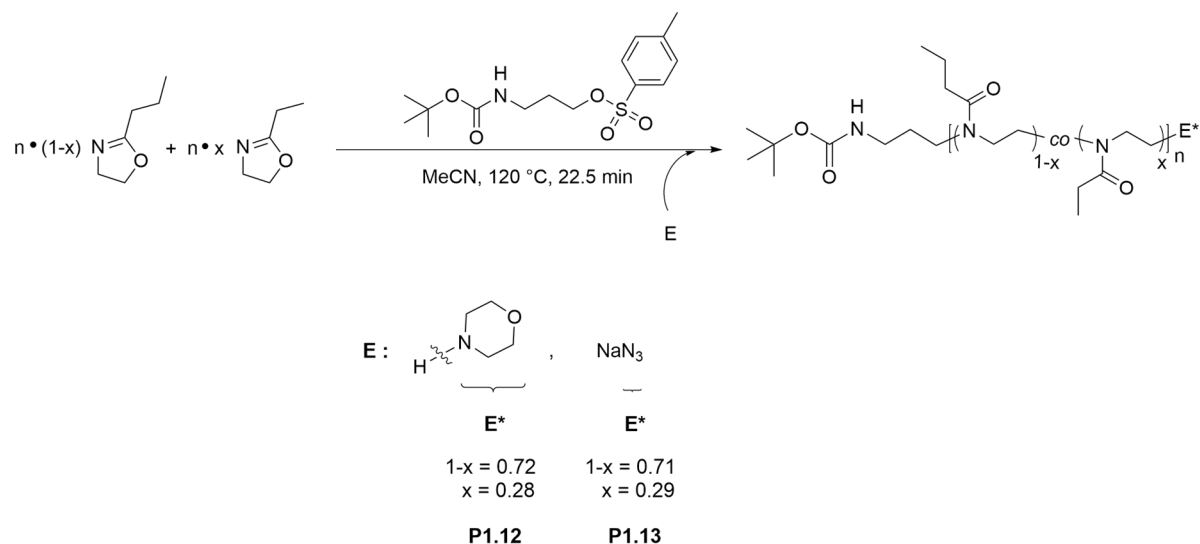
IR (ATR): $\bar{\nu}$ = 3504, 2097, 1630, 1420, 1191 cm⁻¹

Polymer P1.11 (The NMR and IR spectrum are shown in Figure 5.9.)

¹H NMR (500 MHz, CDCl₃) δ 3.58–3.19 (465H), 2.96–2.93 (2H), 2.44–2.12 (243H), 1.84–1.77 (2H), 1.70–1.51 (165H), 1.16–0.99 (102H), 0.98–0.84 (247H) ppm.

IR (ATR): $\bar{\nu}$ = 3506, 2100, 1632, 1417, 1189 cm⁻¹

General Procedure 8: Synthesis of *N*-Boc-Prop-Poly[(*n*PrOxa)-co-(EtOxa)] with different ω -End Groups



*n*PrOxa and EtOxa were filled into a glass vial. To this solution *N*-Boc-aminopropyl tosylate, dissolved in anhydrous acetonitrile, was added in a glovebox. The concentration of monomer was adjusted to 300 mg·ml⁻¹. The polymerization was carried out in a microwave at 120 °C for 22.5 min. Afterwards, the mixture was cooled to room temperature and quenched by adding the termination agent under argon atmosphere. The mixture was stirred at room temperature overnight. The solvent was evaporated, and the polymer redissolved in chloroform (20 ml). The organic phase was washed with saturated aqueous NaHCO₃ solution (2 x 20 ml). Afterwards, the solution was concentrated and precipitated into ice-cold diethyl ether. The polymer was finally redissolved in 1,4-dioxane and freeze dried. The detailed weigh-ins and the corresponding yields are reported in the following Table 6.11.

6 Experimental Section

Table 6.11: Weight-ins of nPrOxa, EtOxa, *N*-Boc-Prop-Tos, the termination agent and the corresponding yield of the reaction. The number in brackets indicates the number of replicate. The relative yields (%) are calculated according to the corresponding weight-in of monomer.

Polymer	nPrOxa / mg (mmol)	EtOxa / mg (mmol)	<i>N</i> -Boc- Prop-Tos / mg (μ mol)	MeCN / mg (ml)	Termination Agent E / mg (mmol)	Yield / mg (%)
P1.12 (1)	461 (4.07)	147 (1.58)	42.5 (129)	1575 (2.0)	34.8 (0.40) ^a	532 (82)
P1.12 (2)	936 (8.27)	327 (3.30)	96.4 (293)	3155 (4.0)	34.8 (0.40) ^a	984 (75)
P1.13 A	468 (4.14) ^a	163 (1.65) ^a	37.2 (113) ^b	1572 (2.0)	65.1 (1.00) ^c	475 (75)
P1.13 A (2)	936 (8.27)	327 (3.30)	96.4 (293)	3155 (4.0)	173 (2.66) ^c	1040 (82)
P1.13 B	468 (4.14) ^b	163 (1.65) ^b	24.8 (75.3) ^b	1572 (2.0)	43.0 (0.67) ^c	400 (63)
P1.13 C	468 (4.14) ^b	163 (1.65) ^b	18.9 (57.4) ^b	1572 (2.0)	32.5 (0.50) ^c	341 (54)
P1.13 D	468 (4.14) ^b	163 (1.65) ^b	12.7 (38.6) ^b	1572 (2.0)	26.2 (0.40) ^c	261 (41)
P1.13 E	468 (4.14) ^b	163 (1.65) ^b	10.4 (31.7) ^b	1572 (2.0)	20.8 (0.32) ^c	263 (42)
P1.13 F	468 (4.14) ^b	163 (1.65) ^b	6.9 (21.2) ^b	1572 (2.0)	13.6 (0.21) ^c	164 (26)
P1.13 G	468 (4.14) ^b	163 (1.65) ^b	5.0 (15.4) ^b	1602 (2.0)	10.0 (0.15) ^c	185 (29)
P1.13 H^d	479 (4.23) ^b	167 (1.68) ^b	5.1 (15.5) ^b	1610 (2.1)	10.0 (0.15) ^c	266 (41)
P1.13 I^e	479 (4.23) ^b	167 (1.68) ^b	5.1 (15.5) ^b	1612 (2.0)	10.0 (0.15) ^c	338 (52)

^a added as 1M methanolic solution

^b added from stock solution

^c after addition of NaN₃ the solution was stirred for 4 h at 80°C and afterwards at room temperature overnight

^d reaction time 37.5 min at 120 °C

^e reaction time 45 min at 120 °C

Spectral data

Polymer P1.12 (The NMR spectrum is shown in Figure S61.)

^1H NMR (400 MHz, CDCl_3) δ 3.72–3.63 (m, 3H), 3.61–3.24 (m, 528H), 3.21–3.08 (m, 2H), 2.51–2.44 (m, 3H), 2.43–2.11 (m, 207H), 1.84–1.73 (m, 2H), 1.71–1.51 (m, 149H), 1.42 (s, 4H), 1.19–1.00 (m, 91H), 1.00–0.86 (m, 222H) ppm.

Spectral data

Polymer P1.13 A (The NMR and IR spectrum are shown in Figure 5.10 and Figure S62.)

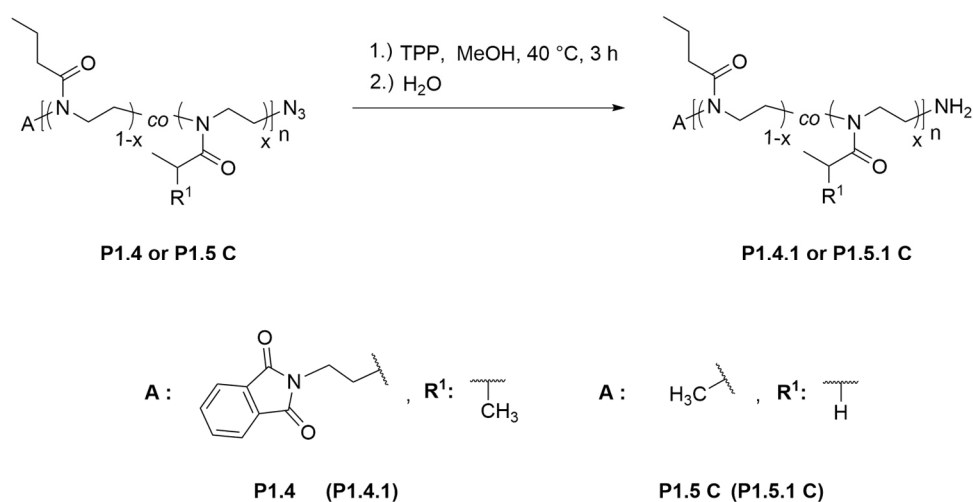
^1H NMR (500 MHz, CDCl_3) δ 3.65–3.23 (m, 436H), 3.23–3.03 (m, 2H), 2.48–2.03 (m, 228H), 1.83–1.71 (m, 2H), 1.71–1.50 (m, 154H), 1.41 (s, 4H), 1.19–1.01 (m, 96H), 1.01–0.82 (m, 231H) ppm.

IR (ATR): $\bar{\nu}$ = 3515, 2100, 1632, 1419, 1190 cm^{-1}

6.6 Post-functionalization Reactions of Poly(2-Oxazoline)s

General Procedure 10: Staudinger Reduction of Azide containing Poly[2-Alkyl-2-oxazoline] Co- and Terpolymers

The reaction was done according to a modified procedure described in literature.¹⁶¹



The azide end-functionalized polymer (1 equiv.) was dissolved in MeOH ($\beta = 30 \text{ mg}\cdot\text{ml}^{-1}$). To the mixture triphenylphosphine (2 equiv.) was added and the mixture was stirred at 40 °C for 3 h. Then a 2-fold volume of cold deionized water with respect to the volume of MeOH was added and the remaining TPP was filtered-off (glass frit porosity 4). The solvents were evaporated under reduced pressure and the remaining viscous liquid was diluted again with cold deionized water (20 ml). The suspension was again filtrated and lyophilized.

The weight-ins are reported in Table 6.12.

Table 6.12: Weight-ins of polymer, TPP and the required volume of EtOH and the corresponding yield of each reaction. The number in brackets indicates the number of replicate. The relative yields (%) are calculated according to the corresponding weight-in of the polymer which was used as educt.

Polymer	Educt Polymer P1. / mg (μmol)	Mass Polymer / mg (μmol)	TPP / mg (mmol)	MeOH / ml	Yield / mg (%)
P1.4.1	4	275 (55)	288 (1.1)	10 ^a	213 (85)
P1.5.1 C (2)	5 C (2)	100 (10)	52 (0.2)	5	86 (86)
P1.5.1 C (3) ^b	5 C (3)	267 (27)	52 (0.2)	10	249 (93)
P1.5.1 C (4)	5 C (4)	3440 (180)	465 (1.8)	100	2880 (84)

^a EtOH was used instead of MeOH

^b The product was additionally purified by dialysis (MWCO = 1.0 kg·mol⁻¹) against EtOH, followed by lyophilization

Spectral data

Polymer P1.4.1 (The NMR and IR spectrum are shown in Figure 5.7.)

¹H NMR (400 MHz, CDCl₃) δ 7.87–7.68 (4H), 3.70–3.13 (292H), 2.99–2.49 (41H), 2.42–1.93 (95H), 1.72–1.51 (72H), 1.18–0.99 (221H), 0.99–0.85 (111H) ppm.

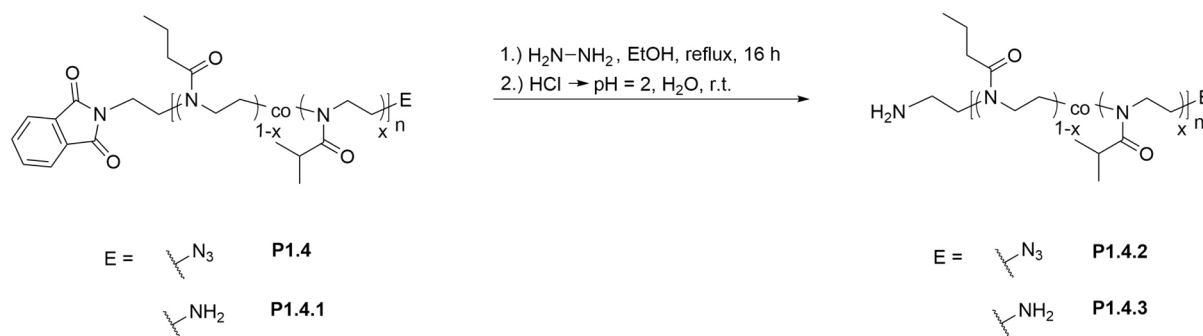
IR (ATR): $\bar{\nu}$ = 3504, 1715, 1632, 1419, 1158, 1087 cm⁻¹

Polymer P1.5.1 C (4) (The NMR and IR spectrum are shown in Figure S63 and Figure S64.)

¹H NMR (500 MHz, CDCl₃) δ 3.64–3.17 (597H), 3.05–2.98 (3H), 2.47–2.12 (304H), 1.71–1.50 (217H), 1.17–1.01 (126H), 1.01–0.83 (325H) ppm.

IR (ATR): $\bar{\nu}$ = 3502, 1632, 1419, 1191 cm⁻¹

General Procedure 11: Hydrazinolysis of Pht-Et-Tos initiated Polymers



The phthalimide end-capped polymer (1 equiv.) was dissolved in EtOH. The concentration was adjusted to $\beta = 5.0 \text{ mg}\cdot\text{ml}^{-1}$. Hydrazine hydrate (10 equiv.) was added and the mixture stirred at reflux overnight. After cooling the solution to room temperature concentrated HCl was added dropwise until pH = 2 was obtained. The solution was filtered and the EtOH removed under reduced pressure. The remaining white residue was redissolved in the same amount of water as the used of EtOH. Then 1M NaOH was added to adjust the pH to 9–10. The aqueous phase was extracted with chloroform (4 x 25 ml) and the organic phase was dried over anhydrous Na_2SO_4 and filtered. The polymer was concentrated under reduced pressure and precipitated into ice-cold diethyl ether. The polymer was dried overnight in vacuo. The weight-ins are reported in the following Table 6.13.

Table 6.13: Weight-ins of the polymer used as educt and hydrazine hydrate and the corresponding yield of the reaction. The number in brackets indicates the number of replicate. The relative yields (%) are calculated according to the corresponding weight-in of polymer.

Polymer	Educt Polymer	Polymer / mg (μmol)	Hydrazine Hydrate / mg (mmol, μl)	Yield / mg (%)
P1.4.2 (1)	1.4 (1)	100 (51)	16.0 (0.51, 16.0)	73 (73)
P1.4.2 (2)^a	1.4 (3)	857 (86)	27.5 (0.85, 26.7)	726 (85)
P1.4.3 (1)	1.4.1 (1)	50 (12)	4.0 (0.12, 4.0)	25 (50)

^a Higher concentration was used ($\beta = 21.4 \text{ mg}\cdot\text{ml}^{-1}$)

Spectral data

Polymer P1.4.2 (Exemplarily shown in Figure 5.7.)

^1H NMR (400 MHz, CDCl_3) δ 3.67–3.18 (8H), 2.99–2.54 (1H), 2.43–2.12 (2H), 1.91–1.50 (3H), 1.20–1.00 (6H), 1.00–0.86 (3H) ppm.

IR (ATR): $\bar{\nu} = 3519, 2104, 1628, 1419, 1158, 1087 \text{ cm}^{-1}$

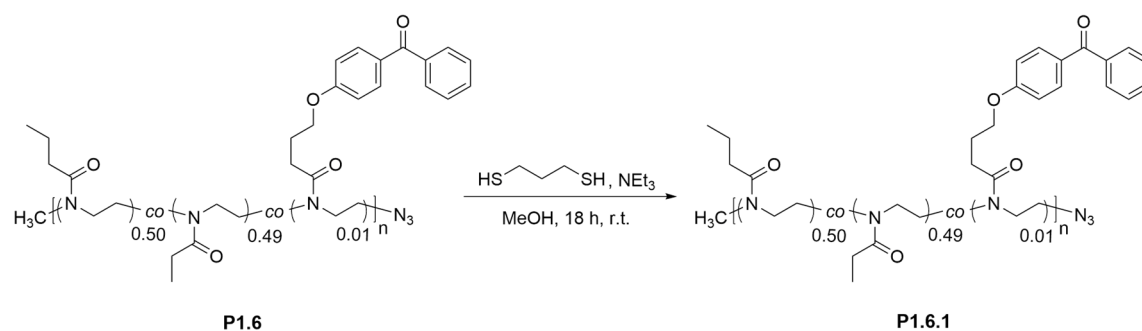
Polymer P1.4.3 (The IR and NMR spectrum are shown in Figure 5.7.)

^1H NMR (400 MHz, CDCl_3) δ 3.63–3.18 (8H), 3.07–2.50 (1H), 2.44–2.12 (2H), 1.73–1.50 (2H), 1.20–1.00 (6H), 1.00–0.84 (3H) ppm.

IR (ATR): $\bar{\nu} = 3493, 1634, 1418, 1198, 1085 \text{ cm}^{-1}$

Reduction of Azide containing Poly[(2-Alkyl-2-oxazoline) Co- and Terpolymers using 1,3-Propanedithiol

The reaction was done according to a modified procedure described in literature.¹⁷³



The azide end functionalized polymer (250 mg, 19 μmol) was dissolved in MeOH (2.5 ml). To the mixture 1,3-propanedithiol (PDT, 163 mg, 1.5 mmol, 150 μl) and triethylamine (151 mg, 1.5 mmol, 208 μl) were added and the mixture was stirred at room temperature overnight. Then the polymer was precipitated into ice-cold diethyl ether. The white solid was collected redissolved in ethanol and residues of impurities filtered-off. Then the solvent was evaporated, and the polymer finally lyophilized from dioxane. Yield: 247 mg (99%)

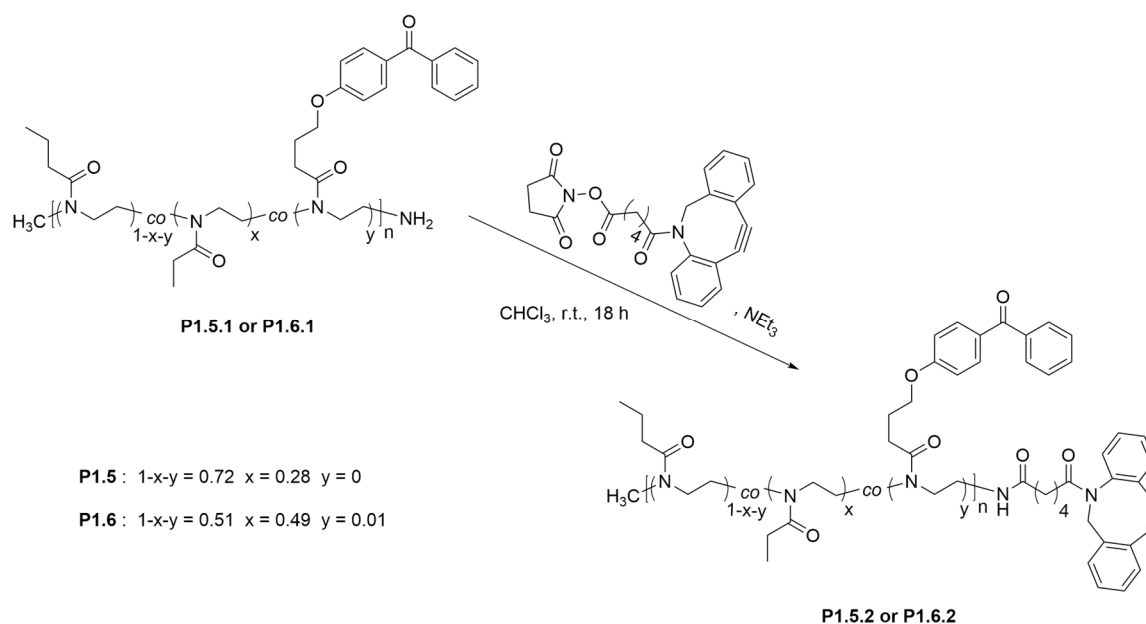
Spectral data

Polymer P1.6.1 (The IR and NMR spectrum are shown in Figure S65 and Figure S66.)

^1H NMR (500 MHz, CDCl_3) δ 7.81–7.40 (7H), 4.13–4.03 (2H), 3.62–3.16 (531H), 3.03–2.97 (3H), 2.48–2.13 (272H), 1.68–1.49 (136H), 1.16–0.98 (196H), 0.98–0.82 (206H) ppm.

IR (ATR): $\bar{\nu}$ = 3497, 1630, 1420, 1195 cm^{-1}

General Procedure 12: DBCO Functionalization of Poly(2-Oxazoline)s



The amino end-functionalized polymer (1 equiv.) was dissolved in chloroform ($\beta = 50 \text{ mg}\cdot\text{ml}^{-1}$). To the mixture DBCO-C₄-NHS (3 equiv.) and triethyl amine (3 equiv.) were added and the mixture was stirred at room temperature overnight. The polymer was precipitated into ice-cold diethyl ether and redissolved in ethanol. Impurities were removed by dialysis against ethanol (MWCO $1.0 \text{ kg}\cdot\text{mol}^{-1}$, 2 days). Finally, the solvent was removed, and the crude product lyophilized from 1,4-dioxane. The weight-ins of each reaction are listed in Table 6.14 on the next page.

Table 6.14: Weight-ins of the polymer used as educt and DBCO-C₄-NHS, NEt₃ and the corresponding yield of the reaction. The number in brackets indicates the number of replicate. The relative yields (%) are calculated according to the corresponding weight-in of polymer.

Polymer	Educt Polymer	Polymer / mg (μmol)	DBCO-C ₄ -NHS / mg (μmol)	NEt ₃ / μl (μmol, mg)	CHCl ₃ / ml	Yield / mg (%)
P1.5.2 (3)	1.5.1 (3)	249 (23.5)	30.3 (70.5)	10.0 (70.5, 7.1)	5.0	181 (73)
P1.5.2 (4)	1.5.1 (4)	2833 (146)	189 (438)	61.0 (438, 44.3)	30 ^a	2785 (92)
P1.6.2	1.6.1	220 (16.3)	21.1 (48.9)	7.0 (48.9, 4.9)	4.4	182 (83)

^a Higher mass concentration was used ($\beta = 95 \text{ mg}\cdot\text{ml}^{-1}$)

Spectral data

Polymer P1.5.2 (4) (Exemplarily shown in Figure 5.4.)

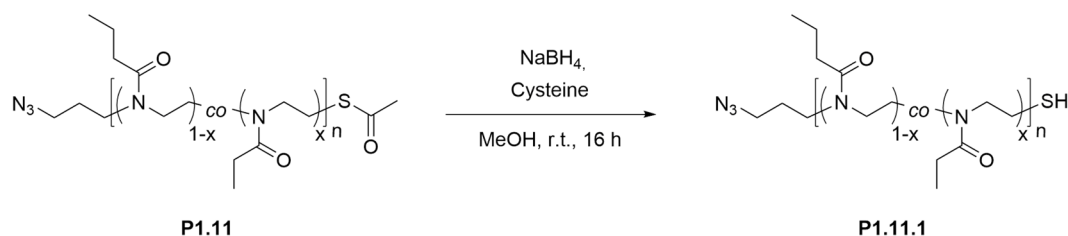
¹H NMR (500 MHz, CDCl₃) δ 7.72–7.63 (1H), 7.44–7.28 (4H), 7.25–7.21 (1H), 4.25–4.02 (2H), 3.60–3.26 (621H), 3.06–2.99 (3H), 2.46–2.14 (316H), 1.73–1.50 (227H), 1.17–1.00 (134H), 1.00–0.84 (337H) ppm.

Polymer P1.6.2 (The NMR spectrum is shown in Figure 5.4.)

¹H NMR (500 MHz, CDCl₃) δ 7.82–7.28 (18H), 4.15–4.05 (4H), 3.66–3.19 (741H), 3.05–2.98 (3H), 2.49–2.16 (380H), 1.72–1.50 (189H), 1.18–1.00 (268H), 1.00–0.74 (281H) ppm.

Synthesis of N₃-Prop-Poly[(nPrOxa)-co-(EtOxa)]-SH

The reaction procedure was adapted from literature.¹⁷⁸



The thioacetate-functionalized polymer (**P1.11**, 200 mg, 16.3 μmol) was dissolved in MeOH (3 ml). Separately, cysteine (3.0 mg, 24.5 μmol) was dissolved in MeOH (3 ml). Both solutions were purged with argon for 15 min. Afterwards, sodium borohydride (1.9 mg, 49 μmol) was added to the cysteine solution. Then the polymer solution was added to the cysteine solution and the resulting mixture was stirred for 16 h at room temperature. The mixture was filtrated, concentrated and the polymer was precipitated into ice-cold diethyl ether. The polymer was redissolved in water and tris(2-carboxyethyl)phosphine hydrochloride (TCEP-HCl, 4.7 mg, 16.3 μmol) was added. The solution was stirred for 2 h at room temperature. Afterwards, the polymer was purified by dialysis (MWCO = 1.0 kg·mol⁻¹) against degassed water over 2 days. Finally, the polymer was lyophilized and obtained as white powder. Yield: 138 mg (69%)

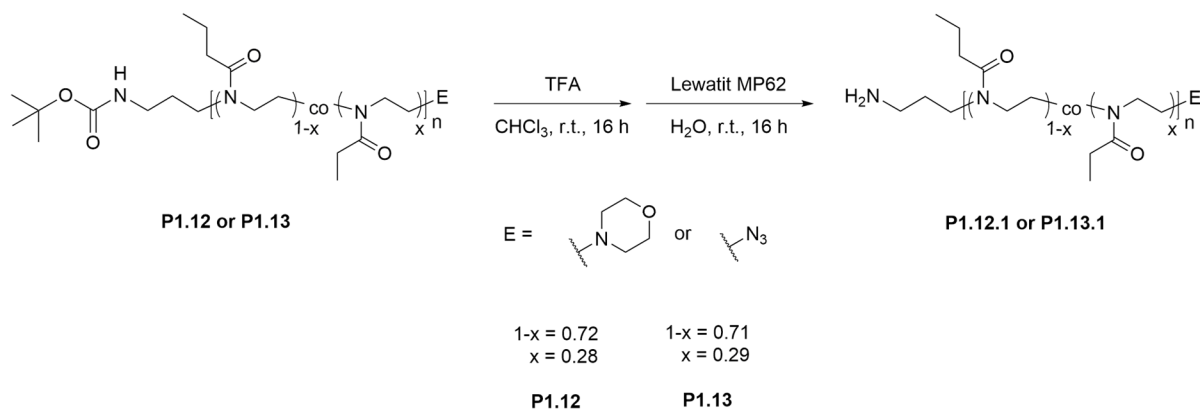
Spectral data

Polymer P1.11.1 (The IR and ¹H NMR spectrum are shown in Figure 5.9.)

¹H NMR (500 MHz, CDCl₃) δ 3.64–3.19 (334H), 2.90–2.76 (2H), 2.46–2.13 (169H), 1.86–1.75 (2H), 1.72–1.52 (120H), 1.18–1.01 (75H), 1.01–0.86 (176H) ppm.

IR (ATR): $\bar{\nu}$ = 3483, 2091, 1634, 1420, 1194 cm⁻¹

General Procedure 13: Deprotection of Boc-protected Amine Moieties in Poly(2-Oxazoline)s



Typically, the Boc-protected polymer (200 or 250 mg) was dissolved in CHCl_3 (3 ml). TFA (640 mg, 6.5 mmol, 0.5 ml) was added and the mixture was stirred for 16 h at room temperature. Then the polymer was recovered by precipitation into ice-cold diethyl ether, dissolved in 1,4-dioxane and dried by lyophilization. The amino end-functionalized polymer was redissolved in water (5 ml) and a weakly basic anion exchanger (Lewatit MP62) was added. The mixture was stirred at room temperature overnight. Finally, the mixture was filtrated, diluted, and lyophilized from water. Weight-in of the polymers are reported in the following Table 6.15.

Table 6.15: Weight-ins of the polymer used as educt, CHCl₃ and the corresponding yield of the reaction. The number in brackets indicates the number of replicate. The relative yields (%) are calculated according to the corresponding weight-in of polymer.

Polymer	Educt Polymer	Polymer / mg (μmol)	Yield / mg (%)
P1.12.1 (1)	P1.12 (1)	125 (4.0) ^a	106 (86)
P1.12.1 (2)	P1.12 (2)	500 (66.7) ^b	435 (87)
P1.13.1 A	P1.13 A	250 (31.5)	174 (69)
P1.13.1 B	P1.13 B	200 (19.0)	45 (23)
P1.13.1 E	P1.13 E	250 (14.9)	128 (51)
P1.13.1 G	P1.13 G	200 (10.4)	95 (48)
P1.13.1 H	P1.13 H	250 (9.8)	122 (49)
P1.13.1 I	P1.13 I	250 (8.6)	196 (78)

^a Half of mass of polymer was used, polymer was not stirred with Lewatit MP62

^b Double mass of polymer was used

Spectral data

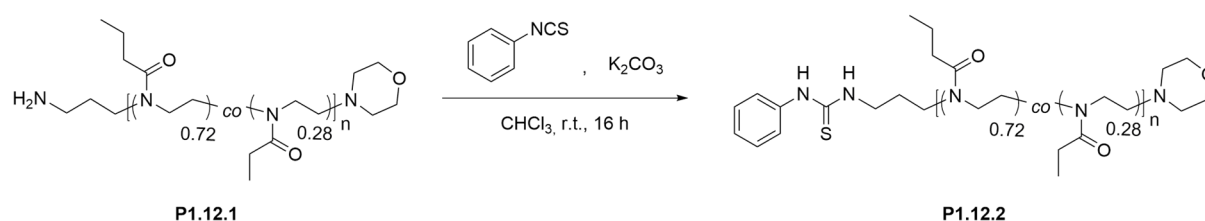
Polymer P1.12.1 (1) (Exemplarily shown in Figure S67.)

¹H NMR (500 MHz, CDCl₃) δ 3.74–3.70 (m, 4H), 3.64–3.34 (m, 528H), 3.01–2.87 (m, 1H), 2.56–2.47 (m, 1H), 2.47–2.13 (m, 278H), 1.79–1.71 (m, 2H), 1.70–1.50 (m, 201H), 1.17–1.01 (m, 114H), 0.99–0.84 (m, 301H) ppm.

Polymer P1.13.1 A (The IR and ¹H NMR spectrum are shown in Figure 5.10 and Figure S68.)

¹H NMR (500 MHz, CDCl₃) δ 3.57–3.28 (m, 509H), 2.79–2.55 (m, 2H), 2.47–2.11 (m, 262H), 1.80–1.71 (m, 2H), 1.70–1.52 (m, 182H), 1.17–1.00 (m, 113H), 1.00–0.84 (m, 273H) ppm.

IR (ATR): $\bar{\nu}$ = 2119, 1635, 1420, 1191 cm⁻¹

General Procedure 14: Thiourea formation of Primary Amino Groups present in Poly(2-Oxazoline)s

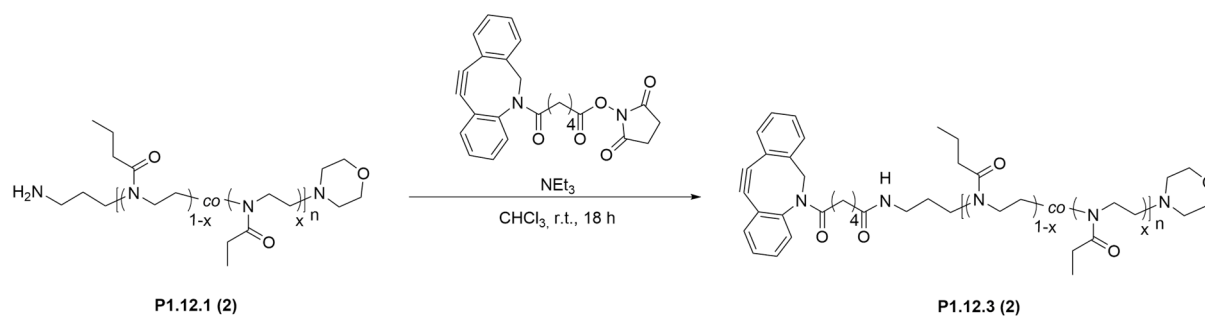
In a dry microwave reaction vial the amino-functionalized polymer (**P1.12.1 (1)**, 103 mg, 17.1 μmol) or (**P1.12.1 (2)**, 100 mg, 16.6 μmol), and K_2CO_3 (25 mg, 1.89 mmol) were dissolved in chloroform (2 ml). Then phenyl isothiocyanate (23.5 mg, 0.17 mmol) was added from a stock solution and the mixture stirred at room temperature for 18 h. Afterwards, the polymer was precipitated twice into ice-cold diethyl ether. The crude product was dissolved followed in 1,4-dioxane and lyophilized. Yields: 54 mg (52%) [**P1.12.2 (1)**] and 61 mg (61%) [**P1.12.2 (2)**]

Spectral data

Polymer P1.12.2 (1) (Exemplarily shown in Figure S69.)

$^1\text{H NMR}$ (500 MHz, $CDCl_3$) δ 7.51–7.28 (m, 5H), 3.70–3.60 (m, 4H), 3.58–3.16 (m, 235H), 2.79–2.59 (m, 0H), 2.51–2.40 (m, 3H), 2.40–2.04 (m, 122H), 1.82–1.67 (m, 2H), 1.67–1.50 (m, 87H), 1.17–0.99 (m, 51H), 1.00–0.83 (m, 132H) ppm.

Synthesis of DBCO-C₄-NH-Poly[(nPrOxa)-co-(EtOxa)]-morpholine



The amino end-functionalized polymer (100 mg, 16.6 μmol , **P1.12.1 (2)**) was dissolved in chloroform (2 ml). Then DBCO-C₄-NHS (16.7 mg, 38.9 μmol) and triethyl amine (3.93 mg, 38.9 μmol , 5.4 μl) were added to the solution and the mixture was stirred at room temperature overnight. The polymer was precipitated into ice-cold diethyl ether and redissolved in ethanol. Impurities were removed by dialysis against ethanol (MWCO = 1.0 $\text{kg}\cdot\text{mol}^{-1}$), followed by freeze drying from 1,4-dioxane. Yield: 80 mg (80%)

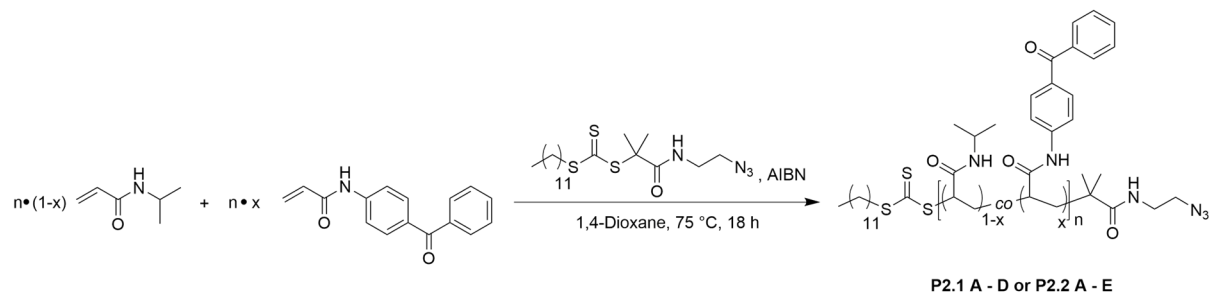
Spectral data

Polymer P1.12.3 (2) (The corresponding ^1H NMR spectrum is shown in Figure S70.)

^1H NMR (500 MHz, CDCl_3) δ 7.44–7.30 (m, 1H), 7.20–6.99 (m, 1H), 3.72–3.62 (m, 2H), 3.62–3.19 (m, 220H), 3.18–3.05 (m, 2H), 2.55–2.44 (m, 2H), 2.45–2.12 (m, 115H), 1.83–1.71 (m, 2H), 1.73–1.50 (m, 83H), 1.20–1.01 (m, 48H), 1.01–0.84 (m, 122H) ppm.

6.7 General Procedures for RAFT-Polymerizations

General Procedure 16: Synthesis of Poly(NiPAm) Homo- and Copolymers using DMP-N₃



P2.1 A - D: NiPAm homopolymers	P2.2 C : 1-x = 0.985 x = 0.015
P2.2 A : 1-x = 0.995 x = 0.005	P2.2 D : 1-x = 0.98 x = 0.02
P2.2 B : 1-x = 0.99 x = 0.01	P2.2 E : 1-x = 0.975 x = 0.025

A dry 10 ml schlenk tube was charged with NiPAm and 1,4-dioxane (8 ml) (**P2.1 A-D**). For polymers which should be photocrosslinkable (**P2.2 A-E**), BPAm was added as comonomer. Afterwards DMP-N₃ and AIBN were added to the mixture and the tube content was purged with argon for 30 min. The final concentration was adjusted to $\beta = 130 \text{ mg}\cdot\text{ml}^{-1}$. Afterwards the tube was placed in a preheated oil bath at 75 °C. The reaction was stopped by cooling the tube with liquid nitrogen and exposure the reaction mixture to air. The polymers were precipitated in ice-cold diethyl ether at least two times, unless otherwise noted, then filtered-off or centrifuged and finally dried in vacuum overnight.

The weight-ins of the monomers, CTA and the corresponding yield of the reaction are reported in Table 6.16.

6 Experimental Section

Table 6.16: Weight-ins of NiPAm, BPAm, 1,4-dioxane, DMP-N₃, AIBN as well as the monomer to DMP-N₃ ratio [M] : [CTA] and the corresponding yield of the reaction. The number in brackets indicates the number of replicate. The relative yields (%) are calculated according to the corresponding weight-in of monomer.

Polymer	NiPAm / g (mmol)	BPAm / mg (μ mol)	DMP-N ₃ / mg (μ mol)	[M ₀] : [CTA]	AIBN / mg (μ mol)	1,4-Dioxane / ml	Yield / g (%)
P2.1 A	1.00 (8.8)	---	153 (353)	25 : 1	5.8 (35.3)	7.9	0.80 (80)
P2.1 B (1)	1.00 (8.8)	---	25.5 (58.9)	150 : 1	1.0 (5.9)	7.9	0.79 (79)
P2.1 B (2)	10.00 (88.3)	---	255 (589)	150 : 1	9.8 (58.9)	80.0	9.32 (93)
P2.1 B (3)	20.00 (176.6)	---	513 (1190)	150 : 1	20.0 (120)	160.0	22.0 (110) ^a
P2.1 C	1.00 (8.8)	---	15.5 (35.7)	247 : 1	0.6 (3.5)	7.9	0.84 (84)
P2.1 D	1.00 (8.8)	---	9.6 (22.1)	400 : 1	0.4 (2.2)	7.9	0.88 (88)
P2.2 A	0.99 (8.8)	11.1 (4.3)	25.5 (58.9)	150 : 1	1.0 (5.9)	7.9	0.83 (83)
P2.2 B (1)	0.98 (8.7)	24.0 (9.6)	25.5 (58.9)	150 : 1	1.0 (5.9)	7.9	0.79 (79)
P2.2 B (2)	9.79 (86.5)	241 (96.0)	256 (589)	150 : 1	10.4 (63.4)	80.0	8.75 (88)
P2.2 C	0.97 (8.6)	33.3 (13.0)	25.1 (58.1)	150 : 1	1.0 (5.8)	7.9	0.86 (86)
P2.2 D	0.96 (8.5)	45.0 (17.0)	25.1 (58.1)	150 : 1	1.0 (5.8)	7.9	0.81 (81)
P2.2 E	0.95 (8.4)	55.2 (22.0)	25.5 (58.9)	150 : 1	1.0 (5.9)	7.9	860 (86)

^a The recorded ¹H NMR spectrum showed 1,4-dioxane present in the polymer

Spectral data

Polymer P2.1 A (The NMR and IR spectrum are shown in Figure 5.12 and Figure S71.)

^1H NMR (400 MHz, CDCl_3) δ 6.25 (26H), 3.99 (31H), 3.47–3.28 (4H), 2.91 (6H), 2.48–1.92 (32H), 1.92–1.21 (85H), 1.13 (192H), 0.86 (3H) ppm.

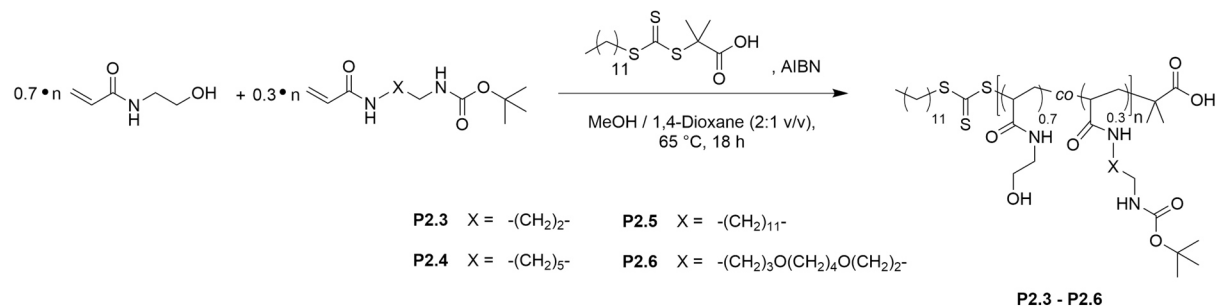
IR (ATR): $\bar{\nu}$ = 3285, 2110, 1636, 1532, 1384, 1250, 1067 cm^{-1}

Polymer P2.2 C (The NMR and IR spectrum are shown in Figure 5.12.)

^1H NMR (400 MHz, CDCl_3) δ 7.83–7.42 (17H), 6.99–5.82 (67H), 4.19–3.80 (80H), 3.48–3.40 (2H), 3.40–3.26 (2H), 2.40–1.95 (74H), 1.94–1.21 (181H), 1.22–0.91 (485H), 0.90–0.83 (3H) ppm.

IR (ATR): $\bar{\nu}$ = 3293, 3072, 2096, 1640, 1529, 1457, 1366, 1255, 1172 cm^{-1}

General Procedure 17: Synthesis of Poly[(HEAm)-*co*-(AXAm-Boc)] Copolymers



In a dry 10 ml schlenk tube 500 mg of the monomers in total were dissolved in a mixture of methanol and 1,4-dioxane (2:1 v/v, 3.7 ml). Then AIBN and DMP were added, and the tube content was purged with argon for 30 min. The final concentration was $\beta = 140 \text{ mg}\cdot\text{ml}^{-1}$. The ratio $[\text{M}]_0 : [\text{BPAm}]_0 : [\text{AIBN}]_0 : [\text{DMP}]$ was chosen to yield polymers with an average molar mass \bar{M}_n of 25 kDa. Afterwards the tube was placed in a preheated oil bath at 65 °C. The reaction was stopped by cooling the tube with liquid nitrogen and exposure the reaction mixture to air. The polymers were precipitated in ethyl acetate at least two times, unless otherwise noted, then filtered-off or centrifuged and finally dried in vacuum overnight.

Table 6.17: Weight-ins of HEAm, the amino-functionalized monomer (AXAm-Boc), DMP, AIBN as well as the monomer to DMP ratio [M] : [CTA] and the corresponding yield of the reaction. The number in brackets indicates the number of replicate. The relative yields (%) are calculated according to the corresponding weight-in of monomer.

Polymer	HEAm / g (mmol)	AXAm- Boc / mg (mmol)	DMP / mg (μ mol)	[M ₀] : [CTA]	AIBN / mg (μ mol)	Yield / mg (%)
P2.3	283 (2.46)	225 (0.99)	7.4 (20.2)	170 : 1	0.66 (4.0)	359 (70)
P2.4	253 (2.20)	241 (0.89)	7.2 (19.7)	156 : 1	0.65 (3.9)	343 (69)
P2.5	227 (1.97)	291 (0.82)	7.65 (21.0)	133 : 1	0.71 (4.3)	148 (28)
P2.6	224 (1.94)	289 (0.81)	7.46 (20.5)	134 : 1	0.67 (4.1)	205 (40)

Spectral data

Polymer P2.3 (The NMR spectrum is shown in Figure 5.15.)

¹H NMR (400 MHz, CD₃OD) δ 8.23–7.69 (25H), 3.89–3.53 (209H), 3.53–3.33 (77H), 3.29–3.00 (200H), 2.37–1.90 (134H), 1.87–1.51 (264H), 1.50–1.41 (329H), 1.33–1.27 (14H), 0.91 (3H) ppm.

Polymer P2.4 (The NMR spectrum is shown in Figure S72.)

¹H NMR (500 MHz, CD₃OD) δ 8.31–7.64 (100H), 3.80–3.56 (185H), 3.56–3.32 (87H), 3.30–2.99 (194H), 2.37–1.89 (124H), 1.84–1.47 (323H), 1.47–1.40 (283H), 1.40–1.31 (144H), 0.90 (3H) ppm.

Polymer P2.5 (The NMR spectrum is shown in Figure S73.)

¹H NMR (500 MHz, CD₃OD) δ 8.26–7.63 (42H), 3.79–3.54 (101H), 3.52–2.96 (175H), 2.32–1.90 (68H), 1.85–1.39 (352H), 1.39–1.26 (300H), 0.91 (3H) ppm.

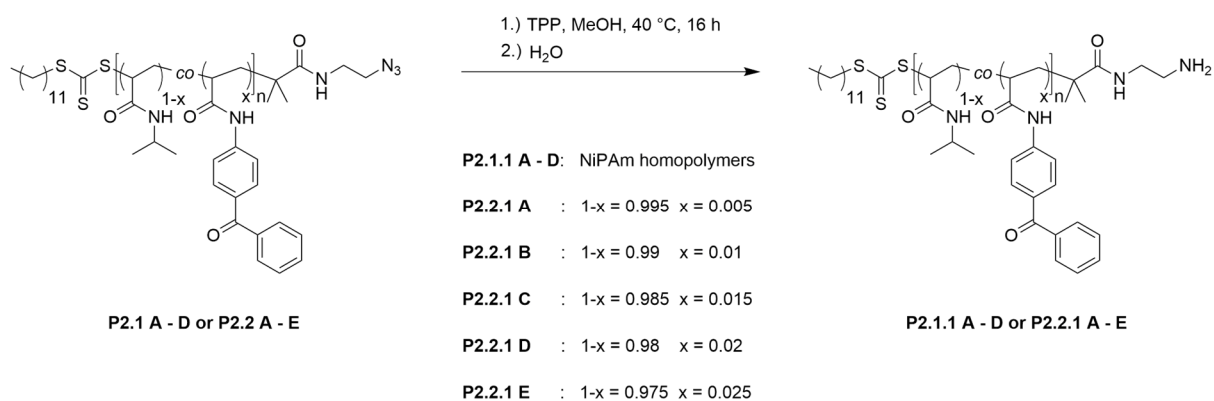
Polymer P2.6 (The NMR spectrum is shown in Figure S74.)

¹H NMR (500 MHz, CD₃OD) δ 8.27–7.75 (53H), 3.85–3.58 (111H), 3.56–3.42 (157H), 3.42–3.24 (86H), 3.21–3.07 (58H), 2.16–1.95 (51H), 1.86–1.71 (99H), 1.70–1.55 (127H), 1.55–1.42 (158H), 1.38–1.28 (20H), 0.93 (3H) ppm.

6.8 Post-functionalization Reactions of Poly(acrylamide)s

General Procedure 18: Staudinger Reduction of Azide Containing Poly(NiPAm) Homo- and Copolymers

The reduction was performed according to a modified procedure described in literature.¹⁶¹



The azide end-functionalized polymer (1 equiv.) was dissolved in MeOH ($\beta = 50 \text{ mg}\cdot\text{ml}^{-1}$). To the mixture triphenylphosphine (TPP, 20 equiv.) was added and the mixture was stirred at 40 °C overnight. Then cold deionized water (double volume as MeOH) was added and the remaining TPP was filtered-off (glass frit porosity 4). The solvents were evaporated under reduced pressure and the remaining viscous liquid was diluted again with cold deionized water ($\beta = 50 \text{ mg}\cdot\text{ml}^{-1}$). The suspension was again filtrated and finally lyophilized.

The weight-ins of the polymer, TPP and the corresponding yield of the reaction are reported in Table 6.18.

Table 6.18: Weight-ins of polymer, TPP, MeOH and the corresponding yield of the reaction. The number in brackets indicates the number of experiment. The relative yields (%) are calculated according to the corresponding weight-in of polymer.

Polymer	Educt Polymer P2.	Polymer / mg (μmol)	TPP / mg (mmol)	MeOH / ml	Yield / mg (%)
P2.1.1 A	1 A	550 (110)	525 (2.0)	11	243 (49)
P2.1.1 B (1)	1 B (1)	500 (33)	176 (0.6)	10	280 (56)
P2.1.1 B (2)	1 B (2)	8300 (280)	1450 (5.5)	160	3620 (44)
P2.1.1 B (3)	1 B (3)	16600 (553)	2900 (11.1)	165 ^a	12495 (75)
P2.1.1 C	1 C	500 (10)	53 (0.2)	10	132 (26)
P2.1.1 D	1 D	505 (6.3)	33 (0.1)	10	100 (20)
P2.2.1 A	2 A	500 (33)	88 (0.3)	10	120 (24)
P2.2.1 B (1)	2 B (1)	502 (17)	90 (0.3)	10	382 (76)
2.1 B (2)	2 B (2)	7742 (258)	1180 (5.2)	80 ^a	6575 (87)
P2.2.1 C	2 C	502 (17)	90 (0.3)	10	177 (35)
P2.2.1 D	2 D	512 (18)	90 (0.3)	10	197 (38)
P2.2.1 E	2 E	505 (17)	90 (0.3)	10	62 (13)

^a The mass concentration was adjusted to $\beta = 100 \text{ mg}\cdot\text{ml}^{-1}$

Spectral data

Polymer P2.1.1 A (The NMR and IR spectrum are shown in Figure S75 and Figure 5.12.)

^1H NMR (400 MHz, CDCl_3) δ 6.23 (29H), 4.12–3.86 (36H), 3.37–3.28 (2H), 2.82–2.64 (8H), 2.38–1.95 (34H), 1.94–1.22 (95H), 1.22–1.01 (229H), 0.87 (3H) ppm.

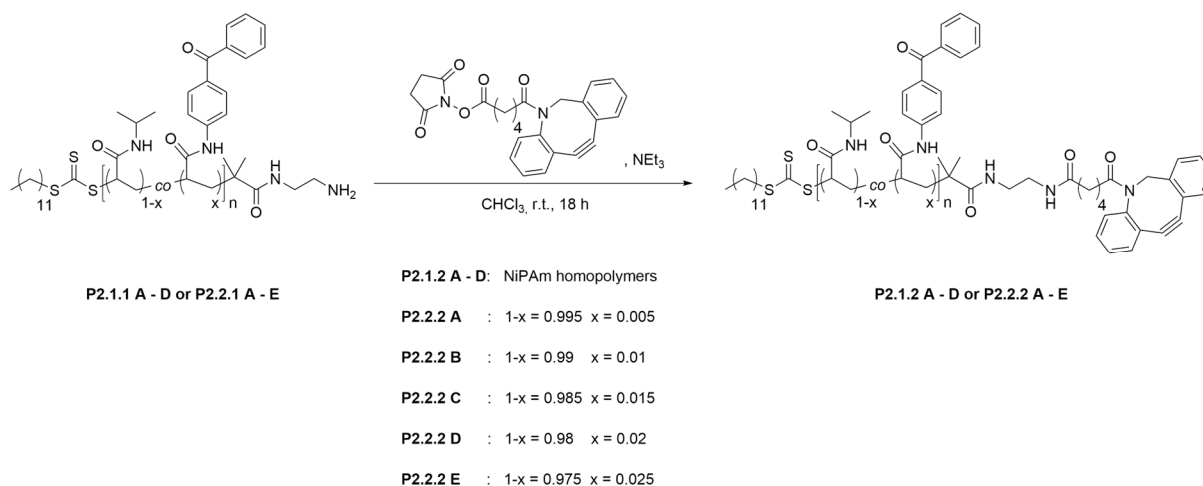
IR (ATR): $\bar{\nu}$ = 3296, 3069, 1641, 1534, 1386 cm^{-1}

Polymer P2.2.1 A (The NMR and IR spectrum are shown in Figure S76 and Figure S77.)

^1H NMR (400 MHz, CDCl_3) δ 7.81–7.41 (16H), 6.93–5.94 (109H), 3.98 (134H), 2.44–1.94 (127H), 1.94–1.21 (312H), 1.12 (820H), 0.86 (3H) ppm.

IR (ATR): $\bar{\nu}$ = 3299, 3070, 1640, 1528, 1459, 1367, 1175 cm^{-1}

General Procedure 19: DBCO-Functionalization of Poly(NiPAm) Homo- and Copolymers



The amino end-functionalized polymer (1 equiv.) was dissolved in chloroform ($\beta = 125 \text{ mg}\cdot\text{ml}^{-1}$). Then, DBCO-C₄-NHS (3 equiv.) and triethyl amine (3 equiv.) was added to the solution and the mixture was stirred at room temperature overnight. The polymer was recovered by precipitation into ice-cold diethyl ether. Further, impurities were removed by dialysis against ethanol ($\text{MWCO} = 1.0 \text{ kg}\cdot\text{mol}^{-1}$), followed by freeze drying from 1,4-dioxane. The weight-ins of the polymer, DBCO-C₄-NHS, NEt_3 , CHCl_3 and the corresponding yield of the reaction are reported in Table 6.19.

Table 6.19: Weight-ins of polymer, DBCO-C₄-NHS, NEt₃, CHCl₃ and the corresponding yield of the reaction. The number in brackets indicates the number of experiment. The relative yields (%) are calculated according to the corresponding weight-in of polymer.

Polymer	Educt Polymer P2.	Polymer / mg (μmol)	DBCO-C₄-NHS / mg (μmol)	NEt₃ / μl (μmol, mg)	CHCl₃ / ml	Yield / g (%)
P2.1.2 A	1.1 A	243 (41)	52.0 (121)	17 (121, 12.2)	1.9	215 (88)
P2.1.2 B (1)	1.1 B (1)	280 (12)	14.0 (35)	5.0 (35, 3.5)	2.2	152 (54)
P2.1.2 B (2)	1.1 B (2)	3610 (121)	156 (363)	50 (363, 36.7)	30	3070 (85)
P2.1.2 B (3)	1.1 B (3)	7500 (280)	363 (843)	117 (843, 85.3)	60	7250 (92)
P2.1.2 C	1.1 C	132 (3.2)	4.0 (9.4)	5.0 (35, 3.5)	2.0 ^a	92 (70)
P2.1.2 D	1.1 D	100 (3.1)	4.0 (9.4)	5.0 (35, 3.5)	2.0 ^a	85 (85)
P2.2.2 A	2.1 A	120 (4.0)	5.1 (12)	5.0 (35, 3.5)	2.0 ^a	78 (65)
P2.2.2 B (1)	2.1 B (1)	382 (13)	17 (39)	5.4 (39, 3.5)	3.1	295 (74)
P2.2.2 B (2)	2.1 B (2)	5870 (196)	253 (587)	81 (587, 59.4)	47	3710 (63)
P2.2.2 C	2.1 C	177 (5.9)	7.6 (18)	2.5 (18, 1.8)	1.4	142 (80)
P2.2.2 D	2.1 D	194 (6.5)	8.4 (19)	5.4 (39, 3.5)	1.6	175 (89)
P2.2.2 E	2.1 E	62 (2.0)	2.7 (6.0)	1.0 (0.75, 0.73)	1.0 ^a	42 (67)

^a The mass concentration was adjusted to $\beta = 62 \text{ mg}\cdot\text{ml}^{-1}$

Spectral data

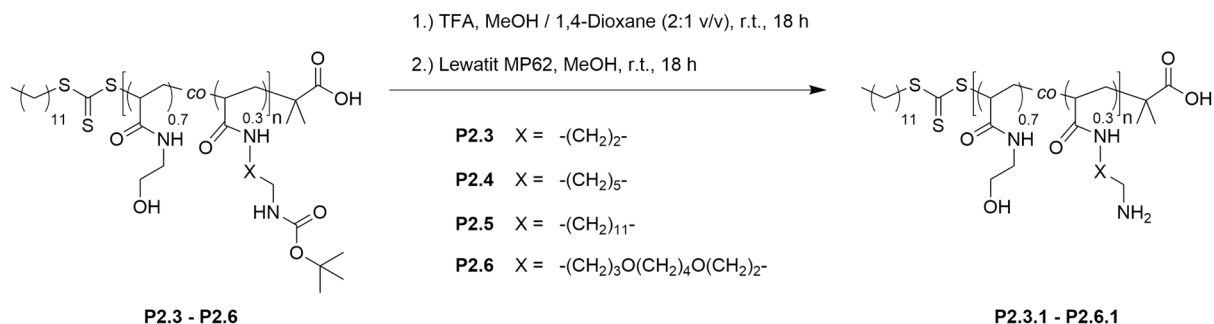
Polymer P2.1.2 A (The NMR spectrum is shown in Figure 5.14.)

^1H NMR (500 MHz, CDCl_3) δ 7.71–7.59 (2H), 7.44–7.27 (4H), 7.18–5.85 (51H), 4.16–3.87 (53H), 3.37–3.29 (2H), 2.41–1.94 (m, 52H), 1.94–1.21 (127H), 1.21–0.98 (333H), 0.89–0.84 (3H) ppm.

Polymer P2.2.2 A (The NMR spectrum is shown in Figure 5.14)

^1H NMR (400 MHz, CDCl_3) δ 7.83–7.42 (14H), 6.91–5.93 (87H), 4.11–3.86 (105H), 3.38–3.26 (2H), 2.41–1.94 (102H), 1.92–1.22 (241H), 1.22–0.90 (648H), 0.88–0.84 (3H) ppm.

General Procedure 20: Deprotection of Amino-Functionalized Poly(Acrylamide)s



The corresponding polymer was dissolved in a mixture of MeOH and 1,4-dioxane (2:1 v/v, $\beta = 125 \text{ mg}\cdot\text{ml}^{-1}$). Then TFA (0.50 ml, 0.745 mg, 6.53 mmol) was added and the mixture stirred at room temperature overnight. Afterwards, the solvent of the reaction mixture was evaporated, and the polymers recovered by precipitation in EtOAc followed by drying in vacuo or lyophilization using water / 1,4-dioxane mixtures as solvents. The deprotected polymers were dissolved in MeOH ($\beta = 62 \text{ mg}\cdot\text{ml}^{-1}$) and stirred with a weakly basic anion exchanger (Lewatit MP 62) overnight. Afterwards, the anion exchanger was filtered-off, subsequently washed with methanol and the solvent was removed. The residue was redissolved in water, passed through a syringe filter (nylon, $0.2 \mu\text{m}$) and dried via lyophilization.

Weight-in of the polymers and the solvents are reported in the following Table 6.20.

Table 6.20: Weight-ins of polymer, MeOH / 1,4-dioxane mixture (2:1 v/v) and the corresponding yield of the reaction. The number in brackets indicates the number of experiment. The relative yields (%) are calculated according to the corresponding weight-in of polymer.

Polymer	Educt Polymer	Polymer / mg (μmol)	MeOH / 1,4-Dioxane (2:1 v/v) / ml	MeOH / ml	Yield / mg (%)
P2.3.1	P2.3	250 (6.4)	2.0	4.0	226 (90)
P2.4.1	P2.4	250 (6.1)	2.0	4.0	199 (80)
P2.5.1	P2.5	121 (3.6)	1.0	2.0	60 (50)
P2.6.1	P2.6	183 (7.0)	1.5	3.0	159 (87)

Spectral data

Polymer P2.3.1 (The NMR spectrum is shown in Figure 5.15.)

^1H NMR (500 MHz, CD_3OD) δ 8.23–7.93 (19H), 3.87–3.57 (328H), 3.57–3.04 (486H), 3.04–2.88 (111H), 2.36–1.94 (222H), 1.94–1.25 (551H), 0.90 (3H) ppm.

Polymer P2.4.1 (The NMR spectrum is shown in Figure S78.)

^1H NMR (500 MHz, CD_3OD) δ 8.46–7.57 (88H), 4.60–4.31 (25H), 3.82–3.57 (233H), 3.57–2.98 (365H), 2.97–2.90 (77H), 2.33–1.83 (207H), 1.83–1.27 (674H), 0.90 (3H) ppm.

Polymer P2.5.1 (The NMR spectrum is shown in Figure S79.)

^1H NMR (500 MHz, CD_3OD) δ 4.52–4.36 (60H), 3.72–3.04 (461H), 2.96–2.89 (31H), 2.32–1.81 (81H), 1.81–1.39 (266H), 1.39–1.23 (316H), 0.90 (3H) ppm.

Polymer P2.6.1 (The NMR spectrum is shown in Figure S80.)

^1H NMR (500 MHz, CD_3OD) δ 8.25–7.61 (22H), 3.86–3.56 (139H), 3.56–3.41 (132H), 3.40–3.17 (101H), 3.17–2.99 (51H), 2.33–1.89 (99H), 1.89–1.28 (260H), 0.92 (3H) ppm.

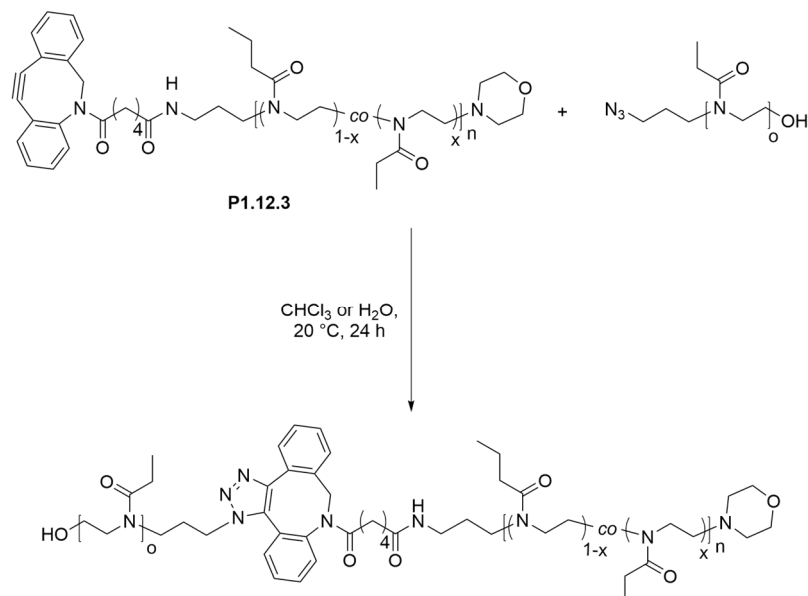
6.9 Procedures for UV/Vis and Irradiation Experiments

Cloud-point (T_c) Determination by UV/Vis Spectroscopy (Turbidity Measurements)

A solution of the corresponding polymer was prepared in salt-free H₂O ($\beta = 5 \text{ mg}\cdot\text{ml}^{-1}$). The solution was filled in a square cuvette (PMMA, 10 mm pathlength) and equilibrated at the starting temperature (typically $T = 20 \text{ }^\circ\text{C}$) for 10 min. The measurement range was commonly $T = 20\text{-}40 \text{ }^\circ\text{C}$. The solution was heated up by a rate of $1 \text{ }^\circ\text{C}\cdot\text{min}^{-1}$ and the transmittance at $\lambda = 600 \text{ nm}$ was measured. Data points were recorded every $t = 10 \text{ s}$. Reaching the target temperature, the solution was hold at this temperature for 5 min and the cooled down by a rate of $1 \text{ }^\circ\text{C}\cdot\text{min}^{-1}$ to the starting temperature. The cloud point T_c and the corresponding uncertainty ΔT_c of the solution were observed by fitting the data using nonlinear curve Boltzmann fit and determining the temperature at the inflection point of the heating curve.

The corresponding graphs are shown in Figure S81 to Figure S85, respectively.

Determining the Coupling Kinetics of a DBCO-end-functionalized Poly(2-Oxazoline) to an Azide containing Polymer by UV/Vis-Spectroscopy



The DBCO end-functionalized polymer (**P1.12.3**, 2.5 mg, 0.3 μmol) was dissolved in chloroform or water (2 ml). To the mixture an azide monofunctionalized polymer (3.0 mg, 0.26 μmol) was added and the mixture was stirred at 20 °C for 24 h. The reaction was followed by UV/Vis spectrometer (Scan every hour, $\lambda = 250 \text{ nm} - 400 \text{ nm}$). After complete reaction, the solvent was evaporated, and the polymer redissolved in DMAc containing LiBr (1 $\text{g}\cdot\text{l}^{-1}$) for determining the molecular mass change by GPC.

Both UV spectra are shown in Figure S86 and Figure S87.

6.10 Experimental Details of Surface Plasmon-Enhanced Fluorescence Spectroscopy (SPFS)

Preparation of gold substrates:

A typical microscope glass slide was cutted to dimensions of 2.0 x 2.5 cm and were then placed in an ultrasonic bath and subsequent sonicated with 1% Hellmanex® solution, distilled water and ethanol (15 min each). Afterwards, the clean glass substrates were blown dry in stream of N₂. Then these substrates were coated with 2 nm Cr and 50 nm Au films by thermal vacuum evaporation (Model HHV FL400, HHV Ltd., UK). After evaporation, the freshly coated Au surfaces were rinsed with ethanol, dried under a stream of nitrogen, and were stored under argon atmosphere until use.

SAM Preparation:

Variant 1: Preparation of mixed thiol-SAMs

(Mercaptoundecyl) triethylene glycol (7.53 mg, 22.3 μmol, 7.53 μl, SPT-0011) and (Mercaptoundecyl) pentaethylene glycol-2-ethoxyacetic acid (1.32 mg, 2.5 μmol, 13.2 μl, SPT-0012) were dissolved in ethanol (25 ml).

Freshly coated glass slides were immersed into the solution overnight and then rinsed with ethanol and blown dry in vacuum.

Variant 2: Preparation of SAM using DTPA-NHS

DTPA-NHS (7.4 mg, 35.2 μmol) was dissolved in chloroform (1 ml). Aliquots of 22.2 μl were added to the previously prepared solutions of **P1.13.1 C** (8.1 mg, 0.8 μmol in 12 ml chloroform) and **P1.13.1 I** (17.4 mg, 0.6 μmol in 12 ml chloroform) and were stirred at room temperature overnight

The freshly coated glass slides were immersed into the resulting solution for 24 h and then rinsed with ethanol and blown dry in vacuum.

Variant 3: Preparation of SAM using thiol-functionalized copolymers

P1.11 (7.8 mg, 0.9 μmol) and **P1.11.1** (9.1 mg, 1.0 μmol) and were dissolved in chloroform (12 ml), respectively.

The freshly coated glass slides were immersed into the resulting solutions for 24 h and then rinsed with ethanol and blown dry in vacuum.

Coupling of the linker polymers to the carboxylic acid groups of the mixed thiol-SAMs:

The carboxylic acid groups were activated using a mixture of NHS (21 mg, 0.2 mmol) and EDC-HCl (75 mg, 0.4 mmol) dissolved in distilled water (1 ml) either during the SPR measurement or a day before by immersing the SAMs into the EDC/NHS solution overnight which was diluted with 9 ml water and spiked with **P1.13.1 I** (10.4 mg, 0.3 μmol).

Fluorescent dye solution:

An aliquot of 1 μl Alexa Flour 647-DBCO dissolved in DMSO ($c = 5.0 \text{ mM}$, 1 ml) was added to PBS buffer (total volume 1 ml).

SPR setup:

The experimental setup was described in literature previously.²³ A schematic representation of the setup is shown in Figure 5.27.

The sensor chips were optically matched to an LASFN9 glass prism by using refractive index matching oil (from Cargille Inc., USA). The HeNe laser ($\lambda_{ex} = 632.8 \text{ nm}$, $P \sim 2 \text{ mW}$) beam was polarized by passing through a polarizer and neutral-density filter (NDF, optical density OD = 2, Linos Plano Optics) in order to reduce the effect of fluorophore bleaching.

A flow-cell (volume of 10 μl) was clamped to the sensor surface to contain liquid samples transported via fluidic tubing with 0.25 mm inner diameter at a flow rate of 50 $\mu\text{l}\cdot\text{min}^{-1}$. The flow-cell consisted of a polydimethylsiloxane (PDMS) gasket and a transparent glass substrate with drilled inlet and outlet ports. On top, a custom-made heating and cooling device was installed to modulate the temperature during the experiments.

The prism and sensor chip assembly with flow-cell and custom-made heating device was

mounted on a rotation stage to control the angle of incidence θ and the angular reflectivity spectra $R(\theta)$ were measured by a photodiode detector connected to a lock-in amplifier (EG&G, USA).

The fluorescence light emitted by the dye at a wavelength around $\lambda_{em} = 670$ nm perpendicular to the surface was collected by a lens (focal length 30 mm, numerical aperture of $NA = 0.2$) and passed through bandpass filters (FBF, transmission wavelength $\lambda = 670$ nm, 670FS10–25, Andover Corporation Optical Filter, USA) and a notch filter (LNF, central stop-band wavelength $\lambda = 632.8$ nm, XNF-632.8–25.0M, CVI Melles Griot, USA). The fluorescence light was collected by an optical fiber (FT400EMT, Thorlabs, UK), which was coupled to an avalanche photodiode photon counter (Count-200-FC, Laser Components, Germany). Its intensity (F) was measured by a counter (53131A, Agilent, USA) in counts per second (cps) and recorded by the software Wasplas (Max Planck Institute for Polymer Research, Mainz, Germany).

SPR measurements:

Variant 1: Measurement of mixed thiol-SAMs

After equilibrating the system with PBS solution ($pH = 7.4$) for 10 min, the mixed thiol-SAMs were incubated with the prepared EDC/NHS solution for 10 min. Afterwards, the gold surface was rinsed with phosphate buffered saline (PBS) solution ($pH = 7.4$) for 1 min and subsequent the surface was rinsed with the prepared polymer solutions (**P1.13.1 B** or **P1.13.1 F**, $\beta = 4.0 \text{ mg}\cdot\text{ml}^{-1}$ in PBS buffer, 5 ml).

Again, the gold surface was rinsed with PBS solution ($pH = 7.4$) for 10 min. Then the sensor was rinsed with the fluorescent dye solution for 10 min and subsequent rinsed with PBS buffer again (10min).

Finally, different sucrose concentrations (1%, 2% and 4%) were passed through the flow-cell for calibration.

Variant 2: Measurement of SAMs and gold surfaces which were pre-reacted with the polymer linkers

After equilibrating the system with PBS solution (pH = 7.4) for 10 min, the sensor was rinsed with the fluorescent dye solution for 1 h and finally rinsed with PBS buffer again (10min).

Temperature-modulation experiments:

First, the sensor substrates were rinsed with distilled and degassed water for 10 min at a flow rate of $100 \mu\text{l}\cdot\text{min}^{-1}$ at 25°C . After additional 5 min equilibration the pump was stopped, and an angular scan was performed. Then, the temperature was increased to 45°C or 60°C and again equilibrated for 5 min a flow rate of $100 \mu\text{l}\cdot\text{min}^{-1}$. Subsequent, an angular scan was performed after stopping of the pump. Afterwards, the temperature was decreased to 25°C . This cycle was repeated at least two times for each sensor chip.

6.11 Experimental Details of the Cell and Transfection Experiments

DNA and Cell Culture

For every test, the 3.7 kb plasmid DNA (pDNA) pGM144³³⁵ was used. It was amplified and purified by Aldevron. Three cell lines were used i.e. A549 (ATCC® CCL-185™; human epithelial lung carcinoma cells), HeLa (ATCC® CCL-2™; human epithelial ovarian carcinoma cells) and C2C12 (ATCC® CRL-1772™; murine myoblast cells). Every cell line was grown in Dulbecco's Modified Eagle Medium (DMEM) supplemented with 10% heat inactivated fetal bovine serum (FBS), 1% L-glutamine and 1% antibiotics (100 units·ml⁻¹ penicillin, 100 µg·ml⁻¹ streptomycin). Incubations were carried out at $T = 37$ °C in a humidified atmosphere containing 5% CO₂. DMEM, FBS, penicillin, and streptomycin were purchased from Invitrogen.

Stock solution preparation of polymers

The polymers **P2.3.1-P2.6.1** and **P2.3.1*-P2.6.1** were used to prepare stock solutions in HEPES (20mM) with concentrations of $\beta = 5$ mg·ml⁻¹. The prepared solutions were stored at $T = -20$ °C prior to use.

Polyplexes preparation:

Polymer/DNA mixtures i.e. polyplexes were prepared in $c = 20$ mM HEPES by adding each polymer solution at different mass ratios over a fixed amount of pDNA in solution. The Mass ratio (MR) of a polymer was defined as the ratio between the mass of the tested polymer and the mass of used pDNA. After mixing of the DNA- and polymer solution in a well-plate, the resulting formulations were kept at room temperature for at least $t = 15$ min before subsequent use in experiments. As reference, bPEI (Sigma, 25 kg·mol⁻¹) was also tested under same experimental conditions.

Fluorescence measurements:

The fluorescent aromatic dye ethidium bromide (EtBr) was used to evaluate DNA condensation within polyplexes, as described in literature.³⁴⁵ After intercalation into free DNA, this stain emits a fluorescence at $\lambda = 590$ nm when excited at $\lambda = 530$ nm. Read-out of the fluorescence intensities were done by using a Mithras² multiplate reader (Berthold).

Gel retardation assay: Polyplexes formation was additionally tested using electrophoresis in 0.8% agarose gels previously stained with EtBr. After 20 min at $U = 100$ V and $I = 90$ mA, the gel was visualized using an UV transilluminator (Fisher Bioblock).

Cell transfection: The transfection experiments were done according to literature.³⁴⁶ Briefly, the day before transfection, the cells were seeded into 96-well plates at a density of 25 000 cells per well. Naked DNA and polyplexes were added dropwise into each well (0.25 μ g of DNA per well) at different MR (1.27-128). After $t = 36$ h incubation at $T = 37$ °C, the culture medium was removed and the cells were lysed by using passive lysis buffer (PLB, 0.5 X, Promega) into each well. For every cell lysate, the chemiluminescence Luciferase Assay System (Promega) was carried out to determine luciferase expression and the BC Assay kit (Uptima) was used to quantify the total protein content. Finally, data were presented as relative light units (RLU) per milligram of total proteins.

Cell viability:

Microscope Images of the cells were taken $t = 20$ h after transfection to check qualitatively the cell viability using a microscope type Olympus IX71 equipped with Axiocam ERc 5s.

After $t = 24$ h, the number of living cells present in each well (resulting from both cell proliferation and cell death that occurred during the experiment) was determined using the ViaLight kit (Lonza). Results were stated as percentages relative to the signal obtained for non-transfected cells (100% cell viability).

7 Appendix

7.1 Spectra of Non-Polymeric Compounds

7.1.1 Additional Spectra of Synthesized Tosylate Initiators

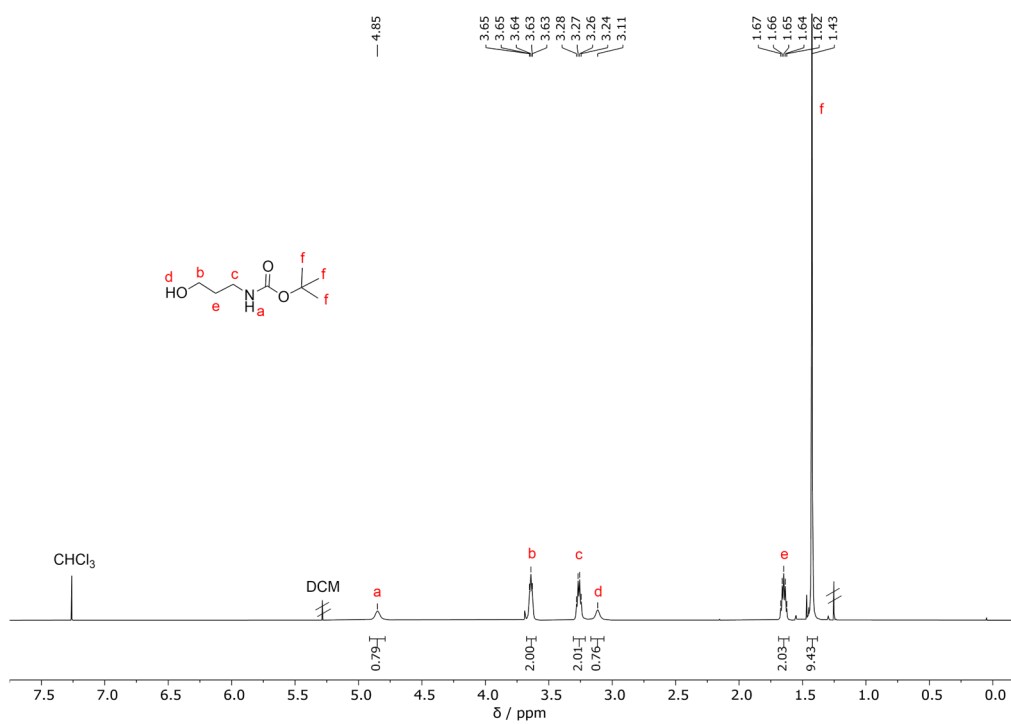


Figure S1: ^1H NMR (500 MHz) spectrum of *N*-Boc-Prop-OH recorded in CDCl_3 .

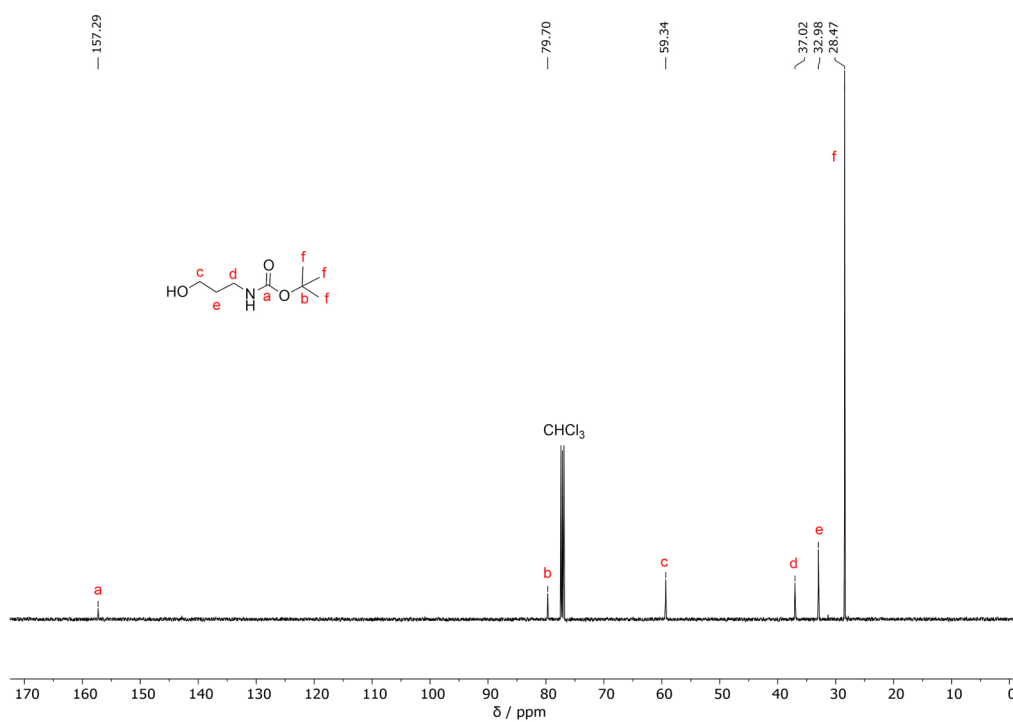


Figure S2: ^{13}C NMR (126 MHz) spectrum of *N*-Boc-Prop-OH recorded in CDCl_3 .

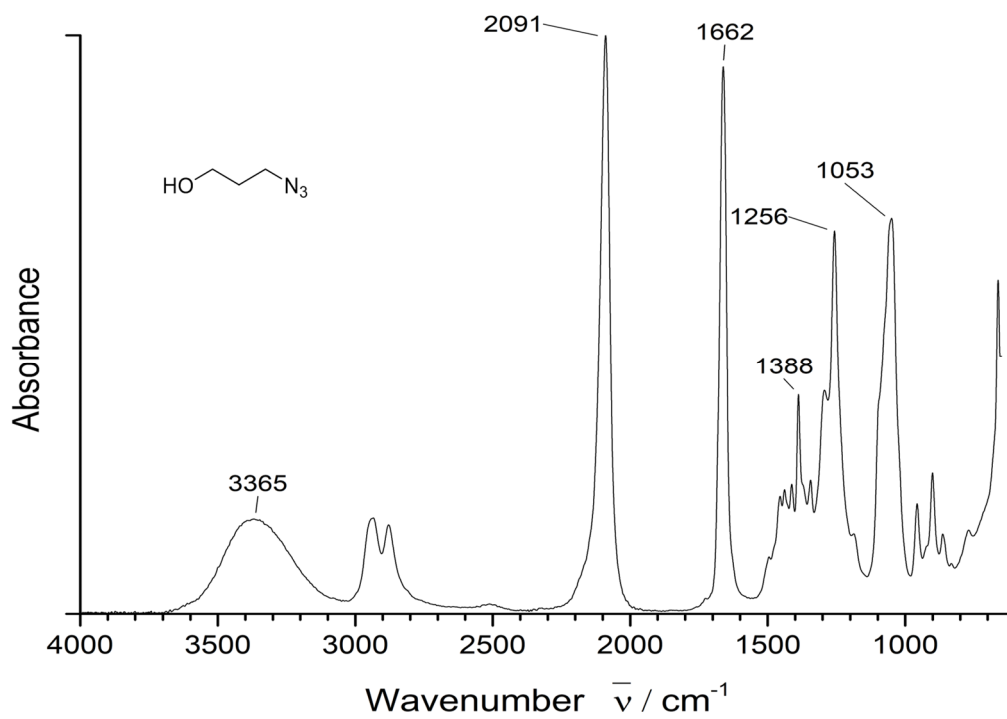


Figure S3: IR spectrum of 3-azidopropanol

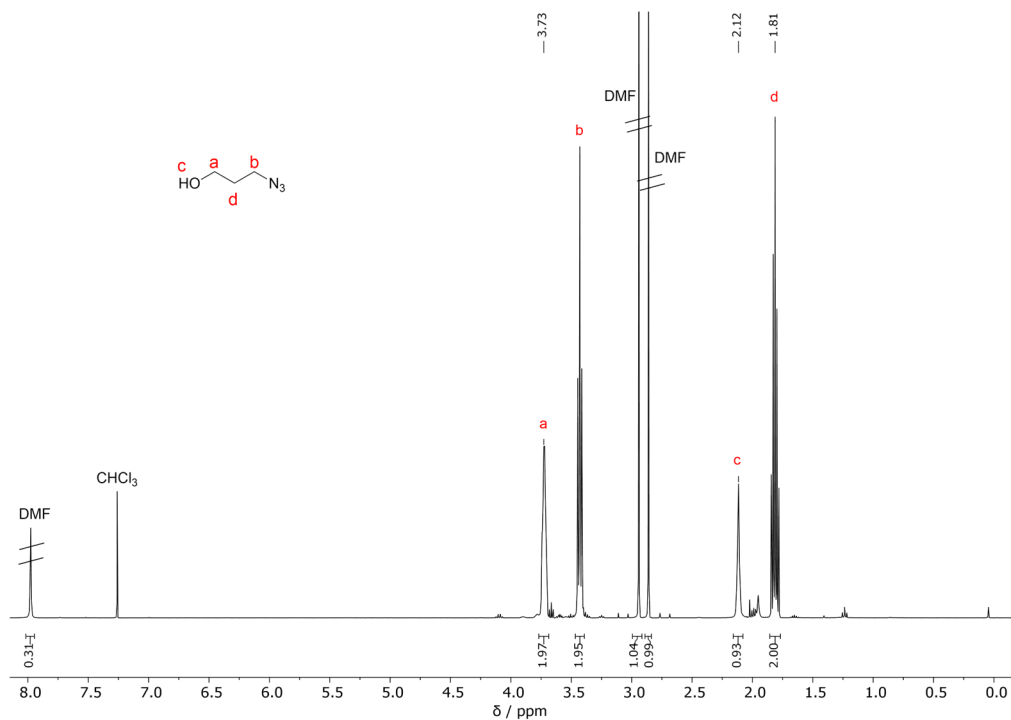


Figure S4: ¹H NMR (400 MHz) spectrum of 3-azidopropanol recorded in CDCl₃.

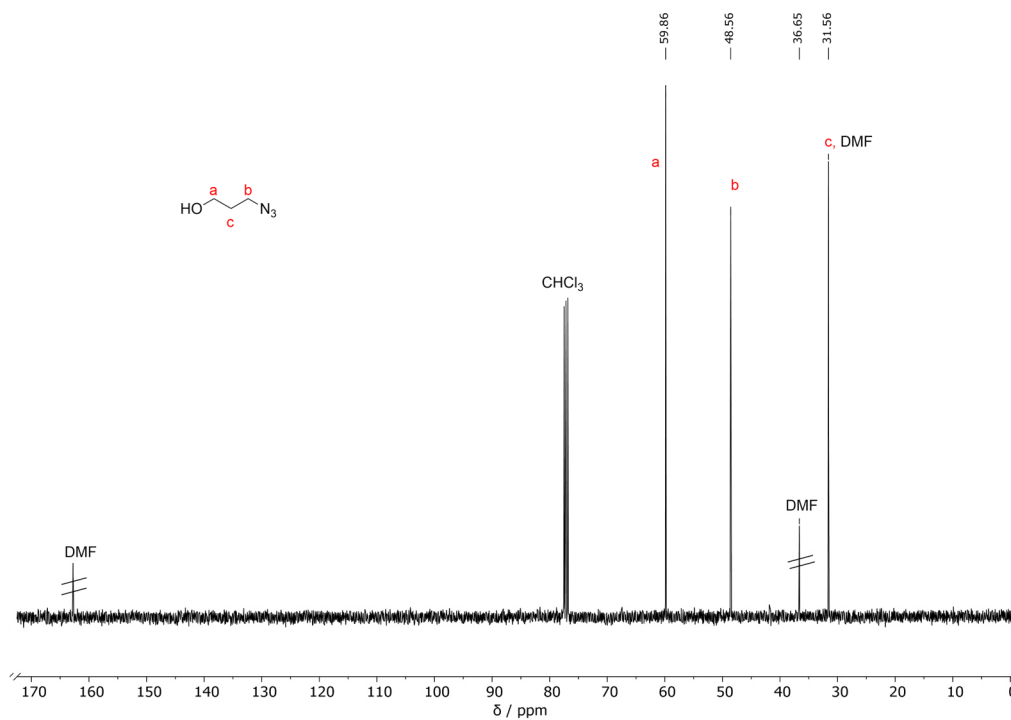


Figure S5: ¹³C NMR (126 MHz) spectrum of 3-azidopropanol recorded in CDCl₃.

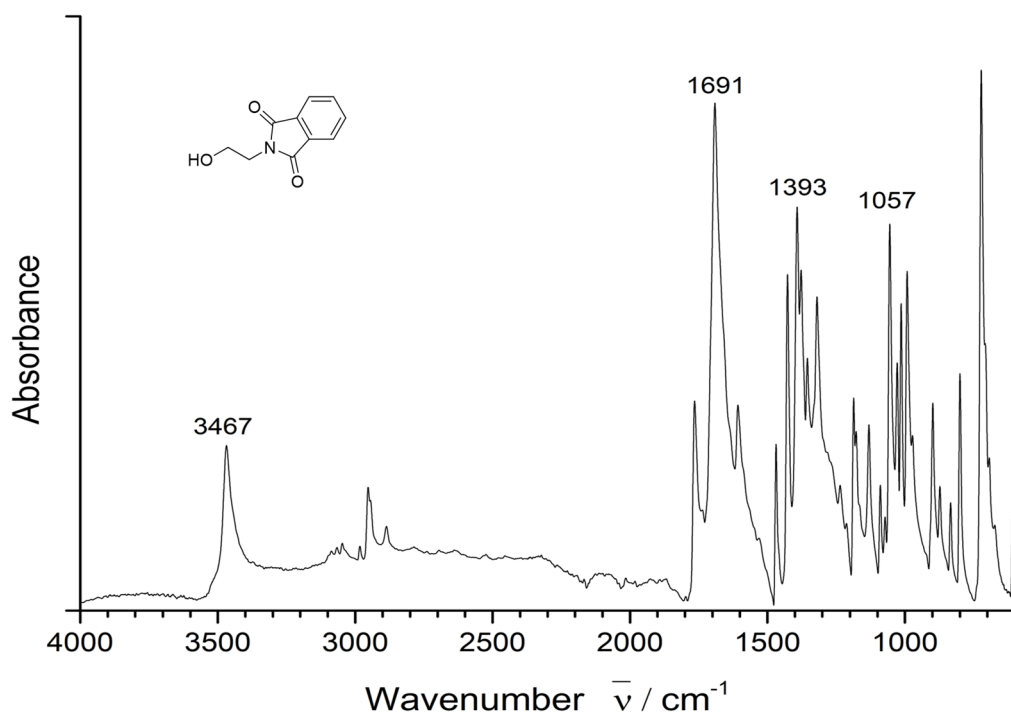


Figure S6: IR spectrum of Pht-Et-OH

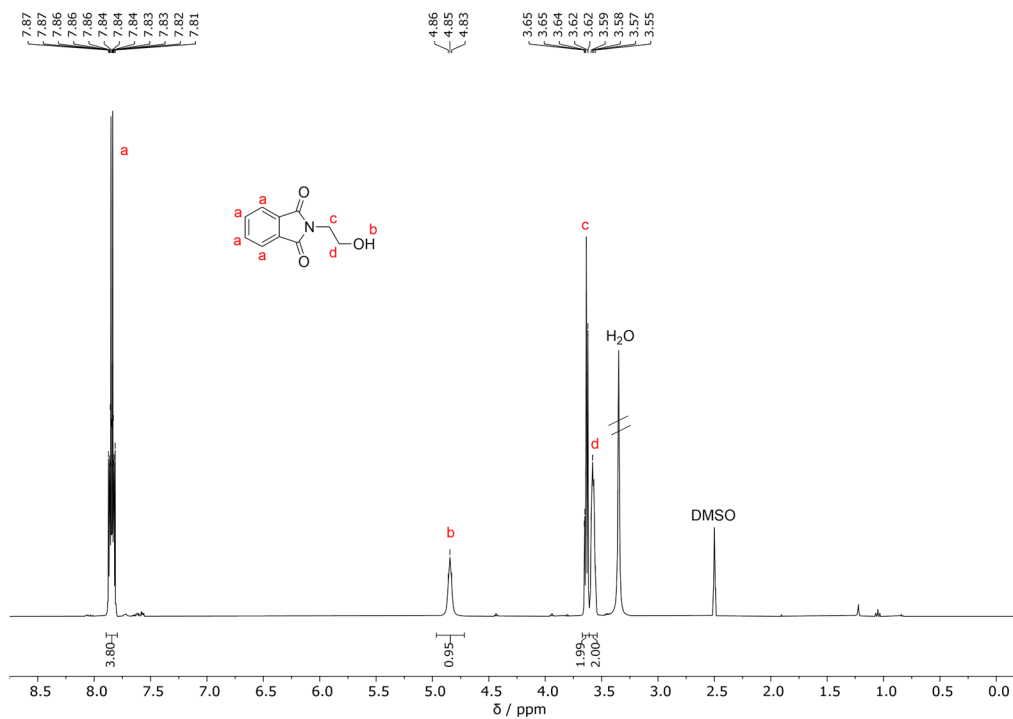


Figure S7: ^1H NMR (400 MHz) spectrum of Pht-Et-OH recorded in DMSO-d_6 .

7 Appendix

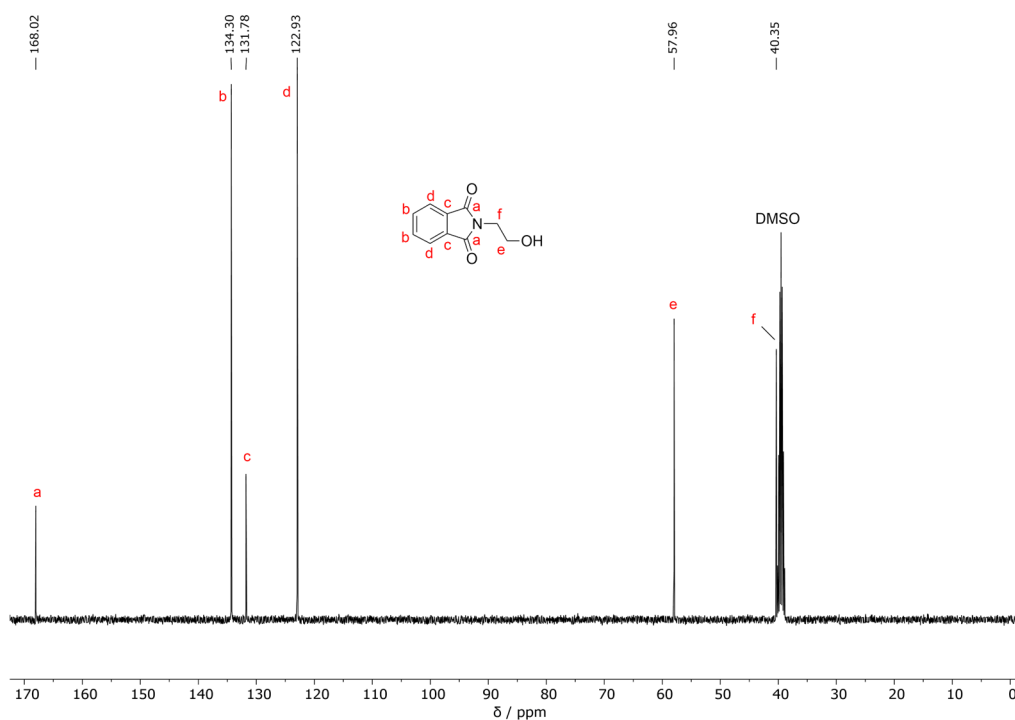


Figure S8: ^{13}C NMR (101 MHz) spectrum of Pht-Et-OH recorded in DMSO-d_6 .

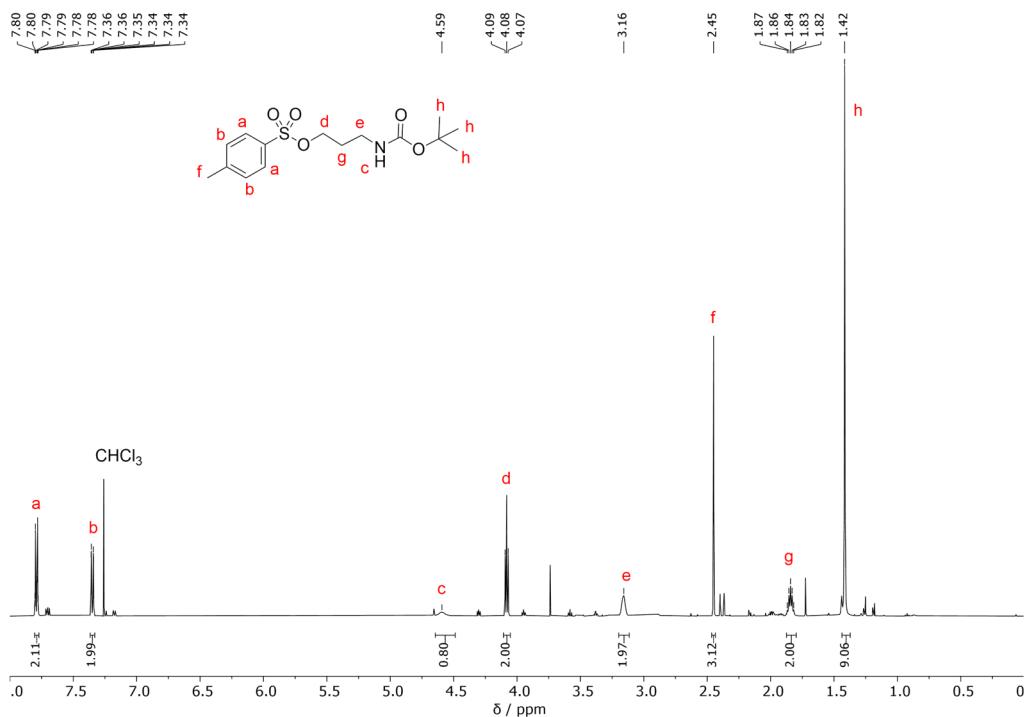


Figure S9: ^1H NMR (500 MHz) spectrum of *N*-Boc-Prop-Tos recorded in CDCl_3 .

7 Appendix

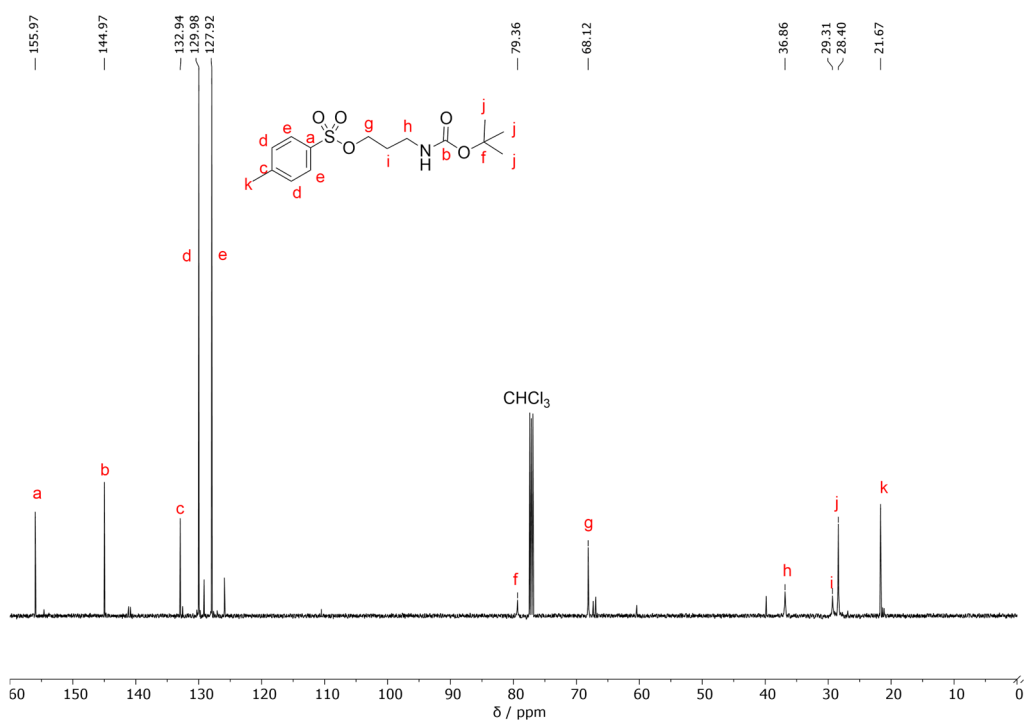


Figure S10: ^{13}C NMR (126 MHz) spectrum of *N*-Boc-Prop-Tos recorded in CDCl_3 .

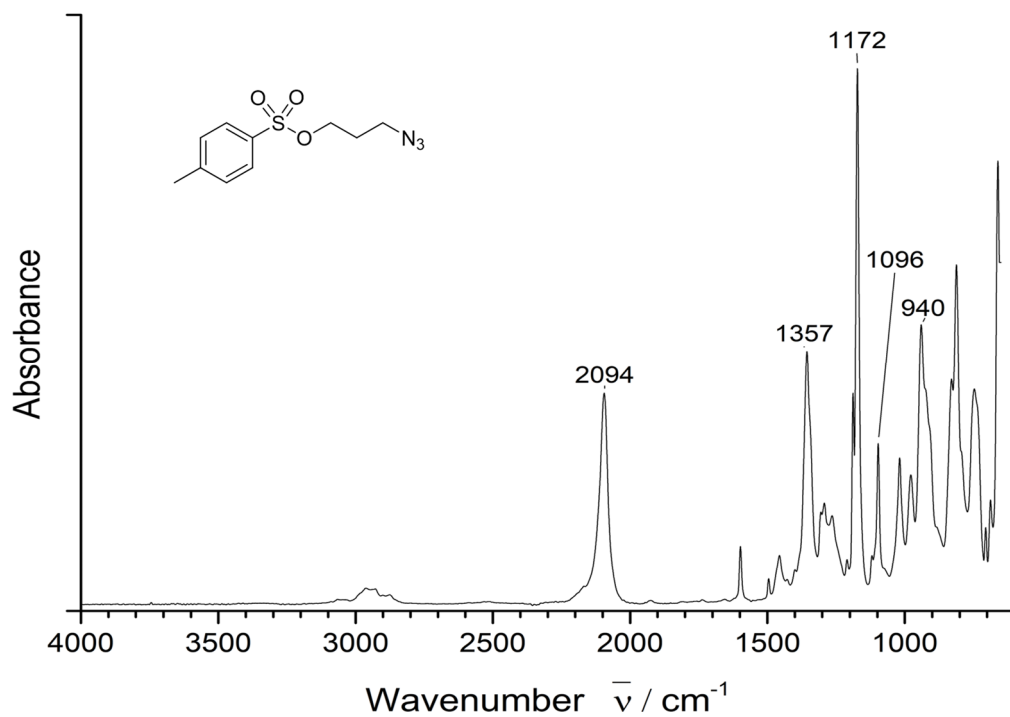


Figure S11: IR spectrum of N_3 -Prop-Tos

7 Appendix

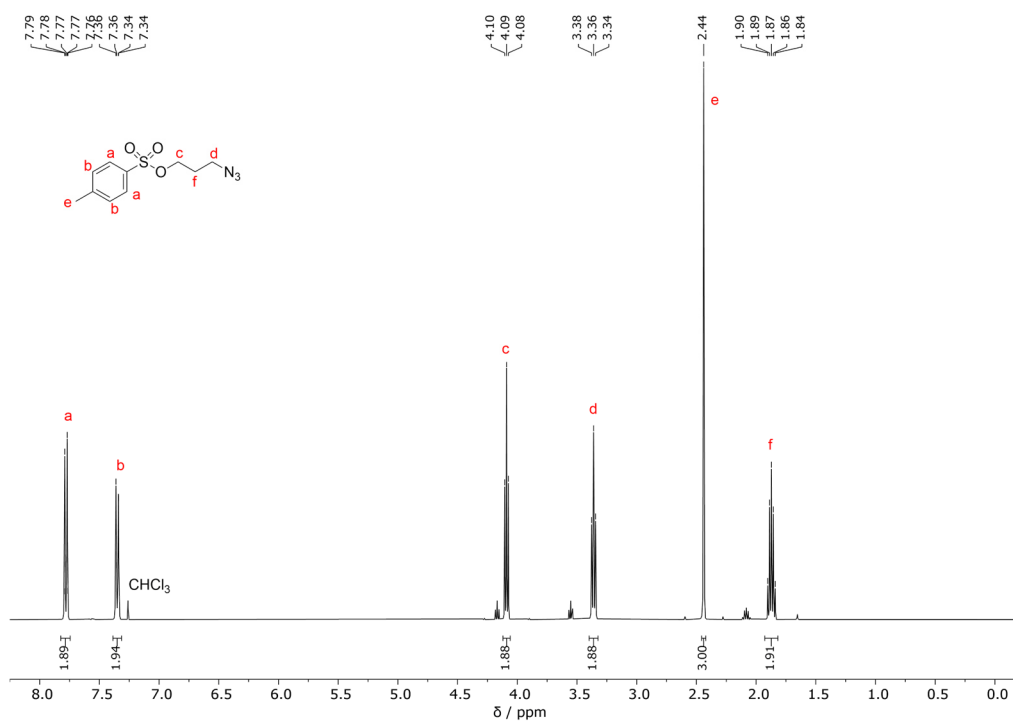


Figure S12: ¹H NMR (400 MHz) spectrum of N₃-Prop-Tos recorded in CDCl₃.

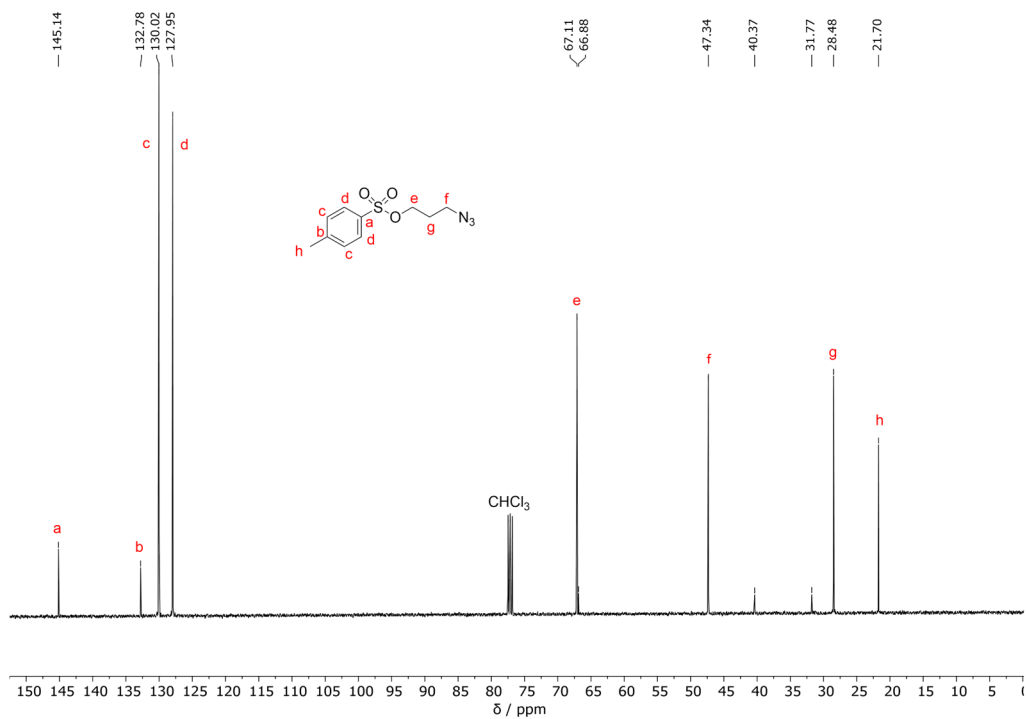


Figure S13: ¹³C NMR (101 MHz) spectrum of N₃-Prop-Tos recorded in CDCl₃.

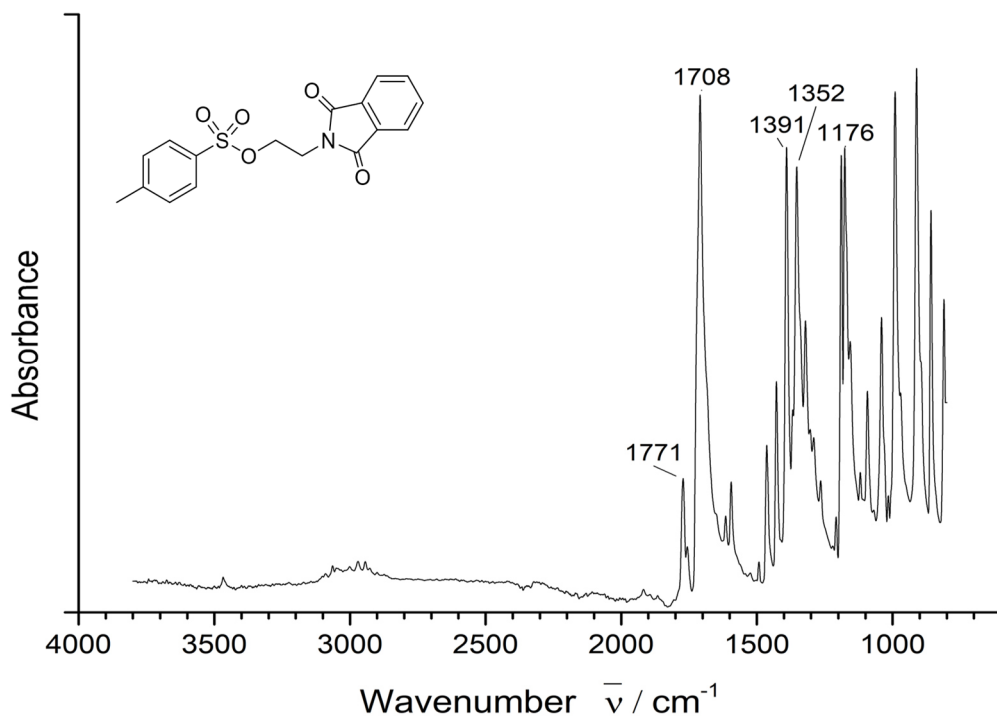


Figure S14: IR spectrum of Pht-Et-Tos

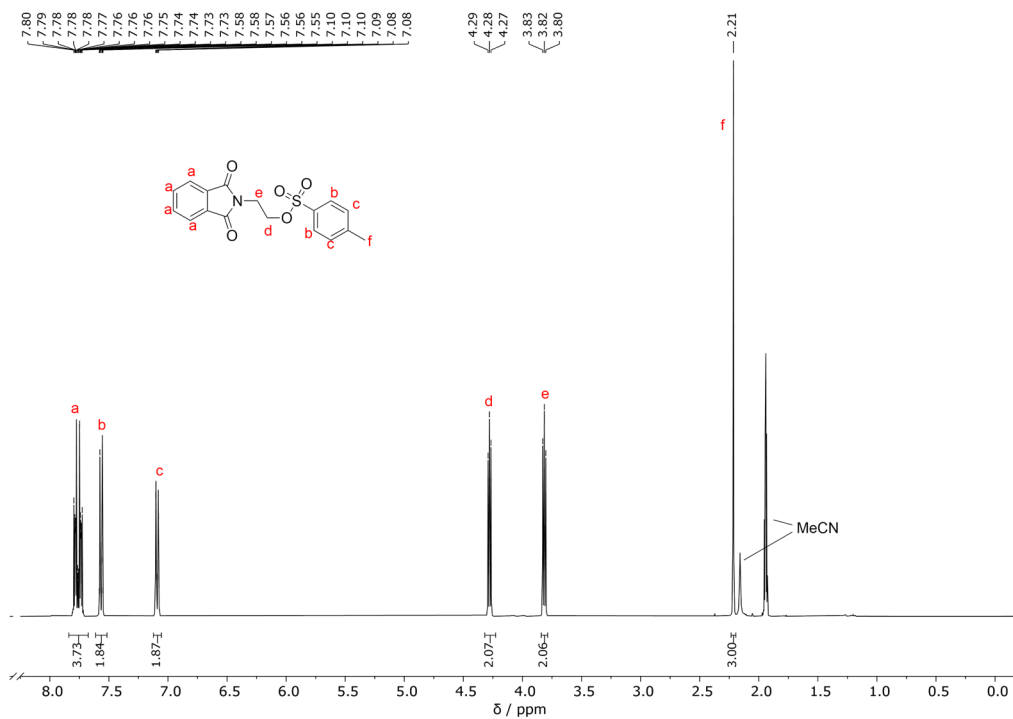


Figure S15: ^1H NMR (400 MHz) spectrum of Pht-Et-Tos recorded in CD_3CN .

7 Appendix

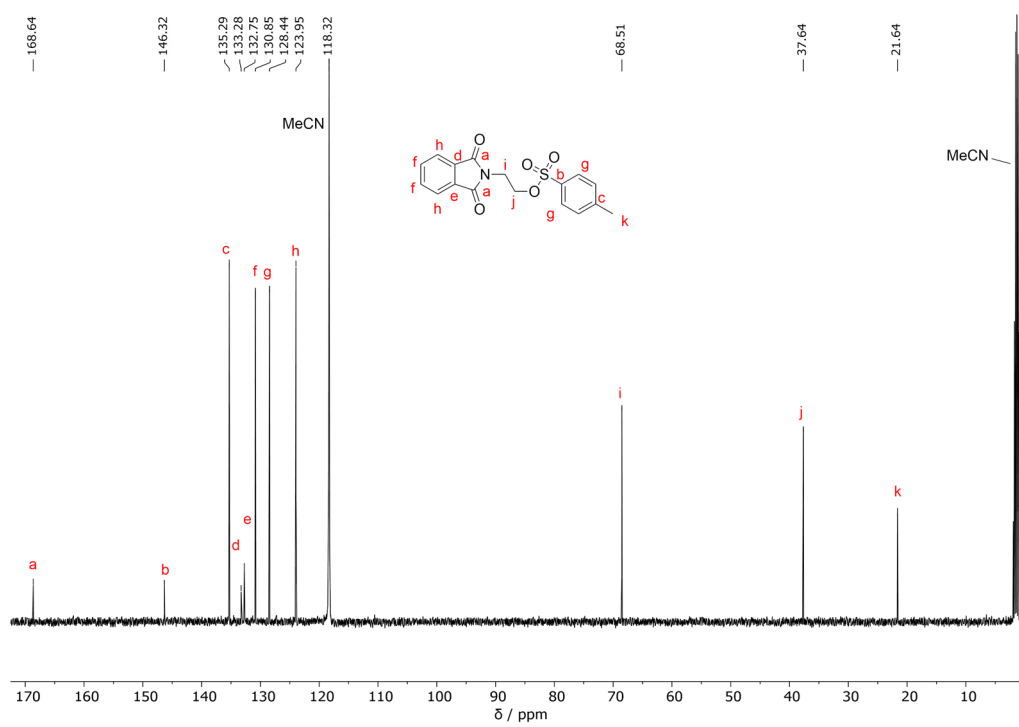


Figure S16: ^{13}C NMR (101 MHz) spectrum of Pht-Et-Tos recorded in CD_3CN .

7.1.2 NMR-Spectra of Oxazoline Monomers

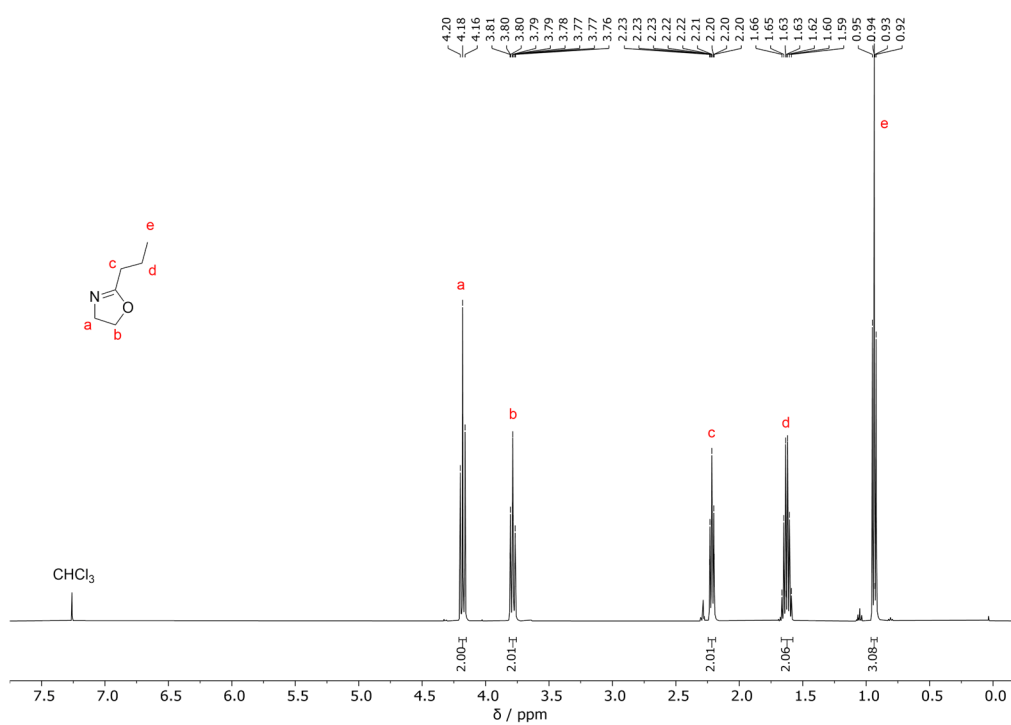


Figure S17: ¹H NMR (500 MHz) spectrum of *n*PrOxa recorded in CDCl₃.

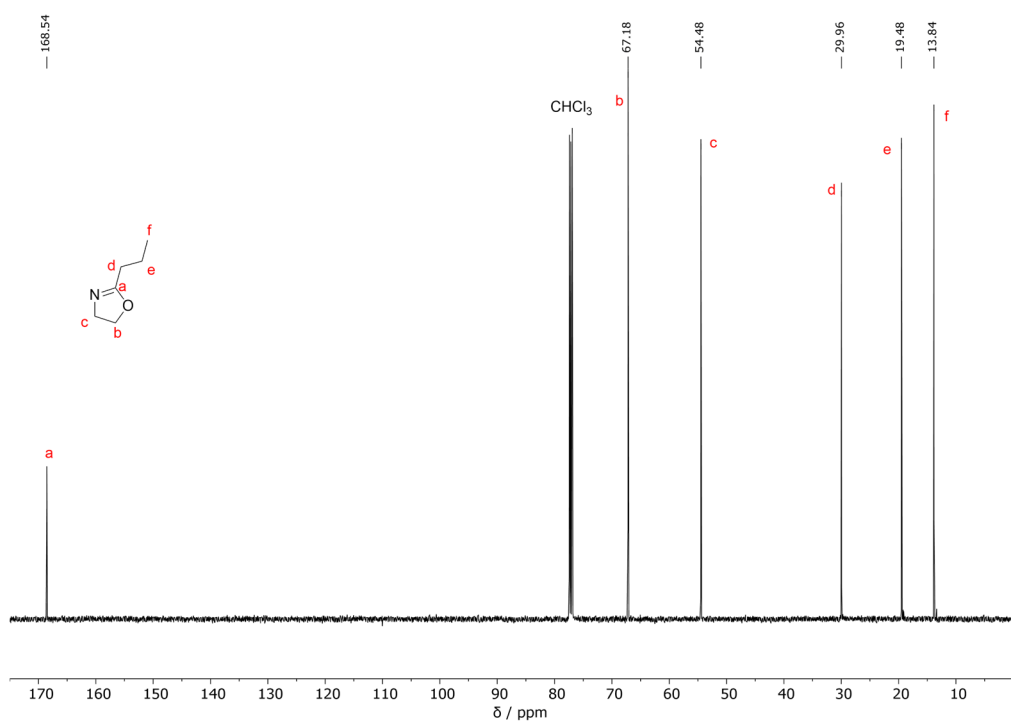


Figure S18: ¹³C NMR (126 MHz) spectrum of *n*PrOxa recorded in CDCl₃.

7 Appendix

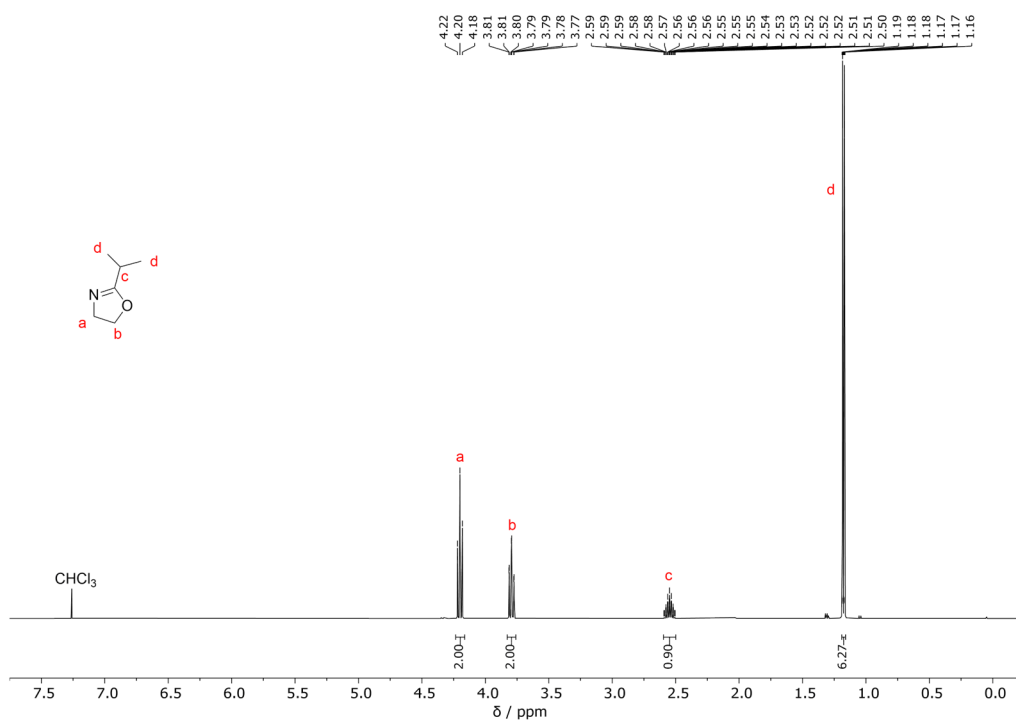


Figure S19: ¹H NMR (500 MHz) spectrum of *i*PrOxa recorded in CDCl₃.

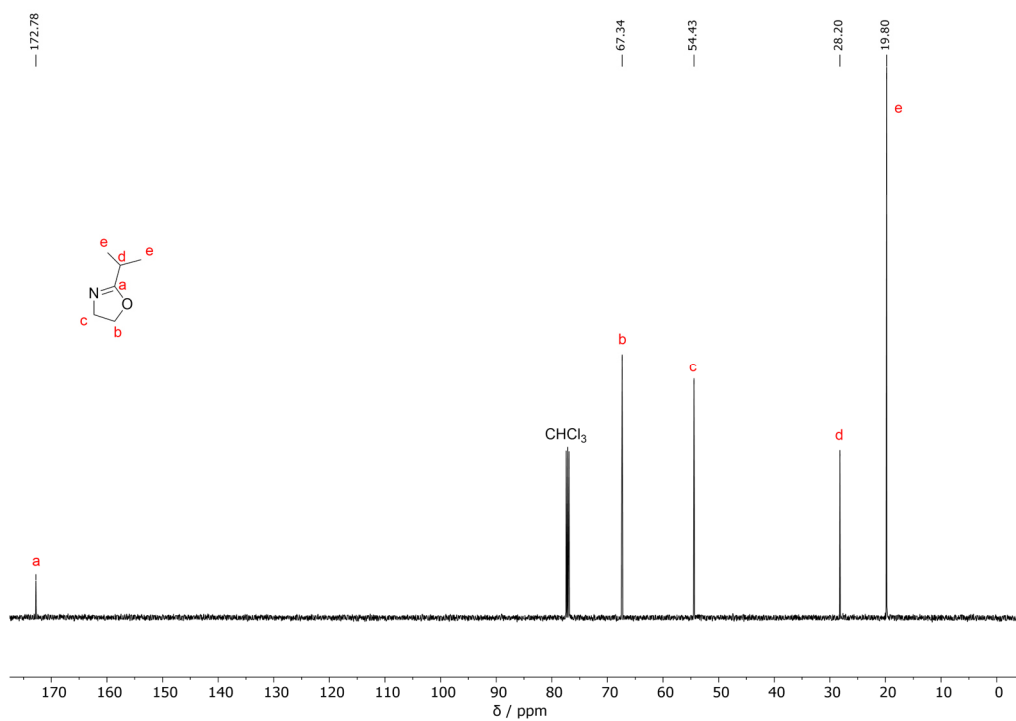


Figure S20: ¹³C NMR (126 MHz) spectrum of *i*PrOxa recorded in CDCl₃.

7.1.3 RAFT-Agents and their Modifications

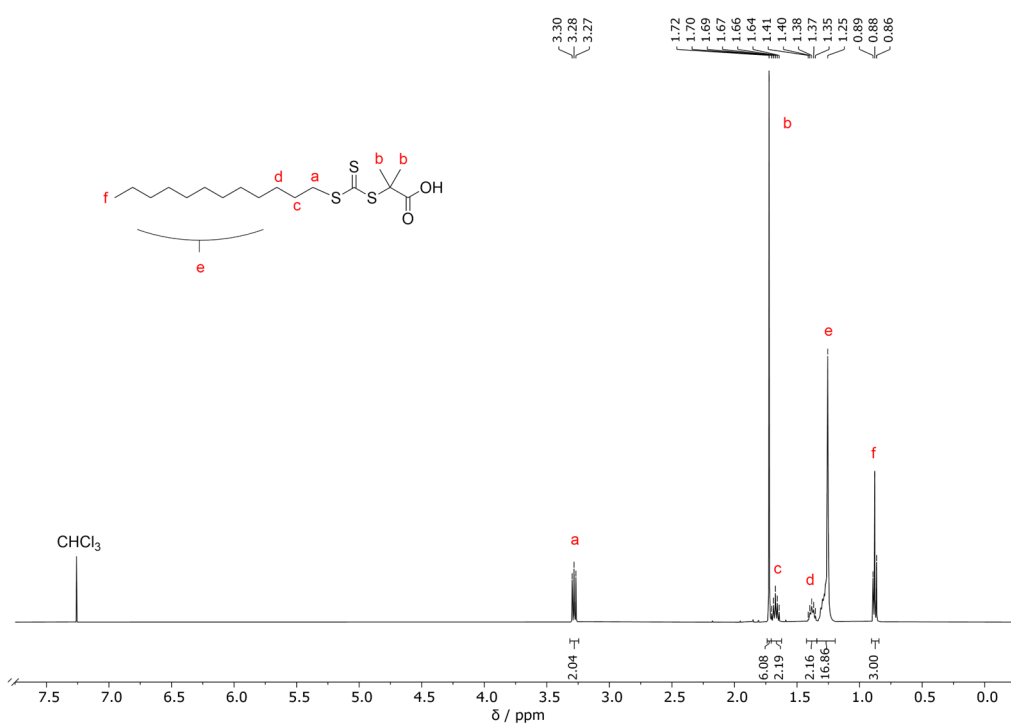


Figure S21: ¹H NMR (500 MHz) spectrum of DMP recorded in CDCl₃.

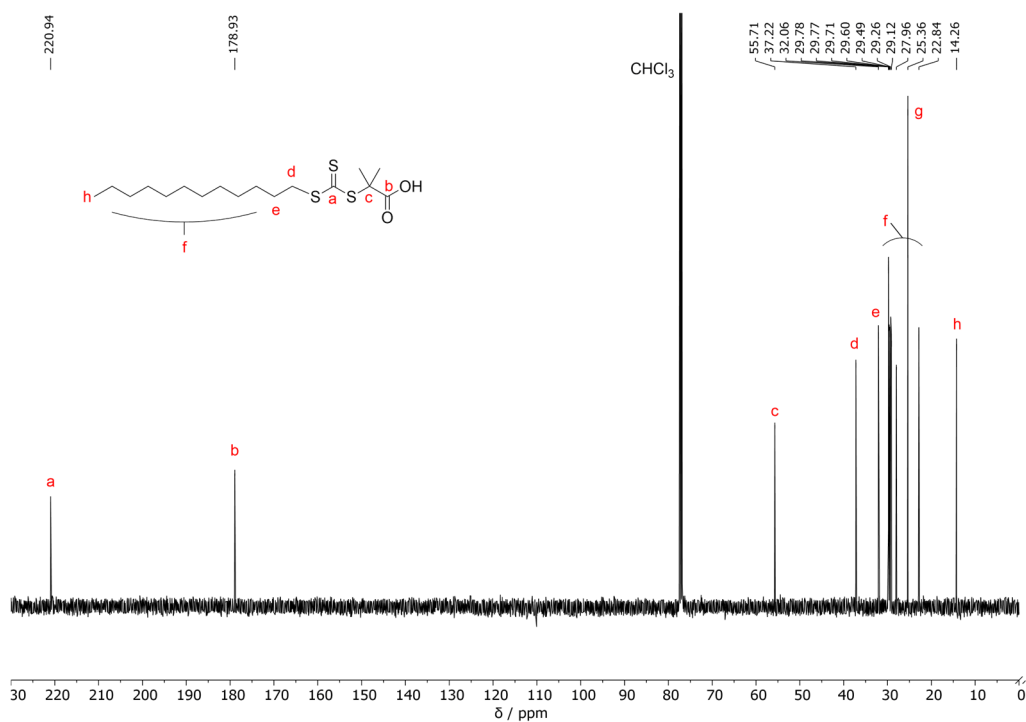


Figure S22: ¹³C NMR (126 MHz) spectrum of DMP recorded in CDCl₃.

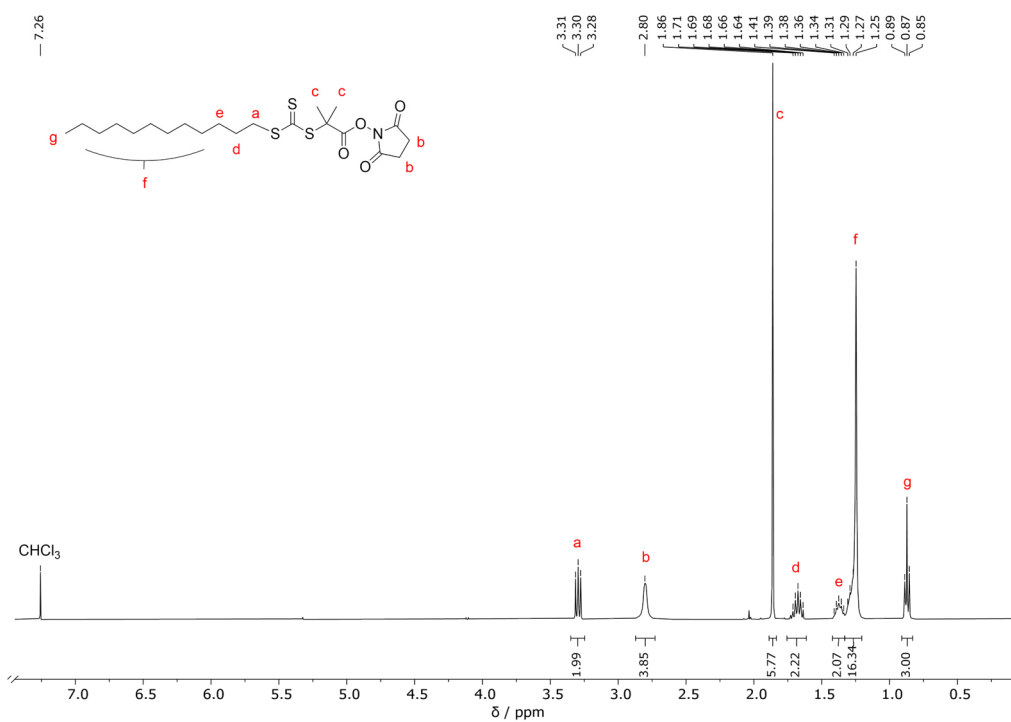


Figure S23: ¹H NMR (400 MHz) spectrum of DMP-NHS recorded in CDCl₃.

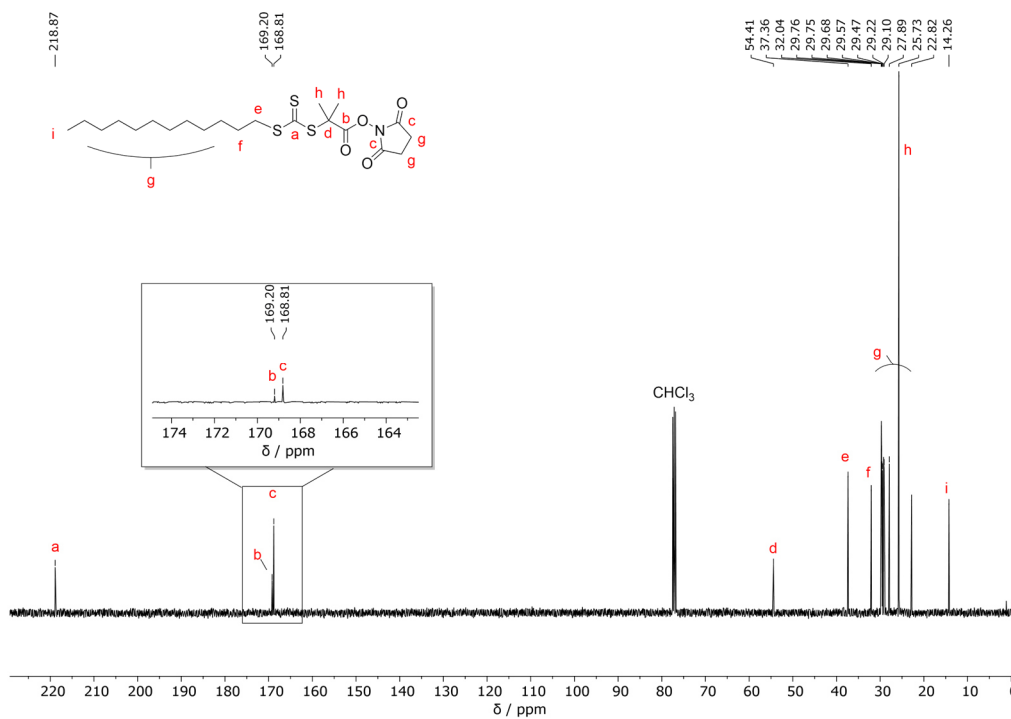


Figure S24: ¹³C NMR (101 MHz) spectrum of DMP-NHS recorded in CDCl₃.

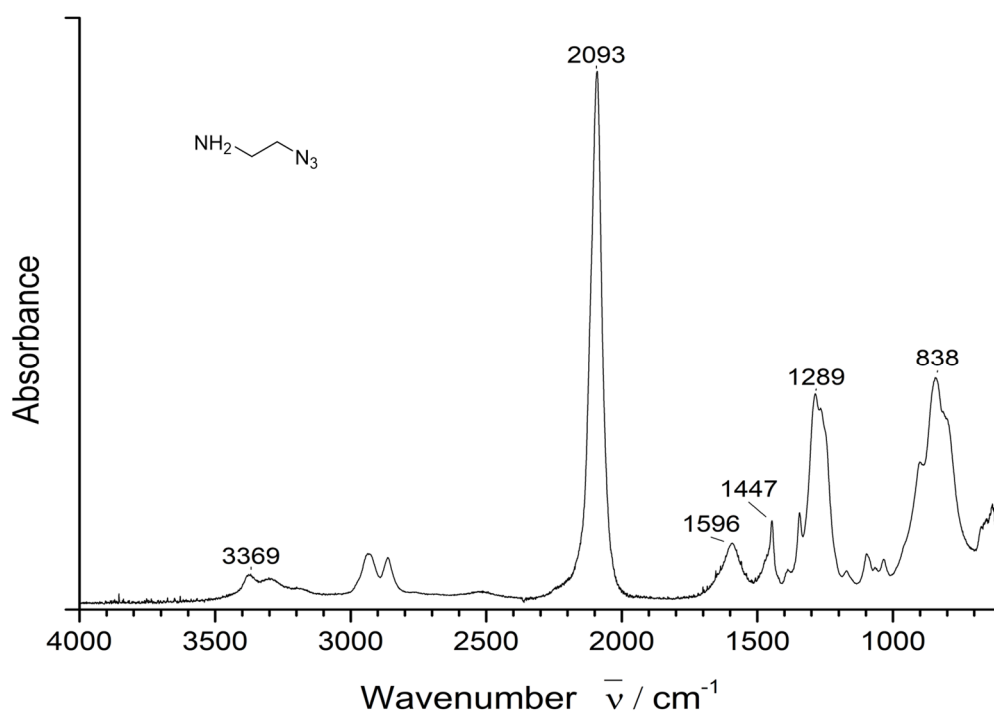


Figure S25: IR spectrum of 2-Azidoethylamine

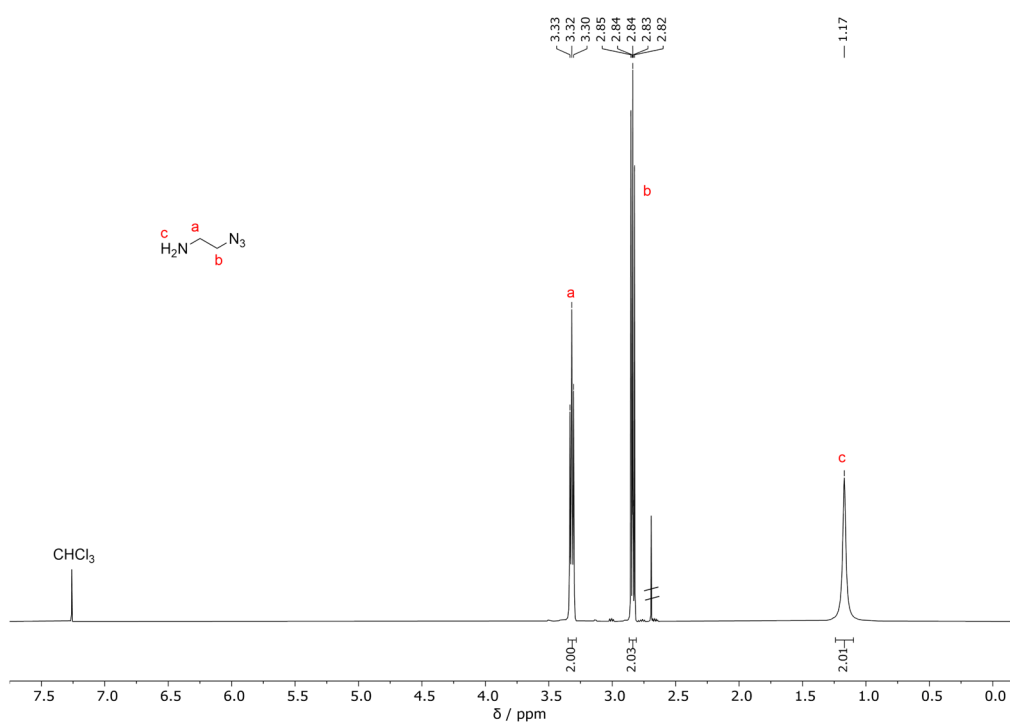


Figure S26: ^1H NMR spectrum (400 MHz) of 2-Azidoethylamine recorded in CDCl_3 .

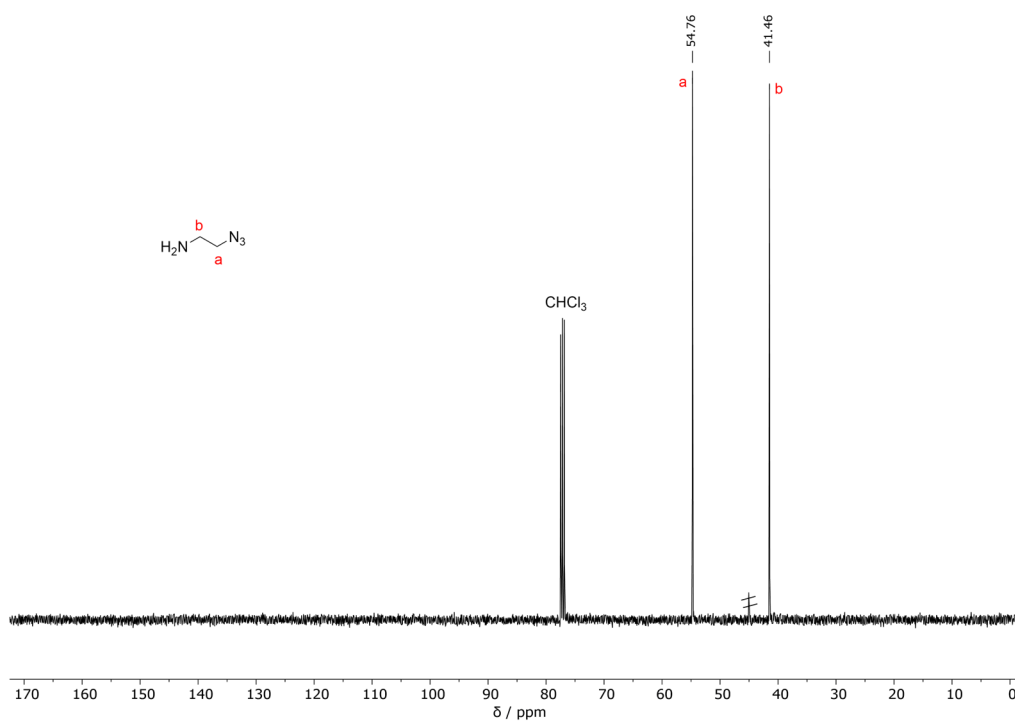


Figure S27: ¹³C NMR spectrum (101 MHz) of 2-Azidoethylamine recorded in CDCl₃.

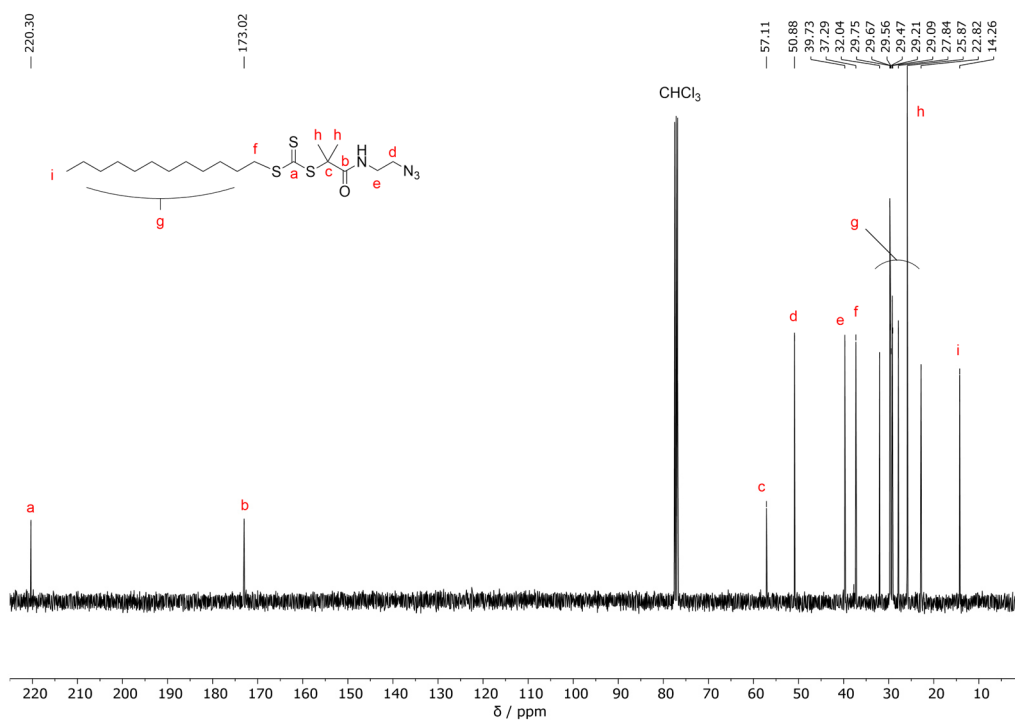


Figure S28: ¹³C NMR (101 MHz) spectrum of DMP-N₃ recorded in CDCl₃.

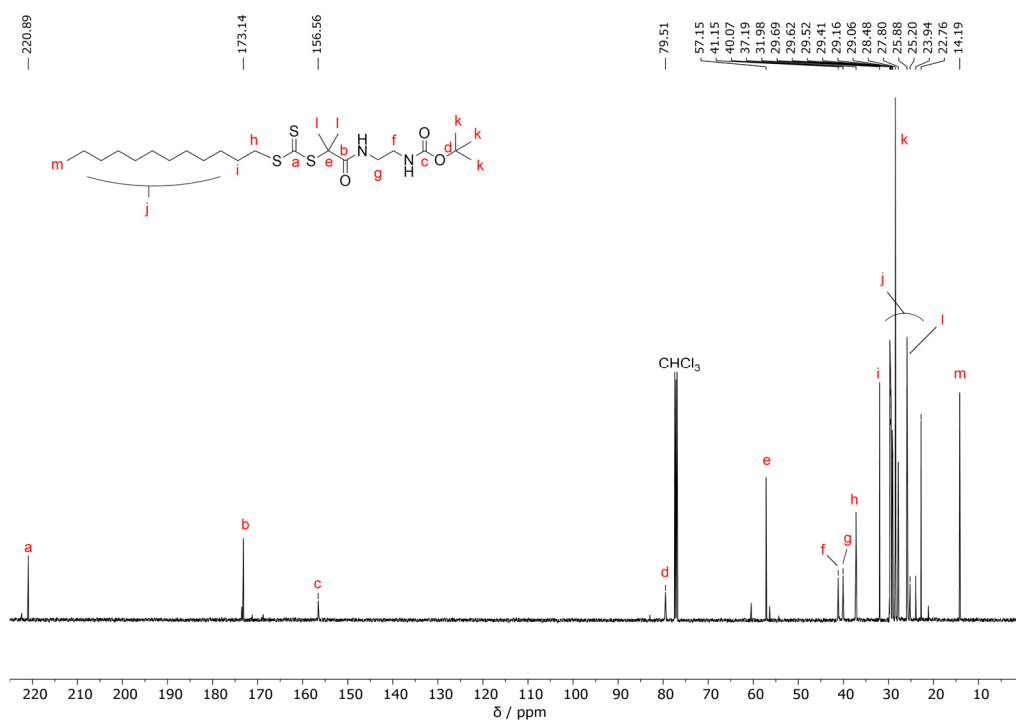


Figure S29: ¹³C NMR spectrum (126 MHz) of DMP-NH-Boc recorded in CDCl₃.

7.1.4 Spectra of Amino-Functionalized Acrylamides and their Precursors

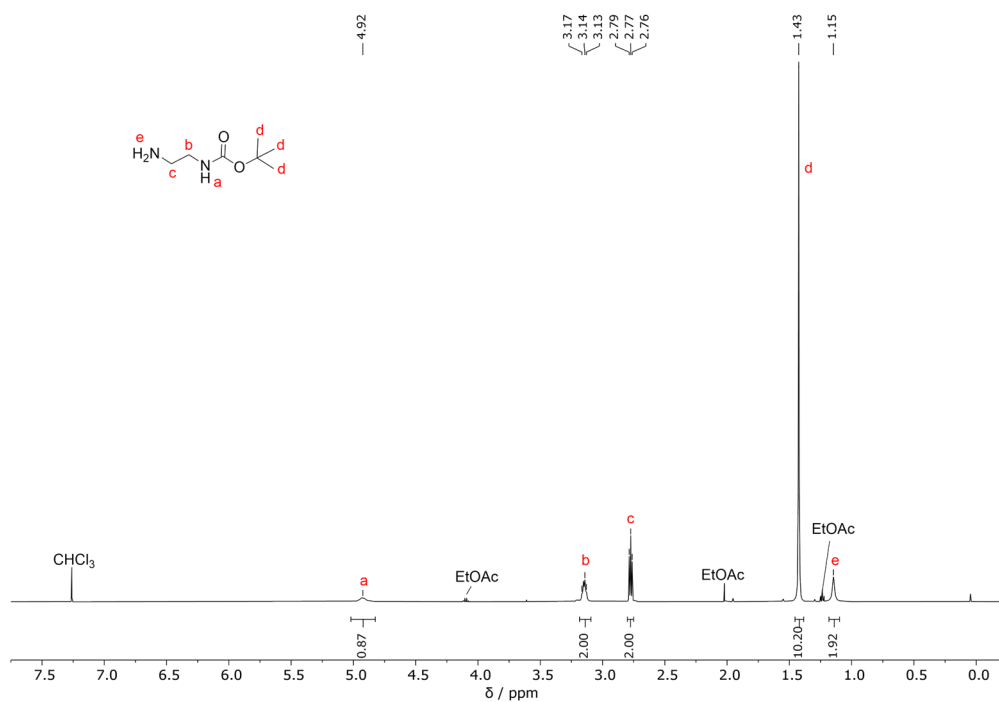


Figure S30: ¹H NMR (500 MHz) spectrum of H₂N-Et-NH-Boc recorded in CDCl₃.

7 Appendix

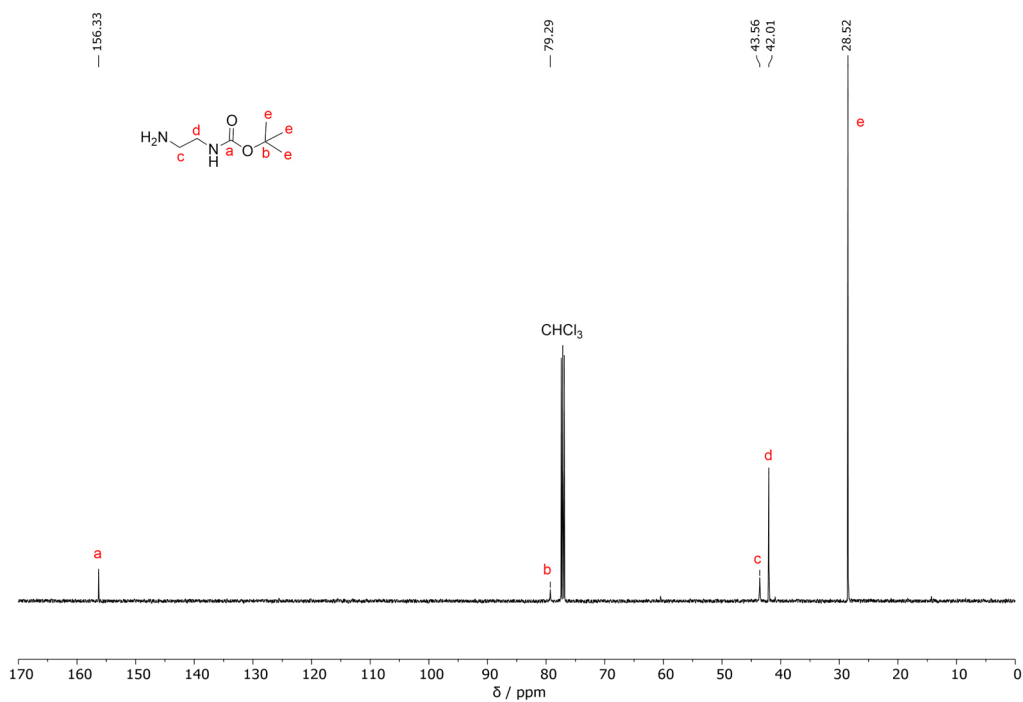


Figure S31: ¹³C NMR (126 MHz) spectrum of H₂N-Et-NH-Boc recorded in CDCl₃.

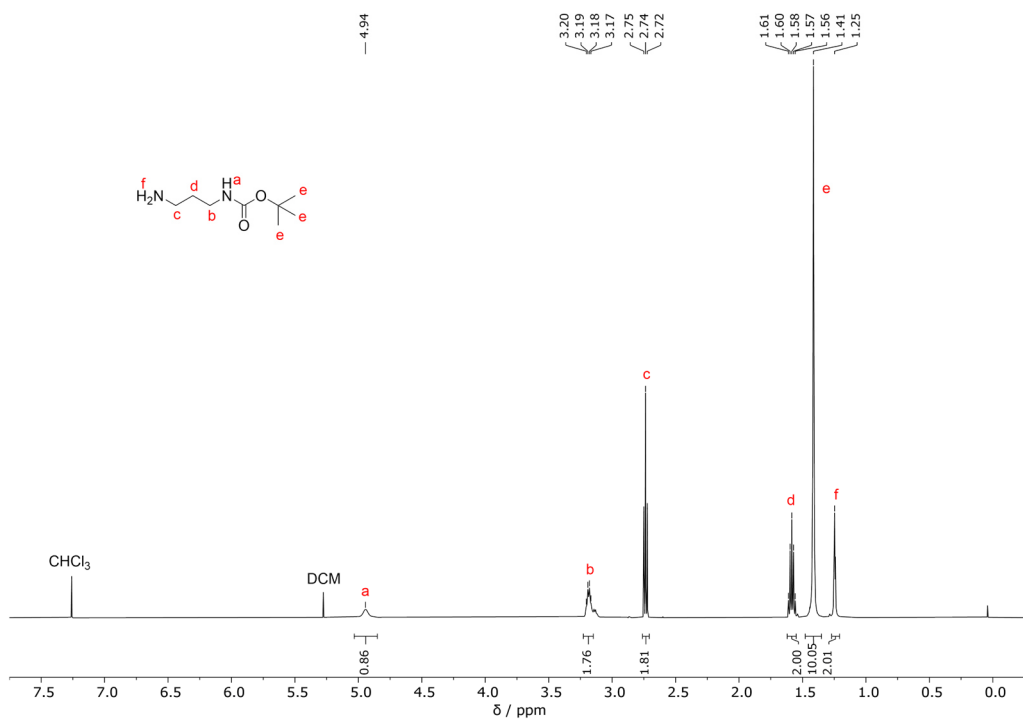


Figure S32: ¹H NMR (500 MHz) spectrum of H₂N-Prop-NH-Boc recorded in CDCl₃.

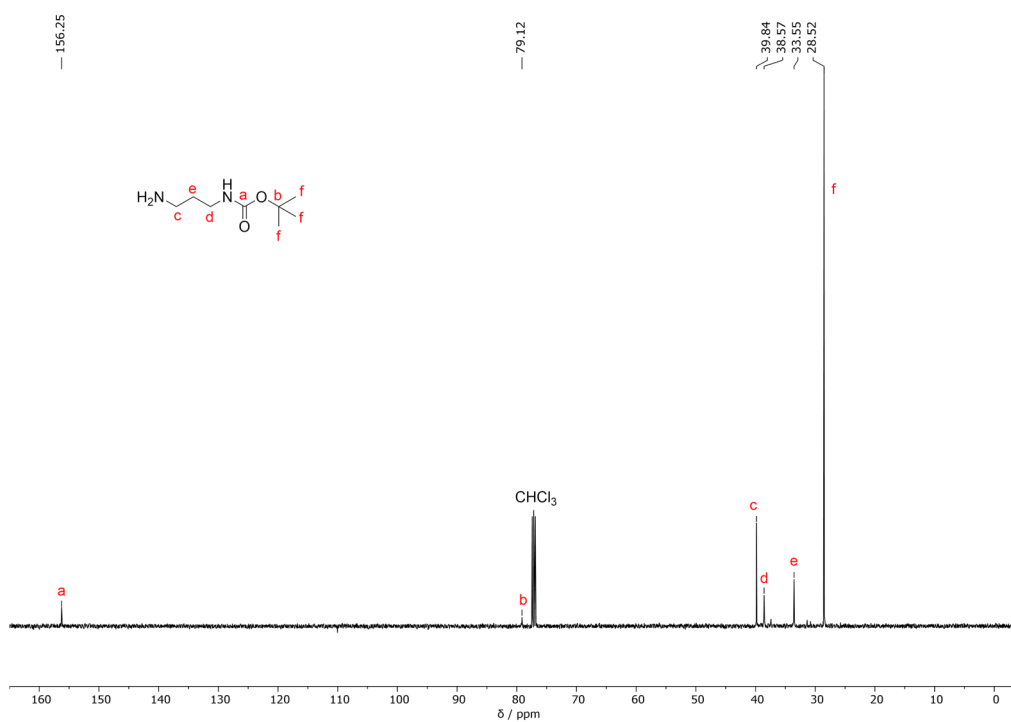


Figure S33: ^{13}C NMR (126 MHz) spectrum of $\text{H}_2\text{N-Prop-NH-Boc}$ recorded in CDCl_3 .

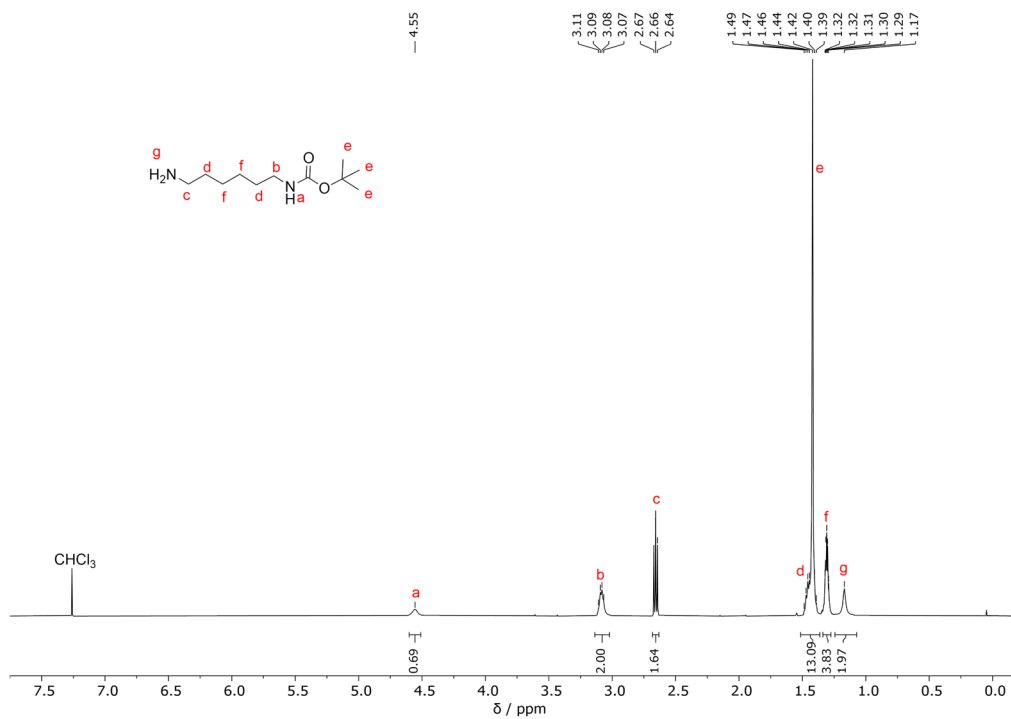


Figure S34: ^1H NMR (500 MHz) spectrum of $\text{H}_2\text{N-Hex-NH-Boc}$ recorded in CDCl_3 .

7 Appendix

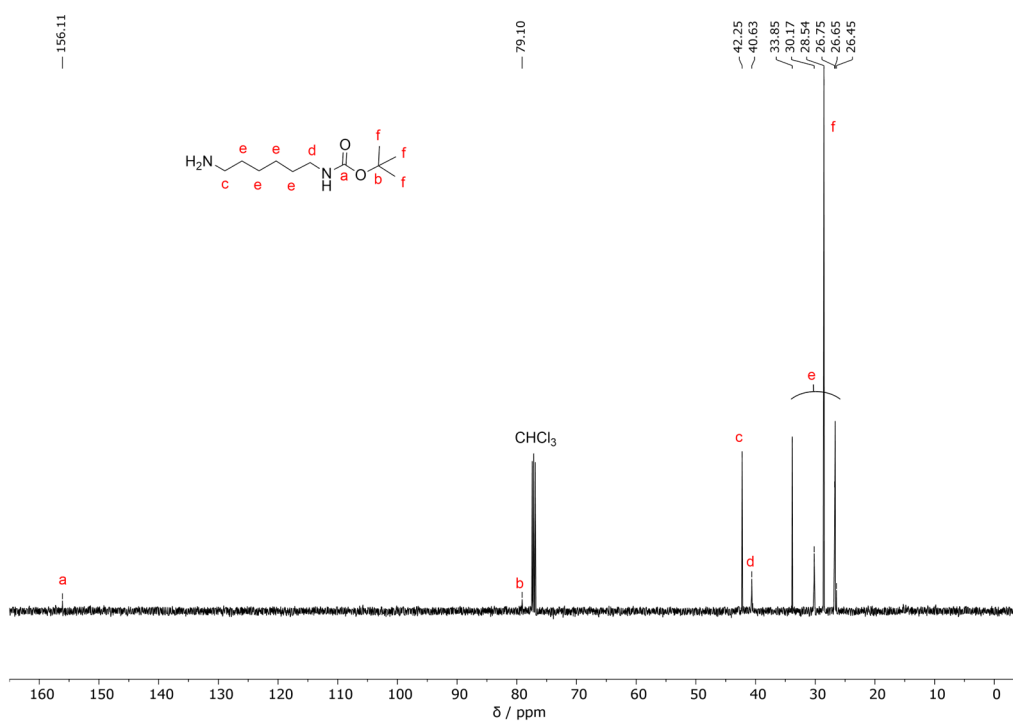


Figure S35: ^{13}C NMR (126 MHz) spectrum of $\text{H}_2\text{N-Hex-NH-Boc}$ recorded in CDCl_3 .

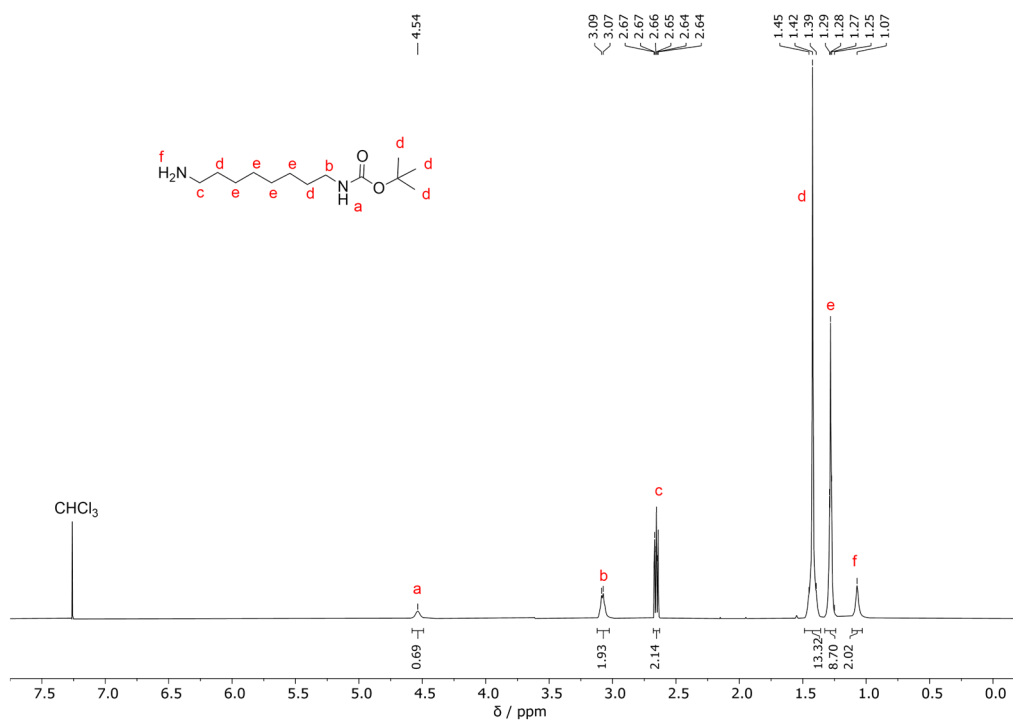


Figure S36: ^1H NMR (500 MHz) spectrum of $\text{H}_2\text{N-Oct-NH-Boc}$ recorded in CDCl_3 .

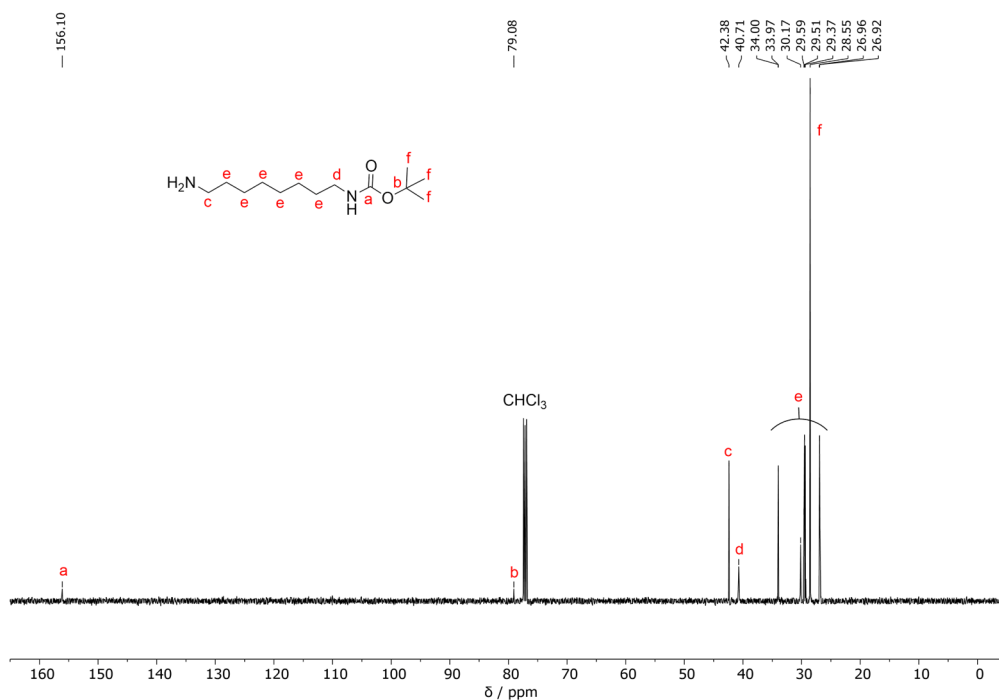


Figure S37: ¹³C NMR (126 MHz) spectrum of H₂N-Oct-NH-Boc recorded in CDCl₃.

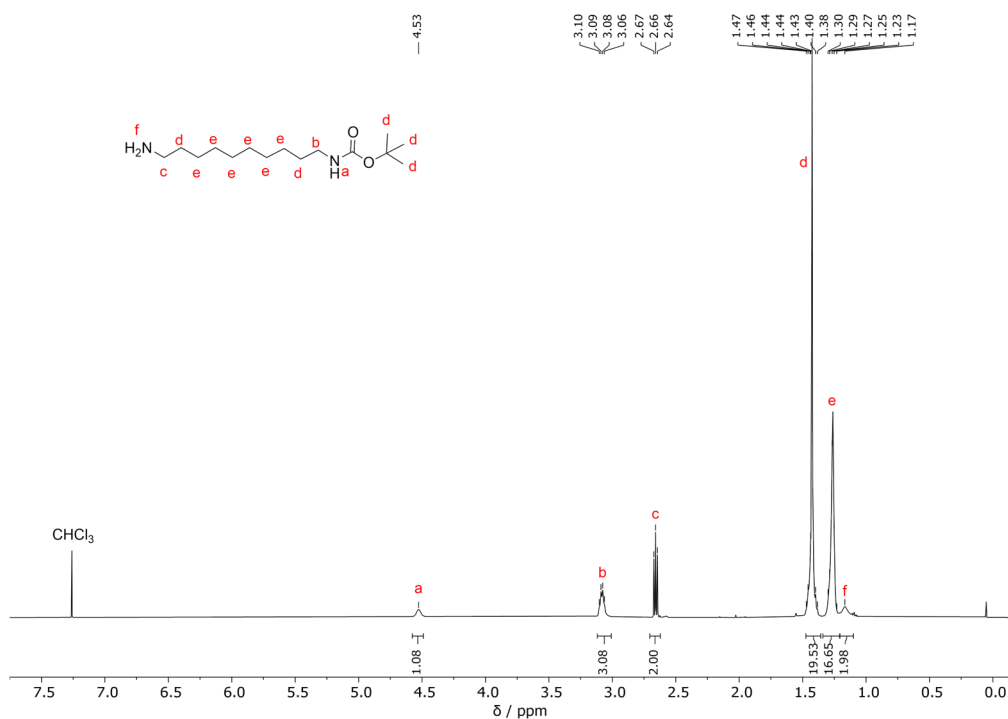


Figure S38: ¹H NMR (500 MHz) spectrum of H₂N-Dec-NH-Boc recorded in CDCl₃.

7 Appendix

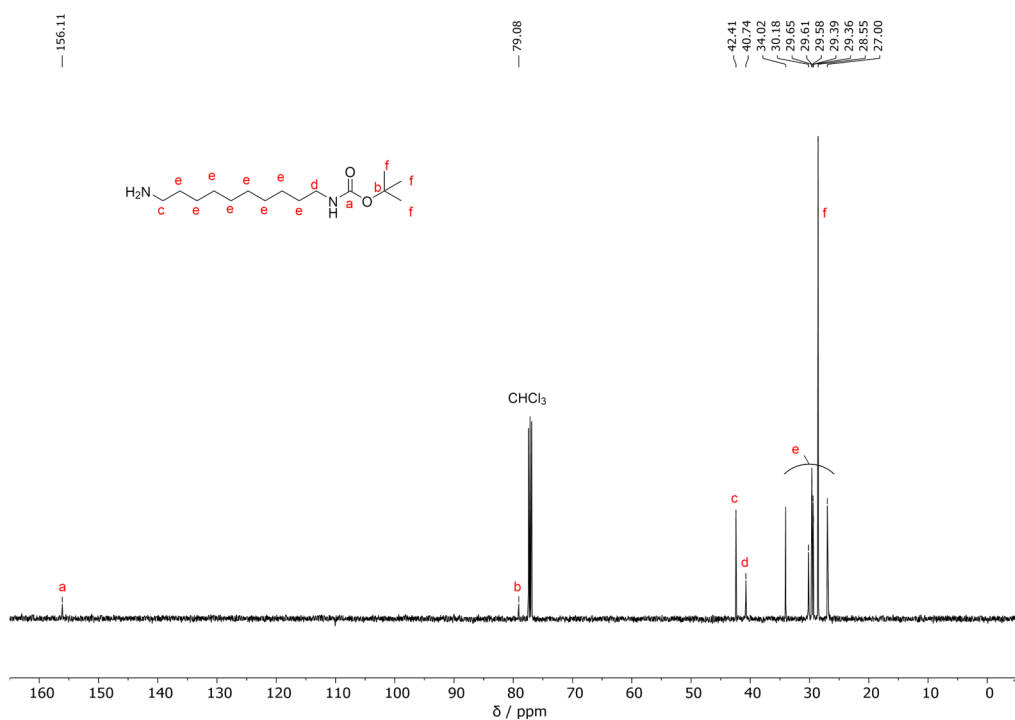


Figure S39: ¹³C NMR (126 MHz) spectrum of H₂N-Dec-NH-Boc recorded in CDCl₃.

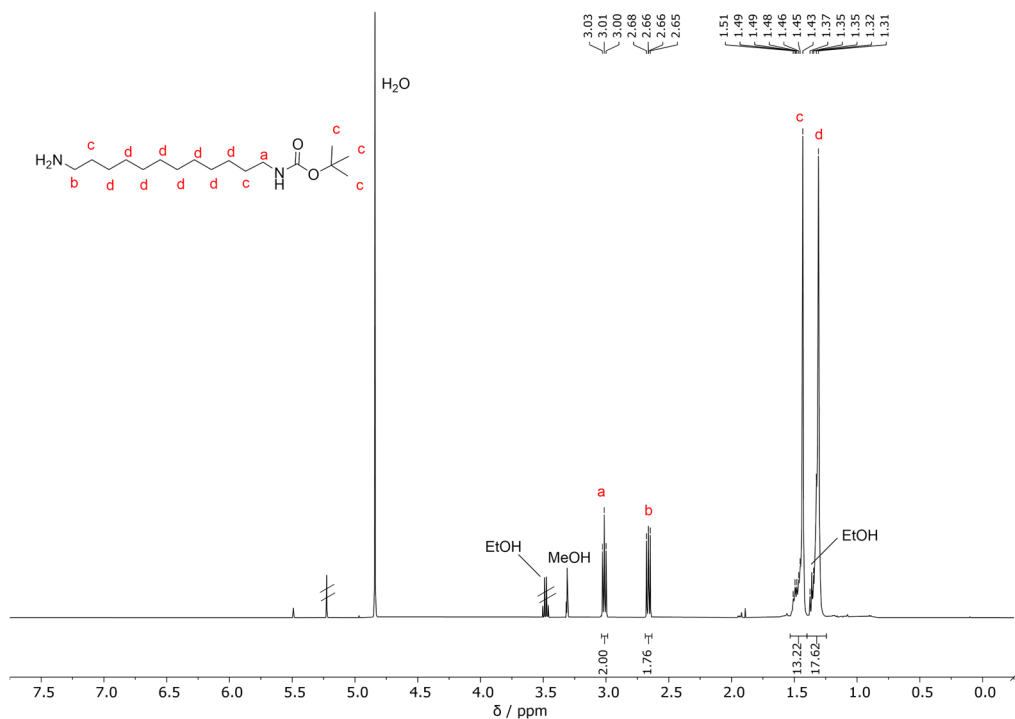


Figure S40: ¹H NMR (500 MHz) spectrum of H₂N-Dod-NH-Boc recorded in CD₃OD. (Spectrum kindly provided by Fiona Diehl)

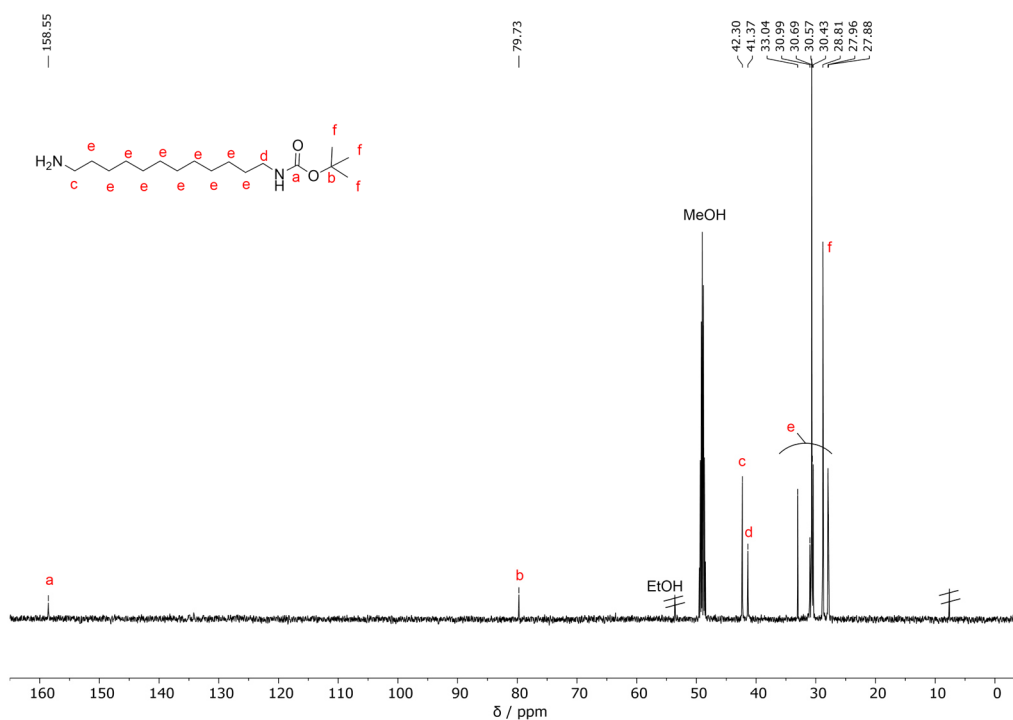


Figure S41: ^{13}C NMR (126 MHz) spectrum of $\text{H}_2\text{N-Dod-NH-Boc}$ recorded in CD_3OD . (Spectrum kindly provided by Fiona Diehl)

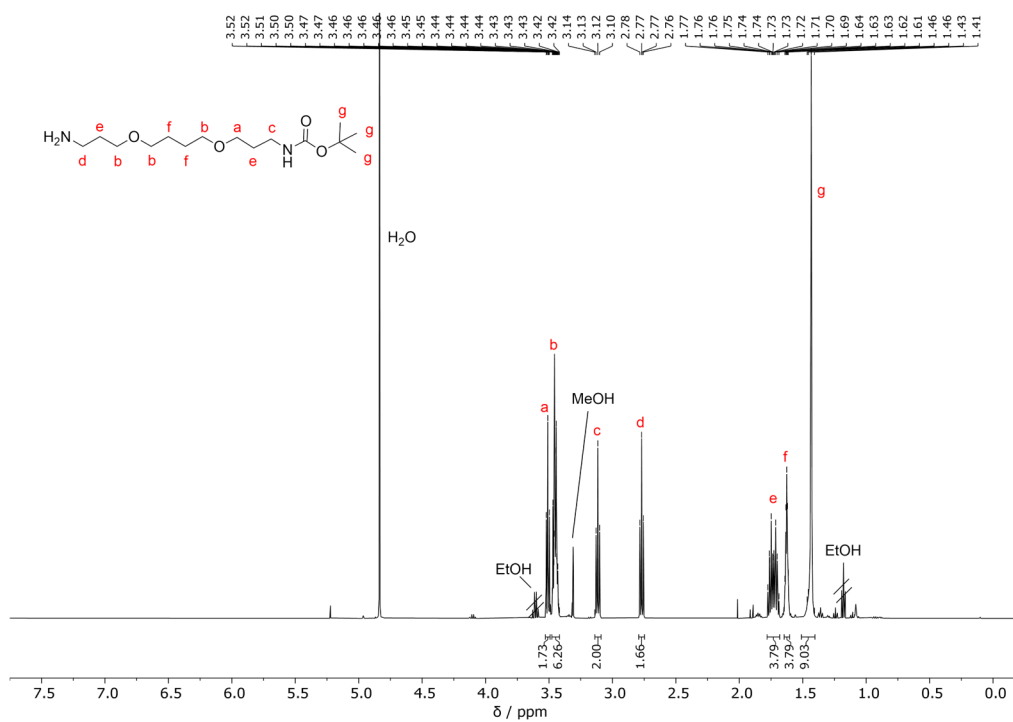


Figure S42: ^1H NMR (500 MHz) spectrum of $\text{H}_2\text{N-PO-NH-Boc}$ recorded in CD_3OD . (Spectrum kindly provided by Fiona Diehl)

7 Appendix

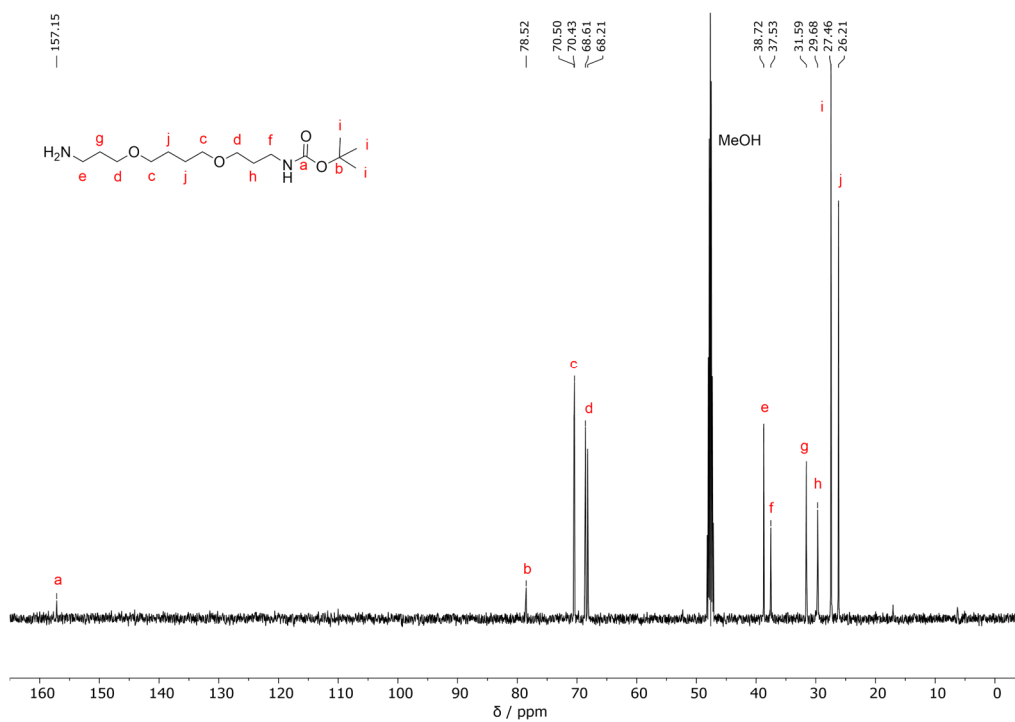


Figure S43: ^{13}C NMR (126 MHz) spectrum of $\text{H}_2\text{N-PO-NH-Boc}$ recorded in CD_3OD . (Spectrum kindly provided by Fiona Diehl)

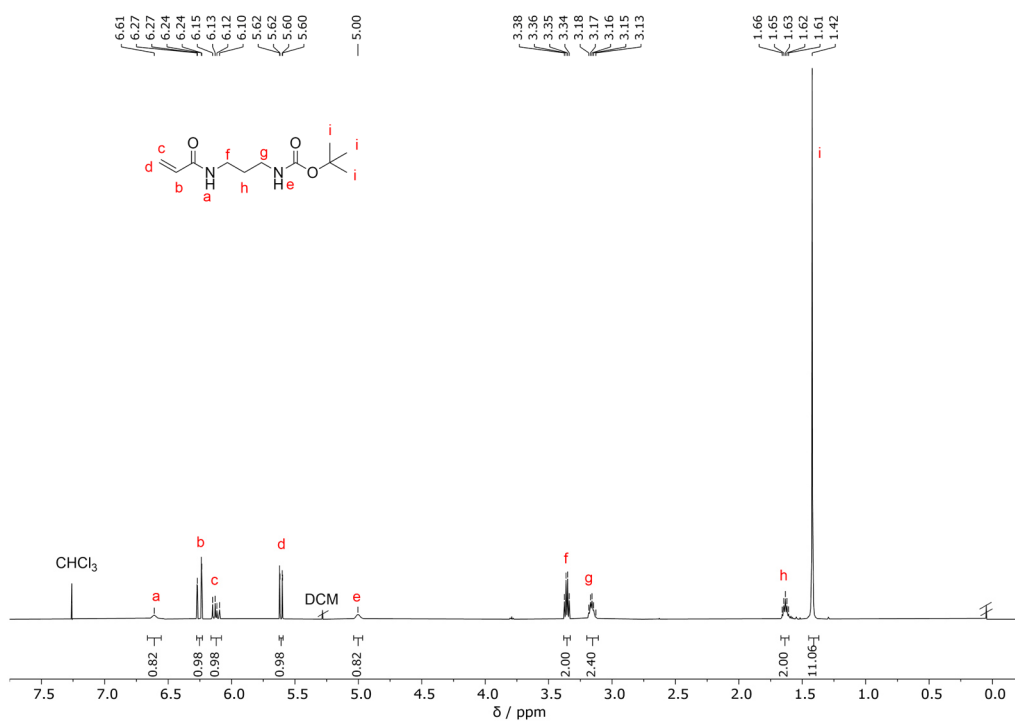


Figure S44: ^1H NMR (500 MHz) spectrum of APAm-Boc recorded in CDCl_3 .

7 Appendix

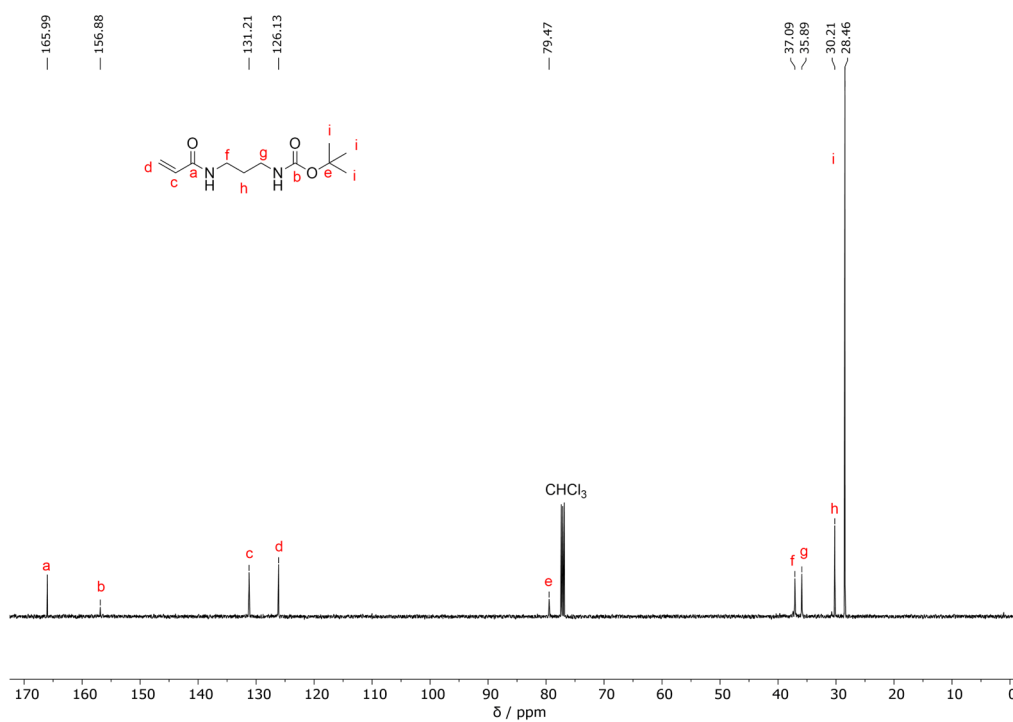


Figure S45: ^{13}C NMR (126 MHz) spectrum of APAm-Boc recorded in CDCl_3 .

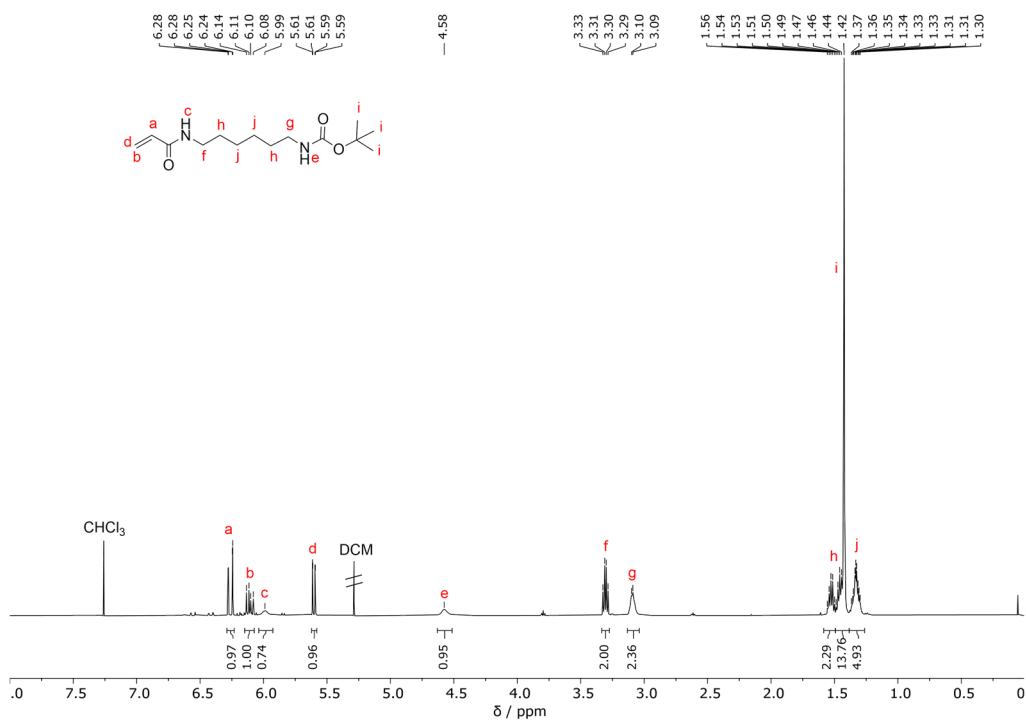


Figure S46: ^1H NMR (500 MHz) spectrum of AHexAm-Boc recorded in CDCl_3 .

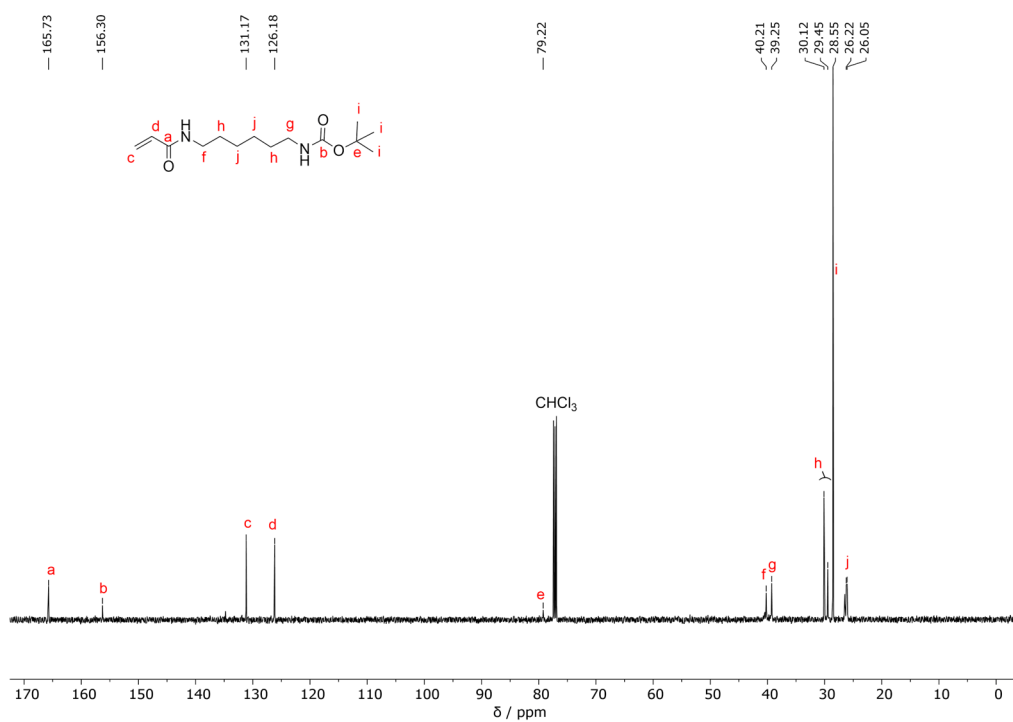


Figure S47: ¹³C NMR (126 MHz) spectrum of AHexAm-Boc recorded in CDCl₃.

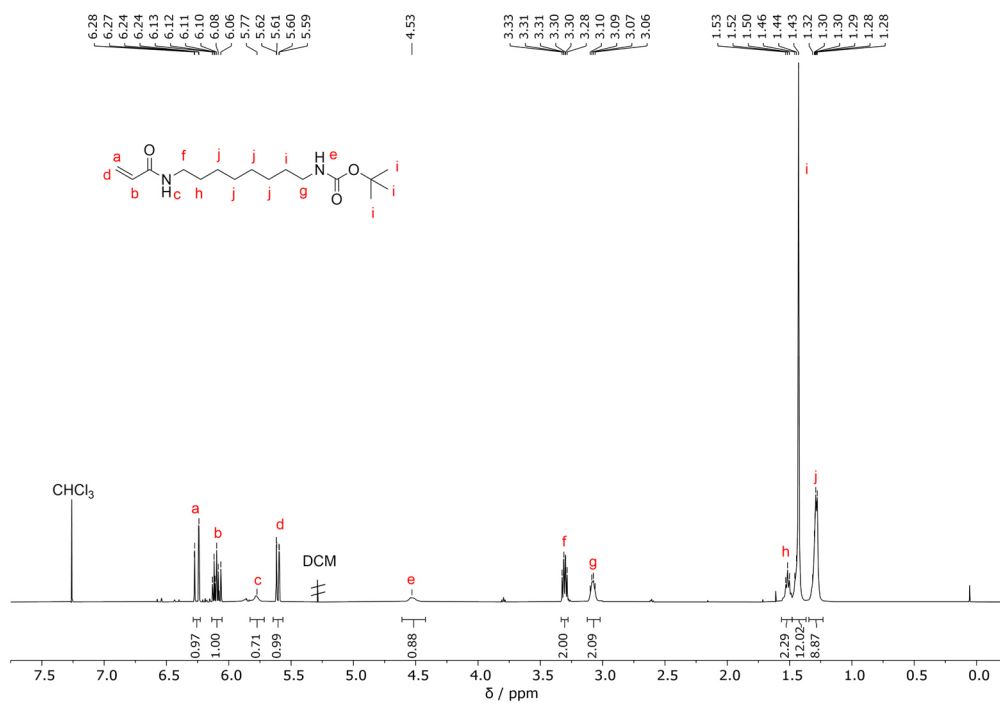


Figure S48: ¹H NMR (500 MHz) spectrum of AOctAm-Boc recorded in CDCl₃.

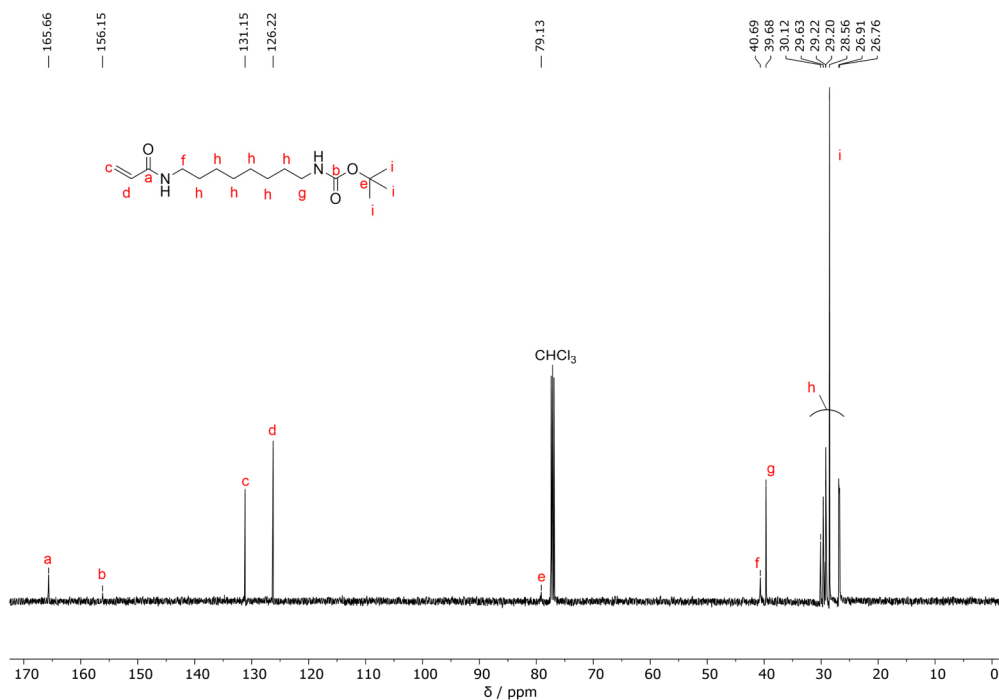


Figure S49: ¹³C NMR (126 MHz) spectrum of AOctAm-Boc recorded in CDCl₃.

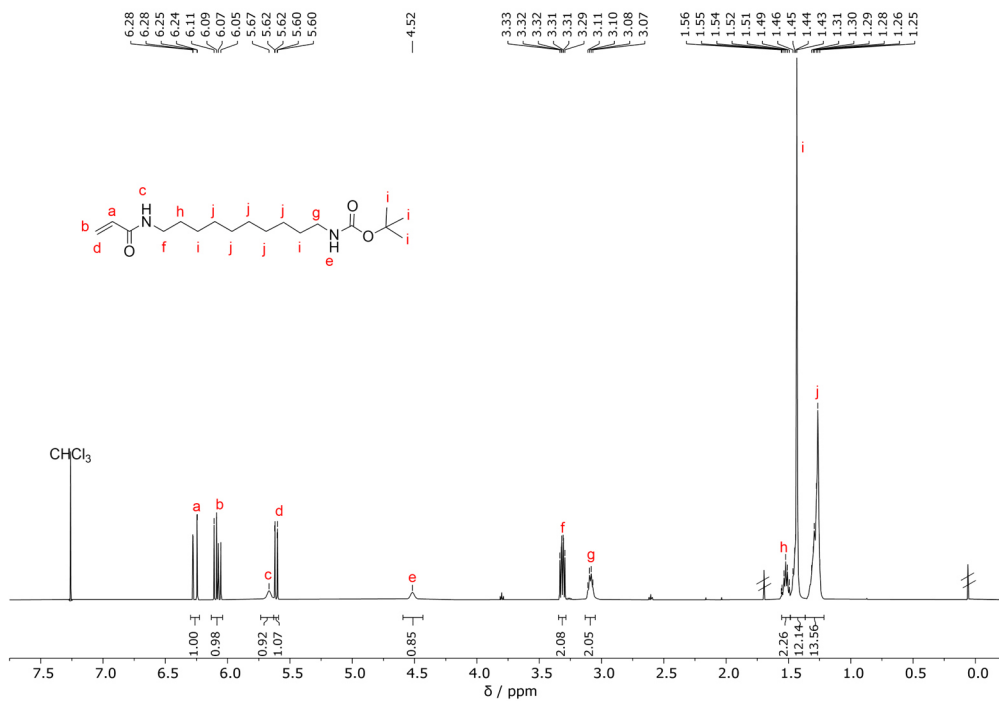


Figure S50: ¹H NMR (500 MHz) spectrum of ADecAm-Boc recorded in CDCl₃.

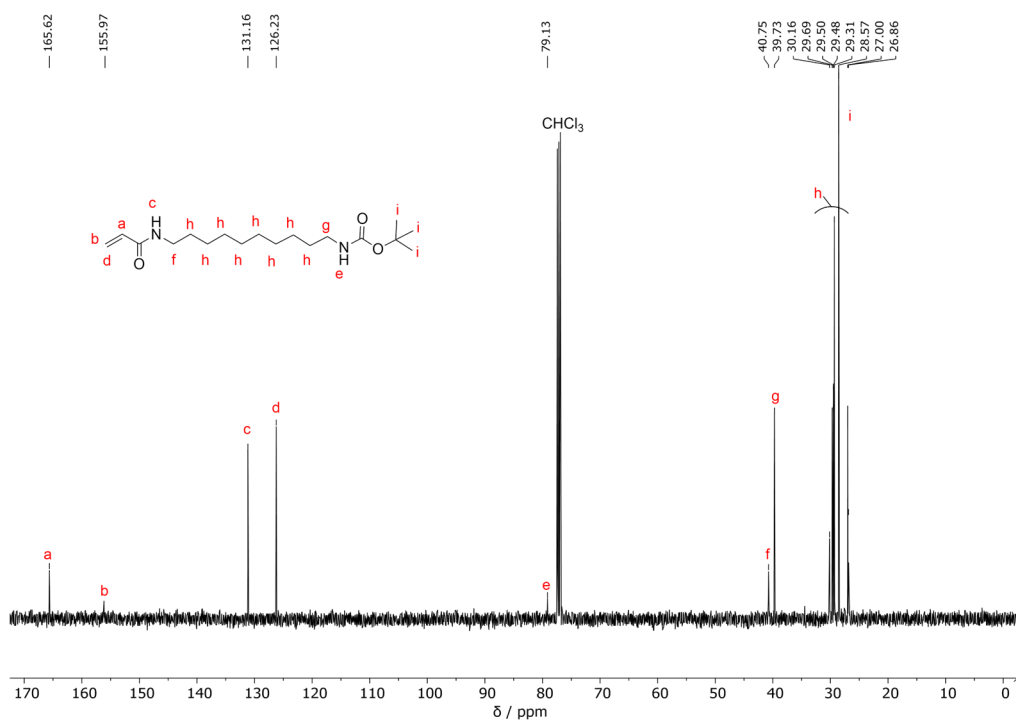


Figure S51: ¹³C NMR (126 MHz) spectrum of ADecAm-Boc recorded in CDCl₃.

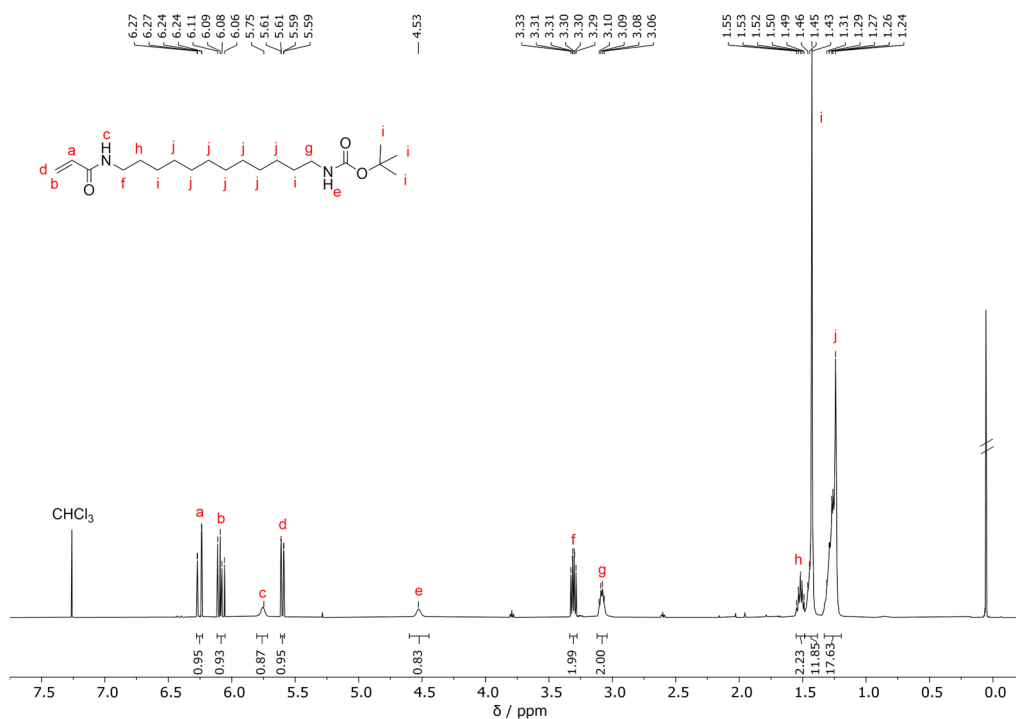


Figure S52: ¹H NMR (500 MHz) spectrum of ADodAm-Boc recorded in CDCl₃. (Spectrum kindly provided by Fiona Diehl)

7 Appendix

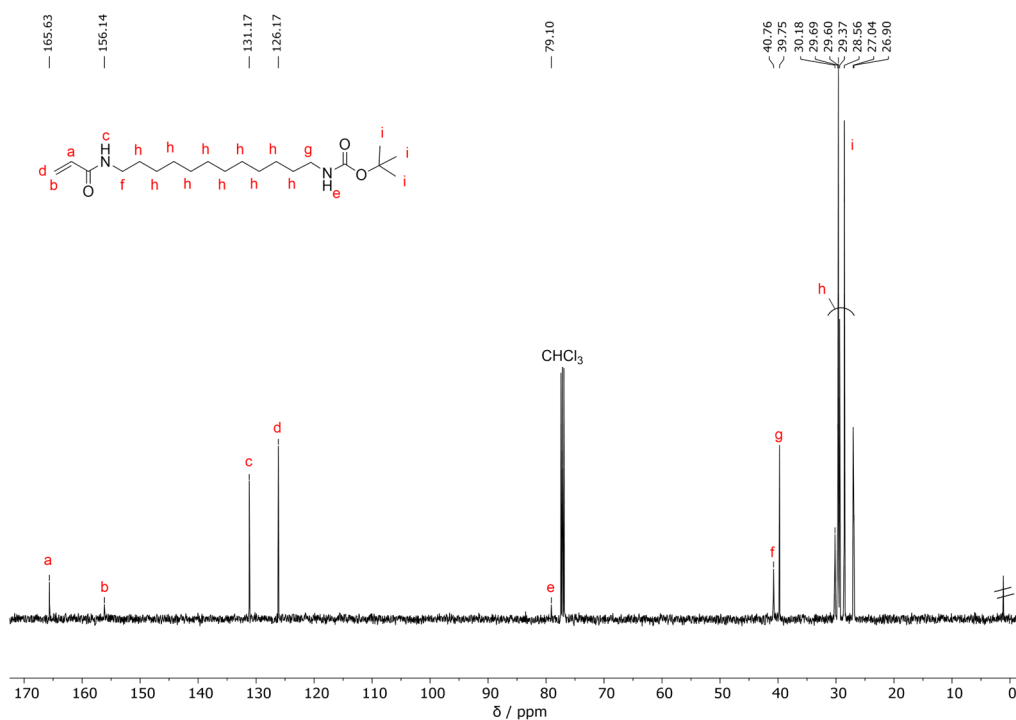


Figure S53: ¹³C NMR (126 MHz) spectrum of ADodAm-Boc recorded in CDCl₃. (Spectrum kindly provided by Fiona Diehl)

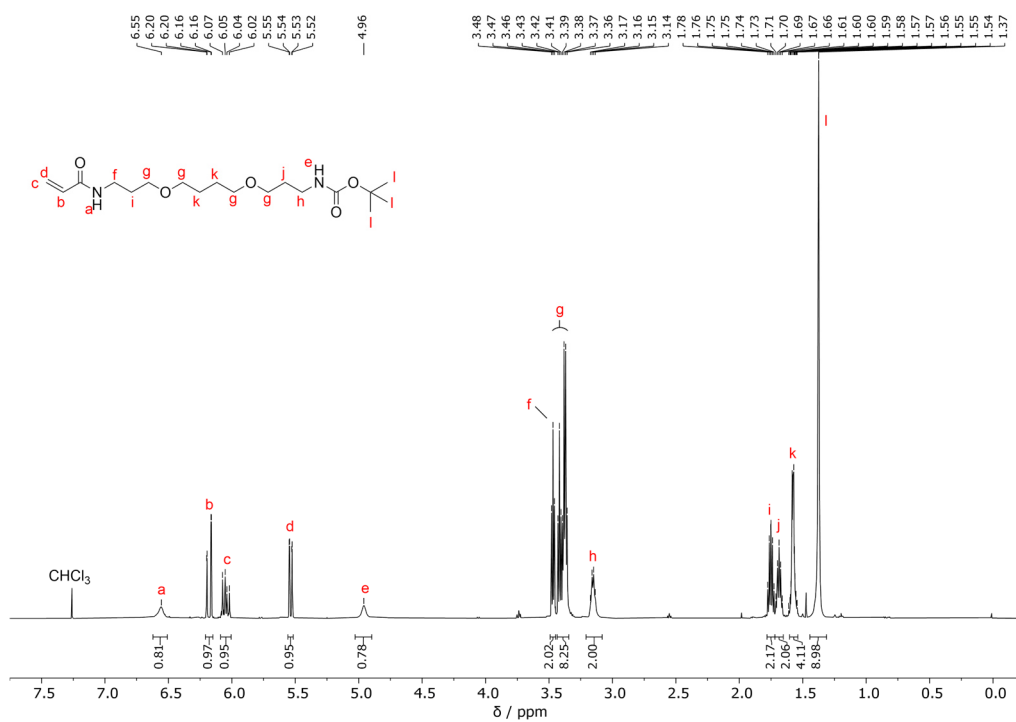


Figure S54: ¹H NMR (500 MHz) spectrum of APOAm-Boc recorded in CDCl₃. (Spectrum kindly provided by Fiona Diehl)

7 Appendix

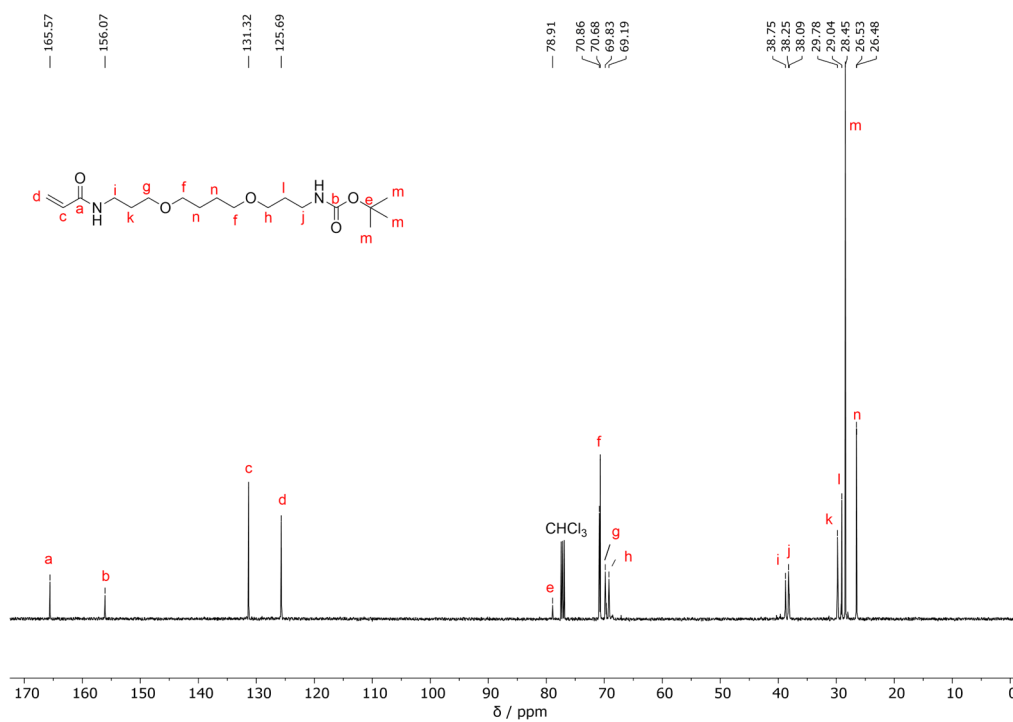


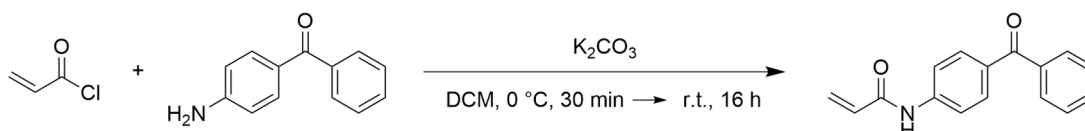
Figure S55: ¹³C NMR (126 MHz) spectrum of APOAm-Boc recorded in CDCl₃. (Spectrum kindly provided by Fiona Diehl)

7.1.5 Additional Experimental Details for the Preparation of Multifunctional Hydrogels

In the following chapter experimental procedure for the synthesis of benzophenone acrylamide (BPAm) and the copolymers **P2.7-P2.15** are given. The procedures were developed and described in the Master's Thesis "*Synthesis of Multifunctional Hydrogel Coatings Using RAFT Polymerization for Potentially Improved Cell-Material Interactions*" Niklas Jung, Universität Siegen, 2016.

Synthesis of Benzophenone acrylamide (BPAm)

The reaction was done according to a modified procedure described in literature.¹²



4-Aminobenzophenone (4.00 g, 20.3 mmol) was dissolved in dichloromethane (60 ml), and the solution was cooled to 0 °C. Anhydrous potassium carbonate (2.80 g, 20.3 mmol) was added and the solution was stirred for 30 min. Acryloyl chloride (2.20 g, 24.3 mmol, 2.0 ml), dissolved in dichloromethane (50 ml), was added drop wise at 0 °C under vigorous stirring. Then the reaction was warmed to room temperature and stirred overnight. The solids were filtrated-off and the organic layer was then extracted with water (3 x 50 ml), saturated sodium bicarbonate (3 x 50 ml), and saturated brine solution (2 x 50 ml). Anhydrous sodium sulfate was added to dry the organic layer, and the solvent was removed rotary evaporation. Then the crude product was recrystallized from DCM three times and dried in high vacuum.

Yield: 3.03 g (12.1 mmol, 60%)

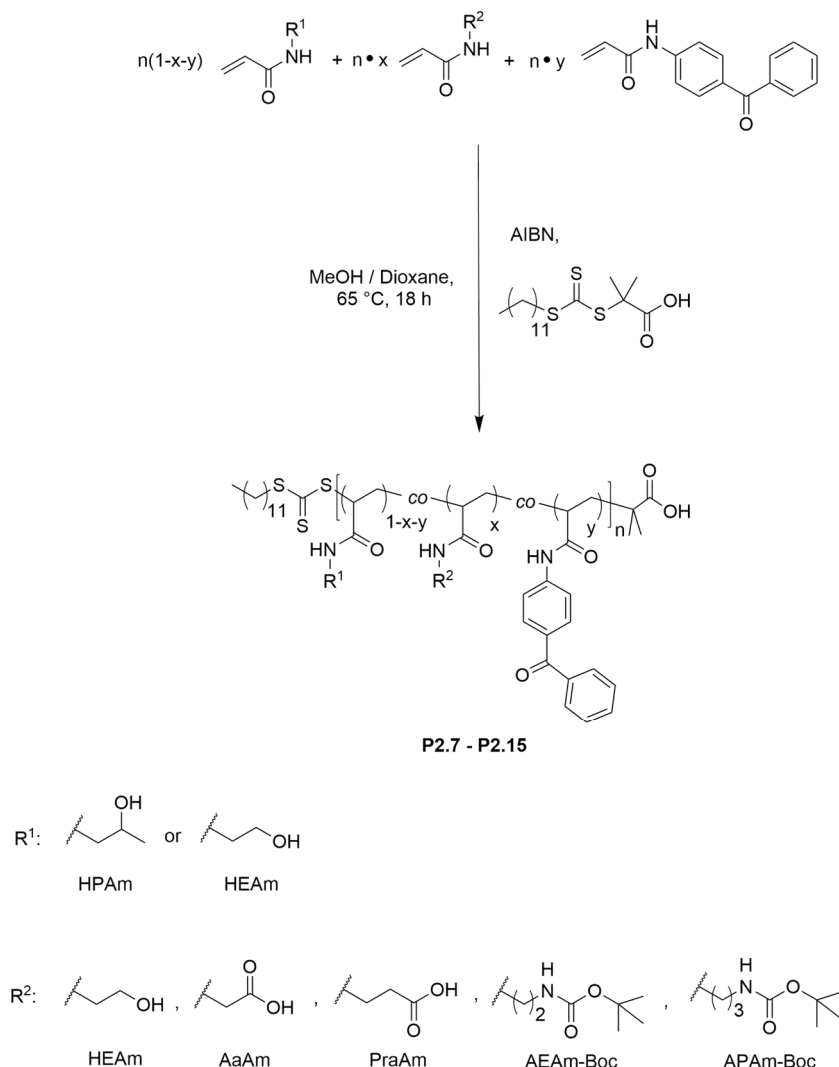
Analytical data:

TLC: silica, hexane : EtOAc 1 : 2 (v/v), R_f: 0.68

¹H NMR (400 MHz, DMSO-d₆): δ 12.59 (s, 1H), 8.43 (t, *J* = 5.9 Hz, 1H), 6.29 (dd, *J* = 17.1, 10.2 Hz, 1H), 6.10 (dd, *J* = 17.2, 2.1 Hz, 1H), 5.62 (dd, *J* = 10.2, 2.1 Hz, 1H), 3.83 (d, *J* = 6.0 Hz, 2H) ppm.

¹³C NMR (101 MHz, DMSO-d₆): δ 171.27, 164.95, 131.33, 125.73, 40.67 ppm.

General Procedure 21: Synthesis of RAFT-Copolymers from Acrylamide Derivatives with 2 mol% BPAm



In a dry 10 ml schlenk tube typically 400 mg of the monomer were dissolved in methanol (2 ml for HPAm, HEAm and 2.4 ml for AaAm, PraAm). To the mixture CTA and initiator were added from stock solutions according to Table S7.1. The ratio $[M]_0 : [BPAm]_0 : [AIBN]_0 : [DMP]$ was chosen to yield polymers with an average molar mass \bar{M}_n of 27.5 kDa. Then AIBN and DMP were added and the tube content was purged with argon for 30 min. The final concentration was $\beta = 140 \text{ mg}\cdot\text{ml}^{-1}$. Afterwards the tube was placed in a preheated oil bath at 65 °C. The reaction was stopped by cooling the tube with liquid nitrogen and exposure the reaction mixture to air. The polymers were precipitated in ethyl acetate at least two times, unless otherwise noted, then filtered-off or centrifuged and finally dried in vacuum overnight.

Table S7.1: Overview of reaction conditions for RAFT-Polymerizations of homopolymers: The polymerizations were performed at a temperature of 65 °C for 18 h and with AIBN as initiator. The masses of DMP and AIBN (0.26 mg, 1.54 mmol) were added each from a stock solution in 1,4-dioxane or in methanol, respectively. The initial weight of BPAm was 2 mol% with respect to the monomer. The concentration was $\beta = 140 \text{ mg}\cdot\text{ml}^{-1}$.

Polymer	Monomer A	Monomer B	Monomer	Monomer	DMP	BPAm	Yield
			A	B	/ mg (μmol)	/ mg (μmol)	/ mg (%)
P2.7 A	HPAm	HEAm	308 (2.38)	97 (0.84)	5.86 (16.10)	16.23 (63.6)	283 (66)
P2.7 B	HPAm	HEAm	212 (1.73)	198 (1.72)	6.28 (17.25)	16.73 (65.6)	307 (73)
P2.7 C	HPAm	HEAm	110 (0.85)	289 (2.51)	6.12 (16.80)	17.2 (67.4)	350 (83)
P2.8	HPAm	AaAm	380 (2.94)	20 (0.15)	5.63 (15.45)	15.58 (61.8)	280 (66)
P2.9	HPAm	PraAm	378 (2.92)	22 (0.15)	5.61 (15.40)	15.58 (61.6)	---
P2.10^a	HPAm	AEAm- Boc	367 (2.84)	32 (0.15)	5.46 (15.00)	15.07 (60.0)	150 (36)
P2.11^a	HPAm	APAm- Boc	366 (2.83)	34 (0.15)	5.44 (14.95)	15.07 (60.0)	147 (35)
P2.12	HEAm	AaAm	377 (3.27)	22 (0.17)	6.28 (17.25)	17.33 (69.0)	286 (67)
P2.13	HEAm	PraAm	375 (3.26)	25 (0.17)	6.24 (17.15)	17.22 (68.6)	---
P2.14^a	HEAm	AEAm- Boc	364 (3.16)	36 (0.17)	6.06 (16.65)	16.72 (66.6)	302 (71)
P2.15^a	HEAm	APAm- Boc	362 (3.14)	38 (0.17)	6.02 (16.55)	16.61 (66.2)	332 (79)

^a Deprotection was done according to procedure described in General Procedure 20 using water instead of MeOH as solvent. After deprotection the corresponding polymers are named **P2.10.1**, **P2.11.1**, **P2.14.1** and **P2.15.1**, respectively.

Well-Plate Preparation for Cell Experiments

Stock Solution Preparation

First, stock solutions (each 1 ml) of the polymers, which should be to be tested, in a water/EtOH mixture (70:30 v/v) were prepared with a final concentration of 25 mg·ml⁻¹.

Additionally, a stock solution (5 ml) of the adhesion polymer (DIS086) in a water/EtOH mixture (70:30 v/v) was prepared with a final concentration of 2.5 mg·ml⁻¹.

Well Plate Coating (fully coated well)

The 24-well plates were first cleaned by rinsing with absolute EtOH and subsequent drying in a vacuum oven under reduced pressure ($T = 40\text{ }^{\circ}\text{C}$, $p = 100\text{ mbar}$) for 2 h. The aliquots of 70 μl of the adhesion polymer, dissolved in a water/EtOH mixture (70:30 v/v), were added to each well and the plates dried in vacuo overnight at elevated temperature ($T = 40\text{ }^{\circ}\text{C}$). Subsequently, the dried films were irradiated with UV-light ($\lambda = 254\text{ nm}$) for 1 h.

Then, 200 μl of the polymer stock solutions were filled into each well and again dried in vacuo overnight at $T = 40\text{ }^{\circ}\text{C}$. Again, the dried films were irradiated with UV-light ($\lambda = 254\text{ nm}$) for 1 h and subsequent the well-plates were sealed with parafilm and stored in a freezer at $T = -18\text{ }^{\circ}\text{C}$ until the respective measurements.

Well Plate Coating (partially coated well)

For the partially coating of each well of a 24-well plate, the same procedure and stock solutions concentrations were used as described above.

In addition to the cleaning with EtOH and subsequent drying in a vacuum oven, the well-plates were blown dry with a stream of nitrogen.

Instead of 70 μl of the adhesion polymer stock solution only one or two drops of this solution were placed in the center of a completely dried well.

Analogue, instead of 200 μl only 10 μl of the polymer stock solutions were placed on top of the small previously coated area of the well.

Note:

The so-called adhesion polymer was prepared previously within the group by Samar Diraoui.

7.2 Polymer Spectra

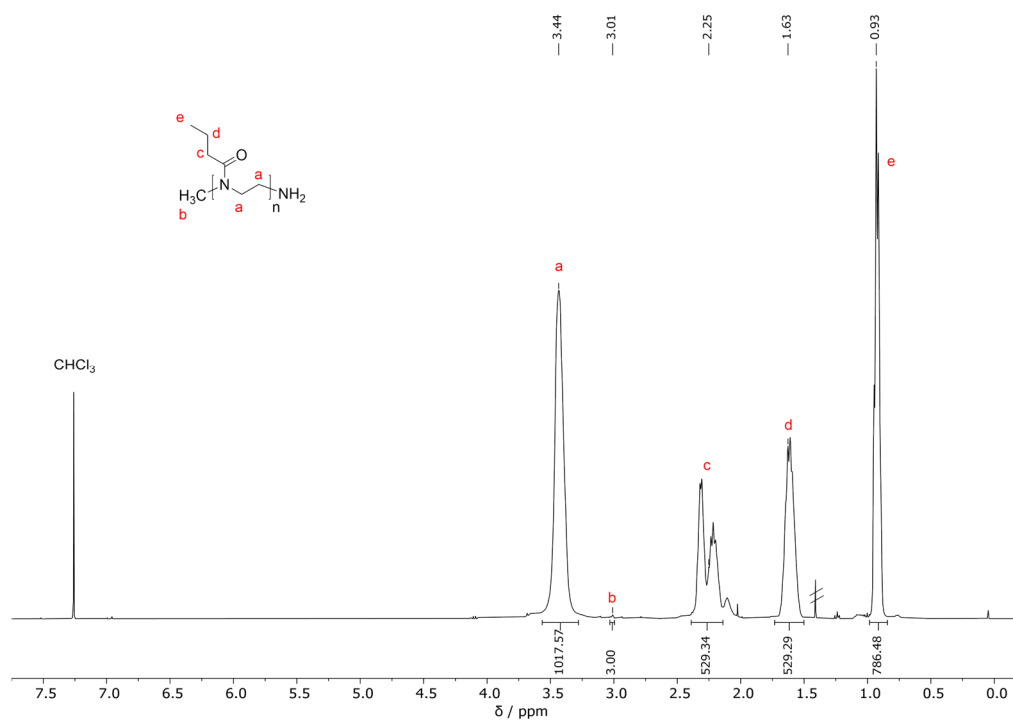


Figure S56: ^1H NMR (400 MHz) spectrum of **P1.1 I** recorded in CDCl_3 .

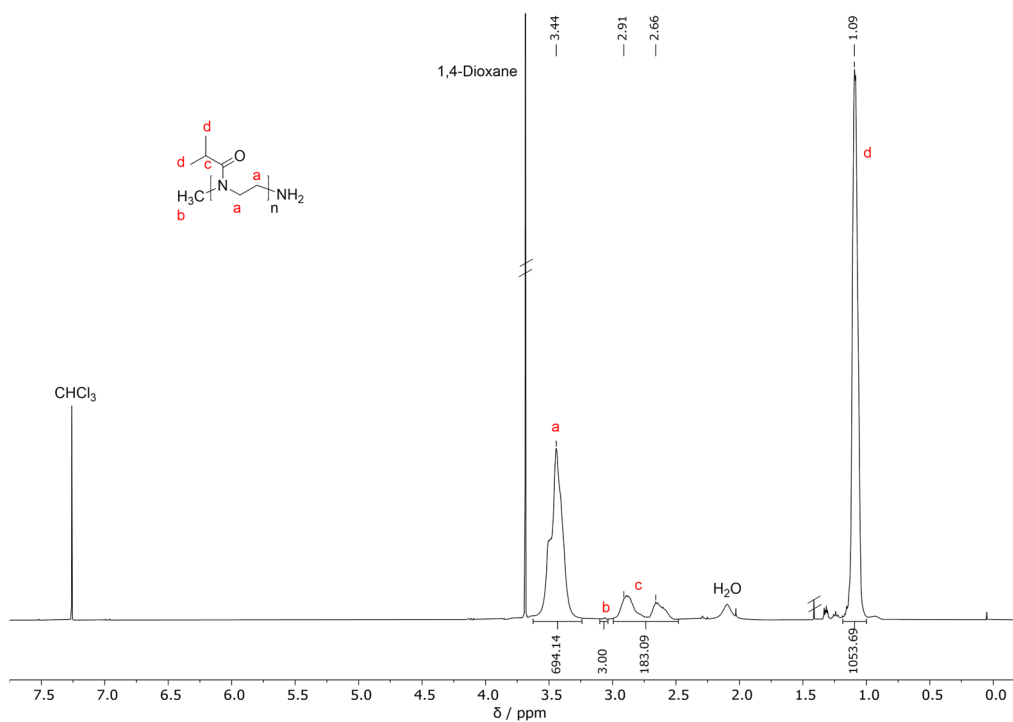


Figure S57: ^1H NMR (400 MHz) spectrum of **P1.2 I** recorded in CDCl_3 .

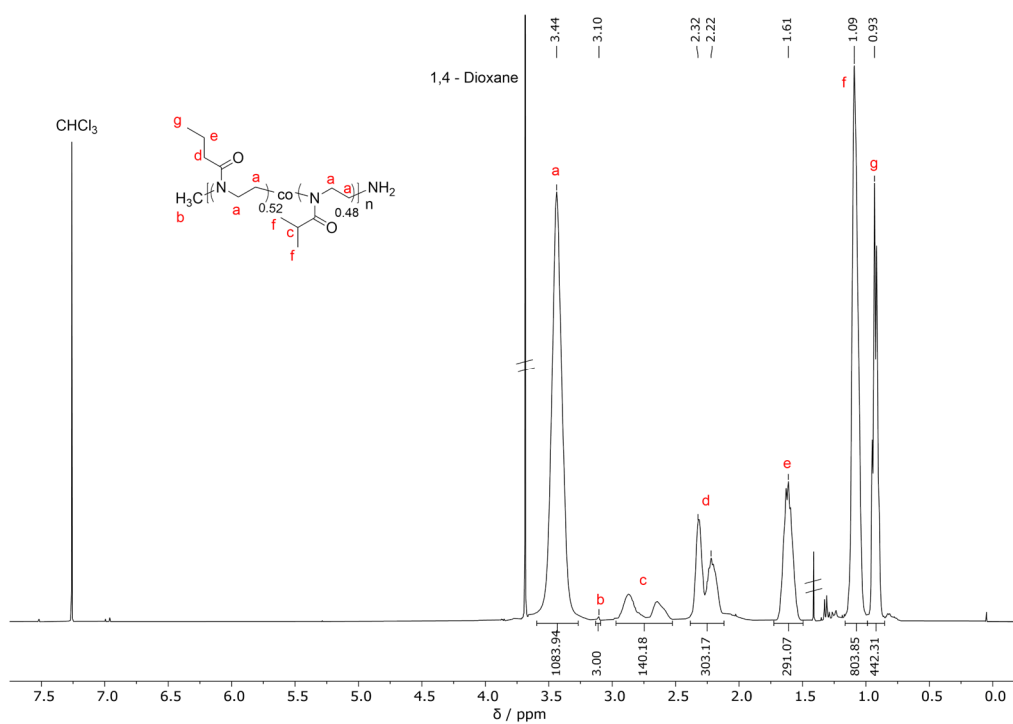


Figure S58: ¹H NMR (400 MHz) spectrum of P1.3 I recorded in CDCl₃.

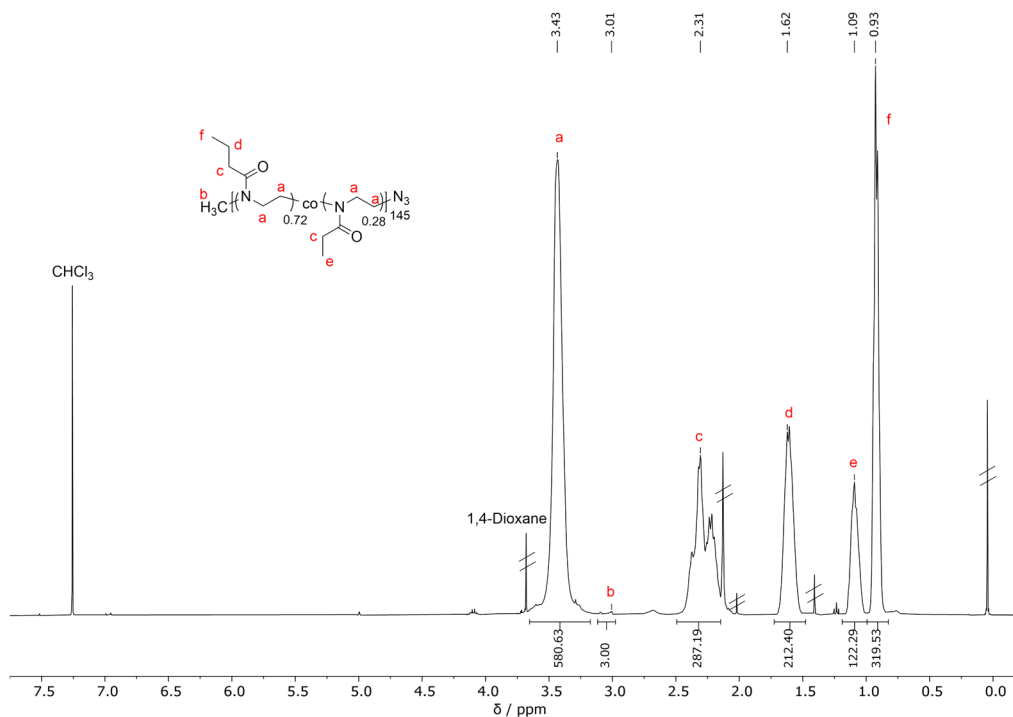


Figure S59: ¹H NMR (400 MHz) spectrum of P1.5 D recorded in CDCl₃.

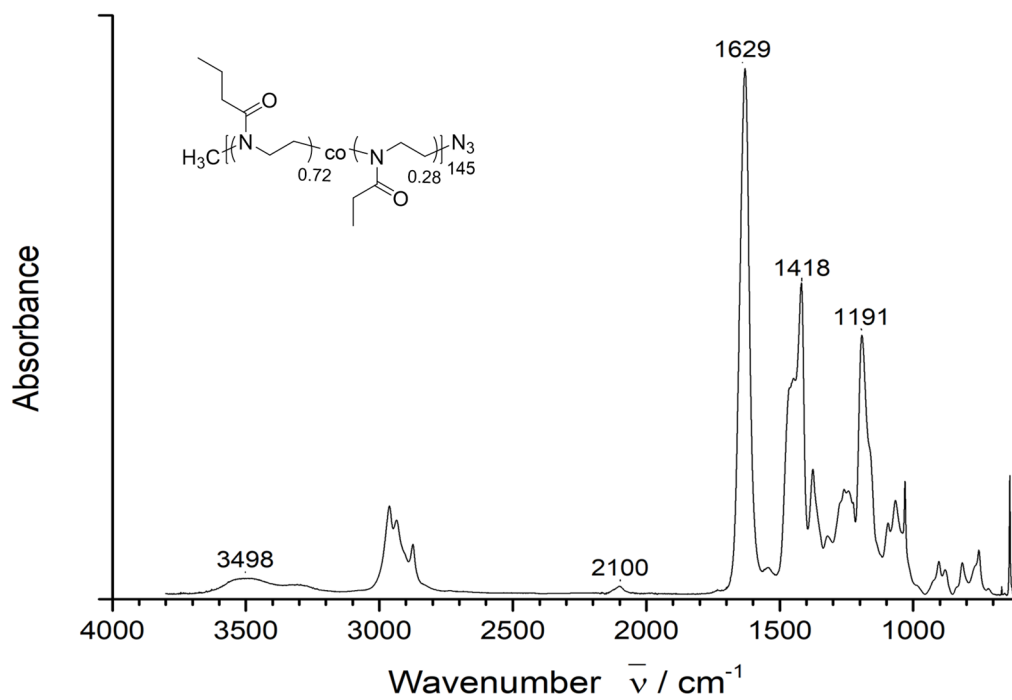


Figure S60: IR spectrum of **P1.5 D**

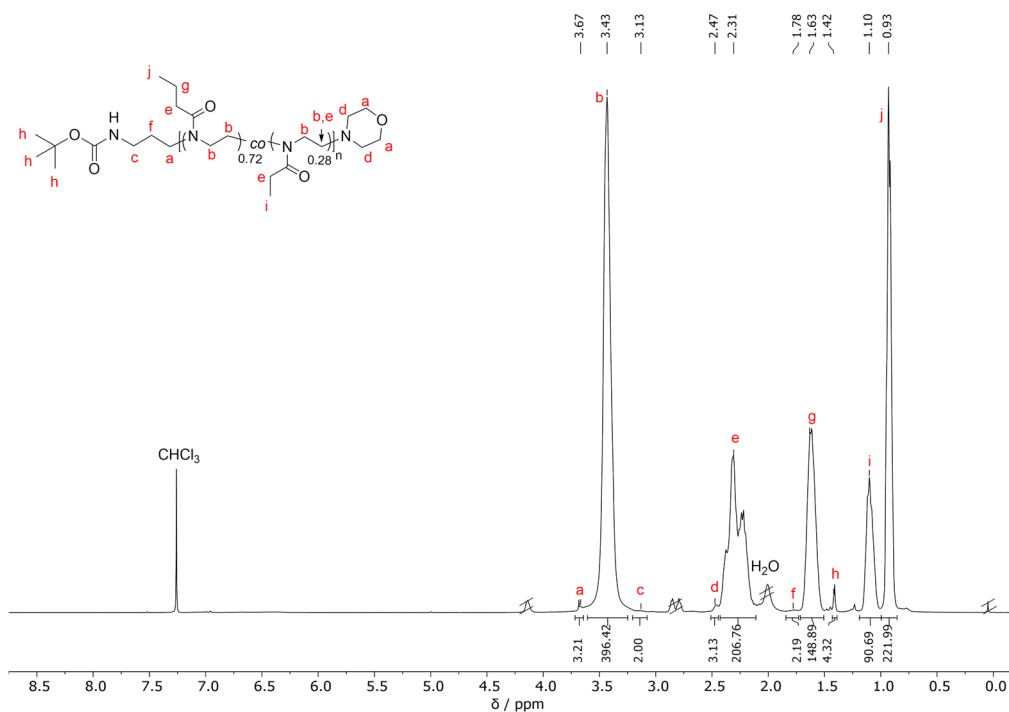


Figure S61: ^1H NMR (400 MHz) spectrum of **P1.12** recorded in CDCl_3 .

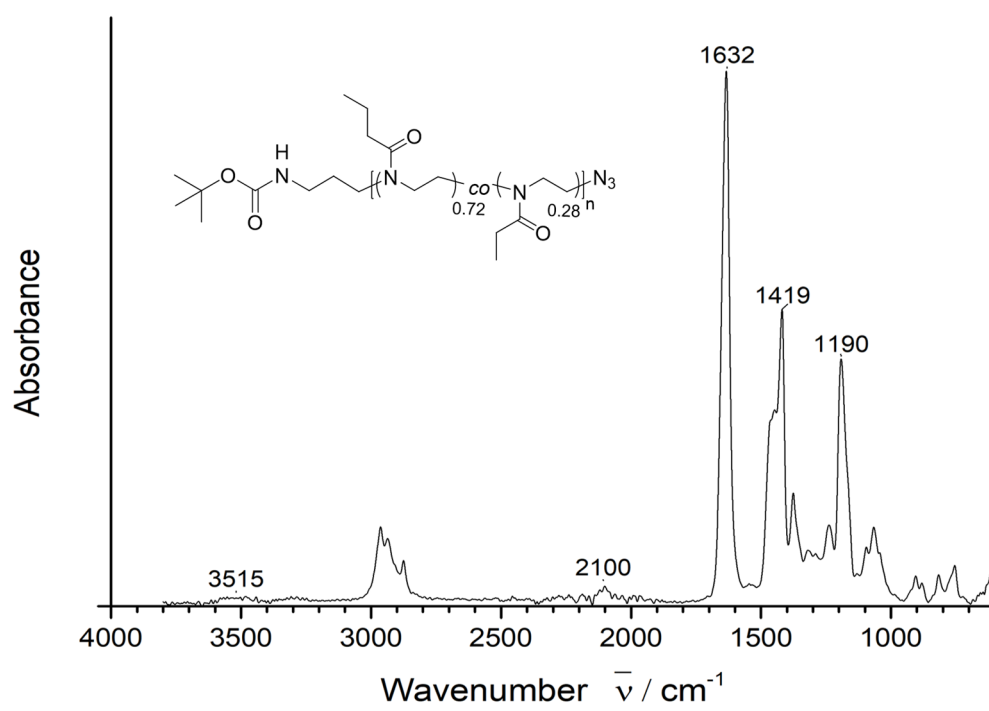


Figure S62: IR spectrum of P1.13 A

7.2.1 Spectra of Postfunctionalized Poly(2-Oxazoline)s

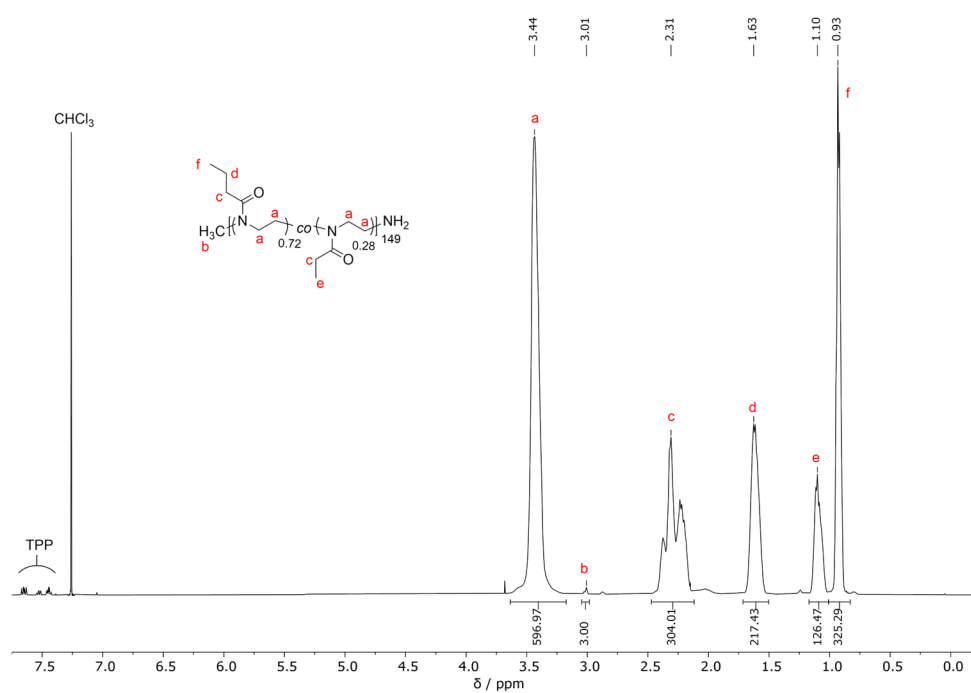


Figure S63: ^1H NMR (500 MHz) spectrum of P1.5.1 (4) recorded in CDCl_3 .

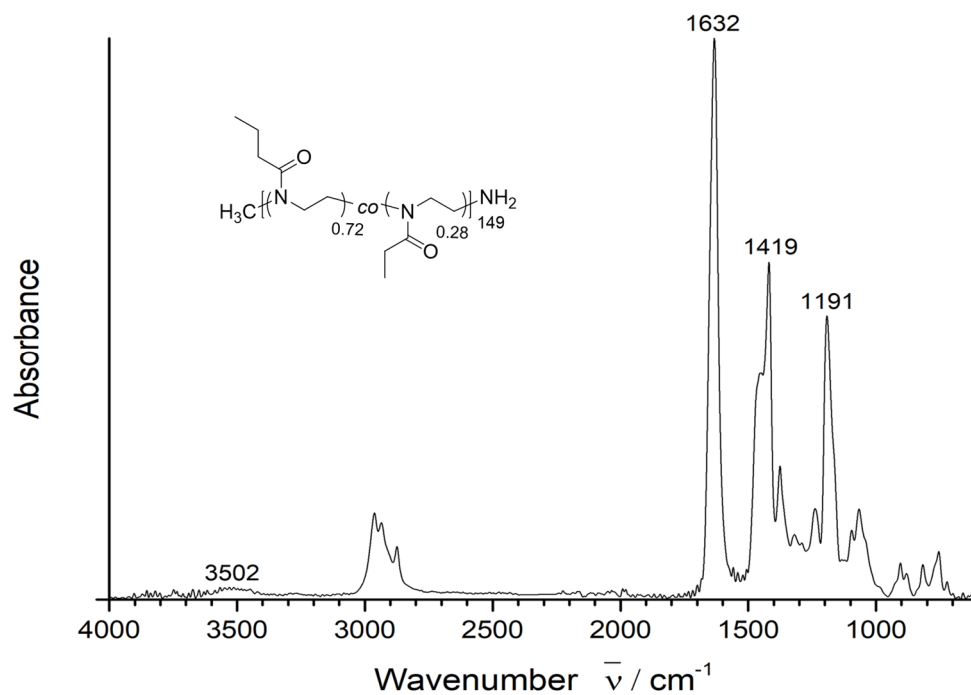


Figure S64: IR spectrum of P1.5.1 (4)

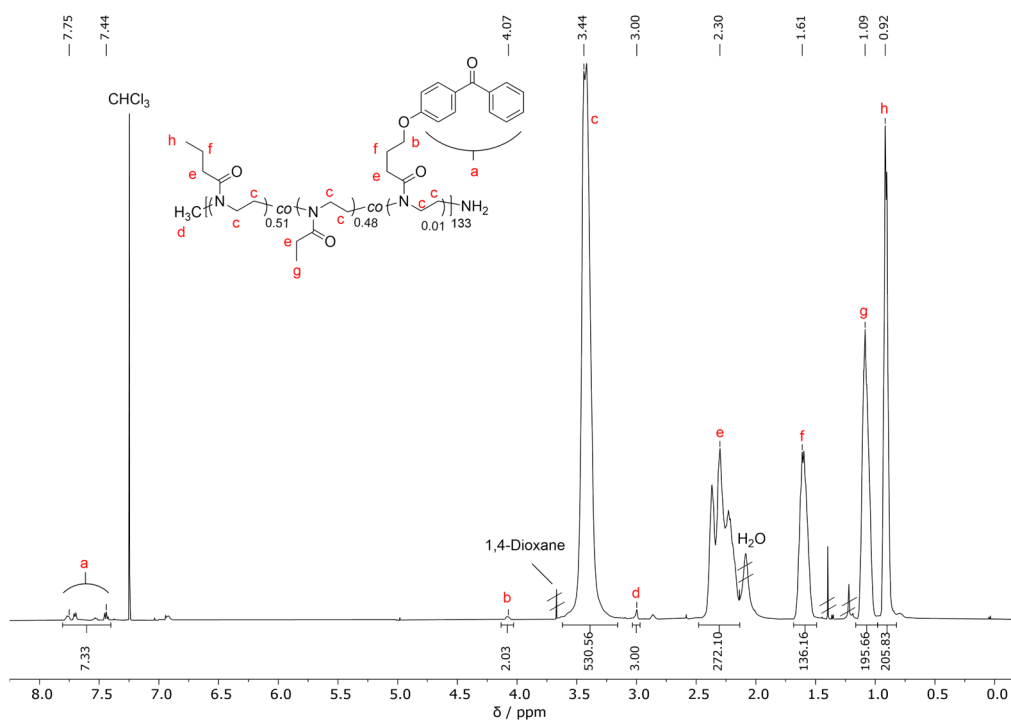


Figure S65: ^1H NMR (500 MHz) spectrum of **P1.6.1** recorded in CDCl_3 .

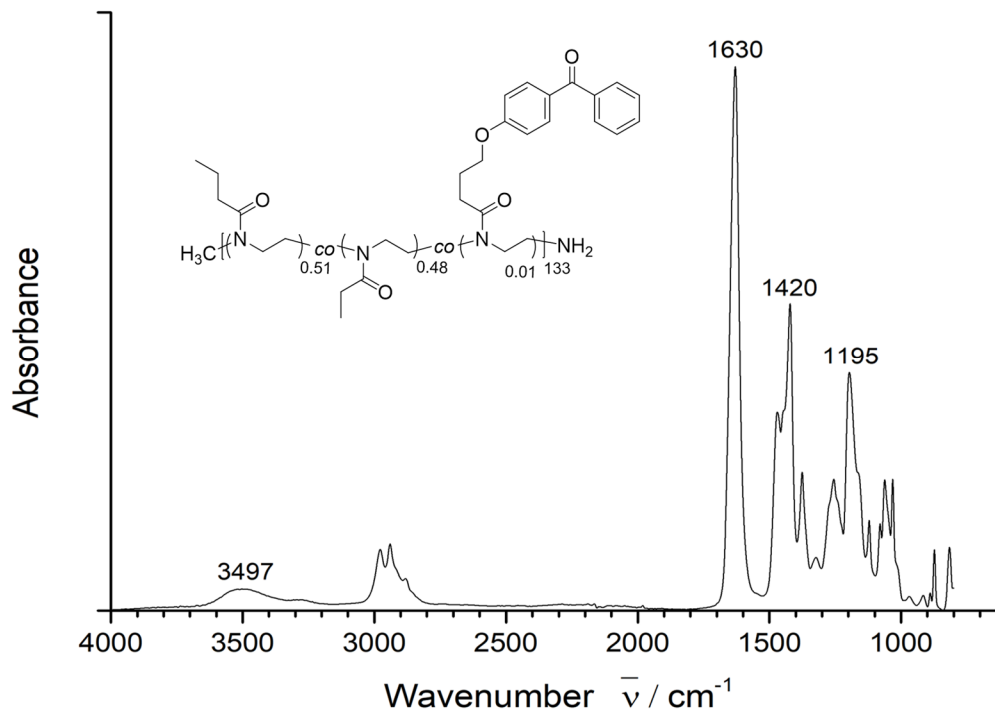


Figure S66: IR spectrum of **P1.6.1**

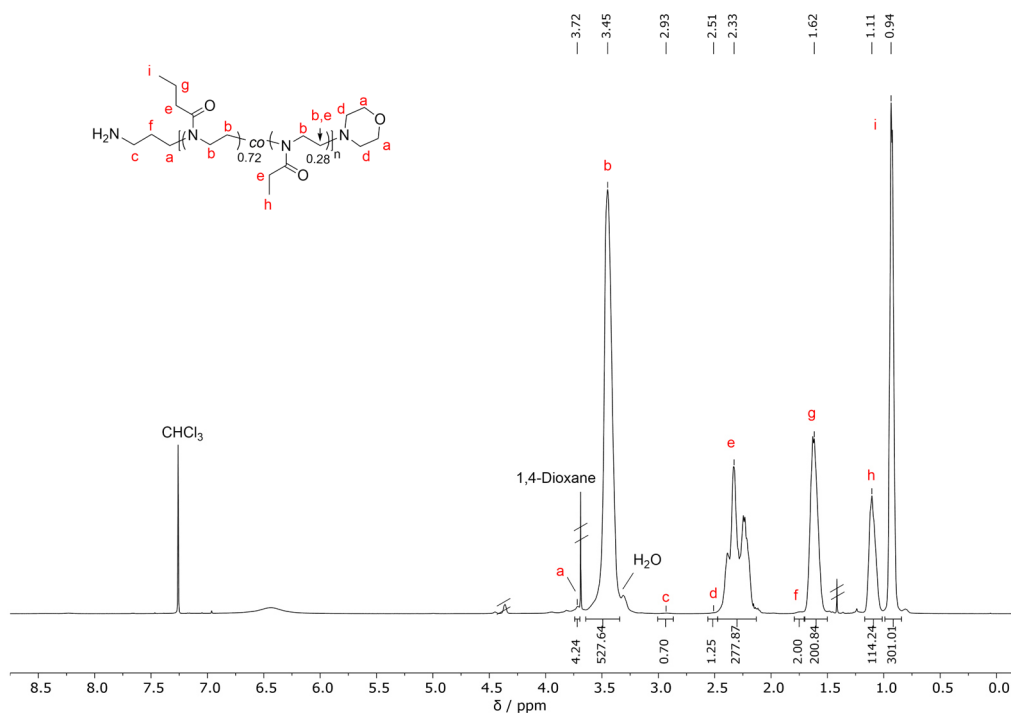


Figure S67: ^1H NMR (500 MHz) spectrum of **P1.12.1 (1)** recorded in CDCl_3 .

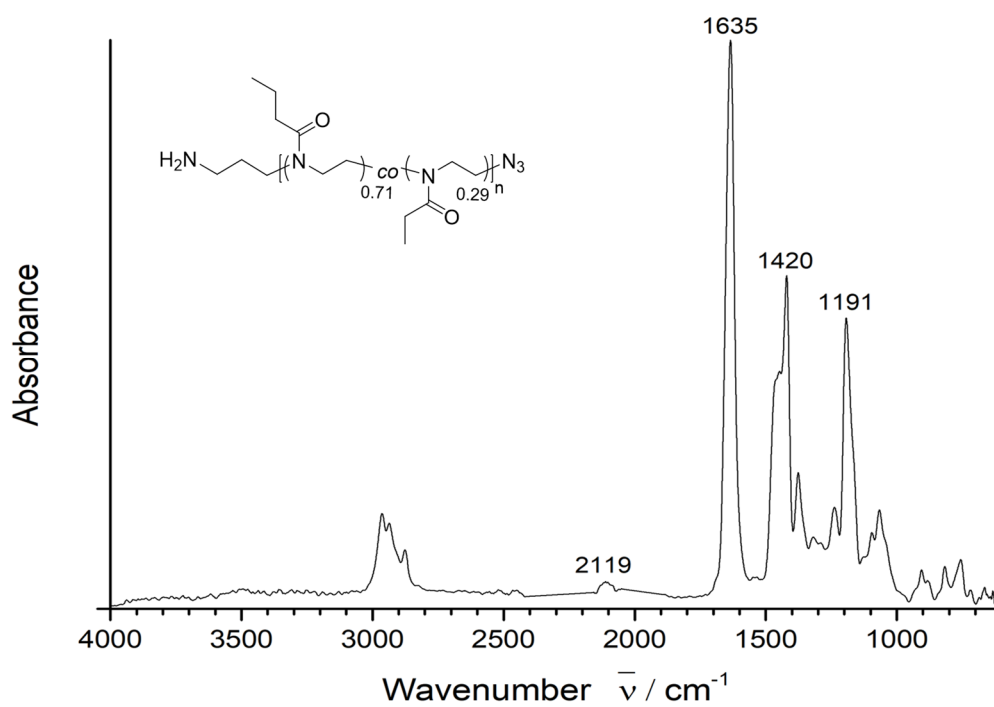


Figure S68: IR spectrum of **P1.13.1 A**

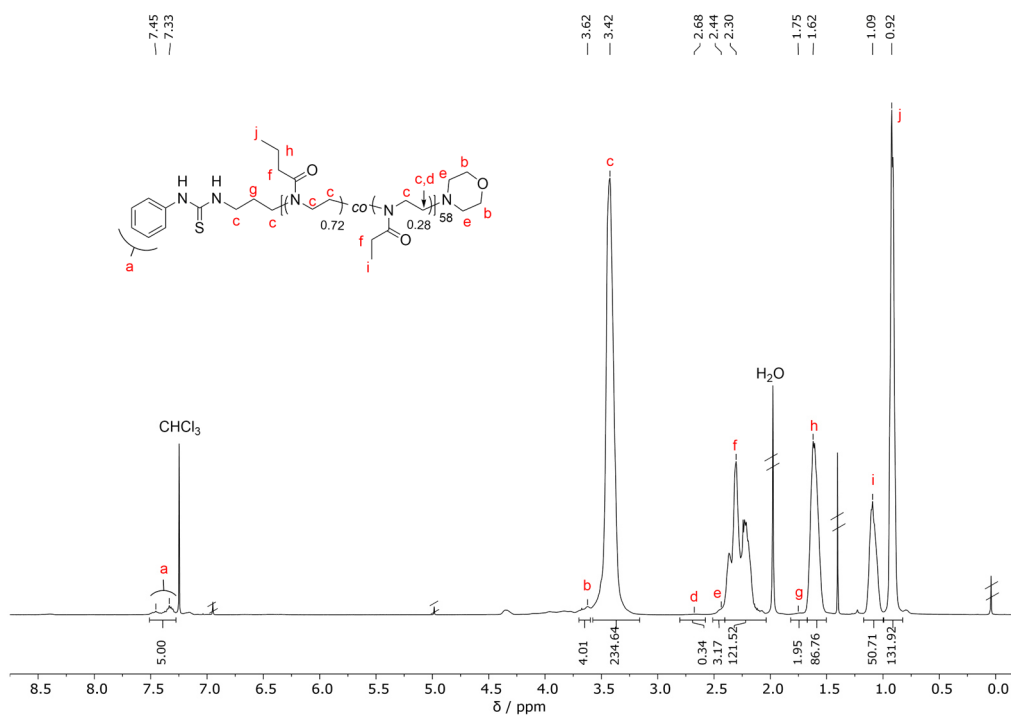


Figure S69: ¹H NMR (500 MHz) spectrum of P1.12.2 (1) recorded in CDCl₃.

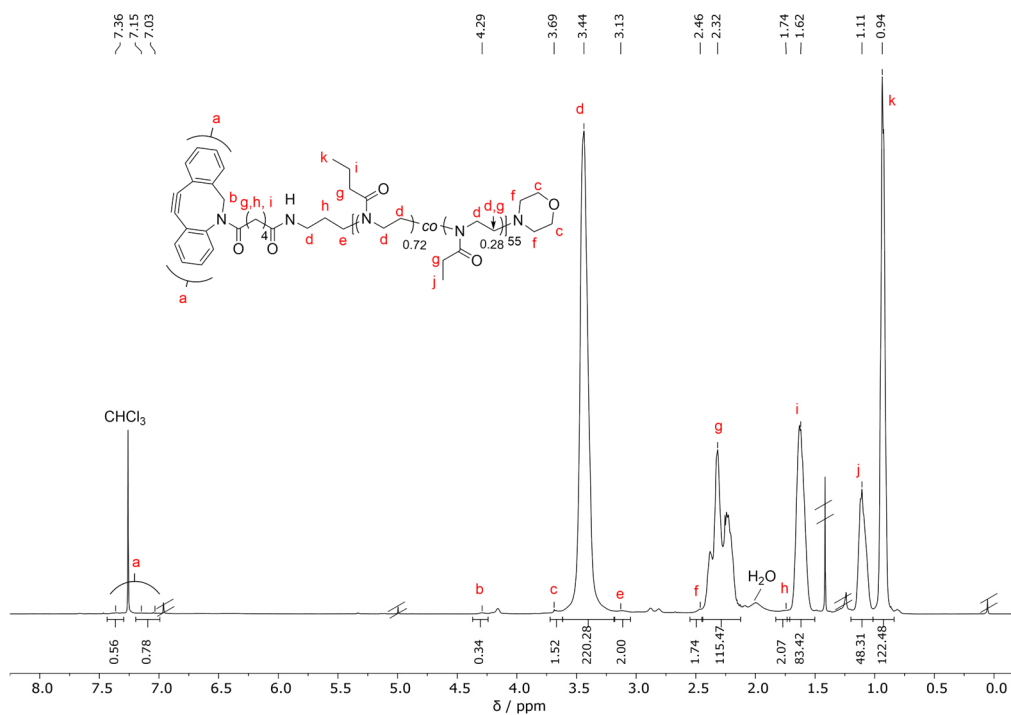
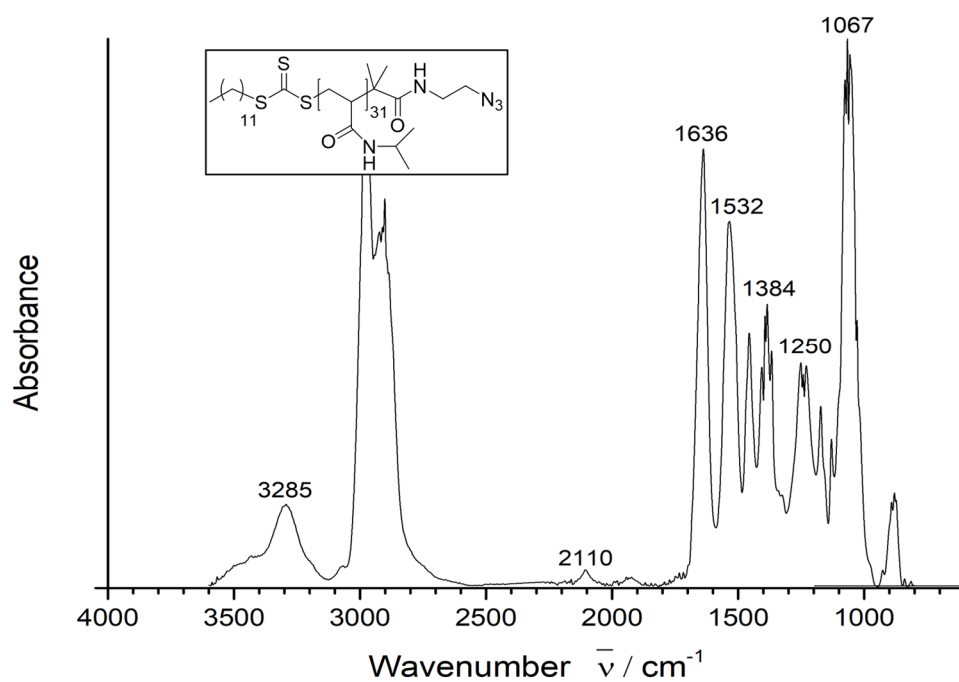
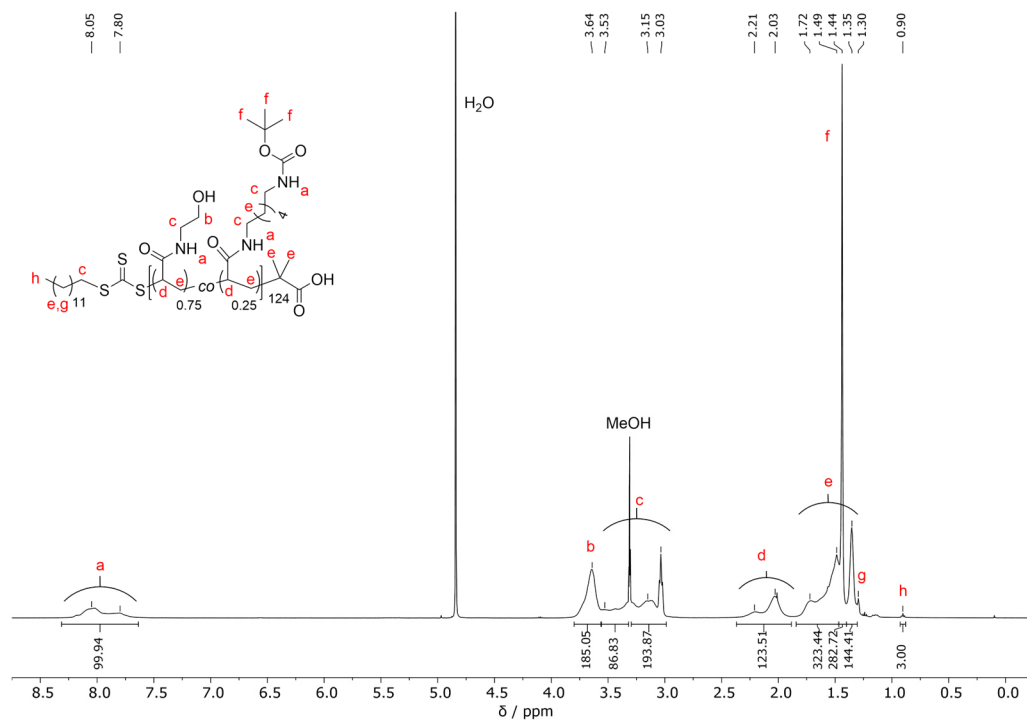


Figure S70: ¹H NMR (500 MHz) spectrum of P1.12.3 (2) recorded in CDCl₃.

7.3 Poly(Acrylamide) Spectra

Figure S71: IR spectrum of **P2.1 A**Figure S72: ^1H NMR (500 MHz) spectrum of **P2.4** recorded in CD_3OD . (Spectrum kindly provided by Fiona Diehl.)

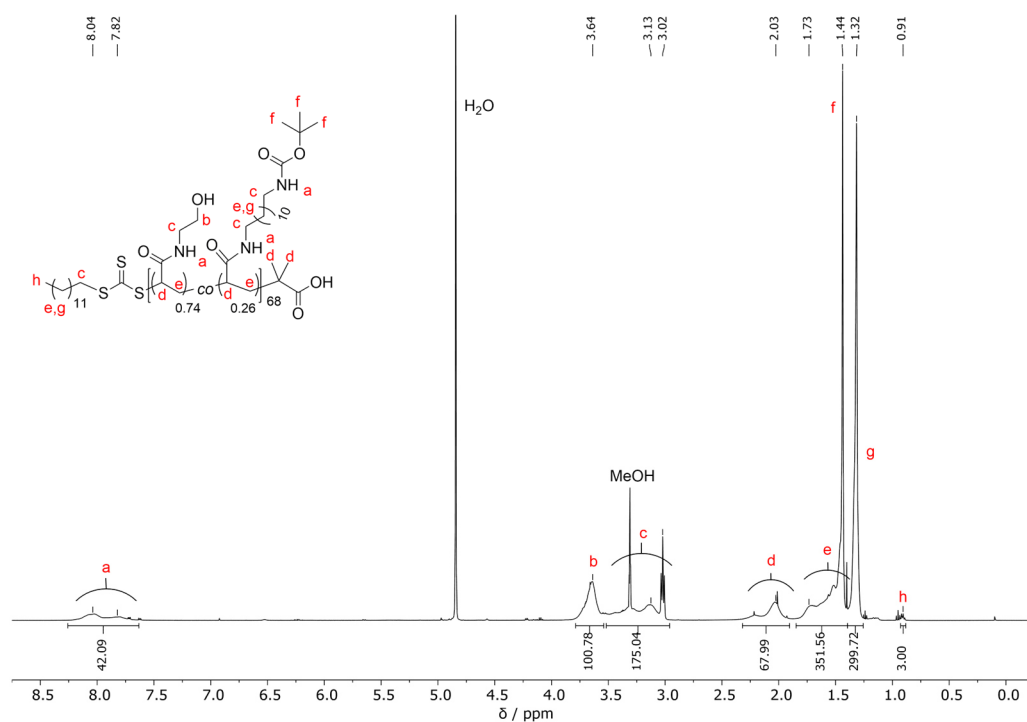


Figure S73: ¹H NMR (500 MHz) spectrum of **P2.5** recorded in CD₃OD. (Spectrum kindly provided by Fiona Diehl.)

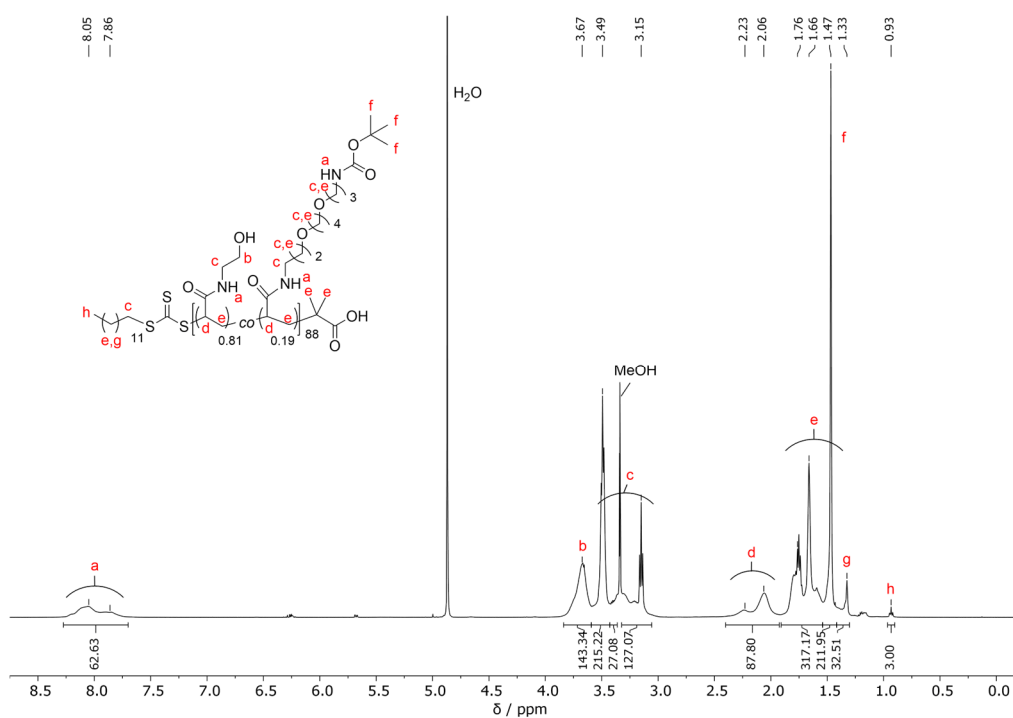


Figure S74: ¹H NMR (500 MHz) spectrum of **P2.6** recorded in CD₃OD. (Spectrum kindly provided by Fiona Diehl.)

7.3.1 Spectra of Post functionalized Poly(Acrylamide)s

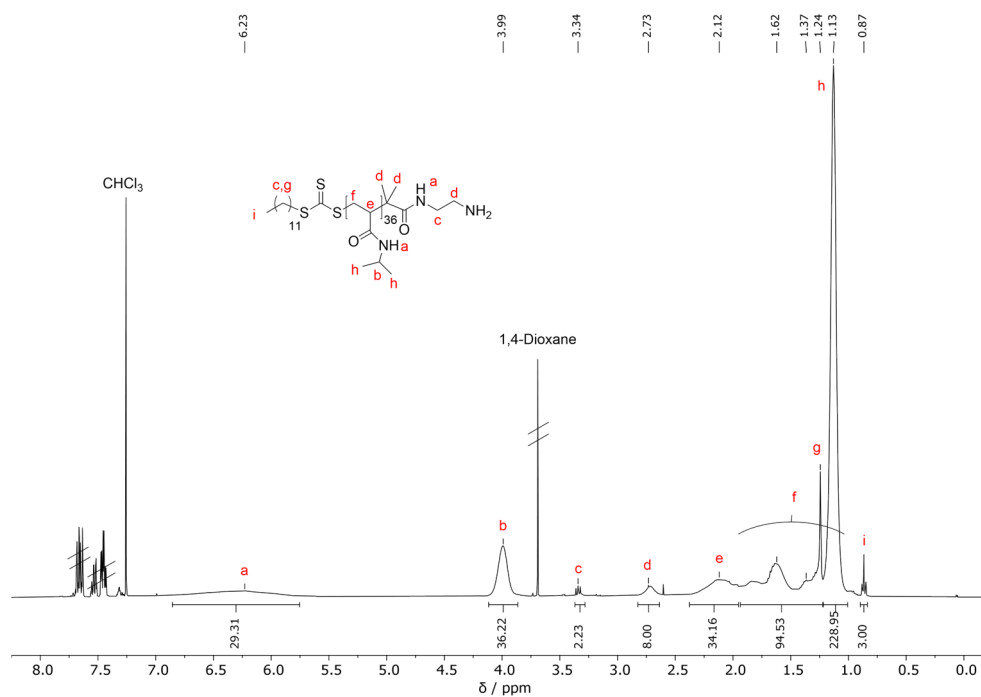


Figure S75: ¹H NMR (400 MHz) spectrum of P2.1.1 A recorded in CDCl₃.

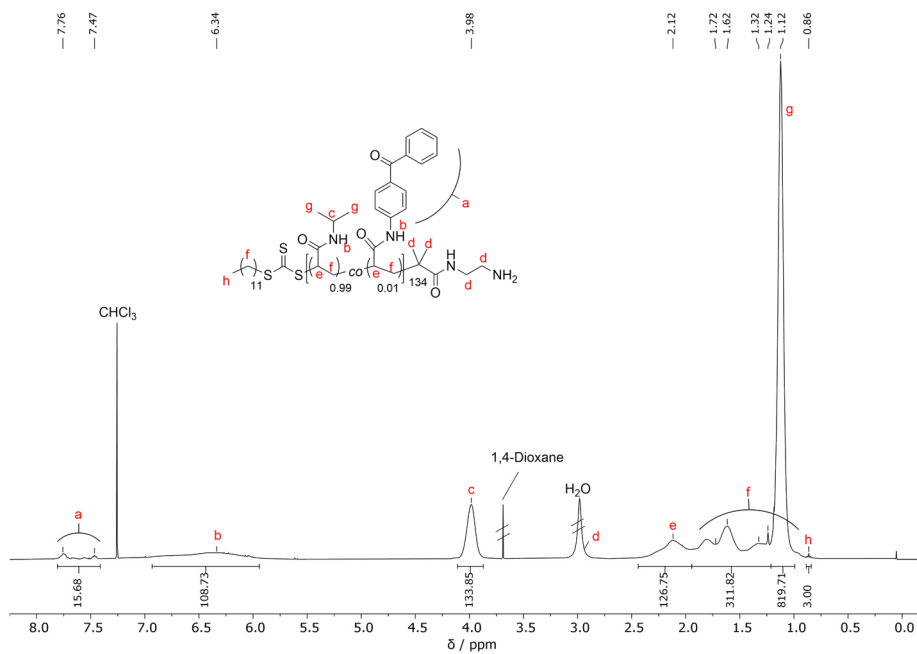


Figure S76: ¹H NMR (400 MHz) spectrum of P2.2.1 A recorded in CDCl₃.

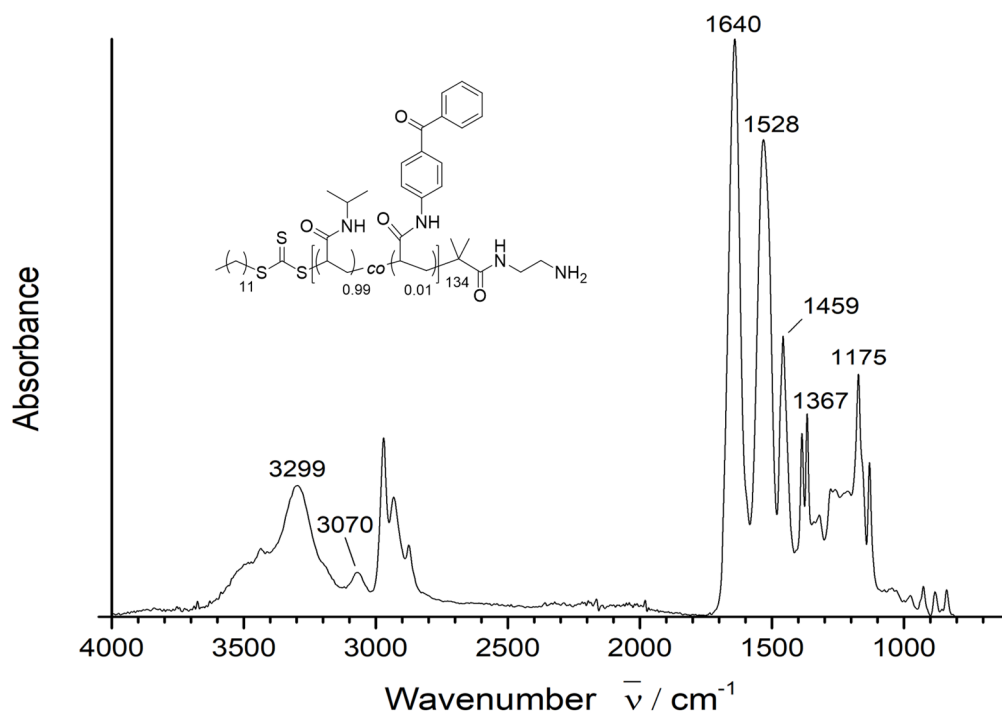


Figure S77: IR spectrum of P2.2.1 A

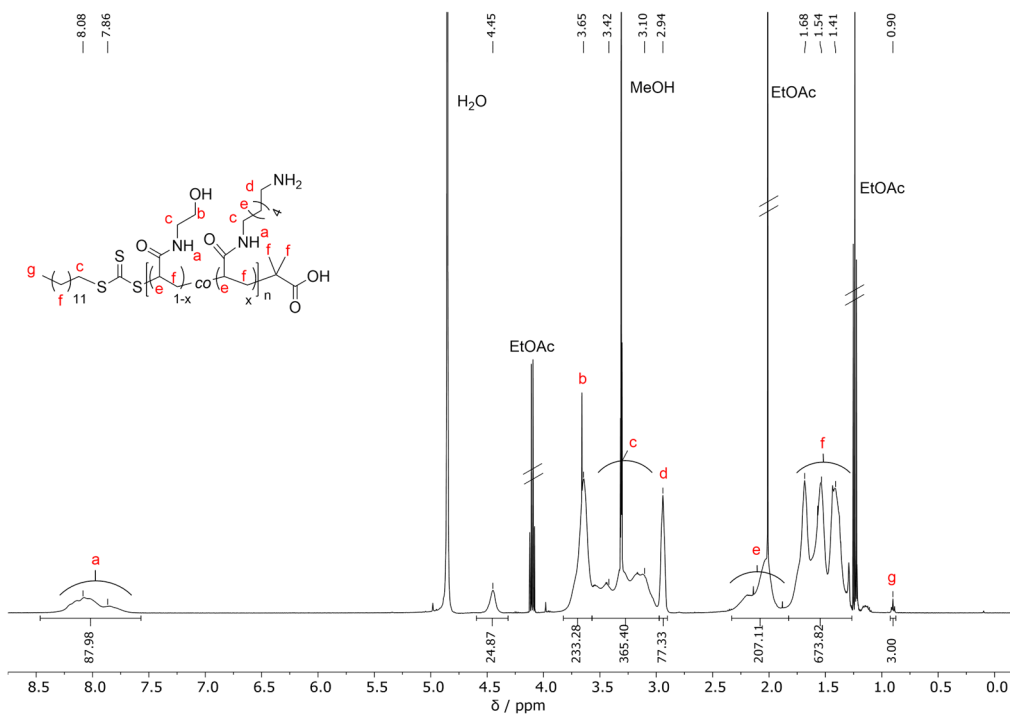


Figure S78: ^1H NMR (500 MHz) spectrum of P2.4.1 recorded in CD_3OD . (Kindly provided by Fiona Diehl.)

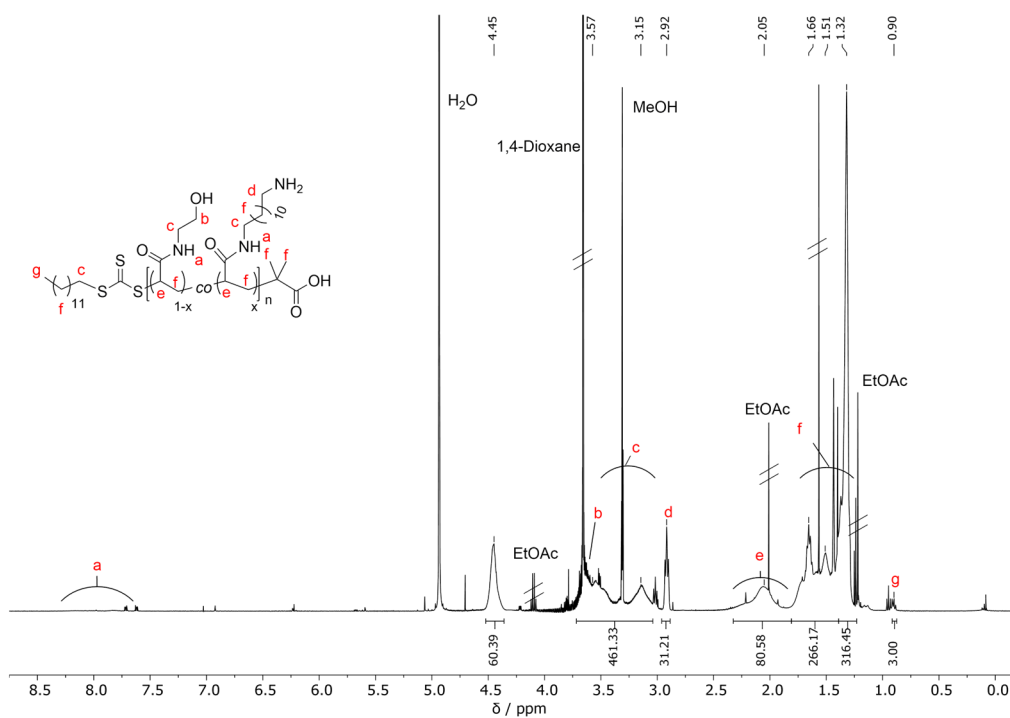


Figure S79: ¹H NMR (500 MHz) spectrum of **P2.5.1** recorded in CD₃OD. (Kindly provided by Fiona Diehl.)

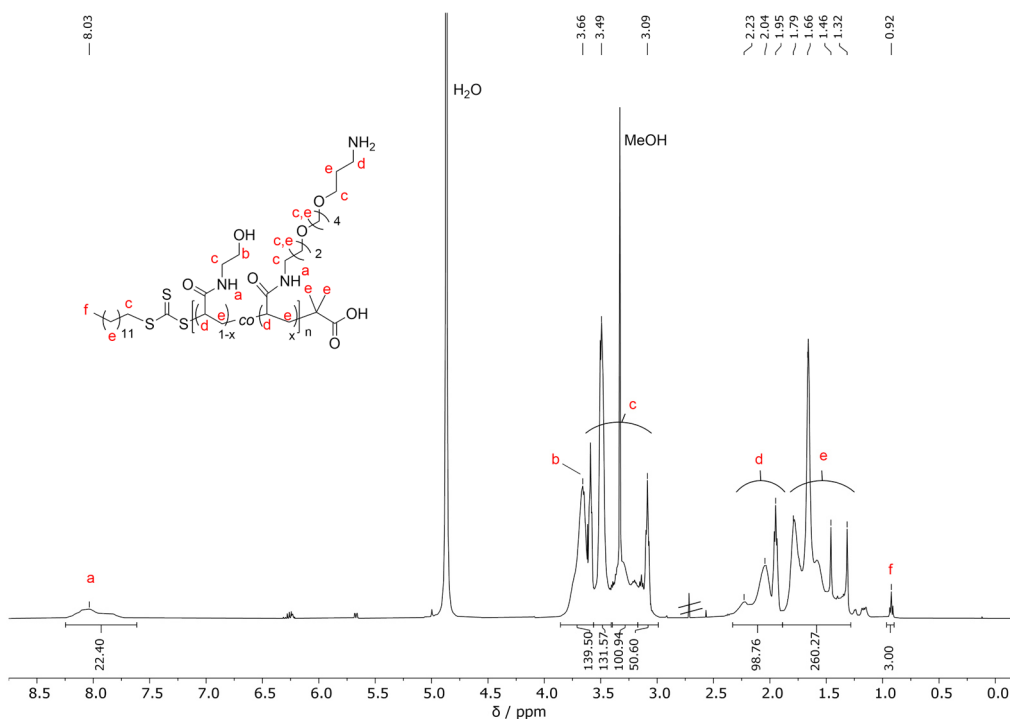


Figure S80: ¹H NMR (500 MHz) spectrum of **P2.6.1** recorded in CD₃OD. (Kindly provided by Fiona Diehl.)

7.4 Additional UV/Vis Spectra

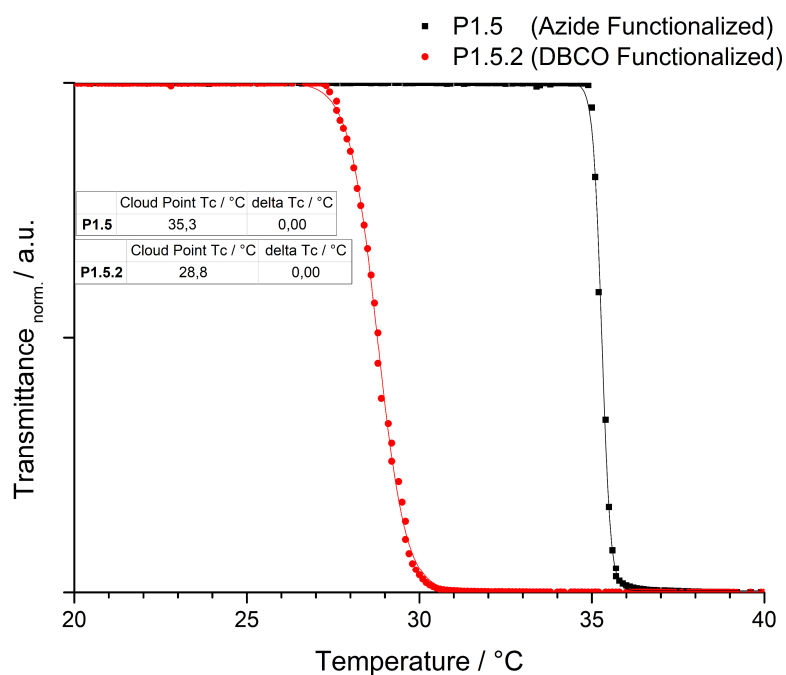


Figure S81: Turbidity measurement in order to determine the Cloud Point of an 0.5 wt% aqueous solution of **P1.5** (black curve) and **P1.5.2** (red curve), respectively.

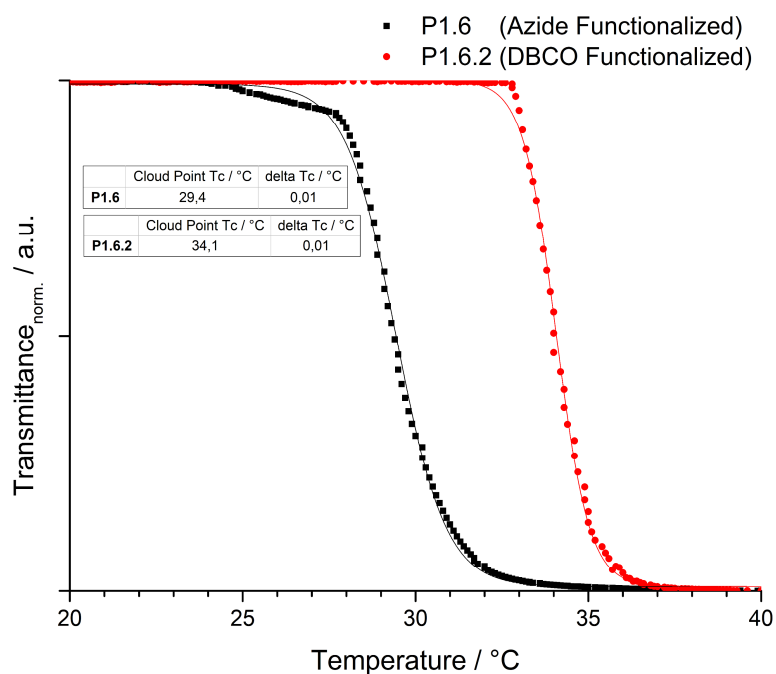


Figure S82: Turbidity measurement in order to determine the Cloud Point of an 0.5 wt% aqueous solution of **P1.6** (black curve) and **P1.6.2** (red curve), respectively.

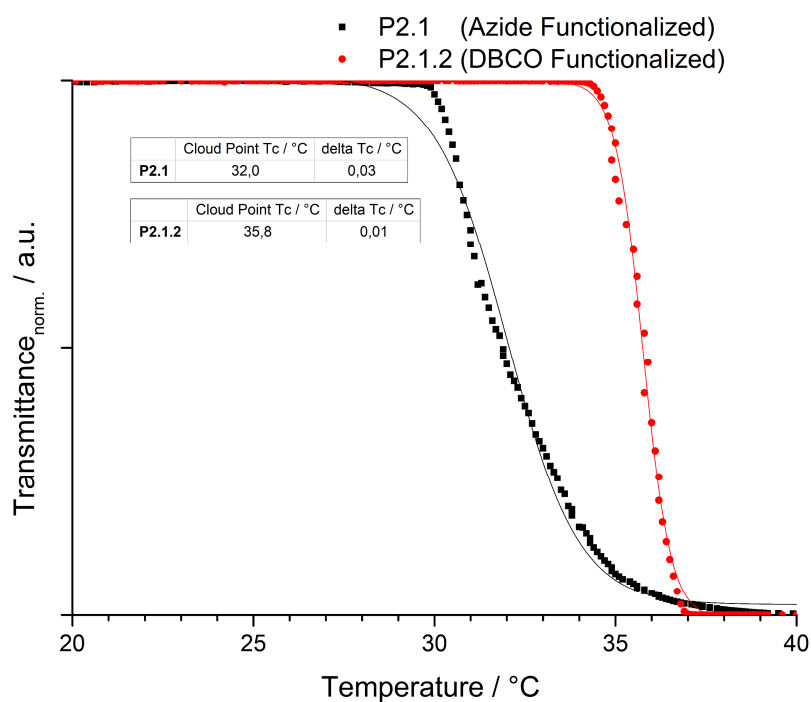


Figure S83: Turbidity measurement in order to determine the Cloud Point of an 0.5 wt% aqueous solution of **P2.1** (black curve) and **P2.1.2** (red curve), respectively.

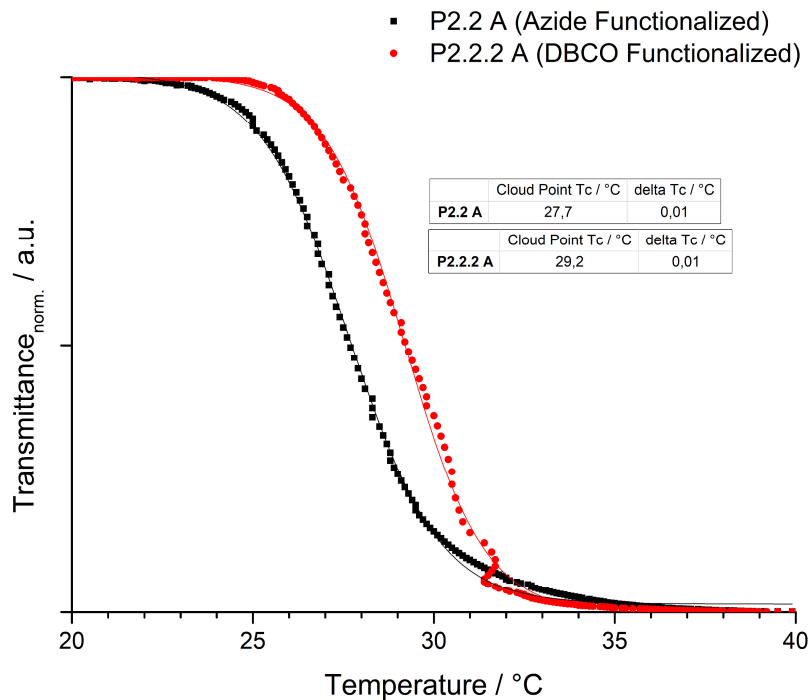


Figure S84: Turbidity measurement in order to determine the Cloud Point of an 0.5 wt% aqueous solution of **P2.2** (black curve) and **P2.2.2** (red curve), respectively.

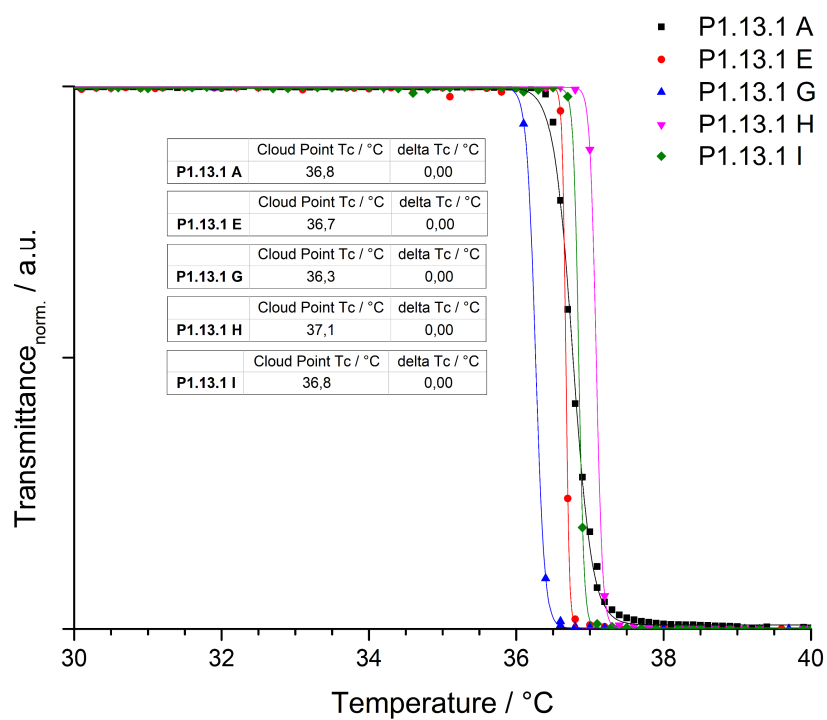


Figure S85: Turbidity measurement in order to determine the Cloud Point of an 0.5 wt% aqueous solution of **P1.13.1 A** (black curve), **P1.13.1 E** (red curve), **P1.13.1 G** (blue curve), **P1.13.1 H** (pink curve) and **P1.13.1 I** (green curve), respectively.

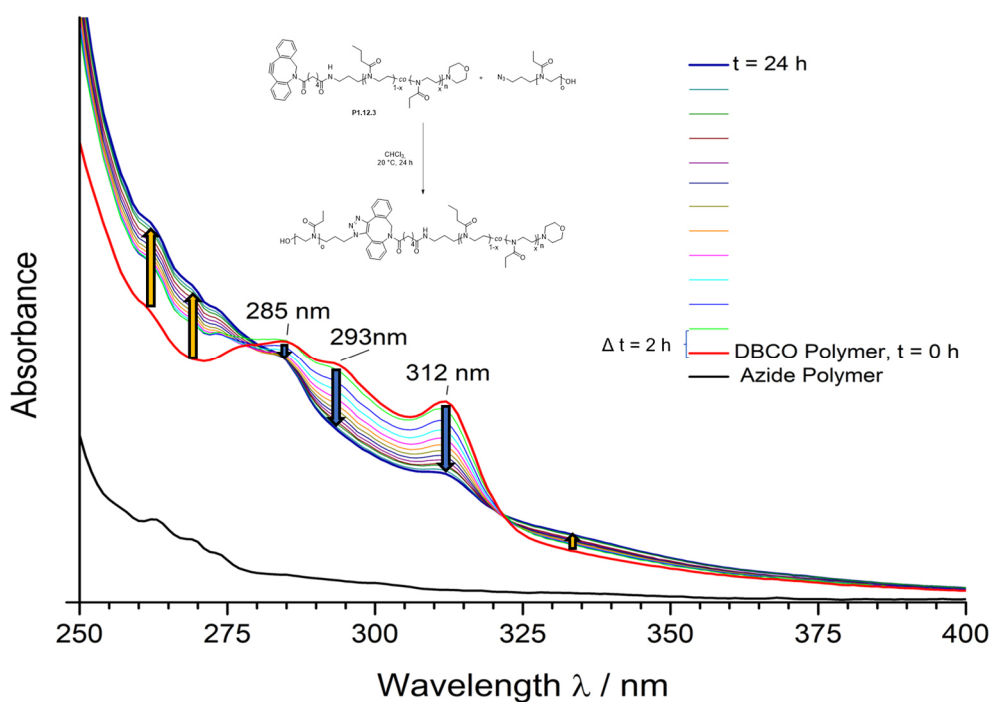


Figure S86: UV/Vis Scans of the coupling reaction between **P1.12.3** and an azide-monomer in CHCl_3 at $T = 20^\circ\text{C}$. The arrows indicate the change in absorbance over time.

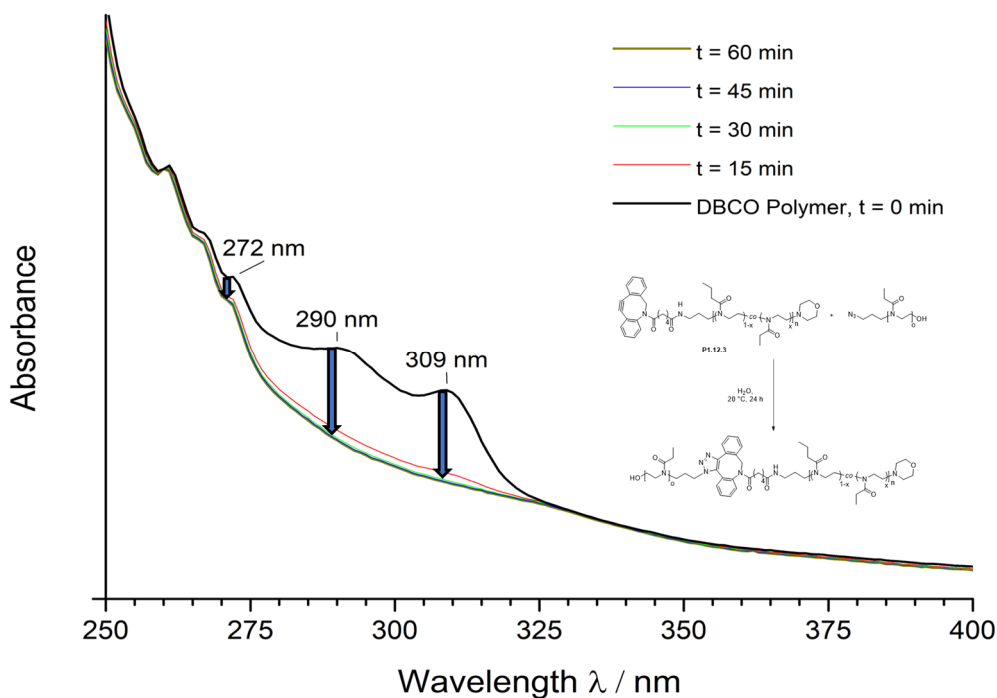


Figure S87: UV/Vis Scans of the coupling reaction between **P1.12.3** and an azide-monomer in H_2O at $T = 20^\circ\text{C}$. The arrows indicate the change in absorbance over time.

7.5 Additional Data Gel Electrophoresis Experiments

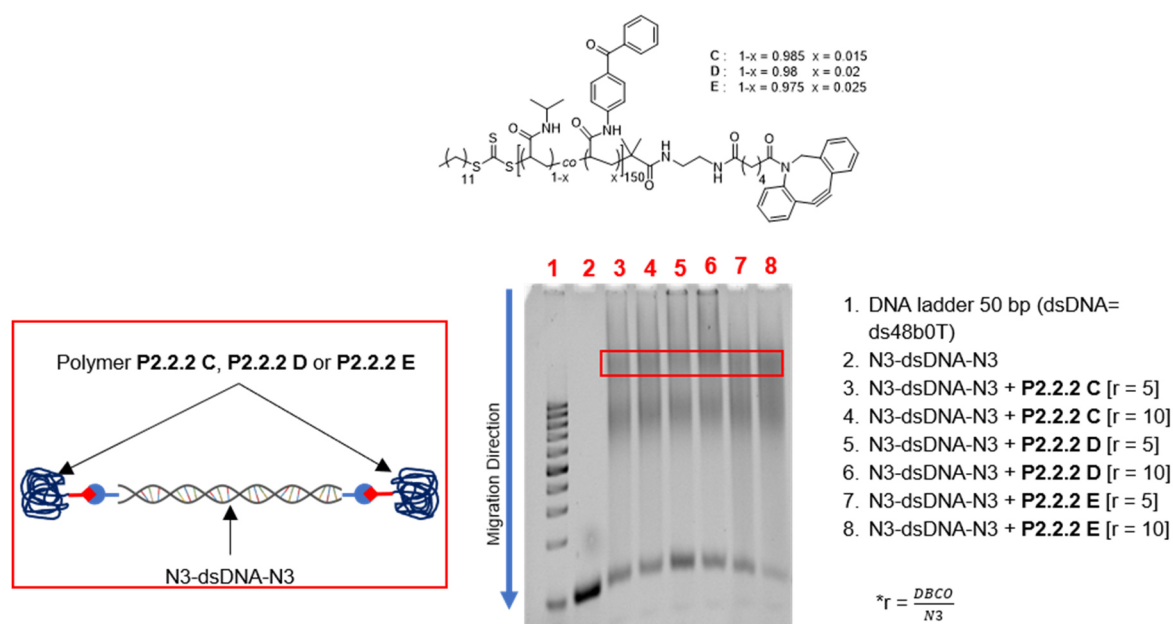


Figure S88: PAGE (5%) electrophoresis pattern of **P2.2.2 B-D** after coupling of N3-dsDNA-N3 in different ratios.

7.6 Additional Data of the SPFS Measurements

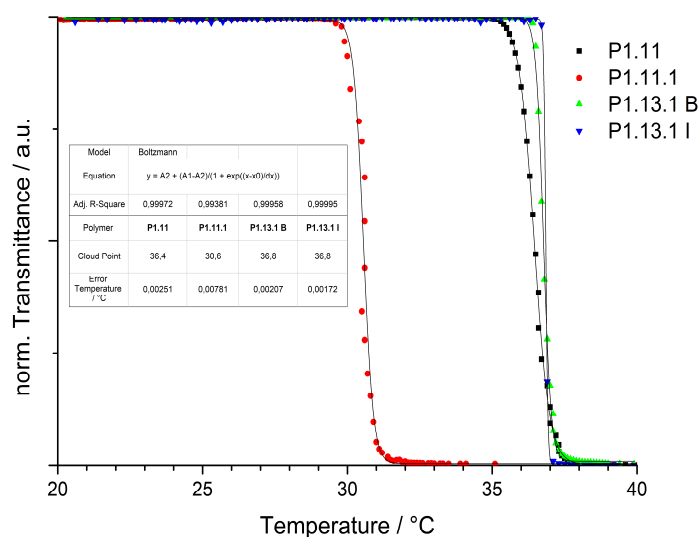


Figure S89: Overview of the turbidity measurements of **P1.11**, **P1.11.1**, **P13.1 B** and **P1.13.1 I** performed using UV-Vis spectroscopy at $\lambda = 600$ nm. T_c was defined as the temperature at the inflection point of the regression curve of the normalized data points obtained for the corresponding copolymer.

7.7 Additional Data of Transfection Experiments

Additional DNA complexation assays performed at different temperatures:

$T = 4\text{ }^{\circ}\text{C}$		HEPES	EtBr	DNA	P2.3.1*	P2.4.1*	P2.5.1*	P2.6.1*	P2.3.1	P2.4.1	P2.5.1	P2.6.1	bPEI
MR = 1.0		0	0	100	103	91	91	103	106	109	115	124	9
MR = 5.0		0	0	106	69	57	27	85	66	39	33	103	15
MR = 10		-3	3	106	45	54	27	69	60	39	24	94	15
MR = 100		-3	3	103	42	48	21	82	54	36	27	88	6

$T = 45\text{ }^{\circ}\text{C}$		HEPES	EtBr	DNA	P2.3.1*	P2.4.1*	P2.5.1*	P2.6.1*	P2.3.1	P2.4.1	P2.5.1	P2.6.1	bPEI
MR = 0.1		-11	0	101	117	107	80	107	117	96	96	80	59
MR = 1.0		-11	0	101	117	85	101	91	101	91	80	112	-5
MR = 10		0	0	96	32	21	-5	59	43	21	5	53	5
MR = 100		-11	0	85	43	21	11	32	21	16	5	37	0

% Fluo	100	90	80	70	60	50	40	30	20	10	0
--------	-----	----	----	----	----	----	----	----	----	----	---

Figure S90: Depiction of the relative fluorescence intensity measured at $T = 4\text{ }^{\circ}\text{C}$ (top) and $T = 45\text{ }^{\circ}\text{C}$ (bottom). The normalized values of the fluorescence compared to the fluorescence of DNA-EtBr complexes were calculated according to equation (5) on page 175. The fluorescence is colored according to the scale bar to guide the eye.

Calculation of N/P ratios:

The number of phosphate atoms n_P of the plasmid DNA, which corresponds directly, to the number of negative charges along the DNA strain, can be estimated by the following equation

$$n_P = \frac{m_{pDNA}}{(N_{BP} \cdot \bar{M}_{BP})} \cdot (2 \cdot N_{BP}) = \frac{2 \cdot m_{pDNA}}{\bar{M}_{BP}} = \frac{2 \cdot (1 \cdot 10^{-6}) \text{ g}}{660 \text{ g} \cdot \text{mol}^{-1}} = 3.03 \cdot 10^{-9} \text{ mol} \quad (9)$$

where m_{pDNA} is the used mass of DNA per test, N_{BP} the number of base pairs, \bar{M}_{BP} the averaged molar mass of a base pair ($M = 660 \text{ g} \cdot \text{mol}^{-1}$), which was found by averaging the calculated molar mass of a cytosine-guanidine and a adenosine-thymine base pair.

Further, the number of amino groups along the tested polymers can be estimated by using the following equation

$$n_{N, Polymer} = \frac{m_{Polymer}}{M_{Polymer}} \cdot \bar{X}_{n, Polymer} \cdot p_{Monomer} = \frac{(1 \cdot 10^{-6}) \text{ g}}{(2.5 \cdot 10^4) \text{ g} \cdot \text{mol}^{-1}} \cdot \bar{X}_{n, Polymer} \cdot p_{Monomer} \quad (10)$$

where $m_{Polymer}$ is the used mass of polymer per test at MR = 1, $M_{Polymer}$ the theoretical molar mass of the polymers ($M = 2.5 \cdot 10^4 \text{ g} \cdot \text{mol}^{-1}$), $\bar{X}_{n, Polymer}$ the theoretical degree of polymerization

and $p_{Monomer}$ the built-in of the amine-containing monomer, which was determined by $^1\text{H NMR}$.

Finally, the N/P ratio can be calculated, considering the mass ratio $MR = \frac{m_{Polymer}}{m_{pDNA}}$, by using the equation

$$N/P = \frac{n_{N,Polymer}}{n_P} \cdot MR \quad (11)$$

The calculated N/P ratios of the used polymers are listed in Figure S91 (below). The built-in of the corresponding monomer and \bar{X}_n of the used polymers can be found in Table 5.13. The \bar{X}_n of PEI was estimated by using a molar mass of $M = 43 \text{ g}\cdot\text{mol}^{-1}$ for an ethyleneimine repeat unit yielding a $\bar{X}_n = 581$.

Table S7.2: List of the calculated N/P ratios according to the used mass ratio and corresponding polymer

Mass ratio MR	N/P Ratios				
	P2.3.1* / P2.3.1	P2.4.1* / P2.4.1	P2.5.1* / P2.5.1	P2.6.1* / P2.6.1	bPEI
0.1	0.06	0.05	0.05	0.03	0.77
1	0.58	0.51	0.46	0.34	7.67
1.27	0.74	0.65	0.58	0.43	9.74
2	1.17	1.03	0.91	0.67	15.34
4	2.33	2.06	1.83	1.34	30.68
5	2.92	2.57	2.28	1.68	38.35
8	4.67	4.12	3.65	2.69	61.35
10	5.83	5.15	4.56	3.36	76.69
16	9.34	8.24	7.30	5.38	122.71
32	18.67	16.47	14.61	10.75	245.41
64	37.34	32.95	29.21	21.51	490.83
100	58.34	51.48	45.65	33.61	766.92
128	74.68	65.89	58.43	43.02	981.66

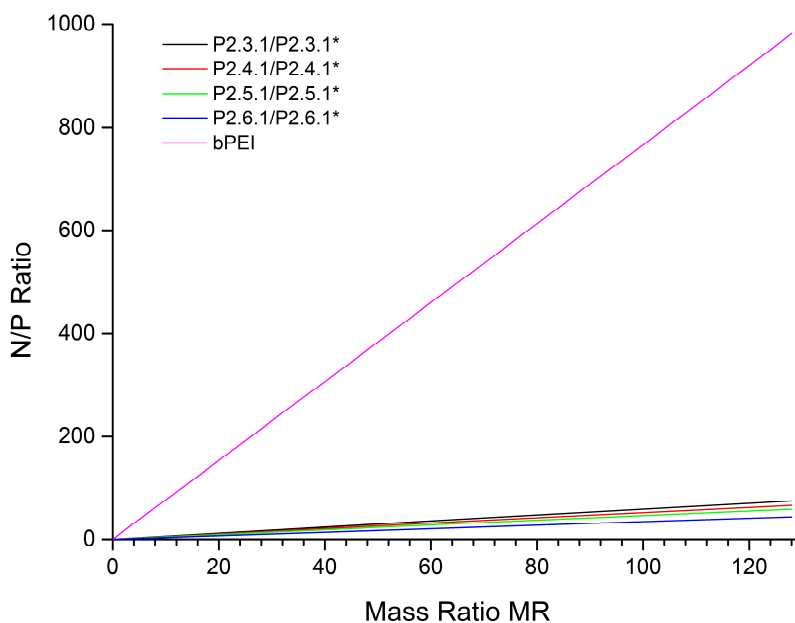


Figure S91: Diagram calculated N/P ratio versus MR of the tested polymers **P2.3.1*-P2.6.1*** and **P2.3.1-P2.6.1** as well as the reference bPEI (magenta curve).

Microscope Images of the other tested cell lines:

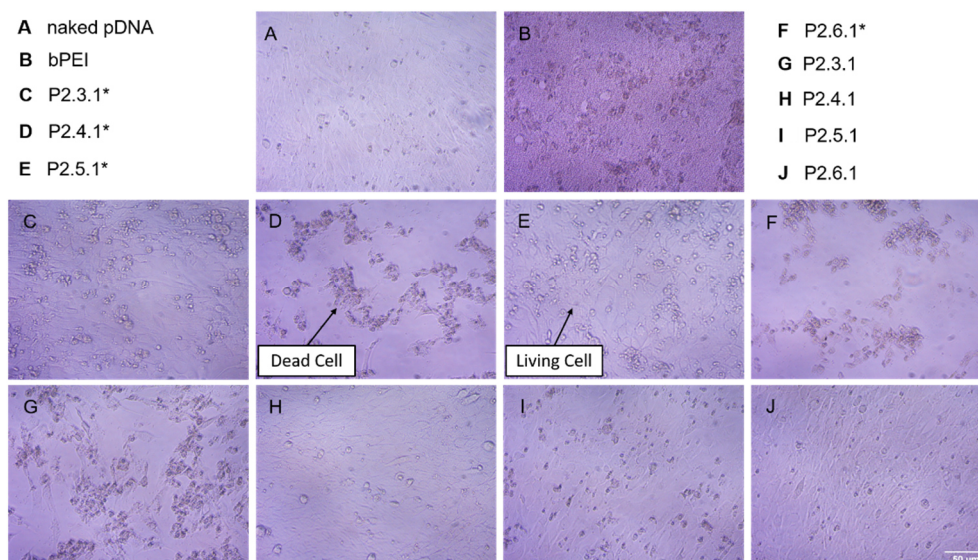


Figure S92: Microscope images of C2C12 cells treated with polyplexes of the tested polymers (MR = 64). In the top row cells are depicted which are employed with pDNA (A) and bPEI-DNA complexes (B). The middle row illustrates the viability of the cells treated with **P2.3.1*-P2.6.1*** polyplexes (C-F) and the bottom row represent the behavior of the cells treated with **P2.3.1-P2.6.1** polyplexes (G-J).

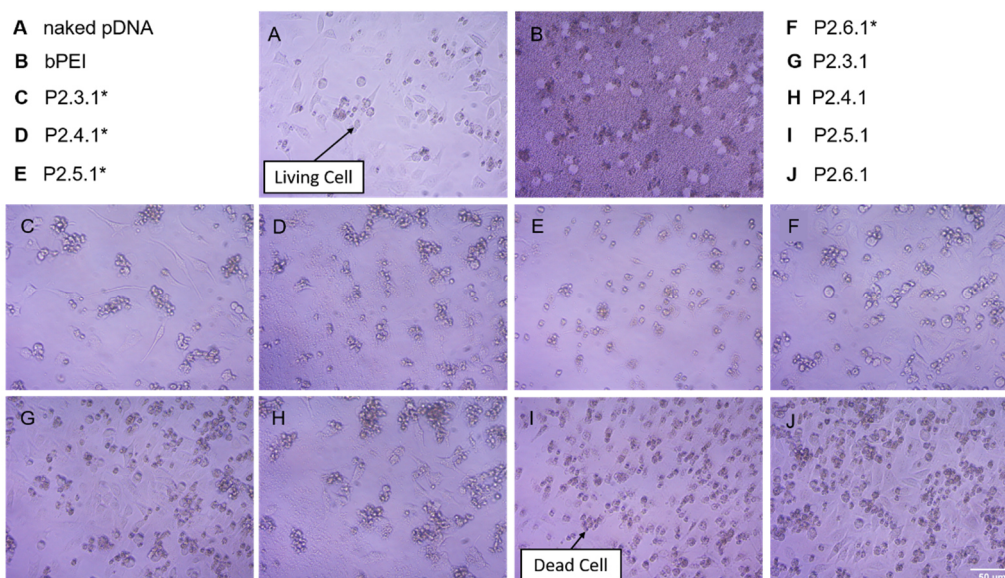


Figure S93: Microscope images of HeLa cells treated with polyplexes of the tested polymers (MR = 64). In the top row cells are depicted which are employed with pDNA (A) and bPEI-DNA complexes (B). The middle row illustrates the viability of the cells treated with **P2.3.1*-P2.6.1*** polyplexes (C-F) and the bottom row represent the behavior of the cells treated with **P2.3.1-P2.6.1** polyplexes (G-J).

Transfection efficiencies and cell viability results of the other used cell lines:

A	HEPES (20mM)	DNA	P2.3.1*	P2.4.1*	P2.5.1*	P2.6.1*	P2.3.1	P2.4.1	P2.5.1	P2.6.1	bPEI	HEPES (20mM)
	1.E+3	1.E+3	2.E+3	2.E+3	2.E+3	2.E+3	3.E+3	3.E+3	2.E+3	3.E+3	1.E+6	6.E+2
	2.E+3	1.E+3	5.E+3	2.E+3	3.E+3	1.E+3	5.E+3	4.E+4	9.E+2	2.E+3	8.E+6	2.E+3
	3.E+3	3.E+2	4.E+3	3.E+4	4.E+3	2.E+3	5.E+3	3.E+3	5.E+3	1.E+3	3.E+6	9.E+2
	2.E+2	1.E+3	7.E+3	3.E+4	3.E+4	1.E+3	4.E+3	2.E+3	7.E+4	3.E+3	3.E+6	9.E+2
	2.E+3	2.E+3	2.E+4	1.E+5	2.E+5	3.E+3	1.E+4	3.E+4	3.E+5	2.E+3	2.E+5	8.E+2
	1.E+3	2.E+3	4.E+4	5.E+4	1.E+5	1.E+4	2.E+5	2.E+4	1.E+5	1.E+3	2.E+3	1.E+2
	1.E+3	2.E+3	8.E+4	2.E+3	4.E+3	2.E+2	8.E+4	3.E+3	3.E+3	1.E+3	1.E+2	1.E+3
	1.E+3	2.E+2	3.E+5	2.E+3	2.E+3	1.E+3	2.E+3	2.E+3	2.E+3	2.E+2	5.E+2	9.E+2

Values given in RLU / mg

B	HEPES (20mM)	DNA	P2.3.1*	P2.4.1*	P2.5.1*	P2.6.1*	P2.3.1	P2.4.1	P2.5.1	P2.6.1	bPEI	HEPES (20mM)
	130	99	123	127	113	63	115	151	128	153	92	53
	160	67	69	103	128	144	73	129	113	126	37	120
	151	128	63	80	105	63	47	92	49	130	88	143
	54	112	47	59	26	121	47	61	97	104	71	128
	88	49	42	67	63	88	45	48	114	105	4	151
	114	126	44	147	125	71	39	99	106	82	0	145
	139	109	87	7	0	77	99	20	0	74	0	125
	85	109	16	0	0	116	11	0	0	107	0	132

Values given in %

Figure S94: Overview of the measured transfection efficiency (A) and the corresponding cell viability of C2C12 cells (B) after 36 h incubation with the polyplexes and lysis of the cells.

7 Appendix

A

	HEPES (20mM)	DNA	P2.3.1*	P2.4.1*	P2.5.1*	P2.6.1*	P2.3.1	P2.4.1	P2.5.1	P2.6.1	bPEI	HEPES (20mM)
MR = 1.27	6.E+2	2.E+3	1.E+4	2.E+3	6.E+2	2.E+3	7.E+2	2.E+3	2.E+3	2.E+3	9.E+7	4.E+3
MR = 2	2.E+3	1.E+3	2.E+6	3.E+4	3.E+3	8.E+2	2.E+5	3.E+3	2.E+3	3.E+4	5.E+7	6.E+2
MR = 4	2.E+3	2.E+3	4.E+5	1.E+5	3.E+3	2.E+3	5.E+5	2.E+5	6.E+3	2.E+4	6.E+7	4.E+3
MR = 8	2.E+3	2.E+3	2.E+5	4.E+5	1.E+5	9.E+4	1.E+6	2.E+5	1.E+5	2.E+6	5.E+7	2.E+3
MR = 16	3.E+3	2.E+3	3.E+5	1.E+5	1.E+4	1.E+5	2.E+5	1.E+5	2.E+4	2.E+4	3.E+7	2.E+3
MR = 32	2.E+3	1.E+4	6.E+6	1.E+5	6.E+3	5.E+5	4.E+5	7.E+5	7.E+3	4.E+4	7.E+5	2.E+3
MR = 64	2.E+3	2.E+3	2.E+5	2.E+5	6.E+3	7.E+4	1.E+6	6.E+4	5.E+3	7.E+4	1.E+3	1.E+3
MR = 128	3.E+3	2.E+3	5.E+5	1.E+3	3.E+3	3.E+4	4.E+5	5.E+6	3.E+3	2.E+4	8.E+2	1.E+3

Values given in RLU / mg

B

	HEPES (20mM)	DNA	P2.3.1*	P2.4.1*	P2.5.1*	P2.6.1*	P2.3.1	P2.4.1	P2.5.1	P2.6.1	bPEI	HEPES (20mM)
MR = 1.27	144	80	49	150	55	42	45	75	78	19	24	32
MR = 2	132	91	58	96	128	150	48	23	112	137	56	31
MR = 4	121	104	38	52	86	159	30	58	80	129	70	55
MR = 8	132	90	30	48	22	78	22	33	52	66	58	71
MR = 16	73	100	40	45	4	69	50	58	11	45	14	118
MR = 32	85	100	57	50	0	71	55	57	1	71	0	109
MR = 64	102	123	69	35	0	91	51	48	0	86	0	98
MR = 128	140	113	67	9	0	109	45	18	0	100	0	71

Values given in %

Figure S95: Overview of the measured transfection efficiency (A) and the corresponding cell viability of HeLa cells (B) after 36 h incubation with the polyplexes and lysis of the cells.

8 References

- (1) Guo, Z.-F.; Zhang, R.; Liang, F.-S. Facile Functionalization of FK506 for Biological Studies by the Thiol–Ene ‘Click’ Reaction. *RSC Adv.* **2014**, *4* (22), 11400–11403. <https://doi.org/10.1039/c3ra47867j>.
- (2) Pak, J. K.; Hesse, M. Synthesis of Penta- *N*-Protected Homocaldopentamine and Its Selective Acylation. *J. Org. Chem.* **1998**, *63* (23), 8200–8204. <https://doi.org/10.1021/jo980689e>.
- (3) Becerra-Cely, L.; Rueda-Espinosa, J.; Ojeda-Porras, A.; Gamba-Sánchez, D. Insights into the Pummerer Synthesis of Oxazolines. *Org. Biomol. Chem.* **2016**, *14* (36), 8474–8485. <https://doi.org/10.1039/C6OB01666A>.
- (4) Petri, C. Synthesis and Characterization of Novel Photocrosslinkable Poly(2-Oxazoline)-Based Hydrogel Systems for the Application as Biosensor Matrix. PhD Thesis, Universität Siegen, 2018.
- (5) Oleszko-Torbus, N.; Utrata-Wesołek, A.; Wałach, W.; Dworak, A. Solution Behavior of Thermoresponsive Random and Gradient Copolymers of 2-*n*-Propyl-2-Oxazoline. *Eur. Polym. J.* **2017**, *88*, 613–622. <https://doi.org/10.1016/j.eurpolymj.2016.11.008>.
- (6) Postma, A.; Davis, T. P.; Evans, R. A.; Li, G.; Moad, G.; O’Shea, M. S. Synthesis of Well-Defined Polystyrene with Primary Amine End Groups through the Use of Phthalimido-Functional RAFT Agents. *Macromolecules* **2006**, *39* (16), 5293–5306. <https://doi.org/10.1021/ma060245h>.
- (7) Zhang, H.; Chen, J.; Zhang, X.; Xiao, C.; Chen, X.; Tao, Y.; Wang, X. Multidentate Comb-Shaped Polypeptides Bearing Trithiocarbonate Functionality: Synthesis and Application for Water-Soluble Quantum Dots. *Biomacromolecules* **2017**, *18* (3), 924–930. <https://doi.org/10.1021/acs.biomac.6b01760>.
- (8) Li, B.; Yuan, Z.; Hung, H.-C.; Ma, J.; Jain, P.; Tsao, C.; Xie, J.; Zhang, P.; Lin, X.; Wu, K.; Jiang, S. Revealing the Immunogenic Risk of Polymers. *Angew. Chem. Int. Ed.* **2018**, *57* (42), 13873–13876. <https://doi.org/10.1002/anie.201808615>.
- (9) Fairbanks, B. D.; Thissen, H.; Maurdev, G.; Pasic, P.; White, J. F.; Meagher, L. Inhibition of Protein and Cell Attachment on Materials Generated from *N*-(2-Hydroxypropyl) Acrylamide. *Biomacromolecules* **2014**, *15* (9), 3259–3266. <https://doi.org/10.1021/bm500654q>.
- (10) Ringear, J.-M.; Griesmar, P.; Caplain, E.; Michiel, M.; Serfaty, S.; Huerou, J.-Y. L.; Marinkova, D.; Yotova, L. Design of Poly(*N*-Acryloylglycine) Materials for Incorporation of Microorganisms. *J. Appl. Polym. Sci.* **2013**, *130* (2), 835–841. <https://doi.org/10.1002/app.39242>.
- (11) Ayala, R.; Zhang, C.; Yang, D.; Hwang, Y.; Aung, A.; Shroff, S. S.; Arce, F. T.; Lal, R.; Arya, G.; Varghese, S. Engineering the Cell–Material Interface for Controlling Stem Cell Adhesion, Migration, and Differentiation. *Biomaterials* **2011**, *32* (15), 3700–3711. <https://doi.org/10.1016/j.biomaterials.2011.02.004>.
- (12) Jia, J.; Sarker, M.; Steinmetz, M. G.; Shukla, R.; Rathore, R. Photochemical Elimination of Leaving Groups from Zwitterionic Intermediates Generated via Electrocyclic Ring Closure of α,β -Unsaturated Anilides. *J. Org. Chem.* **2008**, *73* (22), 8867–8879. <https://doi.org/10.1021/jo8017445>.
- (13) Roy, D.; Sumerlin, B. S. Glucose-Sensitivity of Boronic Acid Block Copolymers at Physiological PH. *ACS Macro Lett.* **2012**, *1* (5), 529–532. <https://doi.org/10.1021/mz300047c>.
- (14) König, S. G.; Krämer, R. Accessing Structurally Diverse Near-Infrared Cyanine Dyes for Folate Receptor-Targeted Cancer Cell Staining. *Chem. - Eur. J.* **2017**, *23* (39), 9306–9312. <https://doi.org/10.1002/chem.201700026>.
- (15) Chiba, K.; Asanuma, M.; Ishikawa, M.; Hashimoto, Y.; Dodo, K.; Sodeoka, M.; Yamaguchi, T. Specific Fluorescence Labeling of Target Proteins by Using a Ligand-4-Azidophthalimide Conjugate. *Chem. Commun.* **2017**, *53* (62), 8751–8754. <https://doi.org/10.1039/C7CC03252H>.
- (16) Howell, L. A.; Gulam, R.; Mueller, A.; O’Connell, M. A.; Searcey, M. Design and Synthesis of Threading Intercalators to Target DNA. *Bioorg. Med. Chem. Lett.* **2010**, *20* (23), 6956–6959. <https://doi.org/10.1016/j.bmcl.2010.09.128>.

References

- (17) Marchetti, C.; Minarini, A.; Tumiatti, V.; Moraca, F.; Parrotta, L.; Alcaro, S.; Rigo, R.; Sissi, C.; Gunaratnam, M.; Ohnmacht, S. A.; Neidle, S.; Milelli, A. Macrocyclic Naphthalene Diimides as G-Quadruplex Binders. *Bioorg. Med. Chem.* **2015**, *23* (13), 3819–3830. <https://doi.org/10.1016/j.bmc.2015.03.076>.
- (18) Novak, S.; Zhang, J.; Kentzinger, E.; Rücker, U.; Portale, G.; Jung, N.; Jonas, U.; Myung, J. S.; Winkler, R. G.; Gompper, G.; Dhont, J. K. G.; Stiakakis, E. DNA Self-Assembly Mediated by Programmable Soft-Patchy Interactions. *ACS Nano* **2020**, 13524–13535. <https://doi.org/10.1021/acsnano.0c05536>.
- (19) Stiakakis, E.; Jung, N.; Adžić, N.; Balandin, T.; Kentzinger, E.; Rücker, U.; Biehl, R.; Dhont, J. K. G.; Jonas, U.; Likos, C. N. Self Assembling Cluster Crystals from DNA Based Dendritic Nanostructures. *Nat. Commun.* **2021**, *12* (1), 7167. <https://doi.org/10.1038/s41467-021-27412-3>.
- (20) Maldovan, M.; Thomas, E. L. Diamond-Structured Photonic Crystals. *Nat. Mater.* **2004**, *3* (9), 593–600. <https://doi.org/10.1038/nmat1201>.
- (21) Liu, W.; Tagawa, M.; Xin, H. L.; Wang, T.; Emamy, H.; Li, H.; Yager, K. G.; Starr, F. W.; Tkachenko, A. V.; Gang, O. Diamond Family of Nanoparticle Superlattices. *Science* **2016**, *351* (6273), 582. <https://doi.org/10.1126/science.aad2080>.
- (22) Jochum, C.; Adžić, N.; Stiakakis, E.; Derrien, T. L.; Luo, D.; Kahl, G.; Likos, C. N. Structure and Stimuli-Responsiveness of All-DNA Dendrimers: Theory and Experiment. *Nanoscale* **2019**, *11* (4), 1604–1617. <https://doi.org/10.1039/C8NR05814H>.
- (23) Sergelen, K.; Fossati, S.; Turupcu, A.; Oostenbrink, C.; Liedberg, B.; Knoll, W.; Dostálek, J. Plasmon Field-Enhanced Fluorescence Energy Transfer for Hairpin Aptamer Assay Readout. *ACS Sens.* **2017**, *2* (7), 916–923. <https://doi.org/10.1021/acssensors.7b00131>.
- (24) Cesana, S.; Kurek, A.; Baur, M. A.; Auernheimer, J.; Nuyken, O. Polymer-Bound Thiol Groups on Poly(2-Oxazoline)s. *Macromol. Rapid Commun.* **2007**, *28* (5), 608–615. <https://doi.org/10.1002/marc.200600737>.
- (25) Jung, N.; Diehl, F.; Jonas, U. Thiol-Substituted Poly(2-Oxazoline)s with Photolabile Protecting Groups—Tandem Network Formation by Light. *Polymers* **2020**, *12* (8), 1767. <https://doi.org/10.3390/polym12081767>.
- (26) Ferruti, P.; Marchisio, M. A.; Barbucci, R. Synthesis, Physico-Chemical Properties and Biomedical Applications of Poly(Amidoamine)s. *Polymer* **1985**, *26* (9), 1336–1348. [https://doi.org/10.1016/0032-3861\(85\)90309-X](https://doi.org/10.1016/0032-3861(85)90309-X).
- (27) Richardson, S. C. W.; Patrick, N. G.; Stella Man, Y. K.; Ferruti, P.; Duncan, R. Poly(Amidoamine)s as Potential Nonviral Vectors: Ability to Form Interpolyelectrolyte Complexes and to Mediate Transfection in Vitro. *Biomacromolecules* **2001**, *2* (3), 1023–1028. <https://doi.org/10.1021/bm010079f>.
- (28) Roy, D.; Brooks, W. L. A.; Sumerlin, B. S. New Directions in Thermoresponsive Polymers. *Chem. Soc. Rev.* **2013**, *42* (17), 7214–7243. <https://doi.org/10.1039/C3CS35499G>.
- (29) Schmaljohann, D. Thermo- and PH-Responsive Polymers in Drug Delivery. *2006 Suppl. Non-Themat. Collect.* **2006**, *58* (15), 1655–1670. <https://doi.org/10.1016/j.addr.2006.09.020>.
- (30) Ward, M. A.; Georgiou, T. K. Thermoresponsive Polymers for Biomedical Applications. *Polymers* **2011**, *3* (3), 1215–1242. <https://doi.org/10.3390/polym3031215>.
- (31) Bordat, A.; Boissenot, T.; Nicolas, J.; Tsapis, N. Thermoresponsive Polymer Nanocarriers for Biomedical Applications. *Phys.-Triggered Nanosyst. Ther. Diagn.* **2019**, *138*, 167–192. <https://doi.org/10.1016/j.addr.2018.10.005>.
- (32) Sponchioni, M.; Capasso Palmiero, U.; Moscatelli, D. Thermo-Responsive Polymers: Applications of Smart Materials in Drug Delivery and Tissue Engineering. *Mater. Sci. Eng. C* **2019**, *102*, 589–605. <https://doi.org/10.1016/j.msec.2019.04.069>.
- (33) Doberenz, F.; Zeng, K.; Willems, C.; Zhang, K.; Groth, T. Thermoresponsive Polymers and Their Biomedical Application in Tissue Engineering – a Review. *J. Mater. Chem. B* **2020**, *8* (4), 607–628. <https://doi.org/10.1039/C9TB02052G>.
- (34) Fujishige, S.; Kubota, K.; Ando, I. Phase Transition of Aqueous Solutions of Poly(N-Isopropylacrylamide) and Poly(N-Isopropylmethacrylamide). *J. Phys. Chem.* **1989**, *93* (8), 3311–3313. <https://doi.org/10.1021/j100345a085>.

- (35) Aseyev, V.; Tenhu, H.; Winnik, F. M. Non-Ionic Thermoresponsive Polymers in Water. In *Self Organized Nanostructures of Amphiphilic Block Copolymers II*; Müller, A. H. E., Borisov, O., Eds.; Springer Berlin Heidelberg: Berlin, Heidelberg, 2010; Vol. 242, pp 29–89.
- (36) Schwenke, K. D. Charles Tanford: The Hydrophobic Effect: Formation of Micelles and Biological Membranes. 200 Seiten, Zahlreiche Abb. Und Tab., John Wiley & Sons, New York, London, Sydney, Toronto 1973. Preis: 7,90 £. *Food Nahr.* **1976**, *20* (4), 449–449. <https://doi.org/10.1002/food.19760200449>.
- (37) Seuring, J.; Agarwal, S. Polymers with Upper Critical Solution Temperature in Aqueous Solution. *Macromol. Rapid Commun.* **2012**, *33* (22), 1898–1920. <https://doi.org/10.1002/marc.201200433>.
- (38) Seuring, J.; Agarwal, S. Polymers with Upper Critical Solution Temperature in Aqueous Solution: Unexpected Properties from Known Building Blocks. *ACS Macro Lett.* **2013**, *2* (7), 597–600. <https://doi.org/10.1021/mz400227y>.
- (39) Niskanen, J.; Tenhu, H. How to Manipulate the Upper Critical Solution Temperature (UCST)? *Polym. Chem.* **2017**, *8* (1), 220–232. <https://doi.org/10.1039/C6PY01612J>.
- (40) Zhang, Y.; Cremer, P. S. Interactions between Macromolecules and Ions: The Hofmeister Series. *Model Syst. Biopolym.* **2006**, *10* (6), 658–663. <https://doi.org/10.1016/j.cbpa.2006.09.020>.
- (41) Zhang, Q.; Weber, C.; Schubert, U. S.; Hoogenboom, R. Thermoresponsive Polymers with Lower Critical Solution Temperature: From Fundamental Aspects and Measuring Techniques to Recommended Turbidimetry Conditions. *Mater. Horiz.* **2017**, *4* (2), 109–116. <https://doi.org/10.1039/C7MH00016B>.
- (42) Scarpa, J. S.; Mueller, D. Dean.; Klotz, I. M. Slow Hydrogen-Deuterium Exchange in a Non- α -Helical Polyamide. *J. Am. Chem. Soc.* **1967**, *89* (24), 6024–6030. <https://doi.org/10.1021/ja01000a006>.
- (43) Schild, H. G. Poly(N-Isopropylacrylamide): Experiment, Theory and Application. *Prog. Polym. Sci.* **1992**, *17* (2), 163–249. [https://doi.org/10.1016/0079-6700\(92\)90023-R](https://doi.org/10.1016/0079-6700(92)90023-R).
- (44) Wang, X.; Qiu, X.; Wu, C. Comparison of the Coil-to-Globule and the Globule-to-Coil Transitions of a Single Poly(N-Isopropylacrylamide) Homopolymer Chain in Water. *Macromolecules* **1998**, *31* (9), 2972–2976. <https://doi.org/10.1021/ma971873p>.
- (45) Xia, Y.; Burke, N. A. D.; Stöver, H. D. H. End Group Effect on the Thermal Response of Narrow-Disperse Poly(N-Isopropylacrylamide) Prepared by Atom Transfer Radical Polymerization. *Macromolecules* **2006**, *39* (6), 2275–2283. <https://doi.org/10.1021/ma0519617>.
- (46) Knop, K.; Hoogenboom, R.; Fischer, D.; Schubert, U. S. Poly(Ethylene Glycol) in Drug Delivery: Pros and Cons as Well as Potential Alternatives. *Angew. Chem. Int. Ed.* **2010**, *49* (36), 6288–6308. <https://doi.org/10.1002/anie.200902672>.
- (47) Alarcón, C. de las H.; Pennadam, S.; Alexander, C. Stimuli Responsive Polymers for Biomedical Applications. *Chem. Soc. Rev.* **2005**, *34* (3), 276–285. <https://doi.org/10.1039/B406727D>.
- (48) Alexandridis, P.; Holzwarth, J. F.; Hatton, T. A. Micellization of Poly(Ethylene Oxide)-Poly(Propylene Oxide)-Poly(Ethylene Oxide) Triblock Copolymers in Aqueous Solutions: Thermodynamics of Copolymer Association. *Macromolecules* **1994**, *27* (9), 2414–2425. <https://doi.org/10.1021/ma00087a009>.
- (49) Lau, A. C. W.; Wu, C. Thermally Sensitive and Biocompatible Poly(N-Vinylcaprolactam): Synthesis and Characterization of High Molar Mass Linear Chains. *Macromolecules* **1999**, *32* (3), 581–584. <https://doi.org/10.1021/ma980850n>.
- (50) Makhaeva, E. E.; Thanh, L. T. M.; Starodoubtsev, S. G.; Khokhlov, A. R. Thermoshinking Behavior of Poly(Vinylcaprolactam) Gels in Aqueous Solution. *Macromol. Chem. Phys.* **1996**, *197* (6), 1973–1982. <https://doi.org/10.1002/macp.1996.021970616>.
- (51) Foster, J. A.; Bruenger, E.; Gray, W. R.; Sandberg, L. B. Isolation and Amino Acid Sequences of Tropoelastin Peptides. *J. Biol. Chem.* **1973**, *248* (8), 2876–2879.
- (52) Rodríguez-Cabello, J. C.; Reguera, J.; Girotti, A.; Arias, F. J.; Alonso, M. Genetic Engineering of Protein-Based Polymers: The Example of Elastinlike Polymers. In *Ordered Polymeric Nanostructures at Surfaces*; Vancso, G. J., Ed.; Advances in Polymer Science; Springer Berlin Heidelberg: Berlin, Heidelberg, 2005; Vol. 200, pp 119–167. https://doi.org/10.1007/12_047.

References

- (53) Urry, D. W. Physical Chemistry of Biological Free Energy Transduction As Demonstrated by Elastic Protein-Based Polymers. *J. Phys. Chem. B* **1997**, *101* (51), 11007–11028. <https://doi.org/10.1021/jp972167t>.
- (54) Tomalia, D. A.; Sheetz, D. P. Homopolymerization of 2-Alkyl- and 2-Aryl-2-Oxazolines. *J. Polym. Sci. [A1]* **1966**, *4* (9), 2253–2265. <https://doi.org/10.1002/pol.1966.150040919>.
- (55) Seeliger, W.; Aufderhaar, E.; Diepers, W.; Feinauer, R.; Nehring, R.; Thier, W.; Hellmann, H. Recent Syntheses and Reactions of Cyclic Imidic Esters. *Angew. Chem. Int. Ed. Engl.* **1966**, *5* (10), 875–888. <https://doi.org/10.1002/anie.196608751>.
- (56) Kagiya, T.; Narisawa, S.; Maeda, T.; Fukui, K. Ring-Opening Polymerization of 2-Substituted 2-Oxazolines. *J. Polym. Sci. [B]* **1966**, *4* (7), 441–445. <https://doi.org/10.1002/pol.1966.110040701>.
- (57) Bassiri, T. G.; Levy, A.; Litt, M. Polymerization of Cyclic Imino Ethers. I. Oxazolines. *J. Polym. Sci. [B]* **1967**, *5* (9), 871–879. <https://doi.org/10.1002/pol.1967.110050927>.
- (58) Saegusa, T.; Kobayashi, S.; Ishiguro, M. A New Route to Optically Active Linear Poly(Propylenimine). *Macromolecules* **1974**, *7* (6), 958–959. <https://doi.org/10.1021/ma60042a054>.
- (59) Saegusa, T.; Hirao, T.; Ito, Y. Polymerization of (4S,5R)-4-Carbomethoxy-5-Methyl-2-Oxazoline. *Macromolecules* **1975**, *8* (1), 87–87. <https://doi.org/10.1021/ma60043a022>.
- (60) Bloksma, M. M.; Schubert, U. S.; Hoogenboom, R. Poly(Cyclic Imino Ether)s Beyond 2-Substituted-2-Oxazolines. *Macromol. Rapid Commun.* **2011**, *32* (18), 1419–1441. <https://doi.org/10.1002/marc.201100138>.
- (61) Lambermont-Thijs, H. M. L.; Fijten, M. W. M.; van der Linden, A. J. (Ton); van Lankvelt, B. M.; Bloksma, M. M.; Schubert, U. S.; Hoogenboom, R. Efficient Cationic Ring-Opening Polymerization of Diverse Cyclic Imino Ethers: Unexpected Copolymerization Behavior. *Macromolecules* **2011**, *44* (11), 4320–4325. <https://doi.org/10.1021/ma200426y>.
- (62) Luxenhofer, R.; Huber, S.; Hytry, J.; Tong, J.; Kabanov, A. V.; Jordan, R. Chiral and Water-Soluble Poly(2-Oxazoline)s. *J. Polym. Sci. Part Polym. Chem.* **2013**, *51* (3), 732–738. <https://doi.org/10.1002/pola.26437>.
- (63) Verbraeken, B.; Monnery, B. D.; Lava, K.; Hoogenboom, R. The Chemistry of Poly(2-Oxazoline)s. In *Encyclopedia of Polymer Science and Technology*; John Wiley & Sons, Inc., Ed.; John Wiley & Sons, Inc.: Hoboken, NJ, USA, 2018; pp 1–59. <https://doi.org/10.1002/0471440264.pst626.pub2>.
- (64) Dworak, A. The Role of Cationic and Covalent Active Centers in the Polymerization of 2-Methyl-2-Oxazoline Initiated with Benzyl Bromide. *Macromol. Chem. Phys.* **1998**, *199* (9), 1843–1849. [https://doi.org/10.1002/\(SICI\)1521-3935\(19980901\)199:9<1843::AID-MACP1843>3.0.CO;2-I](https://doi.org/10.1002/(SICI)1521-3935(19980901)199:9<1843::AID-MACP1843>3.0.CO;2-I).
- (65) Kobayashi, S.; Iijima, S.; Igarashi, T.; Saegusa, T. Synthesis of a Nonionic Polymer Surfactant from Cyclic Imino Ethers by the Initiator Method. *Macromolecules* **1987**, *20* (8), 1729–1734. <https://doi.org/10.1021/ma00174a001>.
- (66) Guillerm, B.; Monge, S.; Lapinte, V.; Robin, J.-J. Novel Investigations on Kinetics and Polymerization Mechanism of Oxazolines Initiated by Iodine. *Macromolecules* **2010**, *43* (14), 5964–5970. <https://doi.org/10.1021/ma1009808>.
- (67) Hayashi, T.; Takasu, A. Design of Electrophoretic and Biocompatible Poly(2-Oxazoline)s Initiated by Perfluoroalkanesulfoneimides and Electrophoretic Deposition with Bioactive Glass. *Biomacromolecules* **2015**, *16* (4), 1259–1266. <https://doi.org/10.1021/acs.biomac.5b00043>.
- (68) Obeid, R.; Scholz, C. Synthesis and Self-Assembly of Well-Defined Poly(Amino Acid) End-Capped Poly(Ethylene Glycol) and Poly(2-Methyl-2-Oxazoline). *Biomacromolecules* **2011**, *12* (10), 3797–3804. <https://doi.org/10.1021/bm201048x>.
- (69) Qiu, L.-Y.; Yan, L.; Zhang, L.; Jin, Y.-M.; Zhao, Q.-H. Folate-Modified Poly(2-Ethyl-2-Oxazoline) as Hydrophilic Corona in Polymeric Micelles for Enhanced Intracellular Doxorubicin Delivery. *Int. J. Pharm.* **2013**, *456* (2), 315–324. <https://doi.org/10.1016/j.ijpharm.2013.08.071>.
- (70) Witzigmann, D.; Wu, D.; Schenk, S. H.; Balasubramanian, V.; Meier, W.; Huwyler, J. Biocompatible Polymer–Peptide Hybrid-Based DNA Nanoparticles for Gene Delivery. *ACS Appl. Mater. Interfaces* **2015**, *7* (19), 10446–10456. <https://doi.org/10.1021/acsami.5b01684>.

References

- (71) Xia, G.; An, Z.; Wang, Y.; Zhao, C.; Li, M.; Li, Z.; Ma, J. Synthesis of a Novel Polymeric Material Folate-Poly(2-Ethyl-2-Oxazoline)-Distearoyl Phosphatidyl Ethanolamine Tri-Block Polymer for Dual Receptor and PH-Sensitive Targeting Liposome. *Chem. Pharm. Bull. (Tokyo)* **2013**, *61* (4), 390–398. <https://doi.org/10.1248/cpb.c12-00951>.
- (72) Bühler, J.; Gietzen, S.; Reuter, A.; Kappel, C.; Fischer, K.; Decker, S.; Schäffel, D.; Koynov, K.; Bros, M.; Tubbe, I.; Grabbe, S.; Schmidt, M. Selective Uptake of Cylindrical Poly(2-Oxazoline) Brush-AntiDEC205 Antibody-OVA Antigen Conjugates into DEC-Positive Dendritic Cells and Subsequent T-Cell Activation. *Chem. – Eur. J.* **2014**, *20* (39), 12405–12410. <https://doi.org/10.1002/chem.201403942>.
- (73) Tang, P.; di Cio, S.; Wang, W.; E. Gautrot, J. Surface-Initiated Poly(Oligo(2-Alkyl-2-Oxazoline)Methacrylate) Brushes. *Langmuir* **2018**, *34* (34), 10019–10027. <https://doi.org/10.1021/acs.langmuir.8b01682>.
- (74) Loukotová, L.; Konefał, R.; Venclíková, K.; Machová, D.; Janoušková, O.; Rabyk, M.; Netopilík, M.; Mázl Chánová, E.; Štěpánek, P.; Hrubý, M. Hybrid Thermoresponsive Graft Constructs of Fungal Polysaccharide β -Glucan: Physico-Chemical and Immunomodulatory Properties. *Eur. Polym. J.* **2018**, *106*, 118–127. <https://doi.org/10.1016/j.eurpolymj.2018.07.004>.
- (75) Saegusa, T.; Ikeda, H. Isomerization Polymerization of 2-Oxazoline. VI. Kinetic Study on the Polymerization of 2-Methyl-2-Oxazoline Initiated by Methyl Iodide. *Macromolecules* **1973**, *6* (6), 808–811. <https://doi.org/10.1021/ma60036a004>.
- (76) Hoogenboom, R.; Paulus, R. M.; Fijten, M. W. M.; Schubert, U. S. Concentration Effects in the Cationic Ring-Opening Polymerization of 2-Ethyl-2-Oxazoline in N,N-Dimethylacetamide. *J. Polym. Sci. Part Polym. Chem.* **2005**, *43* (7), 1487–1497. <https://doi.org/10.1002/pola.20603>.
- (77) Glassner, M.; Vergaelen, M.; Hoogenboom, R. Poly(2-Oxazoline)s: A Comprehensive Overview of Polymer Structures and Their Physical Properties: Poly(2-Oxazoline)s. *Polym. Int.* **2017**. <https://doi.org/10.1002/pi.5457>.
- (78) Taubmann, C.; Luxenhofer, R.; Cesana, S.; Jordan, R. First Aldehyde-Functionalized Poly(2-Oxazoline)s for Chemoselective Ligation. *Macromol. Biosci.* **2005**, *5* (7), 603–612. <https://doi.org/10.1002/mabi.200500059>.
- (79) Cesana, S.; Auernheimer, J.; Jordan, R.; Kessler, H.; Nuyken, O. First Poly(2-Oxazoline)s with Pendant Amino Groups. *Macromol. Chem. Phys.* **2006**, *207* (2), 183–192. <https://doi.org/10.1002/macp.200500495>.
- (80) Bouten, P. J. M.; Hertsen, D.; Vergaelen, M.; Monnery, B. D.; Boerman, M. A.; Goossens, H.; Catak, S.; van Hest, J. C. M.; Van Speybroeck, V.; Hoogenboom, R. Accelerated Living Cationic Ring-Opening Polymerization of a Methyl Ester Functionalized 2-Oxazoline Monomer. *Polym. Chem.* **2015**, *6* (4), 514–518. <https://doi.org/10.1039/C4PY01373E>.
- (81) Nuyken, O.; Maier, G.; Groß, A.; Fischer, H. Systematic Investigations on the Reactivity of Oxazolinium Salts. *Macromol. Chem. Phys.* **1996**, *197* (1), 83–95. <https://doi.org/10.1002/macp.1996.021970106>.
- (82) Kosakowska, K. A.; Dimitrov, P.; Panambur, G.; Grayson, S. M. MALDI-TOF MS Investigation of the Unconventional Termination of Living Polyoxazoline with Ammonia. *J. Polym. Sci. Part Polym. Chem.* **2017**, *55* (8), 1303–1312. <https://doi.org/10.1002/pola.28495>.
- (83) Delaittre, G. Telechelic Poly(2-Oxazoline)s. *Eur. Polym. J.* **2019**, *121*, 109281. <https://doi.org/10.1016/j.eurpolymj.2019.109281>.
- (84) Litt, M.; Levy, A.; Herz, J. Polymerization of Cyclic Imino Ethers. X. Kinetics, Chain Transfer, and Repolymerization. *J. Macromol. Sci. Part - Chem.* **1975**, *9* (5), 703–727. <https://doi.org/10.1080/00222337508065890>.
- (85) Warakomski, J. M.; Thill, B. P. Evidence for Long Chain Branching in Polyethyloxazoline. *J. Polym. Sci. Part Polym. Chem.* **1990**, *28* (13), 3551–3563. <https://doi.org/10.1002/pola.1990.080281303>.
- (86) Levy, A.; Litt, M. Polymerization of Cyclic Iminoethers. V. 1,3-Oxazolines with Hydroxy-, Acetoxy-, and Carboxymethyl-Alkyl Groups in the 2 Position and Their Polymers. *J. Polym. Sci. [A1]* **1968**, *6* (7), 1883–1894. <https://doi.org/10.1002/pol.1968.150060711>.

References

- (87) Van Steenberge, P. H. M.; Verbraeken, B.; Reyniers, M.-F.; Hoogenboom, R.; D'hooge, D. R. Model-Based Visualization and Understanding of Monomer Sequence Formation in Gradient Copoly(2-Oxazoline)s On the Basis of 2-Methyl-2-Oxazoline and 2-Phenyl-2-Oxazoline. *Macromolecules* **2015**, *48* (21), 7765–7773. <https://doi.org/10.1021/acs.macromol.5b01642>.
- (88) Park, J.-S.; Kataoka, K. Precise Control of Lower Critical Solution Temperature of Thermosensitive Poly(2-Isopropyl-2-Oxazoline) via Gradient Copolymerization with 2-Ethyl-2-Oxazoline as a Hydrophilic Comonomer. *Macromolecules* **2006**, *39* (19), 6622–6630. <https://doi.org/10.1021/ma0605548>.
- (89) Diab, C.; Akiyama, Y.; Kataoka, K.; Winnik, F. M. Microcalorimetric Study of the Temperature-Induced Phase Separation in Aqueous Solutions of Poly(2-Isopropyl-2-Oxazolines). *Macromolecules* **2004**, *37* (7), 2556–2562. <https://doi.org/10.1021/ma0358733>.
- (90) Levy, A.; Litt, M. Polymerization of Cyclic Iminoethers. IV. Oxazoline Polymerization in Solvents Containing Different Functional Groups. *J. Polym. Sci. [A1]* **1968**, *6* (1), 63–72. <https://doi.org/10.1002/pol.1968.150060107>.
- (91) Luxenhofer, R.; Schulz, A.; Roques, C.; Li, S.; Bronich, T. K.; Batrakova, E. V.; Jordan, R.; Kabanov, A. V. Doubly Amphiphilic Poly(2-Oxazoline)s as High-Capacity Delivery Systems for Hydrophobic Drugs. *Biomaterials* **2010**, *31* (18), 4972–4979. <https://doi.org/10.1016/j.biomaterials.2010.02.057>.
- (92) de la Rosa, V. R. Poly(2-Oxazoline)s as Materials for Biomedical Applications. *J. Mater. Sci. Mater. Med.* **2014**, *25* (5), 1211–1225. <https://doi.org/10.1007/s10856-013-5034-y>.
- (93) Hoogenboom, R. Poly(2-Oxazoline)s: A Polymer Class with Numerous Potential Applications. *Angew. Chem. Int. Ed.* **2009**, *48* (43), 7978–7994. <https://doi.org/10.1002/anie.200901607>.
- (94) Adams, N.; Schubert, U. S. Poly(2-Oxazolines) in Biological and Biomedical Application Contexts. *Adv. Drug Deliv. Rev.* **2007**, *59* (15), 1504–1520. <https://doi.org/10.1016/j.addr.2007.08.018>.
- (95) Viegas, T. X.; Bentley, M. D.; Harris, J. M.; Fang, Z.; Yoon, K.; Dizman, B.; Weimer, R.; Mero, A.; Pasut, G.; Veronese, F. M. Polyoxazoline: Chemistry, Properties, and Applications in Drug Delivery. *Bioconjug. Chem.* **2011**, *22* (5), 976–986. <https://doi.org/10.1021/bc200049d>.
- (96) Tauhardt, L.; Kempe, K.; Gottschaldt, M.; Schubert, U. S. Poly(2-Oxazoline) Functionalized Surfaces: From Modification to Application. *Chem. Soc. Rev.* **2013**, *42* (20), 7998. <https://doi.org/10.1039/c3cs60161g>.
- (97) Park, J.-S.; Kataoka, K. Comprehensive and Accurate Control of Thermosensitivity of Poly(2-Alkyl-2-Oxazoline)s via Well-Defined Gradient or Random Copolymerization. *Macromolecules* **2007**, *40* (10), 3599–3609. <https://doi.org/10.1021/ma0701181>.
- (98) Hoogenboom, R.; Thijs, H. M. L.; Jochems, M. J. H. C.; van Lankvelt, B. M.; Fijten, M. W. M.; Schubert, U. S. Tuning the LCST of Poly(2-Oxazoline)s by Varying Composition and Molecular Weight: Alternatives to Poly(N-Isopropylacrylamide)? *Chem. Commun.* **2008**, No. 44, 5758–5760. <https://doi.org/10.1039/B813140F>.
- (99) Bloksma, M. M.; Weber, C.; Perevyazko, I. Y.; Kuse, A.; Baumgärtel, A.; Vollrath, A.; Hoogenboom, R.; Schubert, U. S. Poly(2-Cyclopropyl-2-Oxazoline): From Rate Acceleration by Cyclopropyl to Thermoresponsive Properties. *Macromolecules* **2011**, *44* (11), 4057–4064. <https://doi.org/10.1021/ma200514n>.
- (100) Diehl, C.; Schlaad, H. Thermo-Responsive Polyoxazolines with Widely Tuneable LCST. *Macromol. Biosci.* **2009**, *9* (2), 157–161. <https://doi.org/10.1002/mabi.200800213>.
- (101) Zhang, N.; Luxenhofer, R.; Jordan, R. Thermoresponsive Poly(2-Oxazoline) Molecular Brushes by Living Ionic Polymerization: Kinetic Investigations of Pendant Chain Grafting and Cloud Point Modulation by Backbone and Side Chain Length Variation. *Macromol. Chem. Phys.* **2012**, *213* (9), 973–981. <https://doi.org/10.1002/macp.201200015>.
- (102) Weber, C.; Rogers, S.; Vollrath, A.; Hoepfener, S.; Rudolph, T.; Fritz, N.; Hoogenboom, R.; Schubert, U. S. Aqueous Solution Behavior of Comb-Shaped Poly(2-Ethyl-2-Oxazoline). *J. Polym. Sci. Part Polym. Chem.* **2013**, *51* (1), 139–148. <https://doi.org/10.1002/pola.26332>.
- (103) Glassner, M.; Lava, K.; de la Rosa, V. R.; Hoogenboom, R. Tuning the LCST of Poly(2-Cyclopropyl-2-Oxazoline) via Gradient Copolymerization with 2-Ethyl-2-Oxazoline. *J. Polym. Sci. Part Polym. Chem.* **2014**, *52* (21), 3118–3122. <https://doi.org/10.1002/pola.27364>.
- (104) Morgese, G.; Trachsel, L.; Romio, M.; Divandari, M.; Ramakrishna, S. N.; Benetti, E. M. Topological

References

- Polymer Chemistry Enters Surface Science: Linear versus Cyclic Polymer Brushes. *Angew. Chem. Int. Ed.* **2016**, *55* (50), 15583–15588. <https://doi.org/10.1002/anie.201607309>.
- (105) Jung, Y.; Kim, J.-H.; Jang, W.-D. Linear and Cyclic Poly(2-Isopropyl-2-Oxazoline)s for Fine Control of Thermoresponsiveness. *Eur. Polym. J.* **2017**, *88*, 605–612. <https://doi.org/10.1016/j.eurpolymj.2016.09.003>.
- (106) Volet, G.; Chanthavong, V.; Wintgens, V.; Amiel, C. Synthesis of Monoalkyl End-Capped Poly(2-Methyl-2-Oxazoline) and Its Micelle Formation in Aqueous Solution. *Macromolecules* **2005**, *38* (12), 5190–5197. <https://doi.org/10.1021/ma050407u>.
- (107) Huber, S.; Hutter, N.; Jordan, R. Effect of End Group Polarity upon the Lower Critical Solution Temperature of Poly(2-Isopropyl-2-Oxazoline). *Colloid Polym. Sci.* **2008**, *286* (14), 1653–1661. <https://doi.org/10.1007/s00396-008-1942-7>.
- (108) Bloksma, M. M.; Bakker, D. J.; Weber, C.; Hoogenboom, R.; Schubert, U. S. The Effect of Hofmeister Salts on the LCST Transition of Poly(2-Oxazoline)s with Varying Hydrophilicity. *Macromol. Rapid Commun.* **2010**, *31* (8), 724–728. <https://doi.org/10.1002/marc.200900843>.
- (109) Litt, M.; Herz, J. Polymerization of Cyclic Imino Ethers: VII. The Use of the Sessile Drop Method to Investigate the Surface Structure of Poly(N-Acyl and Aroyl Ethyleneimines). *Pap. Present. 43rd Natl. Colloid Symp.* **1969**, *31* (2), 248–252. [https://doi.org/10.1016/0021-9797\(69\)90332-4](https://doi.org/10.1016/0021-9797(69)90332-4).
- (110) Luxenhofer, R.; Han, Y.; Schulz, A.; Tong, J.; He, Z.; Kabanov, A. V.; Jordan, R. Poly(2-Oxazoline)s as Polymer Therapeutics. *Macromol. Rapid Commun.* **2012**, *33* (19), 1613–1631. <https://doi.org/10.1002/marc.201200354>.
- (111) Lorson, T.; Lübtow, M. M.; Wegener, E.; Haider, M. S.; Borova, S.; Nahm, D.; Jordan, R.; Sokolski-Papkov, M.; Kabanov, A. V.; Luxenhofer, R. Poly(2-Oxazoline)s Based Biomaterials: A Comprehensive and Critical Update. *Biomaterials* **2018**, *178*, 204–280. <https://doi.org/10.1016/j.biomaterials.2018.05.022>.
- (112) Krishnan, S.; Weinman, C. J.; Ober, C. K. Advances in Polymers for Anti-Biofouling Surfaces. *J. Mater. Chem.* **2008**, *18* (29), 3405–3413. <https://doi.org/10.1039/b801491d>.
- (113) Moad, G.; Chiefari, J.; Chong, (Bill) Y.K.; Krstina, J.; Mayadunne, R. T.; Postma, A.; Rizzardo, E.; Thang, S. H. Living Free Radical Polymerization with Reversible Addition - Fragmentation Chain Transfer (the Life of RAFT). *Polym. Int.* **2000**, *49* (9), 993–1001. [https://doi.org/10.1002/1097-0126\(200009\)49:9<993::AID-PI506>3.0.CO;2-6](https://doi.org/10.1002/1097-0126(200009)49:9<993::AID-PI506>3.0.CO;2-6).
- (114) Moad, G.; Rizzardo, E.; Thang, S. H. Living Radical Polymerization by the RAFT Process. *Aust. J. Chem.* **2005**, *58* (6), 379–410. <https://doi.org/10.1071/CH05072>.
- (115) Moad, G.; Rizzardo, E.; Thang, S. H. Living Radical Polymerization by the RAFT Process—A First Update. *Aust. J. Chem.* **2006**, *59* (10), 669–692. <https://doi.org/10.1071/CH06250>.
- (116) Moad, G.; Rizzardo, E.; Thang, S. H. Toward Living Radical Polymerization. *Acc. Chem. Res.* **2008**, *41* (9), 1133–1142. <https://doi.org/10.1021/ar800075n>.
- (117) Rizzardo, E.; Chiefari, J.; Mayadunne, R. T. A.; Moad, G.; Thang, S. H. Synthesis of Defined Polymers by Reversible Addition—Fragmentation Chain Transfer: The RAFT Process. In *Controlled/Living Radical Polymerization*; Matyjaszewski, K., Ed.; American Chemical Society: Washington, DC, 2000; Vol. 768, pp 278–296.
- (118) Barner-Kowollik, C. *Handbook of RAFT Polymerization*, 1st ed.; Wiley-VCH Verlag: Weinheim, 2008.
- (119) D’Agosto, F.; Rieger, J.; Lansalot, M. RAFT-Mediated Polymerization-Induced Self-Assembly. *Angew. Chem. Int. Ed.* **2020**, *59* (22), 8368–8392. <https://doi.org/10.1002/anie.201911758>.
- (120) Semsarilar, M.; Perrier, S. “Green” Reversible Addition-Fragmentation Chain-Transfer (RAFT) Polymerization. *Nat. Chem.* **2010**, *2* (10), 811–820. <https://doi.org/10.1038/nchem.853>.
- (121) Phommalsack-Lovan, J.; Chu, Y.; Boyer, C.; Xu, J. PET-RAFT Polymerisation: Towards Green and Precision Polymer Manufacturing. *Chem. Commun.* **2018**, *54* (50), 6591–6606. <https://doi.org/10.1039/C8CC02783H>.
- (122) Aoyagi, N.; Endo, T. Functional RAFT Agents for Radical-Controlled Polymerization: Quantitative Synthesis of Trithiocarbonates Containing Functional Groups as RAFT Agents Using Equivalent Amount of CS₂. *J. Polym. Sci. Part Polym. Chem.* **2009**, *47* (14), 3702–3709. <https://doi.org/10.1002/pola.23410>.
- (123) Willcock, H.; O’Reilly, R. K. End Group Removal and Modification of RAFT Polymers. *Polym. Chem.* **2010**, *1* (2), 149–157. <https://doi.org/10.1039/B9PY00340A>.

References

- (124) Stamenović, M. M.; Espeel, P.; Camp, W. V.; Du Prez, F. E. Norbornenyl-Based RAFT Agents for the Preparation of Functional Polymers via Thiol–Ene Chemistry. *Macromolecules* **2011**, *44* (14), 5619–5630. <https://doi.org/10.1021/ma200799b>.
- (125) Kaupp, M.; Tischer, T.; Hirschbiel, A. F.; Vogt, A. P.; Geckle, U.; Trouillet, V.; Hofe, T.; Stenzel, M. H.; Barner-Kowollik, C. Photo-Sensitive RAFT-Agents for Advanced Microparticle Design. *Macromolecules* **2013**, *46* (17), 6858–6872. <https://doi.org/10.1021/ma401242g>.
- (126) Zhang, L.; Tang, Q.; Weiss, R. A.; Cavicchi, K. A. Synthesis and Characterization of Quaternary Phosphonium-Containing, Trithiocarbonate RAFT Agents. *Polym Chem* **2014**, *5* (18), 5492–5500. <https://doi.org/10.1039/C4PY00615A>.
- (127) Martens, S.; Driessen, F.; Wallyn, S.; Türlüç, O.; Du Prez, F. E.; Espeel, P. One-Pot Modular Synthesis of Functionalized RAFT Agents Derived from a Single Thiolactone Precursor. *ACS Macro Lett.* **2016**, *5* (8), 942–945. <https://doi.org/10.1021/acsmacrolett.6b00499>.
- (128) Moad, G.; Chong, Y. K.; Postma, A.; Rizzardo, E.; Thang, S. H. Advances in RAFT Polymerization: The Synthesis of Polymers with Defined End-Groups. *Polymer* **2005**, *46* (19), 8458–8468. <https://doi.org/10.1016/j.polymer.2004.12.061>.
- (129) Qiu, X.-P.; Winnik, F. M. Facile and Efficient One-Pot Transformation of RAFT Polymer End Groups via a Mild Aminolysis/Michael Addition Sequence. *Macromol. Rapid Commun.* **2006**, *27* (19), 1648–1653. <https://doi.org/10.1002/marc.200600436>.
- (130) Moad, G.; Rizzardo, E.; Thang, S. H. End-Functional Polymers, Thiocarbonylthio Group Removal/Transformation and Reversible Addition–Fragmentation–Chain Transfer (RAFT) Polymerization. *Polym. Int.* **2011**, *60* (1), 9–25. <https://doi.org/10.1002/pi.2988>.
- (131) De, P.; Li, M.; Gondi, S. R.; Sumerlin, B. S. Temperature-Regulated Activity of Responsive Polymer–Protein Conjugates Prepared by Grafting-from via RAFT Polymerization. *J. Am. Chem. Soc.* **2008**, *130* (34), 11288–11289. <https://doi.org/10.1021/ja804495v>.
- (132) Li, M.; Li, H.; De, P.; Sumerlin, B. S. Thermoresponsive Block Copolymer–Protein Conjugates Prepared by Grafting-from via RAFT Polymerization. *Macromol. Rapid Commun.* **2011**, *32* (4), 354–359. <https://doi.org/10.1002/marc.201000619>.
- (133) Trzebicka, B.; Szweda, R.; Kosowski, D.; Szweda, D.; Otulakowski, Ł.; Haladjova, E.; Dworak, A. Thermoresponsive Polymer–Peptide/Protein Conjugates. *Top. Vol. Biomater.* **2017**, *68*, 35–76. <https://doi.org/10.1016/j.progpolymsci.2016.12.004>.
- (134) Ulbrich, K.; Holá, K.; Šubr, V.; Bakandritsos, A.; Tuček, J.; Zbořil, R. Targeted Drug Delivery with Polymers and Magnetic Nanoparticles: Covalent and Noncovalent Approaches, Release Control, and Clinical Studies. *Chem. Rev.* **2016**, *116* (9), 5338–5431. <https://doi.org/10.1021/acs.chemrev.5b00589>.
- (135) Seidi, F.; Jenjob, R.; Crespy, D. Designing Smart Polymer Conjugates for Controlled Release of Payloads. *Chem. Rev.* **2018**, *118* (7), 3965–4036. <https://doi.org/10.1021/acs.chemrev.8b00006>.
- (136) Joubert, F.; Pasparakis, G. Well-Defined Backbone Degradable Polymer–Drug Conjugates Synthesized by Reversible Addition–Fragmentation Chain-Transfer Polymerization. *J. Polym. Sci.* **2020**, *58* (14), 2010–2021. <https://doi.org/10.1002/pol.20200303>.
- (137) Moad, G.; Rizzardo, E.; Thang, S. H. CHAPTER 6. Fundamentals of RAFT Polymerization. In *Polymer Chemistry Series*; Tsarevsky, N. V., Sumerlin, B. S., Eds.; Royal Society of Chemistry: Cambridge, 2013; pp 205–249. <https://doi.org/10.1039/9781849737425-00205>.
- (138) Keddie, D. J. A Guide to the Synthesis of Block Copolymers Using Reversible-Addition Fragmentation Chain Transfer (RAFT) Polymerization. *Chem. Soc. Rev.* **2014**, *43* (2), 496–505. <https://doi.org/10.1039/C3CS60290G>.
- (139) Moad, G. RAFT Polymerization to Form Stimuli-Responsive Polymers. *Polym. Chem.* **2017**, *8* (1), 177–219. <https://doi.org/10.1039/C6PY01849A>.
- (140) Thomas, D. B.; Convertine, A. J.; Hester, R. D.; Lowe, A. B.; McCormick, C. L. Hydrolytic Susceptibility of Dithioester Chain Transfer Agents and Implications in Aqueous RAFT Polymerizations †. *Macromolecules* **2004**, *37* (5), 1735–1741. <https://doi.org/10.1021/ma035572t>.
- (141) Keddie, D. J.; Guerrero-Sanchez, C.; Moad, G.; Rizzardo, E.; Thang, S. H. Switchable Reversible Addition–Fragmentation Chain Transfer (RAFT) Polymerization in Aqueous Solution, *N*, *N*-Dimethylacrylamide. *Macromolecules* **2011**, *44* (17), 6738–6745. <https://doi.org/10.1021/ma200760q>.

- (142) Keddie, D. J.; Moad, G.; Rizzardo, E.; Thang, S. H. RAFT Agent Design and Synthesis. *Macromolecules* **2012**, *45* (13), 5321–5342. <https://doi.org/10.1021/ma300410v>.
- (143) Chiefari, J.; Mayadunne, R.; Moad, C. L.; Moad, G.; Rizzardo, E.; Postma, A.; Skidmore, M. A.; Thang, S. H. Thiocarbonylthio Compounds (S:C(Z)S-R) in Free Radical Polymerization with Reversible Addition-Fragmentation Chain Transfer (RAFT Polymerization) . Effect of the Activating Group Z. *Macromolecules* **2003**, *36* (7), 2273–2283. <https://doi.org/10.1021/ma020883>.
- (144) Destarac, M.; Bzducha, W.; Taton, D.; Gauthier-Gillaizeau, I.; Zard, S. Z. Xanthates as Chain-Transfer Agents in Controlled Radical Polymerization (MADIX): Structural Effect of the O-Alkyl Group. *Macromol. Rapid Commun.* **2002**, *23* (17), 1049–1054. <https://doi.org/10.1002/marc.200290002>.
- (145) Chong, Y. K.; Krstina, J.; Le, T. P. T.; Moad, G.; Postma, A.; Rizzardo, E.; Thang, S. H. Thiocarbonylthio Compounds [SC(Ph)S–R] in Free Radical Polymerization with Reversible Addition-Fragmentation Chain Transfer (RAFT Polymerization). Role of the Free-Radical Leaving Group (R). *Macromolecules* **2003**, *36* (7), 2256–2272. <https://doi.org/10.1021/ma020882h>.
- (146) Moad, G.; Benaglia, M.; Chen, M.; Chiefari, J.; Chong, Y. K.; Keddie, D. J.; Rizzardo, E.; Thang, S. H. Block Copolymer Synthesis through the Use of Switchable RAFT Agents. In *Non-Conventional Functional Block Copolymers*; Theato, P., Kilbinger, A. F. M., Coughlin, E. B., Eds.; American Chemical Society: Washington, DC, 2011; Vol. 1066, pp 81–102.
- (147) Benaglia, M.; Chen, M.; Chong, Y. K.; Moad, G.; Rizzardo, E.; Thang, S. H. Polystyrene- Block - Poly(Vinyl Acetate) through the Use of a Switchable RAFT Agent. *Macromolecules* **2009**, *42* (24), 9384–9386. <https://doi.org/10.1021/ma9021086>.
- (148) Benaglia, M.; Chiefari, J.; Chong, Y. K.; Moad, G.; Rizzardo, E.; Thang, S. H. Universal (Switchable) RAFT Agents. *J. Am. Chem. Soc.* **2009**, *131* (20), 6914–6915. <https://doi.org/10.1021/ja901955n>.
- (149) Chiefari, J.; Chong, Y. K. (Bill); Ercole, F.; Krstina, J.; Jeffery, J.; Le, T. P. T.; Mayadunne, R. T. A.; Meijs, G. F.; Moad, C. L.; Moad, G.; Rizzardo, E.; Thang, S. H. Living Free-Radical Polymerization by Reversible Addition–Fragmentation Chain Transfer: The RAFT Process. *Macromolecules* **1998**, *31* (16), 5559–5562. <https://doi.org/10.1021/ma9804951>.
- (150) Robert J. Young; Peter A. Lovell. *Introduction to Polymers*, 3rd ed.; CRC Press, 2011.
- (151) Moad, G.; Rizzardo, E.; Thang, S. H. Living Radical Polymerization by the RAFT Process – A Third Update. *Aust. J. Chem.* **2012**, *65* (8), 985. <https://doi.org/10.1071/CH12295>.
- (152) Favier, A.; Charreyre, M.-T.; Pichot, C. A Detailed Kinetic Study of the RAFT Polymerization of a Bi-Substituted Acrylamide Derivative: Influence of Experimental Parameters. *Polymer* **2004**, *45* (26), 8661–8674. <https://doi.org/10.1016/j.polymer.2004.10.055>.
- (153) Favier, A.; Charreyre, M.-T. Experimental Requirements for an Efficient Control of Free-Radical Polymerizations via the Reversible Addition-Fragmentation Chain Transfer (RAFT) Process. *Macromol. Rapid Commun.* **2006**, *27* (9), 653–692. <https://doi.org/10.1002/marc.200500839>.
- (154) Moad, G. A Critical Survey of Dithiocarbamate Reversible Addition-Fragmentation Chain Transfer (RAFT) Agents in Radical Polymerization. *J. Polym. Sci. Part Polym. Chem.* **2019**, *57* (3), 216–227. <https://doi.org/10.1002/pola.29199>.
- (155) Li, S.; Han, G.; Zhang, W. Photoregulated Reversible Addition–Fragmentation Chain Transfer (RAFT) Polymerization. *Polym. Chem.* **2020**, *11* (11), 1830–1844. <https://doi.org/10.1039/D0PY00054J>.
- (156) Zhou, J.; Yao, H.; Ma, J. Recent Advances in RAFT-Mediated Surfactant-Free Emulsion Polymerization. *Polym. Chem.* **2018**, *9* (19), 2532–2561. <https://doi.org/10.1039/C8PY00065D>.
- (157) Kobayashi, S.; Masuda, E.; Shoda, S.; Shimano, Y. Synthesis of Acryl- and Methacryl-Type Macromonomers and Telechelics by Utilizing Living Polymerization of 2-Oxazolines. *Macromolecules* **1989**, *22* (7), 2878–2884.
- (158) Heskins, M.; Guillet, J. E. Solution Properties of Poly(N-Isopropylacrylamide). *J. Macromol. Sci. Part - Chem.* **1968**, *2* (8), 1441–1455. <https://doi.org/10.1080/10601326808051910>.

References

- (159) Goossens, H.; Catak, S.; Glassner, M.; de la Rosa, V. R.; Monnery, B. D.; De Proft, F.; Van Speybroeck, V.; Hoogenboom, R. Cationic Ring-Opening Polymerization of 2-Propyl-2-Oxazolines: Understanding Structural Effects on Polymerization Behavior Based on Molecular Modeling. *ACS Macro Lett.* **2013**, *2* (8), 651–654. <https://doi.org/10.1021/mz400293y>.
- (160) Wiesbrock, F.; Hoogenboom, R.; Leenen, M. A. M.; Meier, M. A. R.; Schubert, U. S. Investigation of the Living Cationic Ring-Opening Polymerization of 2-Methyl-, 2-Ethyl-, 2-Nonyl-, and 2-Phenyl-2-Oxazoline in a Single-Mode Microwave Reactor †. *Macromolecules* **2005**, *38* (12), 5025–5034. <https://doi.org/10.1021/ma0474170>.
- (161) Osawa, S.; Ishii, T.; Takemoto, H.; Osada, K.; Kataoka, K. A Facile Amino-Functionalization of Poly(2-Oxazoline)s' Distal End through Sequential Azido End-Capping and Staudinger Reactions. *Eur. Polym. J.* **2017**, *88*, 553–561. <https://doi.org/10.1016/j.eurpolymj.2016.11.029>.
- (162) Fijten, M. W. M.; Haensch, C.; van Lankvelt, B. M.; Hoogenboom, R.; Schubert, U. S. Clickable Poly(2-Oxazoline)s as Versatile Building Blocks. *Macromol. Chem. Phys.* **2008**, *209* (18), 1887–1895. <https://doi.org/10.1002/macp.200800226>.
- (163) Wiesbrock, F.; Hoogenboom, R.; Abeln, C. H.; Schubert, U. S. Single-Mode Microwave Ovens as New Reaction Devices: Accelerating the Living Polymerization of 2-Ethyl-2-Oxazoline. *Macromol. Rapid Commun.* **2004**, *25* (22), 1895–1899. <https://doi.org/10.1002/marc.200400369>.
- (164) Wiesbrock, F.; Hoogenboom, R.; Leenen, M.; van Nispen, S. F. G. M.; van der Loop, M.; Abeln, C. H.; van den Berg, A. M. J.; Schubert, U. S. Microwave-Assisted Synthesis of a 4²-Membered Library of Diblock Copoly(2-Oxazoline)s and Chain-Extended Homo Poly(2-Oxazoline)s and Their Thermal Characterization. *Macromolecules* **2005**, *38* (19), 7957–7966. <https://doi.org/10.1021/ma050437x>.
- (165) Cartwright, I. L.; Hutchinson, D. W.; Armstrong, V. W. The Reaction between Thiols and 8-Azidoadenosine Derivatives. *Nucleic Acids Res.* **1976**, *3* (9), 2331–2340. <https://doi.org/10.1093/nar/3.9.2331>.
- (166) Singh, J.; Singha, T.; Naskar, A.; Kundu, M.; Kumar, R.; Mondal, A.; Ghosh, T.; Maity, T. K. SYNTHESIS AND ANTI-PROLIFERATIVE ACTIVITY OF SOME ISOINDOLINE-1, 3-DIONE DERIVATIVES AGAINST EHRlich'S ASCITES CARCINOMA BEARING MICE MODEL. *Pharmacologyonline* **2011**, No. 2, 976–987.
- (167) Devine, W. G.; Diaz-Gonzalez, R.; Ceballos-Perez, G.; Rojas, D.; Satoh, T.; Tear, W.; Ranade, R. M.; Barros-Álvarez, X.; Hol, W. G. J.; Buckner, F. S.; Navarro, M.; Pollastri, M. P. From Cells to Mice to Target: Characterization of NEU-1053 (SB-443342) and Its Analogues for Treatment of Human African Trypanosomiasis. *ACS Infect. Dis.* **2017**, *3* (3), 225–236. <https://doi.org/10.1021/acscinfdis.6b00202>.
- (168) Kolb, H. C.; Finn, M. G.; Sharpless, K. B. Click Chemistry: Diverse Chemical Function from a Few Good Reactions. *Angew. Chem. Int. Ed.* **2001**, *40* (11), 2004–2021. [https://doi.org/10.1002/1521-3773\(20010601\)40:11<2004::AID-ANIE2004>3.0.CO;2-5](https://doi.org/10.1002/1521-3773(20010601)40:11<2004::AID-ANIE2004>3.0.CO;2-5).
- (169) Binder, W. H.; Sachsenhofer, R. 'Click' Chemistry in Polymer and Materials Science. *Macromol. Rapid Commun.* **2007**, *28* (1), 15–54. <https://doi.org/10.1002/marc.200600625>.
- (170) Staudinger, H.; Meyer, J. Über Neue Organische Phosphorverbindungen III. Phosphinmethylenderivate Und Phosphinimine. *Helv. Chim. Acta* **1919**, *2* (1), 635–646. <https://doi.org/10.1002/hlca.19190020164>.
- (171) Gololobov, Y. G.; Kasukhin, L. F. Recent Advances in the Staudinger Reaction. *Tetrahedron* **1992**, *48* (8), 1353–1406. [https://doi.org/10.1016/S0040-4020\(01\)92229-X](https://doi.org/10.1016/S0040-4020(01)92229-X).
- (172) Tian, W. Q.; Wang, Y. A. Mechanisms of Staudinger Reactions within Density Functional Theory. *J. Org. Chem.* **2004**, *69* (13), 4299–4308. <https://doi.org/10.1021/jo049702n>.
- (173) Lehner, R.; Liu, K.; Wang, X.; Wolf, M.; Hunziker, P. A Comparison of Plasmid DNA Delivery Efficiency and Cytotoxicity of Two Cationic Diblock Polyoxazoline Copolymers. *Nanotechnology* **2017**, *28* (17), 175602.
- (174) Hsiue, G.-H.; Chiang, H.-Z.; Wang, C.-H.; Juang, T.-M. Nonviral Gene Carriers Based on Diblock Copolymers of Poly(2-Ethyl-2-Oxazoline) and Linear Polyethylenimine. *Bioconjug. Chem.* **2006**, *17* (3), 781–786. <https://doi.org/10.1021/bc050317u>.
- (175) Dawson, P.; Muir, T.; Clark-Lewis, I.; Kent, S. Synthesis of Proteins by Native Chemical Ligation. *Science* **1994**, *266* (5186), 776. <https://doi.org/10.1126/science.7973629>.
- (176) Hackenberger, C. P. R.; Schwarzer, D. Chemoselective Ligation and Modification Strategies for Peptides

References

- and Proteins. *Angew. Chem. Int. Ed.* **2008**, *47* (52), 10030–10074. <https://doi.org/10.1002/anie.200801313>.
- (177) Hu, B.-H.; Su, J.; Messersmith, P. B. Hydrogels Cross-Linked by Native Chemical Ligation. *Biomacromolecules* **2009**, *10* (8), 2194–2200. <https://doi.org/10.1021/bm900366e>.
- (178) Blöbbaum, J.; Paulus, I.; Pöppler, A.-C.; Tessmar, J.; Groll, J. Influence of Charged Groups on the Cross-Linking Efficiency and Release of Guest Molecules from Thiol–Ene Cross-Linked Poly(2-Oxazoline) Hydrogels. *J. Mater. Chem. B* **2019**, *7* (10), 1782–1794. <https://doi.org/10.1039/C8TB02575D>.
- (179) Waschinski, C. J.; Tiller, J. C. Poly(Oxazoline)s with Telechelic Antimicrobial Functions. *Biomacromolecules* **2005**, *6* (1), 235–243. <https://doi.org/10.1021/bm049553i>.
- (180) Monnery, B. D.; Jerca, V. V.; Sedlacek, O.; Verbraeken, B.; Cavill, R.; Hoogenboom, R. Defined High Molar Mass Poly(2-Oxazoline)s. *Angew. Chem. Int. Ed.* **2018**, *57* (47), 15400–15404. <https://doi.org/10.1002/anie.201807796>.
- (181) Schild, H. G.; Tirrell, D. A. Microcalorimetric Detection of Lower Critical Solution Temperatures in Aqueous Polymer Solutions. *J. Phys. Chem.* **1990**, *94* (10), 4352–4356. <https://doi.org/10.1021/j100373a088>.
- (182) Priest, J. H.; Murray, S. L.; Nelson, R. J.; Hoffman, A. S. Lower Critical Solution Temperatures of Aqueous Copolymers of N-Isopropylacrylamide and Other N-Substituted Acrylamides. In *Reversible Polymeric Gels and Related Systems*; ACS Symposium Series; American Chemical Society, 1987; Vol. 350, pp 255–264. <https://doi.org/10.1021/bk-1987-0350.ch018>.
- (183) Keddie, D. J.; Moad, G.; Rizzardo, E.; Thang, S. H. RAFT Agent Design and Synthesis. *Macromolecules* **2012**, *45* (13), 5321–5342. <https://doi.org/10.1021/ma300410v>.
- (184) Sperry, J. B.; Minter, C. J.; Tao, J.; Johnson, R.; Duzguner, R.; Hawksworth, M.; Oke, S.; Richardson, P. F.; Barnhart, R.; Bill, D. R.; Giusto, R. A.; Weaver, J. D. Thermal Stability Assessment of Peptide Coupling Reagents Commonly Used in Pharmaceutical Manufacturing. *Org. Process Res. Dev.* **2018**, *22* (9), 1262–1275. <https://doi.org/10.1021/acs.oprd.8b00193>.
- (185) Ganachaud, F.; Monteiro, M. J.; Gilbert, R. G.; Dourges, M.-A.; Thang, S. H.; Rizzardo, E. Molecular Weight Characterization of Poly(N -Isopropylacrylamide) Prepared by Living Free-Radical Polymerization. *Macromolecules* **2000**, *33* (18), 6738–6745. <https://doi.org/10.1021/ma0003102>.
- (186) Namivandi-Zangeneh, R.; Sadrearhami, Z.; Dutta, D.; Willcox, M.; Wong, E. H. H.; Boyer, C. Synergy between Synthetic Antimicrobial Polymer and Antibiotics: A Promising Platform To Combat Multidrug-Resistant Bacteria. *ACS Infect. Dis.* **2019**, *5* (8), 1357–1365. <https://doi.org/10.1021/acsinfecdis.9b00049>.
- (187) Nguyen, T.-K.; Lam, S. J.; Ho, K. K. K.; Kumar, N.; Qiao, G. G.; Egan, S.; Boyer, C.; Wong, E. H. H. Rational Design of Single-Chain Polymeric Nanoparticles That Kill Planktonic and Biofilm Bacteria. *ACS Infect. Dis.* **2017**, *3* (3), 237–248. <https://doi.org/10.1021/acsinfecdis.6b00203>.
- (188) Judzewitsch, P. R.; Zhao, L.; Wong, E. H. H.; Boyer, C. High-Throughput Synthesis of Antimicrobial Copolymers and Rapid Evaluation of Their Bioactivity. *Macromolecules* **2019**, *52* (11), 3975–3986. <https://doi.org/10.1021/acs.macromol.9b00290>.
- (189) Yin, H.; Kanasty, R. L.; Eltoukhy, A. A.; Vegas, A. J.; Dorkin, J. R.; Anderson, D. G. Non-Viral Vectors for Gene-Based Therapy. *Nat. Rev. Genet.* **2014**, *15* (8), 541–555. <https://doi.org/10.1038/nrg3763>.
- (190) Haensler, J.; Szoka, F. C. Polyamidoamine Cascade Polymers Mediate Efficient Transfection of Cells in Culture. *Bioconjug. Chem.* **1993**, *4* (5), 372–379. <https://doi.org/10.1021/bc00023a012>.
- (191) Tang, M.; Szoka, F. The Influence of Polymer Structure on the Interactions of Cationic Polymers with DNA and Morphology of the Resulting Complexes. *Gene Ther.* **1997**, *4* (8), 823–832. <https://doi.org/10.1038/sj.gt.3300454>.
- (192) Determan, M. D.; Cox, J. P.; Seifert, S.; Thiyagarajan, P.; Mallapragada, S. K. Synthesis and Characterization of Temperature and PH-Responsive Pentablock Copolymers. *Polymer* **2005**, *46* (18), 6933–6946. <https://doi.org/10.1016/j.polymer.2005.05.138>.
- (193) Zong, L.; Liu, F.; Chen, D.; Zhang, X.; Ling, C.; Li, A. A Novel Pyridine Based Polymer for Highly Efficient Separation of Nickel from High-Acidity and High-Concentration Cobalt Solutions. *Chem. Eng. J.* **2018**, *334*, 995–1005. <https://doi.org/10.1016/j.cej.2017.10.127>.

References

- (194) Wang, C.; Stewart, R. J.; Kopeček, J. Hybrid Hydrogels Assembled from Synthetic Polymers and Coiled-Coil Protein Domains. *Nature* **1999**, *397* (6718), 417–420. <https://doi.org/10.1038/17092>.
- (195) Toyoda, N.; Yoshida, M.; Otsu, T. Polymers from 1,2-Disubstituted Ethylenic Monomers VI. Monomer-Isomerization Radical Polymerization of Diethyl Maleate. *Polym. J.* **1983**, *15* (4), 255–260. <https://doi.org/10.1295/polymj.15.255>.
- (196) Ragnarsson, U.; Grehn, L. Dual Protection of Amino Functions Involving Boc. *RSC Adv.* **2013**, *3* (41), 18691. <https://doi.org/10.1039/c3ra42956c>.
- (197) Ashworth, I. W.; Cox, B. G.; Meyrick, B. Kinetics and Mechanism of *N*-Boc Cleavage: Evidence of a Second-Order Dependence upon Acid Concentration. *J. Org. Chem.* **2010**, *75* (23), 8117–8125. <https://doi.org/10.1021/jo101767h>.
- (198) Castellaro, S.; Catena, S.; Alfei, S. *Tert*-Butoxycarbonyl Protecting Group Location Induces Different Reactive Behaviors in the Five Possible Isoforms of Tri-Boc-Arginine. *ChemistrySelect* **2018**, *3* (31), 8826–8832. <https://doi.org/10.1002/slct.201801182>.
- (199) Wuts, P. G. M.; Greene, T. W. *Greene's Protective Groups in Organic Synthesis*; John Wiley & Sons, Inc.: Hoboken, NJ, USA, 2006. <https://doi.org/10.1002/0470053488>.
- (200) Zhao, C.; Chen, Q.; Patel, K.; Li, L.; Li, X.; Wang, Q.; Zhang, G.; Zheng, J. Synthesis and Characterization of PH-Sensitive Poly(*N*-2-Hydroxyethyl Acrylamide)–Acrylic Acid (Poly(HEAA/AA)) Nanogels with Antifouling Protection for Controlled Release. *Soft Matter* **2012**, *8* (30), 7848. <https://doi.org/10.1039/c2sm25861g>.
- (201) Seeman, N. C. DNA in a Material World. *Nature* **2003**, *421*, 427–431. <https://doi.org/10.1038/nature01406>.
- (202) Aldaye, F. A.; Palmer, A. L.; Sleiman, H. F. Assembling Materials with DNA as the Guide. *Science* **2008**, *321* (5897), 1795–1799. <https://doi.org/10.1126/science.1154533>.
- (203) Chidchob, P.; Sleiman, H. Supramolecular Chemistry with DNA. In *Macrocyclic and Supramolecular Chemistry*; Izatt, R. M., Ed.; John Wiley & Sons, Ltd: Chichester, UK, 2016; pp 10–37. <https://doi.org/10.1002/9781119053859.ch2>.
- (204) Seeman, N. C. Nucleic Acid Junctions and Lattices. *J. Theor. Biol.* **1982**, *99* (2), 237–247. [https://doi.org/10.1016/0022-5193\(82\)90002-9](https://doi.org/10.1016/0022-5193(82)90002-9).
- (205) Watson, J. D.; Crick, F. H. C. Molecular Structure of Nucleic Acids: A Structure for Deoxyribose Nucleic Acid. *Nature* **1953**, *171* (4356), 737–738. <https://doi.org/10.1038/171737a0>.
- (206) Yakovchuk, P. Base-Stacking and Base-Pairing Contributions into Thermal Stability of the DNA Double Helix. *Nucleic Acids Res.* **2006**, *34* (2), 564–574. <https://doi.org/10.1093/nar/gkj454>.
- (207) Winfree, E.; Liu, F.; Wenzler, L. A.; Seeman, N. C. Design and Self-Assembly of Two-Dimensional DNA Crystals. *Nature* **1998**, *394* (6693), 539–544. <https://doi.org/10.1038/28998>.
- (208) LaBean, T. H.; Yan, H.; Kopatsch, J.; Liu, F.; Winfree, E.; Reif, J. H.; Seeman, N. C. Construction, Analysis, Ligation, and Self-Assembly of DNA Triple Crossover Complexes. *J. Am. Chem. Soc.* **2000**, *122* (9), 1848–1860. <https://doi.org/10.1021/ja993393e>.
- (209) Liu, D.; Wang, M.; Deng, Z.; Walulu, R.; Mao, C. Tensegrity: Construction of Rigid DNA Triangles with Flexible Four-Arm DNA Junctions. *J. Am. Chem. Soc.* **2004**, *126* (8), 2324–2325. <https://doi.org/10.1021/ja031754r>.
- (210) He, Y.; Chen, Y.; Liu, H.; Ribbe, A. E.; Mao, C. Self-Assembly of Hexagonal DNA Two-Dimensional (2D) Arrays. *J. Am. Chem. Soc.* **2005**, *127* (35), 12202–12203. <https://doi.org/10.1021/ja0541938>.
- (211) Mathieu, F.; Liao, S.; Kopatsch, J.; Wang, T.; Mao, C.; Seeman, N. C. Six-Helix Bundles Designed from DNA. *Nano Lett.* **2005**, *5* (4), 661–665. <https://doi.org/10.1021/nl050084f>.
- (212) Yan, H.; Park, S. H.; Finkelstein, G.; Reif, J. H.; LaBean, T. H. DNA-Templated Self-Assembly of Protein Arrays and Highly Conductive Nanowires. *Science* **2003**, *301* (5641), 1882–1884. <https://doi.org/10.1126/science.1089389>.
- (213) Seeman, N. C. DNA Nicks and Nodes and Nanotechnology. *Nano Lett.* **2001**, *1* (1), 22–26. <https://doi.org/10.1021/nl000182v>.
- (214) Rothmund, P. W. K. Folding DNA to Create Nanoscale Shapes and Patterns. *Nature* **2006**, *440* (7082), 297–302. <https://doi.org/10.1038/nature04586>.
- (215) Douglas, S. M.; Dietz, H.; Liedl, T.; Högberg, B.; Graf, F.; Shih, W. M. Self-Assembly of DNA into

References

- Nanoscale Three-Dimensional Shapes. *Nature* **2009**, *459* (7245), 414–418. <https://doi.org/10.1038/nature08016>.
- (216) Ke, Y.; Douglas, S. M.; Liu, M.; Sharma, J.; Cheng, A.; Leung, A.; Liu, Y.; Shih, W. M.; Yan, H. Multilayer DNA Origami Packed on a Square Lattice. *J. Am. Chem. Soc.* **2009**, *131* (43), 15903–15908. <https://doi.org/10.1021/ja906381y>.
- (217) Ke, Y.; Voigt, N. V.; Gothelf, K. V.; Shih, W. M. Multilayer DNA Origami Packed on Hexagonal and Hybrid Lattices. *J. Am. Chem. Soc.* **2012**, *134* (3), 1770–1774. <https://doi.org/10.1021/ja209719k>.
- (218) Wei, B.; Dai, M.; Yin, P. Complex Shapes Self-Assembled from Single-Stranded DNA Tiles. *Nature* **2012**, *485* (7400), 623–626. <https://doi.org/10.1038/nature11075>.
- (219) Bates, F. S.; Fredrickson, G. H. Block Copolymers—Designer Soft Materials. *Phys. Today* **1999**, *52* (2), 32–38. <https://doi.org/10.1063/1.882522>.
- (220) Epps, III, T. H.; O'Reilly, R. K. Block Copolymers: Controlling Nanostructure to Generate Functional Materials – Synthesis, Characterization, and Engineering. *Chem. Sci.* **2016**, *7* (3), 1674–1689. <https://doi.org/10.1039/C5SC03505H>.
- (221) Mai, Y.; Eisenberg, A. Self-Assembly of Block Copolymers. *Chem. Soc. Rev.* **2012**, *41* (18), 5969. <https://doi.org/10.1039/c2cs35115c>.
- (222) Sprouse, D.; Jiang, Y.; Laaser, J. E.; Lodge, T. P.; Reineke, T. M. Tuning Cationic Block Copolymer Micelle Size by PH and Ionic Strength. *Biomacromolecules* **2016**, *17* (9), 2849–2859. <https://doi.org/10.1021/acs.biomac.6b00654>.
- (223) Lodge, T. P. Block Copolymers: Past Successes and Future Challenges. *Macromol. Chem. Phys.* **2003**, *204* (2), 265–273. <https://doi.org/10.1002/macp.200290073>.
- (224) Foster, J. C.; Varlas, S.; Couturaud, B.; Coe, Z.; O'Reilly, R. K. Getting into Shape: Reflections on a New Generation of Cylindrical Nanostructures' Self-Assembly Using Polymer Building Blocks. *J. Am. Chem. Soc.* **2019**, *141* (7), 2742–2753. <https://doi.org/10.1021/jacs.8b08648>.
- (225) Whitesides, G.; Mathias, J.; Seto, C. Molecular Self-Assembly and Nanochemistry: A Chemical Strategy for the Synthesis of Nanostructures. *Science* **1991**, *254* (5036), 1312–1319. <https://doi.org/10.1126/science.1962191>.
- (226) Discher, D. E.; Ahmed, F. POLYMERSOMES. *Annu. Rev. Biomed. Eng.* **2006**, *8* (1), 323–341. <https://doi.org/10.1146/annurev.bioeng.8.061505.095838>.
- (227) Lasic, D. D. Novel Applications of Liposomes. *Trends Biotechnol.* **1998**, *16* (7), 307–321. [https://doi.org/10.1016/S0167-7799\(98\)01220-7](https://doi.org/10.1016/S0167-7799(98)01220-7).
- (228) Carvalho, C. M. L.; Cabral, J. M. S. Reverse Micelles as Reaction Media for Lipases. *Lipase 2000* **2000**, *82* (11), 1063–1085. [https://doi.org/10.1016/S0300-9084\(00\)01187-1](https://doi.org/10.1016/S0300-9084(00)01187-1).
- (229) Malam, Y.; Loizidou, M.; Seifalian, A. M. Liposomes and Nanoparticles: Nanosized Vehicles for Drug Delivery in Cancer. *Trends Pharmacol. Sci.* **2009**, *30* (11), 592–599. <https://doi.org/10.1016/j.tips.2009.08.004>.
- (230) Allen, C.; Maysinger, D.; Eisenberg, A. Nano-Engineering Block Copolymer Aggregates for Drug Delivery. *Colloids Surf. B Biointerfaces* **1999**, *16* (1), 3–27. [https://doi.org/10.1016/S0927-7765\(99\)00058-2](https://doi.org/10.1016/S0927-7765(99)00058-2).
- (231) Jiao, W.; Yang, H.; Wu, Z.; Liu, J.; Zhang, W. Self-Assembled Block Polymer Aggregates in Selective Solution: Controllable Morphology Transitions and Their Applications in Drug Delivery. *Expert Opin. Drug Deliv.* **2020**, *17* (7), 947–961. <https://doi.org/10.1080/17425247.2020.1767582>.
- (232) Taylor, T. M.; Weiss, J.; Davidson, P. M.; Bruce, B. D. Liposomal Nanocapsules in Food Science and Agriculture. *Crit. Rev. Food Sci. Nutr.* **2005**, *45* (7–8), 587–605. <https://doi.org/10.1080/10408390591001135>.
- (233) Kwak, M.; Herrmann, A. Nucleic Acid/Organic Polymer Hybrid Materials: Synthesis, Superstructures, and Applications. *Angew. Chem. Int. Ed.* **2010**, *49* (46), 8574–8587. <https://doi.org/10.1002/anie.200906820>.

- (234) Li, Z.; Zhang, Y.; Fullhart, P.; Mirkin, C. A. Reversible and Chemically Programmable Micelle Assembly with DNA Block-Copolymer Amphiphiles. *Nano Lett.* **2004**, *4* (6), 1055–1058. <https://doi.org/10.1021/nl049628o>.
- (235) Carneiro, K. M. M.; Hamblin, G. D.; Hänni, K. D.; Fakhoury, J.; Nayak, M. K.; Rizis, G.; McLaughlin, C. K.; Bazzi, H. S.; Sleiman, H. F. Stimuli-Responsive Organization of Block Copolymers on DNA Nanotubes. *Chem. Sci.* **2012**, *3* (6), 1980–1986. <https://doi.org/10.1039/C2SC01065H>.
- (236) Wilks, T. R.; Bath, J.; de Vries, J. W.; Raymond, J. E.; Herrmann, A.; Turberfield, A. J.; O'Reilly, R. K. “Giant Surfactants” Created by the Fast and Efficient Functionalization of a DNA Tetrahedron with a Temperature-Responsive Polymer. *ACS Nano* **2013**, *7* (10), 8561–8572. <https://doi.org/10.1021/nm402642a>.
- (237) Edwardson, T. G. W.; Carneiro, K. M. M.; McLaughlin, C. K.; Serpell, C. J.; Sleiman, H. F. Site-Specific Positioning of Dendritic Alkyl Chains on DNA Cages Enables Their Geometry-Dependent Self-Assembly. *Nat. Chem.* **2013**, *5* (10), 868–875. <https://doi.org/10.1038/nchem.1745>.
- (238) Kolb, H. C.; Finn, M. G.; Sharpless, K. B. Click Chemistry: Diverse Chemical Function from a Few Good Reactions. *Angew. Chem. Int. Ed.* **2001**, *40* (11), 2004–2021. [https://doi.org/10.1002/1521-3773\(20010601\)40:11<2004::AID-ANIE2004>3.0.CO;2-5](https://doi.org/10.1002/1521-3773(20010601)40:11<2004::AID-ANIE2004>3.0.CO;2-5).
- (239) Hoyle, C. E.; Bowman, C. N. Thiol-Ene Click Chemistry. *Angew. Chem. Int. Ed.* **2010**, *49* (9), 1540–1573. <https://doi.org/10.1002/anie.200903924>.
- (240) Pickens, C. J.; Johnson, S. N.; Pressnall, M. M.; Leon, M. A.; Berkland, C. J. Practical Considerations, Challenges, and Limitations of Bioconjugation via Azide–Alkyne Cycloaddition. *Bioconjug. Chem.* **2018**, *29* (3), 686–701. <https://doi.org/10.1021/acs.bioconjchem.7b00633>.
- (241) Huisgen, R. 1,3-Dipolar Cycloadditions. Past and Future. *Angew. Chem. Int. Ed. Engl.* **1963**, *2* (10), 565–598. <https://doi.org/10.1002/anie.196305651>.
- (242) Tornøe, C. W.; Christensen, C.; Meldal, M. Peptidotriazoles on Solid Phase: [1,2,3]-Triazoles by Regiospecific Copper(I)-Catalyzed 1,3-Dipolar Cycloadditions of Terminal Alkynes to Azides. *J. Org. Chem.* **2002**, *67* (9), 3057–3064. <https://doi.org/10.1021/jo011148j>.
- (243) Bock, V. D.; Hiemstra, H.; van Maarseveen, J. H. CuI-Catalyzed Alkyne–Azide “Click” Cycloadditions from a Mechanistic and Synthetic Perspective. *Eur. J. Org. Chem.* **2006**, *2006* (1), 51–68. <https://doi.org/10.1002/ejoc.200500483>.
- (244) Hong, V.; Presolski, S.; Ma, C.; Finn, M. G. Analysis and Optimization of Copper-Catalyzed Azide–Alkyne Cycloaddition for Bioconjugation. *Angew. Chem. Int. Ed.* **2009**, *48* (52), 9879–9883. <https://doi.org/10.1002/anie.200905087>.
- (245) Agard, N. J.; Prescher, J. A.; Bertozzi, C. R. A Strain-Promoted [3 + 2] Azide–Alkyne Cycloaddition for Covalent Modification of Biomolecules in Living Systems. *J. Am. Chem. Soc.* **2004**, *126* (46), 15046–15047. <https://doi.org/10.1021/ja044996f>.
- (246) Baskin, J. M.; Prescher, J. A.; Laughlin, S. T.; Agard, N. J.; Chang, P. V.; Miller, I. A.; Lo, A.; Codelli, J. A.; Bertozzi, C. R. Copper-Free Click Chemistry for Dynamic in Vivo Imaging. *Proc. Natl. Acad. Sci. U. S. A.* **2007**, *104* (43), 16793–16797. <https://doi.org/10.1073/pnas.0707090104>.
- (247) Duan, Q.; Miura, Y.; Narumi, A.; Shen, X.; Sato, S.-I.; Satoh, T.; Kakuchi, T. Synthesis and Thermo-responsive Property of End-Functionalized Poly(N-Isopropylacrylamide) with Pyrenyl Group. *J. Polym. Sci. Part Polym. Chem.* **2006**, *44* (3), 1117–1124. <https://doi.org/10.1002/pola.21208>.
- (248) Furyk, S.; Zhang, Y.; Ortiz-Acosta, D.; Cremer, P. S.; Bergbreiter, D. E. Effects of End Group Polarity and Molecular Weight on the Lower Critical Solution Temperature of Poly(N-Isopropylacrylamide). *J. Polym. Sci. Part Polym. Chem.* **2006**, *44* (4), 1492–1501. <https://doi.org/10.1002/pola.21256>.
- (249) Appel, E. A.; del Barrio, J.; Loh, X. J.; Dyson, J.; Scherman, O. A. High Molecular Weight Polyacrylamides by Atom Transfer Radical Polymerization: Enabling Advancements in Water-Based Applications. *J. Polym. Sci. Part Polym. Chem.* **2012**, *50* (1), 181–186. <https://doi.org/10.1002/pola.25041>.
- (250) Li, Y.; Tseng, Y. D.; Kwon, S. Y.; d’Espaux, L.; Bunch, J. S.; McEuen, P. L.; Luo, D. Controlled Assembly of Dendrimer-like DNA. *Nat. Mater.* **2004**, *3* (1), 38–42. <https://doi.org/10.1038/nmat1045>.

References

- (251) Lenz, D. A.; Blaak, R.; Likos, C. N.; Mladek, B. M. Microscopically Resolved Simulations Prove the Existence of Soft Cluster Crystals. *Phys. Rev. Lett.* **2012**, *109* (22), 228301. <https://doi.org/10.1103/PhysRevLett.109.228301>.
- (252) Balibar, S. The Enigma of Supersolidity. *Nature* **2010**, *464* (7286), 176–182. <https://doi.org/10.1038/nature08913>.
- (253) Sciortino, F.; Zaccarelli, E. Soft Heaps and Clumpy Crystals. *Nature* **2013**, *493* (7430), 30–31. <https://doi.org/10.1038/493030a>.
- (254) Dostálek, J.; Knoll, W. Biosensors Based on Surface Plasmon-Enhanced Fluorescence Spectroscopy (Review). *Biointerphases* **2008**, *3* (3), FD12–FD22. <https://doi.org/10.1116/1.2994688>.
- (255) Liebermann, T.; Knoll, W. Surface-Plasmon Field-Enhanced Fluorescence Spectroscopy. *Colloids Surf. Physicochem. Eng. Asp.* **2000**, *171* (1–3), 115–130. [https://doi.org/10.1016/S0927-7757\(99\)00550-6](https://doi.org/10.1016/S0927-7757(99)00550-6).
- (256) Homola, J. Surface Plasmon Resonance Sensors for Detection of Chemical and Biological Species. *Chem. Rev.* **2008**, *108* (2), 462–493. <https://doi.org/10.1021/cr068107d>.
- (257) Chen, C.; Wang, J. Optical Biosensors: An Exhaustive and Comprehensive Review. *Analyst* **2020**, *145* (5), 1605–1628. <https://doi.org/10.1039/C9AN01998G>.
- (258) Kretschmann, E. Die Bestimmung Optischer Konstanten von Metallen Durch Anregung von Oberflächenplasmaschwingungen. *Z. Für Phys. Hadrons Nucl.* **1971**, *241* (4), 313–324. <https://doi.org/10.1007/BF01395428>.
- (259) Tang, Y.; Zeng, X.; Liang, J. Surface Plasmon Resonance: An Introduction to a Surface Spectroscopy Technique. *J. Chem. Educ.* **2010**, *87* (7), 742–746. <https://doi.org/10.1021/ed100186y>.
- (260) Sambles, J. R.; Bradbery, G. W.; Yang, F. Optical Excitation of Surface Plasmons: An Introduction. *Contemp. Phys.* **1991**, *32* (3), 173–183. <https://doi.org/10.1080/00107519108211048>.
- (261) Knoll, W. INTERFACES AND THIN FILMS AS SEEN BY BOUND ELECTROMAGNETIC WAVES. *Annu. Rev. Phys. Chem.* **1998**, *49* (1), 569–638. <https://doi.org/10.1146/annurev.physchem.49.1.569>.
- (262) Spinke, J.; Liley, M.; Guder, H. J.; Angermaier, L.; Knoll, W. Molecular Recognition at Self-Assembled Monolayers: The Construction of Multicomponent Multilayers. *Langmuir* **1993**, *9* (7), 1821–1825. <https://doi.org/10.1021/la00031a033>.
- (263) Noomnarm, U.; Clegg, R. M. Fluorescence Lifetimes: Fundamentals and Interpretations. *Photosynth. Res.* **2009**, *101* (2–3), 181–194. <https://doi.org/10.1007/s11120-009-9457-8>.
- (264) Weber, W. H.; Eagen, C. F. Energy Transfer from an Excited Dye Molecule to the Surface Plasmons of an Adjacent Metal. *Opt. Lett.* **1979**, *4* (8), 236–238. <https://doi.org/10.1364/OL.4.000236>.
- (265) Cortie, M. B.; McDonagh, A. M. Synthesis and Optical Properties of Hybrid and Alloy Plasmonic Nanoparticles. *Chem. Rev.* **2011**, *111* (6), 3713–3735. <https://doi.org/10.1021/cr1002529>.
- (266) Guo, X. Surface Plasmon Resonance Based Biosensor Technique: A Review. *J. Biophotonics* **2012**, *5* (7), 483–501. <https://doi.org/10.1002/jbio.201200015>.
- (267) Kang, Y.; Won, D.-J.; Kim, S. R.; Seo, K.; Choi, H.-S.; Lee, G.; Noh, Z.; Lee, T. S.; Lee, C. Self-Assembled Monolayer of the Aromatic Thioacetate on the Gold Surface. *14th Mol. Electron. Devices Symp.* **2004**, *24* (1), 43–46. <https://doi.org/10.1016/j.msec.2003.09.042>.
- (268) Love, J. C.; Estroff, L. A.; Kriebel, J. K.; Nuzzo, R. G.; Whitesides, G. M. Self-Assembled Monolayers of Thiolates on Metals as a Form of Nanotechnology. *Chem. Rev.* **2005**, *105* (4), 1103–1170. <https://doi.org/10.1021/cr0300789>.
- (269) Béthencourt, M. I.; Srisombat, L.; Chinwangso, P.; Lee, T. R. SAMs on Gold Derived from the Direct Adsorption of Alkanethioacetates Are Inferior to Those Derived from the Direct Adsorption of Alkanethiols. *Langmuir* **2009**, *25* (3), 1265–1271. <https://doi.org/10.1021/la803179q>.
- (270) Mintzer, M. A.; Simanek, E. E. Nonviral Vectors for Gene Delivery. *Chem. Rev.* **2009**, *109* (2), 259–302. <https://doi.org/10.1021/cr800409e>.
- (271) Cavazzana-Calvo, M.; Hacein-Bey, S.; Basile, G. de S.; Gross, F.; Yvon, E.; Nusbaum, P.; Selz, F.; Hue, C.; Certain, S.; Casanova, J.-L.; Bousso, P.; Deist, F. L.; Fischer, A. Gene Therapy of Human Severe Combined Immunodeficiency (SCID)-X1 Disease. *Science* **2000**, *288* (5466), 669. <https://doi.org/10.1126/science.288.5466.669>.

References

- (272) Lundstrom, K. Gene Therapy Today and Tomorrow. *Diseases* **2019**, *7* (2), 37. <https://doi.org/10.3390/diseases7020037>.
- (273) Christopher Boyd, A.; Guo, S.; Huang, L.; Kerem, B.; Oren, Y. S.; Walker, A. J.; Hart, S. L. New Approaches to Genetic Therapies for Cystic Fibrosis. *ECFS Cyst. Fibros. Res.* **2020**, *19*, S54–S59. <https://doi.org/10.1016/j.jcf.2019.12.012>.
- (274) Yan, Z.; McCray Jr, P. B.; Engelhardt, J. F. Advances in Gene Therapy for Cystic Fibrosis Lung Disease. *Hum. Mol. Genet.* **2019**, *28* (R1), R88–R94. <https://doi.org/10.1093/hmg/ddz139>.
- (275) Liu, L.; Li, M.; Xu, M.; Wang, Z.; Zeng, Z.; Li, Y.; Zhang, Y.; You, R.; Li, C.-H.; Guan, Y.-Q. Actively Targeted Gold Nanoparticle Composites Improve Behavior and Cognitive Impairment in Parkinson's Disease Mice. *Mater. Sci. Eng. C* **2020**, *114*, 111028. <https://doi.org/10.1016/j.msec.2020.111028>.
- (276) Kaplitt, M. G.; Feigin, A.; Tang, C.; Fitzsimons, H. L.; Mattis, P.; Lawlor, P. A.; Bland, R. J.; Young, D.; Strybing, K.; Eidelberg, D.; During, M. J. Safety and Tolerability of Gene Therapy with an Adeno-Associated Virus (AAV) Borne GAD Gene for Parkinson's Disease: An Open Label, Phase I Trial. *The Lancet* **2007**, *369* (9579), 2097–2105. [https://doi.org/10.1016/S0140-6736\(07\)60982-9](https://doi.org/10.1016/S0140-6736(07)60982-9).
- (277) Yang, Z. R.; Wang, H. F.; Zhao, J.; Peng, Y. Y.; Wang, J.; Guinn, B.-A.; Huang, L. Q. Recent Developments in the Use of Adenoviruses and Immunotoxins in Cancer Gene Therapy. *Cancer Gene Ther.* **2007**, *14* (7), 599–615. <https://doi.org/10.1038/sj.cgt.7701054>.
- (278) Cheng, R.; Feng, F.; Meng, F.; Deng, C.; Feijen, J.; Zhong, Z. Glutathione-Responsive Nano-Vehicles as a Promising Platform for Targeted Intracellular Drug and Gene Delivery. *J. Controlled Release* **2011**, *152* (1), 2–12. <https://doi.org/10.1016/j.jconrel.2011.01.030>.
- (279) Pardi, N.; Hogan, M. J.; Porter, F. W.; Weissman, D. mRNA Vaccines — a New Era in Vaccinology. *Nat. Rev. Drug Discov.* **2018**, *17* (4), 261–279. <https://doi.org/10.1038/nrd.2017.243>.
- (280) Polack, F. P.; Thomas, S. J.; Kitchin, N.; Absalon, J.; Gurtman, A.; Lockhart, S.; Perez, J. L.; Pérez Marc, G.; Moreira, E. D.; Zerbini, C.; Bailey, R.; Swanson, K. A.; Roychoudhury, S.; Koury, K.; Li, P.; Kalina, W. V.; Cooper, D.; Frenck, R. W., Jr; Hammitt, L. L.; Türeci, Ö.; Nell, H.; Schaefer, A.; Ünal, S.; Tresnan, D. B.; Mather, S.; Dormitzer, P. R.; Şahin, U.; Jansen, K. U.; Gruber, W. C.; C4591001 Clinical Trial Group. Safety and Efficacy of the BNT162b2 mRNA Covid-19 Vaccine. *N. Engl. J. Med.* **2020**, *383* (27), 2603–2615. <https://doi.org/10.1056/NEJMoa2034577>.
- (281) Krammer, F. SARS-CoV-2 Vaccines in Development. *Nature* **2020**, *586* (7830), 516–527. <https://doi.org/10.1038/s41586-020-2798-3>.
- (282) Chen, J.; Wang, K.; Wu, J.; Tian, H.; Chen, X. Polycations for Gene Delivery: Dilemmas and Solutions. *Bioconjug. Chem.* **2019**, *30* (2), 338–349. <https://doi.org/10.1021/acs.bioconjchem.8b00688>.
- (283) Potter, H. Electroporation in Biology: Methods, Applications, and Instrumentation. *Anal. Biochem.* **1988**, *174* (2), 361–373. [https://doi.org/10.1016/0003-2697\(88\)90035-8](https://doi.org/10.1016/0003-2697(88)90035-8).
- (284) Lambrecht, L.; Lopes, A.; Kos, S.; Sersa, G.; Pr at, V.; Vandermeulen, G. Clinical Potential of Electroporation for Gene Therapy and DNA Vaccine Delivery. *Expert Opin. Drug Deliv.* **2016**, *13* (2), 295–310. <https://doi.org/10.1517/17425247.2016.1121990>.
- (285) Wolff, J.; Malone, R.; Williams, P.; Chong, W.; Acsadi, G.; Jani, A.; Felgner, P. Direct Gene Transfer into Mouse Muscle in Vivo. *Science* **1990**, *247* (4949), 1465–1468. <https://doi.org/10.1126/science.1690918>.
- (286) Evans, C. H.; Ghivizzani, S. C.; Robbins, P. D. Gene Delivery to Joints by Intra-Articular Injection. *Hum. Gene Ther.* **2017**, *29* (1), 2–14. <https://doi.org/10.1089/hum.2017.181>.
- (287) Chien, C.-T.; Liu, C.-Y.; Wu, Z.-W.; Chen, P.-J.; Chu, C.-L.; Lin, S.-Y. Co-Caged Gold Nanoclusters and Methyl Motifs Lead to Detoxification of Dendrimers and Allow Cytosolic Access for SiRNA Transfection. *J Mater Chem B* **2014**, *2* (39), 6730–6737. <https://doi.org/10.1039/C4TB01153H>.
- (288) Mislick, K. A.; Baldeschwieler, J. D. Evidence for the Role of Proteoglycans in Cation-Mediated Gene Transfer. *Proc. Natl. Acad. Sci.* **1996**, *93* (22), 12349–12354. <https://doi.org/10.1073/pnas.93.22.12349>.
- (289) Ruponen, M.; Honkakoski, P.; Tammi, M.; Urtti, A. Cell-Surface Glycosaminoglycans Inhibit Cation-Mediated Gene Transfer. *J. Gene Med.* **2004**, *6* (4), 405–414. <https://doi.org/10.1002/jgm.522>.

References

- (290) Billiet, L.; Gomez, J.-P.; Berchel, M.; Jaffrès, P.-A.; Le Gall, T.; Montier, T.; Bertrand, E.; Cheradame, H.; Guégan, P.; Mével, M.; Pitard, B.; Benvegna, T.; Lehn, P.; Pichon, C.; Midoux, P. Gene Transfer by Chemical Vectors, and Endocytosis Routes of Polyplexes, Lipoplexes and Lipopolyplexes in a Myoblast Cell Line. *Biomaterials* **2012**, *33* (10), 2980–2990. <https://doi.org/10.1016/j.biomaterials.2011.12.027>.
- (291) Wattiaux, R.; Laurent, N.; Wattiaux-De Coninck, S.; Jadot, M. Endosomes, Lysosomes: Their Implication in Gene Transfer. *Recent Adv. Cell. Subcell. Mol. Target.* **2000**, *41* (2), 201–208. [https://doi.org/10.1016/S0169-409X\(99\)00066-6](https://doi.org/10.1016/S0169-409X(99)00066-6).
- (292) Behr, J.-P. The Proton Sponge: A Trick to Enter Cells the Viruses Did Not Exploit. *Chim. Int. J. Chem.* **1997**, *51* (1–2), 34–36.
- (293) Benjaminsen, R. V.; Matthebjerg, M. A.; Henriksen, J. R.; Moghimi, S. M.; Andresen, T. L. The Possible "proton Sponge" Effect of Polyethylenimine (PEI) Does Not Include Change in Lysosomal PH. *Mol. Ther. J. Am. Soc. Gene Ther.* **2013**, *21* (1), 149–157. <https://doi.org/10.1038/mt.2012.185>.
- (294) Pouton, C. W.; Seymour, L. W. Key Issues in Non-Viral Gene Delivery IPII of Original Article: S0169-409X(98)00048-9. The Article Was Originally Published in *Advanced Drug Delivery Reviews* 34 (1998) 3–19.1. *Spec. Issue Dedic. Dr Eric Tomlinson Adv. Drug Deliv. Rev. Sel. Most Highly Cited Artic. 1991-1998* **2001**, *46* (1), 187–203. [https://doi.org/10.1016/S0169-409X\(00\)00133-2](https://doi.org/10.1016/S0169-409X(00)00133-2).
- (295) Anson, D. S. The Use of Retroviral Vectors for Gene Therapy-What Are the Risks? A Review of Retroviral Pathogenesis and Its Relevance to Retroviral Vector-Mediated Gene Delivery. *Genet. Vaccines Ther.* **2004**, *2* (1), 9–9. <https://doi.org/10.1186/1479-0556-2-9>.
- (296) Miller, A. D. Retroviral Vectors in Gene Therapy. In *eLS*; American Cancer Society, 2006. <https://doi.org/10.1038/npg.els.0005741>.
- (297) Crystal, R. G. Adenovirus: The First Effective In Vivo Gene Delivery Vector. *Hum. Gene Ther.* **2014**, *25* (1), 3–11. <https://doi.org/10.1089/hum.2013.2527>.
- (298) Lee, C. S.; Bishop, E. S.; Zhang, R.; Yu, X.; Farina, E. M.; Yan, S.; Zhao, C.; Zeng, Z.; Shu, Y.; Wu, X.; Lei, J.; Li, Y.; Zhang, W.; Yang, C.; Wu, K.; Wu, Y.; Ho, S.; Athiviraham, A.; Lee, M. J.; Wolf, J. M.; Reid, R. R.; He, T.-C. Adenovirus-Mediated Gene Delivery: Potential Applications for Gene and Cell-Based Therapies in the New Era of Personalized Medicine. *Genes Dis.* **2017**, *4* (2), 43–63. <https://doi.org/10.1016/j.gendis.2017.04.001>.
- (299) Boussif, O.; Lezoualc'h, F.; Zanta, M. A.; Mergny, M. D.; Scherman, D.; Demeneix, B.; Behr, J. P. A Versatile Vector for Gene and Oligonucleotide Transfer into Cells in Culture and in Vivo: Polyethylenimine. *Proc. Natl. Acad. Sci.* **1995**, *92* (16), 7297. <https://doi.org/10.1073/pnas.92.16.7297>.
- (300) Neu, M.; Fischer, D.; Kissel, T. Recent Advances in Rational Gene Transfer Vector Design Based on Poly(Ethylene Imine) and Its Derivatives. *J. Gene Med.* **2005**, *7* (8), 992–1009. <https://doi.org/10.1002/jgm.773>.
- (301) Wang, Y.; Zheng, M.; Meng, F.; Zhang, J.; Peng, R.; Zhong, Z. Branched Polyethylenimine Derivatives with Reductively Cleavable Periphery for Safe and Efficient In Vitro Gene Transfer. *Biomacromolecules* **2011**, *12* (4), 1032–1040. <https://doi.org/10.1021/bm101364f>.
- (302) van de Wetering, P.; Cherng, J.-Y.; Talsma, H.; Hennink, W. E. Relation between Transfection Efficiency and Cytotoxicity of Poly(2-(Dimethylamino)Ethyl Methacrylate)/Plasmid Complexes. *J. Controlled Release* **1997**, *49* (1), 59–69. [https://doi.org/10.1016/S0168-3659\(97\)00059-X](https://doi.org/10.1016/S0168-3659(97)00059-X).
- (303) Cherng, J.-Y.; van de Wetering, P.; Talsma, H.; Crommelin, D. J. A.; Hennink, W. E. Effect of Size and Serum Proteins on Transfection Efficiency of Poly ((2-Dimethylamino)Ethyl Methacrylate)-Plasmid Nanoparticles. *Pharm. Res.* **1996**, *13* (7), 1038–1042. <https://doi.org/10.1023/A:1016054623543>.
- (304) Funhoff, A. M.; van Nostrum, C. F.; Koning, G. A.; Schuurmans-Nieuwenbroek, N. M. E.; Crommelin, D. J. A.; Hennink, W. E. Endosomal Escape of Polymeric Gene Delivery Complexes Is Not Always Enhanced by Polymers Buffering at Low PH. *Biomacromolecules* **2004**, *5* (1), 32–39. <https://doi.org/10.1021/bm034041+>.
- (305) Dubruel, P.; Christiaens, B.; Vanloo, B.; Bracke, K.; Rosseneu, M.; Vandekerckhove, J.; Schacht, E. Physicochemical and Biological Evaluation of Cationic Polymethacrylates as Vectors for Gene Delivery. *Eur. J. Pharm. Sci.* **2003**, *18* (3–4), 211–220. [https://doi.org/10.1016/S0928-0987\(02\)00280-4](https://doi.org/10.1016/S0928-0987(02)00280-4).

References

- (306) van de Wetering, P.; Cherng, J.-Y.; Talsma, H.; Crommelin, D. J. A.; Hennink, W. E. 2-(Dimethylamino)Ethyl Methacrylate Based (Co)Polymers as Gene Transfer Agents. *J. Controlled Release* **1998**, *53* (1), 145–153. [https://doi.org/10.1016/S0168-3659\(97\)00248-4](https://doi.org/10.1016/S0168-3659(97)00248-4).
- (307) Ferruti, P.; Franchini, J.; Bencini, M.; Ranucci, E.; Zara, G. P.; Serpe, L.; Primo, L.; Cavalli, R. Prevalingly Cationic Agmatine-Based Amphoteric Polyamidoamine as a Nontoxic, Nonhemolytic, and “Stealthlike” DNA Complexing Agent and Transfection Promoter. *Biomacromolecules* **2007**, *8* (5), 1498–1504. <https://doi.org/10.1021/bm061126c>.
- (308) Lin, C.; Zhong, Z.; Lok, M. C.; Jiang, X.; Hennink, W. E.; Feijen, J.; Engbersen, J. F. J. Linear Poly(Amido Amine)s with Secondary and Tertiary Amino Groups and Variable Amounts of Disulfide Linkages: Synthesis and in Vitro Gene Transfer Properties. *Proc. Ninth Eur. Symp. Control. Drug Deliv.* **2006**, *116* (2), 130–137. <https://doi.org/10.1016/j.jconrel.2006.09.009>.
- (309) Yang, J.; Zhang, Q.; Chang, H.; Cheng, Y. Surface-Engineered Dendrimers in Gene Delivery. *Chem. Rev.* **2015**, *115* (11), 5274–5300. <https://doi.org/10.1021/cr500542t>.
- (310) Mintzer, M. A.; Grinstaff, M. W. Biomedical Applications of Dendrimers: A Tutorial. *Chem Soc Rev* **2011**, *40* (1), 173–190. <https://doi.org/10.1039/B901839P>.
- (311) Gupta, B.; Levchenko, T. S.; Torchilin, V. P. Intracellular Delivery of Large Molecules and Small Particles by Cell-Penetrating Proteins and Peptides. *Protein- Pept.-Mediat. Transduct. Mech. Implic. Drug Deliv.* **2005**, *57* (4), 637–651. <https://doi.org/10.1016/j.addr.2004.10.007>.
- (312) Kemp, J. A.; Shim, M. S.; Heo, C. Y.; Kwon, Y. J. “Combo” Nanomedicine: Co-Delivery of Multi-Modal Therapeutics for Efficient, Targeted, and Safe Cancer Therapy. *Deliv. Multi-Modal Ther. Synerg. Ther.* **2016**, *98*, 3–18. <https://doi.org/10.1016/j.addr.2015.10.019>.
- (313) Guan, X.; Guo, Z.; Lin, L.; Chen, J.; Tian, H.; Chen, X. Ultrasensitive PH Triggered Charge/Size Dual-Rebound Gene Delivery System. *Nano Lett.* **2016**, *16* (11), 6823–6831. <https://doi.org/10.1021/acs.nanolett.6b02536>.
- (314) Dash, P. R.; Read, M. L.; Barrett, L. B.; Wolfert, M. A.; Seymour, L. W. Factors Affecting Blood Clearance and in Vivo Distribution of Polyelectrolyte Complexes for Gene Delivery. *Gene Ther.* **1999**, *6* (4), 643–650. <https://doi.org/10.1038/sj.gt.3300843>.
- (315) Ogris, M.; Steinlein, P.; Carotta, S.; Brunner, S.; Wagner, E. DNA/Polyethylenimine Transfection Particles: Influence of Ligands, Polymer Size, and PEGylation on Internalization and Gene Expression. *AAPS PharmSci* **2001**, *3* (3), E21–E21. <https://doi.org/10.1208/ps030321>.
- (316) Tian, H.; Lin, L.; Chen, J.; Chen, X.; Park, T. G.; Maruyama, A. RGD Targeting Hyaluronic Acid Coating System for PEI-PBLG Polycation Gene Carriers. *Asian J Foresight Program Spec. Issue* **2011**, *155* (1), 47–53. <https://doi.org/10.1016/j.jconrel.2011.01.025>.
- (317) Xu, D.-M.; Yao, S.-D.; Liu, Y.-B.; Sheng, K.-L.; Hong, J.; Gong, P.-J.; Dong, L. Size-Dependent Properties of M-PEIs Nanogels for Gene Delivery in Cancer Cells. *Int. J. Pharm.* **2007**, *338* (1), 291–296. <https://doi.org/10.1016/j.ijpharm.2007.01.050>.
- (318) Guo, Z.; Chen, J.; Lin, L.; Guan, X.; Sun, P.; Chen, M.; Tian, H.; Chen, X. PH Triggered Size Increasing Gene Carrier for Efficient Tumor Accumulation and Excellent Antitumor Effect. *ACS Appl. Mater. Interfaces* **2017**, *9* (18), 15297–15306. <https://doi.org/10.1021/acsami.7b02734>.
- (319) Liang, S.; Yang, X.-Z.; Du, X.-J.; Wang, H.-X.; Li, H.-J.; Liu, W.-W.; Yao, Y.-D.; Zhu, Y.-H.; Ma, Y.-C.; Wang, J.; Song, E.-W. Optimizing the Size of Micellar Nanoparticles for Efficient siRNA Delivery. *Adv. Funct. Mater.* **2015**, *25* (30), 4778–4787. <https://doi.org/10.1002/adfm.201501548>.
- (320) Chen, J.; Tian, H.; Dong, X.; Guo, Z.; Jiao, Z.; Li, F.; Kano, A.; Maruyama, A.; Chen, X. Effective Tumor Treatment by VEGF siRNA Complexed with Hydrophobic Poly(Amino Acid)-Modified Polyethylenimine. *Macromol. Biosci.* **2013**, *13* (10), 1438–1446. <https://doi.org/10.1002/mabi.201300211>.
- (321) Godbey, W. T.; Wu, K. K.; Mikos, A. G. Size Matters: Molecular Weight Affects the Efficiency of Poly(Ethylenimine) as a Gene Delivery Vehicle. *J. Biomed. Mater. Res.* **1999**, *45* (3), 268–275. [https://doi.org/10.1002/\(SICI\)1097-4636\(19990605\)45:3<268::AID-JBM15>3.0.CO;2-Q](https://doi.org/10.1002/(SICI)1097-4636(19990605)45:3<268::AID-JBM15>3.0.CO;2-Q).

References

- (322) Petersen, H.; Kunath, K.; Martin, A. L.; Stolnik, S.; Roberts, C. J.; Davies, M. C.; Kissel, T. Star-Shaped Poly(Ethylene Glycol)-Block-Polyethylenimine Copolymers Enhance DNA Condensation of Low Molecular Weight Polyethylenimines. *Biomacromolecules* **2002**, *3* (5), 926–936. <https://doi.org/10.1021/bm025539z>.
- (323) Chen, L.; Tian, H.; Chen, J.; Chen, X.; Huang, Y.; Jing, X. Multi-Armed Poly(L-Glutamic Acid)-Graft-Oligoethylenimine Copolymers as Efficient Nonviral Gene Delivery Vectors. *J. Gene Med.* **2010**, *12* (1), 64–76. <https://doi.org/10.1002/jgm.1405>.
- (324) Jiang, X.; Zhang, J.; Zhou, Y.; Xu, J.; Liu, S. Facile Preparation of Core-Crosslinked Micelles from Azide-Containing Thermoresponsive Double Hydrophilic Diblock Copolymer via Click Chemistry. *J. Polym. Sci. Part Polym. Chem.* **2008**, *46* (3), 860–871. <https://doi.org/10.1002/pola.22430>.
- (325) Liu, S.; Huang, W.; Jin, M.-J.; Fan, B.; Xia, G.-M.; Gao, Z.-G. Inhibition of Murine Breast Cancer Growth and Metastasis by Survivin-Targeted siRNA Using Disulfide Cross-Linked Linear PEI. *Eur. J. Pharm. Sci.* **2016**, *82*, 171–182. <https://doi.org/10.1016/j.ejps.2015.11.009>.
- (326) Liu, Z.; Zhang, Z.; Zhou, C.; Jiao, Y. Hydrophobic Modifications of Cationic Polymers for Gene Delivery. *Top. Issue Biomater.* **2010**, *35* (9), 1144–1162. <https://doi.org/10.1016/j.progpolymsci.2010.04.007>.
- (327) Kuhn, P. S.; Levin, Y.; Barbosa, M. C. Charge Inversion in DNA–Amphiphile Complexes: Possible Application to Gene Therapy. *Phys. Stat. Mech. Its Appl.* **1999**, *274* (1), 8–18. [https://doi.org/10.1016/S0378-4371\(99\)00409-4](https://doi.org/10.1016/S0378-4371(99)00409-4).
- (328) Ong, Z. Y.; Yang, C.; Cheng, W.; Voo, Z. X.; Chin, W.; Hedrick, J. L.; Yang, Y. Y. Biodegradable Cationic Poly(Carbonates): Effect of Varying Side Chain Hydrophobicity on Key Aspects of Gene Transfection. *Acta Biomater.* **2017**, *54*, 201–211. <https://doi.org/10.1016/j.actbio.2017.03.027>.
- (329) Alshamsan, A.; Haddadi, A.; Incani, V.; Samuel, J.; Lavasanifar, A.; Uludağ, H. Formulation and Delivery of siRNA by Oleic Acid and Stearic Acid Modified Polyethylenimine. *Mol. Pharm.* **2009**, *6* (1), 121–133. <https://doi.org/10.1021/mp8000815>.
- (330) M. Molas; A. G. Gomez-Valades; A. Vidal-Alabro; M. Miguel-Turu; J. Bermudez; R. Bartrons and J. C. Perales. Receptor-Mediated Gene Transfer Vectors: Progress Towards Genetic Pharmaceuticals. *Curr. Gene Ther.* **2003**, *3* (5), 468–485. <https://doi.org/10.2174/1566523034578195>.
- (331) Chen, J.; Guan, X.; Hu, Y.; Tian, H.; Chen, X. Peptide-Based and Polypeptide-Based Gene Delivery Systems. In *Polymeric Gene Delivery Systems*; Cheng, Y., Ed.; Springer International Publishing: Cham, 2018; pp 85–112. https://doi.org/10.1007/978-3-319-77866-2_4.
- (332) McKenzie, D. L.; Kwok, K. Y.; Rice, K. G. A Potent New Class of Reductively Activated Peptide Gene Delivery Agents. *J. Biol. Chem.* **2000**, *275* (14), 9970–9977. <https://doi.org/10.1074/jbc.275.14.9970>.
- (333) Bouraoui, A.; Ghanem, R.; Berchel, M.; Deschamps, L.; Vié, V.; Paboeuf, G.; Le Gall, T.; Montier, T.; Jaffrès, P.-A. Branched Lipid Chains to Prepare Cationic Amphiphiles Producing Hexagonal Aggregates: Supramolecular Behavior and Application to Gene Delivery. *Org. Biomol. Chem.* **2020**, *18* (2), 337–345. <https://doi.org/10.1039/C9OB02381J>.
- (334) Zhao, C.; Patel, K.; Aichinger, L. M.; Liu, Z.; Hu, R.; Chen, H.; Li, X.; Li, L.; Zhang, G.; Chang, Y.; Zheng, J. Antifouling and Biodegradable Poly(N-Hydroxyethyl Acrylamide) (PolyHEAA)-Based Nanogels. *RSC Adv.* **2013**, *3* (43), 19991–20000. <https://doi.org/10.1039/C3RA42323A>.
- (335) Hyde, S. C.; Pringle, I. A.; Abdullah, S.; Lawton, A. E.; Davies, L. A.; Varathalingam, A.; Nunez-Alonso, G.; Green, A.-M.; Bazzani, R. P.; Sumner-Jones, S. G.; Chan, M.; Li, H.; Yew, N. S.; Cheng, S. H.; Christopher Boyd, A.; Davies, J. C.; Griesenbach, U.; Porteous, D. J.; Sheppard, D. N.; Munkonge, F. M.; Alton, E. W. F. W.; Gill, D. R. CpG-Free Plasmids Confer Reduced Inflammation and Sustained Pulmonary Gene Expression. *Nat. Biotechnol.* **2008**, *26* (5), 549–551. <https://doi.org/10.1038/nbt1399>.
- (336) Reinhardt, C. G.; Krugh, T. R. A Comparative Study of Ethidium Bromide Complexes with Dinucleotides and DNA: Direct Evidence for Intercalation and Nucleic Acid Sequence Preferences. *Biochemistry* **1978**, *17* (23), 4845–4854. <https://doi.org/10.1021/bi00616a001>.
- (337) Olmsted, J.; Kearns, D. R. Mechanism of Ethidium Bromide Fluorescence Enhancement on Binding to Nucleic Acids. *Biochemistry* **1977**, *16* (16), 3647–3654. <https://doi.org/10.1021/bi00635a022>.

References

- (338) Swami, A.; Kurupati, R. K.; Pathak, A.; Singh, Y.; Kumar, P.; Gupta, K. C. A Unique and Highly Efficient Non-Viral DNA/SiRNA Delivery System Based on PEI-Bisepoxide Nanoparticles. *Biochem. Biophys. Res. Commun.* **2007**, *362* (4), 835–841. <https://doi.org/10.1016/j.bbrc.2007.08.073>.
- (339) Crouch, S. P. M.; Kozlowski, R.; Slater, K. J.; Fletcher, J. The Use of ATP Bioluminescence as a Measure of Cell Proliferation and Cytotoxicity. *J. Immunol. Methods* **1993**, *160* (1), 81–88. [https://doi.org/10.1016/0022-1759\(93\)90011-U](https://doi.org/10.1016/0022-1759(93)90011-U).
- (340) Arndt, T. Luciferin-Luciferase-System. In *Lexikon der Medizinischen Laboratoriumsdiagnostik*; Gressner, A. M., Arndt, T., Eds.; Springer Berlin Heidelberg: Berlin, Heidelberg, 2019; pp 1535–1535. https://doi.org/10.1007/978-3-662-48986-4_1977.
- (341) Smith, P. K.; Krohn, R. I.; Hermanson, G. T.; Mallia, A. K.; Gartner, F. H.; Provenzano, M. D.; Fujimoto, E. K.; Goeke, N. M.; Olson, B. J.; Klenk, D. C. Measurement of Protein Using Bicinchoninic Acid. *Anal. Biochem.* **1985**, *150* (1), 76–85. [https://doi.org/10.1016/0003-2697\(85\)90442-7](https://doi.org/10.1016/0003-2697(85)90442-7).
- (342) Campbell, A. K. *Chemiluminescence: Principles and Applications in Biology and Medicine*; Ellis Horwood series in biomedicine; VCH; E. Horwood: New York, NY, USA : Chichester, England, 1988.
- (343) Armarego, W. L. F.; Perrin, D. D. *Purification of Laboratory Chemicals*, 4. ed., reprint.; Butterworth-Heinemann: Oxford, 2002.
- (344) Benalil, A.; Carboni, B.; Vaultier, M. Synthesis of 1,2-Aminoazides. Conversion to Unsymmetrical Vicinal Diamines by Catalytic Hydrogenation or Reductive Alkylation with Dichloroboranes. *Tetrahedron* **1991**, *47* (38), 8177–8194. [https://doi.org/10.1016/S0040-4020\(01\)91013-0](https://doi.org/10.1016/S0040-4020(01)91013-0).
- (345) Le Gall, T.; Baussanne, I.; Halder, S.; Carmoy, N.; Montier, T.; Lehn, P.; Décout, J.-L. Synthesis and Transfection Properties of a Series of Lipidic Neamine Derivatives. *Bioconjug. Chem.* **2009**, *20* (11), 2032–2046. <https://doi.org/10.1021/bc9000062z>.
- (346) Le Gall, T.; Loizeau, D.; Picquet, E.; Carmoy, N.; Yaouanc, J.-J.; Burel-Deschamps, L.; Delépine, P.; Giamarchi, P.; Jaffrès, P.-A.; Lehn, P.; Montier, T. A Novel Cationic Lipophosphoramidate with Diunsaturated Lipid Chains: Synthesis, Physicochemical Properties, and Transfection Activities. *J. Med. Chem.* **2010**, *53* (4), 1496–1508. <https://doi.org/10.1021/jm900897a>.

Acknowledgements

In erster Linie möchte ich mich bei Prof. Ulrich Jonas für die Möglichkeit der Promotion in seiner Arbeitsgruppe bedanken, wie auch für die Ratschläge und Diskussionen, die zur Durchführung der Promotion sehr hilfreich waren.

Des Weiteren danke ich Dr. Emmanuel Stiakakis vom Forschungszentrum in Jülich für die konstruktive und erfolgreiche Zusammenarbeit während der letzten vier Jahre.

Dr. Tony Le Gall und Prof. Dr. Tristan Montier danke ich für die Möglichkeit die Labore in Brest zu besuchen, um dort sehr interessante Einblicke in die Durchführung von Zellversuchen zu erlangen. Dr. Yann Le Guen danke ich für die Unterstützung bei den Versuchen während des Aufenthalts in Brest und die großartige Gastfreundschaft und die interessanten und auch lustigen Gespräche. Gleichzeitig danke ich auch Dr. Frank Thetiot für seine Gastfreundschaft und die interessanten Unterhaltungen, welche den Aufenthalt in Brest so beeindruckend gemacht haben.

Vielen Dank sagen möchte ich auch Dr. Jakub Dostalek und Prof. Wolfgang Knoll für die Möglichkeit in den Laboren des AIT zu arbeiten und praktische Erfahrungen in der SPR Spektroskopie zu sammeln. Der Biosensor Technologie Gruppe des AIT in Tulln danke ich für die Unterstützung und die großartige Zeit während meines Aufenthalts in Wien.

Weiterhin danke ich Dr. Ulrike Ritz und Kira Vogel vom Universitätsklinikum Mainz für die Durchführung von Zellexperimenten und die konstruktive Zusammenarbeit.

Ein großer Dank gilt Petra Frank für das Korrekturlesen dieser Arbeit, die hilfreichen Tipps und die fachlichen Diskussionen während der letzten Jahre. Danken möchte ich auch Max Meier und Thorben Jaik für die vielen interessanten und teilweise auch sehr lustigen Unterhaltungen nicht nur über Fachliches, sondern so ziemlich alles. Der gesamten Arbeitsgruppe der makromolekularen Chemie danke ich neben der sehr angenehmen Arbeitsatmosphäre mit zahlreichen und konstruktiven Diskussionen, auch für einige großartige Abende und Ausflüge. Weiterhin gilt mein Dank auch den Bachelor- und Masterstudenten, mit denen ich zusammenarbeiten durfte.

Danken möchte ich auch Dr. Thomas Paululat für den stets großartigen und schnellen NMR Service.

Ganz besonders bedanken möchte ich mich bei meiner Familie und Freundin, die mir jederzeit den Rücken freigehalten haben und mir immer mit Rat und Tat zur Seite gestanden haben.

Zuletzt möchte ich bei allen bedanken, die hier nicht erwähnt wurden und die zum Gelingen dieser Dissertation beigetragen haben.